FROM GLYCEROL TO VALUE-ADDED PRODUCTS

EDITED BY: Patrick Cognet and Mohamed Kheireddine Aroua

frontiers Research Topics

About Frontiers

Frontiers is more than just an open-access publisher of scholarly articles: it is a pioneering approach to the world of academia, radically improving the way scholarly research is managed. The grand vision of Frontiers is a world where all people have an equal opportunity to seek, share and generate knowledge. Frontiers provides immediate and permanent online open access to all its publications, but this alone is not enough to realize our grand goals.

Frontiers Journal Series

The Frontiers Journal Series is a multi-tier and interdisciplinary set of open-access, online journals, promising a paradigm shift from the current review, selection and dissemination processes in academic publishing. All Frontiers journals are driven by researchers for researchers; therefore, they constitute a service to the scholarly community. At the same time, the Frontiers Journal Series operates on a revolutionary invention, the tiered publishing system, initially addressing specific communities of scholars, and gradually climbing up to broader public understanding, thus serving the interests of the lay society, too.

Dedication to Quality

Each Frontiers article is a landmark of the highest quality, thanks to genuinely collaborative interactions between authors and review editors, who include some of the world's best academicians. Research must be certified by peers before entering a stream of knowledge that may eventually reach the public - and shape society; therefore, Frontiers only applies the most rigorous and unbiased reviews.
Frontiers revolutionizes research publishing by freely delivering the most outstanding research, evaluated with no bias from both the academic and social point of view. By applying the most advanced information technologies, Frontiers is catapulting scholarly publishing into a new generation.

What are Frontiers Research Topics?

Frontiers Research Topics are very popular trademarks of the Frontiers Journals Series: they are collections of at least ten articles, all centered on a particular subject. With their unique mix of varied contributions from Original Research to Review Articles, Frontiers Research Topics unify the most influential researchers, the latest key findings and historical advances in a hot research area! Find out more on how to host your own Frontiers Research Topic or contribute to one as an author by contacting the Frontiers Editorial Office: researchtopics@frontiersin.org

FROM GLYCEROL TO VALUE-ADDED PRODUCTS

Table of Contents

Check for
updates

Editorial: From Glycerol to Value-Added Products

Mohamed Kheireddine Aroua[1,2] and Patrick Cognet[3]*

[1] Centre for Carbon Dioxide Capture and Utilisation, School of Science and Technology, Sunway University, Subang Jaya, Malaysia, [2] Department of Engineering, Faculty of Science and Technology, Lancaster University, Bailrigg, United Kingdom, [3] Laboratoire de Génie Chimique, Université de Toulouse, CNRS, INPT, UPS, Toulouse, France

Editorial on the Research Topic

From Glycerol to Value-Added Products

Increases in biodiesel production and the demand for oleochemical-based products have led to the generation of huge amounts of crude glycerol, which has given birth to new challenges regarding its sustainable use. Although there is a wide range of potential uses for crude glycerol, there are limited by its degree of purity, which affects its physical, chemical, and biological properties. The chemical transformation of glycerol has thus become a major point of interest for crude glycerol valorization. High added value products can be obtained from glycerol through different pathways, such as oxidation, carbonylation, reforming, acetalyzation, etherification, esterification, dehydration, hydrogenolysis, etc. Starting from a poly-hydroxylated molecule, all these chemical routes generally lead to complex mixtures and are not selective. In order to develop further industrial processes, progresses must be achieved to increase yield and selectivity, reduce reaction times, and ensure that work in media is as clean as possible. The catalyst choice is also of great importance since it impacts the selectivity. Heterogeneous ones must be preferred for an industrial process because they can be easily separated. One other important aspect is the quality of the starting glycerol; it has a great influence on the synthesis performance. This special issue gathers some contributions focused on recent advances in some key aspects of glycerol transformation processes: the crude glycerol purification prior to use for chemical transformation, the use of new synthesis media, the use of non-thermal activation techniques such as electrochemistry and plasma, as well as the synthesis, use, and characterization of new heterogeneous catalysts. These principles are applied to the optimization of the synthesis of key added-value products, such as glycerol carbonate, glycerol oleates, glyceraldehyde, acrolein, glycolic acid, and lactic acid. Process aspects are also considered, such as the purification process or fluidized bed technology.

This special issue is a collection of 3 critical reviews and 10 original research articles.

The use of an electron as a clean reagent is of great interest to the goal of transforming glycerol in added-value products in a sustainable manner. As direct electron transfer for a polyhydroxylated molecule like glycerol would lead to the creation of a variety of products, an indirect electrocatalytic process is envisaged in this special issue. Lee et al. have investigated the use of mixed carbon black-activated carbon electrodes for glycolic and lactic acid production. Glycolic acid was then obtained with good yield and selectivity. On the other hand, Coutanceau et al. have proposed an overview of different catalytic systems and conditions to control the products selectivity obtained from glycerol electrooxidation.

Catalyst deactivation is also a crucial issue to overcome on the road to a sustainable industrial process. Liu et al. have demonstrated the benefits of non-thermal plasma technology to avoid silice-supported silicotungstic acid catalyst deactivation during glycerol dehydration for acrolein production.

Glycerol purity is crucial for its further selective transformation into various products. Therefore, in order to valorize crude glycerol for synthetic purposes, a purification step is necessary.

Abdul Raman et al. propose, in this special issue, a dual-step purification method that includes acidification and ion exchange operations, which allows it to reach a 98.2% purity.

This special issue also focuses on targeted molecules derived from glycerol. de Caro et al. have presented the recent advances concerning glycerol carbonate (GC) synthesis. Amongst the different routes, DMC and glycerol are good precursors, leading to GC through transcarbonation under mild conditions. Bruniaux et al. have reported the selective conversion of glycerol into 3-methoxypropan-1,2diol in mild yields. Al-Saadi et al. have investigated a reactive coupling that associates the transesterification of rapeseed oil into a fatty acid methyl ester and glycerol carbonate in a one-step process by introducing triazabicyclodecene guanidine as a catalyst.

Viable industrial chemical processes imply the use of heterogeneous catalysts for easy product recovery and catalyst recycling. Moreover, catalyst activity strongly relies on its physical properties, such as hydrophilicity/hydrophobicity, acidity, stability to water, etc. Muraza et al. have investigated the performances of natural zeolites and natural clays as low-cost catalysts. For a specific application, such as esterification with oleic acid, new catalysts must be developed, and these should exhibit good proprieties in terms of acidity and hydrophobicity. Kong et al. have developed, characterized, and studied hydrophobic zirconia-silica acid catalysts. They obtained 80% glycerol conversion together with 60% mono-oleate selectivity. Pt-based solid catalysts deposited on various supports have been studied by El Roz et al. when applied to the synthesis of glyceraldehyde from glycerol. The best activity was obtained for $Pt/g-Al_2O_3$, whereas best selectivity was obtained using Pt/SiO_2. Sulphonic acid-functionalized copolymer beads were also synthetized, characterized, and used for solketal synthesis from glycerol. Al-Saadi et al. succeeded in optimizing the process using a two-step acetone feeding process. A technico-economic analysis revealed that this process could compete with the current industrial one. This reaction—the acetalization of glycerol through acid catalysis—was also investigated by Talebian-Kiakalaieh et al. They give, in this special issue, a comprehensive study of the impact of the different operating parameters—a prerequisite for biorefinery development.

To succeed in these industrial implementations, a chemical engineering approach has to be coupled with a chemical one.

For this purpose, Katryniok et al. developed a two-zone fluidized bed reactor to carry out the gas-phase dehydration of glycerol to acrolein, using phosphotungstic acid supported on silica as a catalyst. The fluidization quality, the catalyst mechanical stability, and the influence of the operating conditions were successively studied, thus showing, for example, the crucial part the O_2/glycerol ratio plays for the purposes of conversion and selectivity.

The contributions made to this special issue of "From Glycerol to Value-Added Products" underline the variety of the research work carried out in the field of the valorization of glycerol and processing of raw material at low cost, and they tackle both the reactional aspects as catalysis, processes, and even economic aspects. Many chemical applications have been covered in this special issue, thus showcasing all the potential of glycerol. We hope that the issue will inspire the readers to further contribute to this exciting field of glycerol valorization.

Finally, we would like to thank all authors for their valuable contributions to this special issue, and we wish them success in their research.

AUTHOR CONTRIBUTIONS

MA and PC thank all contributors for their original articles submissions to this special issue.

ACKNOWLEDGMENTS

Check for
updates

A Review on the Catalytic Acetalization of Bio-renewable Glycerol to Fuel Additives

Amin Talebian-Kiakalaieh[1,2], Nor Aishah Saidina Amin[2]*, Neda Najaafi[3] and Sara Tarighi[1]

[1] *Faculty of Petrochemicals, Iran Polymer and Petrochemical Institute (IPPI), Tehran, Iran,* [2] *Chemical Reaction Engineering Group, Faculty of Chemical and Energy Engineering, Universiti Teknologi Malaysia (UTM), Skudai, Malaysia,* [3] *Iran Industrial Design Company, Tehran, Iran*

The last 20 years have seen an unprecedented breakthrough in the biodiesel industry worldwide leads to abundance of glycerol. Therefore, the economic utilization of glycerol to various value-added chemicals is vital for the sustainability of the biodiesel industry. One of the promising processes is acetalization of glycerol to acetals and ketals for applications as fuel additives. These products could be obtained by acid-catalyzed reaction of glycerol with aldehydes and ketones. Application of different supported heterogeneous catalysts such as zeolites, heteropoly acids, metal-based and acid-exchange resins have been evaluated comprehensively in this field. In this review, the glycerol acetalization has been reported, focusing on innovative and potential technologies for sustainable production of solketal. In addition, the impacts of various parameters such as application of different reactants, reaction temperature, water removal, utilization of crude-glycerol on catalytic activity in both batch and continuous processes are discussed. The outcomes of this research will therefore significantly improve the technology required in tomorrow's bio-refineries. This review provides spectacular opportunities for us to use such renewables and will consequently benefit the industry, environment and economy.

Keywords: glycerol, acetalization, fuel additives, heterogeneous catalysts, acetone, ketone

INTRODUCTION

In the early Twentieth century, petroleum exploitation and its cracking to simple hydrocarbons was one of the most influential factors on human life. Fossil fuel has been the main source of energy for almost a century. Current oil production rate reach approximately 12 Mt/day and its demand is predicted to rise dramatically to around 16 Mt/day by 2030 due to the significant increase in the world population and industrial development (Lin and Huber, 2009; Talebian-Kiakalaieh et al., 2014). Various types of environmental concerns such as massive amount of carbon dioxide and the depletion of fossil fuel resources have become the main concerns in maintaining sustainability. Low cost supply of fossil fuel (<100 USD/barrel) will no longer be available by 2040 (Posada et al., 2009). Many efforts are geared toward finding new sources of alternative energy to supplant the current non-renewable fossil fuels. Biomass is selected as a promising alternative source of energy to meet the significant energy demand as well as to reduce environmental concerns. As a result, a new term, "bio-refinery," has emerged recently to describe a facility for converting biomass to food, fuel, and value-added chemicals.

Biodiesel is one of the most important and valuable alternative liquid fuel in the transportation sector. As a substitute to fossil fuels, biodiesel could reduce chemical emissions such as sulfur dioxide (100%), unburned hydrocarbon (68%), and polycyclic aromatic hydrocarbon (80–90%). In addition, biodiesel is environmentally friendly, technically feasible and biodegradable (Fazal et al., 2011). The worldwide production of biodiesel is predicted to increase to 141 billion liters by 2022 from 110 billion liters in 2013, mainly due to the contribution of European Renewable Energy Directive (EU-RED) and Renewable Fuel Standard (RFS) in the United States. This would improve the global production to almost 70% by the year of 2022, compared to its average from 2010 to 2012 (SSI Review, 2014). Hence, it is vital to enhance the economic feasibility of biodiesel production through the modification of three major aspects of the process, namely the raw materials used in the process, the synthesis method, and the byproducts (De Torres et al., 2011).

Briefly, biodiesel is obtained via the transesterification of animal fat or vegetable oils in the presence of methanol under basic catalysis condition (Menchavez et al., 2017). Glycerol as a byproduct is produced at a high 1:10 glycerol to biodiesel weight ratio. The increasing demand for biodiesel caused a glycerol over-supply, thus reducing the commercial price of glycerol to almost 8 cents/lb recently compared to 25 cents/lb in 2004 (Clomburg and Gonzalez, 2013). It is expected the global surge in biodiesel production lead to production of >41.9 billion liter of crude glycerol by 2020 (Nanda et al., 2014a). Fabrication of low cost glycerol is important since it can be transformed to many value-added chemicals (more than 2,000 products) in various reaction pathways (Nanda et al., 2017; Nguyen et al., 2017; Tangestanifard and Ghaziaskar, 2017). Traditionally, glycerol was produced from the production of fatty acids (47%), followed by soaps (24%), fatty alcohols (12%), and the biodiesel industry (9%). However, since 2009 the biodiesel industry is the main producer that supplies over 64% of the glycerol (Abad and Turon, 2012). Thus, glycerol consumption is expected to increase significantly by up to 50% in 2020. Its demand was 2,247.2 kilo tons in 2013 and is expected to reach 3,469.2 kilo tons by 2020 (Ayoub and Abdullah, 2012; Villa et al., 2015).

Traditional uses of glycerol include in the textiles (24%), food and beverages (21%), cosmetics and toiletries (18%), drugs (18%), tobacco (6%), and paper and printing (5%), and others, cannot satisfy the dramatic surge in production of this compound. Thus, it is necessary to find new routes of conversion for this chemical in order to avoid market saturation. **Table 1** lists the possible catalytic processes and products that can be produced from glycerol.

Undoubtedly, one of the most promising glycerol applications is production of fuel additives such as cyclic acetals and ketals with aldehydes and ketones, respectively (Deutsch et al., 2007). Generally, fuel (Wang et al., 2004) and diesel additive (Ribeiro et al., 2007) is a material that improves the cleanliness of different parts of the engine (e.g., carburetor, fuel injector and intake valve), promotes complete combustion, reduces fuel gelling and choking of nozzle, as well as reducing corrosion impact on different parts of the engine. The result is improved engine performance, reduced emission and reduced fuel consumption.
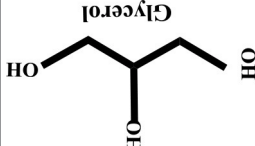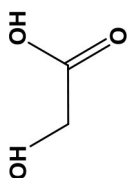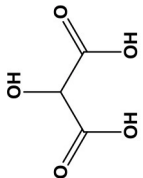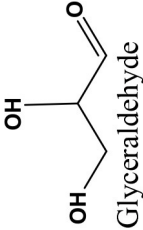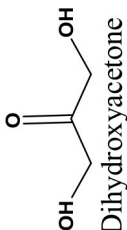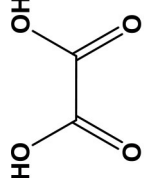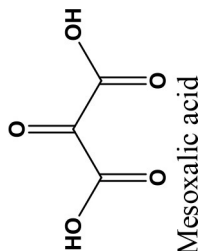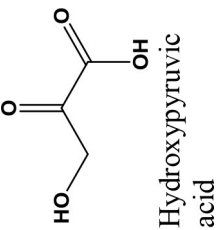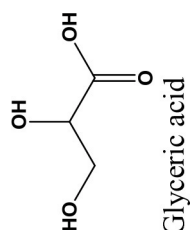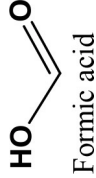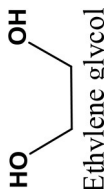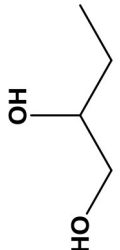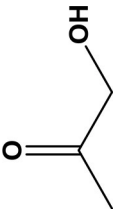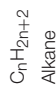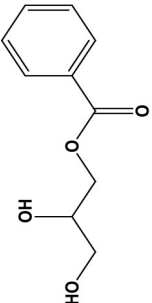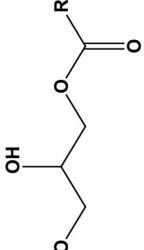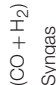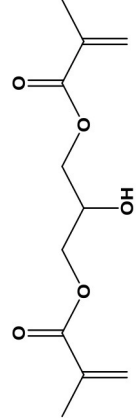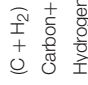
It could significantly reduce the particulate emissions of diesel fuel (Rakopoulos et al., 2008) (e.g., reduction of CO_2 and NO emission) and increase oxygen and air concentration (Lin and Chen, 2006). In addition, it could improve the thermal stability of jet fuels as well as significantly reduce (1–70%) deposits in jet engines (Forester et al., 2003). Methyl tertiary butyl ether (MTBE) was widely used as octane accelerator in gasoline in the early 1980's (Franklin et al., 2000). For more than two decades, it was the most economical oxygenate additive used by the refineries to reduce production cost of Reformulated Gasoline (RFG) (Romanow, 1999). However, the International Agency of Research on Cancer (IARC) classified RFG as a major health risk threat in 2000 (U.S. EPA, 1996). Thus, ketalization reaction between glycerol and acetone where 2, 2-dimethyl-1, 3-dioxolane-4- methanol known as solketal, is formed as the condensation product over an acid catalyst is shown in **Figure 1**. Solketal, an oxygenate fuel additives, could reduce the particulate emission and improve the cold flow properties of liquid transportation fuels (Pariente et al., 2008). It helps to reduce the gum formation, improves the oxidation stability, and enhances the octane number when added to gasoline (Mota et al., 2010). Maksimov et al. (2011) reported its use as a versatile solvent and a plasticizer in the polymer industry and a solubilizing and suspending agent in pharmaceutical preparations. More importantly, the aquatox fish test on the toxicity of the solketal showed that solketal (with a LC50 for fish to be as high as 3,162 ppm) has demonstrated much less environmental toxicity than the common fuel additive, MTBE, with a LC50 of 1,000 ppm (Nanda et al., 2014a).

Thus, the main objective of this review is to collect information about the latest advances in glycerol conversion to oxygenated fuel additives from biomass sources. In addition, the review addresses the critical knowledge gaps for enhancing conversion and selectivity in glycerol acetalization. Fundamentals of reaction mechanisms for the acid-catalyzed conversion of glycerol into solketal are presented. Some aspects such as the influence of various reaction parameters, reactant selection, reaction temperature, catalyst acidity, water removal, and reactor design are exclusively summarized and discussed. Finally, the application of crude-glycerol is discussed in batch and continuous-flow processes.

CATALYTIC ACETALIZATION OF GLYCEROL

Glycerol is an organic compound which is a low toxicity alcohol that consists of a three-carbon chain with a hydroxyl group attached to each carbon. These groups made glycerol hygroscopic and water-soluble. Glycerol has low volatility and low vapor pressure and is nontoxic to both humans and the environment. Physically, glycerol is a clear, colorless, odorless, viscous, and sweet-tasting liquid. **Table 2** lists the physico-chemical characteristics of glycerol (Rahmat et al., 2010). Glycerol was first discovered by K.W. Scheele, a Swedish researcher, in 1779. He produced a material with a sweet taste by heating olive oil with lead oxide. Three decades later, a French chemist, Michel

TABLE 1 | Catalytic conversion of glycerol into value-added chemicals by different processes.

(Continued)

TABLE 1 | Continued

Etherification		
Mono-ethers	Di-ethers	Tri-ether
Oligomerization, Polymerization		
Glycerol 1-monoethers	Polyglycerol methacrylates	
Carboxylation		
Glycerol carbonate		
Acetalization		
Solketal ([1,3] dioxolan-4-yl-methanols)	1,3-dioxane ([1,3] Dioxan-5-ol)	

Different catalytic conversion of glycerol into value-added chemicals.

FIGURE 1 | Reaction mechanism of glycerol with aldehydes/ketones.
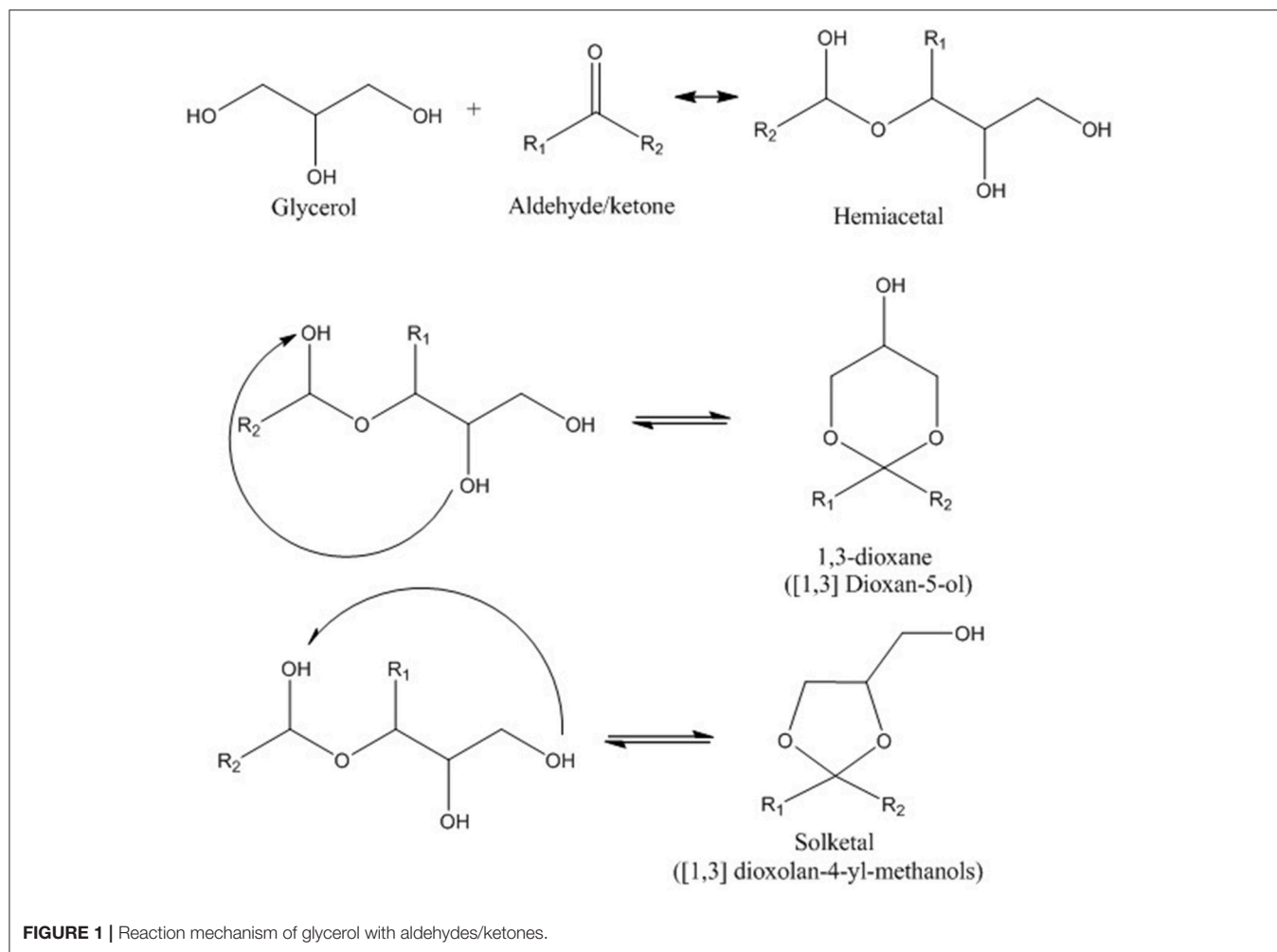
Eugene Chevrel, named it "glycerin." He then proposed fatty acids ethereous chemical formulas along with glycerin formulas in vegetable oils and animal fats. Finally, his study on the production of fatty acids (FA) from the reaction of fatty materials with lime and alkali was reported, which was the first industrial attempt in this field (Gesslein, 1999). It is an irrefutable fact that the discovery of glycerol has brought significant breakthroughs in the production different products. Recent advances in catalyst and bio-refinery industries have provided great opportunities for industrialization of bio-based processes which could produce food, fuel, and chemicals from glycerol.

Based on the literature in the last decades, catalytic acetalization of glycerol process could be categorized by three generations. In fact, the first generation of studies on the catalytic acetalization of glycerol to fuel additives reported in the presence of homogenous catalysts and a solvent. Fischer and co-workers pioneered the synthesis of solketal from glycerol and acetone, catalyzed by hydrogen chloride, in a batch reactor (Fischer, 1895). A few years later, a similar process by Fischer and Pfahler (1920) was applied for the ketalization of glycerol with anhydrous sodium sulfate and hydrogen chloride. Newman and Renoll (1945) reported the preparation of solketal in a three-neck flask

using reflux and mechanical stirrer in 1948. To obtain high solketal yield, they used pTSA monohydrate as the catalyst and petroleum ether as the reaction medium. After the reaction, the products were separated by reducing the pressure and distilling. The drawback of this system was its very long reaction time (21–36 h). Generally, the reaction of glycerol with aldehydes/ketones is conducted under homogenous Lewis catalysts (Ruiz et al., 2010) or mineral acids such as HF, HCl, H_3PO_4, H_2SO_4, and p-toluenesulfonic acid (pTSA) to form solketal (1,2-isopropylidene glycerol, 2,2-dimethyl-1, or 3-dioxolane-4-methanol) (Sato et al., 2008; Coleman and Blankenship, 2010; Suriyapradilok and Kitiyanan, 2011; Nanda et al., 2014a; Sun et al., 2017). The first generation of studies was stopped more than half a century ago due to the economic barriers. Indeed, availability of cheap fossil fuels was the main obstacle for bio-based processes.

The second generation of catalytic acetalization of glycerol performed in the presence of heterogeneous catalysts and a solvent as reaction medium. Indeed, this group of investigations on bio-based glycerol acetalization to fuel additives started after the introduction of large amount of inexpensive glycerol from biodiesel industry at the end of the Twentieth century. Science and technological advances in synthesis of heterogeneous

Properties	Values
Chemical formula	CH_2OH–$CHOH$–CH_2OH
Formula weight	92.09
Form and color	Colorless and liquid
Specific gravity	$1.260^{50/4}$
Melting point	$17.9^{\circ}C$
Boiling point	$290^{\circ}C$
Solubility in 100 parts	
Water	Infinitely
Alcohol	Infinitely
Ether	Insoluble
Vapor pressure in 760 mmHg	$290^{\circ}C$
Heat of fusion at $18.07^{\circ}C$	47.49 cal/g
Viscosity liquid glycerol 100%	10 cP
50%	25 cP
Diffusivity in	$(DL \times 10^5$ sq.cm/s)
i-Amyl alcohol	0.12
Ethanol	0.56
Water	0.94

Specific heat glycerol in aqueous solution (mol%)	$15^{\circ}C$ (cal/g$^{\circ}C$)	$30^{\circ}C$(cal/g$^{\circ}C$)
2.12	0.961	0.960
4.66	0.929	0.924
11.5	0.851	0.841
22.7	0.765	0.758
43.9	0.670	0.672
100	0.555	0.576

catalysts and their applications provide spectacular opportunities for further investigations in this field. In fact, homogenous catalysts like Lewis catalysts and strong mineral acids are known to not only cause difficult purification and product separation, but also environmental and corrosion problems. Several studies were employed to solve the shortcomings of homogenous catalysts using heterogeneous catalysts by evaluating the most important characteristics of a catalyst which are cost, accessibility, efficiency, easy removal, and good activity at mild conditions. One of the earliest studies on the use of heterogeneous acid catalyst was reported by Deutsch et al. (2007). They applied Amberlyst-36 with various solvents (dichloromethane, chloroform, toluene, and benzene) as organic solvents to obtained >62% glycerol conversion in the presence of three different reactants (acetone, benzene, and furfural) in a batch reactor (Deutsch et al., 2007). Application of Hβ and MMT-K10 zeolites were reported in catalytic acetalization of glycerol to fuel additives in the presence of chloroform as solvent and benzaldehyde as reactant. The results indicated that >95% of solketal yield was obtained at glycerol to benzaldhyde molar ratio of 1.1/1 and after 6 h of reaction time (Deutsch et al.,

2007). In addition, toluene is another solvent which was utilized in catalytic acetalization of glycerol by Umbarkar et al. (2009). They reported about 72% glycerol conversion over MoO_3/SiO_2 catalyst at optimum reaction of 1.1/1 molar ration of glycerol to benzaldehyde, reaction temperature of $100^{\circ}C$ and in 8 h. As mentioned earlier, simultaneous application of heterogeneous catalysts and solvent is one of the old methods in catalytic acetalization process and there are limited number of studies in this field in the last decade. However, Nanda et al. (2014b) reported one of the successful studies on application of ethanol as solvent in the presence of Amberlyst-35 as catalyst to reach more than 74% solketal yield at 2/1 molar ratio of glycerol to acetone and quite very low reaction temperature of $25-45^{\circ}C$. Indeed, they could significantly reduce the reaction temperature by application of ethanol as solvent.

Finally, the third generation is solvent free glycerol acetalization reaction by heterogeneous catalysts in batch or continuous processes. In fact, new heterogeneous catalysts are active enough to push the catalytic process to produce desired products (solketal) at high reaction conversion even without solvent (Chen et al., 2018a; Ferreira et al., 2018). In this regard, different types of heterogeneous acid catalysts have been recently applied in the acetalization of various carbonyl compounds with glycerol such as activated carbons, montmorillonite (MMT), zeolites, metal-based catalysts, ionic liquids, supported multi-walled carbon nano-tubes (MWCNTs) or, mesoporous silicates with arylsulphonate group, heteropoly acids, rare-earth triflates, and ion-exchange resins. Thus, the latest trend in catalytic acetalization of glycerol to fuel-additives will be investigated in the following sections. **Table 3** summarizes some of the recent studies related to glycerol acetalization with different aldehydes and ketones in batch and continuous processes. All the reported studies are organized into two main groups of homogenous and heterogeneous catalysts. Also, the heterogeneous catalysts are divided into four categories of zeolite-, heteropoly acid-, metal-, and polymers-based catalysts. As it can clearly be seen, the highest catalytic activity (complete conversions) were observed from the rare-earth triflate catalysts (Pierpont et al., 2015), Ni-Zr/activated carbon catalyst (Khayoon and Hameed, 2013), (L)Ru (II)@SBA-15 (Lazar et al., 2018), Amberlyst-47 (Guemez et al., 2013), and [5%V] Si-ITQ-6 (Vieira et al., 2018). The detail of each reaction process and optimum conditions reported in **Table 3**.

Lack of research studies on different methods of catalyst synthesize (e.g., sol-immobilization) is obvious, which has great influence on the catalyst activity and selectivity. In fact, the majority of reported heterogeneous catalysts synthesized through simple impregnation approach. Also, the photo-catalytic process is a promising strategy in various reaction processes and under mild reaction conditions with altered selectivities, compared with the conventional thermo-catalytic route. Unfortunately, application of photo-catalytic acetalization of glycerol has rarely been reported, while it definitively requires more attention in the future.

In addition to investigating the synthesis of an effective catalyst, the process engineering for economic evaluation was also rarely investigated. The UNISim^{TM} software was used

TABLE 3 | Glycerol acetalization with different aldehydes and ketones in batch and continuous processes.

Type		Catalyst	Optimum condition	Con[c] (%) Y[d] (%)	Description	References
Homogenous		PTSA	MR[a]Gl/F[b] = 1:1 T = 80°C, t = 9 h	Y_{Acetal} = 80	–	Ruiz et al., 2010
		PTSA	MR Gl/Ac[e] = 1:4 t = 12 h	Con = 82	–	Suriyapradilok and Kitiyanan, 2011
		PTSA	MR Gl/Ben[f] = 1:2 T = 140°C, t = 15 min	Con = 67	Microwave assisted, Power = 600 W; Con = 95% without catalyst	Pawar et al., 2014
		H_2SO_4	MR Gl/F = 1.5/1 T = 100°C, t = 4 h	Y_{Acetal} = 89	–	Coleman and Blankenship, 2010
Heterogeneous	Zeolites	Zeolite beta	MR Gl/F = 1/1 T = 100°C, t = 2 h	Y_{Acetal} = 25	–	Ruiz et al., 2010
		Zeolite beta	MR Gl/Ac = 1/2 T = 70°C, t = 1 h	Con = 90	–	da Silva and Mota, 2011
		H beta zeolite	MR Gl/Ac = 1/2 T = 25°C, t = 2 h	Con = 86	–	Manjunathan et al., 2015
		Zeolite USY	MR Gl/Bu[g] = 1/2.5 T = 70°C, t = 4 h	Con = 72	–	Serafim et al., 2011
		Zeolite BEA		Con = 87		
		Zeolite ZSM		Con = 28		
		MMT K10	MR Gl/Ben = 1/2 T = 140°C, t = 15 min	Con = 84	Microwave assisted, Power = 600 W	Roldan et al., 2009
				Con = 95	No catalyst	
		Nb$_5$-HUSY	MR Gl/Ac = ½ T = 40°C, Cat = 2 wt%	Con = 66 $S_{Solketal}$ = 98	–	Ferreira et al., 2018
		MK-10S$_{MW}$	T = 40°C, t = 2 h, Cat = 5 wt%, MR Gl/F = 1/1	Con = 68 $S_{Solketal}$ = 66	Microwave synthesis enhanced reaction conversion	Gutiérrez-Acebo et al., 2018
		[5%V]Si-ITQ-6	T = 60°C, t = 120 min, Ac/Gl = 3/1, Cat = 0.02 g	Con = 100 $S_{Solketal}$ = >95	Acetone washing could reduce the catalyst deactivation after each run	Vieira et al., 2018
		Zr-MO-KIT-6	T = 50°C, t = 4 h, Ac/Gl = 8/1, Cat = 0.05 g	Con = 85.8 $S_{Solketal}$ = 97.8	–	Li et al., 2018a
		Immobilize sulfonic acid on to silica	T = 120°C, t = 8 h	Con = 78	Argon atmosphere in the presence of Benzaldehyde	Adam et al., 2012
		Zeolite beta CP814E	MR Gl/Ac = 1/6 T = 35°C, t = 4 h	Con = 82%	–	Maksimov et al., 2011
		Zeolite beta CP811T1		Con = 85%		
		Zeolite HY		Con = 37%		
Heterogeneous	Zeolites	Hierarchical Zeolite (H/BEA$_5$)	T = 70°C, t = 240 min, MR G/F = 1/1.25, Cat = 10%	Con = 78 $S_{Solketal}$ = 85	–	Sonar et al., 2018
		6.8v-MCM-41	T = 60 °C, t = 60 min, Ac/Gl =6.5, Cat =20 mg	Con = 92 $S_{Solketal}$ = 95	–	Abreu et al., 2018
		ITQ-2	T = 83°C, HMF/Gl = 1/2, Cat =20 wt%, Si/Al = 15	Con = 98 S_{5R+6R} = 100	Products ratio 5R/6R = 2.8	Arias et al., 2018
		MCM-41		Con = 99 S_{5R+6R} =100	Products ratio 5R/6R = 3.9	
	Heteropoly acid	$Cs_{2.5}H_{0.5}PW_{12}O_{40}$	T = 25°C, MR Gl/Ac = 1/6, Cat = 0.25 g/batch, t = 15 min	Con = 95 $S_{Solketal}$ = 98	–	Chen et al., 2018a
		$Cs_{2.5}$/KIT-6	T = 70°C, MR Gl/F = 1/1.2, C_s = 3.83 g/batch, t = 24 h	Con = 95 Y_{GF} = 60	–	Chen et al., 2018b

(Continued)

TABLE 3 | Continued

Type		Catalyst	Optimum condition	Con[c] (%) Y[d] (%)	Description	References
	Acid exchange resins	Nafion SAC 13	MR Gl/Ben = 1/2 T = 140°C, t = 15 min	Con = 81	Microwave assisted, Power = 600 W, Con = 95% without catalyst	Trifoi et al., 2016
		Dowex	MR Gl/Bu = 1/2.5 T = 70°C, t = 4 h	Con = 66	–	Serafim et al., 2011
		Amberlyst 36	MR Gl/F =1/1, T = 100°C, t = 4 h	Y = 55	–	Ruiz et al., 2010
		Amberlyst 15	MR Gl/Ac = 1/2 T = 70°C, t = 1 h	Con = 95	–	
		Amberlyst 15	MR Gl/Ac = 1/2 T = 50°C, P = 8.0 bar t = 6 h	Con = 95	–	
		Amberlyst 47	MR Gl/F = 2/1 T = 80–100°C, t = 3 h	Con = 75	–	Agirre et al., 2011
		Amberlyst 47	MR Gl/Ac = 2/1 t = 10–50°C, t = 4 h	Con = 90		
		Amberlyst 47	MR Gl/But[h] = 3/1 T = 80°C, t = 100 min	Con = 95	–	Guemez et al., 2013
			MR Gl/But = 0.5/1 T = 60°C, t = 4 h	Con = 100		
		Amberlyst 15	MR Gl/F = 1/2 T = 75°C, t = 2 h	Con = 100%	Reactive distillation process	Hasabnis and Mahajani, 2014
Heterogeneous	Metal-based	Ni-activated carbon	MR Gl/Ac = 1/8 T = 45°C, t = 3 h	Con = 98	3% reduction of catalytic activity after the 4th run	Khayoon and Hameed, 2013
		Zr-activated carbon		Con = 67		
		X%Ni-Y%Zr/ activated carbon		Con = 100		
		Ni-MWCNT [i]	MR Gl/Ac = 1/6 T = 40°C, t = 3 h	Con = 96	5% reduction of catalytic activity after 4th run	Khayoon et al., 2014
		Pt-TNT	T = 50°C, t = 24 h, Ac/Gl = 1/1, Cat = 130 mg	Con = 46.7 $S_{Solketal}$ = 10	–	Gomes et al., 2018
		M-AlPO$_4$ M-ZnAlPO$_4$ M-CuAlPO$_4$ M-NiAlPO$_4$ M-CoAlPO$_4$	MR Gl/Ac = 1/8 T = 80°C, t = 1 h	Con = 75	80% reduction of M-NiAlPO$_4$ activity after the 5th run	Zhang et al., 2015
		PTNT	T = 50 °C, MR G/Ac = 1/1, t = 6 h	Con = 40 $S_{Soketal}$ = 20	–	Gomes et al., 2018
		SO$_4$/SnO$_2$	Gl-Fur[j]	Con = 99	–	Mallesham et al., 2014
		TiO$_2$-SiO$_2$	MR Gl/Ac = 1/4 T = 40–90°C, t = 3 h	Con = 98	$Sel^k_{5-membered ring}$ = 95%	Fan et al., 2012
		Mo$_X$/TiO$_2$-ZrO$_2$	MR Gl/Ben = 1/1 T = 60–100°C, t = 90 min	Con = 74	–	Sudarsanam et al., 2013
		Niobium oxyhydroxyde	MR Gl/Ac = 1/4 T = 40°C, t = 1 h	Con = 74	–	Souza et al., 2014, 2015
		Nb$_2$O$_5$	MR Gl/Ac = 1/3 T = 70 °C, t = 6 h	Con = 80	Up to 4 time reusability	Nair et al., 2012
		HC-SZ (SO$_4^2$/ZrO$_2$ coated on cordierite honeycomb monolith)	T = 60°C, MR G/Ac = 1/3, Cat = 0.2 g	Con = 96, $Y_{Solketal}$ = 94	–	Vasantha et al., 2018

(Continued)

TABLE 3 | Continued

Type		Catalyst	Optimum condition	Con[c] (%) Y[d] (%)	Description	References
		Meso-SnO$_2$-350	$T = 60°C$, $t = 30$ min, Ac/Gl $= 1/1$, Cat $= 0.125$ g	Con $= 51.3$ S$_{Solketal} = 98$	Higher selectivity to the solketal in the presence of Acetone compared to the Furfuraldehyde and benzaldehyde	Manjunathan et al., 2018
Heterogeneous	Other catalysts	Rare earth triflate	Gl-Ac $T = 25$ °C	Con $= 100$	–	Pierpont et al., 2015
		Organic-inorganic hybrid catalyst	MR Gl/Ac $= 1/6$ $T = 30°C$, $t = 3$ h	Con $= 94$	Water resistance	Sandesh et al., 2015
		(L)Ru(II)@SBA-15	$T = 25°C$, $t = 20$ min, MR Al/MeOH $= 1/250$	Con $= 100$ S$_{Solketal} = 100$	–	Lazar et al., 2018
		80LS20PS450H$^+$	$T = 40°C$, Cat $= 5$ wt%, MR G/Ac $= 1/6$, $t = 60$ min	Con $= 90$	S$_{Soketal} = 51–53\%$ obtained over Furfural and Methyl levulinate instead of acetone	Konwar et al., 2017
		PrSO$_3$H-SBA-15-400	$T = 90°C$, $t = 8$ h, F/Gl $= 1.5/1$, Cat $= 0.2$ g	S$_{Solektal} = 60$	–	Li et al., 2018b
		Carbon-based catalyst	$T = 28°C$, $t = 30$ min, Ac/Gl $=4/1$, Cat $= 3$ wt%	Con $= >78$ S$_{Solketal} = 73$	–	Mantovani et al., 2018
		Co(II) (Co(III)$_{1.25}$)Al$_{2-0.75}$)O$_4$	$T = 130°C$, $t = 3$ h, 2 g Gl and 12.72 g AC, Cat $= 0.1$ g	Con $= 69.2$ S$_{Solketal} = 98.6$	–	Li et al., 2018c
		Purolite PD206	$T = 40.66°C$, $P = 42.31$ bar, MR Gl/Ac $= 1/4.97$, Feed flow rate $= 0.49$ ml/min, Cat $= 0.5$ g	Normalized exergy destraction $= 6.18\%$, Universal Exergetic efficiency $= 90.36\%$	Optimization and modeling of continuous acetalization process with subcritical acetone	Aghbashloa et al., 2018
		KU-2	MR Gl/Ac $= 1/6$ $T = 60°C$, $t = 4$ h	Con $= 85\%$	–	Maksimov et al., 2011
		Purolite PD 206	MR Gl/Ac $= 5/1$ $T = 20°C$, $P = 120$ bar	Con $= 95\%$	Acetone-solvent	Shirani et al., 2014

^{a}MR, Molar Ratio; ^{b}F, Formaldehyde; ^{c}Con, Conversion (%); ^{d}Y, Yield (%); ^{e}Ac, Acetone; ^{f}Ben, Benzaldehyde; ^{g}Bu, Butanal; ^{h}But, Butiraldehyde; ^{i}MWCNTs, Multiwall carbon nano-tubes; ^{j}Fur, Furfural; ^{k}Sel, Selectivity.

FIGURE 2 | Annual operation costs.

operation costs are shown in **Figure 2**. The results of this study suggest that glycerol acetalization for the production of solketal (fuel-additive) requires more attention and study. Such simulation studies could provide valuable information before large-scale industrialization of glycerol acetalization process. Indeed, researchers could analyses and evaluate different scenarios to evaluate the environmental and economic aspects of this process such as material, energy and production cost.

Zeolite Based (Micro- and Mesoporous) Catalysts

Zeolite is a micro-porous, alumino-silicate mineral conventionally used as commercial adsorbents due to its unique porous characteristics (tunable pore size), acid sites, and high thermal stability (Halgeri and Das, 1999). Zeolites could be used in various applications with a global market of several million tons annually, which includes petrochemical, water purification, gas separator, nuclear, and biogas industries. Among different forms of zeolite, nano-crystalline zeolite Beta and Y showed higher activity than micro-crystalline zeolites due

for the material and energy balances. The proposed plant could consume 432 t/y of glycerol and produce 620.9 t/y of solketal. The solketal cost was 12.29US$/kg. The annual

to their high surface area, lower diffusion path length and more exposed active sites (Taufiqurrahmi et al., 2011).

Despite all the research studies which have been used zeolite catalysts, some studies reported diffusion problems (mass transfer resistance) by utilization of bulk zeolites due to the presence of micro-porous network (Sharma et al., 2011). Thus, researchers have decided to use different metal oxides, metals, or metal nanoparticles as a support for zeolites to overcome these limitations. However, the synthesis procedures are sometimes laborious and require additional costs due to application of noble metals or thermal treatment which in general consume lots of time, energy, and cost. As a result, new concept of "Hierarchical zeolites" have attracted much attention recently. Based on our knowledge, application of supported hierarchical zeolites acid catalysts is reported rarely in this field. Indeed, hierarchical zeolites overcome the drawbacks related to hamper mass transfer and limited accessibility of conventional zeolites by the introduction of secondary, larger porosity within the micro-porous framework (García-Martínez and Li, 2015). In hierarchical meso-micro-porous zeolites, mesopores facilitate the physical transport of reactant molecules, whereas micropores act as nano-reactors to provide both active sites and shape selectivity (Groen et al., 2007). Therefore, hierarchical zeolites have recently been explored as catalysts for reactions that involve bulky molecules and their outstanding activities have been reported (Zhou et al., 2010). There are two approaches to introduce a hierarchical pore structure (connected pore structure) in zeolites. In fact, the bottom up and the top-down methods which hierarchical zeolites are synthesized directly from a silica-alumina gel or by post-treatment of the existing zeolites, respectively. Extra-crystalline, hard, templates such as carbon, (Egeblad et al., 2008) starch, (Park et al., 2009) resins, (Tosheva et al., 2000) and surfactants, (Choi et al., 2006) which are removed by calcination after crystallization to create mesoporosity can be used in the bottom-up approach (Fan et al., 2008). In the top-down approach to achieve hierarchical form, zeolites are post-treated after synthesis. The easiest way to introduce mesoporosity is by dealumination, which can be achieved by steaming and chemical treatments, such as acid leaching which remove the resulting extra-framework alumina. The increased mesoporosity may give rise to increasing rates in bimolecular and oligomeric reaction pathways that require large transition states (Lupulescu and Rimer, 2012). Another way of producing mesopores is desilication which can be done by base leaching. **Figure 3** illustrates bottom-up and top-down methods for synthesizing hierarchical meso-porous zeolites (Vogt and Weckhuysen, 2015). Undoubtedly, application of hierarchical zeolites as one of the catalysts with high activity and selectivity to the desired product should be more studied in the glycerol acetalization process due to its characteristics and acceptable results in other chemical processes particularly as a fluid catalytic cracking (FCC) catalyst in petrochemical industry.

One of the early studies regarding application of zeolites, was performed by da Silva et al. (2009) who investigated different catalysts (K10 MMT, zeolite Beta, amberlyst 15, and p-toluene sulfonic acid) for the conversion of glycerol to fuel-additives in the presence of acetone or formaldehyde. Consequently, the zeolite Beta (Si/Al = 16) reached conversion >95% in 1 h. In fact, high content of Si/Al ratio led to the hydrophobic characteristic of zeolite, which prevents the diffusion of water to inside the pores and acid sites' strength was preserved. Nevertheless, with aqueous formaldehyde solution, the glycerol conversion illustrated a drop to between 60 and 80% for different catalysts (Amberlyst-15, K-10 montmorillonite, p-toluene-sulfonic acid). Indeed the main reason was high amount of water in the reaction medium, which shifts the equilibrium and weakens the acid sites.

Li et al. (2012) reported that mesoporous Lewis acid catalysts could be active in acetalization of glycerol with acetone to produce solketal. A series of three-dimensional mesoporous silicate catalysts (Hf-TUD-1, Zr-TUD-1, Al-TUD-1, and Sn-MCM-41) synthesized and two of these catalysts (Hf-TUD-1 and Zr-TUD-1) showed excellent catalytic activities in solketal production. Indeed, 65 and 64% glycerol conversion obtained over Hf-TUD-1 and Zr-TUD-1 catalysts, respectively, at optimum reaction condition of 2/1 molar ratio of acetone to glycerol, 25 mg of catalyst weigh, at 80°C in 6 h reaction time. The main reasons for such high activity of synthesized catalysts were wide pores (Hf-TUD-1 = 0.6 cm^2/g, Zr-TUD-1 = 0.8 cm^2/g), large specific surface area (Hf-TUD-1 = 715 m^2/g, Zr-TUD-1 = 651 m^2/g), large pore size (Hf-TUD-1 = 4 nm, Zr-TUD-1 = 13.3 nm), the amount of accessible acid sites, and a relatively hydrophobic surface of catalyst. In addition, the active mesoporous materials didn't suffer from leaching and could be efficiently reused in consecutive catalytic cycles. They also proposed a reaction mechanism for acetalization reaction in the presence of Lewis acid catalysts. The Lewis acid metal sites coordinate and activate acetone's carbonyl group. Then, the carbon atom of the carbonyl group is attacked by the primary alcoholic group of glycerol accompanied by the formation of a bond between the carbonyl oxygen atom and the secondary carbon atom of glycerol. Finally, solketal forms through the dehydration step. **Figure 4** displays the detailed reaction mechanism.

Jamil et al. (2017) used different tailored forms of zeolite Beta in the condensation of bio-glycerol with acetone for production of the Solketal. The zeolite Beta catalysts treated with acids (hydrochloric acid, nitric acid, and oxalic acid) exhibited enhanced catalytic activity, irrespective of the nature of the acid used for the de-alumination. The nitric acid-treated beta zeolite sample (AB-2) exhibited a higher conversion than the other acid-treated samples. At optimum conditions (1:6 glycerol to acetone molar ratio, 4 h reaction time, 60°C reaction temperature) the bio-glycerol conversion and solketal yield were 94.26% and 94.21 wt%, respectively. The AB-2 sample was reusable for at least 4 times without any significant loss in its activity with approximately >80% glycerol conversion and >80% solketal yield.

Kowalska-Kus et al. (2017) investigated the glycerol acetalization reaction with acetone in the presence of hierarchical zeolites comprising pores of different diameters (MFI, BEA, and MOR) at 343 K and 1:1 glycerol to acetone molar ratio. The best catalytic performance for glycerol acetalization, which was 100% solketal selectivity at 80% reaction conversion, was achieved over hierarchical (micro/mesoporous) MFI zeolites. A
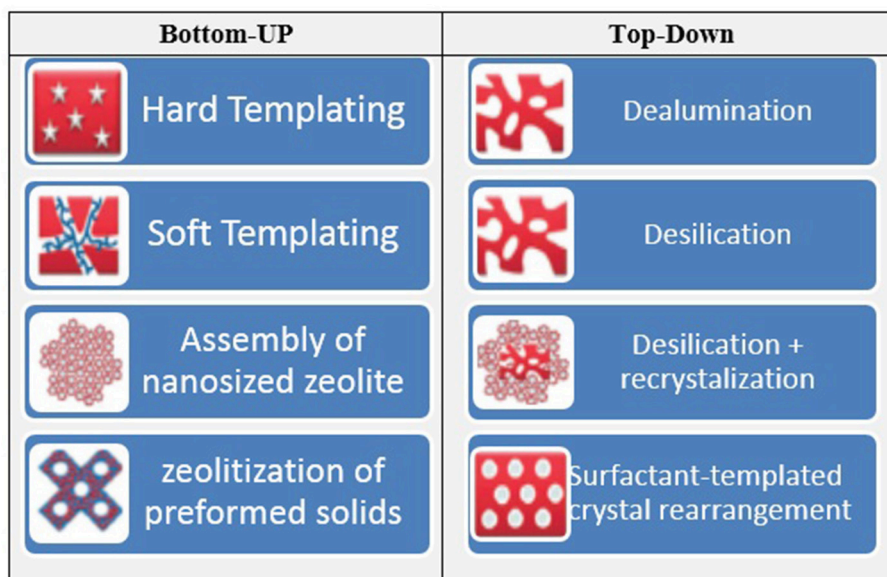
FIGURE 3 | Bottom-up and top-down models for synthesizing hierarchical mesoporous zeolites.
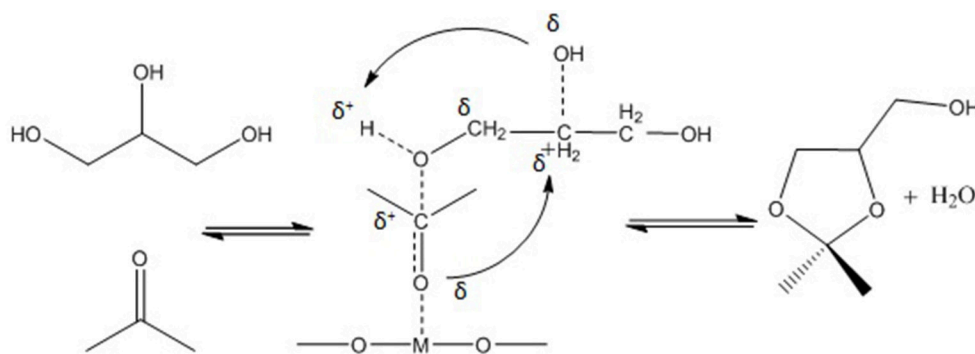
FIGURE 4 | Proposed reaction mechanism for the acetalization of glycerol and acetone over Lewis acid catalyst.

significant increase in reaction conversion and solketal selectivity in the studied reaction resulted from the easier accessibility of the active sites to reagents due to the formation of mesopores by means of desilication of the micro-porous zeolites.

Heteropoly Acid Based Catalysts

Application of heteropoly acid (HPA) has attracted much attention due to its wide applications in biodiesel industry and production of value-added chemical from glycerol. HPAs are highly stable against humidity and air, low toxicity, high solubility in polar solvents, production of less residues than mineral acids, less corrosive, and highly safer than other catalysts (Martin et al., 2012). Tungstophosphoric acid (HPW), silicotungstic acid (HSiW), and Phosphomolybdic acid (HPMo) are three commercially available HPAs. The HPW is a common HPA catalyst which is widely used. HPA catalysts have high ability for adjustment by modifying their central atoms with various

compounds. Researchers have attempted to increase the catalytic activity and long-life stability of the catalysts to achieve the highest fuel-additive yield. The Cs/HPW catalyst displayed one of the highest potential catalyst in acetalization of glycerol with 98% selectivity to solketal at about 95% glycerol conversion (Chen et al., 2018a). HPA's possessed Keggin structure. It is the structural form of α-Keggin anions, which have a general formula of $[XM_{12}O_{40}]^{n-}$, where X, M, and O represent the heteroatom, the addenda atom, and oxygen, respectively (**Figure 5**). The structure self-assembles in acidic aqueous solution and is the most stable structure of polyoxometalate catalysts. Despite the enormous applications of HPA catalysts as active components in various heterogeneous catalytic processes [e.g., glycerol dehydration to acrolein (Talebian-Kiakalaieh et al., 2014), glycerol oxidation to glyceric acid (Talebian-Kiakalaieh et al., 2018)], application of these types of catalysts are rarely reported in glycerol acetalization reaction.

FIGURE 5 | HPA keggin structure.
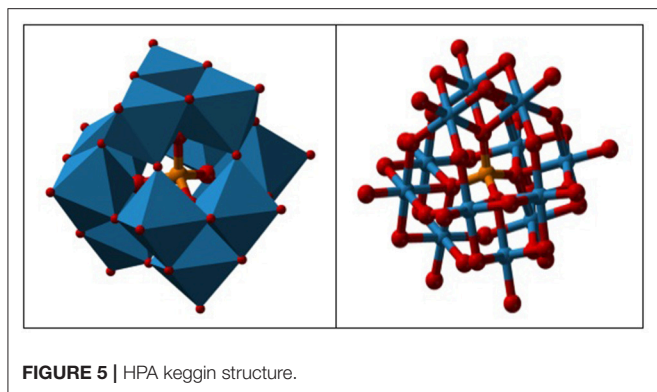
The glycerol acetalization was studied using a series of supported HPAs [HPW, HPMo, HSiW, and molybdosilisic (SiMo)], immobilized in silica catalysts by sol–gel method (Ferreira et al., 2010). As results, all catalysts exhibited high solketal selectivities (near $S_{Solketal} = 98\%$) at quite complete conversions at optimum reaction conditions of 70°C reaction temperature, 0.2 g catalyst weight, 6:1 molar ratio of acetone to glycerol and after 4 h reaction time. Also, the catalytic activities decreased in the following order: HPW-S > SiW-S >PMo-S > SiMo-S. All the catalysts exhibited high stability even after the fourth consecutive run, having lost only 10–13% of their initial activity. In another study, Narkhede and Patel (2014) achieved high selectivity toward solketal using supported SiW with MCM-41 catalysts (30% SiW_{11}/MCM-41, 30% SiW_{12}/MCM-41) in the presence of benzaldehyde. The results indicated that the 30%-SiW_{11}/MCM-41 could reach the highest solketal selectivity of 82 at 85% glycerol conversion at room temperature (30°C), 1/1.2 molar ratio of glycerol to benzaldehyde, 100 mg catalyst weight and in 1 h. Also, tuning of the acidity of the parent SiW led to an increase in the selectivity toward solketal. High activity of these catalysts was attributed to their strength of acidity, wide pores and large specific surface area.

da Silva et al. (2015b) evaluated the activity of various Brønsted acid catalysts e.g., HPW, H_2SO_4, p-toluene sulfonic acid, PMo, or SiW on glycerol ketalization with different ketones (e.g., propanone, butanone, cyclopentanone, and cyclohexanone) at room temperature and in the absence of an auxiliary solvent. The HPW sample exhibited the highest activity among the Brønsted acid catalysts and exhibited high (> 85%) selectivity toward five-membered (solketal) cyclic ketals. The highest (98%) selectivity of solketal is obtained at 288 K reaction temperature, 1 mol% catalyst (HPW) loading, 1:30 glycerol to ketone (propanone) molar ratio. The activity of different tested catalysts was as follows HPW> p-toluene sulfonic acid > PMo > SiW > H_2SO_4 with 83% > 76% > 41% > 40% > 31%, respectively. In addition, the results revealed that the application of various ketones with Brønsted acid catalyst in absence of solvent for ketalization of glycerol has significant influence on product distribution. **Figure 6** summarizes the possible products that can be obtained as a result of different ketone application.

Metal Based Catalysts

Mixed oxides, phosphates, and pyrophosphates have been used in glycerol acetalization to fuel-additives. Metal oxide catalysts such as niobium oxide (Nb_2O_5), tungsten oxides (WO_3), silicon dioxide (SiO_2) have been widely used in various chemical processes. The most important factors about metal-based catalysts are their synthesis method (especially calcination temperature) and their binary or tertiary combinations which have detrimental impact on physicochemical characteristics catalyst (Talebian-Kiakalaieh et al., 2014).

Mallesham et al. (2013) synthesized a series of supported SnO_2 with molybdenum (Mo) and tungsten (W) solid acids catalysts with two different methods of fusion and wet-impregnation. XRD results suggested that solid solutions of nano-crystalline SnO_2 were formed due to the incorporation of Mo and W cations into the SnO_2 lattice. Textural characterization results revealed that all the compounds showed smaller crystallite size, large specific surface area (WO_3-SnO_2 = 32 m^2/g and MoO_3-SnO_2 = 56 m^2/g), and high porosity. Moreover, Raman measurements and TPR results confirmed the formation of more oxygen vacancy defects in the doped catalysts along with facile reduction of the doped SnO_2, respectively. The positive impact of Mo and W oxides on the acidic properties of the SnO_2 was revealed by NH_3-TPD. Total acidity of MoO_3-SnO_2 and WO_3-SnO_2 were 81.45 and 61.81 μmol/g, respectively. The presence of larger number of Brønsted (B) acidic sites vs. Lewis (L) sites (B/L = >95%) was confirmed by pyridine-FTIR characterization. High selectivity to solketal (96%) at approximately 70% glycerol conversion was achieved over the MoO_3-SnO_2 sample at the optimum reaction condition of 1:1 glycerol to acetone molar ratio, 5 wt% catalyst loading in 150 min. In addition, this catalyst reached around 65% solketal selectivity at almost complete glycerol conversion in the presence of furfural (1:1 glycerol to furfural molar ratio) in 120 min. Finally, applications of different mono-substituted furfural compounds (e.g., 5-methylfurfural, 5-nitrofurfural, 5-chlorofurfural, and 5-hydroxymethyl furfural) were evaluated for acetalization of glycerol in the presence of MoO_3/SnO_2 sample. The results confirmed that all the substituted compounds reached lower glycerol conversion than furfural. This observation confirms the impact of steric hindrance induced with substitutes rather than the electronic effects of the substituent (i.e., inductive, resonance and hyper conjugation influences). In detail, the acetalization reaction reached >61% solketal selectivity at >60% glycerol conversion in the presence of different mono-substituted furfural.

In another study, Gonzalez-Arellano et al. (2014b) also evaluated the application of various formaldehyde sources and solventless/solvent-containing systems [Formalin (solvent-less), Para-formaldehyde (water), Para-formaldehyde (solventless)] in the presence of Zr-SBA-16 catalyst with three different Si/Zr ratios (100, 50, and 25) for glycerol acetalization to glycerol formal (GF). Results showed that the Zr–SBA-16(100) sample exhibited 24 and 76% selectivity to the solketal and dioxane, respectively, at 77% glycerol conversion at optimum reaction conditions of 100°C reaction temperature, 1:1 glycerol to para-formaldehyde molar ratio. In addition, the Zr–SBA-16(50)
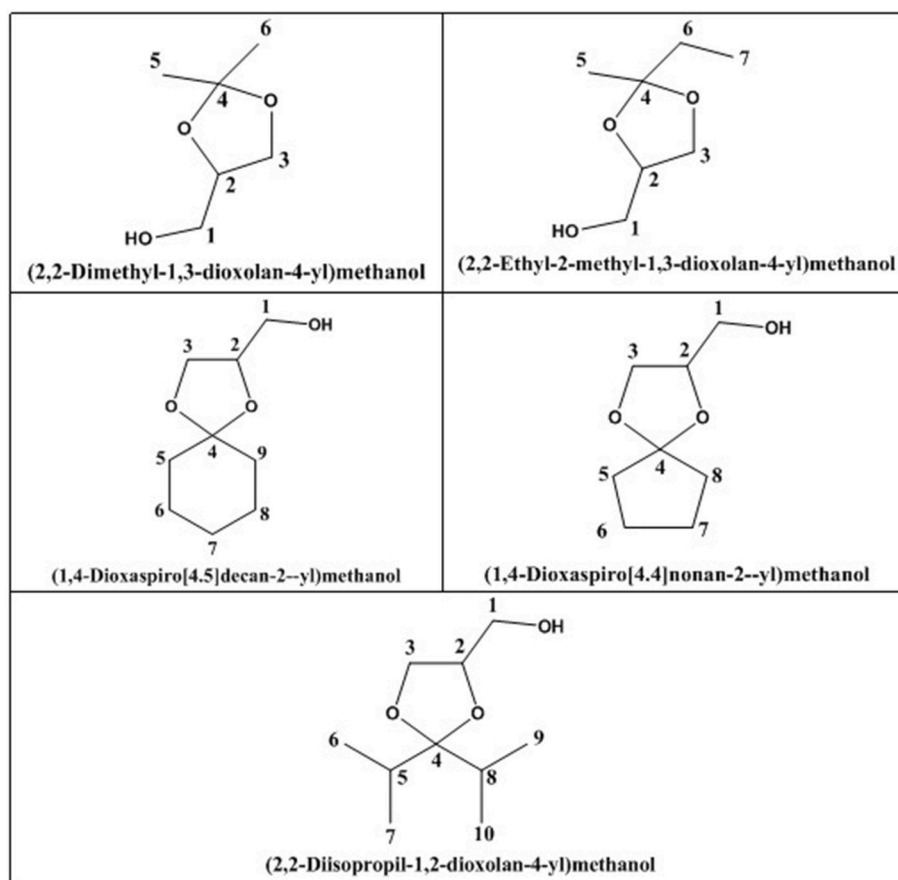
FIGURE 6 | Products with application of various ketones.

sample could be successfully reused up to five times under identical reaction conditions, without any noticeable decrease in activity. The main reason for better stability of Zr-SBA-16 (50) compared to the Zr-SBA-16 (100) was acidity. Indeed, the Zr-SBA-16(50) possessed higher amount of total acidity (116 μmol/g) with Lewis acidic nature (B/L = 36/80) compared to the Zr-SBA-16 (100) with just 40 μmol/g total acidity and with Bronsted acidic nature (B/L = 28/12).

Gonzalez-Arellano et al. (2014a) continued their study on the acetalization of glycerol with different aldehyde sources (para-formaldehyde, benzaldehyde, furfural, and acetone) in the presence of another newly synthesized heterogeneous catalyst, which was supported iron oxide nano-particle system of a mesoporous alumino-silicate heterogeneous catalyst (Fe/Al-SBA-15). The characterization results confirmed that Fe/Al-SBA-15 possessed high surface area (688 m^2/g) with Brønsted acidic nature (88 μmol^{-1}g^{-1}). Experimental results revealed that the product distribution was totally dependent on the use of different aldehyde sources. In fact, acetalization of glycerol with para-formaldehyde results in the production of dioxane (selectivity 66%) as the main product compared to the dioxolane with just 34% selectivity at almost complete glycerol conversion. In contrast, the use of other aldehyde sources led to production

of dioxolane (solketal) as the main product. The product's selectivities (dioxolane/dioxane) were 84%/16% at 70% glycerol conversion, 60%/40% at >95% glycerol conversion, and 99%/1% at 58% glycerol conversion in the presence of benzaldehyde, furfural and acetone, respectively. Finally, the Fe/Al-SBA-15 showed the highest stability after five consecutive runs without significant reduction in catalyst activity in the presence of acetone as the aldehyde source.

Gadamsetti et al. (2015) synthesized a series of supported SBA-15 with molybdenum phosphate (MoPO 5–50 wt%) catalysts for the acetalization of glycerol with acetone. Synthesized catalysts were characterized and the XRD results revealed that unsupported MoPO exhibits the formation of $(MoO_2)_2P_2O_7$ phase and is dispersed well on the SBA-15 surface. Also, Raman spectra characterization confirmed the existence of MoPO species $[(MoO_2)_2P_2O_7]$ in samples with more than 40 wt% MoPO supported on SBA-15. In addition the UV-DRS results revealed the presence of both isolated tetrahedrally and isolated octahedrally coordinated Mo centers in the supported and unsupported MoPO. Finally, the NH$_3$-TPD analysis shows that the total acidity surged from 0.2 to almost 1 mmol/g with MoPO loading from 5 to 40 wt%; however, total acidity dropped by increasing MoPO loading beyond 40 wt%. In contrast, specific

surface area of synthesized catalysts showed a downward trend from 688 to 125 m^2/g for 5 to 50 wt% of MoPO loading. Acidity of catalysts had negative impact on catalytic performance. The 40 wt% MoPO/SBA-15 sample showed the best catalytic activity with 98% Solketal selectivity at complete conversion (100%) at optimal reaction condition of 3:1 molar ratio of acetone to glycerol, 50 mg catalyst loading, room temperature, in 2 h.

da Silva et al. (2017) used solid SnF_2 catalyst for glycerol ketalization with propanone to solketal. The SnF_2 catalyst reached 97% selectivity of solketal at 97% glycerol conversion at optimum condition of glycerol (21.0 mmol), propanone (168.0 mmol) molar ratio (1:8), CH_3CN (15 mL), at room temperature (298 K). Most importantly, this catalyst exhibited incredible stability even after four times recycling and reuse with almost constant reaction conversion and solketal selectivity.

Another recent study on a series of zirconia-based catalysts for the acetalization of glycerol suggested that the activity increased in the order of ZrO_2 < WO_x/ZrO_2 < MoO_x/ZrO_2 < SO_4^{2-}/ZrO_2. In particular, the use of a sulfated zirconia catalyst led to ~98% conversion of glycerol and ~97% selectivity to solketal. The surface acidity and crystalline state of ZrO_2 on the SO_4^{2-}/ZrO_2 catalyst were found to be very influential to the catalytic performances (Reddy et al., 2011).

Kapkowski et al. (2017) synthesized a series of nano-silica supported Re, Ru, Ir, Rh NPs along with different mixture of the metal (Re, Ru, Ir, and Rh) catalysts for acetalization of glycerol with acetone or butanone. It was found that nano-SiO_2 supported Re (1.0%Re/SiO_2) was a highly efficient catalyst in glycerol acetalization reaction for solketal production exhibiting the highest activity (TOF = 620.7 h^{-1}) with 94.1% selectivity to solketal at 100% glycerol conversion. The addition of Ir (1.0% Re.Ir (1:1)/SiO_2) could also slightly improve the solketal selectivity to 96% and catalyst activity to TOF = 630.5 h^{-1} at complete conversion. Although 1.0%Re/SiO_2 favors five-membered cycles, its substitution with Mo alters this selectivity and both five- and six-membered products can be obtained. In detail, the solketal selectivity and catalyst activity decreased to about 78.9% and 336.9 h^{-1}, respectively. Despite the addition of Rh [1.0%RuRh(1:1)/Mo], the solketal selectivity did not increase more than 93.4%.

Priya et al. (2017) used microwave irradiation as a heating source in glycerol acetalization to fuel-additives over different transition-metal-ion-promoted mordenite solid acid catalysts which were synthesized by wet impregnation method. The transition metal ions include Fe, Co, Ni, Cu, and Zn. This approach is considered notably clean and green in this field. The results from the microwave irradiation system were compared to those from other processes that use conventional heating sources to ascertain its efficiency and efficacy. The Cu-Mor catalyst showed the highest activity because of the large number of acidic sites and the synergetic effects of metal particles interacting with mordenite. The activity of synthesized samples is shown in **Figure 7A**. Using Cu-Mor sample and 3:1 acetone/glycerol molar ratio, 98% solketal selectivity at 95% glycerol conversion was obtained in only 15 min. **Figure 7B** illustrates how the glycerol conversion and solketal selectivity in the presence of the best sample of Cu-Mor varies with microwave power. The reaction

mechanism of glycerol acetalization using microwave irradiation and using Cu-Mor catalyst was proposed (**Figure 8**). Finally, the Cu-Mor sample exhibited an excellent reusability of up to four reaction cycles with only a marginal drop in reaction conversion.

Timofeeva et al. (2017) investigated glycerol acetalization with acetone using iso-structural MOFs of the families MIL-100(M) and MIL-53(M) (M = V, Al, Fe, and Cr) and mixed MIL-53(Al/V). The results revealed that the metal ion's type in MIL-100(M) and MIL-53(M) has significant impact on the rate of reaction and selectivity of desired product. The zero point of charge of the surface (pH_{PZC}) values are revealed that the acidity of MIL-100(M) dropped in the following order: MIL-100(V) > MIL−100(Al) > MIL-100(Fe) > MIL-100(Cr). As a result, glycerol conversion decreases in the following order V^{3+} > Al^{3+} > Fe^{3+} > Cr^{3+}. Indeed, literature analysis revealed that isomer selectivity depends on the length of the M-O bond in MIL-53(M) and MIL-100(M). Thus, length of M-O bond in MIL-53(M) and MIL-100(M) change in the following order: (Å): MIL-53(Cr) [2.08 (Serre et al., 2002)] > MIL-53(Al) [1.82–2.00 (Loiseau et al., 2004)] > MIL-47(V) [1.946–1.998 (Karin et al., 2004)] and MIL-100(Cr) [2.18 (Férey et al., 2004)] > MIL-100(Fe) [2.065 (Horcajada et al., 2007)] > MIL-100(Al) [1.831–1.995 (Volkringer et al., 2009)], respectively. The decrease in the length of the M-O bond favors increased formation of solketal for both samples. The solketal selectivities increased from approximately 80, 87, and almost 90% over MIL-100(Cr), MIL-100(Fe), and MIL-100(Al). Similarly, it surged from about 80 to 90%, and then around 97% for MIL-53(Cr), MIL-53(Al), and MIL-53(V), respectively. Evaluation of mixed MIL-53(Al,V) showed that the reaction rate and solketal selectivity rise from 90 to 97.5% with increasing V^{3+} content from 0 to 1% in MIL-53(Al,V). Also, the efficiencies of MIL-100(V) (87 mol/mol) and MIL-47(V) (106.1 mol/mol), were higher than those of H_2SO_4, $SnCl_2$ and p-toluene sulfonic acid with 50.9, 89.6, and 58.9 mol/mol, respectively at 25°C. The MIL-100(V) catalyst exhibited four times recycling and reusability with negligible reduction in glycerol conversion (>80%).

de Carvalho et al. (2017) synthesized a series of titanatenano-tubes (TNTs) by hydrothermal method (sodic and protonic TNTs) to investigate the impact of the type of materials and synthesis time. Physico-chemical characterization results revealed that diversities in the TNT tubular structures with inter wall distances (1.07 to 1.11 nm) depend on the applied synthesis time. TEM, SEM, and XRD characterization results confirmed the enlargement of the layers in the protonic titanates unlike the sodic ones. Sodic TNTs, with long synthesis time of up to 24 h, has the $Na_2Ti_3O_7$ phase, whereas the protonic TNTs has $H_2Ti_3O_7$ ones. Although long hydrothermal treatment times (72 h at 160°C) exhibited a strong impact on the reduction of the structural order of the TNTs, it does improve the textural characteristics and acidities of the solids. Also, mild reaction conditions were ineffective for conversion of glycerol over most synthesized sodic TNTs. The best glycerol conversion was obtained over the HTNT sample synthesized at 72 h, with 44.4% glycerol conversion and 83 and 15% selectivity to solketal and acetal, respectively, and only 2% selectivity to by-products

FIGURE 7 | **(A)** Glycerol acetalization using different mordenite catalysts. **(B)** Effect of microwave power on glycerol acetalization over Cu-Mor catalyst.

FIGURE 8 | Plausible reaction mechanism of glycerol acetalization over metal promoted mordenite catalysts.

(mostly cyclic products) at 50°C and 1:1 acetone to glycerol molar ratio.

Pawar et al. (2015) investigated the glycerol acetalization to fuel-additives using an acid-activated clay catalyst of 6/BBnU/6 in the presence of different ketones (cyclohexanone, Benzaldehyde, Ph-acetaldehyde, Furan aldehyde) in liquid phase. Also, they evaluated the effect of various processes such as

solvent-free, conventional thermal activation, and non-conventional microwave/ultrasonic activation methods to find the best operating conditions. Almost complete (99%) selectivity to solketal at 45% conversion was obtained at 1:1 molar ratio of glycerol to cyclohexanone, at room temperature in 3 h. The optimization results revealed that increasing the reaction temperature to 60 °C, glycerol to cyclohexanone

molar ratio to 3:1 and reaction time to 20 h could significantly increase the reaction conversion to more than 80%. In addition, cyclohexanone showed the best effect on the acetalization reaction among all the tested ketones. The eco-friendly process involving a catalyst, microwave, or ultra-sonication were successfully utilized to achieve a commercially valuable hyacinth fragrance. About 98% selectivity to solketal could be achieved under microwave and ultrasonic processes at 92 and 89% ketone conversion.

In some cases metal-based catalysts support with different types of carbons [e.g., activated carbon (AC), carbon nano-tubes (CNT), and multi wall carbon nano-tube (MWCNT)] (Khayoon and Hameed, 2013; Khayoon et al., 2014). Carbon materials have been proven to be a good catalytic support in liquid phase reactions due to acid and base resistance, porosity, high surface area, excellent electronic properties, surface chemistry control, and the possibility of metal support (Demirel et al., 2007). For instance, CNT's external surface area led metals to be highly exposed and accessible to reactants, which improves the efficiency. All these spectacular characteristics provide more opportunities for further investigation of carbon materials in glycerol acetalization reaction. Application of other types of metal-based catalysts particularly MOFs in this field were rarely reported. These types of catalysts have showed great results in other research areas such as production of biodiesel (Rafiei et al., 2018), due to their physico-chemical characteristics (e.g., large surface area and porosity), and their applications should be accelerated in the glycerol acetalization reaction.

Polymer Based Catalysts

Environmentally friendly chemistry plays an important role in design of a cheap and novel catalyst by utilizing cheaper materials (Kobayashi and Miyamura, 2010). In this regard, different approaches such as micro-encapsulation has been recently recognized as a useful technique to immobilize metal catalysts onto polymers (Akiyama and Kobayashi, 2009). The micro-encapsulation refers to the incorporation of an active substance in a shell or a matrix of a carrier component. The catalysts could be separated from a reaction mixture by simple filtration and recycled, making them suitable for green chemistry processes (Ley et al., 2002). Despite all the recent efforts in this field, the described methods constantly suffers from various issues (e.g., complex systems, tedious processes, difficult control of particles' size and shape, and low activity) (Akiyama and Kobayashi, 2009).

A new and environmentally friendly method was introduced by Konwar et al. (2017) for synthesizing a strong solid acidic meso/macro-porous carbon catalyst from Na-lignosulfonate (LS), which is a byproduct from sulfite pulping. Ice-templated LS was altered to macro/mesoporous solid protonic acid at mild pyrolysis temperature (350–450°C) and through ion/H$^+$ exchanging approach (**Figure 9**). According to the characterization results, the LS-derived components that were synthesized contained heteroatom-doped (O, S) carbon structures that are macro/mesoporous and highly functionalized, as well as a large number of surface -OH, -COOH, and -SO$_3$H groups, making them similar to sulfonated carbon materials.

In addition, these carbon components exhibited very good activity as solid acid catalysts in glycerol acetalization with various bio-based aldehydes and ketones, easily outperforming the commercial acid exchange resins (Amberlite$^®$IR120 and Amberlyst$^®$70). The highest ≥99.5, 53, and 51% selectivities of solketal were obtained at almost complete glycerol conversion in the presence of acetone, methyl levulinate and furfural, respectively in batch processes. In addition, the optimum LS catalyst (80LS20PS450H$^+$) exhibited a large specific surface area (122 m^2/g) and stable -SO$_3$H sites (1.21 mmol/g) revealing excellent potential for continuous production of solketal (reaction condition: 100°C reaction temperature, 60 min time, 50 ml/min N$_2$ flow), maintaining its activity (50% selectivity to solketal at ≥91%conversion of glycerol) even after 90 h reaction time.

For the first time, Qing et al. (2017) used a catalytic active membrane synthesized by immersion phase inversion to accelerate the glycerol conversion in an acetalization reaction by continuous removal of water. Indeed, a highly porous "sponge-like" catalytic layer was immobilized with catalyst Zr(SO$_4$)$_2$_4H$_2$O and coated on a polyvinyl alcohol/polyether sulfone per-evaporation membrane. They compared the catalytic activities in batch reactor, catalytically active membrane reactor, and inert membrane reactor. The results revealed the absence of any type of equilibrium limitations for glycerol conversion in the catalytically active membrane reactor and inert membrane reactor. The impact of different operational conditions on synthesis performance in the catalytically active membrane reactor were evaluated, illustrating that higher feed volume (A/V) ratio and temperature enhanced glycerol conversion due to the enhancement of water removal rate. The highest 93% glycerol conversion was achieved at the optimum condition of 5 wt% catalyst concentration, membrane area to A/V ratio of 50/108, 1.2:1 cyclohexanone to glycerol molar ratio, at 75°C in 25 h reaction time.

Organometallic complex, such as cationic oxorhenium (V) oxazoline complex and [2-(2′-hydroxyphenyl)-2-oxazolinato (-2)] oxorhenium (v), were recently tested for a reaction of glycerol with furfural. As a result, solketal selectivity of 70 at 80% glycerol conversion was obtained at 100°C in 4 h (Wegenhart and Abu-Omar, 2010). Also, Crotti et al. (2010) investigated the organo-iridium derivatives [Cp*IrCl$_2$]$_2$ (Cp* = pentamethylcyclopentadienyl) and [Cp*Ir(Bu$_2$-NHC)Cl$_2$], (Bu$_2$-NHC = 1,3-di-nbutylimidazolylidene) as the catalysts for the acetalization and transacetalization of glycerol with ketones and aldehydes. Solketal was major product in all those catalytic reactions.

IMPACTS OF VARIOUS REACTION PARAMETERS ON CATALYTIC PERFORMANCE

Reaction Temperature

Serafim et al. (2011) evaluated the influence of reaction temperature on the glycerol conversion. It was found that by raising the temperature from 30°C to 70°C, the conversion of
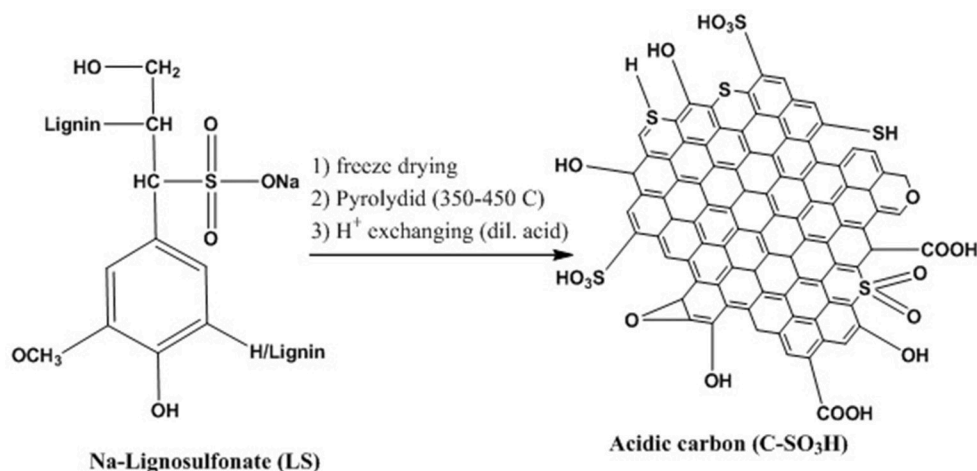
FIGURE 9 | Method for preparing sulfonic acid functionalized carbon materials from LS.

the reaction with butanal was greatly improved from 40 to 87%. Improvement was also observed in the selectivity to solketal. With a similar concept, Khayoon and Hameed (2013) reported a moderate increase in reaction temperature led to increase of glycerol conversion and the reaction successfully formed solketal. Reaction between butyraldehyde and glycerol using Amberlyst 47 catalyst and stoichiometric feed ratio in the temperature range of 50–80°C was performed by Guemez et al. (2013). The total reaction rate increased with temperature although this growth did not affect the final equilibrium conversion. The same results were demonstrated for the reaction of glycerol with formaldehyde and acetaldehyde (Agirre et al., 2011).

In contrast with the aforementioned results and statements, some researchers revealed that product selectivity could be reduced with increasing reaction temperature. Nanda et al. (2014a) showed that a higher temperature lowered the product yield for exothermic reactions. More specifically, the increase in reaction temperature only affected the initial reaction rate. In addition to the mentioned studies, Shirani et al. (2014) reported reduction of solketal yield, by increment of the acetone to glycerol molar ratio as well as the temperature. As the temperature increased, the efficiency of the liquid glycerol molecules with the interaction of the gaseous acetone molecules on the catalyst surface decreases, which caused a lower conversion, yield, and solketal production. Indeed, acetone was vaporized and glycerol was still in the liquid phase while temperature was increased. To enhance the quantity of six-membered cyclic acetal in the mixture, a mild reaction temperature was found to be favorable for the catalytic condensation of glycerol with para-formaldehyde using Amberlyst−36 catalyst (Deutsch et al., 2007).

Application of Various Reactants
Many studies have confirmed that the reactant design has a significant impact on reaction conversion and product selectivity in the glycerol acetalization reaction. Agirre et al. (2011) examined various mole ratios of glycerol and formaldehyde,

using Amberlyst 47 catalyst. The study was performed by altering the molar ratio of glycerol: formaldehyde from 1:1; 1:2 and 1:3, at 353 K. The equilibrium conversion of the formaldehyde increased with rising molar ratio of glycerol. They further applied in excess glycerol for the glycerol and acetaldehyde reaction, which led to 100% conversion of in all cases (Agirre et al., 2013). This finding was in line with Nanda et al. (2014a) on the condensation of glycerol with acetone whereby the glycerol and acetone molar ratio significantly affected the kinetics and thermodynamics of the reaction. When the molar ratios of acetone to glycerol were 1.48:1 and 2.46:1, the solketal yields were 68 and 74%, respectively. The influence of ethanol as a solvent that enhances solubility in acetone was also studied and showed insignificant effect. In another study, the effect of acetone in excess on glycerol conversion was investigated by Ferreira et al. (2010). The glycerol conversion improved with increasing glycerol to acetone molar ratio (from 1:3 to 1:12), while the selectivity to solketal remained constant.

Khayoon and Hameed (2013) stated that in the presence of 5%Ni−1%Zr/AC, the glycerol conversion and the formation of six-membered cyclic ketals were improved by raising the glycerol to acetone molar ratio from 1:4 to 1:8. The same results were reported by Guemez et al. (2013) for glycerol and n-butyraldehyde. When the initial glycerol to butyraldehyde ratio increased from 1:1 to 3:1, the n-butyraldehyde conversion at 80°C and 100 min of reaction time increased from 88 to 98%. When the glycerol to butyraldehyde molar ratio was 0.2, the glycerol conversion reached 100% after 40 min. In another research, the effect of glycerol/butanal molar ratio on the glycerol conversion was investigated (Serafim et al., 2011). In the presence of BEA zeolite catalyst at 80°C, the glycerol conversion after 4 h reaction for glycerol/butanal molar ratio of 1:1 was 71%, whereas the conversion reached 88% in the molar ratio of 1:2.5. However, the further increase of molar ratio (1:6) did not affect the conversion. Applying Amberlyst 15 as a catalyst, Faria et al. (2013) investigated the effect of

various solvents on the production of glycerol ethyl acetalin a simulated moving bed reactor via acetalization of glycerol with acetaldehyde. Compared with acetonitrile, and N,N dimethyl formamide, dimethylsulfoxide solvent exhibited better results owing to its capacity toward the catalyst adsorbents, inertness, and miscibility with the reaction medium. da Silva et al. (2015a) used an available, environmentally friendly, efficient and simple tin-based catalyst for the ketalization of glycerol with different ketones at 25°C. The ketones conversions were 40 and 98% for 4-methyl 2 pentanone and cyclohexanone, respectively.

Water Removal

The acetalization reaction is reported to have a low equilibrium constant (Garcia et al., 2008). Thus, shifting the equilibrium to the product (solketal) side would lead to a higher glycerol conversion. This could be executed by removing the water continuously generated during the reaction or by feeding excess acetone into the reactor. However, the former approach is reported to be the more effective method to break the thermodynamic barriers.

Entrainers have been used in different processes for the continuous elimination of the water from a reaction mixture (Ag, 1998). Benzene, chloroform, and petroleum ethers are some of the entrainers that can be used in this process. The effectiveness of these entrainers is not excellent since their boiling points are higher than acetone. Co-distillation of acetone leads to low efficiency in azeotropic water removal. This obstacle was observed when petroleum ether was used as an entrainer (Chen et al., 2005). The application of phosphorous pentoxide and sodium sulfate as catalyst and desiccant to remove water from the reaction environment has also been reported (Ag, 1998). However, the high amount of catalyst consumption in these cases raises operation costs (He et al., 1992). The aforementioned obstacles could be solved by enhancement of acetone utilization, which not only acts as a reactant but also acts as an entrainer. More importantly, the excess acetone could be recycled and reused in the same process, or even other processes.

Roldan et al. (2009) used membrane batch reactor rather than conventional batch reactor to eliminate water from the reaction environment. Also, Vicente et al. (2010) investigated a two-step batch mode operation for continuous removal of water from the reaction environment. The reaction mixture comprising glycerol, acetone and catalyst was stirred under reflux in a 100 mL flask at 70°C (first step), followed by the removal of produced water as well as acetone by vaporization under vacuum at 70°C. Fresh acetone was added to maintain the liquid level to start a new cycle (second step). After three consecutive steps, 90% solketal yield was obtained at the optimum reaction conditions of 70°C reaction temperature, 5 wt% loading of ArSBA- 15 catalyst, and 30 min reaction time for each step.

Application of Different Types of Processes

Batch reactors commonly encounter drawbacks when scaling up the process. Solketal production in a continuous-flow reactor and in the presence of heterogeneous catalyst is an effective solution because it leads to higher heat and mass transfer efficiency, easy scaling-up of the process along with more environmental

TABLE 4 | Effect of glycerol ether additives on the antiwear properties of heavy cycle oil (ASTM D 2266-01 test method).

Run	Additivies		Average WSD[a] (mm)	ΔWSD[b] (%)
	Type	Amount (ppm)		
1	Additive-free cycle oil		0.94	–
2	Solketal	460	0.71	25
3		980	0.61	35
4		22,470	0.54	43
5	Mixture of di-GTBEs	5,250	0.76	19
6		1,200	0.84	11
7		440	0.88	6
8	STBE/solketal, 70/30	490	0.87	7
9		1,242	0.82	13
10		5,039	0.61	35

[a]Wear spot diameter; [b]Relative change to additive-free cycle oil WSD.

and economic advantages (Noël and Buchwald, 2011). Initial attempts were not successful. For example, Clarkson et al. (2001) used a semi-batch reactor while acetone was fed continuously while the glycerol amount was constant. The main obstacle for a continuous process was glycerol's high viscosity particularly at low temperatures. In another attempt, Monbaliu et al. (2011) designed a continuous process using homogeneous H_2SO_4 as catalyst. However, application of H_2SO_4 made the process not environmentally friendly due to the corrosion and waste disposal problems.

Cablewski et al. (1994) reported on the application of a continuous microwave reactor (CMR) in the production of solketal. A solution of glycerol, acetone and catalyst (pTSA) was pumped into the microwave cavity at a desired temperature, resulting in 84% solketal yield at 13.5 molar ratio of acetone/glycerol, 132°C reaction temperature, 1,175 kPa pressure, 1.2 min residence time and 20 mL/min feed flow rate. However, this process was not appropriate for use with heterogeneous catalysts and low reaction temperatures or for reactants that are incompatible with microwave energy.

For the first time, Samoilov et al. (2016) studied the concurrent ketalisation–alkylation processes in a continuous flow fixed-bed reactor. The results revealed that a continuous single-step process could be effective for glycerol conversion to a mixture of ethers at mild reaction temperature (40–70°C) over a zeolite BEA catalyst. The STBE could be produced at 30% molar yield at optimum reaction conditions of 1:3.4:10 glycerol: TBA: acetone molar ratio and at 45°C. The data in **Table 4** show that solketal has significant influence on the anti-wear characteristics. Application of the glycerol derivatives (e.g., 0.046–2.25 wt%) into hydrocarbon oil can enhance the anti-wear characteristics by 42%. The substitution of the solketal hydroxyl group by TBA produces large hydrocarbon radicals, which could slow down the adsorption of the molecule on metal surfaces by steric hindrance along with a change in the polarity and molecules' surface activity. Moreover, the spatial configuration of the
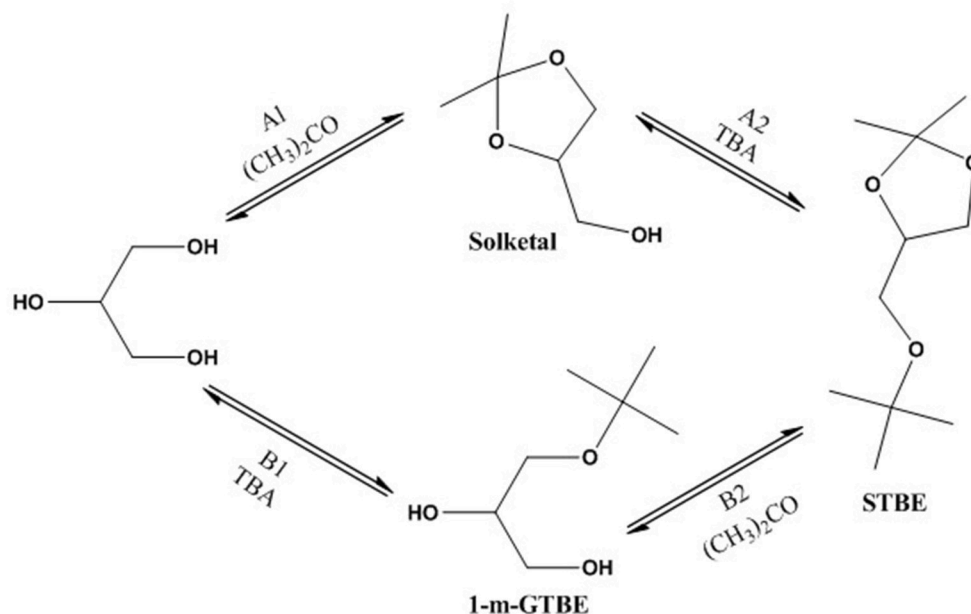
FIGURE 10 | Possible pathways of STBE formation.
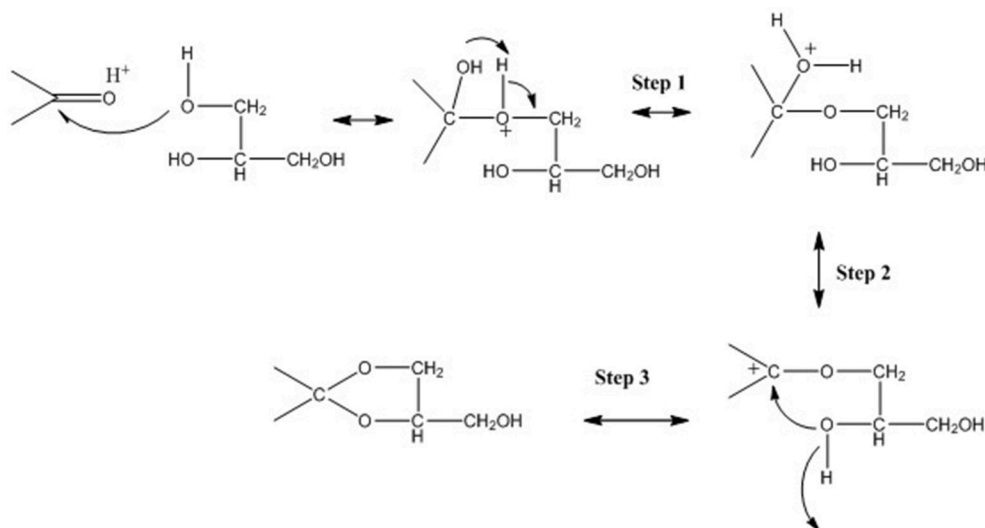
FIGURE 11 | Proposed reaction mechanism for glycerol and acetone acetalization over acid catalyst.

ketal molecule may have a positive impact on the adsorption. **Figure 10** illustrates the different steps of STBE formation. The first route (A) includes glycerol ketalisation (A1) followed by solketal tert-butylation with TBA (A2). The second route (B) includes formation of 1-mono-GTBE (B1) and then ketalisation of ether to STBE (B2).

Recently, Nanda et al. (2014b) developed a continuous-flow reactor based on the "Novel Process Windows" concept with respect to temperature, pressure and/or reactant concentration to enhance the intrinsic kinetics of the reaction for an optimum

yield. Results indicated that they could achieve more than 97% selectivity to solketal at >80% glycerol conversion using different catalysts (H-β zeolite, Amberlyst 36 wet, Amberlyst 35, ZrSO$_4$) at 40°C reaction temperature, 600 psi reaction pressure, 6:1 molar ratio of acetone to glycerol in 15 min reaction time. On the other hand, this system suffered from the catalyst clogging the reactor.

The glycerol acetalization reaction mechanism in the presence of an acid catalyst that leads to the formation of both five- and six-membered rings (ketals) is illustrated in **Figure 11** (Voleva et al., 2012). Nanda et al. (2014a) have also reported

a two-step processes for glycerol acetalization reaction. The surface reaction between glycerol and the adsorbed acetone on the catalyst surface form the hemi-acetal (Step 1), then the carbonyl carbon turns into a carbocation by the removal of a water molecule and deprotonization to form solketal and 1,3-dioxane. The 1,3-dioxane (six membered ring ketal) is the less favorable product because one of the methyl groups is in the axial position of the chaircon formation (Maksimov et al., 2011). Thus, in the majority of cases the resulting product has higher ratio (even up to 99:1) of five-membered ring (solketal) to six-membered ring (5-hydroxy-2,2-dimethyl-1,3-dioxane).

Perreia and Rodrigues (2013) creatively used process intensification for acetal production along with advanced technologies, applying Simulated Moving Bed Membrane Reactor (PermSMBR), and Simulated Moving Bed Reactor (SMBR), for the acetalization of2-butanol and ethanol with acetaldehyde. These reactors achieved high conversion and productivity at low temperatures (10–50°C), while requiring additional operational costs and capitals. This method could be used for the acetalization of glycerol. The reactive distillation with approximately 100% glycerol conversion is the best reactor design since they feature low capital costs and no reactor clogging with the catalyst. Performing the distillation and reaction simultaneously also saves on operational cost.

Gorji and and Ghaziaskar (2016) synthesized mono-acetin by reacting glycerol with acetic acid (first step) followed by solketal production from the reaction of mono-acetin with acetone over Purolite PD 206 catalyst (second step). This method was reported as an economical and easy to scale up process for glycerol conversion to fuel-additives. Results show 69% yield of solketal was achieved at almost complete glycerol conversion at optimal reaction conditions of 5:1 acetone to mono-acetin molar ratio, 0.2 mL/min feed flow rate, and 2.0 g catalyst at ambient temperature of 20°C and 45 bar pressure in the second step.

Application of Crude Glycerol

The key factor for industrial applications of glycerol is its purity level. The crude glycerol obtained from biodiesel production is normally considered as waste by-product in the biodiesel industry since it contains impurities, namely esters, methanol, fatty acids, water, and inorganic salts (matter organic non-glycerol, MONG) (Liang et al., 2010; Rosas et al., 2017). Economically, it is feasible for large-scale biodiesel firms to purify the crude glycerol for further utilizations. Small companies on the other hand cannot afford it; therefore, they have to pay for glycerol disposal or burn it as a waste stream (Wilson, 2002; McCoy, 2006). Heterogeneous catalysts and non-edible oils have been used in the vast majority of studies to produce higher quality biodiesel and glycerol. For example, high quality biodiesel (98.3%) and glycerol (98%) were produced over the Zn-Al heterogeneous solid catalyst (Bournay et al., 2005). Their synthesized catalyst could avoid all the costly purification steps in the direct utilization of crude glycerol. Thus, application of crude-glycerol is another factor that could significantly impact the catalyst activity. Although there have been plenty of studies on the bio-based production of value-added chemicals from

refined glycerol, the same cannot be said regarding the utilization of crude glycerol as feedstock.

da Silva and Mota (2011) evaluated the impact of impurities on the formation of solketal in a batch reactor to enable the utilization of crude glycerol rather than purified glycerol. They investigated the effect of common impurities (e.g., 1% methanol, 10% water, and 15% NaCl) in the acetalization of crude glycerol with various heterogeneous catalysts (e.g., H-beta zeolite and Amberlyst-15). When crude glycerol was used in place of refined glycerol, a dramatic drop in reaction conversion was observed, down to 47 and 50% for Amberlyst-15 and H-beta zeolite catalysts, respectively, compared to 95% reaction conversion for refined glycerol with similar catalysts. In fact, they revealed that methanol had less effect than water and NaCl.

Vicente et al. (2010) reported the application of acid-functionalized SBA-15 catalysts for acetalization of crude glycerol (85.8 wt.%). They obtained 81% conversion of glycerol. However, high Na^+ content in crude glycerol deactivated significantly the sulfonic acid sites due to a cation exchange reaction between Na^+ and H^+.

In another study, Nanda (2015) continued their studies by developing a modified continuous-flow reactor including guard reactors that allow online elimination of impurities from the glycerol feedstock and on-line regeneration of deactivated catalysts. A maximum 78% yield of solketal was achieved using crude glycerol and the modified continuous-flow reactor in only 1 h of on-stream time. They also conducted on-line regeneration of the deactivated catalyst in the guard reactor concurrently with the ketalization experiment using purified (96%) crude-glycerol as feedstock. They found that the catalyst (Amberlyst-36 wet) could be effectively regenerated for four consecutive times even up to 96 h of reaction time with only 11% fall (92 to 81%) in solketal yield (Nanda, 2015). For the catalyst regeneration, a 0.5M H_2SO_4 solution was passed through the guard reactor, followed by a methanol washing of the regenerated catalyst and finally drying the bed with nitrogen for 5 h.

CONCLUDING REMARKS

This review comprehensively summarizes various approaches and strategies for the glycerol conversion to cyclic acetals and ketals processes and recent progress in obtaining higher conversion and selectivity of the desired products. Both homogeneous and heterogeneous acid catalysts can be used in the conversion of glycerol to solketal. The vast majority of studies are conducted over heterogeneous catalysts, which can be easily separated from the system by filtration. Various reaction parameters (e.g., reactor design, temperature, reactants, and nature of catalyst) have significant impact on the catalytic activity in this process.

Recent breakthroughs in catalyst synthesis and characterization lead to unprecedented achievements in this field. Despite various advances, there are still many challenges for increasing selectivity and yield. Indeed, there are spectacular opportunities in catalysis and nano-materials to synthesize a highly active catalyst for glycerol acetalization to specific

useful products. Application of more environmentally friendly processes and materials for catalyst synthesis will be the main objective in the future. For instance, application of microwave radiations could enlarge the specific surface area and increased pore volume.

Investigation on the effect of different reaction parameters on catalytic activity revealed that one of the major obstacles in acetalization reaction is its very low equilibrium constant. As a result, the best remedy for this problem is to shift the equilibrium to the product side (e.g., solketal), by either feeding excess reactant (e.g., acetone) or by removing water generated during the reaction. Also, compared to operation in a batch reactor, similar or even higher product selectivity and relatively shorter reaction time could be achieved with the use of continuous flow reactors. Definitely, more investigation on continuous glycerol acetalization process could be one of the major steps toward industrialization and commercialization of this process in the near future.

The reviewed studies confirm that the acetalization of glycerol is a promising process that could bring significant economic prosperity. In addition to the economic benefits, it also has tangible benefits on the environment by shifting the production of industrial chemicals away from petroleum-based toward bio-based processes. Indeed, fuel additive could improve the cleanliness of different parts of the engine, promote complete combustion, reduce fuel gelling and choking of nozzle, as well as reduce corrosion impact on different parts of the engine.

AUTHOR CONTRIBUTIONS

This research is based on AT-K's postdoctoral fellowship research project. NN assisted in collecting information, the revision process, and manuscript improvement. NA was the corresponding author and AT-K's main supervisor during his Postdoctoral fellowship. ST was AT-K's co-supervisor during his Postdoctoral fellowship.

ACKNOWLEDGMENTS

REFERENCES

Abad, S., and Turon, X. (2012). Valorization of biodiesel derived glycerol as a carbon source to obtain added-value metabolites: focus on polyunsaturated fatty acids. *Biotechnol. Adv.* 30, 733–741. doi: 10.1016/j.biotechadv.2012.01.002

Abreu, A. V., Meyer, C. I., Padro, C., and Martins, L. (2018). Acidic V-MCM-41 catalysts for the liquid-phase ketalization of glycerol with acetone. *Miro. Meso. Matt.* 273, 219–225. doi: 10.1016/j.micromeso.2018.07.006

Adam, F., Batagarawa, M. S., Hello, K. M., and Al-Juaid, S. S. (2012). One-step synthesis of solid sulfonic acid catalyst and its application in the acetalization of glycerol: crystalstructure of−5-hydroxy-2-phenyl-1,3-dioxane trimer. *Chem. Papers* 66, 1048–1058. doi: 10.2478/s11696-012-0203-x

Ag, B. (1998). *Cyclic Acetal or Ketal Preparation From Polyol and Aldehyde or Ketone*. Patent DE19648960 A1.

Aghbashloa, M., Tabatabaei, M., Hosseinpoura, S., Rastegarid, H., and Ghaziaskar, H. S. (2018). Multi-objective exergy-based optimization of continuous glycerol ketalization to synthesize solketal as a biodiesel additive in subcritical acetone. *Energ. Conv. Manage.* 160, 251–261. doi: 10.1016/j.enconman.2018.01.044

Agirre, I., Garcia, I., Requies, J., Barrio, V. L., Guemez, M. B., and Cambra, J. F. (2011). Glycerolacetals, kinetic study of the reaction between glycerol and formaldehyde. *Biomass Bioenergy* 35, 3636–3642. doi: 10.1016/j.biombioe.2011.05.008

Agirre, I., Guemez, M. B., Uguarte, A., Requies, J., Barrio, V. L., and Cambra, J. F. (2013). Glycerolacetals as diesel additives: kinetic study of the reaction between glycerol andacetaldehyde. *Fuel Process. Technol.* 116, 182–188. doi: 10.1016/j.fuproc.2013.05.014

Akiyama, R., and Kobayashi, S. (2009). "Microencapsulated" and related catalysts for organic chemistry and organic synthesis. *Chem Rev.* 109, 594–642. doi: 10.1021/cr800529d

Arias, K. S., Garcia-Ortiz, A., Climent, M. J., Corma, A., and Iborra, S. (2018). Mutual valorization of 5-hydroxymethylfurfural and glycerol into valuable diol monomers with solid acid catalysts. *ACS. Sust. Chem. Eng.* 6, 4239–4245. doi: 10.1021/acssuschemeng.7b04685

Ayoub, M., and Abdullah, A. Z. (2012). Critical review on the current scenario and significance of crude glycerol resulting from biodiesel industry towards more sustainable renewable energy industry. *Renew. Sustain. Energy Rev.* 16, 2671–2686. doi: 10.1016/j.rser.2012.01.054

Bournay, L., Casanave, D., Delfort, B., Hillion, G., and Chodorge, J. A. (2005). New heterogeneous process for biodiesel production: a way to improve the quality and the value of the crude glycerin produced by biodiesel plants. *Catal. Today* 106, 190–192. doi: 10.1016/j.cattod.2005.07.181

Cablewski, T., Faux, A. F., and Strauss, C. R. (1994). Development and application of a continuous microwave reactor for organic synthesis. *J. Org. Chem.* 59, 3408–3412. doi: 10.1021/jo00091a033

Chen, L., Liang, J., Lin, H., Weng, W., Wan, H., and Védrine, J. C. (2005). MCM41 and silica supported MoVTe mixed oxide catalysts for direct oxidation of propane to acrolein. *Appl. Catal. A* 293, 49–55. doi: 10.1016/j.apcata.2005.06.029

Chen, L., Nohair, B., Zhao, D., and Kaliaguine, S. (2018a). Highly efficient glycerol acetalization over supported heteropolyacid catalysts. *Chem. Cat. Chem.* 10, 1918–1925. doi: 10.1002/cctc.201701656

Chen, L., Nohair,B., Zhao, D., and Kaliaguine, S. (2018b). Glycerol acetalization with formaldehyde using heteropolyacid salts supported on mesostructured silica. *Appl. Catal. A Gen.* 549, 207–215. doi: 10.1016/j.apcata.2017.09.027

Choi, M., Cho, H. S., Srivastava, R., Venkatesan, C., Choi, D. H., and Ryoo, R. (2006). Amphiphilic organosilane-directed synthesis of crystalline zeolite with tunable mesoporosity. *Nat. Mater.* 5, 718–723. doi: 10.1038/nmat1705

Clarkson, J. S., Walker, A. J., and Wood, M. A. (2001). Continuous reactor technology for ketal formation: an improved synthesis of solketal. *Org. Process. Res. Dev.* 5, 630–635. doi: 10.1021/op000135p

Clomburg, J. M., and Gonzalez, R. (2013). Anaerobic fermentation of glycerol: a platform for renewable fuels and chemicals. *Trends. Biotechnol.* 31, 20–28. doi: 10.1016/j.tibtech.2012.10.006

Coleman, T., and Blankenship, A. (2010). *Process for the Preparation of Glycerol Formal*. US Patent 0094027.

Crotti, C., Farnetti, E., and Guidolin, N. (2010). Alternative intermediates for glycerol valorization: iridium-catalyzed formation of acetals and ketals. *Green. Chem.* 12, 2225–2231. doi: 10.1039/c0gc00096e

da Silva, C. X. A., Goncalves, V. L. C., and Mota, C. J. A. (2009). Water tolerant zeolite catalyst for the acetalisation of glycerol. *Green. Chem.* 11, 38–41. doi: 10.1039/B813564A

da Silva, C. X. A., and Mota, C. J. A. (2011). The influence of impurities on the acid-catalyzed reaction of glycerol with acetone. *Biomass Bioenerg.* 35, 3547–3551. doi: 10.1016/j.biombioe.2011.05.004

da Silva, M. J., De Oliveira, G. M., and Julio, A. A. (2015a). A highly regioselective and solvent-freeSn(II)-catalyzed glycerol ketals synthesis at room temperature. *Catal. Lett.*145, 769–776. doi: 10.1007/s10562-015-1477-8

da Silva, M. J., Julio, A. A., and Dorgetto, F. C. S. (2015b). Solvent-free heteropolyacid-catalyzed glycerol ketalization at room temperature. *RSC Advance* 5, 44499–44506. doi: 10.1039/C4RA17090C

da Silva, M. J., Rodrigues, F. D. A., and Julio, A. A. (2017). SnF$_2$-catalyzed glycerol ketalization: a friendly environmentally process to synthesize solketal at room temperature over on solid and reusable Lewis acid. *Chem. Eng. J.* 307, 828–835. doi: 10.1016/j.cej.2016.09.002

de Carvalho, D. C., Oliveira, A. C., Ferreira, O. P., Filho, J. M., Tehuacanero-Cuapa, S., and Oliveira, A. C. (2017). Titanate nanotubes as acid catalysts for acetalization of glycerol with acetone: influence of the synthesis time and the role of structure on the catalytic performance. *Chem. Eng. J.* 313, 1454–1467. doi: 10.1016/j.cej.2016.11.047

De Torres, M., Jimenez-oses, G., Mayoral, J. A., and Pires, E. (2011). Fatty acid derivates and their use as CFFP additives in biodiesel. *Bioresour. Technol*. 102, 2590–2594. doi: 10.1016/j.biortech.2010.10.004

Demirel, S., Kern, P., Lucas, M., and Claus, P. (2007). Oxidation of mono-and polyalcohols with gold: comparison of carbon and ceria supported catalysts. *Catal. Today* 122, 292–300. doi: 10.1016/j.cattod.2006.12.002

Deutsch, J., Martin, A., and Lieske, H. (2007). Investigations on heterogeneously catalyzed condensations of glycerol to cyclic acetals. *J. Catal.* 245, 428–435. doi: 10.1016/j.jcat.2006.11.006

Egeblad, K., Christensen, C. H., and Kustova, M. (2008). Templating mesoporous zeolites. *Chem. Mater*. 20, 946–960. doi: 10.1021/cm702224p

Fan, C. N., Xu, C. H., Liu, C. Q., Huang, Z. Y., Liu, J. Y., and Ye, Z. X. (2012). Catalytic acetalization ofbiomass glycerol with acetone over TiO$_2$–SiO$_2$ mixed oxides. *React. Kin. Mech. Cat. Lett.* 107, 189–202. doi: 10.1007/s11144-012-0456-y

Fan, W., Snyder, M. A., Kumar, S., Lee, P. S., Yoo, W. S., McCormick, A. V., et al. (2008). Hierarchical nanofabrication of microporous crystals with ordered mesoporosity. *Nat. Mater*. 7, 984–991. doi: 10.1038/nmat2302

Faria, R. P. V., Pereira, C. S. M., Siva, V. M. T. M., Loureiro, J. M., and Rodrigues, A. E. (2013). Glycerolvalorization as biofuels: selection of a suitable solvent for an innovative processfor the synthesis of GEA. *Chem. Eng. J.* 233, 159–167. doi: 10.1016/j.cej.2013.08.035

Fazal, M. A., Haseeb, A. S. M. A., and Masjuki, H. H. (2011). Biodiesel feasibility study: an evaluation of material compatibility; performance; emission and engine durability. *Ren. Sus. Energ. Rev*. 15, 1314–1324. doi: 10.1016/j.rser.2010.10.004

Férey, G., Serre, C., Mellot-Draznieks, C., Millange, F., Surblé, S., Dutour, J., et al. (2004). A hybrid solid with giant pores prepared by a combination of targeted chemistry, simulation, and powder diffraction. *Angew. Chem*. 116, 6456–6461. doi: 10.1002/ange.200460592

Ferreira, C., Araujo, A., Calvino-Casilda, V., Cutrufello, M. G., Rombi, E., Fonseca, A. M., et al. (2018). Y zeolite-supported niobium pentoxide catalysts for the glycerol acetalization reaction. *Micro. Meso. Mat.* 271, 243–251. doi: 10.1016/j.micromeso.2018.06.010

Ferreira, P., Fonseca, I. M., Ramos, A. M., Vital, J., and Castanheiro, J. E. (2010). Valorisationofglycerol by condensation with acetone over silica-included heteropolyacids. *Appl. Catal. B Environ*. 98, 94–99. doi: 10.1016/j.apcatb.2010.05.018

Fischer, E. (1895). Ueber die verbindungen der zuckermit den alkoholen und ketonen. *Eur. J. Inorg. Chem*. 28, 1145–1167.

Fischer, E., and Pfahler, E. (1920). Uber glycerin-aceton und seine verwendbarkeitzurreindarstellung von α-glyceriden: uber einephosphorsaureverbindungglykois. *Eur. J. Inorg. Chem*. 53, 1606–1621.

Forester, D. R., Robert, S. D. C., Manka, J. S., and Malik, B. B. (2003). *Jet Fuel Additive Concentrate Composition and Fuel Composition and Methods Thereof.* US Patent WO2003106595.

Franklin, P. M., Koshland, C. P., Lucas, D., and Sawyer, R. F. (2000). Clearing the air: using scientific information to regulate reformulated fuels. *Environ. Sci. Technol.* 34, 3857–3863. doi: 10.1021/es0010103

Gadamsetti, S., Rajan, N. P., Rao, G. S., and Chary, K. V. R. (2015). Acetalization of glycerol with acetone to bio fuel additives over supported molybdenum phosphate catalysts. *J. Mol. Cat. A Chem.* 410, 49–57. doi: 10.1016/j.molcata.2015.09.006

Garcia, E., Laca, M., Pe, E., and Garrido, A. (2008). New class of acetal derived from glycerin as abiodiesel fuel component. *Energ. Fuel*. 22, 4274–4280. doi: 10.1021/ef800477m

García-Martínez, J., Li, K. (eds) (2015). *Mesoporous Zeolites: Preparation Characterization and Application* (Weinheim: Wiley-VCH Verlag GmbH & Co KGaA), 1–574.

Gesslein, B. W. (1999). "Humectants in personal care formulation: a practical guide," in *Conditioning Agents for Hair and Skin*, eds R. Schueller, P. Romanowski (New York, NY; Basel: Marcel Dekker, Inc.), 95–6.

Gomes, I. S., de Carvalho, D. C., Oliveira, A. C., Rodriguez-Castellon, E., Tehuacanero-Cuapa, S., Freire, P. T. C., et al. (2018). On the reasons for deactivation of titanate nanotubes with metals catalysts in the acetalization of glycerol with acetone. *Chem. Eng. J.* 334, 1927–1942. doi: 10.1016/j.cej.2017.11.112

Gonzalez-Arellano, C., De, S., and Luque, R. (2014a). Selective glycerol transformations to high value-added products catalysed by alumino-silicate-supported iron oxide nanoparticles. *Catal.Sci. Technol.* 4, 4242–4249. doi: 10.1039/C4CY00714J

Gonzalez-Arellano, C., Parra-Rodriguez, L., and Luque, R. (2014b). Mesoporous Zr–SBA-16 catalysts for glycerol valorization processes: towards bio-renewable formulations. *Catal. Sci. Technol.* 4, 2287–2292. doi: 10.1039/C4CY00230J

Gorji, Y. M., and and Ghaziaskar, H. S. (2016). Optimization of solketalacetin synthesis as a green fuel additive from ketalization of monoacetin with acetone. *Ind. Eng. Chem. Res.* 55, 6904–6910. doi: 10.1021/acs.iecr.6b00929

Groen, J. C., Zhu, W., Brouwer, S., Huynink, S. F., Kapteijn, F., Moulijn, J. A., et al. (2007). Direct demonstration of enhanced diffusion in mesoporous ZSM-5 zeolite obtained via controlled desilication. *J. Am. Chem. Soc.* 129, 355–360. doi: 10.1021/ja065737o

Guemez, M. B., Requies, J., Agirre, I., Arias, P. L., Bario, L., and Cambra, J. F. (2013). Acetalizationreaction between glycerol and n-butyraldehyde using an acidic ion exchangeresin. *Kinet. Model. Chem. Eng. J.* 228, 300–307. doi: 10.1016/j.cej.2013.04.107

Gutiérrez-Acebo, E., Guerrero-Ruiz, F., Centenero, M., Martínez, J. S., Salagre, P., Cesteros, Y. (2018). Effect of using microwaves for catalysts preparation on the catalytic acetalization of glycerol with furfural to obtain fuel additives. *Open Chem.* 16, 386–392. doi: 10.1515/chem-2018-0047

Halgeri, A. B., and Das, J. (1999). Novel catalytic aspects of beta zeolite for alkyl aromatics transformation. *Appl. Catal. A* 181, 347–354. doi: 10.1016/S0926-860X(98)00395-0

Hasabnis, A., and Mahajani, S. (2014). Acetalization of glycerol with formaldehyde byreactive distillation. *Ind. Eng. Chem. Res.* 53, 12279–12287. doi: 10.1021/ie501577q

He, D. Y., Li, Z. J., Li, Z. J., Liu, Y. Q., Qiu, D. X., and Cai, M. S. (1992). Studies on carbohydrates X. A newmethod for the preparation of isopropylidene saccharides. *Synth. Com.* 22, 2653–2658. doi: 10.1080/0039791920802 1665

Horcajada, P., Surblé, S., Serre, C., Hong, D. Y., Seo, Y. K., Chang, J. S., et al. (2007). Synthesis and catalytic properties of MIL-100(Fe), an iron(III) carboxylate with large pores. *Chem. Commun.* 27, 2820–2822. doi: 10.1039/B704325B

Jamil, F., Saxena, S. K., Al-Muhtaseb, A. H., Baawain, M., Al-Abri, M., Viswanandham, N., et al. (2017). Valorization of waste "date seeds" bio-glycerol for synthesizing oxidative green fuel additive. *J. Clean. Prod.* 165, 1090–1096. doi: 10.1016/j.jclepro.2017.07.216

Kapkowski, M., Ambrozkiewicz, W., Siudyga, T., Sitko, R., Szade, J., limontko, J., et al. (2017). Nano silica and molybdenum supported Re, Rh, Ru or Irnanoparticlesfor selective solvent-free glycerol conversion to cyclic acetals with propanone and butanone under mild conditions. *Appl. Catal. B Env.* 202, 335–345. doi: 10.1016/j.apcatb.2016.09.032

Karin, B., Marrot, J., Riou, D., and Férey, G. (2004). A breathing hybrid organic–inorganic solid with very large pores and high magnetic characteristics. *Angew. Chem*. 114, 291–294. doi: 10.1002/1521-3757(20020118)114:2<291::AID-ANGE291>3.0.CO;2-I

Khayoon, M. S., Abbas, A., Hameed, B. H., Triwahyono, S., Jalil, A. A., and Harris, A. T. (2014). Selective acetalization of glycerol with acetone over nickel nanoparticlessupported on multi-walled carbon nano-tubes. *Catal. Lett.* 144, 1009–1015. doi: 10.1007/s10562-014-1221-9

Khayoon, M. S., and Hameed, B. H. (2013). Solventless acetalization of glycerol with acetone tofuel oxygenates over Ni–Zi supported

mesoporous carbon catalyst. *Appl. Catal. A Gen.* 464–465, 191–199. doi: 10.1016/j.apcata.2013.05.035

Kobayashi, S., and Miyamura, H. (2010). Polymer-incarcerated metal (0) cluster catalysts. *Chem Rec.* 10, 271–290. doi: 10.1002/tcr.201000026

Konwar, L. J., Samikannu, A., Maki-Arvela, P., Bostrom, D., and Mikkola, J. (2017). Lignosulfonate-based macro/mesoporous solid protonic acids for acetalization of glycerol to bio-additives. *Appl. Catal. B Environ.* 220, 314–323. doi: 10.1016/j.apcatb.2017.08.061

Kowalska-Kus, J., Held, A., Frankowski, M., and Nowinska, K. (2017). Solketal formation from glycerol and acetone over hierarchical zeolites of different structure as catalysts. *J. Mol. Catal. A Chem.* 426, 205–212. doi: 10.1016/j.molcata.2016.11.018

Lazar, A., Betsy, K. J., Vinod, C. P., and Singh, A. P. (2018). Ru(II)-functionalized SBA-15 as highly chemoselective, acid free and sustainable heterogeneous catalyst for acetalization of aldehydes and ketones. *Cat. Comm.* 104, 62–66. doi: 10.1016/j.catcom.2017.10.016

Ley, S. V., Ramarao, C., Gordon, R. S. G., Holmes, A. B., Morrison, A. J., and McConvey, I. F. (2002). D, Polyurea-encapsulated palladium (II) acetate: a robust and recyclable catalyst for use in conventional and supercritical media. *Chem. Commun.* 10, 1134–1135. doi: 10.1039/b200677b

Li, L., Korányi, T. I., Sels, B. F., and Pescarmona, P. P. (2012). Highly-efficient conversion of glycerol to solketal over heterogeneous Lewis acid catalysts. *Green. Chem.* 14, 1611–1619. doi: 10.1039/C2GC16619D

Li, R., Song, H., and Chen, J. (2018b). Propylsulfonic acid functionalized SBA-15 mesoporous silica as efficient catalysts for the acetalization of glycerol. *Catalysts* 8:297. doi: 10.3390/catal8080297

Li, X., Zheng, L., and Hou, Z. (2018c). Acetalization of glycerol with acetone over Co[II](Co[III]xAl2−x)O4 derived from layered double hydroxide. *Fuel* 233, 565–571. doi: 10.1016/j.fuel.2018.06.096

Li, Z., Miao, Z., Wang, X., Zhao, J., Zhou, J., Si, W., et al. (2018a). One-pot synthesis of ZrMo-KIT-6 solid acid catalyst for solvent-free conversion of glycerol to solketal. *Fuel* 233, 377–387. doi: 10.1016/j.fuel.2018.06.081

Liang, Y., Cui, Y., Trushenski, J., and Blackburn, J. W. (2010). Converting crude glycerol derived from yellow grease to lipids through yeast fermentation. *Bioresour. Technol.* 101, 7581–7586. doi: 10.1016/j.biortech.2010.04.061

Lin, C. Y., and Chen, W. C. (2006). Effects of potassium sulfide content in marine diesel fuel oil on emission characteristics of marine furnaces under varying humidity of inlet air. *Ocean Eng.* 33, 1260–1270. doi: 10.1016/j.oceaneng.2005.06.009

Lin, Y. C., and Huber, G. W. (2009). The critical role of heterogeneous catalysis in lignocellulosic biomass conversion. *Energy Environ. Sci.* 2, 68–80. doi: 10.1039/B814955K

Loiseau, T., Serre, C., Huguenard, C., Fink, G., Taulelle, F., Henry, M., et al. (2004). A rationale for the large breathing of the porous aluminum terephthalate (MIL-53) upon hydration. *Chem. Eur. J.* 10, 1373–1382. doi: 10.1002/chem.200305413

Lupulescu, A. I., and Rimer, J. D. (2012). Tailoring silicalite-1 crystal morphology with molecular modifiers. *Angew. Chem. Int. Ed.* 51, 3345–3349. doi: 10.1002/anie.201107725

Maksimov, L., Nekhaeva, I., Ramazanov, D. N., Arinicheva, Y. A., Dzyubenko, A., and Khadzhiev, S. N. (2011). Preparation of high-octane oxygenate fuel components fromplant-derived polyols. *Pet. Chem.* 51, 61–69. doi: 10.1134/S0965544111010117

Mallesham, B., Sudarsanam, P., Raju, G., and Reddy, B. M. (2013). Design of highly efficient Mo and W-promoted SnO2 solid acids for heterogeneous catalysis: acetalization of bio-glycerol. *Green. Chem.* 15, 478–489. doi: 10.1039/C2GC36152C

Mallesham, B., Sudarsanam, P., and Reddy, B. M. (2014). Eco-friendly synthesis of bio-additivefuels from renewable glycerol using nano-crystalline SnO2- based solid acids. *Catal. Sci. Technol.* 4, 803–813. doi: 10.1039/c3cy00825h

Manjunathan, P., Maradur, S. P., Halgeri, A. B., and Shanbhag, V. (2015). Room temperaturesynthesis of solketal from acetalization of glycerol with acetone: effect ofcristallite size and the role of acidity of beta zeolite. *J. Mol. Catal. A Chem.* 396, 47–54. doi: 10.1016/j.molcata.2014.09.028

Manjunathan, P., Marakatti, V. S., Chandra, P., Kulal, A. B., Umbarkar, S. B., Ravishankar, R., et al. (2018). *Mesoporous tin oxide: an efficient catalyst with versatile applications in acid and oxidation catalysis. *Catal. Today* 309, 61–76. doi: 10.1016/j.cattod.2017.10.009

Mantovani, M., Mandello, D., Goncalves, M., and Carvalho, W. A. (2018). Fructose dehydration promoted by acidic catalysts obtained from biodiesel waste. *Chem. Eng. J.* 348, 860–869. doi: 10.1016/j.cej.2018.05.059

Martin, A., Armbruster, U., and Atia, H. (2012). Recent developments in dehydration of glycerol toward acrolein over heteropoly acids. *Eur. J. Lipid Sci. Technol.* 114, 10–23. doi: 10.1002/ejlt.201100047

McCoy, M. (2006). Glycerin surplus. *Chem. Eng. News* 84, 7–8. doi: 10.1021/cen-v084n006.p007a

Menchavez, R. N., Morra, M. J., and He, B. B. (2017). Co-Production of ethanol and 1,2-propanediol viaGlycerol hydrogenolysis using Ni/Ce–Mg catalysts: effects of catalyst preparation and reaction conditions. *Catalysts* 7:290. doi: 10.3390/catal7100290

Monbaliu, J. C. M., Winter, M., Chevalier, B., Schmidt, F., Jiang, Y., and Hoogendoorn, R. (2011). Effective production of the biodiesel additive STBE by a continuous flowprocess. *Bioresour. Technol.* 102, 9304–9307. doi: 10.1016/j.biortech.2011.07.007

Mota, C. J., da Silva, C. X., Rosenbach, N., Costa, J., and da Silva, F. (2010). Glycerin derivatives as fuel additives: the addition of glycerol/acetone ketal (solketal) in gasolines. *Energ. Fuel.* 24, 2733–2736. doi: 10.1021/ef9015735

Nair, G. S., Adrijanto, E., Alsalme, A., Kozhevnikov, I. V., Cooke, D. J., Brown, D. R., et al. (2012). Glycerol utilization over niobia catalysts. *Catal. Sci. Technol.* 2, 1173–1179. doi: 10.1039/c2cy00335j

Nanda, M. R. (2015). *Catalytic Conversion of Glycerol to Value-Added Chemical Products.* Electronic Thesis and Dissertation Repository, Western University, London, Canada, Paper 3215.

Nanda, M. R., Yuan, Z., Qin, W., Ghaziaskar, H. R., Poirer, M. A., and Xu, C. C. (2014b). Thermodynamic and kinetic studies of a catalytic process to convert glycerol into solketal as an oxygenated fuel additive. *Fuel* 117, 470–477. doi: 10.1016/j.fuel.2013.09.066

Nanda, M. R., Yuan, Z., Qin, W., Ghaziaskar, H. S., Poirier, M. A., and Xu, C. (2014a). A new continuous-flow process for catalytic conversion of glycerol to oxygenated fuel additive: catalyst screening. *Appl. Energ.* 123, 75–81. doi: 10.1016/j.apenergy.2014.02.055

Nanda, M. R., Yuan, Z., Shui, H., and Xu, C. (2017). Selective hydrogenolysis of glycerol and crudeglycerol (a by-product orwaste stream from thebiodiesel industry) to 1,2-propanediol over B2O3Promoted Cu/Al2O3 Catalysts. *Catalysts* 7:196. doi: 10.3390/catal7070196

Narkhede, N., and Patel, A. (2014). Room temperature acetalization of glycerol to cyclicacetals over anchored silicotungstates under solvent free conditions. *R. Soc. Chem. Adv.* 4, 19294–19301. doi: 10.1039/C4RA01851F

Newman, M. S., and Renoll, M. (1945). Improved preparation of isopropylidene glycerol. *J. Am. Chem. Soc.* 67, 1621–1621. doi: 10.1021/ja01225a511

Nguyen, R., Galy, N., Singh, A. K., Paulus, F., Stobener, D., Schlesener, C., et al. (2017). A simple and efficient process for large scaleglycerol oligomerization by microwave Irradiation. *Catalysts* 7:123. doi: 10.3390/catal7040123

Noël, T., and Buchwald, S. L. (2011). Cross-coupling in flow. *Chem. Soc. Rev.* 40, 5010–5029. doi: 10.1039/c1cs15075h

Pariente, S., Tanchoux, N., and Fajula, F. (2008). Etherification of glycerol with ethanol over solid acid catalysts. *Green Chem.* 11, 1256–1261. doi: 10.1039/B905405G

Park, D. H., Kim, S. S., Wang, H., Pinnavaia, T. J., Papapetrou, M. C., Lappas, A. A., et al. (2009). Selective petroleum refining over a zeolite catalyst with small intracrystal mesopores. *Angew. Chem.* 121, 7781–7784. doi: 10.1002/ange.200901551

Pawar, R. R., Gosai, K. A., Bhatt, A. S., Kumaresan, S., Lee, S. M., and Bajaj, H. C. (2015). Clay catalysedrapid valorization of glycerol towards cyclic acetals and ketals. *RSC Adv.* 5, 83985–83996. doi: 10.1039/C5RA15817F

Pawar, R. R., Jadhav, S. V., and Bajaj, H. C. (2014). Microwave-assisted rapid valorization of glycerol towards acetals and ketals. *Chem. Eng. J.* 235, 61–66. doi: 10.1016/j.cej.2013.09.018

Perreia, C. S. M., and Rodrigues, A. E. (2013). Process intensification: new technologies (SMBRandPermSMBR) for the synthesis of acetals. *Catal. Today.* 218–219, 148–152. doi: 10.1016/j.cattod.2013.04.014

Pierpont, A. W., Batista, E. R., Martin, R. L., Chen, W., Kim, J. K., and Hoyt, C. B. (2015). Origins ofthe region-selectivity in the lutetium triflate catalyzed ketalization of acetonewith glycerol: a DFT study. *ACS Catal.* 5, 1013–1019. doi: 10.1021/cs5010932

Posada, J. A., Orrego, C. E., and Cardona, C. A. (2009). Biodiesel production: biotechnological approach. *Int. Rev. Chem. Eng.* 1, 571–580.

Priya, S. S., Selvakannan, P. R., Chary, K. V. R., Kantam, M. L., and Bhargava, S. K. (2017). Solvent-free microwave-assisted synthesis of solketal from glycerol using transition metal ions promoted mordenite solid acid catalysts. *Mol. Catal.* 434, 184–193. doi: 10.1016/j.mcat.2017.03.001

Qing, W., Chen, J., Shi, X., Wu, J., Hu, J., and Zhang, W. (2017). Conversion enhancement for acetalization using a catalytically active membrane in a per-evaporation membrane reactor. *Chem. Eng. J.* 313, 1396–1405. doi: 10.1016/j.cej.2016.11.053

Rafiei, S., Tangestaninejad, S., Horcajada, P., Moghadam, M., Mirkhani, V., Mohammadpoor-Baltork, I., et al. (2018). Efficient biodiesel production using a lipase@ZIF-67 nanobioreactor. *Chem. Eng. J.* 334, 1233–1241. doi: 10.1016/j.cej.2017.10.094

Rahmat, N., Abdullah, A. Z., and Mohamed, A. R. (2010). Recent progress on innovative and potential technologies for glycerol transformation into fuel additives: a critical review. *Renew. Sus. Energ. Rev.* 14, 987–1000. doi: 10.1016/j.rser.2009.11.010

Rakopoulos, C. D., Rakopoulos, D. C., Hountalas, D. T., Giakoumis, E. G., and Andritsakis, E. C. (2008). Performance and emissions of bus engine using blends of diesel fuel with biodiesel of sunflower or cottonseed oils derived from Greek feedstock. *Fuel* 87, 147–157. doi: 10.1016/j.fuel.2007.04.011

Reddy, P. S., Sudarsanam, P., Mallesham, B., Raju, G., and Reddy, B. M. (2011). Acetalisation of glycerol with acetone over zirconia and promoted zirconia catalysts under mild reaction conditions. *Ind. Eng. Chem.* 17, 377–381. doi: 10.1016/j.jiec.2011.05.008

Ribeiro, N. M., Pinto, A. C., and Quintella, C. M. (2007). The role of additives for diesel and diesel blended (ethanol or biodiesel) fuels: a review. *Energ. Fuel* 21, 2433–2445. doi: 10.1021/ef070060r

Roldan, L., Mallada, R., Fraile, J. M., Mayora, J. A., and Menendez, M. (2009). Glycerol upgrading byketalization in a zeolite membrane reactor. *Asia. Pac. J. Chem. Eng.* 4, 279–284. doi: 10.1002/apj.243

Romanow (1999). Perception becomes reality. *Hydrocarbon Process* 78:13.

Rosas, I. P., Conteras, J. L., Salmones, J., Tapia, C., Zeifert, B., Navarrete, J., et al. (2017). Catalytic dehydration of glycerol to acrolein over a catalyst of Pd/LaY zeolite and comparison with the chemical equilibrium. *Catalysts* 7:73. doi: 10.3390/catal7030073

Ruiz, V. E., Velty, A., Santos, L. L., Perez, L. A., Sabater, M. J., and Iborra, S. (2010). Gold Catalysts and solid catalysts for biomass transformations: valorization of glycerol and glycerol – water mixtures through formation of cyclic acetals. *J. Catal.* 271, 351–357. doi: 10.1016/j.jcat.2010.02.023

Samoilov, V. O., Ramazanov, D. N., Nekhaev, A. I., Maximov, A. L., and Bagdasarov, L. N. (2016). Heterogeneous catalytic conversion of glycerol to oxygenated fuel additives. *Fuel* 172, 310–319. doi: 10.1016/j.fuel.2016.01.024

Sandesh, S., Halgeri, A. B., Ganapati, V., and Shanbhag, G. V. (2015). Utilization of renewableresources: condensation of glycerol with acetone at room temperature catalyzedby organic–inorganic hybrid catalyst. *J. Mol. Catal. A Chem.* 401, 73–80. doi: 10.1016/j.molcata.2015.02.015

Sato, S., Araujo, A. S., and Miyano, M. (2008). *Process for the Production of Glycerol Acetals*. US Patent 0207927.

Serafim, H., Fonseca, I. M., Ramos, A. M., Vital, J., and Castanheiro, J. E. (2011). Valorization ofglycerol into fuel additives over zeolites as catalysts. *Chem. Eng. J.* 178, 291–296. doi: 10.1016/j.cej.2011.10.004

Serre, C., Millange, F., Thouvenot, C., Nogues, M., Marsolier, G., Louerand, D., et al. (2002). Very large breathing effect in the first nanoporous chromium(III)-based solids: MIL-53 or Cr^{III}(OH)·{O$_2$C−C$_6$H$_4$−CO$_2$}·{HO$_2$C−C$_6$H$_4$−CO$_2$H}$_x$·H$_2$O$_y$. *J. Am. Chem. Soc.* 124, 13519–13526. doi: 10.1021/ja0276974

Sharma, Y. C., Singh, B., Korstad, B., and Roberts, O. (2011). Advancements in solid acid catalysts for ecofriendly and economically viable synthesis of biodiesel. *Biofuels Bioprod. Biorefin.* 5, 69–92. doi: 10.1002/bbb.253

Shirani, M., Ghaziaskar, H. S., and Xu, C. C. (2014). Optimization of glycerol ketalizationtoproducesolketal as biodiesel additive in a continuous reactor with supercriticalacetone using Purolite PD 206 as catalyst. *Fuel. Proc. Technol.* 124, 206–211. doi: 10.1016/j.fuproc.2014.03.007

Sonar, S. K., Shinde, A. S., Asok, A., Niphadkar, P. S., Mayadevi, S., Joshi, P. N., et al. (2018). Solvent free acetalization of glycerol with formaldehyde over

hierarchical zeolite of BEA topology. *Environ. Prog. Sust. Energ.* 37, 797–807. doi: 10.1002/ep.12742

Souza, T. E., Padula, I. D., Teodoro, M. M. G., Chagas, P., Resende, J. M., Souza, P. P., et al. (2015). Amphiphilic property of niobium oxyhydroxide for waste glycerolconversion to produce solketal. *Catal. Today* 254, 83–89. doi: 10.1016/j.cattod.2014.12.027

Souza, T. E., Portilho, M. F., Souza, P. M. T. J., Souza, P. P., and Oliveira, L. C. A. (2014). Modified niobiumoxyhydroxide catalyst: an acetalization reaction to produce bio-additives forustainable use of waste glycerol. *Chem. Cat. Chem.* 6, 2961–2969. doi: 10.1002/cctc.201402322

SSI Review (2014). *Biofuels Market*. SSI Review.

Sudarsanam, P., Mallesham, B., Prasad, A. N., Reddy, P. S., and Reddy, B. M. (2013). Synthesis ofbio–additive fuels from acetalization of glycerol with benzaldehyde overmolybdenum promoted green solid acid catalysts. *Fuel Proc. Technol.* 106, 539–545. doi: 10.1016/j.fuproc.2012.09.025

Sun, S., He, M., Dai, Y., Li, X., Liu, Z., and Yao, L. (2017). Catalytic acetalization: an efficient strategy forhigh-value utilization of biodiesel-derived glycerol. *Catalysts* 7:184. doi: 10.3390/catal7060184

Suriyapradilok, N., and Kitiyanan, B. (2011). Synthesis of Solketal from glycerol and its reaction with benzyl alcohol. *Energ. Proced.* 9, 63–69. doi: 10.1016/j.egypro.2011.09.008

Talebian-Kiakalaieh, A., Amin, N. A. S., and Hezaveh, H. (2014). Glycerol for renewable acrolein production by catalytic dehydration. *Renew. Sustain. Energy Rev.* 40, 28–59. doi: 10.1016/j.rser.2014.07.168

Talebian-Kiakalaieh, A., Amin, N. A. S., Rajaei, K., and Tarighi, S. (2018). Oxidation of bio-renewable glycerol to value-added chemicals through catalytic and electro-chemical processes. *Appl. Energy* 230, 1347–1379. doi: 10.1016/j.apenergy.2018.09.006

Tangestanifard, M., and Ghaziaskar, H. S. (2017). Arenesulfonic acid-functionalized bentonite ascatalyst in glycerol esterification with acetic acid. *Catalysts* 7:211. doi: 10.3390/catal7070211

Taufiqurrahmi, N., Mohamed, A. R., and Bhatia, S. J. (2011). Nanocrystalline zeolite beta and zeolite Y as catalysts in used palm oil cracking for the production of biofuel. *Nanopart. Res.* 13, 3177–3189. doi: 10.1007/s11051-010-0216-8

Timofeeva, M. N., Panchenko, V. N., Khan, N. A., Hasan, Z., Provirin, I. P., Tsybulya, S. V., et al. (2017). Isostructural metal-carboxylates MIL-100(M) and MIL-53(M) (M: V, Al, Fe and Cr) as catalysts for condensation of glycerol with acetone. *Appl. Catal. A Gen.* 529, 167–174. doi: 10.1016/j.apcata.2016.11.006

Tosheva, L., Valtchev, V., and Sterte, J. (2000). Silicalite-1 containing microspheres prepared using shape-directing macro-templates. *Microporous Mesoporous Mater.* 35, 621–629. doi: 10.1016/S.1387-1811(99)00256-5

Trifoi, A. R., Agachi, P. S., and Pap, T. (2016). Glycerol acetals and ketals as possible diesel additives. A review of their synthesis protocols. *Ren. Sus. Energ. Rev.* 62, 804–814. doi: 10.1016/j.rser.2016.05.013

U.S. EPA (1996) *Oxyfuels Information Needs*. EPA/600/R-96/069 (NTIS PB 96–190665). Washington, DC: U.S. Environmental Protection Agency.

Umbarkar, S. B., Kotbagi, T. V., Biradar, A. V., Pasricha, R., Chanale, J., and Dongare, M. K. (2009). Acetalization of glycerol using mesoporous MoO$_3$/SiO$_2$ solid acid catalyst. *J. Mol. Catal. A Chem.* 310, 150–158. doi: 10.1016/j.molcata.2009.06.010

Vasantha, V. T., Venkatesha, N. J., Shamshuddin, S. Z. M., D'Souza, J. Q., and Reddy, B. G. V. (2018). Sulphated zirconia supported on cordierite honeycomb monolith for effective synthesis of solketal from acetalisation of glycerol with acetone. *Chem. Select.* 3, 602–608. doi: 10.1002/slct.201702186

Vicente, G., Melero, J. A., Morales, G., Paniagua, M., and Martin, E. (2010). Acetalisation of bio-glycerol with acetone to produce solketal over sulfonic mesostructured silicas. *Green Chem.* 12, 899–907. doi: 10.1039/b923681c

Vieira, L. H., Possato, L. G., Chaves, T. F., Pulcinelli, S. H., Santilli, C. V., and Martins, L. (2018). Studies on dispersion and reactivity of vanadium oxides deposited on lamellar ferrierite zeolites for condensation of glycerol into bulky products. *Mol. Catal.* 458, 161–170. doi: 10.1016/j.mcat.2017.11.027

Villa, A., Dimitratos, N., Chan-Thaw, C. E., Hammond, C., Prati, L., and Hutchings, G. (2015). Glycerol oxidation using gold-containing catalysts. *J. Acc. Chem. Res.* 48, 1403–1412. doi: 10.1021/ar500426g

Vogt, E. T. C., and Weckhuysen, B. M. (2015). Fluid catalytic cracking: recent developments on the grand old lady of zeolite catalysis. *Chem. Soc. Rev.* 44, 7342–7370. doi: 10.1039/C5CS00376H

Voleva, V. B., Belostotskaya, I. S., Malkova, V., Komissarova, N. L., Kurkovskaya, L. N., and Usachev, S. V.,(2012). New approach to the synthesis of 1,3-dioxolanes. *Russ. J. Org. Chem.* 48, 638–641. doi: 10.1134/S1070428012050028

Volkringer, C., Popov, D., Loiseau, T., Férey, G., Burghammer, M., Riekel, C., et al. (2009). Synthesis, single-crystal X-ray microdiffraction, and NMR characterizations of the giant pore metal-organic framework aluminum trimesate MIL-100. *Chem. Mater.* 21, 5695–5697. doi: 10.1021/cm901983a

Wang, S., Guin, J. A., Xinhe, B., and Yide, X. (2004). Synthesis of gasoline additives from methanol and olefins over sulfated silica. *Stud. Surf. Sci. Catal.* 147, 439–44. doi: 10.1016/S0167-2991(04)80091-0

Wegenhart, B. L., and Abu-Omar, M. M. (2010). A solvent-free method for making dioxolane and dioxane from the biorenewables glycerol and furfural catalyzed by oxorhenium(V) oxazoline. *Inorg. Chem.* 49, 4741–4743. doi: 10.1021/ic1004352

Wilson, E. K. (2002). Fuel made from vegetable oil leads the pack of alternatives to petroleum products. *Chem. Eng. News* 80, 46–49. doi: 10.1021/cen-v080n021.p046

Zhang, S., Zhao, Z., and Ao, Y. (2015). Design of highly efficient Zn-, Cu-, Ni- and Co-promotedM-AlPO₄solid acids: the acetalization of glycerol with acetone. *Appl. Catal. A Gen.* 496, 32–39. doi: 10.1016/j.apcata.2015.02.006

Zhou, J. A., Hua, Z. L., Zhao, J. J., Gao, Z., Zeng, S. Z., and Shi, J. L. (2010). A micro/mesoporous aluminosilicate: key factors affecting framework crystallization during steam-assisted synthesis and its catalytic property. *J. Mater. Chem.* 20, 6764–6771. doi: 10.1039/C0JM00513D

Conflict of Interest Statement: The authors declare that the research was conducted in the absence of any commercial or financial relationships that could be construed as a potential conflict of interest.

Experimental Determination of Optimal Conditions for Reactive Coupling of Biodiesel Production With *in situ* Glycerol Carbonate Formation in a Triglyceride Transesterification Process

Luma Sh. Al-Saadi, Valentine C. Eze* and Adam P. Harvey

School of Engineering, Newcastle University, Newcastle upon Tyne, United Kingdom

This study investigated a reactive coupling to determine the optimal conditions for transesterification of rapeseed oil (RSO) to fatty acid methyl ester (FAME) and glycerol carbonate (GLC) in a one-step process, and at operating conditions which are compatible with current biodiesel industry. The reactive coupling process was studied by transesterification of RSO with various molar ratios of both methanol and dimethyl carbonate (DMC), using triazabicyclodecene (TBD) guanidine catalyst and reaction temperatures of 50–80°C. The optimal reaction conditions obtained, using a Design of Experiments approach, were a 2:1 methanol-to-RSO molar ratio and 3:1 DMC-to-RSO molar ratio at 60°C. The FAME and GLC conversions at the optimal conditions were 98.0 ± 1.5 and $90.1 \pm 2.2\%$, respectively, after 1 h reaction time using the TBD guanidine catalyst. Increase in the DMC-to-RSO molar ratio from 3:1 to 6:1 slightly improved the GLC conversion to $94.1 \pm 2.8\%$ after 2 h, but this did not enhance the FAME conversion. Methanol substantially improved both FAME and GLC conversions at 1:1–2:1 methanol-to-RSO molar ratios and enhanced the GLC separation from the reaction mixture. It was observed that higher methanol molar ratios (>3:1) enhanced only FAME yields and resulted in lower GLC conversions due to reaction equilibrium limitations. At a 6:1 methanol-to-RSO molar ratio, 98.4% FAME and 73.3% GLC yields were obtained at 3:1 DMC-to-RSO molar ratio and 60°C. This study demonstrates that formation of low value crude glycerol can be reduced by over 90% compared to conventional biodiesel production, with significant conversion to GLC, a far more valuable product.

Keywords: reactive coupling, FAME, glycerol carbonate, biodiesel, design of experiment

INTRODUCTION

Fatty acid alkyl esters are usually produced by a transesterification of triglyceride-containing feedstocks (vegetable oils, animal fat etc.) with short chain alcohols. The most commonly used alcohol is methanol due to its low price and availability (Zabeti et al., 2009), and such triglyceride transesterification process produces fatty acid methyl esters (FAMEs) as the main product and

glycerol as a by-product. Mixtures of fatty acid alkyl esters (≥96.5% according EN14214) produced during transesterification are used as biodiesel, a renewable alternative to petro-diesel, and this accounts for about 82% of the biofuels production in the EU (Demirbas and Balat, 2006). Conventional biodiesel production uses homogeneous base-catalyzed transesterification process in the presence of alkali metal hydroxides and methoxides (NaOH, KOH, NaOCH$_3$, KOCH$_3$), especially sodium methoxide which accounts for than 60% of the commercial biodiesel plants (Huber et al., 2006). Base catalysts are the most commonly used methods of catalysis in processing of vegetable oil feedstock containing low levels of free fatty acids (FFAs), due to the faster reaction rates of the base-catalyzed transesterification, typically about 4,000 times faster than acid catalysts at moderate temperatures (Cervero et al., 2008). However, for biodiesel productions from low-grade vegetable oil feedstock containing high levels of FFAs (≥0.5 wt%) and water content above 0.3 wt%, acid catalysts are required to avoid soap formations. Such low-grade feedstock would require a one-stage acid-catalyzed transesterification or a two-stage process involving an acid-catalyzed initial FFA pre-treatment step followed by a base-catalyzed triglyceride transesterification (Canakci and Van Gerpen, 2003; Moser, 2009). Some studies have also shown that organic bases such as guanidine, especially the triazabicyclodecene (TBD) guanidine, are active for catalysis of triglyceride transesterification (Schuchardt et al., 1995; Bromberg et al., 2010). A major advantage of the TBD guanidine over alkali metal hydroxides and methoxides is that it does not cause triglyceride and FAME saponification side reactions (Schuchardt et al., 1995), whereas such side reactions have been reported for homogeneous alkali metal catalysts (Phan et al., 2012; Eze et al., 2014, 2018). The TBD guanidine can also be grafted onto supports such as silica and used as a stable heterogeneous catalyst (Derrien et al., 1998; Sercheli and Vargas, 1999; Meloni et al., 2011; Nguyen et al., 2013).

In conventional triglyceride transesterification, crude glycerol constitutes about 10–20% (v/v) of the product stream (Ayoub and Abdullah, 2012; Quispe et al., 2013). This crude glycerol by-product needs to be either purified for further use or discarded as a waste which leads to environmental problems. The co-production of crude glycerol in the conventional biodiesel processes has little economic advantage for biodiesel plants, as the huge rise in global glycerol production has caused its oversupply, significantly reducing the glycerol price (Rodrigues et al., 2012). It has been predicted that the worldwide glycerol surplus will rise to over 6 million tons in 2025 (Ciriminna et al., 2014). Therefore, it is important to find a way to upgrade the glycerol into valuable chemicals such as 1,3-propanediol (Mu et al., 2006), citric acid (Papanikolaou et al., 2002), polyhydroxyalkanoates (PHA) (Ashby et al., 2004), solketal (Mota et al., 2010; Eze and Harvey, 2018), and glycerol carbonate (GLC) (Esteban et al., 2015; Ishak et al., 2016). It has been reported that one of the most promising processes for valorisation of glycerol is through conversion to GLC, a valuable chemical in industrial productions of polymers and a non-toxic electrolyte for batteries (Ishak et al., 2016). GLC is also classed as a "green" solvent and significantly

more valuable than glycerol. It is usually produced by reacting glycerol with DMC using a base catalyst (Teng et al., 2016). Bulk productions of GLC is envisaged in from a glycerol output of substantially large biodiesel plants, hence, *in situ* conversions of the glycerol by-product to GLC inside the transesterification reactor would be of potential advantage. This would minimize process costs for additional steps required for crude glycerol purification and subsequent valorisation.

Consequently, there has been significant recent research interest in replacement of methanol with dimethyl carbonate (DMC) in biodiesel production reactions to minimize crude glycerol production (Zhang et al., 2010; Seong et al., 2011; Rathore et al., 2014; Fan et al., 2017; Lee et al., 2017). The reactions of triglyceride with DMC to produce FAME and GLC instead of glycerol are shown in **Figure 1**. Dimethyl carbonate is a versatile, eco-friendly, non-corrosive, and non-toxic chemical (Dhawan and Yadav, 2017), which is usually produced via oxidative carbonylation of methanol (Zhou et al., 2015). A maximum FAME yield of 96.2% was reported (Zhang et al., 2010) for transesterification at 9:1 DMC to palm oil molar ratio, 8.5 wt% KOH catalyst, 8 h reaction time, and 75°C temperature.

It has also been shown that ≥96% FAME yield was achieved after 45 min for transesterification of jatropha and pongamia oils with DMC or diethyl carbonates under supercritical conditions of 325°C and 150 bar at 40:1 molar ratio of DMC or diethyl carbonate to oil (Rathore et al., 2014). Enzymatic catalysis has been shown to be suitable for triglyceride transesterification with DMC (Seong et al., 2011; Lee et al., 2017). This method was used to achieve optimal yields of 96.3% FAME and 99.7% GLC after 48 h, for reactions at 9.27:1 DMC to soybean oil molar ratio, 52.56°C reaction temperature, and 116.76 g L^{-1} of enzyme concentration in the reaction mixture (Lee et al., 2017). Another study also used enzyme catalysis to achieve maximum conversions of 84.9% biodiesel and 92.0% GLC after 48 h, for transesterification at 6:1 DMC to soybean oil molar ratio, 60°C reaction temperature, and 100 g L^{-1} Novozym 435 enzyme concentration, with tert-butanol as a solvent (Seong et al., 2011). A glycerol-free biodiesel production has been reported elsewhere, where maximum FAME yield of 95.7% was obtained after 5 h for reactions at 5:1 DMC to rapeseed oil (RSO) molar ratio and 110°C temperature, using 25 wt% of sulfonated imidazolium ionic liquid as catalyst (Fan et al., 2017). A triglyceride transesterification using a combination of both methanol and DMC have been reported (Dhawan and Yadav, 2017), where 97.3% conversion of soybean oil and 93.2% selectivity of GLC after 3 h were obtained, for reactions at 90:30:1 of methanol-DMC-soybean oil molar ratio, 150°C temperature, and 12.5 g L^{-1} of hydrotalcite catalyst loading.

The existing biodiesel production methodologies using DMC have inherent severe operational disadvantages arising from the high reaction temperatures (Rathore et al., 2014; Dhawan and Yadav, 2017; Fan et al., 2017), long reaction times (Zhang et al., 2010; Seong et al., 2011; Fan et al., 2017; Lee et al., 2017), and requirements of excessively large molar ratios of DMC and DMC/methanol (Rathore et al., 2014; Dhawan and Yadav, 2017). These technical setbacks must be overcome before triglyceride transesterification with DMC could be considered of process

FIGURE 1 | Reaction of triglyceride and DMC.
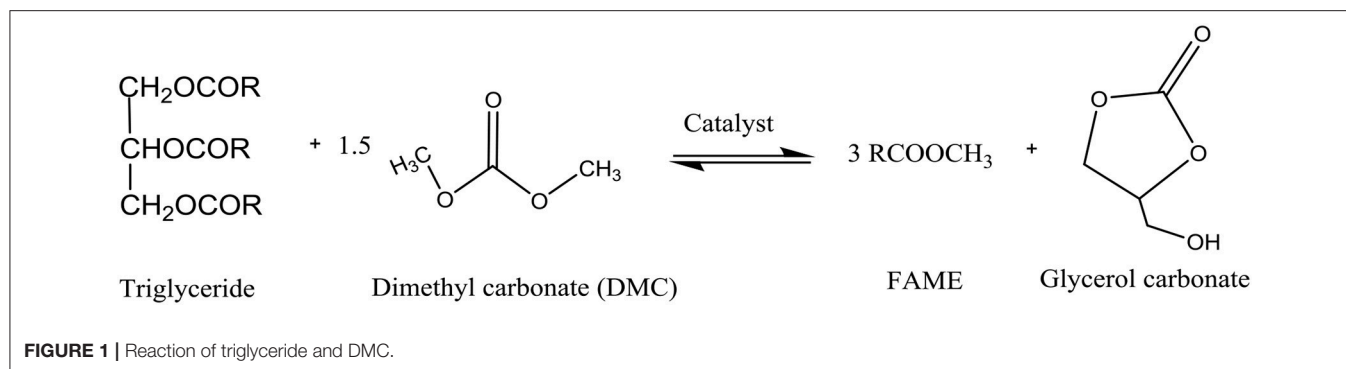
economic advantage compared to the present conventional biodiesel technology. The use of large excesses of DMC and DMC/methanol in the existing studies is uneconomical, and this would particularly be counter-productive to the desire to achieve process advantage by producing biodiesel and valorising the crude glycerol *in situ* to form GLC.

A process simulation and economic analysis of biodiesel production have shown that the amount of energy required for excess methanol recovery was about 23% of the total energy consumption in a conventional biodiesel production reaction using 6:1 methanol to oil molar ratio (Lee et al., 2011). The energy requirement proportionally increases to about 37% and 46% of the total energy consumption of the conventional biodiesel process for 9:1 and 12:1 methanol to oil molar ratios, respectively. Therefore, the existing methods for biodiesel and GLC co-productions are very expensive due to use of energy-intensive operational conditions, and in some cases, partly due to costly enzymatic catalysts. This makes it difficult to commercialize such strategies as they may not compare favorably with the conventional biodiesel process.

The aim of this work was to develop a novel biodiesel process by the application of *in situ* reactive coupling to produce FAME and GLC. It is envisaged that this process would run on less than stoichiometric methanol requirement of 3:1, where small amounts of methanol could be applied to initialize the triglyceride transesterification step. The presence of DMC would convert the reactively-formed crude glycerol into GLC, a highly valuable product, and the reactions of the DMC with glycerol would generate methanol to sustain the triglyceride transesterification. Base-catalyzed triglyceride transesterification is essentially rapid at 60°C, atmospheric pressure, and methanol to oil molar ratio of 3:1, however, the equilibrium FAME conversion is limited to <80% (Eze et al., 2014). Therefore, reactive coupling of the triglyceride transesterification with DMC would accelerate the reactions at moderate process conditions, whereas equilibrium limitation in the FAME conversions would be substantially eliminated by transformations of the reactively-formed glycerol to form GLC. This strategy would potentially allow for use of less methanol and DMC, and operations at moderate reaction conditions. Reactive coupling of the triglyceride transesterification to FAME with *in situ* valorisation of the crude glycerol to GLC at ∼60°C, atmospheric pressure, and DMC/methanol to oil molar ratios <6:1 required in the biodiesel

conventional process is paramount to economic viability and acceptability in the biodiesel industry. TBD guanidine catalyst was selected for the experimental investigation to avoid soap formations due to the low methanol molar ratio envisaged. The TBD guanidine catalyst does not cause triglyceride and FAME saponification side reactions (Schuchardt et al., 1995).

EXPERIMENTAL METHODS

Materials
Anhydrous methanol (99.8% purity), DMC (99% purity), triazabicyclodecene guanidine (99% purity), acetic acid (99% purity), 2-propanol (99.5% purity), methyl heptadecanoate (99.0% purity), and GLC (90% purity) were purchased from Sigma-Aldrich, whilst the RSO used was supplied from Henry Colbeck Ltd, UK. The RSO used in the experiments contained ≥99 wt% triglycerides, 0.06 wt% FFA (oleic acid) and 0.01 wt% water.

Experimental Procedure
The experiments were carried out using a 250 mL sealed batch reactor equipped with a temperature-controlled hot plate magnetic stirrer (IKA® RCT basic IKAMAG™ safety control). The required amount of RSO, methanol and DMC (20 mL total volume) was heated in the batch reactor to the reaction temperature (50–80°C), followed by the addition of 5 wt.% TBD-guanidine based on the RSO. The reaction mixture was mixed vigorously using the magnetic stirrer at 600 rpm to ensure that the reaction was mass transfer independent, based on existing studies on homogenous biodiesel production reactions (Noureddini and Zhu, 1997; Vicente et al., 2005; Eze et al., 2014). The ranges of process parameters studied were methanol-to-RSO molar ratios from 0:1 to 6:1, DMC-to-RSO molar ratios from 1:1 to 6:1, and reaction temperatures of 50–80°C. These range of process parameters were screened using Design of Experiments, response surface methodology. Known amounts (about 1 mL) of samples were collected from the reaction mixture at time intervals from 1 min to 2 h and quenched using calculated amounts of acetic acid. These samples were analyzed using a gas chromatograph (GC) to monitor the extents of conversions of the RSO to FAME and GLC were monitored. The use of 2 h reaction time was based on preliminary results which showed that this period is sufficient to reach the equilibrium conversions. The

product samples settled into two distinct phases in the reactions where methanol was used, with upper layers consisting mainly of biodiesel/DMC and a lower layer containing GLC, residual glycerol, methanol, and catalyst. Statistical significance for the investigated parameters were analyzed using the Minitab 17 statistical software at a significance level of 0.05, corresponding to confidence level of 95%. Therefore, the effects of the reaction parameters on the FAME and GLC yields were considered to be statistically significant at p-values < 0.05, otherwise, a null hypothesis was returned, and the studied parameters are not statistically significant ($p \geq 0.05$).

Analytical Methods

The collected samples were homogenized by adding a known weight (0.5 mL) of 2-propanol to obtain uniform mixtures for the GC quantifications of the FAME and GLC conversions. About 50–80 mg of the homogenized sample was measured into a 2 mL GC vial, followed by the addition of 1 mL of a 10 mg mL^{-1} of methyl heptadecanoate prepared in in a 2-propanol. The prepared samples were analyzed using a 6890 Hewlett Packard gas chromatograph by injection of 1 μL of sample with a 5 μL SGE GC syringe. The GC was equipped with a fused silica capillary column of 30 m length, 0.32 mm internal diameter, and film thickness of 0.25 μm. The GC oven temperature programme was: 120°C held for 5 min initially and ramped from 120°C to 260°C at a heating rate of 15 °C /min, and held for another 15 min. The injector and flame ionization detector (FID) temperatures were set at 250 °C and 260 °C, respectively. FAME content in the samples were quantified using the BS EN 14103:2003 (BSI, 2003), whereas the GLC was quantified using a calibration data which were obtained from the response factors of the solutions of GLC and the methyl heptadecanoate standard prepared in a 2-propanol. The yields of FAME and GLC were calculated using Equations (1) and (2), respectively. Fatty acid profile of the produced FAME was obtained using Equation (3) and compared with the fatty acid profile of the RSO feedstock, as shown in **Table 1**. The fatty acid profiles of the FAME and RSO were similar, indicating no modification in the fatty acid composition of the RSO by the reactively-coupled transesterification process.

$$FAME\ yield\ (\%) = \frac{FAME\ content\ of\ the\ sample}{Maximum\ theoretical\ FAME} * 100 \quad (1)$$

$$GLC\ yield\ (\%) = \frac{GLC\ content\ of\ the\ sample}{Maximum\ theoretical\ GLC} * 100 \quad (2)$$

$$Fatty\ acid\ content\ (\%) =$$
$$\frac{Peak\ area\ of\ a\ specific\ FAME}{Total\ peak\ areas\ of\ all\ FAMEs\ in\ the\ sample} * 100 \quad (3)$$

RESULTS AND DISCUSSION

Trend in the Process Parameters

The effects of the process parameters on the formations of FAME and GLC at the reaction conditions of methanol-to-oil molar ratios from 0:1 to 2:1, DMC-to-oil molar ratios from 1:1 to 3:1,

TABLE 1 | Fatty acid profile of the RSO feedstock and the FAME obtained from reactively coupled biodiesel and GLC productions.

Type of fatty acids	Molecular formula of the fatty acids (C_nH_{2n+1} COOH)	Fatty acids profile (wt. %) for the RSO[a]	FAME fatty acids profile (wt. %) for biodiesel-GLC
Palmitic (C16:0)	$C_{15}H_{31}COOH$	4.71	5.12
Stearic (C18:0)	$C_{17}H_{35}COOH$	1.52	1.62
Oleic (C18:1)	$C_{17}H_{33}COOH$	61.47	60.92
Linoleic (C18:2)	$C_{17}H_{31}COOH$	19.79	19.14
Linolenic (C18:3)	$C_{17}H_{29}COOH$	9.26	9.97
Arachidic (C20:0)	$C_{19}H_{39}COOH$	0.59	0.53
Icosenoic (C20:1)	$C_{19}H_{37}COOH$	1.37	1.62
Behenic (C22:0)	$C_{21}H_{43}COOH$	0.32	0.26
Erucic (C22:1)	$C_{21}H_{41}COOH$	0.57	0.80

[a]RSO fatty acid profile from Henry Colbeck Ltd. product datasheet.

and reaction temperatures of 50–80°C are shown in **Table 2**, indicating average values of FAME and GLC yields and the standard errors from duplicate experiments. The results clearly demonstrate that the equilibrium yields in absence of methanol were 70–82% for FAME and 56–78.8% for GLC for the reactions at 50–80°C, and 1–3: 1 molar ratios of DMC to RSO. This indicates that without methanol, high (≥ 90) FAME and GLC yields cannot be achieved at moderate reaction temperatures, which is consistent with findings elsewhere (Zhang et al., 2010), where $<40\%$ FAME yield was reported at 3:1 DMC to palm oil molar ratios, 75°C temperature, and 8.5% KOH catalyst. The reported lower FAME yield of $<40\%$ could be due to triglyceride and FAME saponification side reactions which usually occurs at large alkali metal hydroxide (8.5 wt% KOH) concentrations (Phan et al., 2012; Eze et al., 2014, 2018). The use of TBD guanidine in this study prevented such deleterious side reactions.

Additions of 1–2:1 methanol to RSO molar ratios substantially enhanced the FAME and GLC yields, as these increased to 84–98% for FAME and 68.9–91% for the GLC for reactions at 2–3:1 DMC-to-RSO molar ratios and 50–80°C temperatures. The data in **Table 2** were analyzed using a response surface model in Minitab statistical software to obtain empirical models shown in Equation (4) for the FAME yields and Equation (5) for the GLC, where X_1 is methanol/ RSO molar ratio, X_2 is DMC/RSO molar ratio, and X_3 is reaction temperature (°C).

$$
\begin{aligned}
FAME\ yield(\%) = {} & 80.3 + 30.4X_1 + 16.2X_2 - 0.77X_3 - 3.98X_1^2 \\
& - 1.66X_2^2 + 0.0077X_3^2 - 0.36X_1X_2 - 0.183X_1X_3 \\
& - 0.095X_2X_3 \quad (4)
\end{aligned}
$$

$$
\begin{aligned}
GLC\ yield(\%) = {} & 14.7 - 0.7X_1 + 19.0X_2 + 0.39X_3 + 4.04X_1^2 \\
& - 0.41X_2^2 + 0.0040X_3^2 + 1.97X_1X_2 - 0.096X_1X_3 \\
& - 0.183X_2X_3 \quad (5)
\end{aligned}
$$

The experimental and the model data for the FAME and GLC yields indicated a high level of agreement between the experimental and predicted data. The p-values for the effects of methanol, DMC and temperature on FAME yield were

TABLE 2 | FAME and GLC yields from duplicate experiments at various reaction conditions for the design of experiment.

Methanol/RSO molar ratio	DMC/RSO molar ratio	Temperatures (°C)	Average FAME yields (%)	Average GLC yields (%)
1	2	65	90.0 ± 4.1	70.0 ± 4.0
0	3	65	79.8 ± 3.1	77.6 ± 3.7
1	2	65	90.1 ± 3.8	68.9 ± 1.6
1	3	80	84.0 ± 1.7	79.0 ± 4.2
1	1	50	93.3 ± 1.8	57.6 ± 3.3
2	2	80	97.0 ± 1.6	91.0 ± 4.2
1	3	50	98.0 ± 1.8	76.7 ± 3.8
2	1	65	89.6 ± 4.8	66.8 ± 5.4
2	2	50	98.0 ± 1.5	75.0 ± 5.5
0	2	80	82.0 ± 1.9	78.8 ± 6.8
0	2	50	73.0 ± 3.0	56.0 ± 6.5
2	3	65	98.0 ± 2.6	86.8 ± 5.4
1	2	65	90.0 ± 5.2	72.7 ± 3.8
0	1	65	70.0 ± 1.8	65.5 ± 4.9
1	1	80	84.0 ± 4.2	70.9 ± 6.2
3[a]	3	60	97.6 ± 2.8	91.7 ± 4.6
6[a]	3	60	98.4 ± 2.0	73.3 ± 6.0
2[a]	6	60	98.1 ± 3.1	94.1 ± 2.8

[a]Experiments outside the design of experiment space.

0.03, 0.175, and 0.305. This showed that only methanol had a significant effect ($p < 0.05$) on the FAME yield (Lee et al., 2017), whereas DMC and temperature had no significant effects on the FAME yields at the reaction temperature of 50–80°C. The non-significant effect of DMC and temperature in the studied range is because near-equilibrium FAME yields were obtained at low levels of DMC (1:1 DMC to RSO molar ratio) and at 50°C, such that further increases in DMC did not have any significant effect on FAME yield. The p-values for the effects of methanol, DMC and temperature on the GLC yield were 0.033, 0.008, and 0.012, respectively ($p < 0.05$ for all parameters), indicating that all the reaction parameters investigated had significant effects on the GLC yields (Lee et al., 2017).

Process Parameters Interactions and Optimal Fame Yields in a Reactive Coupling

Interaction plots for the process parameters in the empirical model for the FAME yield are shown in **Figure 2**. It can be seen in the interaction plot between DMC and methanol (**Figure 2A**) that increase in the methanol to RSO molar ratio resulted in higher FAME yields. For instance, ≥95% FAME yields were obtained after 2 h reaction time at only 2:1 methanol to RSO molar ratio and 2–3:1 DMC to RSO molar ratio, and 65°C temperature. These FAME yields which were achieved at substantially lower DMC to oil and less than stoichiometric requirement of methanol, compares well with the values of 92–97% reported using extreme reaction conditions, such as high reaction temperatures between 110 and 325°C (Rathore et al., 2014; Dhawan and Yadav, 2017; Fan et al., 2017), long reaction times in the range of 5–48 h (Zhang et al., 2010; Seong et al.,

2011; Fan et al., 2017; Lee et al., 2017), large molar ratios (40:1) of DMC to oil (Rathore et al., 2014), and excessively large methanol/DMC/oil (90:30:1) molar ratios (Dhawan and Yadav, 2017). Higher DMC to RSO molar ratio also enhanced the FAME yields, as this increased from 75% at 1:1 DMC to RSO molar ratio to 81% at 3:1 DMC to RSO molar ratio, for reactions at 65°C in the absence of methanol. However, the FAME yields increased from 81 to 90% on addition of only 1:1 methanol to RSO molar ratio at the 3:1 DMC to RSO molar ratio and 65°C (**Figure 2A**).

Clearly, FAME yields ≥95% were obtained at various reaction conditions in the presence of methanol at moderate reaction conditions. It has been reported that 96.2% of FAME yield was obtained after 8 h for transesterification at 6:1 DMC to palm oil molar ratio at refluxing temperatures of 75°C, and using 8.5 wt% KOH catalyst (Zhang et al., 2010), whereas 95.8% FAME yield was achieved after 5 h for transesterification at 5:1 DMC to RSO molar ratio, 110 °C, and 2 wt% of sulfonated imidazolium ionic liquid as a catalyst (Fan et al., 2017). Similar, FAME yields were obtained in this study even at shorter reaction time (1–2 h), DMC to RSO molar ratios of 1–3:1, 1–2:1 methanol to RSO molar ratios and temperature ≤ 80°C. Our findings strongly demonstrate that an optimized reactively coupled triglyceride transesterification and glycerol transformation to GLC is a more efficient strategy for glycerol-free biodiesel process. The reactive coupling strategy is an efficient synergistic process which uses methanol generated from the reaction of DMC with the reactively-formed glycerol to sustain the triglyceride transesterification. As shown in **Figures 2B,C**, temperature has a very weak effect on the FAME yield within the parameter space investigated. Therefore, it is preferable to operate below 65°C, the ambient pressure boiling point of methanol, as this removes the need for operating at pressure.
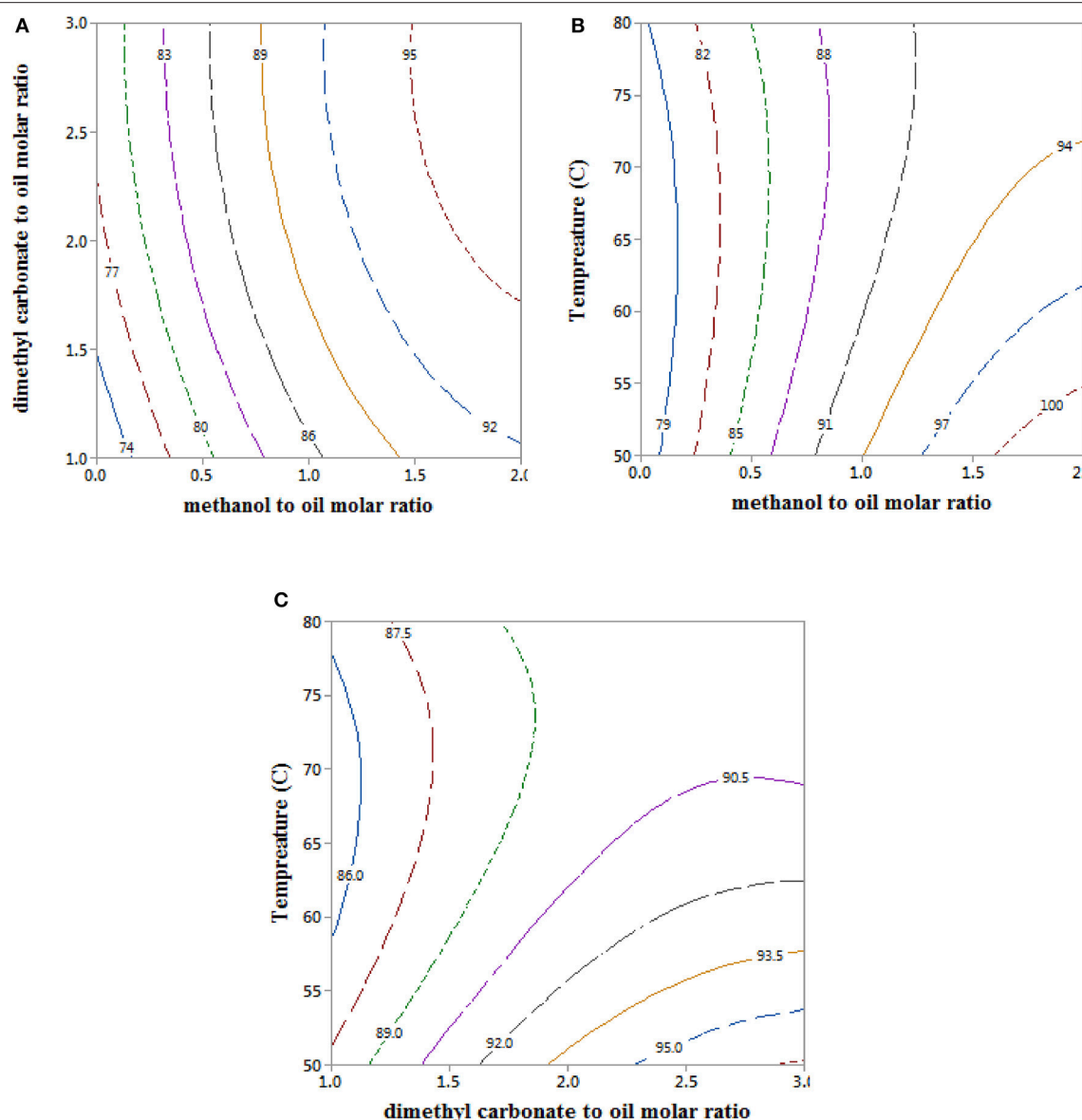
FIGURE 2 | Contour plots for the effect of DMC, methanol, and temperature on the FAME yields for reactive coupling of RSO transesterification with *in situ* crude glycerol valorisation to GLC. **(A)** Interaction between DMC and MeOH to RSO molar ratio at 65°C, **(B)** interaction between temperature and methanol to RSO molar ratio at 2DMC and **(C)** interaction between temperature and DMC at 1 MeOH.

Interactions of Process Parameters and Optimal GLC Yields in a Reactive Coupling

Figure 3 shows the interaction effect of operating variables on the GLC yields, indicating that increasing DMC molar ratios (**Figure 3A**) and reaction temperature (**Figure 3C**) had positive effects on the GLC yields of GLC. This observation suggests that the GLC formation is more endothermic than the formations of FAME. The observed trends in the GLC yields with the increase DMC and temperature are consistent with existing studies on the effects, of DMC (Zhang et al., 2010; Okoye et al., 2016; Fan et al., 2017) and reaction temperature (Lanjekar and Rathod, 2013; Ishak et al., 2016; Okoye et al., 2016), on GLC formations.

It has also been reported that the equilibrium rate constants for GLC formations in the reactions of glycerol with DMC increased from 2.903 at 40°C to 3.81 at 50°C, 4.92 at 60°C, and 6.20 at 70°C (Li and Wang, 2011), indicating a strong interaction between equilibrium GLC yields with the reaction temperatures.

It can be seen from the contour plot in **Figure 3B** that increasing the methanol to RSO molar ratio led to increased GLC yields, as the presence of methanol in the reaction mixture increased the initial rate of formation of FAME and glycerol by transesterification. This led to higher glycerol concentration in the reaction mixture, and consequently increased rates of
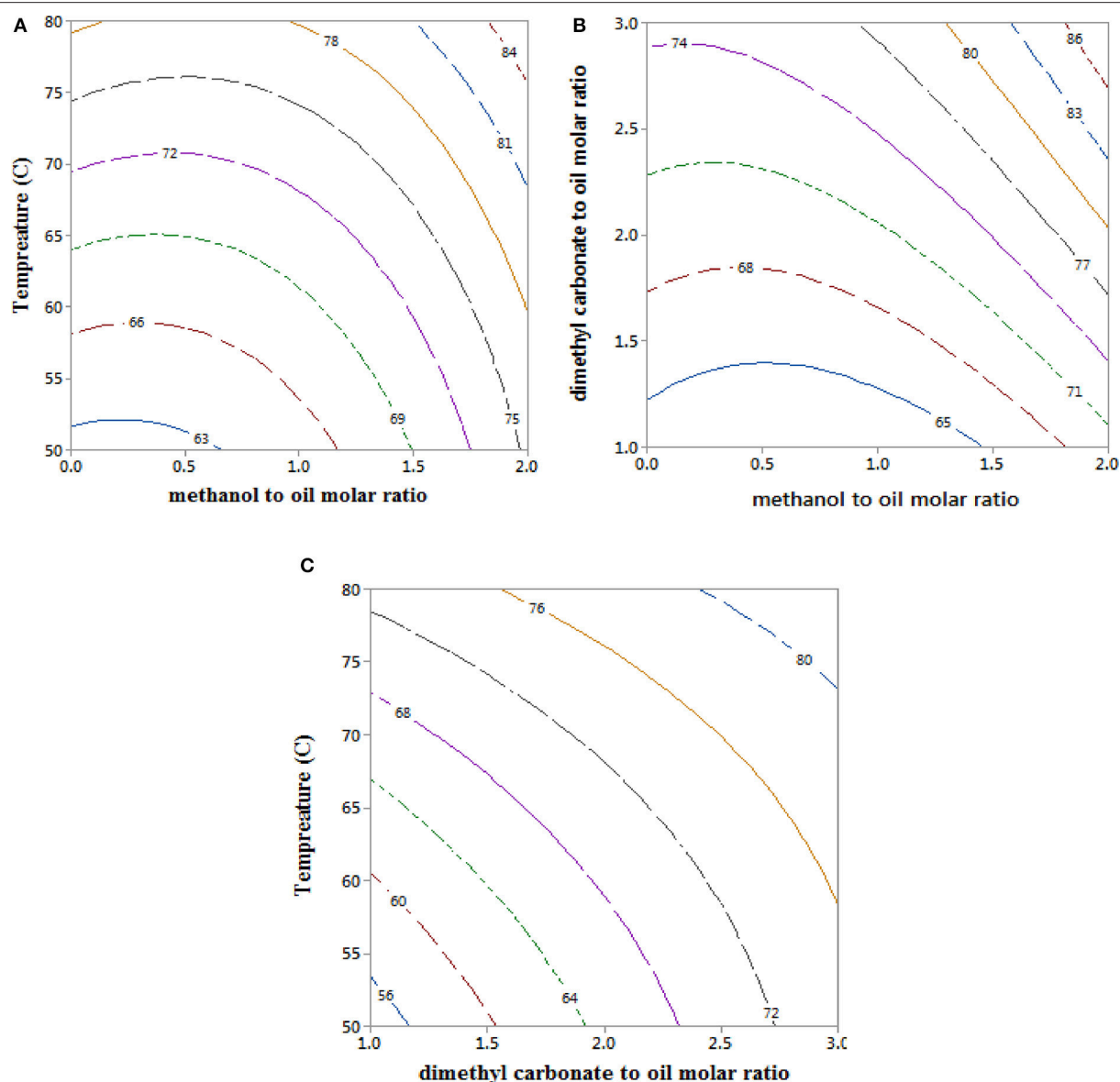
FIGURE 3 | Contour plots for the effect of DMC, methanol, and temperature on the GLC yields for reactive coupling of RSO transesterification with *in situ* crude glycerol valorisation to GLC. **(A)** Interaction between temperature and MeOH at 2 DMC, **(B)** interaction between DMC and MeOH to RSO molar ratio at 65°C and **(C)** interaction between temperature and DMC at 1 MeOH.

reaction with DMC to form GLC. However, at methanol to RSO molar ratios above 3:1, there was a substantial decline in the GLC yield (**Table 2**), which was attributed to the effect of reverse reaction between GLC and methanol. For instance, the GLC yields decreased from about 90.1–91.7% at 2:1–3:1 methanol-to-RSO molar ratio to 73.3% at 6:1 methanol molar ratio, for reactive coupling at 3:1 DMC-to-RSO molar ratio and 60°C temperature using the TBD guanidine catalyst. Although methanol is required to accelerate the RSO transesterification part of the reaction, excess of methanol in the reaction system leads to lower equilibrium GLC conversion due to thermodynamic equilibrium limitations.

Additionally, it was observed that additions of methanol resulted in separation of reaction product into two distinct phases of FAME-rich and GLC-rich layers which allows for ease of separation. In absence of methanol, the GLC formed dissolved in the DMC and FAME to form one phase, which would incur greater downstream separation costs. The optimized reaction conditions by response surface method analysis of the experimental data, showed that high FAME and GLC yields could be achieved at methanol to RSO molar ratio of 2:1 and 3:1 DMC to RSO molar ratio at 60°C. The predicted optimal reaction condition was validated as shown in **Figure 4**, and the results showed that about 90% FAME and 79.9% GLC conversion can

FIGURE 4 | FAME and GLC yields for reactive coupling of RSO transesterification with 2:1 methanol to RSO molar ratio, 3:1 DMC to RSO molar ratio, 60°C reaction temperature, and 5 wt% TBD guanidine.

FIGURE 5 | Proposed reaction scheme for triglyceride transesterification with methanol and *in situ* reactive coupling of the by-product glycerol with DMC to form GLC.
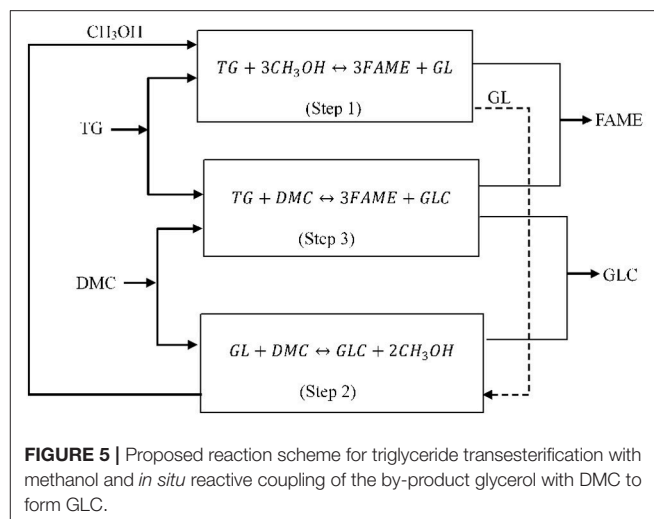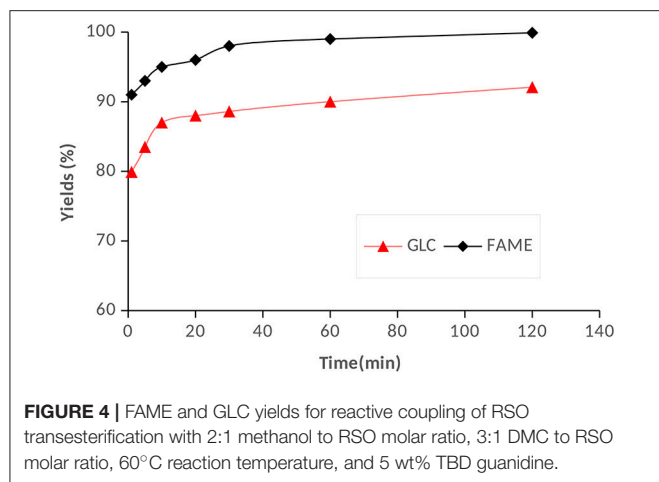
be obtained after only 1 min reaction time. The products yield increased to 98.0 ± 1.5% for FAME and 90.1 ± 2.2% for GLC after 60 min, whereas the equilibrium conversions after 2 h reaction time were about 99 and 92% for FAME and GLC, respectively. At the optimized equilibrium FAME and GLC conversions, the upper layer after separation contained mainly of FAME (~85 wt%) and unreacted DMC (~14 wt%). There was a negligible amount of GLC (≤0.5 wt.%) and no glycerol was detected in the upper layer after separation. The bottom layer contained mainly of GLC (60.8 wt%), glycerol (4.3 wt%), FAME (9.6 wt %), and about one mole equivalent of unreacted methanol (16.5 wt%)**.** Therefore, the GLC produced can be relatively easily recovered from the bottom layer through distillation and the unreacted methanol recycled into the process. The energy cost for unreacted methanol recovery in this study is substantially lower than required for 3 moles of unreacted methanol that remains for the conventional base-catalyzed biodiesel production using 6:1 methanol-to-oil molar ratio (Lee et al., 2011). Therefore, apart from the productions of highly valuable GLC, the reactive coupling process requires less methanol, and reduces the cost of unreacted methanol recovery by over 60%. The unreacted DMC in the FAME at the optimal condition was 14 wt%, which is within the range of 1–20 vol% DMC that has been reported to be suitable in reducing smoke opacity and NOx emissions substantially when blended in diesel fuels (Zhang et al., 2005; Rounce et al., 2010). Therefore, it is envisaged that the unreacted DMC would not be separated, as the combustion characteristics of the biodiesel would be improved by the presence of DMC, an oxygenate fuel additive (Zhang et al., 2005; Rounce et al., 2010; Fan et al., 2017).

Proposed Reaction Scheme in the Reactive Coupling for FAME and GLC Formations

Based on the findings from this study and understandings of the biodiesel reaction process, a reaction scheme in **Figure 5** has been proposed for the base-catalyzed triglyceride transesterification with *in situ* transformation of the reactively-formed glycerol to GLC. The reactive coupling is a particularly complex chemical process as illustrated by the reaction scheme. The reaction

is initiated by generation of methoxide ion (CH_3O^-) by the interaction of methanol and base catalyst such as the TBD guanidine, as shown in Equation (6). The methanol in the system reacts with the triglyceride (TG) to form FAME and glycerol (GL) as shown in the **Figure 5** (Step 1), through the interactions of the CH_3O^- catalytic species with the TG.

$$TBD + CH_3OH \leftrightarrow CH_3O^- + TBDH^+ \qquad (6)$$
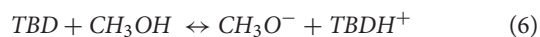
The glycerol by-product is continually removed from the transesterification reaction equilibrium, by reactive coupling with DMC to from GLC (**Figure 5**, Step 2), which generates two moles methanol for every one mole of glycerol converted to GLC. The generated methanol is deprotonated by the base catalyst to form more CH_3O^- which sustains the triglyceride transesterification side of the reactive coupling. The diglyceride (DG) and monoglyceride (MG) intermediates can also be removed from the transesterification equilibrium reaction by reacting with DMC.

The proposed reaction scheme involves formations of CH_3O^- catalytic species via deprotonation of methanol by the TBD guanidine catalyst, as shown in Equation (6). In view of the superbasicity of the TBD, with a pKa of about 25.5 in aprotic solvents (Pratt et al., 2006), deprotonation of methanol by TBD was expected. It has been reported elsewhere that TBD functions by deprotonating or activating alcohols for nucleophilic attack on the substrates during reactions (Kaljurand et al., 2005). However, no experimental data exists to show whether the mode of catalysis was via alkoxide nucleophilic attack from deprotonated alcohol. Measurements of the conductivities of TBD/methanol and TBD/DMC of different TBD molar concentrations were used in this work to investigate any change in ionic conductivity, which would be expected if there are formations of methoxide ions. The conductivities of the TBD solutions were measured using CDM210 conductivity meter (Radiometer Analytical) at 16.8°C. There was a huge rise in conductivity of methanol in the presence of TBD as shown in **Figure 6**. When TBD was dissolved in DMC, there was

FIGURE 6 | Conductivity of methanol at different TBD guanidine molar concentrations.
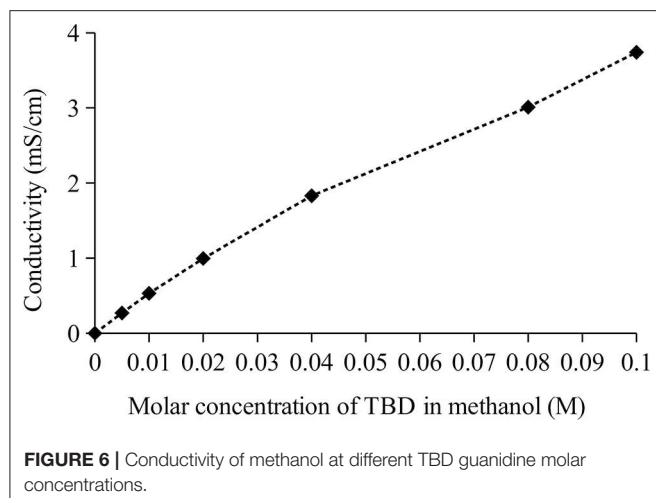
a negligible change in conductivities, with 0.00 mS/cm for DMC only (0.0M TBD) and 0.16 mS/cm for 0.1M TBD in DMC.

The high levels of conductivity of TBD/methanol solutions are consistent with formations of methoxide ions. As shown in **Figure 6**, the conductivities were 0.00 mS/cm for methanol only (0.0M TBD), rising to 3.74 mS/cm for 0.1M TBD in methanol. The change in the methanol conductivity with TBD concentration follows a general trend in conductivity for formations of ions from weak acids and bases due to equilibrium limitations (Martínez, 2018).

Generally, the triglyceride transesterification process occurs via three consecutive step-wise reversible reactions (Mittelbach and Trathnigg, 1990; Darnoko and Cheryan, 2000; Vicente et al., 2005), which are shown Equations (7)–(9). However, in the reactively-coupled transesterification process for simultaneous productions of FAME and GLC, these conventional equilibrium reactions are disrupted. The removal of DG, MG, and GL through reactive coupling with DMC greatly minimizes the reverse reactions in the TG transesterification. The reactive coupling process has enormous advantage, such that use of methanol above the stoichiometric molar ratio of 3:1 would no longer be required. This ensures very efficient methanol utilization and hugely reduces the cost of methanol recovery in the downstream process in biodiesel plants.

$$TG + CH_3OH \leftrightarrow FAME + DG \qquad (7)$$

$$DG + CH_3OH \leftrightarrow FAME + MG \qquad (8)$$

$$MG + CH_3OH \leftrightarrow FAME + GL \qquad (9)$$

As shown in the **Figure 5** (Step 3), triglyceride transesterification also occurs with only DMC. However, this reaction was found to be more energy intensive, and requires high reaction temperature to achieve high FAME and GLC conversions. Therefore, reliance on the reactions in Step 3 for co-productions of FAME and GLC would not be economical due to its energy intensive operation. This study strongly demonstrated that high FAME and GLC conversions are only possible through optimized reactive coupling of the triglyceride transesterification and *in situ* glycerol transformation to GLC. To achieve high FAME and GLC yields, the use of methanol must be optimized. It was experimentally observed that use of > 3:1 methanol to RSO molar ratios resulted in lower GLC yields, although the FAME yields were not affected. This observation was attributed to the reverse reaction of glycerol and DMC shown in **Figure 5** (Step 2), in which excess methanol could lead to shift in the equilibrium conversions toward glycerol according to the Le Chatelier's principle. Optimal values of 3:1 DMC to oil molar ratio is recommended for the reactive coupling. Although use of DMC above 3:1 DMC to RSO molar ratio did not have any adverse effects on the equilibrium FAME and GLC conversions, the reaction rates were proportionately slowed down due to dilution of the reacting mixtures by excess DMC. Therefore, this study hypothesizes that less than molar stoichiometric amount of methanol (2:1) is required to initialize the triglyceride transesterification side of the reactive coupling, while 3:1 of DMC to oil will be required for the *in situ* glycerol conversions to GLC, to achieve both high FAME and GLC yields at much more favorable and moderate process conditions.

CONCLUSIONS

This study investigated a reactive coupling reaction for optimal transesterification of RSO to FAME and GLC in a one-step process, and at operating conditions which are compatible with current biodiesel industry. The reactive coupling process was studied at various molar ratios of both methanol and DMC to the triglyceride [rapeseed oil ("RSO")], using a TBD guanidine catalyst and reaction temperatures of 50–80°C. The optimal reaction conditions identified, using a Design of Experiments approach, were a 2:1 methanol-to-RSO molar ratio and 3:1 DMC -to-RSO molar ratio at 60°C. The FAME and GLC conversions at these conditions were 98.0 ± 1.5% and 90.1 ± 2.2%, respectively, after 1 h reaction time using the TBD guanidine catalyst. Increasing the DMC-to-RSO molar ratio from 3:1 to 6:1 slightly improved the GLC conversion to 94.1 ± 2.8% after 2 h, but did not increase FAME conversion. Methanol substantially improved both FAME and GLC conversions at 1:1–2:1 methanol-to-RSO molar ratios and enhanced the GLC separation from the reaction mixture. It was observed that higher methanol molar ratios (>3:1) enhanced only FAME conversions, with the excess methanol resulting in lower GLC conversions, achieving 73.3% GLC yield for a 6:1 methanol-to-RSO molar ratio, a DMC-to-RSO molar ratio of 3:1 and 60°C. This study clearly demonstrates that formation of the low value crude glycerol in conventional biodiesel processing can be greatly reduced, by over 90%, with proportionate formation of GLC as a more valuable product. This biodiesel production through reactive coupling minimizes the methanol requirement, whilst simultaneously producing GLC, thereby improving the economics of biodiesel production, and rendering the process "greener," as crude glycerol waste is reduced.

AUTHOR CONTRIBUTIONS

AH and VE designed the experimental programme, and the experimental data were collected by LA-S. Initial draft of the manuscript was written by LA-S, VE. The overall supervisions of the experimental work and review of the manuscript were carried out by AH.

REFERENCES

Ashby, R., Solaiman, D. Y., and Foglia, T. (2004). Bacterial poly(Hydroxyalkanoate) polymer production from the biodiesel co-product stream. *J. Polymers Environ.* 12, 105–112. doi: 10.1023/B:JOOE.0000038541.54263.d9

Ayoub, M., and Abdullah, A. Z. (2012). Critical review on the current scenario and significance of crude glycerol resulting from biodiesel industry towards more sustainable renewable energy industry. *Renew. Sustain. Energy Rev.* 16, 2671–2686. doi: 10.1016/j.rser.2012.01.054

Bromberg, L., Fasoli, E., Alvarez, M., Hatton, T. A., and Barletta, G. L. (2010). Biguanide-, imine-, and guanidine-based networks as catalysts for transesterification of vegetable oil. *Reactive Funct. Polym.* 70, 433–441. doi: 10.1016/j.reactfunctpolym.2010.04.003

BSI (2003). *Fat and Oil Derivatives - Fatty Acid Methyl Esters (Fame) For Diesel Engines - Determination of Esters and Linolenic Acid Methyl Ester Contents, in Designation BS EN 14103*. London.

Canakci, M., and Van Gerpen, J. (2003). A pilot plant to produce biodiesel from high free fatty acid feedstocks. *Trans. Am. Soc. Agri. Eng.* 46, 945–954. doi: 10.13031/2013.13949

Cervero, J. M., Coca, J., and Luque, S. (2008). Production of biodiesel from vegetable oils. *Grasas y Aceites* 59, 76–83. doi: 10.3989/gya.2008.v59.i1.494

Ciriminna, R., Della Pina, C., Rossi, M., and Pagliaro, M. (2014). Understanding the glycerol market. *Eur. J. Lipid Sci. Technol.* 116, 1432–1439. doi: 10.1002/ejlt.201400229

Darnoko, D and Cheryan, M. (2000). Kinetics of palm oil transesterification in a batch reactor. *J. Am. Oil Chem. Soc.* 77, 1263–1267. doi: 10.1007/s11746-000-0198-y

Demirbas, M.F., and Balat, M. (2006). Recent advances on the production and utilization trends of bio-fuels: a global perspective. *Energy Conv. Manag.* 47, 2371–2381. doi: 10.1016/j.enconman.2005.11.014

Derrien, A., Renard, G., and Brunel, D. (1998). Guanidine linked to micelle-templated mesoporous silicates as base catalyst for transesterification. *Studies Surf. Sci. Catal.* 117, 445–452. doi: 10.1016/S0167-2991(98)81023-9

Dhawan, M.S., and Yadav, G. D. (2017). Insight into a catalytic process for simultaneous production of biodiesel and glycerol carbonate from triglycerides. *Catalysis Today* 309, 161–171. doi: 10.1016/j.cattod.2017.08.020

Esteban, J., Domínguez, E., Ladero, M., Ochoa, F. G. (2015). Kinetics of the production of glycerol carbonate by transesterification of glycerol with dimethyl and ethylene carbonate using potassium methoxide, a highly active catalyst. *Fuel Process Technol.* 138(Suppl. C), 243–251. doi: 10.1016/j.fuproc.2015.06.012

Eze, V.C. and Harvey, A. P. (2018). Continuous reactive coupling of glycerol and acetone A strategy for triglyceride transesterification and in-situ valorisation of glycerol by-product. *Chem. Eng. J.* 347, 41–51. doi: 10.1016/j.cej.2018.04.078

Eze, V. C., Phan, A. N., and Harvey, A. P. (2018). Intensified one-step biodiesel production from high water and free fatty acid waste cooking oils. *Fuel* 220, 567–574. doi: 10.1016/j.fuel.2018.02.050

Eze, V. C., Phan, A. N., and Harvey, A. P. (2014). A more robust model of the biodiesel reaction, allowing identification of process conditions for significantly enhanced rate and water tolerance. *Bioresour. Technol.* 156, 222–231. doi: 10.1016/j.biortech.2014.01.028

Fan, P., Wang, J., Xing, S., Yang, L., Yang, G., Fu, J., et al. (2017). Synthesis of glycerol-free biodiesel with dimethyl carbonate over sulfonated imidazolium ionic liquid. *Energy Fuels.* 31, 4090–4095. doi: 10.1021/acs.energyfuels.7b00115

Huber, G. W., Iborra, S., and Corma, A. (2006). Synthesis of transportation fuels from biomass: Chemistry, catalysts, and engineering. *Chem. Rev.* 106, 4044–4098. doi: 10.1021/cr068360d

Ishak, Z.I., AsrinaSairi, N., Alias, Y., Taieb Aroua, M. K., and Yusoff, R. (2016). Production of glycerol carbonate from glycerol with aid of ionic liquid as catalyst. *Chem. Eng. J.* 297(Suppl. C), 128–138. doi: 10.1016/j.cej.2016.03.104

Kaljurand, I., Kütt, A., Soovӓli, L., Rodima, T., Mäemets, V., Leito, I., et al. (2005). Extension of the self-consistent spectrophotometric basicity scale in acetonitrile to a full span of 28 pKa units: unification of different basicity scales. *J. Org. Chem.* 70, 1019–1028. doi: 10.1021/jo048252w

Lanjekar, K., and Rathod, V. K. (2013). Utilization of glycerol for the production of glycerol carbonate through greener route. *J. Environ. Chem. Eng.* 1, 1231–1236. doi: 10.1016/j.jece.2013.09.015

Lee, S., Posarac, D., and Ellis, N. (2011). Process simulation and economic analysis of biodiesel production processes using fresh and waste vegetable oil and supercritical methanol. *Chem. Eng. Res. Design.* 89, 26262642. doi: 10.1016/j.cherd.2011.05.011

Lee, Y., Lee, J. H, Yanga, H. J., Jang M., Kim, J. R., Byun, E. H., et al. (2017). Efficient simultaneous production of biodiesel and glycerol carbonate via statistical optimization. *J. Ind. Eng. Chem.* 51, 49–53. doi: 10.1016/j.jiec.2017.03.010

Li, J., and Wang, T. (2011). Chemical equilibrium of glycerol carbonate synthesis from glycerol. *J. Chem. Thermodynam.* 43, 731–736. doi: 10.1016/j.jct.2010.12.013

Martínez, L. (2018). Measuring the conductivity of very dilute electrolyte solutions, drop by drop. *Quimica Nova.* 41, 814–817. doi: 10.21577/0100-4042.20170216

Meloni, D., Monaci, R., Zedde, Z., Cutrufello, M. G., Fiorilli, I., et al. (2011). Transesterification of soybean oil on guanidine base-functionalized SBA-15 catalysts. *Appl. Catal. B Environ.* 102, 505–514. doi: 10.1016/j.apcatb.2010.12.032

Mittelbach, M., and Trathnigg, B. (1990). Kinetics of alkaline catalyzed methanolysis of sunflower oil. *Lipid. Fett.* 92, 145–148.

Moser, B. (2009). Biodiesel production, properties, and feedstocks. *In Vitro Cell. Dev. Biol. Plant* 45, 229–266. doi: 10.1007/s11627-009-9204-z

Mota, C. J. A., da Silva, C. X. A., Rosenbach, N., Costa, J., and da Silva, F. (2010). Glycerin derivatives as fuel additives: the addition of glycerol/acetone ketal (Solketal) in gasolines. *Energy Fuels* 24, 2733–2736. doi: 10.1021/ef9015735

Mu, Y., Teng, H., Zhang, D. J., Wang, W., and Xiu, Z. L. (2006). Microbial production of 1,3-propanediol by Klebsiella pneumoniae using crude glycerol from biodiesel preparations. *Biotechnol. Lett.* 28, 1755–1759. doi: 10.1007/s10529-006-9154-z

Nguyen, P. T., Nohair, B., Mighri, N., and Kaliaguine, S. (2013). TBD-functionalized mesoporous silica: synthesis and catalytic activity in corn oil transesterification. *Microporous Mesoporous Materials* 180, 293–300. doi: 10.1016/j.micromeso.2013.07.001

Noureddini, H., and Zhu, D. (1997). Kinetics of transesterification of soybean oil. *J. Am. Oil Chem. Soc.* 74, 1457–1463. doi: 10.1007/s11746-997-0254-2

Okoye, P.U., Abdullah, A. Z., and Hameed, B. H. (2016). Glycerol carbonate synthesis from glycerol and dimethyl carbonate using trisodium phosphate. *J. Taiwan Instit. Chem. Eng.* 68(Suppl. C), 51–58. doi: 10.1016/j.jtice.2016.09.011

Papanikolaou, S., Muniglia, L., Chevalot, I., Aggelis, G., and Marc, I. (2002). Yarrowia lipolytica as a potential producer of citric acid from raw glycerol. *J. Appl. Microbiol.* 92, 737–744. doi: 10.1046/j.1365-2672.2002.01577.x

Phan, A.N., Harvey, A.P, and Eze, V. (2012). Rapid production of biodiesel in mesoscale oscillatory baffled reactors. *Chem. Eng. Technol.* 35, 1214–1220. doi: 10.1002/ceat.201200031

Pratt, R. C., Lohmeijer, B. G., Long, D. A., Waymouth, R. M., and Hedrick, J. L. (2006). Triazabicyclodecene: a simple bifunctional organocatalyst for acyl transfer and ring-opening polymerization of cyclic esters. *J. Am. Chem. Soc.* 128, 4556–4557. doi: 10.1021/ja060662+

Quispe, C. A. G., Coronado, C. J. R., and Carvalho, J. A. Jr. (2013). Glycerol: Production, consumption, prices, characterization and new trends in combustion. *Renewable Sustain. Energy Rev.* 27, 475–493. doi: 10.1016/j.rser.2013.06.017

Rathore, V., Tyagi, S., Newalkar, B., and Badoni, R. P. (2014). Glycerin-free synthesis of jatropha and pongamia biodiesel in supercritical dimethyl and diethyl carbonate. *Ind. Eng. Chem. Res.* 53, 10525–10533. doi: 10.1021/ie5011614

Rodrigues, R., Isoda, N., Gonçalves, M., Figueiredo, F. C. A., Mandelli, D., and Carvalh, W. A. (2012). Effect of niobia and alumina as support for Pt catalysts in the hydrogenolysis of glycerol. *Chem. Eng. J.* 198–199, 457–467. doi: 10.1016/j.cej.2012.06.002

Rounce, P., Tsolakis, A., Leung, P., and York, A. P. E. (2010). A comparison of diesel and biodiesel emissions using dimethyl carbonate as an oxygenated additive. *Energy Fuels* 24, 4812–4819. doi: 10.1021/ef100103z

Schuchardt, U, Vargas, R.M., and Gelbard, G. (1995). Alkylguanidines as catalysts for the transesterification of rapeseed oil. *J. Mol. Catal. A. Chem.* 99, 65–70. doi: 10.1016/1381-1169(95)00039-9

Seong, P. J., Jeon, B. W., Lee, M., Cho, D. H., Kim, D. K., Jung, K. S., et al. et al. (2011). Enzymatic coproduction of biodiesel and glycerol carbonate from soybean oil and dimethyl carbonate. *Enzyme Microbial Technol.* 48, 505–509. doi: 10.1016/j.enzmictec.2011.02.009

Sercheli, R., Vargas, R.M, and Schuchardt, U. (1999). Alkylguanidine-catalyzed heterogeneous transesterification of soybean oil. *J. Am. Oil Chem. Soc.* 76, 1207–1210. doi: 10.1007/s11746-999-0095-2

Teng, W.K., Ngoh, G. C., Yusoff, R., and Aroua, M. K. (2016). Microwave-assisted transesterification of industrial grade crude glycerol for the production of glycerol carbonate. *Chem. Eng. J.* 284(Suppl. C), 469–477. doi: 10.1016/j.cej.2015.08.108

Vicente, G., Martínez, M., Aracil, J., and Esteban, A. (2005). Kinetics of sunflower oil methanolysis. *Ind. Eng. Chem. Res.* 44, 5447–5454. doi: 10.1021/ie040208j

Zabeti, M., Wan Daud, W. M. A., and Aroua, M.K. (2009). Activity of solid catalysts for biodiesel production: a review. *Fuel Process. Technol.* 90, 770–777. doi: 10.1016/j.fuproc.2009.03.010

Zhang, G. D., Liu, H., Xia, X. X, Zhang, W. G., Fang, J. H. (2005). Effects of dimethyl carbonate fuel additive on diesel engine performances. *Proc. Insti. Mechan. Eng. Part D J. Automob. Eng.* 219, 897–903. doi: 10.1243/095440705X28358

Zhang, L., Sheng, B., Xin, Z., Liu, Q., and Sun, S. (2010). Kinetics of transesterification of palm oil and dimethyl carbonate for biodiesel production at the catalysis of heterogeneous base catalyst. *Bioresour. Technol.* 101, 8144–8150. doi: 10.1016/j.biortech.2010.05.069

Zhou, Y., Wang, S., Xiao, M., Han, D., Lu, Y., and Menga, Y. (2015). Formation of dimethyl carbonate on nature clay supported bimetallic copper-nickel catalysts. *J. Cleaner Production* 103 (Suppl. C), 925–933. doi: 10.1016/j.jclepro.2014.08.075

Conflict of Interest Statement: The authors declare that the research was conducted in the absence of any commercial or financial relationships that could be construed as a potential conflict of interest.

Selective Electrooxidation of Glycerol Into Value-Added Chemicals: A Short Overview

Christophe Coutanceau *, Stève Baranton and Roméo S. Bitty Kouamé

IC2MP, MediaCat Group, UMR CNRS-Université de Poitiers n° 7285, Poitiers, France

A comprehensive overview of the catalysts developed for the electrooxidation of glycerol with the aim of producing selectively value-added compounds is proposed in the present contribution. By presenting the main results reported in the literature on glycerol electrooxidation in acidic and alkaline media, using different kinds of catalytic materials (monometallic catalysts based on platinum group metals and non-noble metals, multimetallic alloys, or modification of surfaces by adatoms, etc.) and under different experimental conditions, some general trends concerning the effects of catalyst composition and structure, of reaction medium and of the electrode potential to enhance the activity for the glycerol oxidation reaction and of the selectivity toward a unique value-added product will be presented and discussed. The objective is to provide a guideline for the development of electrochemical systems which allow performing the electrooxidation of glycerol at the rate and selectivity as high as possible.

Keywords: activity, catalysts, electrooxidation, glycerol, HPLC, *in situ* IR, selectivity

INTRODUCTION

Glycerol is now considered as a largely available, inexpensive, and inherently renewable compound, which could be used as platform molecule for fine chemistry. The trans-esterification reaction in presence of methanol (methanolysis) of vegetable oil to produce biodiesel leads to ca. 10 wt.% of glycerol as side product (Clacens et al., 2002; Dasari et al., 2005). In the case of bio-ethanol production by anaerobic fermentation, significant amount of glycerol is also formed (several wt.%) (Aldiguier et al., 2004). The increasing demand of biofuels worldwide inevitably generated large production of glycerol in amounts much higher than that needed for industries, and therefore important stocks (Ciriminna et al., 2014). It can then be considered as a waste from biofuel industries. For this reason, several heterogeneous, homogeneous, or bio- catalysis processes have been developed to transform glycerol into energy and/or value-added compounds (Behr et al., 2008; Ilie et al., 2011) such as esters, glycerol carbonates, ethers, acetals, or ketals (Pagliaro, 2017). These new usages of glycerol provide a good opportunity for cutting down the production costs of biofuels, which are currently more expensive than fossil fuels and need state exemption to taxation to reach the market.

Amongst the species derived from glycerol, all C3 oxidation compounds (glyceraldehyde, dihydroxyacetone, glyceric acid, tartronic acid, hydroxypyruvic acid, and mesoxalic acid) have economic and/or industrial interests (Behr et al., 2008). But these compounds are generally produced either by enzymatic (microbial) processes (in the case of dihydroxyacetone da Silva et al., 2009, as an example) or by using strong oxidants (permanganate, nitric acid,

chromic acid, etc.). Microbial processes lead generally to high selectivity, but to low conversion rates; moreover, other important drawbacks of such processes concern microbe separation, control of byproducts and disposal of waste water produced by the industrial process (Aarthy et al., 2014). The use of stoichiometric oxidants does not allow the control of the reaction selectivity and leads to the formation of large number of products and by-products (Behr et al., 2008). For these reasons, it has been proposed to develop catalytic processes to increase the conversion and simultaneously to control the selectivity of the oxidation reactions (Carrettin et al., 2004). Generally, the catalytic reactions are performed at ca. 50–60°C pressurized with oxygen (Katryniok et al., 2011; Villa et al., 2015), which can be detrimental for the selectivity.

In this context, electrocatalysis and electrochemical methods for glycerol oxidation have certainly a role to play. In electrochemical methods, the glycerol oxidation can be performed at room temperature, i.e., without external power supply for the heater and without temperature control system, and in the only presence of water and electrolyte (Na^+ or K^+/OH^- in alkaline media and H^+/SO_4^{2-} or ClO_4^- in acidic media). Co-reactants are water as oxygen source, which avoid to work under pressurized oxygen conditions or in presence of oxidative agents in the reaction medium (in electrochemical methods, water molecules can be activated at the solid electrode materials to provide extra-oxygen atoms for the oxidation reaction of organic compounds), solid electrode materials (immobilized catalysts), and electrons, which can make electrocatalysis a more sustainable process than catalysis. Moreover, the activity of electrocatalysts and selectivity of the reaction toward a given reaction product can be accurately tuned and enhanced through the control of the structure/composition of the electrocatalyst and of the electrode potential. Indeed, these parameters control both the glycerol and water adsorption (activation) at the catalytic surface and further the route of oxidation and the reaction product distribution (Simões et al., 2012; Coutanceau et al., 2014; Zalineeva et al., 2014; Cobos-Gonzalez et al., 2016). At last, the electrochemical oxidation of glycerol into value-added compounds at the anode of an electrosynthesis reactor (**Figure 1**) can be accompanied by electric energy production (in fuel cell mode) (Bambagioni et al., 2009; Benipal et al., 2017) or hydrogen production (in electrolysis cell mode) (Bambagioni et al., 2010; Chen et al., 2014), which both can bring higher economical interest to the process.

The current contribution aims at presenting a short overview of the achievements in glycerol electrooxidation toward value-added compounds. By presenting the main results reported in acidic and alkaline media, using different kinds of catalytic materials and under different experimental conditions, some trends concerning the selective electrooxidation of glycerol will be presented. The objective is to provide a guideline for the development of electrochemical systems allowing performing the electrooxidation of glycerol at the highest rate and highest selectivity possible. This requirement is mandatory for decreasing the E-factor, as determined by Sheldon (Sheldon, 2017), of the electrochemical processes down to 0 by only providing valuable outputs (value-added chemicals and energy or hydrogen) from an industrial waste.

EXPERIMENTAL

Synthesis of Catalysts by a Water-Oil-Microemulsion Method (Boutonnet et al., 1982; Coutanceau et al., 2008)

Hexachloroplatinic acid hexahydrate ($H_2PtCl_6 \bullet 6H_2O$), tetrachloroauric acid trihydrate ($HAuCl_4 \bullet 3H_2O$), potassium tetrachloropalladate (K_2PdCl_4), nickel chloride ($NiCl_2$) and bismuth chloride ($BiCl_3$) purchased form from Alfa Aesar (99 % purity) were used as metal salt precursors for the syntheses. Aqueous solutions were prepared in ultrapure water (MilliQ, Millipore, 18.2 MΩ cm) with total concentration in metal salts of 0.1 mol L^{-1} from appropriate weights of metal salts to reach the desired atomic ratios. A 1.6 mL aliquot of a metal salt solution was placed into a flask containing a homogenous mixture of 37.0 g of n-heptane (Sigma Aldrich, HPLC grade) as oil phase and 16.1 g of polyethylene glycol dodecyl ether (Brij® L4, Sigma Aldrich) as surfactant, under continuous stirring conditions until a stable and translucent microemulsion was obtained. The microemulsion consisted in nanodroplets of aqueous solution containing the metal salts protected by the surfactant and in suspension in the continuous n-heptane phase. The metal salts in nanodroplets were then reduced by addition to the mixture of 100 to 200 mg of solid sodium borohydride ($NaBH_4$, 99 % purity, Sigma Aldrich) to reach a large excess. After the reaction was completed (hydrogen evolution has stopped), appropriate amount of carbon powder (Vulcan XC72, CABOT) pre-treated under $N_2(g)$ at 400 °C for 4 h was directly added to the colloidal solution to reach a metal loading of ca. 40 wt.%. After sonication for ca. 15 min, the mixture was filtered under vacuum on a hydrophilic polyvinylidene difluoride (PVDF) membrane (0.22 mm Durapore membrane filter from Millipore). The carbon-supported metal nanoparticle material was washed several times with acetone and ultrapure water and dried overnight in an oven at 60°C. At last, the catalytic powder was thermally treated for 2 h at 200°C under air atmosphere to remove any remaining surfactant.

Electrochemical Measurements

The electrochemical setup consisted in a computer-controlled Voltalab PGZ 402 potentiostat. The solutions were prepared from NaOH (Semiconductor grade 99.99% purity, Sigma-Aldrich), ultrapure water and glycerol (Sigma-Aldrich, Reagent Plus, purity ≥ 99%). The electrochemical experiments were carried out at 20°C in N_2-purged (U-quality, l'Air liquid) 0.1 or 1.0 mol L^{-1} NaOH electrolyte containing 0.1 mol L^{-1} glycerol, using a conventional thermostated three-electrode electrochemical cell. The working electrode was prepared by deposition of a catalytic ink onto a glassy carbon disc (0.071 cm^{-2} geometric surface area). The catalytic ink consisted in the dispersion of 17.7 mg of catalytic powder in 2.117 mL of ultrapure water, 0.529 mL of 2-propanol (LC-MS CHROMASOLV, Fulka), and 0.354 mL of

FIGURE 1 | Working principles of **(A)** an acidic or alkaline solid polymer glycerol fuel cell and **(B)** an acidic or alkaline solid polymer glycerol electrolysis cell.
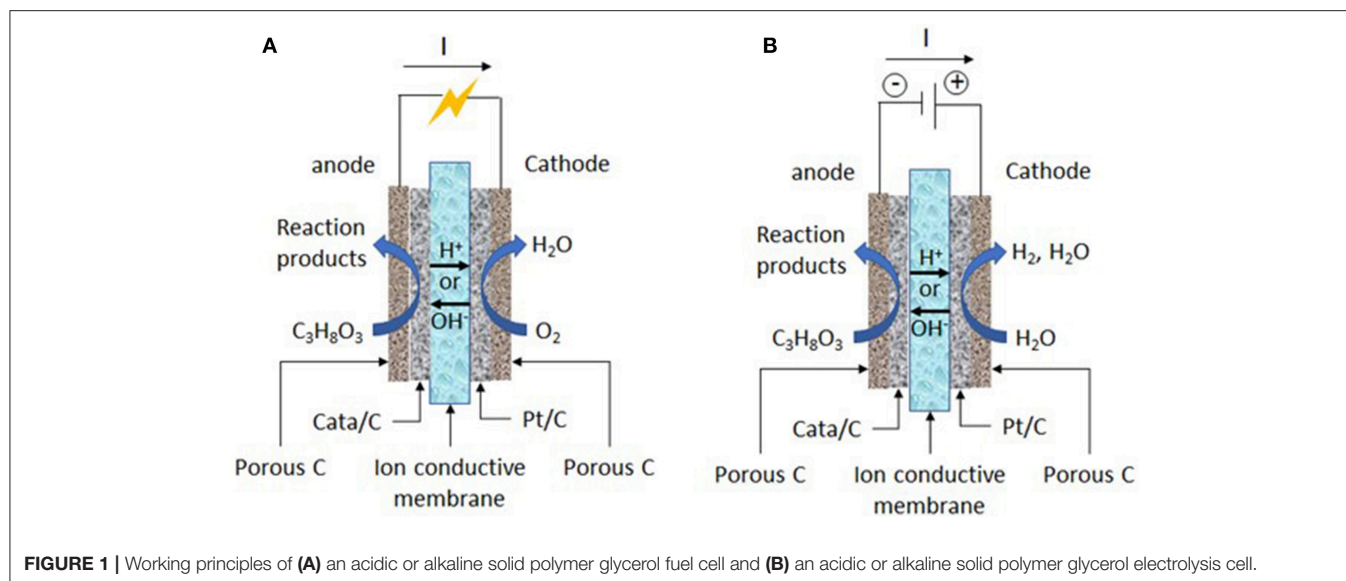
Nafion solution (5 wt % Nafion perfluorinated resin solution in aliphatic alcohols, Sigma Aldrich). After homogenization by sonication (about 30 s), 3 μL of catalytic ink was dipped using a microsyringe on the freshly polished glassy carbon disc, leading to a metal loading of 100 μg_{metal} cm^{-2}. The solvent was then evaporated in a stream of pure nitrogen at room temperature. The counter electrode was a glassy carbon plate (4 cm^2 geometric surface area), and the reference electrode was a reversible hydrogen electrode (RHE).

In situ Infrared Spectroscopy

In situ Fourier transform infrared spectroscopy (FTIRS) experiments were performed on a Bruker IFS 66 FTIR spectrometer modified for beam reflection on the electrode surface at a 65° incident angle. To remove interferences from atmospheric water and CO_2 the beam path was evacuated. An Infrared Associates liquid nitrogen-cooled HgCdTe detector was used. The spectral resolution was 4 cm^{-1}, and each spectrum was obtained by averaging 512 spectra recorded for 35 s. Spectra were recorded every 0.05 V during the linear voltammetry carried out at 1 mV s^{-1} from 0.1 to 1.2 V vs. RHE. The experimental details of the electrochemical setup for SPAIRS (single potential alteration IR spectroscopy) are described elsewhere (Beden and Lamy, 1988; Kabbabi et al., 1998). The method of spectrum normalization involved that negative absorption bands corresponded to the formation of species at the electrode surface and positive absorption bands corresponded to the consumption of species at the electrode surface.

Chronoamperometry Experiment

The electrolysis test was carried out in a recirculation mode at 20°C with a 2.0 M glycerol and 0.5 M NaOH aqueous solution in a 5 cm^2 geometric surface area filter press-like single electrolysis cell at a flow rate of 20 mL min^{-1}. The $U_{cell}(t)$ curves were recorded by using a DC power supply (E3614A from Agilent) to fix the cell voltage and Digital

Multimeters (34405A from Agilent) to record the cell voltage and the applied current. The electrodes (cathode: 1.6 mg cm^{-2} Pt loading; anode: 1.6 mg cm^{-2} metal loading; both electrodes: 20 wt.% PTFE, 0.8 mg cm^{-2} Nafion) for chronoamperometry measurements were prepared by depositing an ink consisting in a mixture of Nafion (5 wt. % from Aldrich) solution, ultrapure water and the catalytic powder, on a carbon porous layer (CPL). The CPLs (4 mg cm^{-2} of a mixture of carbon powder and 20 wt. % PTFE) were made from a carbon cloth (Electrochem Inc.) on which was brushed an ink made of Vulcan XC 72 carbon powder and PTFE dissolved in isopropanol. The electrodes (cathode and anodes) were separated by a simple blotting paper and mechanically pressed in the electrolysis cell.

ELECTRO-OXIDATION OF GLYCEROL IN ACIDIC MEDIA

Mono-Metallic Catalytic Materials

Because very few electrode materials are sufficiently stable or active in acidic medium, the electro-oxidation of glycerol has essentially been studied on platinum and platinum-based surfaces. It has been considered for a long time that platinum was unavoidable in such media to activate the dissociative adsorption of alcohols at its surface (Hogarth and Ralph, 2002; Venancio et al., 2002; Léger et al., 2005), leading to adsorbed species which could be further oxidized and desorbed at relatively high rates. However, it has been proposed recently that gold could also present some activity toward glycerol electrooxidation in acidic medium (Valter et al., 2018). This result was very surprising as previous works established that gold wasn't an active material in acidic media for alcohol oxidation (Beden et al., 1987; Kwon et al., 2011a). This discrepancy was attributed by Valter et al. to the nature of the electrolyte used for the oxidation reaction (Valter et al., 2018). Beden et al. (1987)

and Kwon et al. (2011b) performed their experiments in 0.5 M H_2SO_4, whereas Valter et al. (2018) used 0.1 M $HClO_4$ as supporting electrolyte. These last authors proposed that the stronger adsorption of sulfate ions than that of perchlorate ions on gold surface (Angerstein-Kozlowska et al., 1986) could be responsible for the lack of Au surface activity for glycerol electrooxidation in 0.5 M H_2SO_4 electrolyte. Based only on a DFT study, they explored the most thermodynamically favorable pathway on Au (111) in the potential range below 1.0 V vs. RHE, where no O and/or OH species are adsorbed on the gold surface. They proposed the formation of dihydroxyacetone and 2,3-dihydroxy-2-propenal from the low electrode potential value of 0.39 V vs. RHE (reversible hydrogen electrode), the formation of CO from 0.5 V vs. RHE and glyceraldehyde from 0.6 V vs. RHE, both these last species being expected to remain adsorbed on the surface. But, no experimental evidences were given to support this reaction pathway. Moreover, the presence of CO indicated that the breaking of the C-C bond occurred, meaning low selectivity in C3 products, and moreover the activity, as determined from the current densities recorded by cyclic voltammetry for 0.1 M glycerol electrooxidation in 0.1 M $HClO_4$ electrolyte, remained very low (which could be explained by the blocking of the surface by CO and glyceraldehyde for potential lower than 1.0 V vs. RHE).

Up to now, platinum still remains the best catalytic materials in acidic media either for the oxygen reduction reaction (Gasteiger et al., 2005) in a fuel cell, or for the water reduction reaction (Mamaca et al., 2012) in an electrolysis cell and for alcohol oxidation reactions (Léger et al., 2005) in both cases. From kinetics study based on chromatographic analysis of reaction products formed at different potentials in 0.5 M H_2SO_4 on a bare Pt electrode, Roquet et al. proposed several mechanisms of glycerol oxidation according to the potential range (Roquet et al., 1994). At low potentials, where the platinum surface is not or weakly covered by hydroxide species, Pt led to very high selectivity toward glyceraldehyde (ca. 97 % at 0.75 V vs. RHE), whereas at potential higher than 1.0 V vs. RHE, where Pt is covered by an oxide layer, the selectivity decreased (56 % at 1.30 V vs. RHE) and other products such as glyceric acid, formic acid, and glycolic acid were detected. The proposed mechanism involved the O-adsorption as first adsorption step: no OH coverage:

$$Pt + C_2H_5O_2 - CH_2OH \rightarrow C_2H_5O_2 - CH_2O - Pt$$
$$+ 1e^- + 1H^+ \tag{1}$$

$$C_2H_5O_2 - CH_2O - Pt \rightarrow Pt + C_2H_5O_2 - CHO$$
$$+ 1e^- + 1H^+ \tag{2}$$

weak OH coverage:

$$Pt + H_2O \rightarrow Pt - OH + H^+ + e^- \tag{3}$$

$$C_2H_5O_2 - CH_2O - Pt + Pt - OH \rightarrow C_2H_5O_2 - COOH$$
$$+ 2Pt + 2H^+ + 2e^- \tag{4}$$

O coverage:

$$2Pt + 2H_2O \rightarrow 2PtO + 4H^+ + 4e^- \tag{5}$$

$$2PtO + C_2H_5O_2 - CH_2OH$$
$$\rightarrow \underset{\underset{Pt-O}{|}}{CH_2OH} - \underset{\underset{O-Pt}{|}}{COH} - CHOH + 2H^+ + 2e^- \tag{6}$$

$$\underset{\underset{Pt-O}{|}}{CH_2OH} - \underset{\underset{O-Pt}{|}}{COH} - CHOH \rightarrow 2Pt + CH_2OH - COOH$$
$$+ HCOOH \tag{7}$$
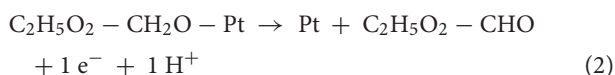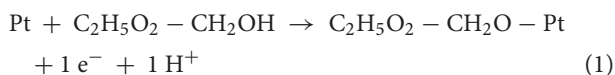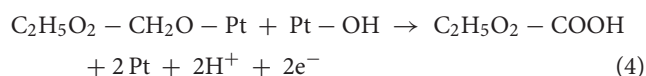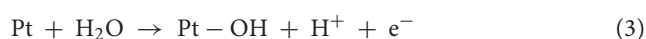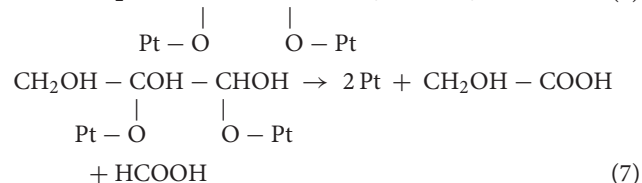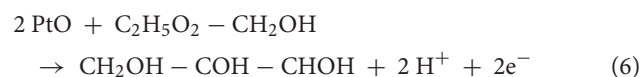
Kwon et al. (2012) performed same kind of measurements on a carbon supported Pt/C catalyst and obtained also a very high selectivity toward glyceraldehyde and small amount of glyceric acid for potential lower than 0.9 V. For higher potentials, they observed also a decrease in glyceraldehyde selectivity, with the formation of compounds of higher oxidation levels such as glyceric acid, formic acid, and glycolic acid, both the latter involving the breaking of the C-C bond. They detected also by in situ FTIRS measurements the production of CO_2 at potentials higher than 1.1 V vs. RHE. According to their study the increase of the selectivity toward glycolic and formic acids was accompanied with a drastic decrease of the selectivity toward glyceraldehyde and glyceric acid; they proposed that glyceraldehyde and glyceric acid acted as reaction intermediates, conversely to the mechanism proposed by Roquet et al. (1994) were glycolic and formic acids appeared as primary products (Equation 7). More recently, high selectivity toward glyceraldehyde at 1.136 V vs. RHE (99.2) for the oxidation of 0.1M glycerol in 0.5 M H_2SO_4 have been reported on highly-dispersed Pt nanoclusters loaded on 3D graphene-like microporous carbon (Lee et al., 2019). Actually, these authors proposed that the glycerol/Pt molar ratio (195 or 433), the applied anode potential (1.097 V or 1.136 V) and the reaction time (10 or 6 h) could change the glycerol conversion from 91.8 to 2.3 % together with an increase in glyceraldehyde selectivity from 2.5 to 99.2 (Kim et al., 2014; Lee et al., 2019).

Both the mechanisms proposed by Roquet et al. (1994) and Kwon et al. (2012) involve the ability of platinum to break the C-C bond, at least at medium and high electrode potentials. However, Schnaidt et al. (2011) studied the adsorption/oxidation of glycerol, glyceraldehyde, and glyceric acid in 0.5 M H_2SO_4 using combined spectroelectrochemical DEMS/ATR-FTIRS (differential electrochemical mass spectroscopy/attenuated total reflectance—Fourier transform infrared spectroscopy) set-up. Highly sensitive in situ ATR-FTIR was used to monitor the development of glycerol adlayer as a function of potential or time, whereas online DEMS was used to detect the volatile products formed. First these authors observed for glycerol adsorption/oxidation ATR-FTIRS absorption bands assigned to the formation of linearly and multiply bonded CO_{ads}, adsorbed glyceroyl and adsorbed glycerate species. The dissociative adsorption of glycerol into CO_{ads} occurred for potential between 0.2 and 0.6 V vs. RHE. For potentials higher than 0.5 V vs. RHE, the formation of CO_2 could be detected although in small amount indicating that incomplete oxidation of glycerol

into C3 compounds prevailed under these conditions. The formation of CO_{ads} at low potentials and of CO_2 at potentials higher than 0.5 V vs. RHE was confirmed by Gomes et al. from investigation of the electrooxidation of 0.1 M glycerol in 0.1 M H_2SO_4 and 0.1 M $HClO_4$ electrolyte on low Miller-index Pt crystalline surface orientations, Pt (100), Pt (110), and Pt (111), followed by *in situ* FTIR spectroscopy (Gomes et al., 2012). They also observed the formation of carbonyl species for potentials higher than 0.3 V vs. RHE. From their study on the adsorption/oxidation of glyceraldehyde and glyceric acid. Schnaidt et al. (2011) proposed also that glyceraldehyde was an intermediate for the formation of both CO_{ads} and glyceric acid. They found also that glyceric acid was a dead end in the electrochemical oxidation of glycerol. But, the detection of adsorbed CO species from glycerol adsorption speaks for a mechanism starting with a C-adsorption step rather than an O-adsorption step as proposed by Roquet et al. (1994). Moreover, the proposition that glyceric acid is a dead end in the electrochemical oxidation of glycerol is in contradiction with the mechanism proposed by Kwon et al. (2012) for the formation of glycolic, oxalic, formic acid and CO_2 at high potentials.

The study of glycerol electrooxidation as a function of its concentration on platinum surfaces in 0.1 M $HClO_4$ performed by Gomes et al. (2013) shed light on some mechanistic aspects of this reaction. First, they confirmed that the adsorption of glycerol led to the formation of CO_{ads} from low potentials. Second, they showed that the electrooxidation of glycerol on Pt was strongly influenced by the concentration of this alcohol. At high glycerol concentrations, a denser coverage than at low concentrations of the Pt surface by glycerol adsorbates occurred, which led to delay the formation of adsorbed OH species on the platinum surface and further the CO_{ads} desorption into CO_2 through a Langmuir-Hinshelwood mechanism ($CO_{ads} + OH_{ads} \rightarrow CO_2 + H^+ + e^-$), and glyceraldehyde, which is the preferentially formed products at low and medium potentials, contributed significantly to the formation of the CO_{ads} layer, in agreement with the observation of Schnaidt et al. (2011). Moreover, Gomes et al. (2013) found that the formation of carboxylic acids at medium and high potentials occurred in a parallel pathway and was not affected by the glycerol concentration. At high potentials carboxylic acids were partly oxidize and participated to the production of CO_2.

(Kongjao et al., 2011) performed electrochemical reforming of a 0.5 M glycerol at a current of 4.5 A in an electrochemical reactor fitted with two Pt electrodes (66.49 and 124.34 cm^2 geometric surface area for the anode and cathode, respectively) in a monochamber cell without separation of the cathodic and anodic compartments. Therefore, their analysis by gas chromatography indicated the formation of reduction products (at the cathode) and oxidation products (at the anode) from glycerol. Concerning the oxidation products, glyceraldehyde, C1 and C2 acids were obtained as reaction products. No C3 carboxylic acid was detected. It is likely that the anode potential (which was not controlled in the experiments) reached for a current of 4.5 A was very high (higher than 1.0 V vs. RHE). Under such conditions, the C-C bond occurred in a large extent leading to low weight carboxylic acids and to CO_2.

Although it is obvious that further investigations are needed to determine the mechanism of glycerol electro-oxidation on platinum surface, a general reaction scheme on platinum can be proposed (**Figure 2**).

Multi-Metallic Catalytic Materials

Studies on glycerol adsorption and electro-oxidation at platinum surfaces have revealed that the type and the density of adsorbed species from glycerol on the catalytic surface greatly influenced the mechanism and the formation of final products. A classical approach to increase the activity and the selectivity of platinum consists in modifying its surface by other atoms, alloyed or deposited as ad-atoms. It is indeed known for a long time that the modification of Pt surfaces by foreign atoms has an important effect on the amount and composition of chemisorbed species. This effect will change the course of electrooxidation of adsorbed species and change the activity and selectivity of the catalyst (Podlovchenko et al., 1966; Smirnova et al., 1988). On platinum surfaces, it has been evidenced that adsorbed species, such as CO or aldehydes, were formed from low electrode potentials and blocked the surface. It has also been evidenced that the removal of such adsorbed species needed the presence of adsorbed OH species to allow further oxidation through the Langmuir-Hinshelwood mechanism. Therefore, by changing the balance between the sites blocked by adsorbed species (Pt sites) and the sites activating water to form adsorbed OH species (foreign atom sites), the activity and the selectivity of the catalyst can be enhanced by allowing a bi-functional mechanism occurring (Watanabe and Motoo, 1975). This effect is called the third body effect (Schmidt et al., 2000). Another effect of the presence of foreign atoms at the platinum surface consists in diluting the Pt surface atoms, which limits the mean number of adjacent Pt atoms and further leads to change the nature of adsorbed species and the strength of their adsorption (Adzic, 1984).

Ruthenium is a co-catalyst often used for the electro-oxidation of alcohols. In particular, PtRu/C catalysts displayed higher activity and stability than Pt/C catalyst for the glycerol electro-oxidation (Kim et al., 2011). The best atomic composition in term of activity was found to be Pt_5Ru_5/C, with an onset potential for glycerol oxidation of 0.448 V vs. RHE against 0.635 V vs. RHE for Pt/C. Chronoamperometry measurements at 1.1 V vs. RHE were performed for 7 h for the oxidation of 0.1 M glycerol in 0.5 M H_2SO_4 on Pt/C and Pt_5Ru_5/C (1.0 mg cm^{-2} metal loading) as anodes at 60 °C (Kim et al., 2017). Higher current densities were obtained with the $Pt_{0.5}Ru_{0.5}$/C anode than with the Pt/C anode, confirming the higher activity of the former catalyst. Moreover, the product distributions determined using high-performance liquid chromatography were different for both catalysts; glyceraldehyde, glyceric acid, and glycolic acid were detected for both catalysts but with different rates, and dihydroxyacetone was only detected with the Pt_5Ru_5/C catalyst. The authors determined the total mass balance and found that it was 100 % with the Pt/C catalyst, whereas it decreased to 80 % with the Pt_5Ru_5/C catalyst. They concluded that the Pt_5Ru_5/C catalyst also promoted the breaking of the C-C bond leading to the formation of formic acid and CO_2.
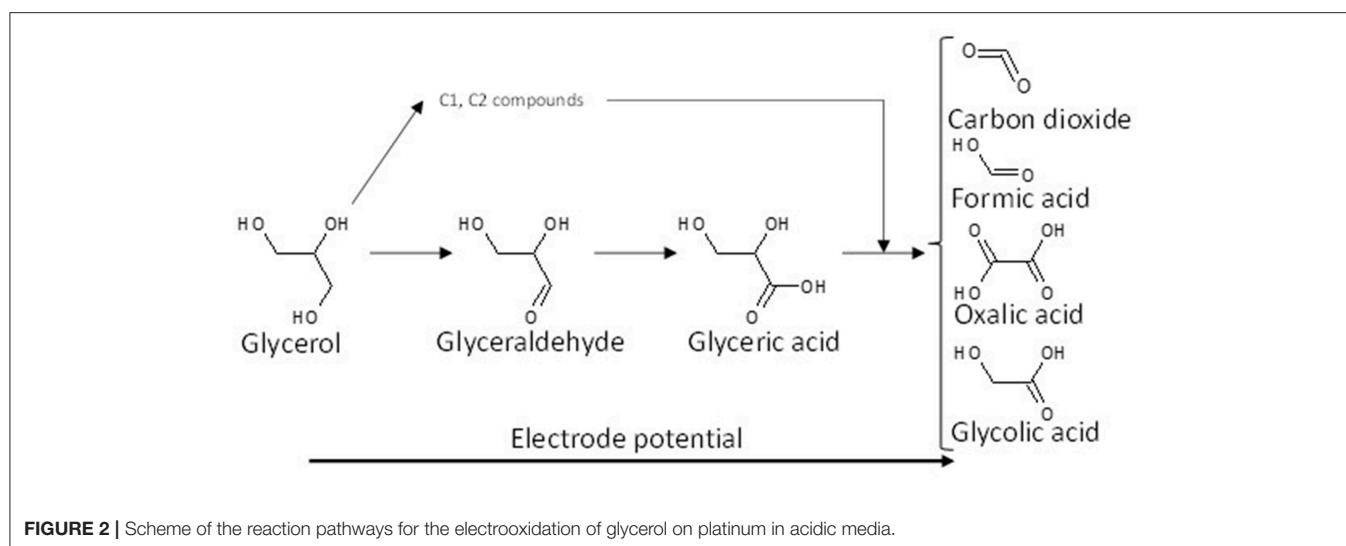
FIGURE 2 | Scheme of the reaction pathways for the electrooxidation of glycerol on platinum in acidic media.

The effect of the modification of platinum surfaces by metals from p-group on the electro-oxidation of glycerol has also been studied. Bismuth is known for a long time to be an excellent co-catalyst for alcohol and biomass conversion by heterogeneous catalysis (Gallezot, 1997). Kwon et al. (2012) compared the activity and selectivity of a Pt/C, a Bi-modified Pt/C and a Pt/C catalyst in Bi-saturated solution. The onset potential for glycerol electrooxidation decreased from ca. 0.5 V to ca. 0.47 V and ca. 0.4 V vs. RHE for Pt/C, Bi-modified Pt/C and Pt/C in Bi-saturated solution, respectively. But the most important results were that the presence of bismuth in solution, and further the high Bi coverage of the Pt surface, avoided the formation of adsorbed CO species and oriented the reaction toward the activation of the secondary alcohol group to produce dihydroxyacetone with very high selectivity at low electrode potentials, whereas on pure Pt the formation of glyceraldehyde was predominant at low electrode potentials. The effect of the modification of platinum by adatoms irreversibly adsorbed on a carbon supported platinum electrode, antimony (Sb), lead (Pb), indium (In), and tin (Sn), has also been studied toward the glycerol electro-oxidation (Kwon et al., 2014). Sb as adatoms displayed the highest activity and allowed achieving a very high selectivity toward dihydroxyacetone from very low potentials, with an onset potential of ca. 0.35 V vs. RHE shifted by ca. 150 mV with respect to that with Pt/C. Both Sb and Bi promoted the secondary alcohol oxidation, whereas Pb, In, and Sn promoted the oxidation of the primary alcohol groups toward glyceraldehyde at low electrode potentials. For all catalysts, glyceric acid was detected at medium potentials and glycolic acid at high potentials. **Figure 3** shows the general reaction scheme of glycerol electrooxidation on platinum modified by p-group elements. The study of Pb@Pt core-shell structures agreed with this reaction mechanism (Silva et al., 2016). The structural and geometric effects induced by the core-shell structure improved the direct oxidation of formic acid into carbon dioxide, limiting the CO surface coverage and hence increasing the catalytic activity. Although these studies are very

interesting in a fundamental point of view, the implementation of such system for DHA production is likely avoided for cosmetic, food, or pharmaceutical applications because of the presence of antimony or bismuth in solution.

ELECTRO-OXIDATION OF GLYCEROL IN ALKALINE MEDIA

In acidic media, the electro-oxidation of glycerol involves the use of platinum. The advantage of alkaline media is that kinetics of alcohol electrooxidation is faster than in acidic ones (Wang et al., 2003). Indeed, Koper et al. proposed that in alkaline media the first deprotonation step for the electrooxidation of alcohols to form alkoxide species was base catalyzed, and that the second deprotonation step depended on the catalytic ability of the surface (Kwon et al., 2011a). This could explain the higher activity toward alcohol electrooxidation not only of gold, but also of platinum in alkaline media than in acidic media. Then other metals than platinum can be used to perform this reaction. Moreover, non-noble metals are more stable in alkaline media. For example, gold, which displays no or very low activity in acidic media, becomes very active in alkaline media; nickel-based catalysts, which are not stable in acidic media, can be used in alkaline media. Hence, a larger panel of electrocatalytic materials, including platinum (Simões et al., 2011; Cobos-Gonzalez et al., 2016; Da Silva et al., 2017) palladium (Bambagioni et al., 2010; Simões et al., 2012; Wang et al., 2016), gold (Jeffery and Camara, 2010; Simões et al., 2010; Gomes et al., 2014; Ottoni et al., 2016), nickel (Oliveira et al., 2013, 2014; Lin et al., 2017; Houache et al., 2018), rhodium (Pagliaro et al., 2017), etc., -based catalysts, could be evaluated for the glycerol oxidation reactions.

Non-platinum Group Metals

It is known that nickel is an active material for alcohol electrooxidation in alkaline media. It is generally admitted that
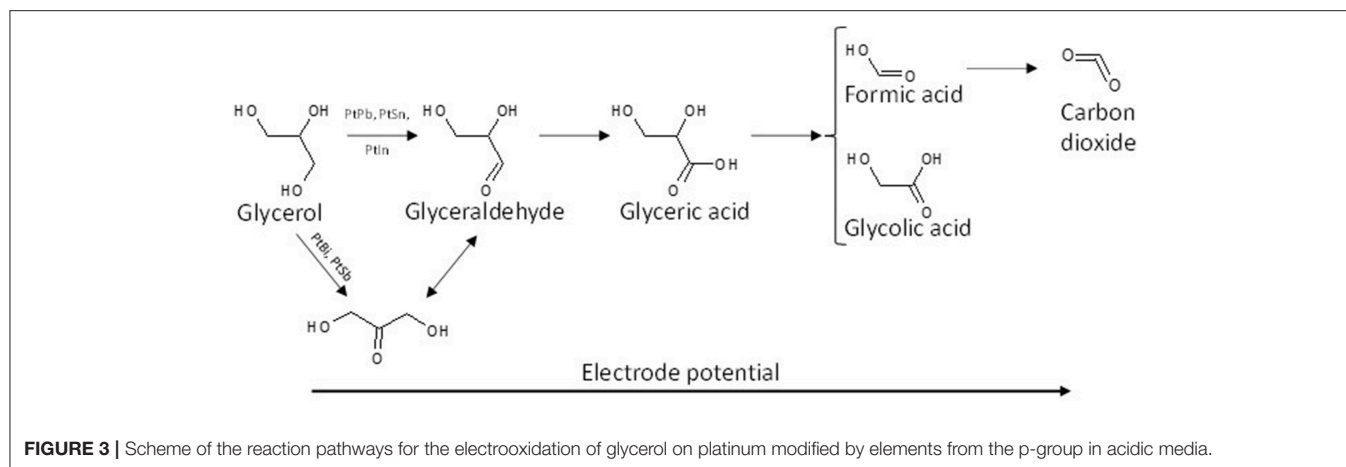
FIGURE 3 | Scheme of the reaction pathways for the electrooxidation of glycerol on platinum modified by elements from the p-group in acidic media.

the electrooxidation of alcohol starts simultaneously with the $Ni^{II}(OH)_2 \rightarrow Ni^{III}OOH$ transition at high potentials. This transition occurs from the onset potential of ca. 1.3 V vs. RHE. Fleischmann et al. (1971, 1972) proposed that the early steps of alcohol electrooxidation in alkaline media on nickel occurred according to the following equations:

$$Ni(OH)_2 + OH^- \rightarrow NiOOH + H_2O + e^- \qquad (8)$$

$$NiOOH + R-CH_2OH + OH^- \rightarrow Ni(OH)_2 + H_2O$$
$$+ R-CHO + e^- \qquad (9)$$

$$R-CHO + 3\,OH^- \rightarrow R-COO^- + 2\,H_2O + 2\,e^- \quad (10)$$

Therefore, according to this mechanism the oxidation of glycerol could only occur for potentials higher than 1.3 V vs. RHE, i.e., in a very oxidative potential range. However, the onset potential of glycerol oxidation is shifted toward a lower potential of ca. 1.1 V vs. RHE, i.e. 200 mV less than the potential for the $Ni^{II}(OH)_2 \rightarrow Ni^{III}OOH$ transition. This effect was already observed (Tehrani and Ab Ghani, 2012; Oliveira et al., 2013) and was attributed to the fact that the very early steps of the transformation of $Ni(OH)_2$ to NiOOH was primordial to start the glycerol oxidation reaction. Houache et al. (2018) performed *in-situ* photo-elastic modulations infrared reflection absorption spectroscopy (PM-IRRAS) measurements coupled with electrochemical experiments for the oxidation at different constant potentials (from ca. 1.27 V to ca. 1.47 V vs. RHE, i.e., in the potential range of the early stages of glycerol oxidation) of 0.1 M glycerol in 1.0 M KOH aqueous electrolyte. They were able to analyze simultaneously the products formed on the Ni surface and in the bulk solution, and detected glyceraldehyde, carbonyl, carboxylate ions, and some carbon dioxide. They attributed the absorption band at ca. 1,700 cm^{-1} to glyceraldehyde and carbonyl species. However, according to Oliveira et al. (2013), the br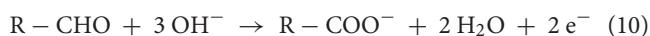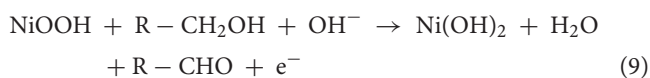oad band at ca. 1,700 cm^{-1} is characteristic of the stretching vibration of the C=O carbonyl group in a C-COO$^-$ structure. Therefore, in the potential range from 1.2 to 1.6 V vs. RHE, the electrooxidation of glycerol seems to involve the C-C bond breaking and leads mainly to the formation of formate and glycolate species, even if the formation of C3 carboxylates cannot be discarded. Indeed, Oliveira et al. (2013) confirmed these results by HPLC analysis of reaction products after long-term electrolysis at 1.6 V vs. RHE of 0.1 M glycerol in 0.1 M NaOH electrolyte. For higher potentials than 1.6 V vs. RHE, important production of CO_2 was also observed by *in situ* infrared spectroscopy. The determination of reaction intermediates by *in situ* FTIRS and the product distribution by HPLC didn't point out the formation of glyceraldehyde, which was however stipulated by Fleischmann et al. (1971, 1972) as the second step of glycerol electro-oxidation (Equation 9). This could be due to the very oxidative anode potential (1.6 V vs. RHE for the long-term electrolysis), which made glyceraldehyde very reactive, oxidizing rapidly this molecule into glycerate, glycolate, formate, carbonate, and even CO_2.

In order to increase both activity and selectivity, attempts were done to modify nickel by other metals, such as Co and Fe (Oliveira et al., 2013, 2014). The modification of Ni by Co led to the formation of larger amount of CO_2, which was explained by the lower potential for the $Co^{II}(OH)_2 \rightarrow Co^{III}OOH$ transition than for the $Ni^{II}(OH)_2 \rightarrow Ni^{III}OOH$ transition. The modification of Ni by Co, Fe or CoFe did not change significantly the onset potential of glycerol electrooxidation which remained always higher than 1.1 V vs. RHE but had an effect on the reaction product distribution (Oliveira et al., 2014). But, the main products were still formate, glycolate and other carboxylates.

Platinum Group Metals

Platinum, palladium and gold are the main studied materials from the platinum group metals for the electrooxidation of glycerol in alkaline media. The onset potential for glycerol electrooxidation is close to 0.4 V on both nanostructured Pt/C (Simões et al., 2010) and polycrystalline Pt disc (Kwon and Koper, 2010), whereas (Simões et al., 2010) showed that it was closed to 0.6 V vs. RHE at Pd/C and Au/C nanostructured catalysts. As in acidic media, platinum displays a better activity at lower electrode potentials. Consequently, it was measured that at low potential (from 0.4 to 0.8 V vs. RHE), the activation energy is lower on Pt than on Pd and Au (Habibi and Razmi, 2012).

This trend reverts at high potential (> 0.8 V vs. RHE) and Au then possesses the lowest activation energy in addition to a good poisoning tolerance. *In situ* infrared spectroscopy measurements and HPLC analysis or reaction products were also performed on such materials.

On a polycrystalline Pt disc electrode, Kwon and Koper (2010) showed that the first glycerol oxidation products was glycerate from 0.35 V to 0.8 V vs. RHE; then secondary products, glycolate and formate, were produced through glycerate oxidation and C-C bond breaking from 0.4 V vs. RHE; at last the ternary product, oxalate acid, coming from the oxidation of glycolate was detected from 0.6 V vs. RHE. In addition, tartronate formation coming from glycerate oxidation without C-C bond breaking was observed over the 0.6–1.0 V vs. RHE potential range. The same conclusion was obtained by (Simões et al., 2010, 2011, 2012) for glycerol electrooxidation on Pt/C nanostructured catalyst, but they observed also infrared absorption bands at ca. 1,150 cm^{-1} and 1,310 cm^{-1} that they attributed to the formation of glyceraldehyde (**Figure 4A**). These authors also showed that although the onset potential was shifted by ca. 200 mV toward higher potential, the same product as with platinum were obtained with Pd/C, i.e., mainly glyceraldehyde, glycerate with IR bands at ca. 1,380 cm^{-1} and 1,575 cm^{-1}, tartronate and/or mesoxalate ions with IR band at ca. 1,575 cm^{-1} (**Figure 4B**). In addition, they observed the infrared absorption band at ca. 1,335 cm^{-1} relative to the formation of dihydroxyacetone with both catalysts, but with a very low relative intensity. It is worth to note that over the 0.05 to 1.15 V vs. RHE potential range of the experiments, no CO_2 formation, giving rise to an infrared absorption band at ca. 2,343 cm^{-1} (Dailey et al., 1998; Dubau et al., 2003), was observed, whereas the presence of an absorption band at 1,950 cm^{-1} on Pt/C and 1,900 cm^{-1} on Pd/C catalyst, the positions and intensities of which are both dependent on the electrode potentials, was due to the formation of adsorbed CO species (bridge bonded CO) on platinum (Couto et al., 2001) and palladium (Jiang et al., 2001) surfaces, respectively. This means that these materials are able to break the C-C bond in a very low extent, to produce also C1 and C2 species which were not detected. All these *in situ* infrared results were confirmed by HPLC analysis at different potentials (Simões et al., 2011).

Simões et al. (2010, 2012), Kwon and Koper (2010), and Jeffery and Camara (2010) studied the electrooxidation of glycerol on Au surface. Combining HPLC with voltrammetry measurements at a polycrystalline Au electrode, Kwon and Koper (2010) detected first glycerate from 0.6 V vs. RHE and then glycolate and formate from 0.8 V vs. RHE. Using *in situ* infrared spectroscopy, (Simões et al., 2010, 2012) and Jeffery and Camara (2010) observed on nanostructured Au/C catalyst and polycrystalline Au electrode, respectively, an absorption band at ca. 1,351 cm^{-1} (**Figure 4C**) which corresponded to the formation hydroxypyruvate, in additions to that of glyceraldehyde and other carboxylates (Simões et al., 2010, 2012). The formation of hydroxypyruvate indicate that the secondary alcohol function is activated and oxidized into ketone on Au surfaces. At potentials higher than 1.3 V,

the formation of CO_2 occurred indicating the breaking of the C-C bonds and therefore the destruction of the carbon chain.

These observations indicate clearly that the nature of the catalytic metal can orient the reaction pathway. Platinum and palladium seem to favor the activation and oxidation of primary alcohol functions toward glyceraldehyde and further toward carboxylates, whereas on Au surfaces the secondary alcohol can be activated leading to the formation of hydroxypyruvate. Hydroxyacetone was also detected on Pt/C and Pd/C, but no hydroxypyruvate. Simões et al. (2012) proposed then that the isomerization equilibrium between dihydroxyacetone and glyceraldehyde could be displaced toward the formation of the aldehyde on the Pt/C and Pd/C catalysts comparatively to the Au/C catalyst. A general reaction scheme of glycerol electrooxidation on platinum group metals is proposed in **Figure 5**.

The use of platinum group metals as catalytic materials allowed to decrease the onset potential for glycerol electrooxidation and to increase the selectivity toward C3 oxidized compounds, compared to non-noble catalytic materials. This remark suggests that decreasing still more the onset potential for this reaction may help to increase the selectivity toward a given product. This can be made by varying the composition and the structure of Pt, Pd, and Au-based catalysts.

For example, Gomes et al. (2014) studied the effect of the modification of gold by silver. They found that the bimetallic catalysts led to lower onset potential for glycerol electrooxidation than the Au/C and to higher reaction rate. But, they also found that Ag addition influenced the mechanism of glycerol electrooxidation, favoring the C-C bond breaking, leading to the selective formation of formate.

The effect of the modification of Pd catalysts by metals from the d-group, such as Ni (Simões et al., 2010, 2012; Holade et al., 2013), Ru (Dash and Munichandraiah, 2015), Au (Simões et al., 2010, 2012; Ottoni et al., 2016), and Ag (Holade et al., 2013) has also been studied and the electrocatalytic activity and selectivity of bimetallic Pd_xAu_x/C, Pd_xNi_{1-x}/C, Pd_xRu_{1-x}/C and Pd_xAg_{1-x} catalysts toward glycerol electrooxidation have been estimated. Although it is admitted that the modification of Pd by Ni, Ru, Au, or Ag led to a shift of the onset of glycerol oxidation toward lower potentials than that on pure Au and Pd metals, i.e., an increase of the activity at lower electrode potentials, the selectivity of the catalysts was essentially the same as for pure Pd. Bambagioni et al. (2010) developed a very active Pd-(Ni-Zn)/C catalyst for glycerol electrooxidation and performed electrolysis measurements at room temperature for the oxidation of glycerol (10 wt%) in 2 M KOH at effective potentials between 0.6 and 0.7 V in an alkaline electrolyzer with a MEA made of a Pd–(Ni–Zn)/C/Ni mesh anode, an E-TEK Pt/C cathode on carbon paper, and a Tokuyama A006 anion conductive membrane (active surface area of 5 cm^2). Under such experimental conditions, in addition to hydrogen produced at the Pt/C cathode, they obtained a mixture of products at the anode; liquid chromatography and ^{13}C NMR analyses indicated that glycerate, tartronate, glycolate, oxalate, formate, and carbonate
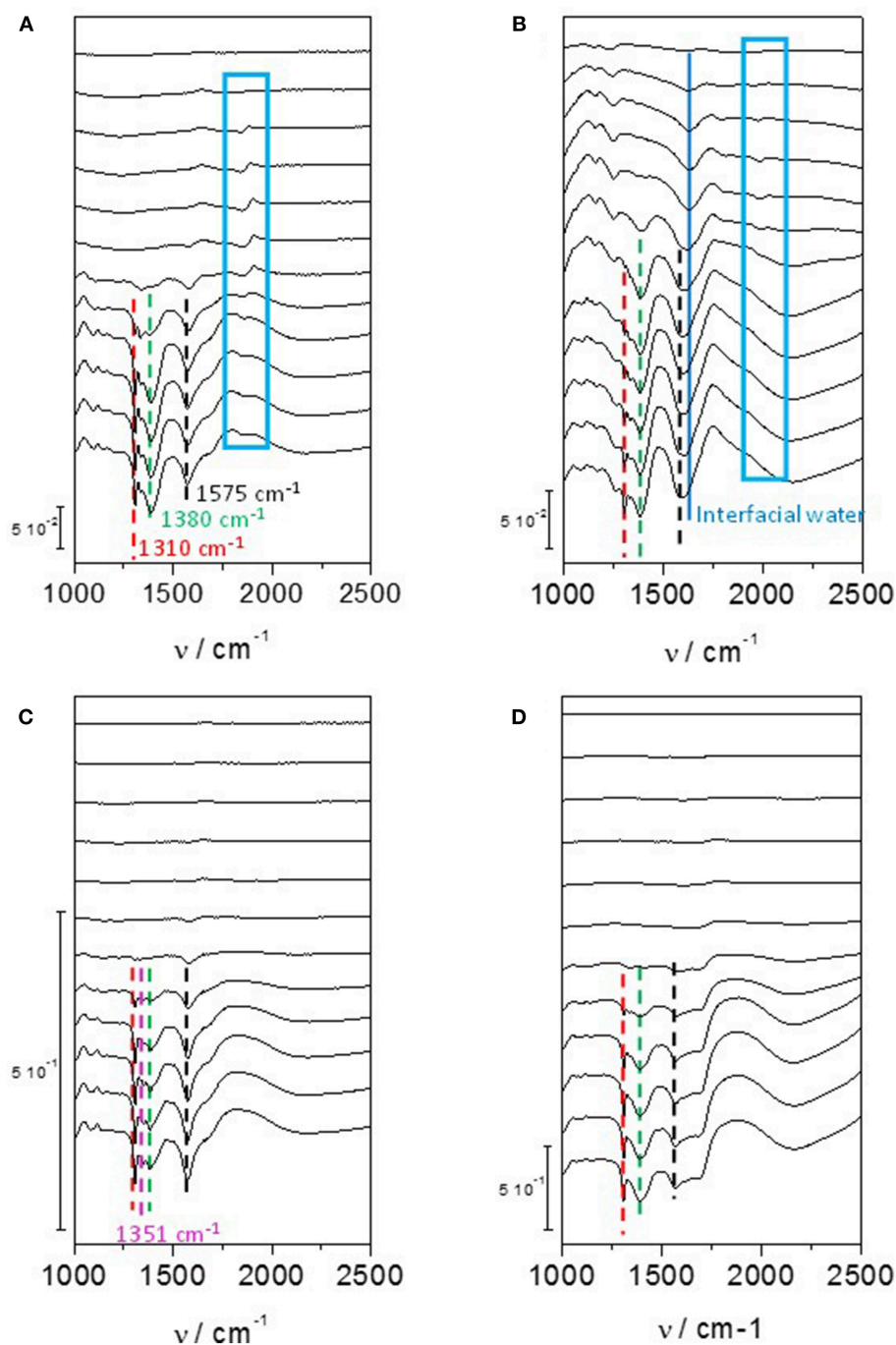
FIGURE 4 | Infrared spectra recorded in the 1,200–2,500 cm^{-1} range for 0.1 M glycerol oxidation in 0.1 M NaOH from 0.05 V to 1.15 V vs. RHE on **(A)** Pd/C, **(B)** Pt/C, **(C)** Au/C, and **(D)** Pd$_9$Bi$_1$/C prepared by the Water-in-Oil microemulsion method ($T = 20\,^{\circ}$C, scan rate: 1 mV s^{-1}, resolution 4 cm^{-1}). The dotted bars show the infrared absorption band at ca. 1,310 cm^{-1} (red), ca. 1,380 cm^{-1} (green), ca. 1,175 cm^{-1} (black) and in the case of Au/C at ca. 1,351 cm^{-1} (pink). The dark blue plain line shows the position of the Infrared absorption band relative to interfacial water and the blue boxes shows the infrared absorption bands related to adsorbed CO species on Pd/C and Pt/C catalysts (Simões et al., 2010, 2011, 2012).

were formed with glycerate and tartronate representing more than 70 % of the formed products.

Modification of palladium by p-group elements, such as indium (Serov et al., 2013), bismuth (Coutanceau et al., 2014; Zalineeva et al., 2014), and tin (Zalineeva et al., 2015), wad also studied for glycerol electrooxidation. Zalineeva et al. (2013), Zalineeva et al. (2015) studied the effect of the coverage of Pd-shaped nanoparticles by bismuth adatoms on
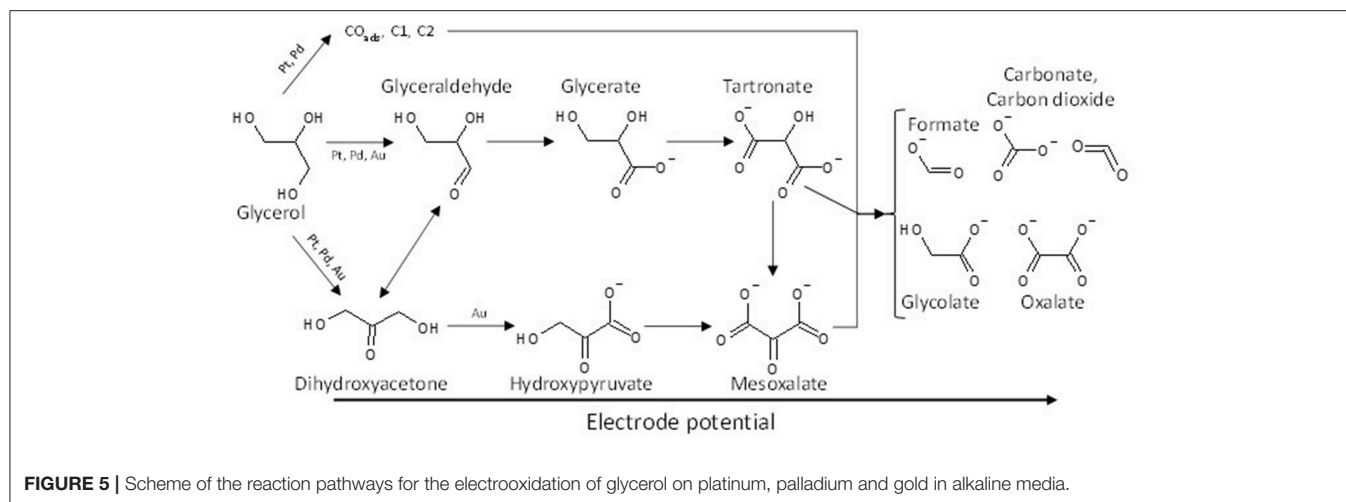
FIGURE 5 | Scheme of the reaction pathways for the electrooxidation of glycerol on platinum, palladium and gold in alkaline media.

FIGURE 6 | Influence of the coverage of a Pd surface by Bi adatoms on selectivity of glycerol oxidation reaction (Zalineeva et al., 2015).

the electrooxidation of glycerol. On pure Pd nanoparticles, they observed a higher electrocatalytic activity with nano-cubes (ca. 10 nm edges) presenting mainly extended (100) surface domains than with nano-octahedrons (ca. 8 nm tip to tip) presenting mainly extended (111) surface domains; spherical Pd nanoparticles (ca. 5 nm diameter) without preferential surface domain orientations led to the lowest activity. They also observed that the modification of the Pd surfaces by spontaneous adsorption of bismuth enhanced the activity for glycerol electrooxidation and that the coverage level of Pd by Bi adatoms did affect the reaction pathway of glycerol electrooxidation as a function of the electrode potential (**Figure 6**). Bi-coverages between 0.2 and 0.3 appeared to greatly limit the formation of CO_2 and carbonate, i.e., the breaking of the C-C bond, and to increase the selectivity toward C3 compounds, particularly dihydroxyacetone and hydroxypyruvate.

Simões et al. (2011, 2012) observed that a Pd_9Bi_1 (atomic ratio) catalyst and a Pt catalyst dispersed on a carbon powder (Vulcan XC 72) at 40 wt%, both with nanoparticles mean size of ca. 5 nm and prepared by the water-in-oil microemulsion method, led to the same activity toward glycerol electrooxidation from the onset potential of 0.4 V vs. RHE (against 0.6 V vs. RHE for Pd/C, **Figure 7**). The same mechanism as for Pt/C was also observed on Pd_9Bi_1/C with the formation of glyceraldehyde and glycerate at potentials lower than 0.8 V vs. RHE and carboxylates at higher potentials (**Figure 4D**). Zalineeva et al. (2014) prepared self-supported Pd_xBi catalysts having a nanofoam structure by the sacrificial support method. *In situ* Fourier transform infrared spectroscopy highlighted the high selectivity as a function of the electrode potential: aldehyde and ketone at low potentials, hydroxypyruvate at moderate potentials, and CO_2 at high potentials. The formation of hydroxypyruvate with high selectivity at moderate potentials (between 0.6 to

0.8 V vs. RHE), which was not observed with other Pd-based catalysts, demonstrated the importance of the catalyst structure/morphology on the selectivity. This unique catalytic behavior was explained in terms of confinement of reactants and intermediates in the catalyst pores acting as nanoreactors. These authors also synthesized self-supported Pd_1Sn_x catalysts displaying the same nanofoam structure as Pd_1Bi_x catalysts. The Pd_1Sn_1 material displayed the lowest glycerol oxidation onset potential (ca. 0.55 V vs. RHE) and led to the higher

current density. According to *in situ* Fourier transform infrared spectroscopy, the formation of glyceraldehyde and glycerate did occur as soon as the Pd_1Sn_1 catalyst become active for the glycerol electrooxidation. No evidence of the C-C bond breaking leading to the formation of C1 compounds was observed at high potentials. Pd-Sn was then shown as being extremely selective toward the formation of C3 carboxylates from 0.55 V vs. RHE.

Simões et al. (2011, 2012) also studied the catalytic behavior of Pt and PtPd nanoparticles modified by bismuth clusters prepared by the water-in-oil microemulsion method. The addition of bismuth led to a dramatic decrease of the glycerol oxidation onset potential from 0.4 V vs. RHE on Pt/C to ca. 0.2 V vs.
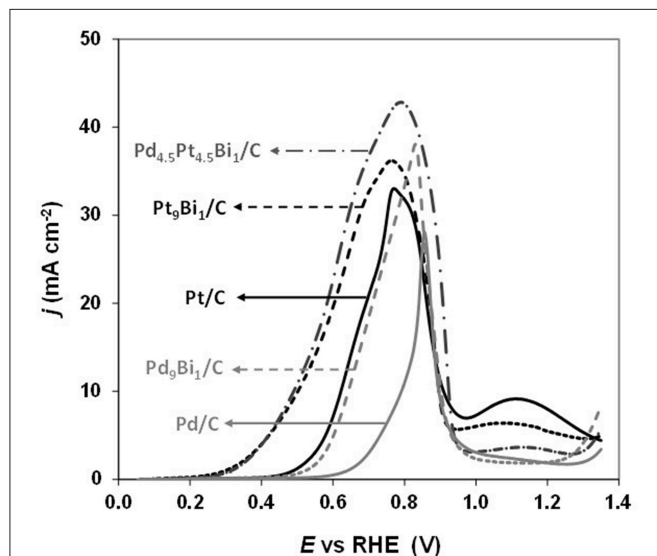
FIGURE 7 | Polarization curves recorded for the oxidation of 0.1 M glycerol in N_2-purged 1.0 M NaOH electrolyte on Pt/C, Pd/C, Pd_9Bi_1/C, Pt_9Bi_1/C and $Pd_{4.5}Pt_{4.5}Bi_1$/C catalysts synthesized by the Water-in-Oil microemulsion method (scan rate = 10 mVs^{-1}, T = 20°C) (Simões et al., 2011, 2012).
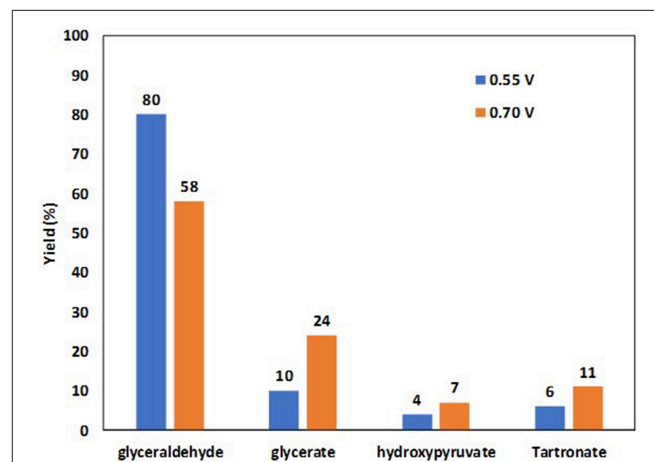
FIGURE 9 | Yields in glyceraldehyde, glycerate, hydroxypyruvate and tartronate obtained by HPLC analyses of the reaction products after 4 h of electrolysis at cell voltages of 0.55 and 0.70 V (2.0 M glycerol in 0.5 M NaOH electrolyte, T = 20°C) at a Pt_9Bi_1/C anode (Cobos-Gonzalez et al., 2016).
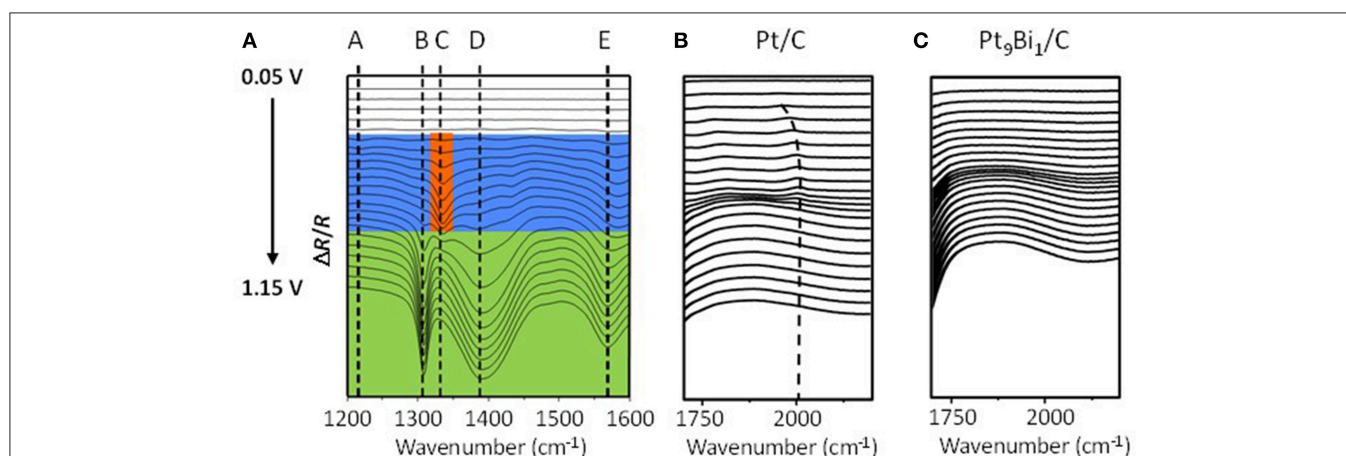
FIGURE 8 | (A) Infrared spectra recorded in the 1,200–1,600 cm^{-1} range during 0.1 mol L^{-1} glycerol oxidation in 1.0 mol L^{-1} NaOH electrolyte from 0.05 V to 1.15 V vs. RHE on a Pt_9Bi_1/C catalysts prepared by the Water-in-Oil microemulsion method (T = 20°C, scan rate: 1 mV s^{-1}, resolution 4 cm^{-1}); **(B,C)** Infrared spectra recorded in the 1,700–2,300 cm^{-1} range during 0.1 mol L^{-1} glycerol oxidation in 1.0 mol L^{-1} NaOH electrolyte from 0.05 V to 1.15 V vs. RHE on **(B)** a Pt/C catalyst and **(C)** a $Pt_{0.9}Bi_{0.1}$/C catalyst (T = 20 °C, can rate: 1 mV s^{-1}, resolution 4 cm^{-1}) (Simões et al., 2011, 2012).

RHE on Pt_9Bi_1/C and $Pt_{4.5}Pd_{4.5}Bi_1$/C catalysts, which made these catalysts among the most active ones at low electrode potentials. On *in situ* infrared spectra recorded for the electrooxidation of 0.1 M glycerol in 1.0 M NaOH electrolyte on Pt_9Bi_1/C (**Figure 8A**), a first absorption band appearing at ca. 1,225 cm^{-1} as soon as 0.2 V vs. RHE, i.e., as soon as the Pt_9Bi_1/C catalyst started to be active for glycerol oxidation, was assigned to the formation of glyceraldehyde. Another band at ca. 1335 cm^{-1} appeared from ca. 0.3 V to ca. 0.7 V which corresponded to the formation of dihydroxyacetone. For higher potentials, the absorption peaks located at ca. 1310 cm^{-1}, 1385 cm^{-1}, and 1570 cm^{-1} were assigned to the formation of glycerate and other carboxylate ions. The very high selectivity at low potentials of Pt_9Bi_1/C and $Pt_{4.5}Pd_{4.5}Bi_1$/C toward aldehyde and ketones was explained in terms of absence of water activation on these catalysts for potential lower than 0.6 V vs. RHE, and further the non-occurrence of the bifunctional mechanism. At last, *in situ* infrared measurements indicated that the presence of Bi led to avoid the formation of adsorbed CO species on the Pt surface since the absorption bands between ca. 1,950 and 2,000 cm^{-1} assigned to adsorbed CO species visible on Pt/C (**Figure 8B**) could not be detected in spectra recorded on Pt_9Bi_1/C (**Figure 8C**) for the glycerol oxidation. This meant that the presence of bismuth made Pt less efficient for the C-C bond breaking and further that $Pt_{0.9}Bi_{0.1}$/C led to higher selectivity into C3 compounds.

Cobos-Gonzalez et al. (2016) confirmed these *in situ* infrared spectroscopy results by HPLC analysis of reaction products obtained after chroamperometry measurements in an electrolysis cell fitted with a 5 cm^2 Pt/C cathode for the hydrogen evolution reaction, a $Pt_{0.9}Bi_{0.1}$/C anode for the glycerol oxidation reaction (metal loading of the electrodes 1.6 mg cm^{-2} and Nafion loading ca. 0.8 mg cm^{-2}) placed on each side of a simple blotting paper as separator and mechanically pressed in the cell. The measurements were performed at 20°C in a 2 M glycerol and 0.5 M NaOH aqueous solution at cell voltages of 0.55 V and 0.7 V for 240 min. **Figure 9** displays the yields obtained in the different compounds. At a cell voltage of 0.55 V (corresponding to an anode potential of ca. 0.6 V vs. RHE, considering that hydrogen evolution reaction at Pt/C is a rapid reaction and that the cathode potential remained close to −0.05 V vs. RHE), a very high selectivity into the formation of glyceraldehyde was obtained (yield of ca. 80 %), whereas at 0.70 V (corresponding to an anode potential of ca. 0.75 V vs. RHE) the selectivity toward carboxylate increased at the expense of that of glyceraldehyde (yield of ca. 58 %).

Recently, Zhou et al. (2013) studied the selective electrooxidation of glycerol on Pt_xAu_y@Ag catalysts. Pt_4Au_6@Ag displayed the highest activity in both acidic and alkaline media, the higher current densities being reached in alkaline medium. The product distribution from glycerol oxidation at 0.5, 0.7, 0.9, 1.1, and 1.3 V were analyzed by HPLC, and it was found that the catalysts led to a mixture of nine C1 to C3 acids together with glyceraldehyde and dihydroxyacetone. However, the Pt_4Au_6@Ag catalyst allowed obtaining the largest DHA selectivity of 77 % at 1.1 V.

CONCLUSION

A comprehensive short overview of the electrooxidation of glycerol with the aim at producing value-added chemicals is presented in this contribution. The objective was to highlight some trends which could allow increasing both the glycerol conversion rate and the selectivity toward given compounds or chemical functions.

In acidic media, platinum is unavoidable for this electrocatalytic reaction. On pure platinum, the onset glycerol oxidation potential achieved was not lower than 0.4 V vs. RHE and a relatively low selectivity (mixture of compounds) was obtained. The modification of platinum by p-group elements allowed decreasing the onset potential and obtaining high selectivity toward dihydroxyacetone (with Bi and Sb) or glyceraldehyde (with Pb, Sn, and In) over a small potential range before a mixture of C3, C2, and C1 carboxylic acids started to be formed.

In alkaline media, non-noble metals, particularly nickel-based catalysts, become stable and active for the electrooxidation of glycerol. But the reaction occurs at very high potentials (higher than 1.1 V vs. RHE) and with low selectivity into C3 compounds, leading to a mixture of C3, C2, and C1 molecules. Gold also become active in alkaline media, as active as palladium, leading both to an onset potential of ca. 0.6 V vs. RHE. However, gold is less prone to poisoning by adsorbed species than Pd, which make it more selective toward C3 carboxylates and hydroxypyruvate. Pt remains still the most active materials in alkaline media, with an onset potential of ca. 0.4 V vs. RHE but leads to the same reaction pathway as Pd involving the formation of glyceraldehyde and dihydroxyacetone as first intermediates and glycerate/tartronate as secondary reaction products, as well as C-C bond breaking with adsorbed CO species and C1 to C3 compounds.

The modification of Pd/C nanocatalysts by d-group elements decreases the onset potential of glycerol oxidation, but does not change the selectivity, which remains the same as with pure Pd/C or pure Pt/C. The modification of Pd catalysts by p-group elements, such as bismuth and Sn, also leads to lower onset potentials of glycerol oxidation and higher activity and to changes in selectivity. The first important observation is that the presence of bismuth and tin on Pd surfaces leads to avoid the dissociative adsorption of glycerol (C-C bond breaking) and the formation of adsorbed CO species. Therefore, the selectivity toward C3 carboxylates is enhanced. It is worst also to note that the structure and morphology of the catalysts play a role for the selectivity the selectivity: glycerate and tartronate with Pd/C and hydroxypyruvate with Pd nanofoam.

The modification of Pt/C by bismuth leads to decrease the onset potential of glycerol oxidation to very low values (ca. 0.2 V vs. RHE). As for Pd, it leads to avoid the C-C bond breaking over a large potential range. The very wide potential range of activity provides different potential regions where different selectivities are obtained. Between 0.2 V vs. RHE and 0. 55 V vs. RHE, a Pt_9Bi_1/C catalyst display very high selectivity toward glyceraldehyde and dihydroxyacetone, whereas for potential between 0. 6 and 1.0 V vs. RHE, this catalyst presents very high selectivity into C3 carboxylates, particularly glycerate.

From these results, it seems that a lower onset potential of glycerol oxidation, a wider potential range of activity of a catalyst and a lower ability of the catalytic surface to adsorb dissociatively glycerol are the key parameters for achieving the best selectivity toward a unique desired compound at the best conversion rate.

AUTHOR CONTRIBUTIONS

All authors listed have made a substantial, direct and intellectual contribution to the work, and approved it for publication.

REFERENCES

Aarthy, M., Saravanan, P., Gowthaman, M. K., Rose, C., and Kamini, N. R. (2014). Enzymatic transesterification for production of biodiesel using yeast lipases: an overview. *Chem. Eng. Res. Des.* 92, 1591–1601. doi: 10.1016/j.cherd.2014.04.008

Adzic, R. R. (1984). "Electrocatalysis on surfaces modified by foreign metal adatoms," in *Advances in Electrochemistry and Electrochemical Engineering*, eds H. Gerisher, C. W. Tobias (New York, NY: Wiley- Interscience), 159–260.

Aldiguier, A. S., Alfenore, S., Cameleyre, X., Goma, G., Uribelarrea, J. L., Guillouet, S. E., et al. (2004). Synergistic temperature and ethanol effect on *Saccharomyces cerevisiae* dynamic behaviour in ethanol bio-fuel production. *Bioprocess. Biosyst. Eng.* 26, 217–222. doi: 10.1007/s00449-004-0352-6

Angerstein-Kozlowska, H., Conway, B. E., Hamelin, A., and Stoicoviciu, L. (1986). Elementary steps of electrochemical oxidation of single-crystal planes of Au - I. chemical basis of processes involving geometry of anions and the electrode surfaces. *Electrochim. Acta* 31, 1051–1061. doi: 10.1016/0013-4686(86)80020-2

Bambagioni, V., Bevilacqua, M., Bianchini, C., Filippi, J., Lavacchi, A., Marchionni, A., et al. (2010). Selfsustainable production of hydrogen, chemicals, and energy from renewable alcohols by electrocatalysis. *ChemSusChem* 3, 851–855. doi: 10.1002/cssc.201000103

Bambagioni, V., Bianchini, C., Marchionni, A., Filippi, J., Vizza, F., Teddy, J., et al. (2009). Pd and Pt–Ru anode electrocatalysts supported on multi-walled carbon nanotubes and their use in passive and active direct alcohol fuel cells with an anion-exchange membrane (alcohol = methanol, ethanol, glycerol). *J. Power Sources* 190, 241–251. doi: 10.1016/j.jpowsour.2009.01.044

Beden, B., Çetin, I., Kahyaoglu, A., Takky, D., and Lamy, C. (1987). Electrocatalytic oxidation of saturated oxygenated compounds on gold electrodes. *J. Catal.* 104, 37–46. doi: 10.1016/0021-9517(87)90334-4

Beden, B., and Lamy, C. (1988). Infrared reflectance spectroscopy, in "*Spectroelectrochemistry: Theory and Practice*", ed R. J. Gale (New York, NY: Plenum Press), 189–261.

Behr, A., Eilting, J., Irawadi, K., Leschinski, J., and Lindner, F. (2008). Improved utilisation of renewable resources: new important derivatives of glycerol. *Green Chem.* 10, 13–30. doi: 10.1039/B710561D

Benipal, N., Qi, J., Gentile, J. C., and Li, W. (2017). Direct glycerol fuel cell with polytetrafluoroethylene (PTFE) thin film separator. *Renew. Energ.* 105, 647–655 doi: 10.1016/j.renene.2016.12.028

Boutonnet, M., Kizling, J., Stenius, P., and Maire, G. (1982). The preparation of monodisperse colloidal metal particles from microemulsions. *Colloids Surf.* 5, 209–225. doi: 10.1016/0166-6622(82)80079-6

Carrettin, S., McMorn, P., Johnston, P., Griffin, K., Kiely, C. J., Attard, G. A., et al. (2004). Oxidation of glycerol using supported gold catalysts. *Top. Catal.* 27, 131–136. doi: 10.1023/B:TOCA.0000013547.35106.0d

Chen, Y. X., Lavacchi, A., Miller, H. A., Bevilacqua, M., Filippi, J., Innocenti, M., et al. (2014). Nanotechnology makes biomass electrolysis more energy efficient than water electrolysis. *Nat. Commun.* 5, 4036:1–6. doi: 10.1038/ncomms5036

Ciminna, R., Della Pina, C., Rossi, M., and Pagliar, M. (2014). Understanding the glycerol market. *Eur. J. Lipid Sci. Technol.* 116, 1432–1439. doi: 10.1002/ejlt.201400229

Clacens, J. M., Pouilloux, Y., and Barrault, J. (2002). Selective etherification of glycerol to polyglycerols over impregnated basic MCM-41 type mesoporous catalysts. *Appl. Catal. A.* 227, 181–190. doi: 10.1016/S0926-860X(01)00920-6

Cobos-Gonzalez, J., Baranton, S., and Coutanceau, C. (2016). Development of bi-modified PtPd nanocatalysts for the electrochemical reforming of polyols into hydrogen and value-added chemicals. *ChemElectroChem.* 3, 1694–1704. doi: 10.1002/celc.201600147

Coutanceau, C., Brimaud, S., Dubau, L., Lamy, C., Léger, J. M., Rousseau, S., et al. (2008). Review of different methods for developing nanoelectrocatalysts for the oxidation of organic compounds. *Electrochim. Acta* 53, 6865–6880. doi: 10.1016/j.electacta.2007.12.043

Coutanceau, C., Zalineeva, A., Baranton, S., and Simões, M. (2014). Modification of palladium surfaces by bismuth adatoms or clusters: effect on electrochemical activity and selectivity towards polyol electrooxidation. *Int. J. Hyd. Energy* 39, 15877–15886. doi: 10.1016/j.ijhydene.2014.03.076

Couto, A., Rincón, A., Pérez, M. C., and Gutiérrez, C. (2001). Adsorption and electrooxidation of carbon monoxide on polycrystalline platinum at pH 0.3–13. *Electrochim. Acta* 46, 1285–1296. doi: 10.1016/S0013-4686(00)00714-3

da Silva, G. P., Mack, M., and Contiero, J. (2009). Glycerol: a promising and abundant carbon source for industrial microbiology. *Biotechnol. Adv.* 27, 30–39. doi: 10.1016/j.biotechadv.2008.07.006

Da Silva, R. G., Neto, S. A., Kokoh, K. B., and De Andrade, A. R. (2017). Electroconversion of glycerol in alkaline medium: from generation of energy to formation of value-added products. *J. Power Sources* 351, 174–182 doi: 10.1016/j.jpowsour.2017.03.101

Dailey, A., Shin, J., and Korzeniewski, C. (1998). Ethylene glycol electrochemical oxidation at platinum probed by ion chromatography and infrared spectroscopy. *Electrochim. Acta* 44, 1147–1152. doi: 10.1016/S0013-4686(98)00217-5

Dasari, M. A., Kiatsimkul, P. P., Sutterlin, W. R., and Suppes, G. J. (2005). Low-pressure hydrogenolysis of glycerol to propylene glycol. *Appl. Catal. A.* 281, 225–231. doi: 10.1016/j.apcata.2004.11.033

Dash, S., and Munichandraiah, N. (2015). Nanoflowers of PdRu on PEDOT for electrooxidation of glycerol and its analysis. *Electrochim. Acta* 180, 339–352. doi: 10.1016/j.electacta.2015.07.020

Dubau, L., Hahn, F., Coutanceau, C., Léger, J.-M., and Lamy, C. (2003). On the structure effects of bimetallic PtRu electrocatalysts towards methanol oxidation. *J. Electroanal. Chem.* 554–555, 407–415. doi: 10.1016/S0022-0728(03)00308-5

Fleischmann, M., Korinek, K., and Pletcher, D. (1971). The oxidation of organic compounds at a nickel anode in alkaline solution. *J. Electroanal. Chem.* 31, 39–49. doi: 10.1016/S0022-0728(71)80040-2

Fleischmann, M., Korinek, K., and Pletcher, D. (1972). The kinetics and mechanism of the oxidation of amines and alcohols at oxide-covered nickel, silver, copper, and cobalt electrodes. *J. Chem. Soc. Perkin Trans.* 2, 1396–1403 doi: 10.1039/p29720001396

Gallezot, P. (1997). Selective oxidation with air on metal catalysts. *Catal. Today* 37, 405–418. doi: 10.1016/S0920-5861(97)00024-2

Gasteiger, H. A., Kocha, S. S., Sompalli, B., and Wagner, F. T. (2005). Activity benchmarks and requirements for Pt, Pt-alloy, and non-Pt

oxygen reduction catalysts for PEMFCs. *Appl. Catal. B: Env.* 56, 9–35. doi: 10.1016/j.apcatb.2004.06.021

Gomes, J. F., Castelo de Paula, F. B., Gasparotto, L. H. S., and Tremiliosi-Filho, G. (2012). The influence of the Pt crystalline surface orientation on the glycerol electro-oxidation in acidic media. *Electrochim. Acta* 76, 88–93 doi: 10.1016/j.electacta.2012.04.144

Gomes, J. F., Garcia, A. C., Gasparotto, L. H. S., de Souza, N. E., Ferreira, E. B., Pires, C., et al. (2014). Influence of silver on the glycerol electro-oxidation over AuAg/C catalysts in alkaline medium: a cyclic voltammetry and in situ FTIR spectroscopy study. *Electrochim. Acta* 144, 361–368 doi: 10.1016/j.electacta.2014.08.035

Gomes, J. F., Martins, C. A., Giz, M. J., Tremiliosi-Filho, G., and Camara, G. A. (2013). Insights into the adsorption and electro-oxidation of glycerol: Self-inhibition and concentration effects. *J. Catal.* 301, 154–161. doi: 10.1016/j.jcat.2013.02.007

Habibi, E., and Razmi, H. (2012). Glycerol electrooxidation on Pd, Pt and Au nanoparticles supported on carbon ceramic electrode in alkaline media. *Int. J. Hyd. Energy* 37, 16800–16809 doi: 10.1016/j.ijhydene.2012.08.127

Hogarth, M. P., and Ralph, T. R. (2002). Catalysis for low temperature fuel cells, Part III: challenges for the direct methanol fuel cell. *Met. Rev.* 46, 146–164.

Holade, Y., Morais, C., Servat, K., Napporn, T. W., and Kokoh, K. B. (2013). Toward the electrochemical valorization of glycerol: fourier transform infrared spectroscopic and chromatographic studies. *ACS Catal.* 3, 2403–2411. doi: 10.1021/cs400559d

Houache, M. S. E., Cossar, E., Ntais, S., and Baranova, E. A. (2018). Electrochemical modification of nickel surfaces for efficient glycerol electrooxidation. *J. Power Sources* 375, 310–319. doi: 10.1016/j.jpowsour.2017.08.089

Ilie, A., Simoes, M., Baranton, S., Coutanceau, C., and Martemianov, S. (2011). Influence of operational parameters and of catalytic materials on electrical performance of direct glycerol solid alkaline membrane fuel cells. *J. Power Sources* 196, 4965–4971. doi: 10.1016/j.jpowsour.2011.02.003

Jeffery, D. Z., and Camara, G. A. (2010). The formation of carbon dioxide during glycerol electrooxidation in alkaline media: first spectroscopic evidences. *Electrochem. Commn.* 12, 1129–1132. doi: 10.1016/j.elecom.2010.06.001

Jiang, Y.-X., Sun, S.-G., and Ding, N. (2001). Novel phenomenon of enhancement of IR absorption of CO adsorbed on nanoparticles of Pd confined in supercages of Y-zeolite. *Chem. Phys. Lett.* 344, 463–470. doi: 10.1016/S0009-2614(01)00812-0

Kabbabi, A., Faure, R., Durand, R., Beden, B., Hahn, F., Léger, J .-M., et al. (1998). *In situ* FTIRS study of the electrocatalytic oxidation of carbon monoxide and methanol at platinum–ruthenium bulk alloy electrodes. *J. Electroanal. Chem.* 444, 41–53. doi: 10.1016/S0022-0728(97)00558-5

Katryniok, B., Kimura, H., Skrzynska, E., Girardon, J.-S., Fongarland, P., Capron, M., et al. (2011). Selective catalytic oxidation of glycerol: perspectives for high value chemicals. *Green Chem.* 13, 1960–1979. doi: 10.1039/c1gc15320j

Kim, H. J., Lee, J., Green, S. K., Huber, G. W., and Kim, W. B. (2014). Selective glycerol oxidation by electrocatalytic dehydrogenation. *ChemSusChem* 7, 1051–1056. doi: 10.1002/cssc.201301218

Kim, H. J., M., Choi, S., Green, S., Tompsett, G. A., Lee, S. H., et al. (2011). Highly active and stable PtRuSn/C catalyst for electrooxidations of ethylene glycol and glycerol. *Appl. Catal. B: Env*. 101, 366–375. doi: 10.1016/j.apcatb.2010.10.005

Kim, Y., Woo Kim, H., Lee, S., Han, J., Lee, D., Kim, J.-R., et al. (2017). The role of ruthenium on carbon-supported PtRu catalysts for electrocatalytic glycerol oxidation under acidic conditions. *ChemCatChem* 9, 1683–1690. doi: 10.1002/cctc.201601325

Kongjao, S., Damronglerd, S., and Hunsom, M. (2011). Electrochemical reforming of an acidic aqueous glycerol solution on Pt electrodes. *J Appl. Electrochem.* 41, 215–222. doi: 10.1007/s10800-010-0226-3

Kwon, Y., Birdja, Y., Spanos, I., Rodriguez, P., and Koper, M. T. M. (2012). Highly selective electro-oxidation of glycerol to dihydroxyacetone on platinum in the presence of bismuth. *ACS Catal.* 2, 759–764. doi: 10.1021/cs200599g

Kwon, Y., Hersbach, T. J. P., and Koper, M. T. M. (2014). Electro-oxidation of glycerol on platinum modified by adatoms: activity and selectivity effects. *Top Catal.* 57, 1272–1276. doi: 10.1007/s11244-014-0292-6

Kwon, Y., and Koper, M. T. (2010). Combining voltammetry with HPLC: application to electro-oxidation of glycerol. *Anal. Chem.* 82, 5420–5424. doi: 10.1021/ac101058t

Kwon, Y., Lai, S. C. S., Rodriguez, P., and Koper, M. T. M. (2011a). Electrocatalytic oxidation of alcohols on gold in alkaline media: base or gold catalysis? *J. Am. Chem. Soc.* 133, 6914–6917. doi: 10.1021/ja200976j

Kwon, Y., Schouten, K. J. P., and Koper, M. T. M. (2011b). Mechanism of the catalytic oxidation of glycerol on polycrystalline gold and platinum electrodes. *ChemCatChem* 3, 1176–1185. doi: 10.1002/cctc.201100023

Lee, D., Kim, Y., Kwon, Y., Lee, J., Kim, T.-W., Noh, Y., et al. (2019). Boosting the electrocatalytic glycerol oxidation performance with highly-dispersed Pt nanoclusters loaded on 3D graphene-like microporous carbon. *Appl. Catal. B: Env.* 245, 555–558. doi: 10.1016/j.apcatb.2019.01.022

Léger, J.-M., Rousseau, S., Coutanceau, C., Hahn, F., and Lamy, C. (2005). How bimetallic electrocatalysts does work for reactions involved in fuel cells?: example of ethanol oxidation and comparison to methanol. *Electrochim. Acta* 50, 5118–5125. doi: 10.1016/j.electacta.2005.01.051

Lin, Q., Wei, Y., Liu, W., Yu, Y., and Hu, J. (2017). Electrocatalytic oxidation of ethylene glycol and glycerol on nickel ion implanted-modified indium tin oxide electrode. *Int. J. Hydr Energy* 42, 1403–1411 doi: 10.1016/j.ijhydene.2016.10.011

Mamaca, N., Mayousse, E., Arrii-Clacens, S., Napporn, T. W., Servat, K., Guillet, N., et al. (2012). Electrochemical activity of ruthenium and iridium-based catalysts for oxygen evolution reaction. *Appl. Catal. B: Env.* 111/112, 376–380. doi: 10.1016/j.apcatb.2011.10.020

Oliveira, V. L., Morais, C., Servat, K., Napporn, T. W., Tremiliosi-Filho, G., and Kokoh, K. B. (2013). Glycerol oxidation on nickel based nanocatalysts in alkaline medium – identification of the reaction products. *J. Electroanal. Chem.* 703, 56–62. doi: 10.1016/j.jelechem.2013.05.021

Oliveira, V. L., Morais, C., Servat, K., Napporn, T. W., Tremiliosi-Filho, G., and Kokoh, K. B. (2014). Studies of the reaction products resulted from glycerol electrooxidation on Ni-based materials in alkaline medium. *Electrochim. Acta* 117, 255–262. doi: 10.1016/j.electacta.2013.11.127

Ottoni, C. A., da Silva, S. G., De Souza, R. F. B., and Neto, A. O. (2016). Glycerol oxidation reaction using PdAu/C electrocatalysts. *Ionics* 22, 1167–1175 doi: 10.1007/s11581-015-1631-8

Pagliaro, M. (2017). *Glycerol: The Renewable Platform Chemical*. Amsterdam: Elsevier.

Pagliaro, M. V., Bellini, M., Bevilacqua, M., Filippi, J., Folliero, M. G., Marchionni, A., et al. (2017). Carbon supported Rh nanoparticles for the production of hydrogen and chemicals by the electroreforming of biomass-derived alcohols. *RSC Adv.* 7, 13971–13978. doi: 10.1039/C7RA00044H

Podlovchenko, B. I., Petrii, O. A., Frumkin, A. N., and Lal, H. (1966). The behavior of a platinized-platinum electrode in solutions of alcohols containing more than one carbon atom, aldehydes and formic acid. *J. Electroanal. Chem.* 11, 12–25. doi: 10.1016/0022-0728(66)80053-0

Roquet, L., Belgsir, E. M., Léger, J.-M., and Lamy, C. (1994). Kinetics and mechanisms of the electrocatalytic oxidation of glycerol as investigated by chromatographic analysis of the reaction products: potential and pH effects. *Electrochim Acta* 39, 2387–2394. doi: 10.1016/0013-4686(94)E0190-Y

Schmidt, T. J., Behm, R. J., Grgur, B. N., Markovic, N. M., and Ross Jr, P. N. (2000). Formic Acid oxidation on pure and Bi-modified Pt(111): temperature effects. *Langmuir* 16, 8159–8166. doi: 10.1021/la000339z

Schnaidt, J., Heinen, M., Denot, D., Jusys, Z., and Behm, R. J. (2011). Electrooxidation of glycerol studied by combined in situ IR spectroscopy and online mass spectrometry under continuous flow conditions. *J. Electroanal. Chem.* 661, 250–264. doi: 10.1016/j.jelechem.2011.08.011

Serov, A., Martinez, U., and Atanassov, P. (2013). Novel Pd–In catalysts for alcohols electrooxidation in alkaline media. *Electrochem. Commun.* 34, 185–188. doi: 10.1016/j.elecom.2013.06.003

Sheldon, R. A. (2017). The E factor 25 years on: the rise of green chemistry and sustainability. *Green. Chem.* 19, 18–43. doi: 10.1039/C6GC02157C

Silva, L. S. R., López-Suárez, F. E., Perez-Cadenas, M., Santos, S. F., da Costa, L. P., Eguiluz, K. I. B., et al. (2016). Synthesis and characterization of highly active Pb$_x$@Pt$_y$/C core-shell nanoparticles toward glycerol electrooxidation. *Appl. Catal. B: Env.* 198, 38–48 doi: 10.1016/j.apcatb.2016.04.046

Simões, M., Baranton, S., and Coutanceau, C. (2010). Electro-oxidation of glycerol at Pd based nano-catalysts for an application in alkaline fuel cells for chemicals and energy cogeneration. *Appl. Catal. B: Env.* 93, 354–362 doi: 10.1016/j.apcatb.2009.10.008

Simões, M., Baranton, S., and Coutanceau, C. (2011). Enhancement of catalytic properties for glycerol electrooxidation on Pt and Pd nanoparticles induced by Bi surface modification. *Appl. Catal. B: Env.* 110, 40–49. doi: 10.1016/j.apcatb.2011.08.020

Simões, M., Baranton, S., and Coutanceau, C. (2012). Electrochemical valorization of glycerol. *ChemSusChem* 5, 2106–2124. doi: 10.1002/cssc.201200335

Smirnova, N. W., Petrii, O. A., and Grzejdziak, A. (1988). Effect of ad-atoms on the electro-oxidation of ethylene glycol and oxalic acid on platinized platinum. *J. Electroanal. Chem.* 251, 73–87. doi: 10.1016/0022-0728(88)80386-3

Tehrani, R. M. A., and Ab Ghani, S. (2012). Electrocatalysis of free glycerol at a nanonickel modified graphite electrode and its determination in biodiesel. *Electrochim. Acta* 70, 153–157. doi: 10.1016/j.electacta.2012.03.044

Valter, M., Busch, M., Wickman, B., Grönbeck, H., Baltrusaitis, J., and Hellman, A. (2018). Electrooxidation of glycerol on gold in acidic medium: a combined experimental and DFT Study. *J. Phys. Chem. C* 122, 10489–10494. doi: 10.1021/acs.jpcc.8b02685

Venancio, E. C., Napporn, W. T., and Motheo, A. J. (2002). Electro-oxidation of glycerol on platinum dispersed in polyaniline matrices. *Electrochim. Acta* 47, 1495–1501. doi: 10.1016/S0013-4686(01)00877-5

Villa, A., Dimitratos, N., Chan-Thaw, C. E., Hammond, C., Prati, L., and Hutchings, G. J. (2015). Glycerol oxidation using gold-containing catalysts. *Acc. Chem. Res.* 48, 1403–1412. doi: 10.1021/ar500426g

Wang, W., Kang, Y., Yang, Y., Liu, Y., Chai, D., and Lei, Z. (2016). PdSn alloy supported on phenanthroline-functionalized carbon as highly active electrocatalysts for glycerol oxidation. *Int. J. Hydro Energy* 41, 1272–1280 doi: 10.1016/j.ijhydene.2015.11.017

Wang, Y., Li, L., Hu, L., Zhuang, L., Lu, J., and Xu, B. (2003). A feasibility analysis for alkaline membrane direct methanol fuel cell: thermodynamic disadvantages versus kinetic advantages. *Electrochem. Commun.* 5, 662–666. doi: 10.1016/S1388-2481(03)00148-6

Watanabe, M., and Motoo, S. (1975). Electrocatalysis by ad-atoms. 2. enhancement of oxidation of methanol on platinum by ruthenium ad-atoms. *J. Electroanal. Chem.* 60, 267–273. doi: 10.1016/S0022-0728(75)80261-0

Zalineeva, A., Baranton, S., and Coutanceau, C. (2013). Bi-modified palladium nanocubes for glycerol electrooxidation. *Electrochem. Comm.* 34, 335–338. doi: 10.1016/j.elecom.2013.07.022

Zalineeva, A., Baranton, S., and Coutanceau, C. (2015). How do Bi-modified palladium nanoparticles work towards glycerol electrooxidation? an in situ FTIR study. *Elecrtochim. Acta* 176, 705–717. doi: 10.1016/j.electacta.2015.07.073

Zalineeva, A., Padilla, M., Martinez, U., Serov, A., Artyushkova, K., Baranton, S., et al. (2014). Self-supported Pd-Bi catalysts for the electrooxidation of glycerol in alkaline media. *J. Am. Chem. Soc.* 136, 3937–3945. doi: 10.1021/ja412429f

Zhou, Y., Shen, Y., and Xi, J. (2013). Seed-mediated synthesis of $Pt_xAu_y@Ag$ electrocatalysts for the selective oxidation of glycerol. *Appl. Catal. B: Env.* 245, 604–612 doi: 10.1016/j.apcatb.2019.01.009

Extending Catalyst Life in Glycerol-to-Acrolein Conversion Using Non-thermal Plasma

Lu Liu[1], Xiaofei Philip Ye[1]*, Benjamin Katryniok[2], Mickaël Capron[2], Sébastien Paul[2] and Franck Dumeignil[2]

[1] Department of Biosystems Engineering and Soil Science, The University of Tennessee, Knoxville, TN, United States, [2] Univ. Lille, CNRS, Centrale Lille, ENSCL, Univ. Artois, UMR 8181 - UCCS - Unité de Catalyse et Chimie du Solide, Lille, France

Booming biodiesel production worldwide demands valorization of its byproduct of glycerol. Acrolein, an important intermediate chemical, can be produced by gas-phase glycerol dehydration catalyzed by solid acids. Because catalysts that lead to high acrolein selectivity usually deactivate rapidly due to the formation of coke that blocks the active sites on their surface, one major challenge of this method is how to extend the service life of the catalyst. Silica-supported silicotungstic acid (HSiW-Si) is a good example of such a catalyst that shows good activity in glycerol dehydration to acrolein initially, but deactivates quickly. In this study, HSiW-Si was selected to probe the potential of using non-thermal plasma with oxygen-containing gas as the discharge gas (NTP-O$_2$) to solve the catalyst deactivation problem. NTP-O$_2$ was found to be effective in coke removal and catalyst regeneration at low temperatures without damaging the Keggin structure of the HSiW-Si catalyst.

Keywords: non-thermal plasma, glycerol, acrolein, coking, deactivation, catalyst regeneration

INTRODUCTION

Acrolein, the simplest unsaturated aldehyde, is an important intermediate leading to many useful chemicals and materials, such as methionine, and acrylic acid and its esters (Liu et al., 2012). The manufacturing method for acrolein has been partial oxidation of propylene since the 1950s (Weigert and Haschke, 1976). The market demand for propylene far exceeds its availability. Securing this raw material supply is now becoming highly strategic in a tough competition among downstream applications. Recently, an alternative scheme for acrolein production from glycerol has become a promising candidate, since glycerol, which is co-produced with biodiesel, has become abundantly available (Cheng et al., 2013; Katryniok et al., 2013; Zou et al., 2016). This value-added synthesis from glycerol to acrolein could alleviate propylene supply issue while providing a sustainable approach for backing up the biodiesel industry viability.

Highly efficient solid acid catalysts are the key in the gas-phase reaction to produce bio-based acrolein from glycerol. Suitable acidity of the catalysts leads to a high selectivity to acrolein, but unfortunately also results in severe coke formation, and consequently, the deactivation of the catalysts (Alhanash et al., 2010). Good glycerol conversion and acrolein yield have been achieved with many solid acid catalysts (Chai et al., 2007; Tsukuda et al., 2007; Atia et al., 2008; Alhanash et al., 2010), with the major remaining challenge being how to extend the service life of the catalyst (Katryniok et al., 2009, 2010, 2013; Liu et al., 2012). If the catalyst deactivation problem cannot

be solved, industrialization of this bio-based acrolein production from glycerol is not promising. Therefore, studies focusing on extending the catalyst life are necessary.

Silicotungstic acid ($H_4SiW_{12}O_{40}$, hereafter abbreviated as HSiW) is a commercially available heteropoly acid, and supported HSiW has been proven as one of the best performers among many studied catalysts in achieving high yield for the glycerol-to-acrolein conversion (Tsukuda et al., 2007; Atia et al., 2008; Liu et al., 2012). However, because of its strong acidity, supported HSiW unavoidably suffers from severe deactivation due to coke formation. The Keggin structure (Wu et al., 1996; Timofeeva, 2003), the most important feature of HSiW, is retained intact after coke formation (Kozhevnikov, 2007). Deposited coke has been reported to occur as an amorphous form, and its existence would not alter any crystalline structure of the catalyst (Wang et al., 2009, 2010; Alhanash et al., 2010). Therefore, supported HSiW can be regenerated to regain the acid catalytic activity if the deposited coke is removed.

Carbonaceous coke is a distribution of polynuclear aromatic substances of aliphatic and alicyclic compounds usually formed via condensation, hydrogen abstraction, polymerization, and repetitions of these reactions (Khan and Al-Jalal, 2008). The terms "soft" and "hard" refer to the relative properties of coke those are associated with the structural complexity and degree of polymerization of the carbonaceous substances. "Harder" coke is more complex in structure and more difficult to burn off. Catalyst deactivation due to coking is common in industrial chemical production processes; an example is catalytic cracking of petroleum fractions (Khan and Al-Jalal, 2008). The routine treatment is to flush the catalyst bed with oxygen-containing gas at elevated temperatures, usually 450–600°C, but depending on the catalyst characteristics and specific reactions, higher temperatures (600–800°C) may be required to remove the coke (Tanabe, 1989; Khan and Al-Jalal, 2004; Chai et al., 2008). A problem encountered is that the Keggin structure of HSiW can only be maintained up to 400°C (Atia et al., 2008) [one study claims up to only 300°C (Bardin and Davis, 2000)], depending on the characteristics of the supports. Consequently, regeneration using the high-temperature combustion approach will remove the coke only at the cost of reducing catalytic activity afterwards, due to the damage of the Keggin structure and consequently significant loss of activity (Atia et al., 2008; Katryniok et al., 2012). Therefore, this conventional decoking treatment is not suitable for regenerating supported HSiW for the acrolein production process.

Non-thermal plasma (NTP) can initiate the formation of ions, free radicals, and other highly reactive intermediates at low temperatures. In an O_2-containing atmosphere, NTP can convert the O_2 molecule into many highly reactive oxygen species, including the triplet ground-state oxygen atom $O(^3P)$, the metastable oxygen atom $O(^1D)$, the metastable oxygen molecule $O_2(^1\Delta g)$, and ozone O_3 (Fridman, 2008). When humidity is present, additional highly reactive species are formed, such as H_2O^+, free H atoms, and OH radicals (Fridman, 2008). Most of these species are highly oxidative and can oxidize substances that fail to be oxidized by O_2 or air under mild temperature conditions. Therefore, non-thermal

plasma with oxygen-containing gas as the discharge gas (NTP-O_2) is very likely to contribute to solving the deactivation problem of a solid acid catalyst having low thermal stability. Regenerating deactivated catalysts is a challenging issue of industrial importance; depending on the catalyst's characteristics and the reaction in which it is used, the deactivated catalysts can vary significantly in their coke profile, and thus they may vary in term of how difficult it is for them to be regenerated (Silva et al., 2004). Therefore, it is worth expending some effort on regenerating a promising acid catalyst deactivated in the glycerol-dehydration process.

The objective of this study was to investigate the effectiveness of NTP-O_2 in the coke removal (decoking) and regeneration of deactivated solid acid catalysts to increase the potential of bio-based acrolein production in industrial applications.

MATERIALS AND METHODS

Catalyst and Catalytic Reaction

Silica-supported silicotungstic acid (HSiW-Si) would be a good catalyst for acrolein production from glycerol if it did not deactivate so quickly (Tsukuda et al., 2007). Therefore, HSiW-Si was chosen as an excellent candidate to explore the potential of applying NTP-O_2 to extending catalyst service life. The experiments in this study were designed to evaluate whether NTP-O_2 can be effective in removing the coke from catalyst surface and regenerating the deactivated catalyst. Ultimately, the method developed in this study for glycerol dehydration to acrolein could be applied to other catalytic reactions using solid catalysts that have relatively low thermal stability.

Mesoporous silica granules (SiO_2, Davicat® Si1252) were supplied by Grace-Davison (Columbia, MD, USA). The silica granules have particle sizes of 1 to 3 mm, an average pore diameter of 11 nm, and an average surface area of 390 m^2/g. Silicotungstic acid (HSiW) was purchased from Sigma Aldrich (St. Louis, MO, USA), and it was loaded on the catalyst support by the impregnation method. Briefly, HSiW of 10 wt.% on the basis of the silica support (Si) was dissolved in deionized water to make a 0.04 g/mL solution. The silica, which was previously calcined at 300°C in a muffle furnace for 2 h, was added to the HSiW solution. The mixture was set at room temperature for 24 h to reach the adsorption-desorption equilibrium. The resultant HSiW-Si solids were first dried at 55°C for 24 h, followed by further drying at 105°C for 6 h to complete dryness, and then calcined at 300°C in a muffle furnace for 2 h before the 2nd impregnation. The procedures were repeated for another 10 wt.% HSiW loading. Hence, a catalyst consisting of 20 wt.% HSiW on silica was obtained.

The as-obtained silica-supported HSiW catalyst (HSiW-Si) was used as a catalyst for the glycerol dehydration reaction (275°C, 7.5 h Time-On-Stream) that was carried out in a down-flow packed-bed reactor at atmospheric pressure (**Figure 1**). The reactor was made of a quartz tube (length 300 mm, ID 19.35 mm, OD 25.3 mm), which was heated by a heating tape evenly wrapped around the outer wall of the quartz tube. The heating tape was controlled by a PID temperature controller to maintain the desired temperature of the catalyst bed. The

FIGURE 1 | Experimental setup for glycerol dehydration at reaction temperature of 275°C (The optional elements inside dashed lines were used for the experiments described in section Evaluation of *in situ* Catalyst Regeneration by NTP).
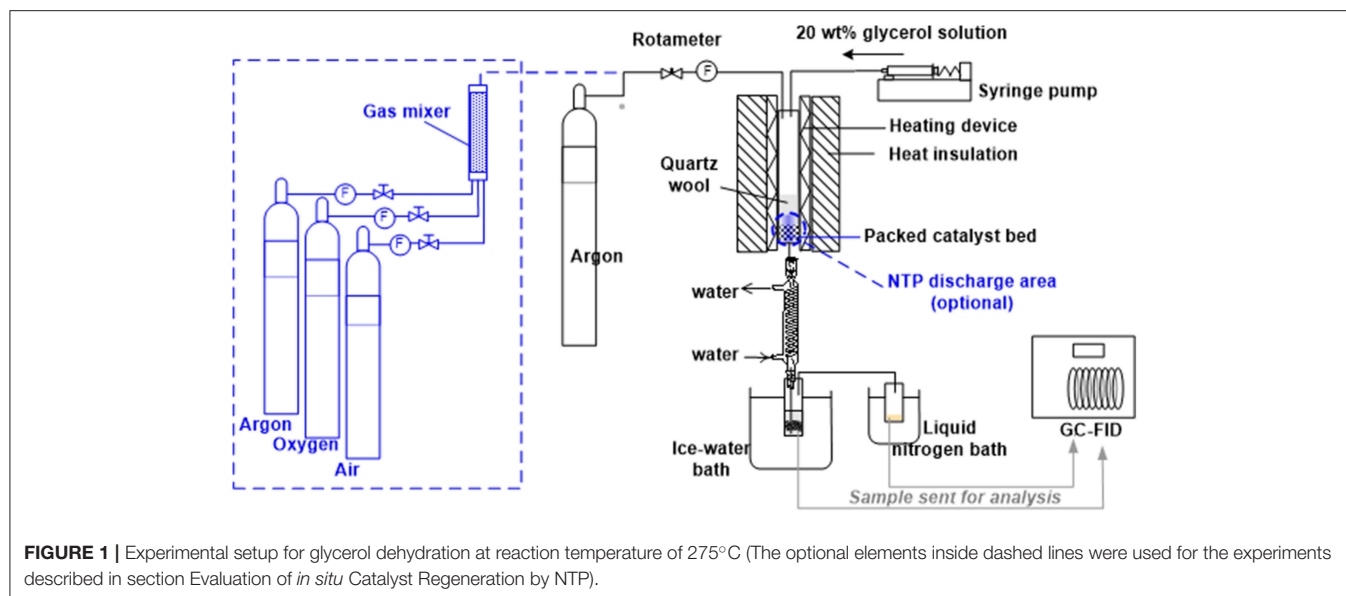
reactor had an external layer of thermal insulation to minimize the heat loss to the surroundings. Seven milliliter of HSiW-Si (~3.2 g) were packed at the lower end of the reactor, leaving a sufficient path length for the carrier gas and the glycerol feed to be preheated to the desired temperature before reaching the catalyst bed. The glycerol solution (20 wt.% of glycerol in water) was fed by a syringe pump at 6 mL/h feeding rate, resulting in an 84 h^{-1} gas hourly space velocity (GHSV) of glycerol. The flow rate of carrier gas argon (Ar) was regulated at 60 mL/min. The temperature of the catalyst bed was controlled at 275°C during the glycerol dehydration. Reaction effluent was first passed through a condenser with flowing tap water, and the majority of the liquid product was condensed in a 50 mL vial immersed in an ice-water cold bath (1st condensation stage). Any product that was not condensed in the first condensation stage was collected in a 20 mL vial that was immersed in a liquid nitrogen bath (2nd condensation stage). During the dehydration reaction, samples were collected every 1.5 h and analyzed using a gas chromatography equipped with a flame ionization detector (GC-FID) and a VB-WAX capillary column (Valco Instrument Co. Inc., USA).

Powder X-ray diffraction (XRD) was used to examine whether the silica-supported HSiW underwent any structural change after being used in the dehydration reaction. Solid-State Cross-Polarization Magic Angle Spinning Carbon-13 Nuclear Magnetic Resonance (CP/MAS ^{13}C-NMR) was performed on spent HSiW-Si with and without NTP-O_2 treatment to study the change of coke structure (**Supplementary Material**).

NTP Generation

Non-thermal plasma was generated by a wire-to-cylinder configuration of dielectric barrier discharge (DBD) as shown in **Figure 2**. DBD is a simple NTP generation approach that can be found in many other applications [e.g., (Kogelschat, 2002)]. An Inconel wire was inserted in the

axial direction of the quartz reactor tube, and connected to the high-voltage port of a transformer. Copper tape was wrapped around the outside wall of the quartz tube, and connected to the ground. The wire and copper tape served as two electrodes, while the quartz wall served as the dielectric barrier. AC waveform was generated by an inverter (solid-state drive SSD110 model, PTI, Racine, WI) followed by a voltage transformer (55-HLH10102/D115, PTI, Racine, WI). The waveform of the NTP discharge was monitored via an oscilloscope (WaveLet™ series, LeCroy, Chestnut Ridge, NY). A capacitor (2 μF) was inserted in the circuit to create a phase lag to generate Lissajous figure for the calculation of power consumption by NTP (Manley, 1943; Kraus et al., 2001; Subrahmanyam et al., 2005).

Evaluation of Coke Removal by NTP

We first designed two types of tests to evaluate NTP's effect in coke removal.

Test 1: Monitoring NTP decoking process using temperature programmed reaction (TPR)

This test was completed using a system that was constructed based on a ChemBET PULSAR™ TPR/TPD (Quantachrome Instruments, Boynton Beach, FL, USA) with a homemade DBD cell (electrical configuration is depicted in **Figure 2**). Schematic flow diagram of the test is shown in **Figure 3**. The spent HSiW-Si was collected from a glycerol dehydration run after 7.5 h Time-On-Stream (TOS) as described in section Catalyst and Catalytic Reaction; 100 mg of this spent catalyst was placed in the DBD cell, and heat could be applied as an option using a heating tape. A gas blend (5% O_2 in He) was fed into the system at 30 mL/min, going through the DBD cell, and traveling through a liquid nitrogen (LN) trap before reaching a thermal conductivity detector (TCD). Helium could not be condensed in the LN trap and would pass through. Oxygen could also pass

FIGURE 2 | Schematics of the electrical setup for the NTP generation and the section of DBD cell.
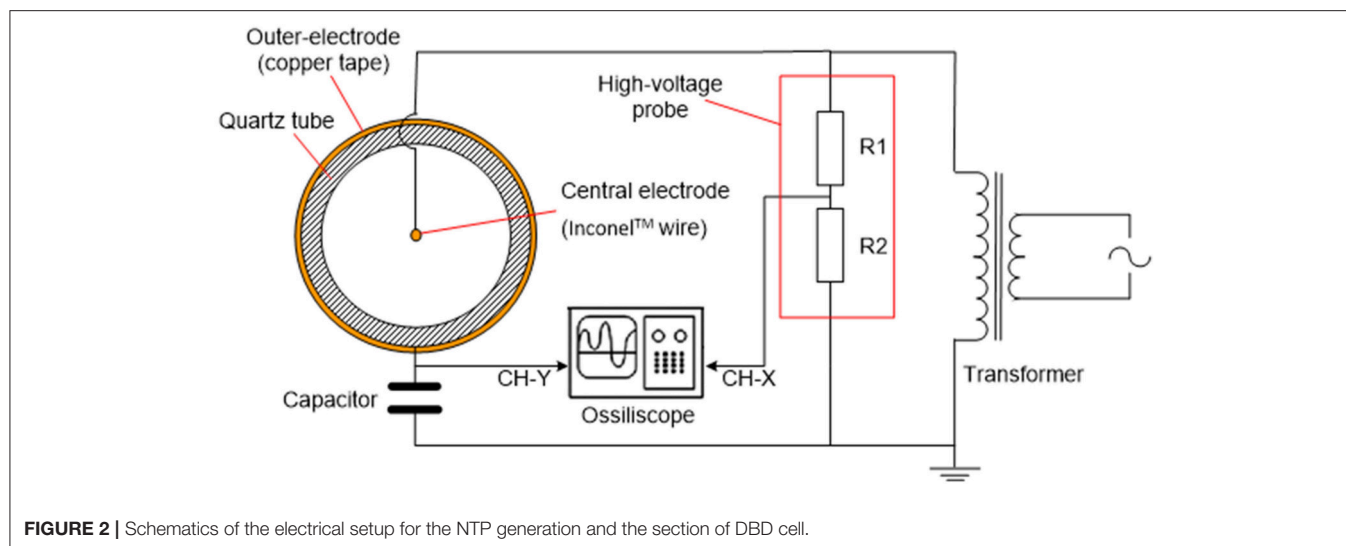
through the LN trap, because the 5% concentration was far below its saturation vapor pressure (Bayraktar and Kugler, 2002). Four NTP discharge field strengths (3.0, 4.8, 6.6, and 8.4 kV/cm), which were defined as the discharge voltage divided by the discharge gap length, were first studied at ambient temperature (25°C). Then the optimal NTP field strength was used to study the temperature effect at 25, 100, 150, and 200°C. A blank test was first conducted using fresh catalyst that was not used in a dehydration reaction. The DBD cell was loaded with 100 mg fresh catalyst with only helium or a 5% O_2 in He gas blend flowing through the cell; NTP discharge was applied to the cell at the designed field strength levels. The purpose of the blank test was to obtain the baseline signal for each discharge strength. Thus, the TCD signal was able to qualitatively reflect the decoking process when a spent catalyst is used.

Test 2: Evaluating NTP de-coked spent catalyst using temperature programmed oxidation (TPO).

The amount of coke removal by NTP-O_2 was also evaluated by temperature-programmed oxidation (TPO), characterizing the spent catalyst after a specific NTP decoking treatment. Characteristics of the remaining coke on the catalyst surface after NTP-O_2 treatment were obtained to evaluate the coke-removal effectiveness of each NTP-O_2 condition (from Test 1).

The experiment was conducted with the ChemBET PULSAR™ TPR/TPD, and the flow diagram is similar to **Figure 3**; the only difference was that instead of the NTP application, programmed heating was applied to the reaction cell. Catalyst sample (100 mg) was pretreated on the ChemBET at 300°C in nitrogen atmosphere prior to the TPO experiment, which was conducted with a temperature program from 25 to 900°C at a heating rate of 10°C/min. A gas blend (5% O_2 in He) was fed

into the reaction cell at 70 mL/min; the effluent gas was then passing through a liquid nitrogen trap before reaching the TCD detector. Oxidation products such CO_X was condensed, but the background gas helium and the unconsumed oxygen could pass through and detected by the TCD.

Evaluation of *in situ* Catalyst Regeneration by NTP

This part of experiments focused on the catalyst performance for glycerol dehydration after *in situ* NTP regeneration treatment. The catalyst was kept inside the packed-bed reactor (**Figure 1**) and regeneration with NTP-O_2 treatment was directly applied *in situ*. This was an indirect evaluation in term of coke removal, but a direct evaluation in term of whether the catalyst could be regenerated and the catalyst's performance could be regained.

The experiment proceeded as follows: after 7.5 h of glycerol dehydration as described in section Catalyst and Catalytic Reaction, the glycerol feed was stopped. Instead of pure argon, different oxygen-containing gases were fed into the reactor, and NTP discharge was applied to the catalyst bed region with the aim of regenerating the catalyst. After 2 h of the NTP-O_2 application, NTP was stopped; the carrier gas was changed back to pure argon, and the glycerol feed was restarted. The glycerol-dehydration reaction was continued for a few hours, and glycerol conversion (Equation 1) and acrolein selectivity (Equation 2) were used to evaluate the catalyst performance.

$$X_{glycerol} = \frac{n_{reacted}}{n_{feed}} \times 100\% = \frac{n_{feed} - n_{quantified}}{n_{feed}} \times 100\% \quad (1)$$

where $X_{glycerol}$ is glycerol conversion (mol%), $n_{reacted}$ is the moles of glycerol reacted, and n_{feed} is the moles of glycerol in the feed, $n_{quantified}$ is the remaining glycerol in the collected sample quantified by GC.

$$S_{acrolein} = \frac{n_{c-acrolein}}{n_{c-gly-reacted}} \times 100\% \quad (2)$$

FIGURE 3 | Schematics of the experiment setup to monitor NTP decoking process using TPR.
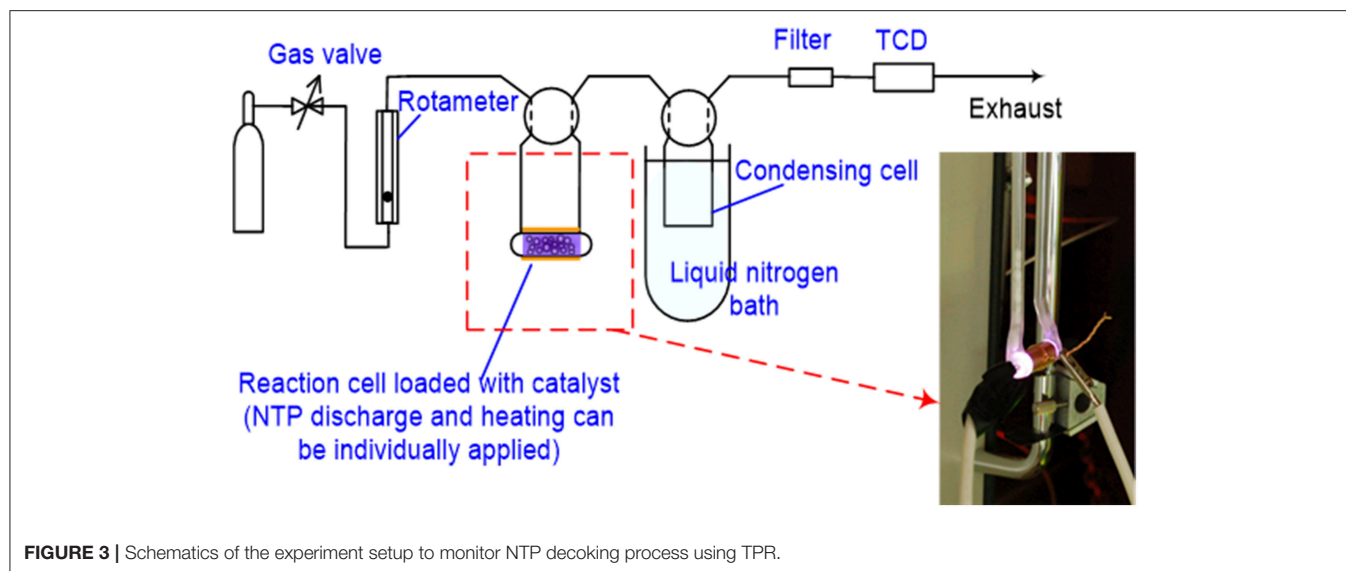
where $S_{acrolein}$ is the selectivity to acrolein (mol%), $n_{c-acrolein}$ is the moles of carbon in the produced acrolein, and $n_{c-gly-reacted}$ is the moles of carbon in the converted glycerol.

The elements inside dash lines in **Figure 1** are designed for the experiment described in this section. NTP was integrated into the reactor system using the electrical setup as described in **Figure 2**, and the discharge zone started from 25.4 mm upstream of the catalyst bed and terminated at the end of the catalyst bed (a cylindrical NTP zone with 19.35 mm in diameter and 50.8 mm in height), including both a pre-bed discharge and an on-bed discharge zone.

The selected NTP field strength and operating temperature were based on the optimal condition found after evaluating the coke removal (section Evaluation of Coke Removal by NTP). Three different oxygen-containing discharge gases were compared: (1) 20% oxygen blended in argon, (2) air, which can be viewed as ~20% oxygen blended in nitrogen, and (3) pure oxygen. The total gas flow rate was fixed at 30 mL/min.

RESULTS

Overview

The X-ray diffraction results (**Supplementary Figure S1**) showed no difference between the fresh HSiW-Si and the spent HSiW-Si that was collected after a 7.5-h glycerol dehydration test (section Catalyst and Catalytic Reaction); this result agreed with previous publications (Wang et al., 2009, 2010; Alhanash et al., 2010) in that the deposited coke was amorphous and would not change the crystalline structure of the catalyst on which it was deposited.

CP/MAS ^{13}C-NMR analysis revealed that the relative abundance of aromatic and unsaturated C in NTP-treated spent catalyst decreased while that of C connected to heteroatoms of O significantly increased (**Supplementary Figure S2**), comparing with spent catalyst without NTP treatment. This confirms that oxidation is the main mechanism for coke removal by the NTP-O$_2$.

We found that the NTP field strength, operation temperature, and the nature of the discharge gas were all able to influence the coke removal effectiveness; these results are presented in section Evaluation of Coke Removal by NTP. More importantly, we discovered NTP's positive role in regenerating the deactivated catalyst *in situ* for the glycerol-to-acrolein conversion (section Evaluation of *in situ* Catalyst Regeneration by NTP); a comparison of the results for the different discharge gases is also presented hereafter.

Evaluation of Coke Removal by NTP
Effect of NTP Field Strength

The effect of the NTP field strength was first studied by monitoring the decoking process (section Evaluation of Coke Removal by NTP Test 1). Here we first explain how the real-time TPR monitoring served the function of examining coke removal from the baseline signal. **Figure 4** displays the baseline signals obtained using fresh HSiW-Si with different NTP field strengths. The baseline collected on the fresh catalyst with pure helium showed no baseline shift regardless of how large a NTP discharge field strength was applied, suggesting that the excited helium species were transient and vanished as soon as they left the discharge zone. On the contrary, the background collected on the fresh catalyst with 5% O$_2$ in He mixture showed some signal changes when the NTP was applied. Each baseline curve of NTP-O$_2$ displayed a characteristic initial overshoot followed by stabilization to a constant. An increasing trend of the stabilized baseline was observed as the NTP field strength increased from 3.0 to 8.4 kV/cm.

The NTP discharge excited molecular oxygen into new species, such as ozone, O (^{1}D), O (^{3}P) and other surface oxygen species. Except for ozone, all the other strong oxidants were short-lived. As soon as these short-lived oxygen species left the discharge zone, they recombined back to molecular oxygen. Ozone (O$_3$) has a lifetime of over a day at room temperature, so it would not convert back to molecular oxygen in the effluent after

FIGURE 4 | Baselines of TCD signal collected for monitoring decoking process using fresh catalyst at different field strengths with pure He or 5% O_2 in He.

FIGURE 5 | TCD signals for the real-time monitoring of the decoking process at different NTP field strengths at room temperature; 3.0, 4.8, 6.6, and 8.4 kV/cm indicate the field strength of NTP-O_2 with 5% O_2 in He.

FIGURE 6 | TPO characterization of the spent catalyst both without NTP-O_2 treatment and after regeneration with NTP-O_2 at different field strengths.

leaving the discharge zone. Therefore, the gaseous effluent after the discharge cell packed with fresh catalyst was composed of O_2, O_3 and He. However, the O_3 condensed and could be observed as a layer of navy-blue liquid in the liquid nitrogen trap; it could not reach the TCD detector. Therefore, essentially what TCD could detect was the consumption of oxygen. The initial overshoot was probably caused by the presence of porous materials (HSiW-Si) that adsorbed some O_2 at different field strengths. An increasing trend of the stabilized baseline was observed as the field strength of the plasma increased from 3.0 to 8.4 kV/cm, suggesting that the ozone yield increased along with the increase of the NTP field strength. For a given condition, the ozone concentration should be a constant. Therefore, after subtracting the baseline from the signal obtained during the NTP-O_2 treatment of the spent HSiW-Si, which was at least eight times larger than the baseline signal, any signal change would be caused by the ongoing reaction with the carbonaceous coke species deposited on the catalyst surface.

Figure 5 shows the result of monitoring the decoking process at the various NTP field strengths after subtracting the corresponding baseline. There was an equilibrium between the distribution of molecular oxygen, which could be detected by TCD, and other O species generated by NTP. When the reactive O species reacted with some surface carbonaceous coke, the consumption of these species drove forward the reactions of O_2 to the reactive species, such as ozone and O radicals, causing the consumption of O_2. Upon each NTP application with different field strength, the signal first reached to a maximum, indicating fast oxidation of coke and consumption of O_2. Coke was the limiting reactant while the oxidative species formed in NTP-O_2 were in excess. It is reasonable to state that "soft" coke was consumed first, leaving the "hard" coke to be oxidized at slower rates, as indicated by the level-off of the TCD signal.

Therefore, **Figure 5** implies that the effectiveness of coke removal increased with increasing NTP field strength; the effectiveness rose in the following order: 3.0 kV/cm < 4.8 kV/cm < 6.6 kV/cm < 8.4 kV/cm. It is noteworthy that at the field strength of 3.0 kV/cm, there was barely any coke removal. From
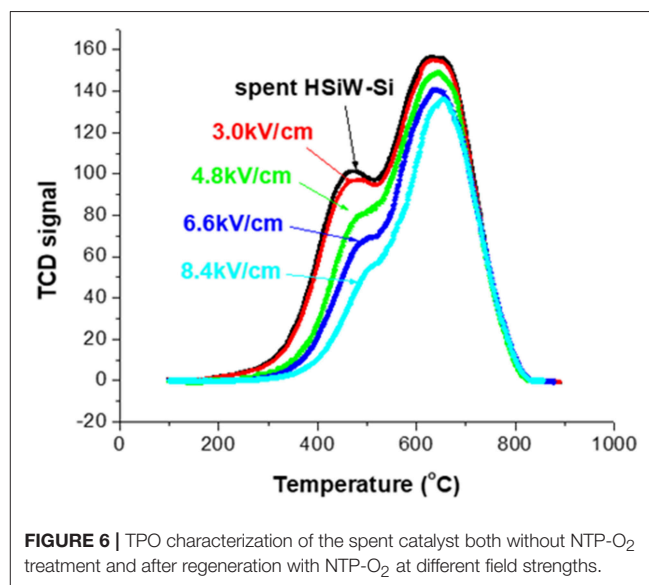
3.0 to 4.8 kV/cm, there was a drastic change in coke removal, indicating the activation of decoking by the NTP. We used a Lissajous figure to calculate the NTP power consumption, a method developed by Manley (Manley, 1943) that has been used in many studies [e.g., (Kraus et al., 2001; Subrahmanyam et al., 2005)]. The calculated power was as 0.05, 0.43, 0.84, and 1.27 W, corresponding to the field strength of 3.0, 4.8, 6.6 and 8.4 kV/cm, respectively.

Figure 6 presents the TPO characterization (section Evaluation of Coke Removal by NTP Test 2) result of the spent catalyst without NTP treatment, and after 1.5 h of NTP-O_2 treatment at different NTP field strengths. There is only a slight difference in the TPO profile between the untreated spent catalyst
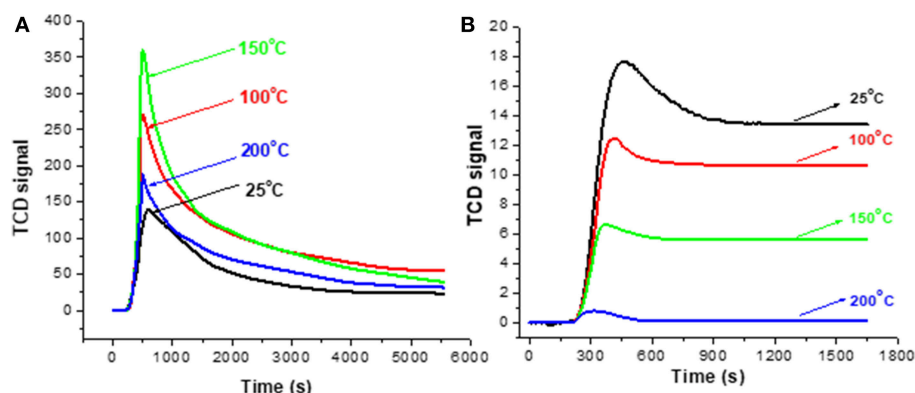
FIGURE 7 | TCD signals for the real-time monitoring of the decoking process with 8.4 kV/cm NTP-O_2 at different temperatures **(A)**; baseline profiles collected using fresh catalyst **(B)**.

and the spent catalyst after the 1.5-h treatment by NTP-O_2 at the field strength of 3.0 kV/cm. For the rest of the investigated field strengths, the TPO curves showed a decreasing trend with the increasing NTP field strength. Although the reduction of TCD signal intensity was more significant in the "soft" coke region (peak at ∼450°C), the reduction was also observed in the "hard" coke region (peak at ∼650°C).

The results of the above two tests showed that the coke removal was more effective at higher NTP field-strengths. Therefore, the field strength of 8.4 kV/cm, at which the maximum coke removal was observed, was employed for the following tests.

Effect of Operation Temperature

Test 1 (section Evaluation of Coke Removal by NTP) was repeated with extra control of the DBD cell temperature and **Figure 7** depicts the results of monitoring the decoking process. The stabilized baseline using fresh HSiW-Si (**Figure 7B**) decreased in the order of 25°C > 100°C > 150°C > 200°C, and the stabilized baseline at 200°C was nearly zero. The relative positions of the stabilized baselines at different operation temperatures suggest that ozone (O_3) concentration decreased as the operation temperature increased. It is well known that ozone decomposes faster at high temperatures; almost no O_3 existed at 200°C. **Figure 7A** displays the signal profile during NTP-O_2 treatment at different temperatures. The signal intensity was descending in the order of 150°C > 100°C > 200°C > 25°C, suggesting that the effectiveness of the coke removal decreased in this order. Therefore, the order of coke removal effectiveness does not quite follow the sequence of the ozone concentration as suggested in **Figure 7B**. This inconsistency implies that the ozone concentration was not the major factor that determined the effectiveness of the coke removal.

A consistent trend was exhibited by TPO characterization of the spent HSiW-Si after the 8.4 kV/cm NTP treatment at different temperatures, as shown in **Figure 8**. Coke was largely reduced after the NTP-O_2 treatment at 100°C, and even more so at 150°C. However, the trend reversed as the temperature further increased to 200°C, and more coke, especially hard coke, remained on the catalyst compared to those being treated at

100 and 150°C. The results also confirmed that the reactive oxygen species formed under NTP discharge were able to react with some hard coke (around 600–700°C), especially when the NTP regeneration was operated at a proper temperature. Among the investigated temperatures, the most effective coke removal occurred at 150°C.

Both of the TPR and TPO tests consistently showed that operating the NTP-O_2 decoking at 150°C provided more effective coke removal compared to the other investigated temperatures.

Time Dependence of Coke Removal

Figure 9 shows the time dependence of coke removal at the NTP condition of 8.4 kV/cm and 150°C. The percentage of coke deposit was defined as the weight difference between the fresh catalyst and the coked catalyst divided by the weight of fresh catalyst. Although the strong oxidizing species in NTP were able to react with hard coke, the reaction rate is likely to be much lower in comparison to that with soft coke, which was likely removed first. This is one reason for that the decrease of coke deposit in **Figure 9** became slower at the longer treatment times. Also, the diffusion of short-lived atomic oxygen into the pores was unlikely, so when the more exposed surface coke was consumed, the decoking process would become more difficult. When soft coke was oxidized, CO_2 was formed and flushed off the surface, directly resulting in the weight decrease of the spent catalyst. In contrast, for oxidation of hard coke, the reaction rate might be slow, and the oxidation of hard coke started by converting it to an oxygen-rich intermediate, or breaking it down into a smaller structure (Deitz and Bitner, 1973; Smith and Chughtai, 1995; Mawhinney and Yates, 2001). Consequently, oxidizing hard coke most likely did not directly generate CO_2, leaving the total mass barely changed. This conceivably explains why the coke removal rate slowed down with time, even though NTP-O_2 was able to react with hard coke.

Evaluation of *in situ* Catalyst Regeneration by NTP

Coke removal usually resulted in catalyst regeneration, but not always, e.g., in case if some active sites on the catalyst were
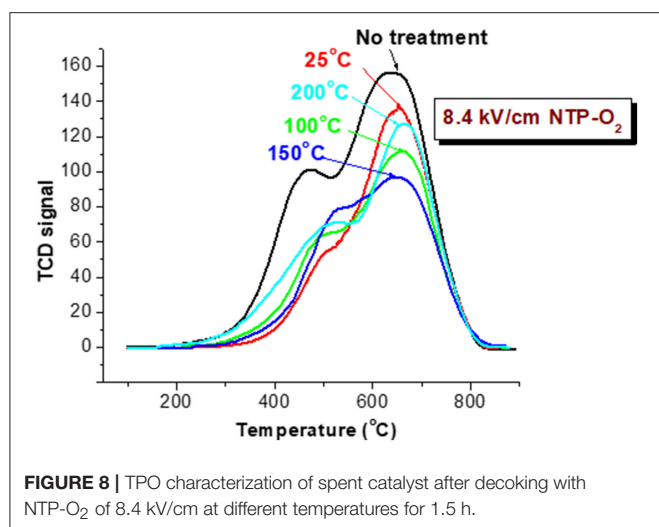
FIGURE 8 | TPO characterization of spent catalyst after decoking with NTP-O_2 of 8.4 kV/cm at different temperatures for 1.5 h.

damaged during coke removal, catalytic performance would not be regained. The NTP-O_2 effect in catalyst regeneration was directly tested via periodic *in situ* regeneration at 8.4 kV/cm and 150°C. The results of periodic regeneration using 20% O_2 in argon, air, and pure oxygen are presented in **Figures 10A–C**, respectively. The reason that 20% O_2 was used here was because we wanted to make the comparison of Ar as the discharge gas to N_2 as the discharge gas (in the case of air) at similar O_2 concentration. A control test is presented in **Figure 10D**, for which there was no NTP application during the 2 h of flushing the reactor with 20% O_2 in Ar. Evidently, the NTP application regenerated the catalyst *in situ*, showing as the rebound of glycerol conversion after each session of regeneration. The NTP with 20% O_2 in Ar showed the best effectiveness, with a descending order of effectiveness as NTP-O_2 in Ar > NTP-pure $O_2 \geq$ NTP-O_2 in N_2. In contrast, flushing the reactor with 20% O_2 in Ar without NTP had no effect for regeneration. Based on the results shown previously in **Figure 9**, a 2-h NTP treatment was unlikely to completely remove surface coke. The results here show that the catalytic activity could be regained to some extent even with the partial regeneration. However, because of the fact that coke was not thoroughly removed, the catalyst after partial regeneration might be prone to somewhat faster deactivation. This explains why, overall, a slightly decreasing trend in glycerol conversion was observed after each regeneration. Nevertheless, the purpose of this experiment to examine the influence of the discharge gas on the regeneration was achieved.
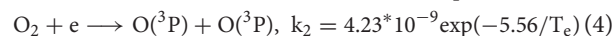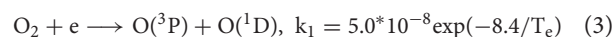
DISCUSSION

Overall Discussion

Regarding that partial coke removal could significantly restore catalytic activity, the "indirect deactivation mechanism" (Tanabe, 1989) was probably the predominant mechanism causing the deactivation of the HSiW-Si catalyst during glycerol dehydration. **Figure 11** illustrates this "indirect deactivation mechanism." Silica had relatively small pores

(average ~11 nm). Some coke formed near the mouth of the pores, narrowing or blocking the entrance into the pores, wherein lots of active sites were located (**Figure 11C**). All of these internal active sites became inaccessible if the pore entrance was blocked. Similarly, once these "entrance blockers" were removed or partially removed, a significant amount of active sites became accessible again for the reactant to contact. Therefore, even partial coke removal greatly revived the catalytic activity.

The situation of *in situ* NTP-O_2 with the presence of the catalyst is complex, and to the best knowledge of the authors, such a situation has rarely been discussed in the past. In the NTP-O_2 plasma system, the possible oxygen species include ozone (O_3), O_2 molecules in the ground state ($O_2(X^3\Sigma^-)$), O_2 molecules in the excited state ($O_2(a^1\Delta^-)$ and $O_2(b^1\Sigma_g^+)$), atomic oxygen in the ground state ($O(^3P)$), atomic oxygen in the excited state ($O(^1D)$), and oxygen ions (O_2^+, O^+, and O^-). Among them, the most effective oxidants are ozone and atomic oxygen. Since non-thermal plasma is an electron-driven process (Fridman, 2008), atomic oxygen is most likely to be firstly generated via dissociation in the Schumann-Runge band (Equation 3) and in the Herzberg band (Equation 4; Falkenstein, 1999). Herzberg-band dissociation has a higher efficiency than Schumann-Runge-band dissociation (Falkenstein, 1999), because the ground-state oxygen atom $O(^3P)$ is relatively more stable than the excited-state oxygen atom $O(^1D)$, and also because $O(^1D)$ could be easily quenched into $O(^3P)$ (Equation 5); $O(^3P)$ was possibly the most predominant atomic oxidant (Bogaerts, 2009; Mok et al., 2009).

$$O_2 + e \longrightarrow O(^3P) + O(^1D), \ k_1 = 5.0^*10^{-8}\exp(-8.4/T_e) \quad (3)$$
$$O_2 + e \longrightarrow O(^3P) + O(^3P), \ k_2 = 4.23^*10^{-9}\exp(-5.56/T_e) \ (4)$$
$$O(^1D) + M \rightarrow O(^3P) + M \quad (5)$$

where T_e is electron temperature, k is the reaction rate constant, and M is any other types of molecule.

It was proven that atomic oxygen could rapidly react with carbonaceous species (Blackwood and McTaggart, 1958; Marsh et al., 1963; Pattabiraman et al., 1990). Some researchers have claimed that the atomic oxygen is a stronger oxidant than ozone, and is capable of providing a faster rate when reacting with carbonaceous species (Smith and Chughtai, 1995; Falkenstein, 1999; Pieck et al., 2005; Khan and Al-Jalal, 2006). Some plausible overall reactions are listed in the following Equations 6 through 8 (Khan and Al-Jalal, 2006). The very detailed mechanism was not quite clear; however, it was generally thought that the O attacks the carbonaceous compound preferentially via the delocalized π bonds.

$$C_xH_yO_z + O + e \rightarrow C_{x-1}H_yO_z + CO + e \quad (6)$$
$$C_xH_yO_z + O + e \rightarrow C_{x-1}H_{y-1}O_z + H + CO + e \quad (7)$$
$$CO + O + e \rightarrow CO_2 + e \quad (8)$$
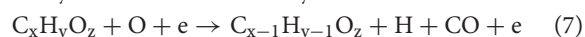
Ozone is another effective strong oxidant that has been previously reported as being reactive with carbonaceous species (Pieck et al., 1994; Smith and Chughtai, 1995; Mawhinney and Yates, 2001; Subrahmanyam et al., 2005).
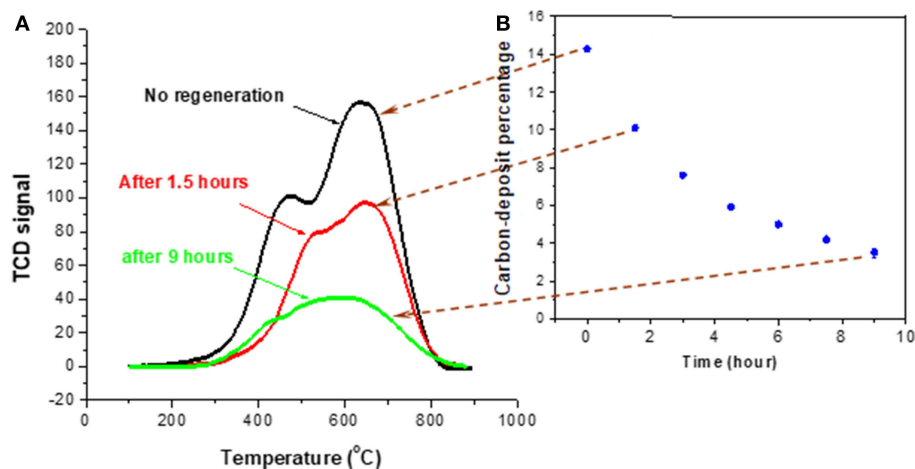
FIGURE 9 | TPO characterization of spent catalyst after decoking at 150°C using 8.4 kV/cm NTP-O$_2$ for different times **(A)**; percentage of coke deposit as a function of decoking time **(B)**.
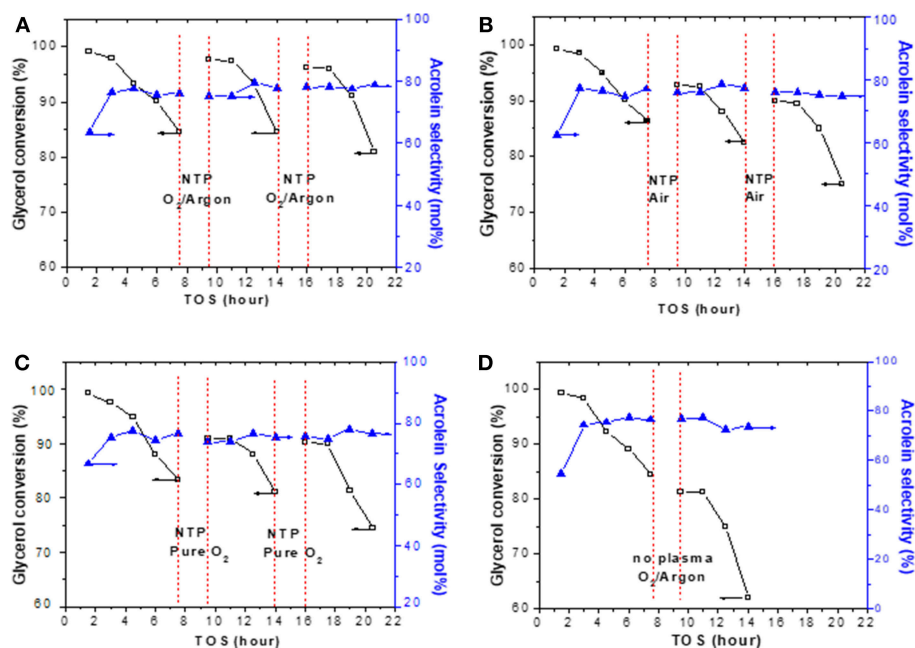
FIGURE 10 | Effects of *in situ* regeneration by NTP using **(A)** 20% O$_2$ in Ar, **(B)** air, and **(C)** pure oxygen, in comparison to **(D)** flushing with 20% O$_2$ in Ar without NTP. Each regeneration was conducted at 8.4 kV/cm and 150°C for 2 h.

Ozone is generated via three-body collisions (Equation 9), involving the molecular oxygen, the ground-state atomic oxygen, and another gas molecule M; ozone is decomposed via Equation (10) (Mok et al., 2009). Both processes consume some atomic oxygen. The general process of ozone reacting with carbonaceous species is summarized in Equation (11) (Smith and Chughtai, 1995).

$$O_2 + O\,(^3P) + M \rightarrow O_3 + M, \quad k_3 = 8.6{*}10^{-31}T^{-1.25} \quad (9)$$

$$O_3 + O\,(^3P) \rightarrow 2O_2, \quad k_2 = 9.5{*}10^{-12}\exp(-2300/T) \quad (10)$$
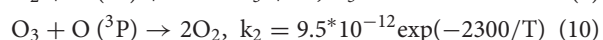
where T is the overall gas temperature.

$$C_n + O_3 \rightarrow \text{Functional groups } (-COOH, -C-OH, -C \\ = O) \rightarrow \ldots \rightarrow CO_2 \quad (11)$$
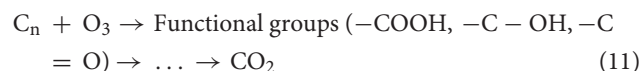
Possible mechanisms of ozone reaction with the functional groups in surface coke have been discussed previously (Deitz and Bitner, 1973; Smith and Chughtai, 1995; Mawhinney and Yates, 2001). For examples, if a carbon-carbon double bond was located at the end of an aliphatic carbon chain, the ozone addition
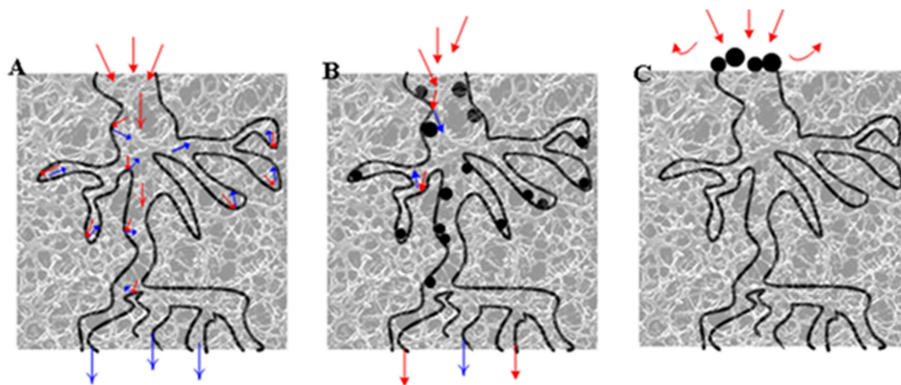
FIGURE 11 | Illustration of catalyst pores **(A)** fresh catalyst; **(B)** coke relatively evenly distributed on the active sites, and glycerol molecules only could not reach the active sites covered by coke (direct deactivation); **(C)** coke deposit on the mouth of pore entrance, and glycerol molecules could not reach the active sites that were still "available" (indirect deactivation). Red arrows denote the path of glycerol, blue arrows denote the path of product (acrolein), and the black dots denote the coke.

could directly reduce the number of carbons and release one mole of CO_2; if a carbon-carbon double bond was located within an aromatic carbonaceous compound, then the ozone insertion may have opened up the ring structure, significantly lowering its stability and thus lowering the activation energy for further oxidization and increasing the reactivity. The process could have continued in a step-by-step fashion, breaking the larger molecule into smaller molecules, and eventually converting all to CO_x, which could be pumped out of the system.

Some of the oxidizing species could also chemically bind to the catalyst surface, existing as oxidizing surface-species. The active surface species are assigned to three categories: surface atomic oxygen (denoted as O-S), adsorbed excited oxygen (O_2^*-S) and adsorbed ozone (O_3-S) (Equations 12–14). It is possible that the reactions with the carbonaceous species proceeded via two different pathways. First, the active O species in the gas phase directly attacked the surface coke, which would be O_3, O, or O^* directly interacting with coke. Second, the reactive surface O species (O-S, O_2^*-S, and O_3-S) migrated to the surface and reacted with the neighboring coke.

$$O_3 + S \rightarrow O_3 - S \qquad (12)$$

$$O_2(^1\Delta P) + S \rightarrow O_2(^1\Delta P) - S\,(O_2^* - S) \qquad (13)$$

$$O(^3P) + S \rightarrow O(^3P) - S \text{ or } O(^1D) + S \rightarrow O(^1D) - S\,(14)$$

Conventional combustion method of a substance with molecular oxygen is an exothermal process. The operation requires a very strict temperature controlling and heat release system to avoid temperature runoff, which would result in the permanent deactivation of catalyst (such as sintering; Pieck et al., 1994), and more importantly, potential safety issues for a plant. Regeneration with NTP-O_2 at a mild temperature condition could best preserve the catalyst properties. Therefore, in general, it would be beneficial if a process that can remove coke at a low tem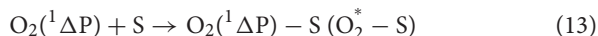perature is developed. The coke on the acid catalyst HSiW-Si from glycerol dehydration was more distributed toward the hard coke region compared to most spent cracking metal catalysts (Tanable et al., 1989; Li and Brown, 1999). Therefore, our concept

proved for a more difficult model compound (coked acid catalyst HSiW-Si) is very likely to be applicable to metal catalysts, which are sensitive to sintering. Some modifications of the catalyst, such as doping with palladium metals (Kozhevnikov, 2007), may significantly modify the coke distribution (to the softer end) and lead to more efficient regeneration.

Effects of NTP Field Strength (Figures 5, 6)

As the field strength increased, the electrons became more energetic and a larger number of energized electrons was generated in the system. As a result, the dissociation of the molecular oxygen was facilitated, and more atomic oxygen was formed. Ozone was generated via the three-body collision, and atomic oxygen was the limiting substrate. Therefore, if all other parameters remained the same, the ozone concentration was likely to increase as the field strength increased (Teranishi et al., 2009). With the application of a more intense plasma field, more reactive oxygen species were generated, and more energy that could be efficiently transferred to the oxidation processes was available in the system. As a result, coke removal effectiveness increased along with the field strength. However, there were also decomposition/recombination reactions that converted the reactive oxygen species back to molecular O_2, as shown in Equations 15 and 16. As a result, the density (or concentration) of ozone and atomic oxygen would not further increase as the NTP field strength increased, and it was more likely to be an asymptotic function of field strength increasing toward a saturation point. This statement agrees with a previous finding by Sung et al. that ozone concentration in an atmosphere of oxygen increased with the increase of the discharge power until approaching a saturation point (Sung and Sakoda, 2005). This explained that while coke removal increased with NTP field strength, the increasing trend leveled off.

$$O_3 + O\,(^3P) \rightarrow 2\,O_2 \qquad (15)$$

$$O\,(^3P) + O\,(^3P)(+M) \rightarrow O_2 + e\,(+M) \qquad (16)$$
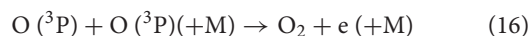
Effects of Operation Temperature (Figures 7, 8)

The experimental results showed that operating the NTP-O_2 regeneration at 150°C provided more effective coke removal than operating at any other temperatures investigated. The majority of oxidizing species were ozone and atomic oxygen, and maybe some OH radicals. The kinetic equations for ozone show that low temperature favors ozone formation (Equation 9), while high temperature favors ozone decomposition (Equation 10); both processes consume some atomic oxygen. At higher temperatures, less ozone is formed. Because the ozone concentration is reduced in the first place, there is a limited amount of atomic oxygen that would be consequently consumed according to Equation (10). Although few ozone molecules could exist at temperature conditions above 200°C (as indicated in **Figure 7B**), atomization of oxygen molecules is feasible at 300°C (Khan and Al-Jalal, 2004). Some believe that atomic oxygen is an even stronger oxidizing species than ozone (Smith and Chughtai, 1995; Falkenstein, 1999; Silva et al., 2004; Pieck et al., 2005; Khan and Al-Jalal, 2006). Atomic oxygen is a short-lived species, and it may not be able to diffuse deeply into a pore within its lifetime. However, higher temperature increases the kinetic velocity of atomic oxygen, facilitating deeper penetration into the catalyst and increasing the collision probability with more carbonaceous molecules (Khan and Al-Jalal, 2006). Consequently, the reaction of atomic oxygen with coke would be enhanced. Nonetheless, when the oxygen atoms move faster at elevated temperatures, the odds of their collision with another oxygen atom increased, increasing the possibility of recombination back to molecular oxygen (Equation 17). As the temperature increases, the rate of oxidation with carbonaceous coke by atomic oxygen and/or ozone also increases significantly. All these factors interacting and counteracting with each other resulted in the optimal operation occurring at a mildly elevated temperature, thus in our study, coke removal at 150°C showed the greatest effectiveness among all the investigated temperatures.

$$O\,(^3P) + O\,(^3P) \rightarrow O_2 \tag{17}$$
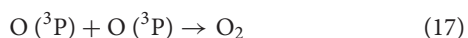
It is possible that the fluidized bed reactor would facilitate the catalyst regeneration process, because of the complex balance existing in diffusion and lifetime for atomic oxygen and ozone.

Time Dependence (Figure 9)

It is rather difficult for the short-lived NTP species ($O(^3P)$, $O(^1D)$ and OH) generated in the gas-phase and/or on catalyst surface to diffuse deeply into the catalyst pore due to their short lifetimes. The relatively long lifetime of ozone would make it diffuse into the pores easily (Holzer et al., 2002); however, ozone is much larger in molecular size than atomic oxygen, and its steric hindrance is therefore larger than that of atomic oxygen. Therefore, ozone would not diffuse into pores as easily as atomic oxygen because of the steric effect (Deitz and Bitner, 1973). As the result, the diffusion of highly reactive oxidants into the porous catalyst might be another important issue limiting the rate of further coke removal, slowing down the removal as the coke on top of the surface is consumed. These reasons may explain

TABLE 1 | Relevant reactions in NTP-O_2 conditioned with different discharge gases.

Discharge gas[a]	Relevant reactions in the specific NTP-O_2
O_2	$e + O_2 \rightarrow 2\,O + e$ $\qquad$ $e + O_2 \rightarrow O_2^+ + 2e$ $\qquad$ $e + O_2^+ \rightarrow 2\,O^*$
Ar	$e + Ar \rightarrow Ar^* + e$ $\quad$ where Ar* is the excited state, or Ar radical
	$Ar^* \rightarrow Ar^M$ $\quad$ where Ar^M is the metastable states of Ar from Ar
	$Ar^M + O_2 \rightarrow Ar + O + O$ $\qquad$ $Ar^M + O \rightarrow Ar + O^*$
	$Ar^+ + O_2 \rightarrow O_2^+ + Ar$ $\qquad$ $O_2^+ + e \rightarrow O + O$
N_2	$e + N_2 \rightarrow 2\,N + e$ $\qquad$ $e + N_2 \rightarrow N_2^+ + 2e$
	$O^+ + N_2 \rightarrow NO^+ + N$ $\qquad$ $O_2^+ + N_2 \rightarrow NO^+ + NO$
	$N_2^+ + O_2 \rightarrow NO^+ + NO$

[a]The gas component present with a larger percentage than O_2; to be specific, O_2 relates to our case of using pure oxygen; Ar relates to our case of using 20% O_2 blended in argon; N_2 relates to our case of using air (~20% O_2 blended in N_2).

why the coke removal rate slowed down with time, even though NTP-O_2 was able to react with hard coke. The coke removal rate decreased with the increasing regeneration time. These reactions would continue as long as the basic graphitic structure and carbon-carbon double bonds still exist (Takeuchi and Itoh, 1993), although the reaction rate varied.

Effects of Discharge Gas (Figure 10)

Plausible reactions under NTP with different background gases are listed in **Table 1** (Khan and Al-Jalal, 2004; Sung and Sakoda, 2005). The metastable state of argon (Ar^M), formed from Ar radical (Ar*) via radioactive decay, had a very small probability of transition for further decay, and instead, they were more likely to transfer energy to oxygen molecules via collisions, generating O atoms and thus ozone. Also, the presence of a large number of Ar atoms created an inhibiting "wall" between oxygen atoms and oxygen atoms or ozone, preventing these active oxygen species from recombining into molecular oxygen. Consequently, the density of atomic oxygen and ozone in the presence of Ar as the background gas might be higher than that when pure O_2 was used. Similarly, the background N_2 could also have provided the same "wall-effect." However, ionizing N_2 requires much higher energy/field strength, and the ionized N species might react with the active oxygen species, forming NO_x (Fridman, 2008); such reactions competitively consumed a part of the highly reactive oxygen species, resulting in a decrease in the regeneration effectiveness. Generally, a noble gas, such as Ar and He, can be ionized most easily. Therefore, at a given NTP field strength, the electron energy and the number of electrons were significantly higher in the system with Ar as a background gas than those in the other two systems (Snyder and Anderson, 1998; Okumoto et al., 2001). Forming atomic N, comparing to forming atomic Ar or O, costs a much larger amount of energy (Fridman, 2008), and the dissociation of nitrogen competitively consumed a certain amount of energy available in the system. The presence of nitrogen added to the complexity of the gaseous-electron processes and downgraded the electron energy density. Studies have shown that the rate of atomic oxygen formation in a

mixture with argon was an order of magnitude higher than that in a mixture with nitrogen (Snyder and Anderson, 1998; Khan and Al-Jalal, 2006). These factors might account for our result in that the regeneration effectiveness decreased as NTP-O$_2$ in Ar > NTP-O$_2$ > NTP-O$_2$ in N$_2$. All the discussion associated with argon should be presumably applicable to any noble gas, such as helium.

CONCLUSIONS

Silica-supported silicotungstic acid (HSiW-Si), which shows good performance in glycerol dehydration initially but deactivates quickly, was chosen to probe the potential of using non-thermal plasma with oxygen-containing gas (NTP-O$_2$) to solve the catalyst deactivation problem. This study proved that NTP-O$_2$ is a viable method to regenerate supported HSiW, which cannot be accomplished by the conventional combustion method due to its low thermal stability. The existence of strong oxidizing agents produced in NTP (e.g., O$_3$, atomic oxygen, and active surface oxygen species) made it possible to oxidize coke at a much lower temperature compared to the conventional combustion method. NTP-O$_2$ at higher field strengths was more effective in coke removal; however, the improvement in the coke removal exhibited an asymptotic tendency, indicating the limitation or slow rate in removing hard coke. Among the investigated field strengths and temperature conditions, operating NTP-O$_2$ at 8.4 kV/cm and 150°C provided the most effective coke removal. Longer NTP-O$_2$ treatment time to the spent catalyst would certainly regenerate the catalyst more thoroughly; however, a balance between the treatment time and the regeneration outcome needs to be found, since the coke removal becomes slower while longer time means more energy consumption.

It is likely that HSiW-Si was deactivated via an indirect mechanism, since partial decoking by NTP-O$_2$ could regenerate the catalyst to a large degree. NTP-O$_2$ with argon as background gas showed better regeneration effectiveness than that with nitrogen as background gas; also, diluting oxygen with argon showed better regeneration effectiveness than using pure oxygen. This comparison is presumably applicable to other noble gases like helium as well.

NTP-O$_2$ could react with both soft coke and hard coke. For the soft coke, NTP-O$_2$ could likely convert it to CO/CO$_2$ that could be flushed off catalyst surface, resulting in weight loss of the spent catalyst. On the other hand for the hard coke, the active oxidants in NTP reacted with them and formed some intermediate oxygenated surface compounds, shifting the coke distribution to the soft coke. NTP-O$_2$ could significantly lower coke-removal temperature, and this method is presumably applicable to other catalysts (and other reactions) with low thermal stability that suffer from coking deactivation.

AUTHOR CONTRIBUTIONS

XY conceived the study and directed the experimental work conducted by LL. Catalyst characterizations were done collaboratively by LL, XY, BK, MC, SP, and FD. LL drafted the manuscript. All authors participated in the revision and approved the manuscript.

ACKNOWLEDGMENTS

SUPPLEMENTARY MATERIAL

The Supplementary Material for this article can be found online at: https://www.frontiersin.org/articles/10.3389/fchem.2019.00108/full#supplementary-material

REFERENCES

Alhanash, A., Kozhevnikova, E. F., and Kozhevnikov, I. V. (2010). Gas-phase dehydration of glycerol to acrolein catalysed by caesium heteropoly salt. *Appl. Catal. A Gen.* 378, 11–18. doi: 10.1016/j.apcata.2010.01.043

Atia, H., Armbrusterh, U., and Martin, A. (2008). Dehydration of glycerol in gas phase using heteropolyacid catalysts as active compounds. *J. Catal.* 258, 71–82. doi: 10.1016/j.jcat.2008.05.027

Bardin, B. B., and Davis, R. J. (2000). Effect of water on silica-supported phosphotungstic acid catalysts for 1-butene double bond shift and alkane skeletal isomerization. *Appl. Catal. A Gen.* 200, 219–231. doi: 10.1016/S0926-860X(00)00651-7

Bayraktar, O., and Kugler, E. L. (2002). Characterization of coke on equilibrium fluid catalytic cracking catalysts by temperature-programmed oxidation. *Appl. Catal. A Gen.* 233, 197–213. doi: 10.1016/S0926-860X(02)00142-4

Blackwood, J. D., and McTaggart, F. K. (1958). The oxidation of carbon with atomic oxygen. *Aust. J. Chem.* 12, 114–121. doi: 10.1071/CH9590114

Bogaerts, A. (2009). Effects of oxygen addition to argon glow discharges: a hybrid Monte Carlo-fluid modeling investigation. *Spectrochim. Acta Part B Atom. Spectr.* 64, 1266–1279. doi: 10.1016/j.sab.2009.10.003

Chai, S.-H., Wang, H.-P., Liang, Y., and Xu, B.-Q. (2007). Sustainable production of acrolein: investigation of solid acid-base catalysts for gas-phase dehydration of glycerol. *Green Chem.* 9, 1130–1136. doi: 10.1039/b702200j

Chai, S.-H., Wang, H.-P., Liang, Y., and Xu, B.-Q. (2008). Sustainable production of acrolein: gas-phase dehydration of glycerol over 12-tungstophosphoric acid supported on ZrO$_2$ and SiO$_2$. *Green Chem.* 10, 1087–1093. doi: 10.1039/b805373a

Cheng, L., Liu, L., and Ye, X. P. (2013). Acrolein production from crude glycerol in sub- and super-critical water. *J. Am. Oil Chem. Soc.* 90, 601–610. doi: 10.1007/s11746-012-2189-5

Deitz, V. R., and Bitner, J. L. (1973). Interaction of ozone with adsorbent charcoal. *Carbon* 11, 393–398. doi: 10.1016/0008-6223(73)90079-1

Falkenstein, Z. (1999). Effects of the O$_2$ concentration on the removal efficiency of volatile organic compounds with dielectric barrier discharges in Ar and N$_2$. *J. Appl. Phys.* 85, 81–89. doi: 10.1063/1.369484

Fridman, A. (2008). *Plasma Chemistry.* New York, NY: Cambridge University Press. doi: 10.1017/CBO9780511546075

Holzer, F., Roland, U., and Kopinke, F. D. (2002). Combination of non-thermal plasma and heterogeneous catalysis for oxidation of volatile organic

compounds Part 1: accessibility of the intra-particle volume. *Appl. Catal. B Environ.* 38, 163–181. doi: 10.1016/S0926-3373(02)00040-1

Katryniok, B., Paul, S., Belliere-Baca, V., Rey, P., Dumeignil, A. F., and Abdullah, A. Z. (2010). Glycerol dehydration to acrolein in the context of new uses of glycerol. *Green Chem.* 12, 2079–2098. doi: 10.1039/c0gc00307g

Katryniok, B., Paul, S., Capron, M., Bellière-Baca, V., Rey, P., and Dumeignil, F. (2012). Regeneration of Silica-supported silicotungstic acid as a catalyst for the dehydration of glycerol. *ChemSusChem* 5, 1298–1306. doi: 10.1002/cssc.201100635

Katryniok, B., Paul, S., Capron, M., and Dumeignil, F. (2009). Towards the sustainable production of acrolein by glycerol Dehydration. *ChemSusChem* 2, 719–730. doi: 10.1002/cssc.200900134

Katryniok, B., Paul, S., and Dumeignil, F. (2013). Recent developments in the field of catalytic dehydration of glycerol to acrolein. *ACS Catal.* 3, 1819–1834. doi: 10.1021/cs400354p

Khan, M. A., and Al-Jalal, A. A. (2004). Enhanced decoking of a coked zeolite catalyst using a glow discharge in Ar-O$_2$ gas mixture. *Appl. Catal. A Gen.* 272, 141–149. doi: 10.1016/j.apcata.2004.05.027

Khan, M. A., and Al-Jalal, A. M. (2006). Cumulative contributions of 3s-np (n >= 3) transitions in comparing O atom densities in low-pressure Ar-O$_2$ and He-O$_2$ glow discharges. *Appl. Phys. Lett.* 89, 171501–171503. doi: 10.1063/1.2364464

Khan, M. A., and Al-Jalal, A. M. (2008). Dissociation of O$_2$ in low pressure glow discharges in He-O$_2$, Ne-O$_2$, and Ar-O$_2$ gas mixtures. *J. Appl. Phys.* 104, 123302–123305. doi: 10.1063/1.3043886

Kogelschat, U. (2002). Dielectric-barrier discharges: their history, discharge physics, and industrial applications. *Plasma Chem. Plasma Process.* 23, 1–46. doi: 10.1023/A:1022470901385

Kozhevnikov, I. V. (2007). Sustainable heterogeneous acid catalysis by heteropoly acids. *J. Mol. Catal. A Chem.* 262, 86–92. doi: 10.1016/j.molcata.2006.08.072

Kraus, M., Eliasson, B., Kogelschatz, U., and Wokaun, A. (2001). CO$_2$ reforming of methane by the combination of dielectric-barrier discharges and catalysis. *Phys. Chem. Chemical Phys.* 3, 294–300. doi: 10.1039/b007015g

Li, C. E., and Brown, T. C. (1999). Temperature-programmed oxidation of coke deposited by 1-octene on cracking catalysts. *Energy Fuels* 13, 888–894. doi: 10.1021/ef980265n

Liu, L. (2011). *Roles of Non-thermal Plasma in Gas-phase Glycerol Dehydration Catalyzed by Supported Silicotungstic Acid.* Ph.D. dissertation, The University of Tennessee.

Liu, L., Ye, X. P., and Bozell, J. J. (2012). A comparative review of petroleum-based and bio-based acrolein production. *ChemSusChem* 5, 1162–1180. doi: 10.1002/cssc.201100447

Manley, T. C. (1943). The electric characteristics of the ozonator discharge. *Trans. Electrochem. Soc.* 84, 83–96. doi: 10.1149/1.3071556

Marsh, H., O'hair E., Reed, R., and Wynne-Jones, W. F. K. (1963). Reaction of atomic oxygen with Carbon. *Nature* 198, 1195–1196. doi: 10.1038/1981195a0

Mawhinney, D. B., and Yates, J. T. (2001). FTIR study of the oxidation of amouphous carbon by ozone at 300K –Direct COOH formation. *Carbon* 39, 1167–1173. doi: 10.1016/S0008-6223(00)00238-4

Mok, Y. S., Koh, D. J., Shin, D. N., and Kim, K. T. (2009). Gaseous ozone decomposition using a nonthermal plasma reactor with adsorbent and dielectric pellets. *Kor. J. Chem. Eng.* 26, 1613–1619. doi: 10.1007/s11814-009-0248-x

Okumoto, M., Kim, H. H., Takashima, K., Katsura, S., and Mizuno, A. (2001). Reactivity of methane in nonthermal plasma in the presence of oxygen and inert gases at atmospheric pressure. *IEEE Trans. Ind. Appl.* 37, 1618–2001. doi: 10.1109/28.968169

Pattabiraman, P., Rodriguez, N. M., Jang, B. Z., and Baker, R. T. K. (1990). A study of the interaction of atomic oxygen with various carbonaceous materials. *Carbon* 28, 867–878. doi: 10.1016/0008-6223(90)90335-V

Pieck, C. L., Jablonski, E. L., and Parera, J. M. (1994). "Regeneration of coked Pt-Re/Al$_2$O$_3$ catalyst by burning with oxygen and ozone," in *Catalyst Deactivation*, eds. B. Delmon, and G. F. Froment (Amsterdam: Elsevier Science Publ B V), 289–295. doi: 10.1016/S0167-2991(08)62752-4

Pieck, C. L., Vera, C. R., Querini, C. A., and Parera, J. A. (2005). Differences in coke burning-off from Pt-Sn/Al$_2$O$_3$ catalyst with oxygen or ozone. *Appl. Catal. A Gen.* 278, 173–180. doi: 10.1016/j.apcata.2004.05.001

Silva, A. O. S., Souza, M. J. B., Aquino, J. M. F. B., Fernandes, V. J., and Araújo, A. S. (2004). Coke removal of the HZSM-12 zeolite with different silica/alumina ratio. *J. Therm. Anal. Calorim.* 75, 699–704. doi: 10.1023/B:JTAN.0000027165.62244.ea

Smith, D. M., and Chughtai, A. R. (1995). The surface structure and reactivity of black carbon. *Colloids Surf. A Physicochem. Eng. Aspects* 105, 47–77. doi: 10.1016/0927-7757(95)03337-1

Snyder, H. R., and Anderson, G. K. (1998). Effect of air and oxygen content on the dielectric barrier discharge decomposition of chlorobenzene. *IEEE Trans. Plasma Sci.* 26, 1695–1699. doi: 10.1109/27.747888

Subrahmanyam, C., Bulushev, D. A., and Kiwi-Minsker, L. (2005). Dynamic behaviour of activated carbon catalysts during ozone decomposition at room temperature. *Appl. Catal. B Environ.* 61, 98–106. doi: 10.1016/j.apcatb.2005.04.013

Sung, Y. M., and Sakoda, T. (2005). Optimum conditions for ozone formation in a micro dielectric barrier discharge. *Surf. Coat. Technol.* 197, 148–153. doi: 10.1016/j.surfcoat.2004.09.031

Takeuchi, T., and Itoh, T. (1993). Removal of ozone from air by activated carbon treatment. *Sep. Sci. Technol.* 3, 168–175. doi: 10.1016/0956-9618(93)80017-L

Tanabe, K. (1989). *Solid Acids and Bases: Their Catalytic Properties.* Tokyo: Elsevier.

Tanable, K., Misono, M., Ono, M., and Hattori, H. (1989). *New Solid Acids and Bases. Their Catalytic Properties.* Tokyo: Elsevier.

Teranishi, K., Shimomura, N., Suzuki, S., and Itoh, H. (2009). Development of dielectric barrier discharge-type ozone generator constructed with piezoelectric transformers: effect of dielectric electrode materials on ozone generation. *Plasma Sour. Sci. Technol.* 18:045011. doi: 10.1088/0963-0252/18/4/045011

Timofeeva, M. N. (2003). Acid catalysis by heteropoly acids. *Appl. Catal. A Gen.* 256, 19–35. doi: 10.1016/S0926-860X(03)00386-7

Tsukuda, E., Sato, S., Takahashi, R., and Sodesawa, T. (2007). Production of acrolein from glycerol over silica-supported heteropoly acids. *Catal. Commun.* 8, 1349–1353. doi: 10.1016/j.catcom.2006.12.006

Wang, F., Dubois, J.-L., and Ueda, W. (2009). Catalytic dehydration of glycerol over vanadium phosphate oxides in the presence of molecular oxygen. *J. Catal.* 268, 260–267. doi: 10.1016/j.jcat.2009.09.024

Wang, F., Dubois, J.-L., and Ueda, W. (2010). Catalytic performance of vanadium pyrophosphate oxides (VPO) in the oxidative dehydration of glycerol. *Appl. Catal. A Gen.* 376, 25–32. doi: 10.1016/j.apcata.2009.11.031

Weigert, W. M., and Haschke, H. (1976). *Acrolein and Derivatives.* New York, NY: Marcel Dekker, Inc.

Wu, Y., Ye, X., Yang, X., Wang, X., Chu, W., and Hu, Y. (1996). Heterogenization of heteropolyacids: a general discussion on the preparation of supported acid catalysts. *Ind. Eng. Chem. Res.* 35, 2546–2560. doi: 10.1021/ie950473s

Zou, B., Ren, S., and Ye, X. P. (2016). Glycerol dehydration to acrolein catalyzed by ZSM-5 Zeolite in Supercritical Carbon Dioxide Medium. *ChemSusChem* 9, 3268–3271. doi: 10.1002/cssc.201601020

Selective Electrochemical Conversion of Glycerol to Glycolic Acid and Lactic Acid on a Mixed Carbon-Black Activated Carbon Electrode in a Single Compartment Electrochemical Cell

Ching Shya Lee[1,2]*, Mohamed Kheireddine Aroua[3,4]*, Wan Ashri Wan Daud[1], Patrick Cognet[2], Yolande Pérès[2] and Mohammed A. Ajeel[5]

[1] Department of Chemical Engineering, Faculty of Engineering, University of Malaya, Kuala Lumpur, Malaysia, [2] Laboratoire de Génie Chimique, Université de Toulouse, CNRS, INP, UPS, Toulouse, France, [3] Centre for Carbon Dioxide Capture and Utilization (CCDCU), School of Science and Technology, Sunway University, Bandar Sunway, Malaysia, [4] Department of Engineering, Lancaster University, Lancaster, United Kingdom, [5] Department of Chemistry, Al-Karkh University of Science, Baghdad, Iraq

In recent years, the rapid swift increase in world biodiesel production has caused an oversupply of its by-product, glycerol. Therefore, extensive research is done worldwide to convert glycerol into numerous high added-value chemicals i.e., glyceric acid, 1,2-propanediol, acrolein, glycerol carbonate, dihydroxyacetone, etc. Hydroxyl acids, glycolic acid and lactic acid, which comprise of carboxyl and alcohol functional groups, are the focus of this study. They are chemicals that are commonly found in the cosmetic industry as an antioxidant or exfoliator and a chemical source of emulsifier in the food industry, respectively. The aim of this study is to selectively convert glycerol into these acids in a single compartment electrochemical cell. For the first time, electrochemical conversion was performed on the mixed carbon-black activated carbon composite (CBAC) with Amberlyst-15 as acid catalyst. To the best of our knowledge, conversion of glycerol to glycolic and lactic acids via electrochemical studies using this electrode has not been reported yet. Two operating parameters i.e., catalyst dosage (6.4–12.8% w/v) and reaction temperature [room temperature (300 K) to 353 K] were tested. At 353 K, the selectivity of glycolic acid can reach up to 72% (with a yield of 66%), using 9.6% w/v catalyst. Under the same temperature, lactic acid achieved its highest selectivity (20.7%) and yield (18.6%) at low catalyst dosage, 6.4% w/v.

Keywords: glycerol, electro-oxidation, electro-reduction, lactic acid, glycolic acid

INTRODUCTION

Glycolic and lactic acids are hydroxyl acids consisting of carboxyl and alcohol groups. Glycolic acid is extensively used as a chemical exfoliator or antioxidant in the cosmetic industry. Similarly, lactic acid also shows broad applications in cosmetic and pharmaceutical industries. Considering the increasing demand of both acids in the cosmetic industry, the international market of lactic and

glycolic acids has grown rapidly and is expected to reach USD $382 million (Research and Markets, 2015) and USD $2.78 billion (Grand_View_Research, 2016) by 2020, respectively.

Previous studies demonstrated that glycolic and lactic acids can be synthesized from a glycerol oxidation process (Kumar et al., 2008; Zhou et al., 2008; Lakshmanan et al., 2013; Purushothaman et al., 2014). The product variation is extremely reliant on the catalyst structure, especially the porosity of the catalyst support, and the type of metal catalyst and its particle size. Additionally, reaction conditions such as reaction temperature, the acidity or basicity of the medium and mole ratio of metal to substrate are also key factors that could influence the product selectivity (Katryniok et al., 2011; Bagheri et al., 2015; Wang et al., 2015). **Table 1** shows the product selectivity and yield of glycolic and lactic acids which were obtained through the catalytic reaction from glycerol. From the study carried out by Lux et al., lactic acid was produced through a hybrid process of combining the electrochemical and catalytic process. In this approach, glycerol was initially converted to dihydroxyacetone and glyceraldehyde via electrochemical oxidation and then be catalytically converted to lactic acid. While the product selectivity of lactic acid is high, this process required complicated reaction set-up (Lux et al., 2010). In view of the work carried out by Lux et al., a single compartment electrochemical process is presented in this study in order to convert lactic acid from glycerol in a single step reaction.

Furthermore, as compared to the catalytic process that is usually conducted under high temperature and high pressure conditions, this study has focused on the electrochemical approach, which is performed over a new electrode: the mixed carbon-black activated carbon electrode (CBAC). The electrochemical process is a simple and robust process which can operate under low reaction temperature and ambient pressure. In agreement to the study by Zhou et al. (2018), electrochemical valorization of glycerol offers an absolutely green route to produce high added-value compounds. They studied a series of electrocatalyst from graphene nano-sheet supported Pt to oxidize glycerol to glycolic acid. A maximum selectivity of 65.4 % glycolic acid was obtained at applied potential 0.2 V (Zhou et al., 2018). Dai et al. (2017) studied the electrochemical conversion of glycerol to lactic acid on AuPt nanoparticle. At potential 0.45 V, the selectivity for lactic acid was up to 73%. In another study, Lam et al. (2017) produced lactic acid from glycerol over cobalt-based oxidative catalyst under galvanostatic mode with 43% of selectivity.

Although electrochemical conversion of glycerol to glycolic and lactic acids has been previously explored (Fashedemi et al., 2015; Hunsom and Saila, 2015; Saila and Hunsom, 2015; Dai et al., 2017; Lam et al., 2017; Zhou et al., 2018), all the studies deployed expensive materials for working electrodes, such as gold, platinum, palladium etc. In this study, the electrode material (activated carbon) consumed is greener and more cost effective compared to the noble metal electrode. The cost of the noble metal and activated carbon (per gram) are presented in **Table 2** (Sigma_Aldrich[1]). The new carbon-based cathode

electrodes (CBAC) were investigated by the author in an earlier study to produce 1,2-propanediol (1,2-PDO) from electro-reduction of glycerol. The selectivity of 1,2-PDO was reported as high as 86 % on CBAC electrode (Lee et al., 2017). Due to the high selectivity and reduction in material costs in the first attempt (Lee et al., 2017), this new electrode is proposed in the present study. The effect of catalyst dosage and reaction temperature will be explored and the reaction mechanism is proposed.

METHODOLOGY

Electrode Preparation

In this work, similar carbon electrode was prepared as reported by Lee et al. (2017) in her first study on the electro-reduction of glycerol (Lee et al., 2017). This carbon electrode was used as the cathode electrode in this current effort. The CBAC electrode (with geometrical surface area of 3.5 cm^2) was prepared by blending 20 wt.%. carbon black (99% purity, specific surface area of 550 m^2/g and average particle size of 13 nm; Alfa-chemicals, Malaysia) and 80 wt.% activated carbon (99.5% purity, specific surface area of 950 m^2/g and average particle size of 100 μm,; Sigma Aldrich[1]) to a total weight of 1.0 g.

Later, 80% v/v 1,3-propanediol and 20% v/v polytetrafluoroethylene were added into the pre-mixed carbon powder to form a liquid-to-powder proportion of 2:1. The slurry was hard-pressed carefully to a round shape mold and dried in the oven based on the subsequent heating program: 373 K (2 h), 453 K (1 h), 523 K (1 h), and lastly 623 K for 30 min to allow the powder to dry completely and improve the electrode rigidity (Ajeel et al., 2015). The appearance of the electrode was characterized by scanning electron microscopy (SEM) equipped with an energy-dispersive E-ray (EDX) analyse (Hitachi SU-8000, Japan). The active surface areas of the electrode was acquired from the Cottrell equation as follows,

$$I = \frac{nFAD^{1/2}C_0}{\pi^{1/2}t^{1/2}} \tag{1}$$

where I is the current (A), D is the diffusion coefficient (6.20 × 10^{-6} cm^2/s), F is the Faraday constant 96487 (C/mol), A is the active surface area of the electrode (cm^2), t is the time (s), n is the number of electrons and C_0 is the bulk concentration of K$_4$Fe(CN)$_6$ (mol/cm^3).

Electrochemical Conversion

Electrochemical experiment was carried out in a single compartment electrochemical cell as shown in **Figure 1**. The cell was filled with 0.1 L of 0.30 M of 99% purity glycerol solution and the reaction was performed over Pt anode electrode (geometrical surface area: 33 cm^2) and CBAC cathode electrode (geometrical surface area: 3.5 cm^2) for 8 h. A constant current at 2.0 A was supplied to the system by a DC power supply. In this study, Amberlyst-15 was used as an acid catalyst. The acid catalyst was investigated by the author in an earlier study. It showed that the strong sulfonic acid group in the Amberlyst-15 can enhance

TABLE 1 | The product yield and selectivity of glycolic and lactic acids; and glycerol conversion attained from the previous catalytic approaches.

Type of catalyst	Conditions	Glycerol conversion (%)	Lactic acid		Glycolic acid		References
			Y (%)	S (%)	Y (%)	S (%)	
Au/C (1% CB)	T: 333 K P O$_2$: 1 Mpa	100			–	40	Demirel-Gülen et al., 2005
Au/C (5% CB)	Time: 3 h NaOH medium	100			–	36	
Au/C	T: 323 K P O$_2$: 0.3 Mpa	90			–	17.0	Dimitratos et al., 2006
Pd/C	NaOH medium	90			–	5.6	
Pt	T: 333 K	40			–	22	Rodrigues et al., 2013
Pt/C	P O$_2$: 0.3 Mpa	81			–	19	
Au/C	Time: 3 h	61			–	18	
Pt/C-Au/C	NaOH medium	98			–	20	
Ptt/S-CNFs	T: 333 K P O$_2$: 0.4 MPa Time: 6 h	89.9			–	8.9	Zhang et al., 2015
Au/PUF (295 nm)	T: 333 K	30			–	76	Gil et al., 2014
Au/PUF (236 nm)	P O$_2$: 0.5 MPa	30			–	74	
Au/PUF (111 nm)	Time: 1 h	30			–	50	
Au/PUF (138 nm)	NaOH medium	30			–	55	
Pt/MCN N amount: 3.3 g	T: 333 K P O$_2$: 0.3 MPa	88.5			–	12.1	Wang et al., 2015
N amount: 2.7 g	Time: 4 h	63.1			–	6.3	
AuPd/C + Mg(OH)$_2$	Au: Pd = 1: 1.85 Catalyst = 1% wt T: 60°C Time: 4 h P O$_2$: 3 bar	40			–	10	Fu et al., 2018
AuPd/C + NaHCO$_3$	T: 60°C	30			–	10	
Bi-AuPt/Ac	O$_2$ flow: 15 ml/min	31.5				14.3	Motta et al., 2018
Pt/C (NaOH)	T: 473 K P H$_2$: 4 MPa Time: 5 h	20 92 (5 h)	–	0.62 0.48			Maris and Davis, 2007
Ru/C (NaOH)		20 100 (5 h)	–	0.47 0.34			
Pt/C (CaO)		30 100 (5 h)	–	0.58 0.58			
Ru/C (CaO)		20 85 (5 h)	–	0.54 0.48			
Alkaline metal-hydroxide	T: 573 K Time: 1.5 h						Shen et al., 2009
KOH		>90	90.0	–			
NaOH		>90	87.1	–			
LiOH		>90	81.2	–			
Au-Pt/TiO$_2$	T: 363 K P: 0.1 MPa NaOH medium	30	–	85.6			Shen et al., 2010
Ir-based catalyst	T: 433 K P N$_2$: 0.1 MPa Time: 15 h KOH medium	34.8	–	>95			Sharninghausen et al., 2014
Au-Pt/nCeO$_2$	T: 373 K P O$_2$: 0.5 MPa Time: 30 min NaOH medium	99	–	80			Purushothaman et al., 2014
Au/CeO$_2$	T: 363 K P O$_2$: 0.1 MPa NaOH medium	98	–	83			Lakshmanan et al., 2013

(Continued)

TABLE 1 | Continued

Type of catalyst	Conditions	Glycerol conversion (%)	Lactic acid		Glycolic acid		References
			Y (%)	S (%)	Y (%)	S (%)	
Ru/La$_2$O$_3$	T: 453 K P H$_2$: 5 MPa Time: 10 h	31.5	–	8.5			Feng et al., 2014
Ru/MgO		60.4	–	21.3			
Ru/CeO$_2$		85.2	–	3.1			
Pt/C	T: 363 K P O$_2$: 0.1 MPa Time: 6 h LiOH medium	100	–	69.3			Zhang et al., 2016
Pd/C	T: 503 K P O$_2$: 0.1 MPa Time: 3 h NaOH medium	99	–	68			Arcanjo et al., 2016
Pt/C		99	–	74			
Ir(NHC-PhSO$_3$)(CO)$_2$	T: 115°C Time: 3 h (microwave)		–	91			Finn et al., 2018
	Time: 24 h (conventional)		–	8			
Pt/ZnO	T: 260°C P: 46 atm Time: 30 h	60	60				Bruno et al., 2018

T, Temperature; P, Pressure; atm, atmospheric; Y, Yield; S, Selectivity.

TABLE 2 | The price of noble metal and activated carbon (adapted form Lee et al., 2017).

Type of material	Price (USD $/g)	% Purity	CAS number
Platinum**	2015.00	99	7440-06-4
Palladium**	1260.00	99	7440-05-3
Rhodium**	506.00	99	7440-16-6
Gold**	347.00	99	7440-57-5
Activated carbon*	0.11	99	7782-40-3

**In the form of nanopowder.
*In the form of powder.

the glycerol conversion, product selectivity and yield (Lee et al., 2017). The effect of catalyst dosage (6.4, 9.6, and 12.8% w/v) and reaction temperature [room temperature (300 K), 323 and 353 K] were studied.

Characterization and Quantification of the Electrochemical Conversion

The products obtained were characterized by gas chromatography-mass spectroscopy (GC-MS) (Agilent Model 7890, United States) and quantified by gas chromatography (Agilent Model 6890, United States) equipped with a flame ionization detector (FID). Compounds were separated by a ZB-Wax column (30 m × 0.25 mm × 0.25 mm) (Phenomenex, United States). The obtained chromatograms were compared with the MS library and chemical standards. Glycerol, glycolic
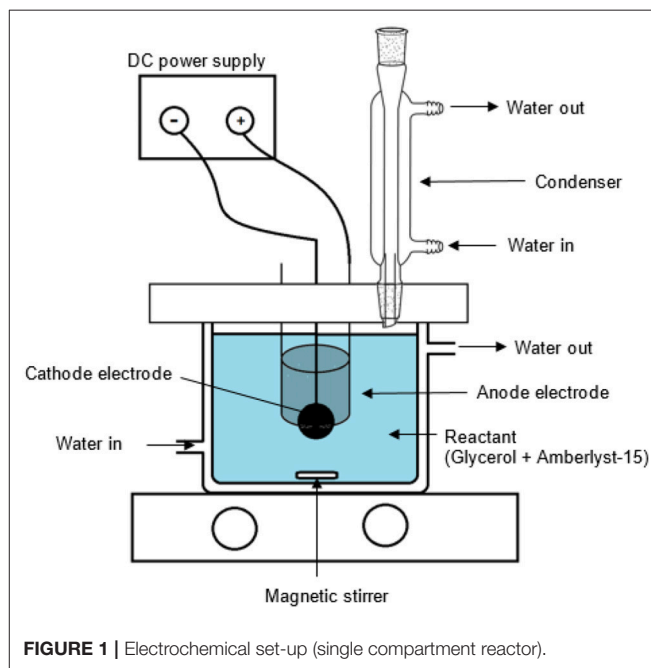
FIGURE 1 | Electrochemical set-up (single compartment reactor).

acid and lactic acid were analyzed using the following procedure: the front inlet temperature was controlled at 240°C. Initially, the oven temperature was fixed at 45°C and maintained for 5 min. Later, it was ramped at 10°C/min to reach 240°C at the final temperature and maintained for another 5 min. The
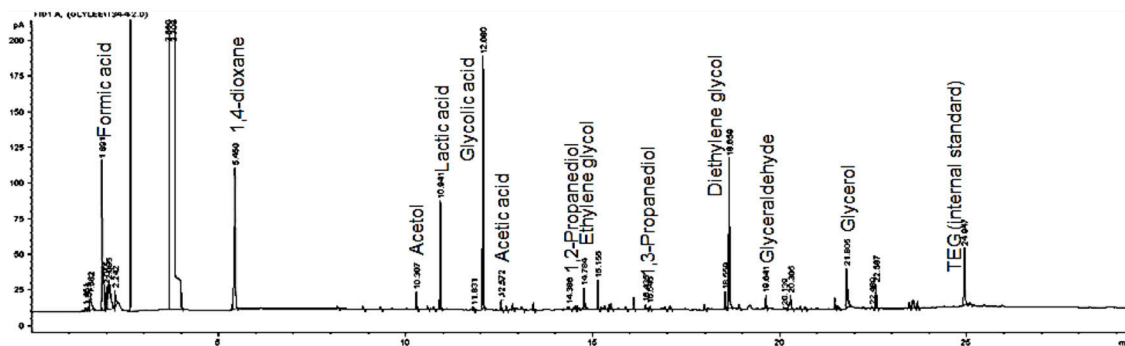
FIGURE 2 | GC chromatogram of the products obtained from the electrochemical conversion of glycerol.

sample injection was 1 μL. Glycerol conversion, product selectivity as well as yield were calculated based on the Equations (2–4), respectively.

$$Glycerol\ conversion\ (\%) = \frac{Gycerol\ converted\ (C\ mole)}{Total\ glycerol\ in\ reactant\ (C\ mole)} \times 100\ \% \quad (2)$$

$$Product\ selectivity\ (\%) = \frac{Product\ (C\ mole)}{Total\ of\ all\ products\ in\ liquid\ phase\ (C\ mole)} \times 100\ \% \quad (3)$$

$$Product\ yield\ (\%) = \frac{Product\ (C\ mole)}{Total\ glycerol\ in\ reactant\ (C\ mole)} \times 100\ \% \quad (4)$$

RESULTS AND DISCUSSION

Electrochemical Conversion

Based on the GC chromatogram as shown in **Figure 2**, the main compounds obtained from this study are glycolic acid and lactic acid. Other compounds i.e., ethylene glycol, acetic acid, formic acid, acetaldehyde, 1,3-propanediol (1,3-PDO), glyceraldehyde, acetol and 1,2-propanediol (1,2-PDO) were produced in small amount.

Reaction Mechanism

In the electrochemical study, glycerol can possibly be oxidized via one of two pathways namely glyceraldehyde pathway or dihydroxyacetone (DHA) pathway. Based on a review published in 2012, the pathway's option can be determined by a few parameters, i.e., electrode material, applied potential, and pH of the reaction medium. In this case study, DHA pathway was involved (Simões et al., 2012). However, DHA was undetectable in the GC analysis. Whereby, it might have gone through the enolization process in the acidic condition (Van De Vyver et al., 2015), and further oxidized into pyruvic acid (PA).

Since the electrochemical process was studied in a single compartment; lactic acid can be formed straightway via electroreduction of PA (Martin et al., 2005, 2006), and so PA was not detected in the analysis too. In addition, the activated carbon-based cathode electrode that was specially prepared for this study is highly porous (SEM image in **Figure 3**), Intermediate compounds that were produced from oxidation and dehydration processes (e.g., hydroxypropanal, pyruvic acid, and acetol) could be trapped or held in the porous surface thus enhancing the electrochemical reduction process (Qi et al., 2014) (**Scheme 1**).
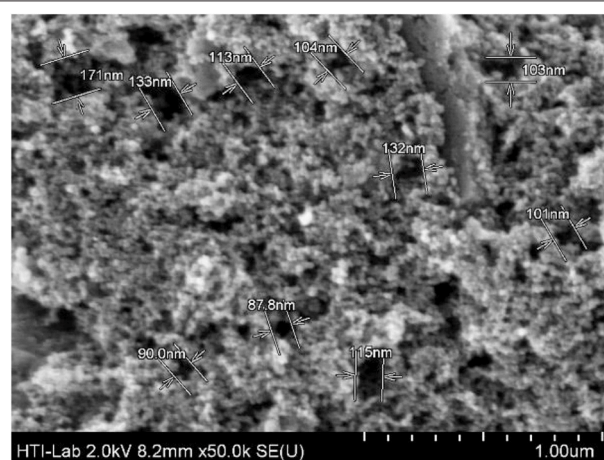
FIGURE 3 | SEM image of CBAC electrode (pore sizes: 90−170 nm).

1,3-PDO and 1,2-PDO were most likely formed from the electroreduction of hydroxylpropanal and acetol, respectively (Hunsom and Saila, 2015). At the anodic region, glycolic acid was likely produced via oxidation of glycerol through C-C bond cleavage. When glycolic acid continued to oxidize, acetic acid could be formed (Gomes et al., 2013). The proposed mechanism is shown in **Scheme 2**.

Effect of Catalyst Dosage

To study the catalyst dosage for Amberlyst-15, the catalyst dosage was varied ranging from 6.4 to 12.8% w/v. Other parameters such as temperature (353 k), and applied electric current (2.0 A) were maintained constant for 8 h. The glycerol conversion rate is described in **Figure 4**. When the catalyst dosage increases, the conversion rate increased from 0.635 to 0.724 h^{-1}. As seen in **Figure 5**, the product distributions varied when the catalyst dosage increased. The highest glycolic acid yield was achieved after 6 h with selectivity of 72.0%, using 9.6% w/v of catalyst. However, lactic acid preferred at low catalyst dosage (6.4% w/v), 18.6% of yield was obtained after 6 h of reaction. After a critical dosage of catalyst, the conversion slightly reduced.
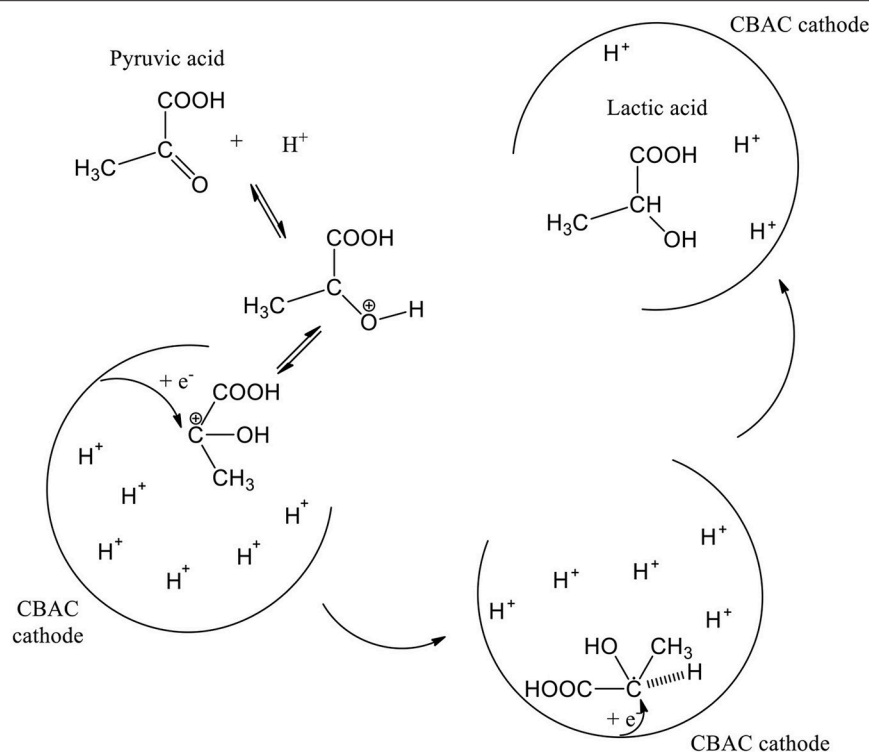
SCHEME 1 | Formation of lactic acid on the porous surface of CBAC cathode electrode.

It can be attributed to the poisoning effect of catalyst. The products may compete with the reactant for the active sites thus causing a self-inhibitive effect, decreasing the conversion rate and yields (Bühler et al., 2002; Farma et al., 2013). In this case study, glycolic acid competed with glycerol and further oxidized into other compounds, for example CO_2. **Figure 6** illustrates the glycerol conversion. In all cases, overall the conversions were above 99%.

Effect of Temperature

To study the optimal temperature for electrochemical conversion, the temperature was varied ranging from room temperature (300 K) to 353 K, while keeping other variables constant at 2.0 A and 9.6% w/v of catalyst. Results depicted in **Figure 7** show that the glycerol conversion rates increased with an increase in temperature. At 300 K and 323 K, the conversion rates were around 0.400 h^{-1}. It increased to 0.724 h^{-1}, when the temperature reached 353 K.

During the electrochemical process, a temperature increase accelerates the breakage of C-C bond, thus converting the glycerol into glycolic acid. Highest glycolic acid yield was achieved at 66.1% with selectivity of 72.0% after 6 h of reaction. In addition, an increase in temperature could also enhance OH adsorption on the Pt anode electrode thus reducing the barrier for O-H and C-H dissociations, and subsequently improving the oxidation performance (Beden et al., 1987; Yang et al., 2012; Zhang et al., 2012). Higher temperatures yielded higher production of lactic acid yield (14.8%). This could be due to

the thickness of the diffusion layer which is effectively reduced (Gupta et al., 1984), thus improving the diffusion rate of intermediate compounds such as pyruvic acid to the CBAC cathode electrode which accelerates the formation of lactic acid. **Figure 8** illustrates the products distribution for the three trials. Acetic acid and formic acid were found in all trials. Other compounds e.g., acetaldehyde, ethylene glycol, ethyl acetate and diethylene glycol were observed inconsistently. Overall, 90% glycerol conversion was achieved at the three temperatures, ranging from 300 to 353 K. The results are displayed in **Figure 9**.

Energy Consumption

Energy consumptions in electrochemical conversion of glycerol were examined depending on the operating parameters such as catalyst dosage and temperature. The values were calculated using Equation (5):

$$E_{Gly\ Conv.} = \frac{iU\Delta t}{(C_o - C_t)V} \tag{5}$$

Where, $E_{Gly\ Conv.}$ is energy consumption in glycerol conversion (kWh/kg), i is current (A), U is voltage (V), Δt is time (h), C_0 is initial glycerol concentration (g/L), C_t is final glycerol concentration (g/L), and V is volume (L).

The energy consumption values for glycerol conversion after 8 h of reaction at 2.0 A are tabulated in **Table 3**. Both parameters show similar energy consumed, in the range of 9–12 kWh/kg, due to the conversion of all trials are above 90%.

SCHEME 2 | Proposed reaction mechanism of the overall electrochemical conversion for glycerol.

FIGURE 4 | First-order kinetic model of the electrochemical conversion of glycerol at catalyst dosage ranging from 6.4 to 12.8% w/v. Other parameters such as temperature (353 k), and applied electric current (2.0 A) was maintained constant for 8 h.
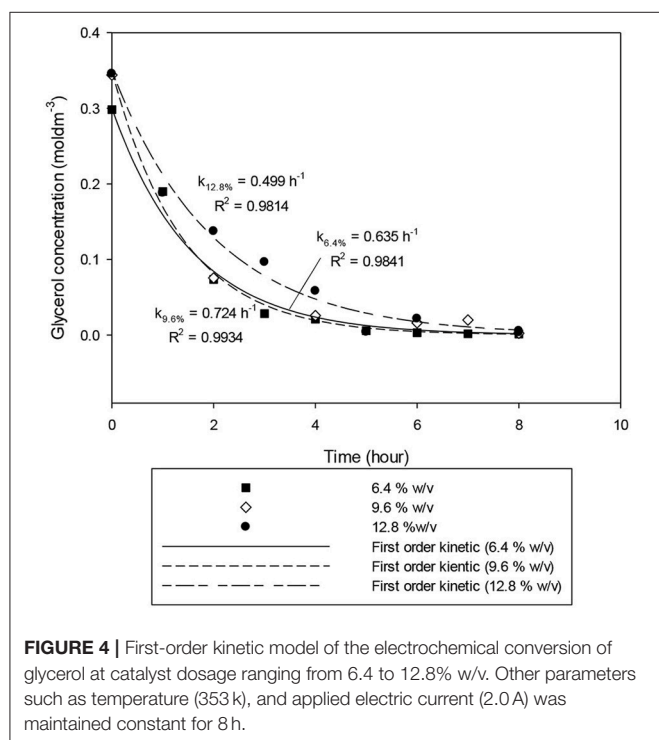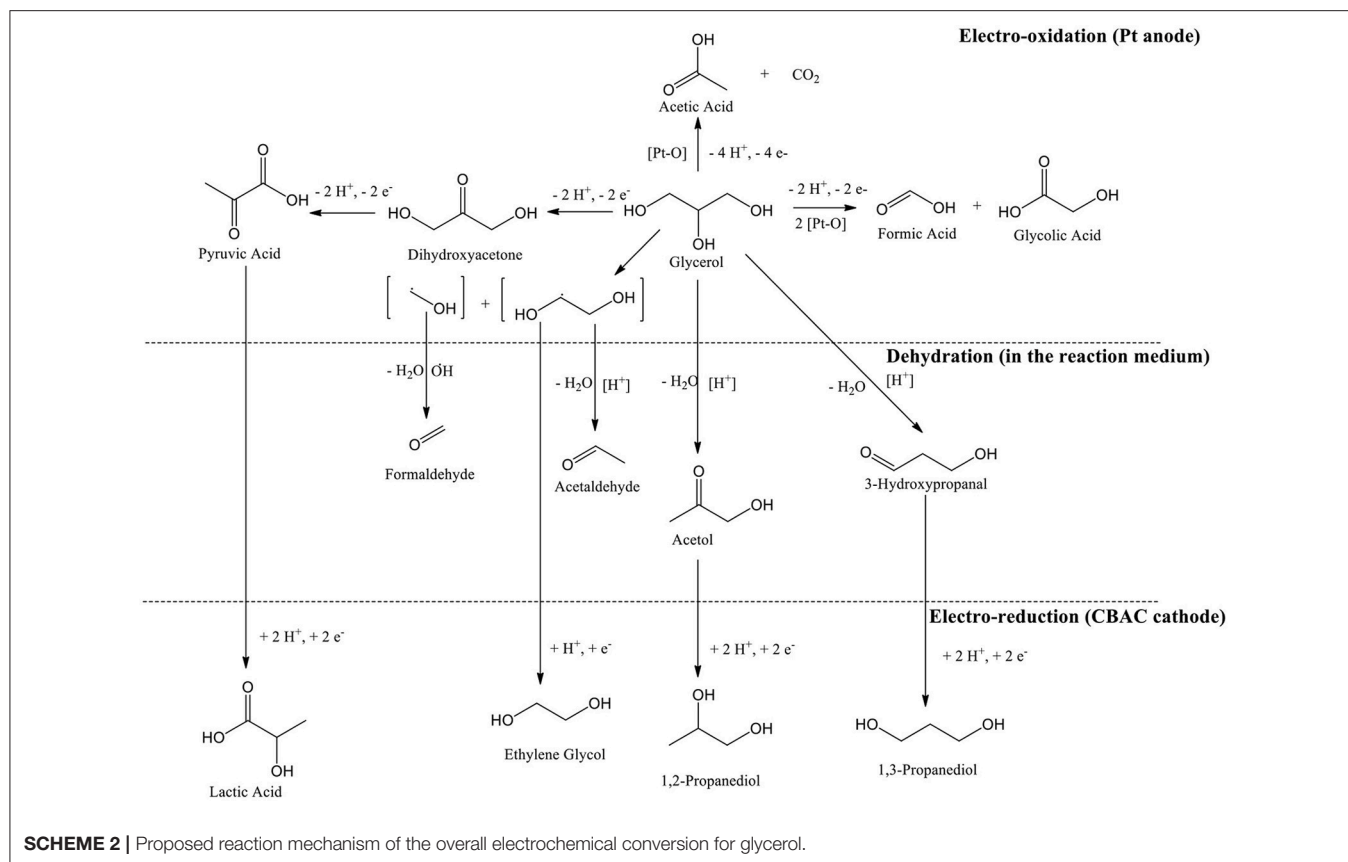
Research Outlook

The proposed electrochemical method resulted in a comparable or higher selectivity of glycolic acid with that previously reported in the studies tabulated in **Table 1**, which is about 72.0%. Nevertheless, the method proposed in this work is simpler, requiring at lower temperature and ambient pressure, which save energy and cost. The catalyst used can accelerate the reaction by enhancing the electron transfer between the electrolyte and electrode (Francke and Little, 2014), thus avoiding over-oxidation to other inauspicious by-products, i.e., acetic acid.

Based on the experimental results, lactic acid's yield and selectivity are lower as compared to the past published works (**Table 1**). Although the results are unpromising, the newly prepared in-house carbon-based electrode (CBAC electrode) appeared to be more cost-effective than the metal-based catalyst used in the reported chemical conversion studies (Arcanjo et al., 2016; Zhang et al., 2016). In accordance with (Qi et al., 2014) and Zhang et al. (2014), pore sizes is the key factor to stimulate the product selectivity, by controlling the activated carbon ratio in the upcoming trials the lactic acid selectivity could be boosted (Qi et al., 2014; Zhang et al., 2014).

Nevertheless, the main challenge for this work lies on separation and purification studies. This is always an

FIGURE 5 | Product distribution of the electrochemical conversion of glycerol at catalyst dosage ranging from **(A)** 6.4, **(B)** 9.6 to **(C)** 12.8% w/v. Other parameters such as temperature (353 k), and applied electric current (2.0 A) was maintained constant for 8 h.

FIGURE 6 | Glycerol conversion from the electrochemical conversion of glycerol at catalyst dosage ranging from 6.4 to 12.8% w/v. Other parameters such as temperature (353 k), and applied electric current (2.0 A) was maintained constant for 8 h.

FIGURE 7 | First-order kinetic model of the electrochemical conversion of glycerol at operating temperature ranging from room temperature (300 K) to 353 K. Other parameters such as applied electric current (2.0 A) and catalyst dosage (9.6% w/v) were maintained for 8 h.

important step in downstream operation to recover those valuable compounds produced from the reaction. The traditional separation methods include solvent extraction, crystallization, ion exchange, precipitation and acidification as well as adsorption. Nowadays, these methods become less popular because they hardly meet the modern green chemistry requirement (Anastas and Breen, 1997). Membrane technologies have attracted significant interests in recent years. Nano-filtration, electro-deionization, and electro-dialysis are the common separation methods that have been widely studied (Huang et al., 2007; González et al., 2008;
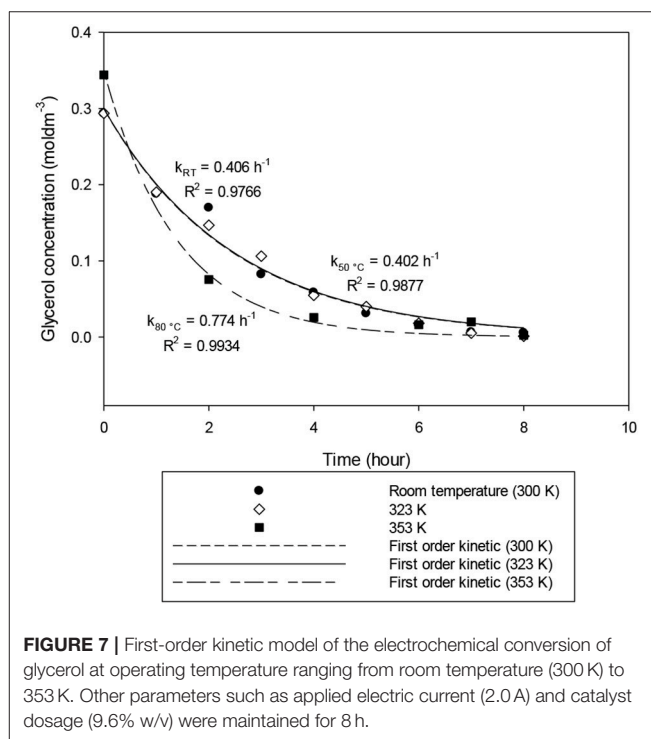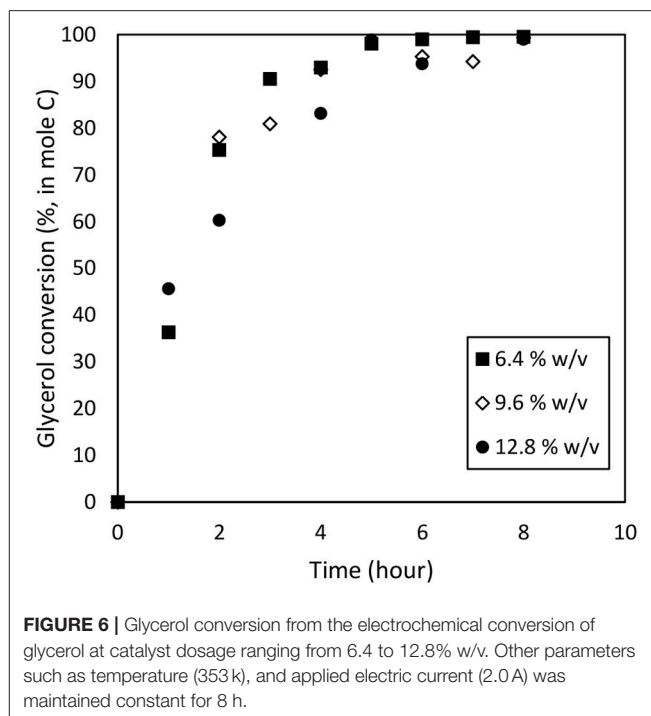
FIGURE 9 | Glycerol conversion from the electrochemical study at operating temperature ranging from room temperature (300 K) to 353 K. Other parameters such as applied electric current (2.0 A) and catalyst dosage (9.6% w/v) were maintained for 8 h.

TABLE 3 | Energy consumption in electrochemical conversion of glycerol depending on operating parameters.

Operating parameters	Reaction conditions	Energy consumption of glycerol conversion (kWh/kg)
Catalyst Dosage	Glycerol Concentration: 0.3 M Volume: 0.1 L Current: 2.0 A Catalyst: 6.4–12.8 % w/v Potential: 15.4–20.4 V	9.0–12.8
Reaction temperature	Glycerol concentration: 0.3 M Volume: 0.1 L Current: 2.0 A Catalyst: 300–353 K Potential: 15.4–16.8 V	9.0–12.7

FIGURE 8 | Product distribution from the electrochemical conversion of glycerol at operating temperature ranging from **(A)** room temperature (300 K); **(B)** 323 K to **(C)** 353 K. Other parameters such as applied electric current (2.0 A) and catalyst dosage (9.6% w/v) were maintained for 8 h.

Boontawan et al., 2011). Electro-dialysis which consists of a cation-selective membrane, an anion-selective membrane in a two-compartment cell is suggested for future product purification as it has been extensively reported in the previous literatures for recovery of pyruvate (Zeli and Vasić-Rački, 2005), glycine (Elisseeva et al., 2002), formic acid (Luo et al., 2002), lactate (Boniardi et al., 1996; Danner et al., 2000; Madzingaidzo et al., 2002; Hábová et al., 2004), and propionate (Fidaleo and Moresi, 2006).

CONCLUSIONS

In this study, the single compartment electrochemical conversion for glycerol was examined. Glycerol was successfully converted to glycolic acid and lactic acid on the Pt anode electrode and the new activated carbon-based cathode electrode: CBAC electrode. Based on the optimization study, the experimental

conditions favorable to glycolic acid production were a 353 K temperature with 9.6% w/v Amberlyst-15, leading to the highest yield of 66.1% and selectivity of 72.0%. Lactic acid was preferably generated at 353 K with the presence of 6.4% w/v Amberlyst-15. In this conditions, the highest yield obtained was 18.6% with selectivity of 20.7%. The highest glycerol conversions achieved were around 99%. These findings successfully provide a new route to convert glycerol to lactic acid via one step electrochemical process.

DATA AVAILABILITY

All datasets generated for this study are included in the manuscript and/or the supplementary files.

AUTHOR CONTRIBUTIONS

ACKNOWLEDGMENTS

REFERENCES

Ajeel, M. A., Aroua, M. K., and Daud, W. M., (2015). Anodic Degradation of 2-chlorophenol by carbon black diamond and activated carbon composite electrodes. *Electrochim. Acta* 180, 22–28. doi: 10.1016/j.electacta.2015.08.062

Anastas, P. T., and Breen, J. J. (1997). Design for the environment and green chemistry: the heart and soul of industrial ecology. *J. Cleaner Produc.* 5, 97–102. doi: 10.1016/S0959-6526(97)00025-5

Arcanjo, M. R. A., Silva I. J. Jr, Rodríguez-Castellón, E., Infantes-Molina, A., and Vieira, R. S. (2016). Conversion of glycerol into lactic acid using Pd or Pt supported on carbon as catalyst. *Catal. Today.* 279, 317–326. doi: 10.1016/j.cattod.2016.02.015

Bagheri, S., Julkapli, N. M., and Yehye, W. A. (2015). Catalytic conversion of biodiesel derived raw glycerol to value added products. *Renew. Sustain. Energy Rev.* 41, 113–127. doi: 10.1016/j.rser.2014.08.031

Beden, B., Çetin, I., Kahyaoglu, A., Takky, D., and Lamy, C. (1987). Electrocatalytic oxidation of saturated oxygenated compounds on gold electrodes. *J. Catal.* 104, 37–46. doi: 10.1016/0021-9517(87)90334-4

Boniardi, N., Rota, R., Nano, G., and Mazza, B. (1996). Analysis of the sodium lactate concentration process by electrodialysis. *Separat. Technol.* 6, 43–54. doi: 10.1016/0956-9618(96)00139-7

Boontawan, P., Kanchanathawee, S., and Boontawan, A. (2011). Extractive fermentation of l-(+)-lactic acid by Pediococcus pentosaceus using electrodeionization (EDI) technique. *Biochem. Eng. J.* 54, 192–199. doi: 10.1016/j.bej.2011.02.021

Bruno, A. M., Chagas, C. A., Souza, M. M. V. M., and Manfro, R. L. (2018). Lactic acid production from glycerol in alkaline medium using Pt-based catalysts in continuous flow reaction system. *Renew. Energy* 118, 160–171. doi: 10.1016/j.renene.2017.11.014

Bühler, W., Dinjus, E., Ederer, H. J., Kruse, A., and Mas, C. (2002). Ionic reactions and pyrolysis of glycerol as competing reaction pathways in near- and supercritical water. *J. Supercrit. Fluids* 22, 37–53. doi: 10.1016/S0896-8446(01)00105-X

Dai, C., Sun, L., Liao, H., Khezri, B., Webster, R. D., Fisher, A. C., and Xu, Z. J. (2017). Electrochemical production of lactic acid from glycerol oxidation catalyzed by AuPt nanoparticles. *J. Catal.* 356, 14–21. doi: 10.1016/j.jcat.2017.10.010

Danner, H., Madzingaidzo, L., Holzer, M., Mayrhuber, L., and Braun, R. (2000). Extraction and purification of lactic acid from silages. *Bioresour. Technol.* 75, 181–187. doi: 10.1016/S0960-8524(00)00068-7

Demirel-Gülen, S., Lucas, M., and Claus, P. (2005). Liquid phase oxidation of glycerol over carbon supported gold catalysts. *Catal. Today* 102–103, 166–172. doi: 10.1016/j.cattod.2005.02.033

Dimitratos, N., Lopez-Sanchez, J. A., Lennon, D., Porta, F., Prati, L., and Villa, A. (2006). Effect of particle size on monometallic and bimetallic (Au,Pd)/C on the liquid phase oxidation of glycerol. *Catal. Lett.* 108, 147–153. doi: 10.1007/s10562-006-0036-8

Elisseeva, T. V., Shaposhnik, V. A., and Luschik, I. G. (2002). Demineralization and separation of amino acids by electrodialysis with ion-exchange membranes. *Desalination.* 149, 405–409. doi: 10.1016/S0011-9164(02)00763-4

Farma, R., Deraman, M., Awitdrus, A., Talib, I. A., Taer, E., Basri, N. H., et al. (2013). Preparation of highly porous binderless activated carbon electrodes from fibres of oil palm empty fruit bunches for application in supercapacitors. *Bioresour. Technol.* 132, 254–261. doi: 10.1016/j.biortech.2013.01.044

Fashedemi, O. O., Miller, H. A., Marchionni, A., Vizza, F., and Ozoemena, K. I. (2015). Electro-oxidation of ethylene glycol and glycerol at palladium-decorated FeCo@Fe core-shell nanocatalysts for alkaline direct alcohol fuel cells: functionalized MWCNT supports and impact on product selectivity. *J. Mater. Chem. A* 3, 7145–7156. doi: 10.1039/C5TA00076A

Feng, J., Xiong, W., Xu, B., Jiang, W., Wang, J., and Chen, H. (2014). Basic oxide-supported Ru catalysts for liquid phase glycerol hydrogenolysis in an additive-free system. *Catal. Commun.* 46, 98–102. doi: 10.1016/j.catcom.2013.11.031

Fidaleo, M., and Moresi, M. (2006). Assessment of the main engineering parameters controlling the electrodialytic recovery of sodium propionate from aqueous solutions. *J. Food Eng.* 76, 218–231. doi: 10.1016/j.jfoodeng.2005.05.010

Finn, M., Ridenour, J. A., Heltzel, J., Cahill, C., and Voutchkova-Kostal, A. (2018). Next-generation water-soluble homogeneous catalysts for conversion of glycerol to lactic acid. *Organometallics* 37, 1400–1409. doi: 10.1021/acs.organomet.8b00081

Francke, R., and Little, R. D. (2014). Redox catalysis in organic electrosynthesis: basic principles and recent developments. *Chem. Soc. Rev.* 43, 2492–2521. doi: 10.1039/c3cs60464k

Fu, J., He, Q., Miedziak, P. J., Brett, G. L., Huang, X., Pattisson, S., Douthwaite, M., and Hutchings, G. J. (2018). The Role of Mg(OH)2 in the So-Called "Base-Free" Oxidation of Glycerol with AuPd Catalysts. *Chem. A Eur. J.* 24, 2396–2402. doi: 10.1002/chem.201704151

Gil, S., Cuenca, N., Romero, A., Valverde, J. L., and Sánchez-Silva, L. (2014). Optimization of the synthesis procedure of microparticles containing gold for the selective oxidation of glycerol. *Appl. Catal. A* 472, 11–20. doi: 10.1016/j.apcata.2013.12.008

Gomes, J. F., Martins, C., Giz, M. J., Tremiliosi-Filho, G., and Camara, G. A. (2013). Insights into the adsorption and electro-oxidation of glycerol: Self-inhibition and concentration effects. *J. Catal.* 301, 154–161. doi: 10.1016/j.jcat.2013.02.007

González, M. I., Alvarez, S., Riera, F. A., and Álvarez, R. (2008). Lactic acid recovery from whey ultrafiltrate fermentation broths and artificial solutions by nanofiltration. *Desalination* 228, 84–96. doi: 10.1016/j.desal.2007.08.009

Grand_View_Research, I. (2016). *Global Glycolic Acid Market by Application (Personal Care, Household Cleaning, Industrial) is Expected to Reach USD 277.8 Million by 2020 [Online]. Grand View Research, Inc.* Available online at : https://www.grandviewresearch.com/press-release/global-glycolic-acid-market (Accessed 14 July 2016).

Gupta, O. P., Chauhan, M., and Loomba, R. (1984). Study of the variation in the cathode potential with temperature in Ni-Cd alloy plating from a sulphate bath. *Surface Technol.* 21, 155–160. doi: 10.1016/0376-4583(84)90158-4

Hábová, V., Melzoch, K., Rychtera, M., and Sekavov,á, B. (2004). Electrodialysis as a useful technique for lactic acid separation from a model solution and a fermentation broth. *Desalination* 162, 361–372. doi: 10.1016/S0011-9164(04)00070-0

Huang, C., Xu, T., Zhang, Y., Xue, Y., and Chen, G. (2007). Application of electrodialysis to the production of organic acids: State-of-the-art and recent developments. *J. Membrane Sci.* 288, 1–12. doi: 10.1016/j.memsci.2006.11.026

Hunsom, M., and Saila, P. (2015). Electrochemical conversion of enriched crude glycerol: effect of operating parameters. *Renew. Energy* 74, 227–236. doi: 10.1016/j.renene.2014.08.008

Katryniok, B., Kimura, H., Skrzynska, E., Girardon, J.-S., Fongarland, P., Capron, M., et al. (2011). Selective catalytic oxidation of glycerol: perspectives for high value chemicals. *Green Chem.* 13, 1960–1979. doi: 10.1039/c1gc15320j

Kumar, K. S., Haridoss, P., and Seshadri, S. K. (2008). Synthesis and characterization of electrodeposited Ni-Pd alloy electrodes for methanol oxidation. *Surface Coat. Technol.* 202, 1764–1770. doi: 10.1016/j.surfcoat.2007.07.035

Lakshmanan, P., Upare, P. P., Le, N.-T., Hwang, Y. K., Hwang, D. W., Lee, U. H., et al. (2013). Facile synthesis of CeO2-supported gold nanoparticle catalysts for selective oxidation of glycerol into lactic acid. *Appl. Catal. A* 468, 260–268. doi: 10.1016/j.apcata.2013.08.048

Lam, C. H., Bloomfield, A. J., and Anastas, P. T. (2017). A switchable route to valuable commodity chemicals from glycerol via electrocatalytic oxidation with an earth abundant metal oxidation catalyst. *Green Chem.* 19, 1958–1968. doi: 10.1039/C7GC00371D

Lee, C. S., Aroua, M. K., Wan Daud, W. M. A., Cognet, P., Pérès, Y., and Ajeel, M. A. (2017). Selective electroreduction of glycerol to 1,2-propanediol on a mixed carbon-black activated carbon electrode and a mixed carbon black-diamond electrode. *BioResources* 13, 115–130. doi: 10.15376/biores.13.1.115-130

Luo, G. S., Pan, S., and Liu, J. G. (2002). Use of the electrodialysis process to concentrate a formic acid solution. *Desalination* 150, 227–234. doi: 10.1016/S0011-9164(02)00978-5

Lux, S., Stehring, P., and Siebenhofer, M. (2010). Lactic acid production as a new approach for exploitation of glycerol. *Separat. Sci. Technol.* 45, 1921–1927. doi: 10.1080/01496395.2010.493824

Madzingaidzo, L., Danner, H., and Braun, R. (2002). Process development and optimisation of lactic acid purification using electrodialysis. *J. Biotechnol.* 96, 223–239. doi: 10.1016/S0168-1656(02)00049-4

Maris, E. P., and Davis, R. J. (2007). Hydrogenolysis of glycerol over carbon-supported Ru and Pt catalysts. *J. Catal.* 249, 328–337. doi: 10.1016/j.jcat.2007.05.008

Martin, C., Huser, H., Servat, K., and Kokoh, K. B. (2005). Electrosynthesis of lactic acid on copper and lead cathodes in aqueous media. *Electrochim. Acta* 51, 111–117. doi: 10.1016/j.electacta.2005.04.008

Martin, C., Huser, H., Servat, K., and Kokoh, K. B. (2006). Electrosynthesis of lactic acid and 2,3-dimethyltartaric acid from pyruvic acid on lead cathode in aqueous medium. *Tetrahedron Lett.* 47, 3459–3462. doi: 10.1016/j.tetlet.2006.03.035

Motta, D., Trujillo, F. J. S., Dimitratos, N., Villa, A., and Prati, L. (2018). An investigation on AuPt and AuPt-Bi on granular carbon as catalysts for the oxidation of glycerol under continuous flow conditions. *Catal. Today* 308, 50–57. doi: 10.1016/j.cattod.2017.10.012

Purushothaman, R. K. P., Van Haveren, J., Van Es, D. S., Melián-Cabrera, I., Meeldijk, J. D., and Heeres, H. J. (2014). An efficient one pot conversion of glycerol to lactic acid using bimetallic gold-platinum catalysts on a nanocrystalline CeO2 support. *Appl. Catal. B* 147, 92–100. doi: 10.1016/j.apcatb.2013.07.068

Qi, J., Xin, L., Chadderdon, D. J., Qiu, Y., Jiang, Y., Benipal, N., Liang, C., and Li, W. (2014). Electrocatalytic selective oxidation of glycerol to tartronate on Au/C anode catalysts in anion exchange membrane fuel cells with electricity cogeneration. *Appl. Catal. B-Environ.* 154, 360–368. doi: 10.1016/j.apcatb.2014.02.040

Research and Markets (2015). *Lactic Acid Market by Application (Biodegradable Polymer, Food and Beverage, Personal Care and Pharmaceutical) and Polylactic Acid Market by Application, and by Geography–Global Trends and Forecasts to 2020 [Online]*. Research and Markets. Available online at: http://www.researchandmarkets.com/reports/3505450/lactic-acid-market-by-application-biodegradable?gclid=CI_58sSV7M0CFS8z0wodAj4Iqw (Accessed July14, 2016).

Rodrigues, E. G., Pereira, M. F. R., Chen, X., Delgado, J. J., and Órfão, J.J.M. (2013). Selective oxidation of glycerol over platinum-based catalysts supported on carbon nanotubes. *Indus. Eng. Chem. Res.* 52, 17390–17398. doi: 10.1021/ie402331u

Saila, P., and Hunsom, M. (2015). Effect of additives on one-pot electrochemical conversion of enriched crude glycerol. *Korean J. Chem. Eng.* 32, 2412–2417. doi: 10.1007/s11814-015-0066-2

Sharninghausen, L. S., Campos, J., Manas, M. G., and Crabtree, R. H. (2014). Efficient selective and atom economic catalytic conversion of glycerol to lactic acid. *Nat. Commun.* 5:5084. doi: 10.1038/ncomms6084

Shen, Y., Zhang, S., Li, H., Ren, Y., and Liu, H. (2010). Efficient Synthesis of lactic acid by aerobic oxidation of glycerol on Au–Pt/TiO2 Catalysts. *Chem. A Eur. J.* 16, 7368–7371. doi: 10.1002/chem.201000740

Shen, Z., Jin, F., Zhang, Y., Wu, B., Kishita, A., Tohji, K., and Kishida, H. (2009). Effect of alkaline catalysts on hydrothermal conversion of glycerin into lactic acid. *Indus. Eng. Chem. Res.* 48, 8920–8925. doi: 10.1021/ie900937d

Simões, M., Baranton, S., and Coutanceau, C. (2012). Electrochemical Valorisation of Glycerol. *ChemSusChem* 5, 2106–2124. doi: 10.1002/cssc.201200335

Van De Vyver, S., Odermatt, C., Romero, K., Prasomsri, T., and Román-Leshkov, Y. (2015). Solid lewis acids catalyze the carbon-carbon coupling between carbohydrates and formaldehyde. *ACS Catal.* 5, 972–977. doi: 10.1021/cs5015964

Wang, F., Shao, S., Liu, C.-L., Xu, C.-L., Yang, R.-Z., and Dong, W.-S. (2015). Selective oxidation of glycerol over Pt supported on mesoporous carbon nitride in base-free aqueous solution. *Chem. Eng. J.* 264, 336–343. doi: 10.1016/j.cej.2014.11.115

Yang, F., Hanna, M., and Sun, R. (2012). Value-added uses for crude glycerol–a byproduct of biodiesel production. *Biotechnol. Biofuels* 5, 13. doi: 10.1186/1754-6834-5-13

Zeli,ć, B., and Vasić-Rački, Ã. (2005). Process development and modeling of pyruvate recovery from a model solution and fermentation broth. *Desalination* 174, 267–276. doi: 10.1016/j.desal.2004.09.016

Zhang, C., Wang, T., Liu, X., and Ding, Y. (2016). Selective oxidation of glycerol to lactic acid over activated carbon supported Pt catalyst in alkaline solution. *Chinese J. Catal.* 37, 502–509. doi: 10.1016/S1872-2067(15)61055-5

Zhang, M., Nie, R., Wang, L., Shi, J., Du, W., and Hou, Z. (2015). Selective oxidation of glycerol over carbon nanofibers supported Pt catalysts in a base-free aqueous solution. *Catal. Commun.* 59, 5–9. doi: 10.1016/j.catcom.2014.09.036

Zhang, Z., Xin, L., and Li, W. (2012). Electrocatalytic oxidation of glycerol on Pt/C in anion-exchange membrane fuel cell: Cogeneration of electricity and valuable chemicals. *Appl. Catal. B* 119–120, 40–48. doi: 10.1016/j.apcatb.2012.02.009

Zhang, Z., Xin, L., Qi, J., Chadderdon, D. J., Sun, K., Warsko, K. M., and Li, W. (2014). Selective electro-oxidation of glycerol to tartronate or mesoxalate on Au nanoparticle catalyst via electrode potential tuning in anion-exchange membrane electro-catalytic flow reactor. *Appl. Catal. B* 147, 871–878. doi: 10.1016/j.apcatb.2013.10.018

Zhou, C., Beltramini, J. N., Fan, Y.-X., and Lu, G. Q. (2008). Chemoselective catalytic conversion of glycerol as a biorenewable source to valuable commodity chemicals. *Chem. Soc. Rev.* 37, 527–549. doi: 10.1039/B707343G

Zhou, Y., Shen, Y., and Piao, J. (2018). Sustainable conversion of glycerol into value-added chemicals by selective electro-oxidation on pt-based catalysts. *ChemElectroChem* 5, 1624–1624. doi: 10.1002/celc.201800691

Catalytic Dehydration of Glycerol to Acrolein in a Two-Zone Fluidized Bed Reactor

Benjamin Katryniok[1], Roger Meléndez[1], Virginie Bellière-Baca[2], Patrick Rey[2], Franck Dumeignil[1], Nouria Fatah[1] and Sébastien Paul[1]*

[1] CNRS, Centrale Lille, ENSCL, Univ. Lille, Univ. Artois, UMR 8181 - UCCS - Unité de Catalyse et Chimie du Solide, Lille, France, [2] ADISSEO France SAS, Antony, France

The gas-phase catalytic dehydration of glycerol to acrolein was carried out in a Two-Zone Fluidized-Bed Reactor (TZFBR) using a 20 wt. % phosphotungstic acid ($H_3PW_{12}O_{40}$) catalyst supported on CARIACT-Q10 commercial silica. In the first step, a hydrodynamic study of the reactor was performed. A quality of fluidization of more than 80% was obtained. In the second step, the mechanical stability of the catalyst was studied. It was found that only the external layer of active phase is eliminated under the conditions of operation whereas the global composition of the catalyst was not significantly affected after 44 h of fluidization. Finally, in a third step, the influence of the main operating parameters on the overall catalytic performances (glycerol/oxygen molar ratio and relative volumes of the reaction and regeneration zones) was investigated, showing notably the importance of the O_2/glycerol ratio, resulting in an inverse trend between conversion and selectivity. Increasing O_2/glycerol ratio led to higher conversion (lower coke deposit as shown by TGA analysis), but to the detriment of the selectivity to acrolein, supposedly due to the presence of O_2 in the reaction zone causing the degradation of glycerol and acrolein.

Keywords: glycerol, dehydration, acrolein, heterogeneous catalysis, two-zone fluidized bed reactor

INTRODUCTION

The glut of glycerol issued from the industrial process of vegetable oil transesterification for the production of biodiesel has led to numerous studies on the gas-phase dehydration of glycerol to acrolein in the past 10 years (Katryniok et al., 2009, 2010, 2013; Voegele, 2011). This reaction is generally catalyzed by solids exhibiting acid properties, which can be classified in three distinct groups: (i) supported Keggin-type heteropolyacids (HPA), (ii) zeolites, and (iii) metal oxides such as WO_3-ZrO_2 or Nb_2O_5 (Katryniok et al., 2010). In the first and second groups, the catalysts are efficient during the first hours under stream but they suffer from rapid deactivation because of coke formation blocking the access of reactants to the acid active sites. For example, the best Keggin-type HPA catalyst studied by Alhanash et al. (2010) initially reached a glycerol conversion of 100% and an acrolein selectivity of 98%, but the performances rapidly decreased after 6 h under stream (loss of roughly 40% of conversion). In the third group, the rate of deactivation by coking is generally lower and good performances can be kept at least during 200 h under stream. However, the performances—and especially the initial performances—are generally lower (acrolein yield in the range 60–70%) than those observed on the catalysts of groups 1 and 2 (acrolein yield in the range 85–95% or even more). As an illustration, the zirconium-niobium mixed oxides studied by

Lauriol-Garbay et al. still exhibited 82% conversion of glycerol and a selectivity to acrolein of 72 % after 177 h on stream, while, initially, full glycerol conversion, and roughly 70% of selectivity to acrolein were reached (Lauriol-Garbey et al., 2011). Hence, irrespective of the type of acid catalyst used to carry out the glycerol dehydration reaction, the deactivation by coking unavoidably occurs. This notably prevented the commercialization of the acrolein production from glycerol until now. Indeed, the unavoidable deactivation phenomenon impedes the development of a competitive process which would be necessary for cost-effective industrial exploitation.

Then, in parallel to the optimization of the heterogeneous catalyst properties, an adequate regeneration technology of the catalyst would be highly desirable. Some groups worked on that aspect, and **Table 1** summarizes the three main regeneration technologies proposed so far.

The first approach consists in co-feeding oxygen (or hydrogen) in the reactor to eliminate the coke immediately after its formation on the catalyst. In this case, continuous regeneration of the catalyst is achieved, but the risk of yielding explosive conditions in the reactor and the possible formation of side products issued from subsequent reactions of acrolein or of other products with oxygen (or hydrogen) are serious disadvantages which acted as barriers to wider application of this solution.

To isolate glycerol and acrolein from oxygen (or hydrogen), a cyclic regeneration strategy (possibly using intermediate purges with an inert gas to avoid any risk of yielding explosive atmospheres), sometimes called "semi-regenerative process," can be chosen. However, in this case, the process productivity is low because of the frequent need to stop the reaction for regenerating the catalyst. A solution could be to work with a two-reactor configuration in the so-called switch mode (one reactor being in operation when the second one is in the regeneration mode), but then the capital expenditure of the process is substantially higher.

Another solution was proposed to avoid the interruption of the production of acrolein. It consists in using a fluidized catalytic cracking (FCC)-like process often called "moving-bed reactor." In such a configuration, two separate reactors placed in a loop configuration are used for the reaction and the regeneration steps, respectively. A continuous regeneration is carried out in this case. It was first employed by Corma et al. (2008) and O'Connor et al. (2008) with zeolite-based catalysts. The authors used a MicroDowner reactor to simulate the industrial fluid catalytic cracking process. Temperatures were in the range of

290–650°C with contact times of 0.5–30 s. The highest yields in acrolein were relatively low (around 55 to 60%) at 350°C, using a ZSM-5 catalyst, at low contact times of 0.5–2 s, which corresponds to WHSVs in the range of 300 to 1,300 h^{-1}. The disadvantage of a conventional FCC-like reactor is the complexity of the system, consisting of two independent riser and regeneration reactors, thus demanding high investment costs.

Finally, in the 80s, a new reactor concept was developed by Wheelock where both the reaction and the regeneration take place in the same volume, thus involving reduced capital expenditure from the resulting process (Wheelock, 1997). The reactor can roughly be described as a single fluidized bed, where the reactant is injected in the middle of the bed via a nozzle (**Figure 1**). The regenerating agent (oxygen or hydrogen) is injected in the fluidized bed at the bottom of the reactor. Thus, two zones can be distinguished: the bottom zone, where the catalyst is only in contact with the regenerating agent, and the top zone, where the catalyst is in contact with the reactant gas. The corresponding concept—called Two-Zone Fluidized-Bed Reactor (TZFBR)—was applied for regeneration of an ethanol-reforming coked catalyst, (Pérez-Moreno et al., 2012) but also and mainly for decoupling the oxidation and reduction steps of catalyzed reactions following a Mars and Van Krevelen mechanism [i.e., styrene synthesis, (Cocco and Castor, 2001) oxidative dehydrogenation of butane and propane] (Soler et al., 1999; Gascón et al., 2005; Lobera et al., 2009).

In our previous studies, we have shown that Keggin-type heteropolyacids supported on silica can give excellent initial performances in glycerol dehydration to acrolein with yields larger than 90%, but also suffer from fast deactivation by coking (Katryniok et al., 2012). This makes this kind of catalyst an excellent candidate to be studied in a TZFBR. The idea is to check if it would be possible to maintain the initial excellent performances by continuously eliminating the coke formed on the catalyst surface and porosity during the reaction. Therefore, in the present work, a TZFBR was used to carry out the glycerol dehydration to acrolein catalyzed by a Keggin-type heteropolyacid (20 wt.% of phosphotungstic acid, $H_3PW_{12}O_{40}$)

TABLE 1 | Main regeneration technologies proposed to extend the life of glycerol dehydration catalysts.

Regeneration technology	Main disadvantages
Co-feeding of oxygen or hydrogen	Risk of explosive conditions Formation of side products
Cyclic regeneration with oxygen or air under flow or by pulse injection	Loss of productivity High capital costs (spare reactor)
Continuous regeneration by FCC-like technology (2 fluidized-bed in series)	Attrition of catalyst particles High capital expenditure

FIGURE 1 | Schematics of the Two-Zone Fluidized-Bed Reactor (TZFBR) concept.
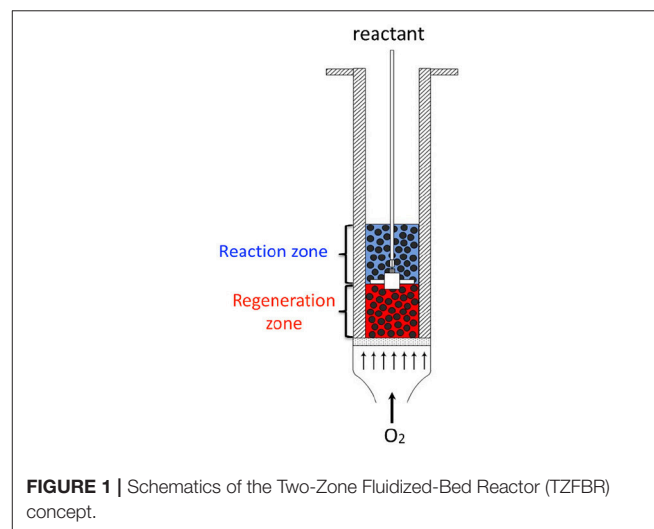
supported on CARIACT-Q10 commercial silica. The TZFBR design made it possible to simultaneously conduct the two steps of the process, namely the reaction of glycerol dehydration and the regeneration by oxygen of the coked catalyst, in a single reactor. The feasibility of the continuous acrolein production from glycerol was therefore shown for the first time using this reactor technology (Pariente et al., 2012).

EXPERIMENTAL

A schematic diagram of the experimental set-up (TZFBR) used in this work is illustrated in **Figure 2**. The fixed bed (Zone 1), the fluidized bed reactor (Zone 2), and the disengagement zone (Zone 3) were all made of stainless steel 304. The fixed bed had an inner diameter of 50 mm and a total height of 225 mm. The main objective of this fixed bed was to efficiently pre-heat the fluidization gas before it entered the fluidization column. Therefore, it was filled with SiC beads (2 mm diameter) to improve heat transfer. A porous plate 70 mm in diameter and 2 mm thick made of Inconel and presenting a pore size of 40–50 μm was used as a gas distributor for Zones 1 and 2. The fluidization column had a 50 mm inner diameter and a total height of 700 mm. It was equipped with three thermocouples in order to check the temperature homogeneity along the fluidized-bed during the reaction. A pressure probe was installed at a distance of 2.5 cm over the distributor plate (bottom of the fluidization column). The pressure probe was connected to a system of U-tube manometers to determine the pressure drop (ΔP) through the fluidized bed with reference to the atmospheric pressure. The disengagement zone (Zone 3) had an internal diameter of 85 mm in the upper section, of 50 mm in the bottom section, and a total height of 275 mm total. This disengagement zone enabled the reduction of the gas velocity and prevented the entrainment of most of the catalyst particles by the gas flow. However, for the attrition test (see below for description) a cyclone (not shown on **Figure 2**) with an internal diameter of 15 mm and a total height of 60 mm was installed at the outlet of Zone 3. Its main function was to recover any small particles which could be possibly formed by attrition (erosion) of the catalyst and then subsequently dragged in the gas flow. The cyclone was removed during catalytic experiments to avoid acrolein condensation in the cold spot, as the attrition test showed that the formation of fine particles was negligible (see below).

Finally, a feed tube equipped with a nozzle was installed inside the fluidization column. The feed tube was used to inject the evaporated glycerol aqueous solution directly in the catalytic fluidized bed. The feed tube position could be changed vertically to increase or decrease the volumes of the reaction and regeneration zones correspondingly.

The reaction conditions used were as follows: An aqueous solution of 20 wt.% glycerol was fed with a volumetric flow of 0.5 mL/min by a HPLC pump (Gilson 305). The feed was progressively pre-heated at 200°C before entering into an evaporator at 230°C in order to ensure complete evaporation of the solution. A mixture of air and nitrogen was used as fluidization gas. It contained 0, 1, 3, 6, or 21 mol.% of oxygen and its flow was monitored by a Q-Flow rotameter from Voegtlin. The air flowrate was set by a Brooks mass flow controller.

In a first step of the study, the quality of the fluidization was checked at 275°C using 96 g of catalyst, which corresponded to a fixed bed height of 10 cm. Moreover, an attrition test was also performed at 275°C during 44 h. Air was employed as a fluidization gas to conduct these experiments, which were carried out in the absence of glycerol.

In a second step, catalytic tests were performed using 96 g of catalyst. The nozzle for the injection of the glycerol solution was placed at 5 or 8 cm from the distributor, thus modifying the volumes of the reaction and regeneration zones. The reaction temperature was 275°C. When the desired temperature was reached (after around 4 h because of the thermal inertia of the TZFBR), the glycerol feed started to be injected in the fluidized-bed reactor via the inlet nozzle (this is the t0 considered in **Figures 7–10**). A further period of 4 h was required for stabilizing the glycerol feed in the TZFBR. This step, which was carried out using pure nitrogen as fluidizing gas, is important to enable formation of a layer of coke on the catalyst before starting the oxygen injection in the system. In the absence of coke, the oxygen would react with glycerol or acrolein in the upper part of the fluidized bed, notably leading to the formation of byproducts.

Then, after the 4 h of stabilization, the fluidizing nitrogen flow was mixed with 2.7, 3.6, 11, or 21 NL/h of air in order to obtain an oxygen/glycerol molar ratio of 0.3, 0.4, 1.3, or 2.4, respectively. The catalytic performances were measured over 3 days (55 h under stream in total), as follows: The first day, after glycerol feed stabilization, two cold traps were collected (between 4 and 6 h under stream) and then the test was left to run overnight. The second day (between 20 and 30 h under stream) 5 cold-traps were collected and analyzed. Finally, the third day (between 45 and 55 h under stream) 4 cold-traps were collected and analyzed and then the test was stopped.

The products and the non-reacted glycerol were recovered using a cold trap at the outlet of the set-up. They were analyzed off-line on an Agilent 5890 gas chromatograph equipped with a FID detector and a CB-WAX column (L: 30 m, ID: 53 μm). Acrolein was the main product found in the cold trap, with very small traces of hydroxyacetone, acrylic acid, acetaldehyde and propionaldehyde, which were not taken into account in the calculation of the carbon balance. In the operating conditions where the glycerol was not fully converted, cyclic acetals resulting from the reaction between glycerol and acrolein were also detected but not quantified and hence were not included in the carbon balance either. Finally, CO_2 was also formed but, because of its high dilution in the fluidizing gas, it was impossible to quantify it and consider it for the carbon balance calculation.

The glycerol conversion (X), the product's selectivities (S), and yields (Y) and the carbon balance were calculated as follows:

$$X = 1 - \frac{\dot{n}_{glycerol(0)}}{\dot{n}_{glycerol(i)}} \tag{1}$$

$$S = \left(\frac{\gamma_i}{\gamma_{glycerol}}\right) * \left(\frac{\dot{n}_i}{\dot{n}_{glycerol(i)} - \dot{n}_{glycerol(o)}}\right) x100 \tag{2}$$

$$Y = S * X \tag{3}$$

$$BC = \frac{\sum \gamma_i * \dot{n}_i + \gamma_{glycerol} * \dot{n}_{glycerol(o)}}{\gamma_{glycerol} * \dot{n}_{glycerol(i)}} \tag{4}$$

Where γ_i is the number of carbon atoms in the product i, $\gamma_{glycerol}$ the number of carbon atoms in glycerol (i.e., 3) and $\dot{n}_i$ and $\dot{n}_{glycerol}$ the molar flowrates of product i and of glycerol, respectively. (o) and (i) refer to the outlet and the inlet, respectively.
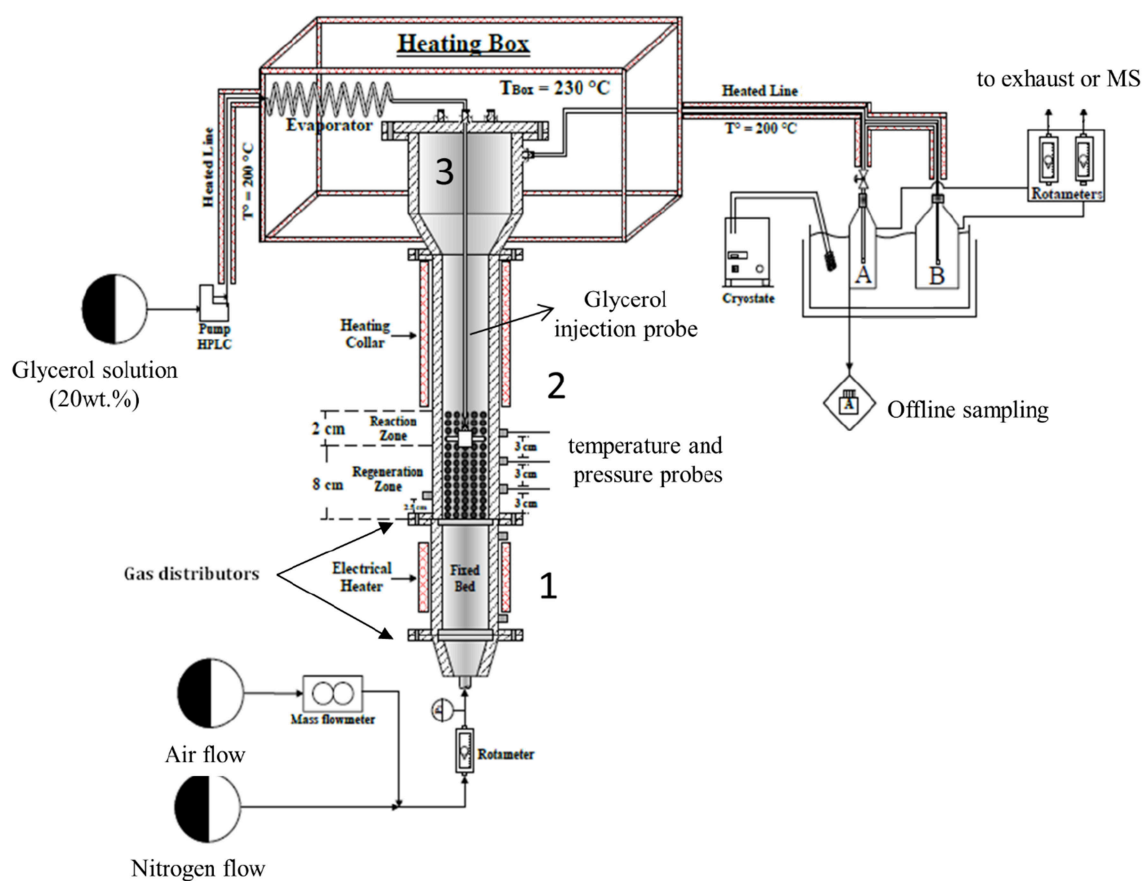
FIGURE 2 | Schematics of the TZFBR setup.

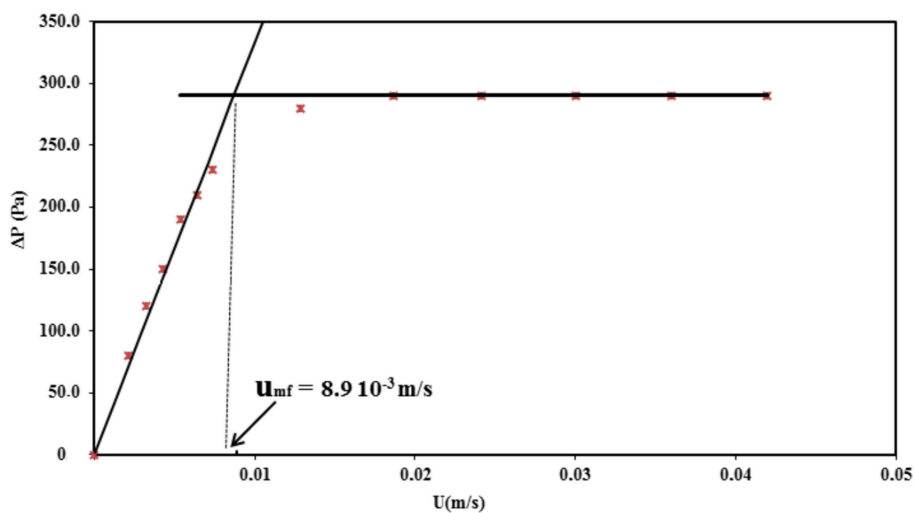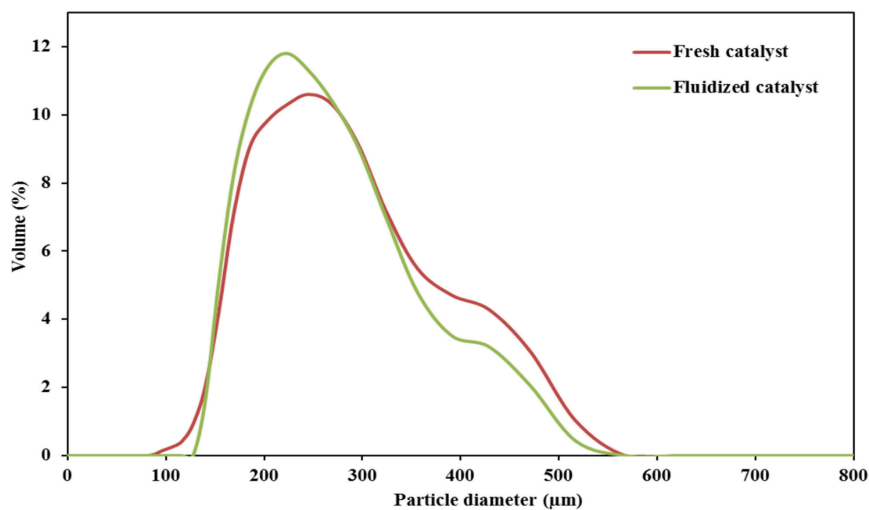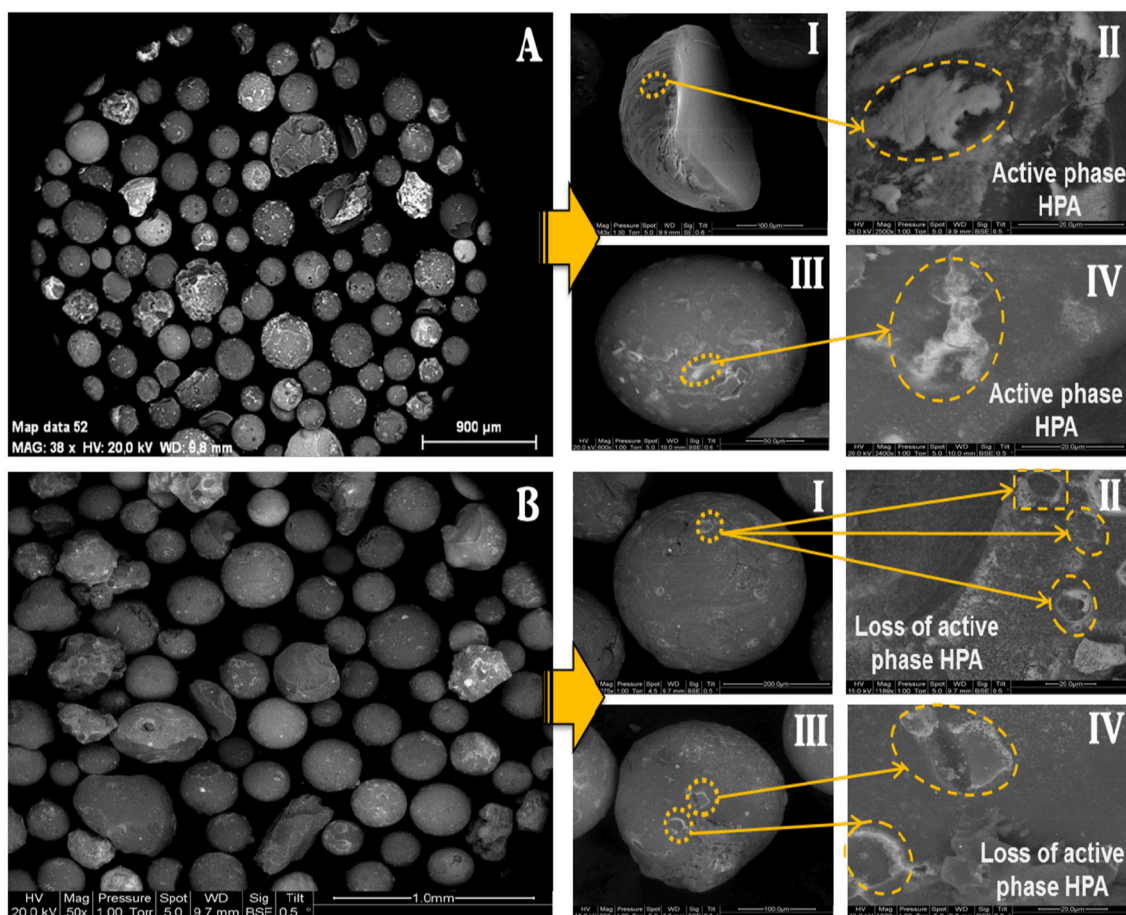**FIGURE 3 |** Pressure drop as a function of the gas velocity at 275°C using the gas velocity decreasing branch.

FIGURE 4 | Particles' size distribution of the fresh catalyst and after a 44 h attrition test in the TZBR at 275°C.

FIGURE 5 | Scanning Electron Micrographs of **(A)** the fresh catalyst, and **(B)** the catalyst after attrition test (after 44 h of fluidization at 275°C).

Raman spectroscopy was carried out on an ISA Dilor-Jobin Yvon-SPEX Horiba instrument at room temperature using a laser beam of 532 nm, a confocal hole size of 50 μm and acquisition times of 30 s and 200 s for fresh and fluidized catalyst, respectively, and 60 s for the catalyst after reaction. The analysis was performed from 200 to 1,600 cm^{-1}.

The ICP-MS analyses were performed using a Thermo-Fisher X7 ICP-MS to determine the experimental quantity of silicon and tungsten of the catalyst after fluidization.

Scanning electron microscopy (SEM) images were taken with a Philips SEM 505 scanning microscope equipped with an EDX Philips 505 microprobe at 5 and 20 keV.

TGA and DSC analyses of used and of fresh catalysts were carried out under air (flow rate 100 mL/min). The samples were heated from room temperature to 550°C at a temperature ramp of 3°C/min in a Labsys TGA-DTA 1,600 apparatus.

The surface areas, pore sizes, and total pore volumes of the catalysts before and after reaction were measured by N$_2$ adsorption-desorption. A Micromeritics ASAP 2000 was employed to carry out these experiments. The samples were degassed at 130°C before analysis. The specific surface area, S$_{BET}$, was calculated using the linear part of the BET plot. The isotherms were obtained at −196°C. The mesoporous size distributions were obtained by applying the Barrett-Joyner-Halenda (BJH) equation to the desorption branch of isotherms. The estimation of the total pore volume was made from the N$_2$ uptake at a P/P0 value of 0.995.

A L230 Beckman-Coulter light scattering laser was employed in order to measure the particle size of the catalyst before and after catalytic test. Ethanol was used as a solvent in order to avoid the agglomeration of particles during the analysis.

In order to study the nature of the carbonaceous species deposited on the catalyst after catalytic tests, cross-polarization (CP), and magic angle spinning (MAS) ^{13}C-NMR (CPMAS ^{13}C-NMR) spectroscopy was carried out. The spectroscopy experiments were conducted on Bruker ASX400 (9.4 T) spectrometers operating at frequencies 100.6 MHz and using a 4 mm rotor probe. The rotor spinning rate was 10 kHz.

RESULTS AND DISCUSSION

Hydrodynamic Study

A hydrodynamic study was first carried out to check the fluidization quality, which has a direct impact on the catalytic performances. The study was performed at 275°C, corresponding thus to the reaction temperature. Hydrodynamic parameters

TABLE 2 | Physical and textural properties of the catalyst before and after the attrition test.

Parameter	Fresh catalyst	Catalyst after fluidization
Particle diameter	245 μm	233 μm
Surface area	230 m^2/g	230 m^2/g
Pore volume	0.92 cm^3/g	1.01 cm^3/g

such as the quality of fluidization and minimum fluidization velocity were determined. As mentioned before, an attrition study of the catalyst was also carried out.

In order to avoid the hysteresis phenomenon during the measurement of the pressure drop (ΔP) with the increasing velocity of the gas, all the measurements of the ΔP curves were carried out while decreasing the superficial gas velocity (U) (**Figure 3**). This curve enables determining the minimum fluidization velocity u_{mf} by applying the standardized Richardson's method (Richardson et al., 1971) u_{mf} is thus located at the intersection of the sloping line corresponding to the linear increase of ΔP in the fixed bed and of the horizontal line corresponding to the fluidized regime (**Figure 3**). The as-determined minimum fluidization velocity for the catalyst was 8.9.10^{-3} m/s.

Using **Figure 3**, it was also possible to evaluate the quantity of solid participating in the fluidization, described by the so-called "fluidization quality," further noted as α and defined as follows:

$$\alpha = \frac{\Delta P_{experimental}}{(m.g/A)} \tag{5}$$

Where $\Delta P_{experimental}$ corresponds to the ΔP measured when the fluidization regime is reached (i.e., the horizontal line on **Figure 3**), m is the mass of catalyst loaded in the reactor (96 g), g the standard gravity (9.81 m.s^{-2}), and A the cross-section of the catalytic bed (1.96.10^{-3} m^2 corresponding to an internal diameter of 5 cm).

The fluidization quality was 83%, meaning that more than 80% of the catalyst participated in the fluidization, the remainder being probably located in dead zones of the reactor. Such a high fluidization quality in a small-scale fluidized bed reactor can be considered as very good, offering reassurance for the appropriate design of the TZFBR used herein.

Attrition Test for Catalysts

In a fluidized bed, the attrition of catalyst particles is most of the time unavoidable. In general, the attrition phenomenon can be classified into two main types: particles' fragmentation and surface abrasion. These phenomena could lead to a certain loss in the active phase fraction located on the outer surface of the particles and thus to a decrease in the catalytic performances. In order to verify the mechanical stability of the particles, an attrition experiment was carried out in the fluidized bed. The TZFBR was loaded with 96 g of fresh catalyst and then fluidized during 44 h with air at 275°C, without any glycerol feed, and using a gas velocity roughly twice as much as the minimum fluidization velocity u_{mf} determined previously (namely 18.6.10^{-3} m/s). Note that it also corresponded to the velocity selected for the subsequent catalytic tests. In those conditions, the height of the fluidized bed was around 15 cm. For this experiment, the cool-trap system (**Figure 2**) was replaced by a cyclone so as to recover the small particles possibly elutriated out by the gas during the test. The particles of the catalyst were recovered in the TZFBR after the attrition test and subsequently analyzed by light scattering laser, SEM, nitrogen physisorption, Raman spectroscopy and elemental analysis (ICP-MS).

In **Figure 4**, it can be noticed that the size distribution curve of the fluidized catalyst is slightly less broad than that of the fresh one. This indicates a slight abrasion of the catalyst after the attrition test. The recovered mass of the catalyst was 94 g after the attrition test (corresponding to 98% of the initial loading). No particles were collected in the cyclone. The loss of 2 wt.% is within the experimental accuracy and thus does not constitute strong evidence of the elutriation of fine particles.

The SEM images of the catalyst particles before and after the attrition test are presented in **Figure 5**. It was observed that the fluidized catalyst substantially keeps the same morphology as that of the fresh one, meaning that no fragmentation occurred during the fluidization process. However, it seems that the active phase deposited on the external surface of the support in plate-like spots (**Figures 5 A-II,IV**) was somewhat eroded after 44 h of fluidization, with some tear-like damage marks detected on the surface of the particles (**Figures 5 B-II,IV**).

Similarly, the comparison of the physical and textural properties (**Table 2**) such as the particle diameter, the specific surface area and the pore volume of the catalyst before and after 44 h of fluidization (attrition test) did not show any significant change. Only a slight decrease in the mean particle diameter determined by light scattering granulometry from 245 to 233 μm was observed after fluidization. One can assume that this resulted from the abrasion phenomenon.

In order to evidence the hypothesis of an abrasion, the surface of the catalyst was analyzed by Raman spectroscopy. In fact, the collision and friction between particles during the fluidization could lead to a loss of the active phase ($H_3PW_{12}O_{40}$) by abrasion from the catalyst surface, which would be easily evidenced due to the specific Raman bands of phosphotungstic acid. Raman spectra were recorded for several particles of fresh and used catalysts for comparison. **Figure 6** shows the exemplary Raman spectra for a fresh (left) and a used catalyst particle (right). It is very clear that the fresh catalyst exhibits the typical bands of $H_3PW_{12}O_{40}$, notably the W=O stretching vibration at $\approx$ 1,000 cm^{-1} whereas for the used catalyst almost no active phase was detected on the outer surface (Thouvenot et al., 1984). This evidenced clearly the abrasion of the HPA from the external surface of the catalyst. Nevertheless, as the Raman technique is a surface-sensitive technique, one cannot draw conclusions

regarding the behavior of the active phase present in the pores of the catalyst.

Therefore, in order to complete the Raman study and to estimate the loss of active phase during the attrition test, ICP-MS analyses of the fresh and used catalysts were done. From **Table 3**, where the calculated amounts of both HPA and support are reported, it can be noted that the compositions in HPA for the fresh and the used catalysts were close to the theoretical weight percentages expected (19 and 18 $\pm$ 1 vs. 20 wt.% for the fresh and used samples, respectively). It can therefore be concluded that the catalyst did not undergo a significant loss of active phase after 44 h of fluidization. Nevertheless, as said above, the SEM analysis showed a slight abrasion of the active phase on the external surface of the catalyst. It is believed that the particles produced by the abrasion are very fine and elutriated by the gas stream from the reactor and cannot be trapped in the cyclone, which was not sufficiently efficient to handle such fine particles. Consequently, from the analysis of physical and textural properties as well as the Raman, SEM and ICP-MS analysis, it may be asserted that the catalyst particles undergo a slight loss of active phase by mechanical abrasion during the fluidization. However, the loss of active phase remains limited to the catalyst's external surface and is not significant in comparison to the amount of active phase, which is present in the internal porosity of the silica support.

Catalytic Tests

The stability of the catalytic performances in a TZFBR depends on the balance between the rates of the coking of the catalyst under dehydration reaction conditions and of the regeneration of the catalyst in the presence of oxygen in the fluidizing gas. If the regeneration is not sufficiently efficient, coke will accumulate on the surface and in the pores of the catalyst, causing its progressive deactivation. If the regeneration is effective, the formation of coke and the oxidative removal are balanced, avoiding thus

TABLE 3 | Weight percentages of active phase and support obtained by ICP-MS.

Compound	Fresh catalyst	Fluidized catalyst
$H_3PW_{12}O_{40}$	19 $\pm$ 1 wt.%	18 $\pm$ 1 wt.%
SiO_2	81 $\pm$ 1 wt.%	82 $\pm$ 1 wt.%
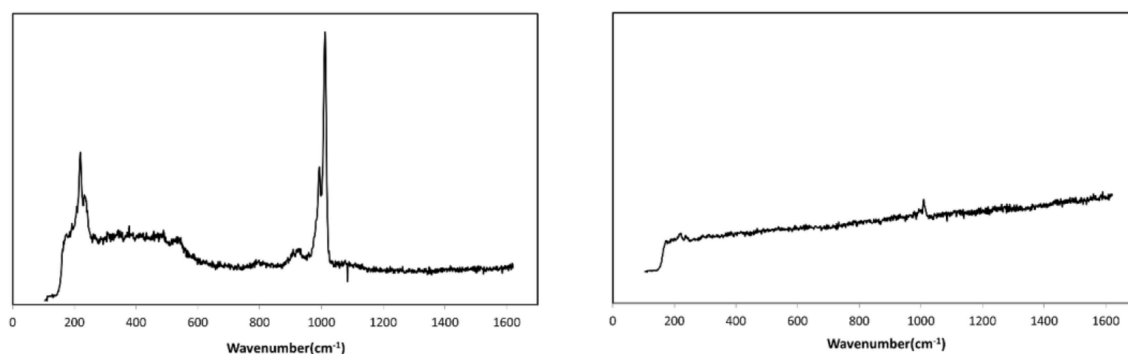
FIGURE 6 | Raman spectra of fresh **(Left)** and fluidized catalyst particle **(Right)** (attrition test: 44 h of fluidization).

the over-accumulation of carbonaceous species. On the other hand, if too much oxygen is present in the reaction zone, it will react with glycerol, acrolein, or others to yield undesired products. Hence, the tuning of the operating conditions of the TZFBR must be very precise to find a good compromise. In order to better control this aspect, two parameters were studied in this work: (i) the relative volumes of the regeneration and reaction zones, and (ii) the oxygen/glycerol molar ratio. The total height (and consequently volume) of the fluidized-bed is constant at a given set of operating conditions (about 15 cm height in our case) but, as mentioned before, the respective volumes of the regeneration and reaction zones can be modified by adjusting the vertical position of the injection nozzle of the glycerol feed. Moreover, the oxygen/glycerol ratio can be tuned using different amounts of air mixed with the nitrogen flow in the fluidization gas.

Influence of the Volumes of the Reaction and Regeneration Zones

In order to observe the influence of the relative volumes of the regeneration and reaction zones, the vertical position of the glycerol injection nozzle was varied. More precisely, the glycerol feed was injected at 5 and 8 cm above the gas distributor. Considering that the fluidized bed's total height was 15 cm, the regeneration and reaction zones' heights were 5 and 10 cm, respectively, in the first case, and 8 and 7 cm, respectively, in the second configuration. In other words, the reaction zone was twice the size of the regeneration zone in the first case ($V_{reaction}/V_{regeneration} = 2$) and roughly the same size in the second configuration ($V_{reaction}/V_{regeneration} = 1$).

The glycerol conversion and acrolein selectivity vs. time on stream are shown in **Figures 7**, **8**, respectively. **Figure 7** shows that a larger regeneration zone led to a lower conversion during
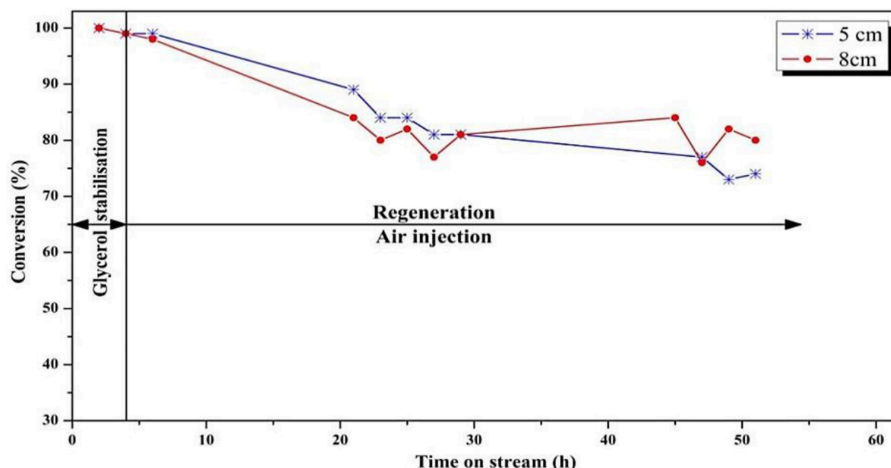
FIGURE 7 | Influence of position of the feed injection in the fluidized-bed on the conversion of glycerol ($T = 275°C$, O$_2$/Gly $= 0.4$, gas velocity $= 1.86.10^{-2}$ m/s). Five centimeters correspond to $V_{reaction}/V_{regeneration} = 2$ whereas 8 cm correspond to $V_{reaction}/V_{regeneration} = 1$.
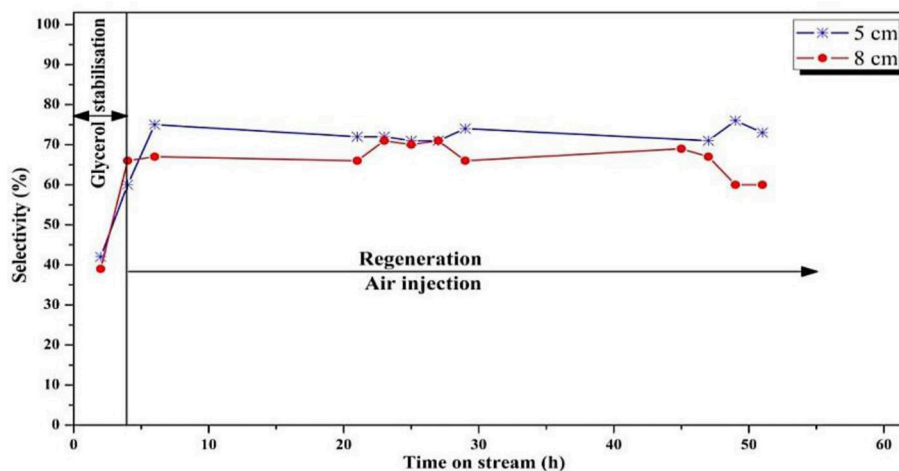
FIGURE 8 | Influence of position of the feed injection nozzle in the fluidized bed on the selectivity to acrolein ($T = 275°C$, O$_2$/Gly $= 0.4$, gas velocity $= 1.86.10^{-2}$ m/s). Five centimeters correspond to $V_{reaction}/V_{regeneration} = 2$ whereas 8 cm correspond to $V_{reaction}/V_{regeneration} = 1$.

the first 20 h on stream, which then remained rather constant until the end of the test (50 h), meaning that the catalyst reached a steady state after 20 h of reaction. On the other hand, with a smaller regeneration zone, it seems that the catalyst showed a constant deactivation, without reaching a steady-state. With respect to the accuracy of ± 2% in the conversion measurement, one can state that the difference observed between both experiments was significant, meaning that a too-small regeneration zone ($V_{reaction}/V_{regeneration} = 2$) did not enable continuous regeneration of the coked catalyst.

Concerning the acrolein selectivity (**Figure 8**), quite similar values (65–70%) were observed in both experiments. Only small amounts of byproducts such as acetaldehyde (2%), acetone (1%), propionaldehyde (1%), and hydroxyacetone (3%) were

observed. Carbon balances of 84 and 80% for the smaller and the larger regeneration zone were, respectively, observed. The incondensable CO and CO_2 gas quantities could not be measured because of dilution that was too high in the fluidization gas outlet stream, and are hence not included in the carbon balance, explaining the low values.

Influence of the Oxygen/Glycerol Molar Ratio

Catalytic tests were performed using various oxygen/glycerol molar ratios, namely 0 (only nitrogen is injected in the fluidisation gas), 0.3, 0.4, 1.3, and 2.4 at 275°C with $V_{reaction}/V_{regeneration} = 1$ (injection nozzle at 8 cm above the gas distributor). The results are given in **Figures 9**, **10** for glycerol conversion and acrolein selectivity, respectively.
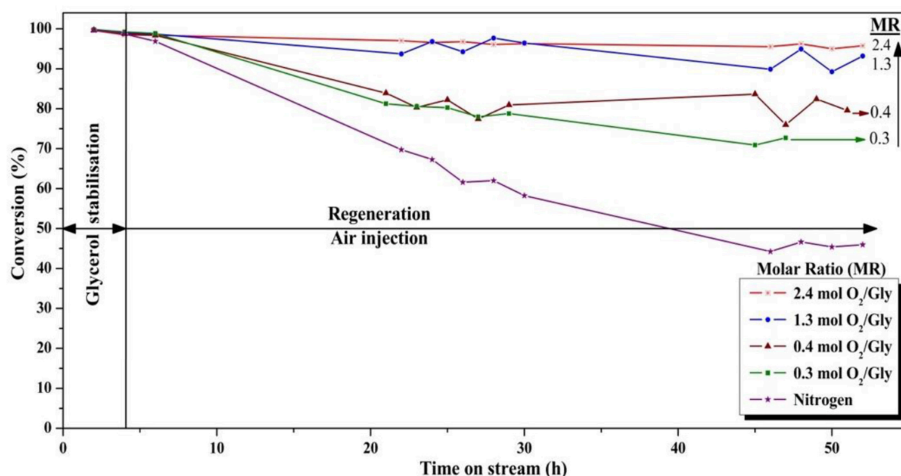
FIGURE 9 | Influence of the oxygen/glycerol molar ratio on the conversion of glycerol ($T = 275°$C, position of the feed injection nozzle = 8 cm above the gas distributor, gas velocity = $1.86.10^{-2}$ m/s).
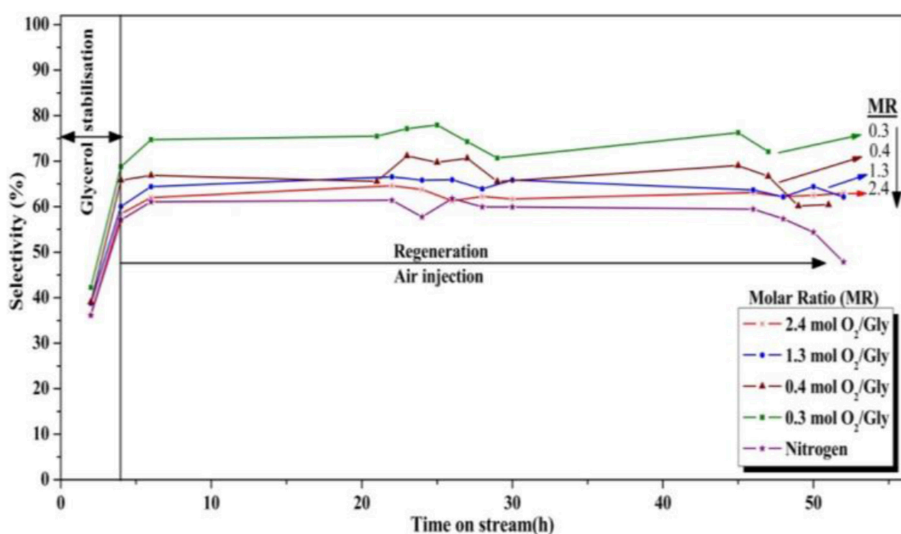
FIGURE 10 | Influence of the oxygen/glycerol molar ratio on the selectivity to acrolein ($T = 275°$C, position of the feed injection nozzle = 8 cm above the gas distributor, gas velocity = $1.86\ 10^{-2}$ m/s).

The use of higher quantities of oxygen in the feed was clearly found to be favorable for the glycerol conversion. With an oxygen/glycerol molar ratio of 2.4, a high and stable conversion of ca. 96% was observed during the 52 h of the experiment, which is remarkable. The conversion decreased in the same order as that of the oxygen-to-glycerol molar ratio, with 75, 80, and 90% after 52 h on stream for molar ratios of 0.3, 0.4, and 1.3, respectively. It is worth mentioning that for a ratio of 1.3, a high conversion of glycerol around 95% was observed during the first 30 h, with a slight decrease of 5 points after 52 h. When no oxygen was injected, a fast deactivation of the catalyst occurred as expected, and no more than 45% of the fed glycerol were converted after 52 h under stream.

On the other hand, high O_2/glycerol molar ratios led to a decrease in acrolein selectivity (**Figure 10**). While a high selectivity to acrolein ($\approx$ 75%) was observed at a molar ratio of 0.3, it was only 60% when using a molar ratio of 2.4. This decrease in acrolein selectivity can be explained by the decomposition of the as-formed acrolein in oxygen excess. In fact, based on a rough calculation, an O_2/Gly ratio of 0.3 should roughly allow the oxidization of carbonaceous species corresponding to a carbon selectivity of 15%. Hence, when using larger amounts of oxygen for the regeneration, one can suppose that significant parts of the introduced oxygen are not consumed in the regeneration zone for the combustion of the deposited coke, whereby the unreacted oxygen can interact with glycerol or acrolein in the reaction zone, causing notably total oxidation to CO_x. Next to acrolein, only small amounts of condensable byproducts such as acetaldehyde (3%), propionaldehyde (1%), and acrylic acid (1%) were observed.
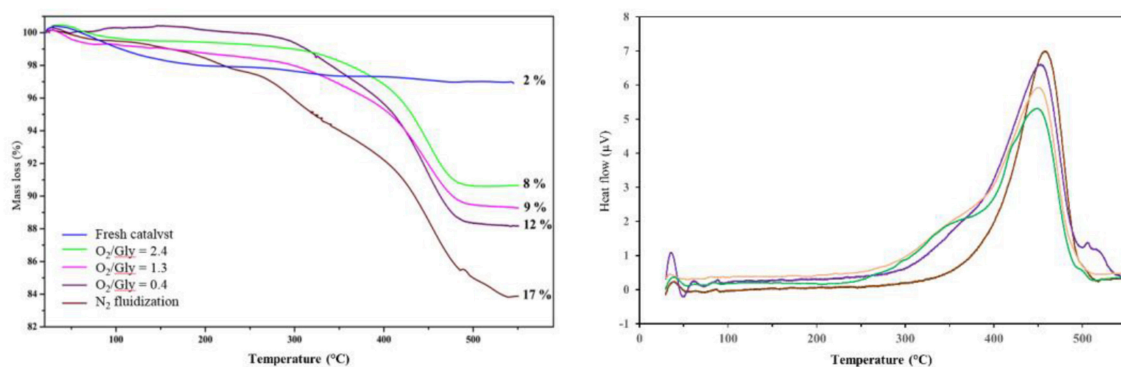
FIGURE 11 | Influence of the oxygen/glycerol molar ratio on the amount of coke after test, determined by TGA **(Left)** analysis and DSC **(Right)**.
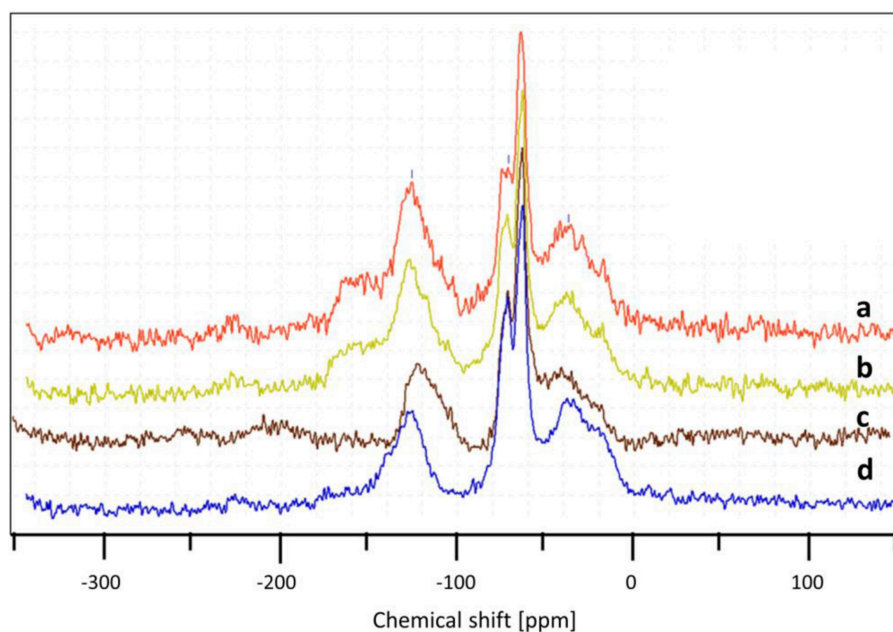
FIGURE 12 | Influence of the oxygen/glycerol molar ratio on the nature of carbonaceous species after test, determined by ^{13}C CP MAS NMR for (O_2/Gly) = 2.4 **(a)**, 1.3 **(b)**, 0.4 **(c)**, and pure nitrogen **(d)**.

Surprisingly, the selectivity to acrolein was found to be very low in total absence of oxygen in the feed. The surface of the catalyst was probably already too covered by coke after the 4-h stabilization period, preventing the reactant from accessing the selective active sites where acrolein is formed by glycerol conversion. Moreover, the quality of fluidization can be significantly affected for strongly coked catalyst.

Nevertheless, it is noteworthy that in the best conditions tested in the present study (O_2/Gly =1.3 and 2.4), a stable yield in acrolein of around 60–65% could be maintained, which would have been impossible in a fixed-bed reactor without oxygen injection.

In order to check the influence of the O_2/Gly ratio on the amount of coke formed on the catalyst, the particles recovered after the test were analyzed by TGA and DSC (**Figure 11**). The results showed the formation of carbonaceous species for all catalyst, but in different extents depending on the amount of oxygen injected in the TZFBR. In all cases, the loss of the carbonaceous species was accompanied by an exothermal peak, corresponding to the burning of the coke. Concerning the quantification, the amount of coke increased when decreasing the O_2/Gly ratio from 8 wt.% (O_2/Gly = 2.4) to 17 wt.% (no oxygen in the fluidization gas). Considering the stable performance observed for a O_2/Gly ratio of 2.4, one can conclude that 8 wt.% of carbonaceous species are still acceptable for obtaining full conversion. In addition to the quantification of the deposed carbonaceous species, the latter were characterized using solid-state NMR on the ^{13}C carbon with cross-polarization (CP) and magic-angle spinning (MAS). From the results (**Figure 12**), no significant change is observed in the nature of the carbonaceous species deposited on the catalyst under various molar ratios of oxygen or on the catalyst employed under pure nitrogen. This can be explained by the fact that ^{13}C CP-MAS NMR is a non-quantitative technique. Nevertheless, one can note that the coke for all catalysts is basically composed by an aliphatic part (peaks around −37, −64, −71 ppm) and an aromatic part (peak around −125 ppm).

CONCLUSION

The TZFBR concept was applied to the dehydration of glycerol to acrolein using a heteropolyacid-based supported catalyst.

The catalyst was easily synthesized by wet impregnation of a commercial silica. The hydrodynamic behavior of the TZFBR shows good mixing, illustrated by the fluidization quality being superior to 80% at a reaction temperature of 275°C. The mechanical stability of the catalyst was controlled by performing an attrition test of the catalyst particles in the TZFBR at 275°C over 44 h in the absence of glycerol. The results show good mechanical resistance of the catalyst, whereby only a small quantity of active phase on its external surface was elutriated.

Concerning the catalytic results, the effect of the O_2/glycerol ratio and of the size of the reaction/regeneration zone was studied, showing that a regeneration zone that was too small ($V_{reaction}/V_{regeneration}$ = 2) did not allow efficient catalyst regeneration. Concerning the O_2/glycerol ratio, an inverse trend between conversion and selectivity was found: increasing the O_2/glycerol ratio led to higher conversion (and lower coke deposit as shown by TGA analysis), but at the expense of the selectivity to acrolein, supposedly due to the presence of O_2 in the reaction zone then burning glycerol and acrolein.

DATA AVAILABILITY

All datasets generated for this study are included in the manuscript and/or the supplementary files.

AUTHOR CONTRIBUTIONS

RM: experiments, interpretation, writing of the first draft; SP, BK, NF, and FD: design of the study, experiments design, supervision, interpretation, and writing; VB-B and PR: design of the study, supervision, interpretation, and writing. All authors contributed to manuscript revision, read, and approved the submitted version.

ACKNOWLEDGMENTS

REFERENCES

Alhanash, A., Kozhevnikova, E. F., and Kozhevnikov, I. V. (2010). Gas-phase dehydration of glycerol to acrolein catalysed by caesium heteropoly salt. *Appl. Catal.* 378, 11–18. doi: 10.1016/j.apcata.2010.01.043

Cocco, R. A., and Castor, W. M. (2001). *Dehydrogenation of an Alkyl Aromatic Compound and Catalyst Regeneration in a Fluidized Bed Reactor*. Patent WO 01/44146 A1.

Corma, A., Huber, G. W., Sauvanaud, L., and O'Connor, P. (2008). Biomass to chemicals: catalytic conversion of glycerol/water mixtures into acrolein, reaction network. *J. Catal.* 257, 163–171. doi: 10.1016/j.jcat.2008.04.016

Gascón, J., Téllez, C., Herguido, J., and Menéndez, M. (2005). A two-zone fluidized bed reactor for catalytic propane dehydrogenation. *Chem. Eng. J.* 106, 91–96. doi: 10.1016/j.cej.2004.11.005

Katryniok, B., Paul, S., Capron, M., Bellière-Baca, V., Rey, P., and Dumeignil, F. (2012). Regeneration of silica-supported silicotungstic acid as a catalyst for the dehydration of glycerol. *ChemSusChem* 5, 1298–1306. doi: 10.1002/cssc.201100635

Katryniok, B., Paul, S., Capron, M., and Dumeignil, F. (2009). Towards the sustainable production of acrolein by glycerol dehydration. *ChemSusChem* 2, 719–730. doi: 10.1002/cssc.200900134

Katryniok, B., Paul, S., and Dumeignil, F. (2013). Recent developments in the field of catalytic dehydration of glycerol to acrolein. *ACS Catal.* 3, 1819–1834. doi: 10.1021/cs400354p

Katryniok, B., Paul, S., Rey, P., Bellière-Baca, V., and Dumeignil, F. (2010). Glycerol dehydration to acrolein in the context of new uses of glycerol. *Green Chem.* 12, 2079–2098. doi: 10.1039/C0GC00307G

Lauriol-Garbey, P., Millet, J. M. M., Loridant, S., Belliere-Baca, V., and Rey, P. (2011). Erratum to "New efficient and long life catalyst for gas-phase glycerol dehydration to acrolein" [J. Catal. 280 (2011) 68–76]. *J Catal.* 281:361. doi: 10.1016/j.jcat.2011.05.013

Lobera, M. P., Téllez, C., Herguido, J., and Menéndez, M. (2009). Pt–Sn/MgAl₂O₄ as *n*-butane dehydrogenation catalyst in a two-zone fluidized-bed reactor. *Ind. Eng. Chem. Res.* 48, 6573–6578. doi: 10.1021/ie900381p

O'Connor, P., Corma, C. A., Huber, G., and Savanaud, L. A. (2008). *Process for Production of Acrolein and Other Oxygenated Compounds From Glycerol in a Transported Bed Reactor*. Patent WO 2008052993 A2.

Pariente, S., Bellière-Baca, V., Paul, S., and Fatah, N. (2012). *Process for Obtaining Acrolein by Catalytic Dehydration of Glycerol or Glycerin*. Patent WO 2012056166 A1.

Pérez-Moreno, L., Soler, J., Herguido, J., and Menéndez, M. (2012). Stable steam reforming of ethanol in a two-zone fluidized-bed reactor. *Ind. Eng. Chem. Res.* 51, 8840–8848. doi: 10.1021/ie201968u

Richardson, J. F., Davidson, J. F., Harroson, S., and Fluidization, D. (1971). *Fluidization*. London: Academic Press Ed.

Soler, J., López Nieto, J. M., Herguido, J., Menéndez, M., and Santamaría, J. (1999). Oxidative dehydrogenation of *n*-butane in a two-zone fluidized-bed reactor. *Ind. Eng. Chem. Res.* 38, 90–97.

Thouvenot, R., Fournier, M., Franck, R., and Rocchiccioli-Deltcheff, C. (1984). Vibrational investigations of polyoxometalates. 3. Isomerism in molybdenum(VI) and tungsten(VI) compounds related to the Keggin structure. *Inorg. Chem.* 23, 589–605. doi: 10.1021/ic00173a022

Voegele, E. (2011). *Report Outlines Global Biodiesel Production*. Biodiesel Magazine 06/2011, 30.

Wheelock, T. D. (1997). *Cyclic Process for Oxidation of Calcium Sulfide*. Patent US 5,653,955.

Conflict of Interest Statement: VB-B and PR are employed by ADISSEO Company.

The remaining authors declare that the research was conducted in the absence of any commercial or financial relationships that could be construed as a potential conflict of interest.

Glycerol to Glyceraldehyde Oxidation Reaction Over Pt-Based Catalysts Under Base-Free Conditions

Ayman El Roz[1], Pascal Fongarland[2], Franck Dumeignil[1] and Mickael Capron[1]*

[1] CNRS, Centrale Lille, ENSCL, Université d'Artois, UMR 8181-UCCS-Unité de Catalyse et Chimie du Solide, Université de Lille, Lille, France, [2] Laboratoire de Génie des Procédés Catalytiques, Université Lyon 1, Villeurbanne, France

Glycerol valorization through partial oxidation is a good way of obtaining many different molecules with high added value such as glyceric acid, tartronic acid, dihydroxyacetone, etc. Among the potential products, glyceraldehyde is an interesting chemical compound for its various applications in different domains such as organic chemistry, medical, and cosmetic industries. In the present paper, we studied the effect of different supports on the glycerol oxidation reaction in a batch reactor applying base-free conditions. The tested catalysts were Pt-based materials deposited on various supports (i.e., SiO_2, TiO_2, ZSM-5, γ-Al_2O_3), which were synthesized using a deposition method followed by a chemical reduction. The catalysts were extensively characterized (BET, ICP, XRD, TEM, XPS), highlighting differences in terms of specific surface areas, textural properties, and Pt nanoparticles sizes. We evidenced a direct relation between glycerol conversion and glyceraldehyde selectivity (i.e., an increase in glycerol conversion leads to a decrease in glyceraldehyde selectivity). The Pt/γ-Al_2O_3 catalysts exhibited the highest activity, but their selectivity to glyceraldehyde significantly decreased with time on stream. Pt/SiO_2 presented the highest selectivity to glyceraldehyde owing to a slower reaction rate, which allows envisioning technical opportunities to continuously extract the formed glyceraldehyde from the mixture.

Keywords: glycerol, oxidation, base-free conditions, platinum, glyceraldehyde

INTRODUCTION

Biomass efficient valorization is an important challenge to ensure the viability of our various industrial sectors (Katryniok et al., 2011; Skrzynska et al., 2015). In fact, the increasing demand for energy, combined with the environmental issues related to climate change, motivates the promotion of the use of renewable energies and biofuels, as well as of the replacement of the fossil raw materials traditionally used in the chemical industry with bioresources (Purushothaman et al., 2014). In this context, biodiesel is obtained by catalytic transesterification of the vegetables oil or animal fat with short chain alcohols, mainly methanol (Ftouni et al., 2015). The main by-product of this reaction is glycerol (accounting for 10 wt.% based on the initial plant oil quantity). The valorization of this molecule has been intensively studied in several ways, including advanced transformations to value added compounds (Katryniok et al., 2011). Its upgrading by heterogeneous catalysis has been particularly studied, in gas phase to produce for instance acrolein (Katryniok et al., 2009, 2010; Lauriol-Garbey et al., 2011), acrylonitrile (Liebig et al., 2013) or H_2 (El Doukkali et al., 2014) but also in liquid phase including conversion to esters or glycerol ethers by

esterification or etherification, to *1,2*-propanediol or *1,3*-propanediol by hydrogenolysis (Alhanash et al., 2008). The glycerol partial oxidation in the liquid phase can lead to various products such as aldehydes (glyceraldehyde), ketones (dihydroxyacetone), and carboxylic acids (glyceric acid, tartronic acid, glycolic acid, etc.) (Katryniok et al., 2011; Mimura et al., 2014; Skrzynska et al., 2016, 2019; Zaid et al., 2017).

In this paper, we focus on the glycerol oxidation using noble metal catalysts to obtain glyceraldehyde in base free media. Glyceraldehyde is an industrially important chemical compound, which has found applications in the cosmetic industry, organic chemistry and, in pharmaceutical applications. The main difficulty lies in the control of the catalytic selectivity with many possible products through networks of consecutive reactions (Skrzynska et al., 2015; Díaz et al., 2017), which can also ultimately lead to low value products, such as oxalic acid or carbon dioxide. Until now, most of the heterogeneous catalysts used for the oxidation of glycerol are based on noble metals such as platinum, palladium, gold, or even silver (Carrettin et al., 2002, 2003; Zhang et al., 2012; Skrzynska et al., 2014; Ftouni et al., 2015). According to the various studies reported in the literature, it is clear that the gold-based catalysts are active only in basic solution. Under these conditions, glycerol oxidation over supported gold catalysts promotes the production of acids under their salt form, with the necessity of an additional step to recover the desired acids in their native form, yielding a high quantity of waste (i.e., salts resulting from the neutralization). The use of the Ag based catalyst, in basic media, leads to the formation of glycolic acid resulting in an oxidative C-C bond cleavage. On the other hand, the platinum based catalysts enable the conversion of glycerol in both acidic and basic solutions and can be selective for the formation of glyceraldehyde in acidic solution or base-free solutions (Carrettin et al., 2002, 2003; Zhang et al., 2012; Skrzynska et al., 2014; Wang et al., 2014; Li and Zaera, 2015). In these previous studies, authors evidence that selectivity is a critical issue. This issue may be solved by tuning the *ad hoc* noble metal(s)/support couple and adjusting the proper process conditions.

EXPERIMENTAL

Materials

Anhydrous glycerol 99%, from Sigma-Aldrich was used for the catalytic tests, and H_2SO_4 from Sigma Aldrich was used for HPLC analysis. Different supports were used for the synthesis of the catalysts: SiO_2 MCM-41 from ACS Material and three oxide supports, gamma alumina, titanium oxide, and zeolite ZSM-5, all from Alfa Aesar. Potassium platinum (+IV) chloride and pure sodium hydroxide both from Sigma-Aldrich were used as precursors for the preparation of the Pt-supported catalysts, while sodium borohydride (>96% $NaBH_4$) from Sigma-Aldrich was used as reducing agent and sodium hydroxide (NaOH ≥98%) from Sigma-Aldrich was used to adjust the pH.

Catalysts Preparation

The platinum-based materials deposited on various supports (i.e., SiO_2, TiO_2, γ-Al_2O_3, ZSM-5) were prepared by chemical reduction in the liquid phase. Each powdered oxidic support (about 5 g) was suspended in 75 cm^3 of ultrapure water and stirred for 60 min at 67°C. Then, a solution containing 0.3736 g $K_2PtCl_6.6H_2O$ (Sigma Aldrich, ≥98%) dissolved in 25 cm^3 of ultrapure water was added dropwise to this suspension to obtain a platinum loading of about 1.5 wt.% relative to the support in the final material. The temperature of the reaction mixture was maintained at 67°C for 60 min under stirring. Sodium borohydride was used as a reducing agent to reduce the platinum metal. The amount of reducing agent was adjusted with respect to the amount of platinum precursor, each time using a 2-fold stoichiometric excess [11]. The as-obtained gray mixture was further stirred at 67°C, after adjusting the pH to 7 with a 0.3 M solution of sodium hydroxide. The suspension was then mixed at 67°C for 90 min and a gray solid was recovered by filtration, washed with 100 cm^3 of distilled water and dried at 110°C for 24 h prior testing. A series of catalysts with a nominal content of platinum of 1.5 wt.% was then obtained.

Catalysts' Characterization

The textural properties (specific surface area, pore volume and mean pore size) of the catalysts were analyzed by N_2 adsorption-desorption using a Micromeritics Tristar-II 3020 instrument. Prior to the analysis, the samples were outgassed at 110°C for 7 h under vacuum. To determine the Pt loading in the catalysts, inductively coupled plasma-atomic emission spectroscopy (ICP-AES, Vista Pro Varian) was used. The samples were prepared by dissolving the catalysts in a Hot Block/HCl/HNO$_3$ digestion. The dispersion of Pt is determined by H_2 chemisorption using Micromeritics Autochem II 2920 instrument. Prior to the analysis, pure H_2 (i.e., 30 mL/min) was used to reduce the samples at 500°C (i.e., 10°C/min); Then an Ar flux (i.e., 50 mL/min) was used for 1 h at 500°C before a return to room temperature and 10 injections (20 μL) of H_2 in Ar were carried out. The crystalline phases present in the catalysts were analyzed by XRD at ambient temperature on Bruker D8 Advance instrument, equipped with a CuKα source ($\lambda = 0.154$ nm). The samples were scanned at a rate of 0.02° over the 5° ≤ 2θ ≤ 90° range with an integration time of 0.5 s. The diffractograms were indexed using the JCPDS database. The oxidation state of platinum and its quantification on the surface of catalysts were determined by XPS analysis (AXIS Ultra Kratos) using a monochromatized aluminum source (AlKα = 1486.6 eV, 150 W), and the value of the C1s core level (285 eV) was used for the calibration of the energy scale. Curve fitting was performed using the Casa XPS software applying a Shirley-type background subtraction. To determine the size of the platinum particles, transmission electron microscopy analysis was used. TEM FEI Tecnai G2-20 twin, working with an accelerating potential of 200 kV and equipped with a slow-scan CCD camera, enabled the observation of samples with a very high resolution (2–5 nm scale). The samples for TEM were prepared from a diluted suspension of catalyst in ethanol. A drop of suspension was placed on a Lacey carbon-coated grid and allowed to dry in air. The particle size distribution was calculated by counting over 200 particles over multiple areas using the ImageJ software.

Catalytic Performance Evaluation

The glycerol oxidation reaction in the liquid phase was carried out in a 300 cm^3 semi-batch stainless steel reactor (PARR 5500 HP Series Compact Reactors), equipped with a thermocouple and a thermo-regulated oxygen supply system. For each experiment, 200 cm^3 of an 0.1 M glycerol aqueous solution were heated to 80°C. The reaction was started at the temperature of 80°C when 0.5 g of the selected catalyst was introduced into the reactor immediately pressurized with 2 bar oxygen (t_0). The products were periodically sampled and analyzed with an Agilent 1260 HPLC, equipped with an Aminex HPX-87H column (300 × 7.8 mm) and a reflective index detector (RID). A solution of H_2SO_4 (0.0025 M) in deionized water (flow rate: 0.5 cm^3·min^{-1}) was used as an eluent. The identification and quantification of the reaction products were performed using the corresponding calibration curves plotted upfront.

RESULTS AND DISCUSSION

Catalysts Characterization

BET

The results of the textural analysis of the catalysts are presented in **Table 1**. Compared to supports alone, no change can be noted in terms of specific surface area for Pt/SiO$_2$, Pt/TiO$_2$, Pt/ZSM-5, and Pt/γ-Al$_2$O$_3$. The silica-supported catalyst (SiO$_2$-MCM 41) exhibits the largest specific surface area (i.e., 625 m^2/g) and the largest pore volume (0.575 cm^3/g), but an average pore diameter of 2.7 nm. Pt/ZSM-5 and Pt/TiO$_2$ have lower specific surface areas of 358 and 167 m^2/g, respectively (**Table 2**). It can be noted that Pt/γ-Al$_2$O$_3$ has the lowest specific surface area (57 m^2/g), but a higher pore diameter than the other studied materials (25.7 nm).

XRD

The diffractograms of catalysts are presented in **Figure 1**. The diffractogram of the TiO$_2$ support (**Figure 1A**) shows well resolved diffraction peaks, characteristic of the crystallized anatase phase in a tetragonal face-centered system (PDF 00-021-1272). There is no significant change in the diffractogram after platinum addition is observed. **Figure 1B** shows the diffractogram of the catalyst supported on gamma-alumina (PDF 001-1303). The diffractograms of the catalyst support

TABLE 1 | List of the prepared catalysts with the corresponding acronyms, specific surface area (SSA$_{BET}$), the BJH desorption branch-deduced average pore diameter (d$_{pores}$) and the BJH desorption branch-derived cumulative pore volume (V$_{pores}$).

Catalyst	Pt loading (ICP)/Me wt.%	Pt dispersion (H$_2$ chemisorption)/%
Pt/SiO$_2$	1.20	1
Pt/ZSM5	1.36	1.5
Pt/TiO$_2$	1.15	24.5
Pt/γ-Al$_2$O$_3$	1.29	32.7
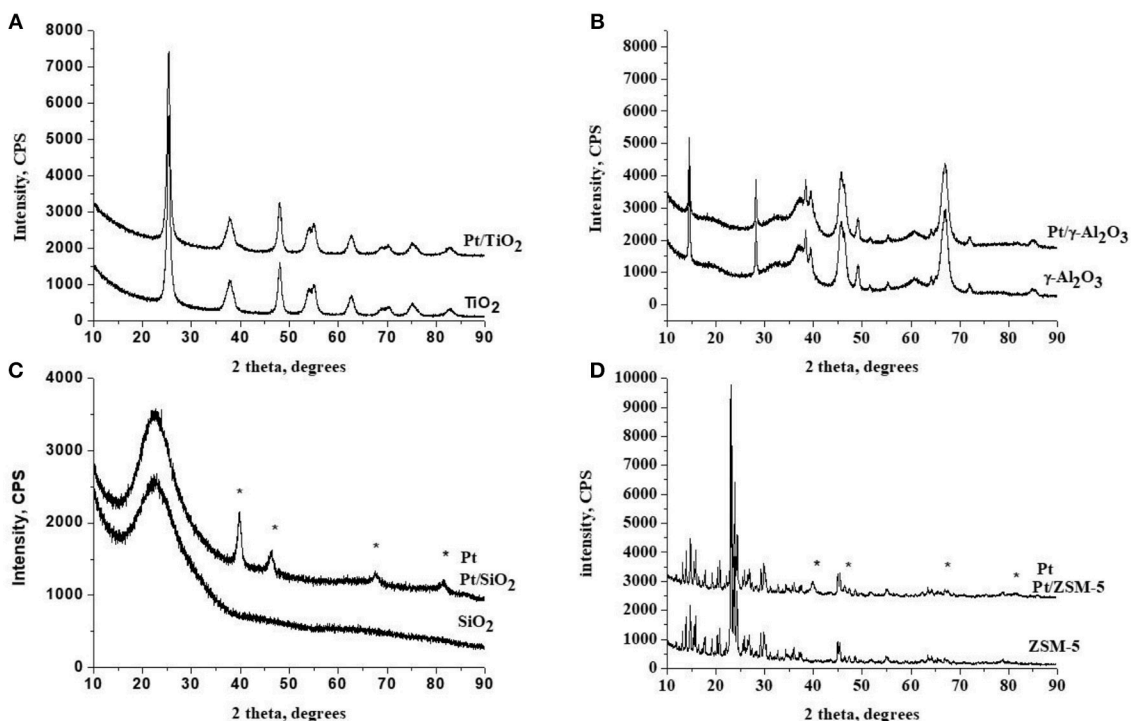
FIGURE 1 | X-ray diffractograms of the fresh catalysts and of the corresponding supports with the position of the main diffraction lines expected for the metallic particles. Symbols (*) corresponds to: Pt. **(A)** TiO$_2$ as support, **(B)** γ-Al$_2$O$_3$ as support, **(C)** SiO$_2$ as support and **(D)** ZSM-5 as support.
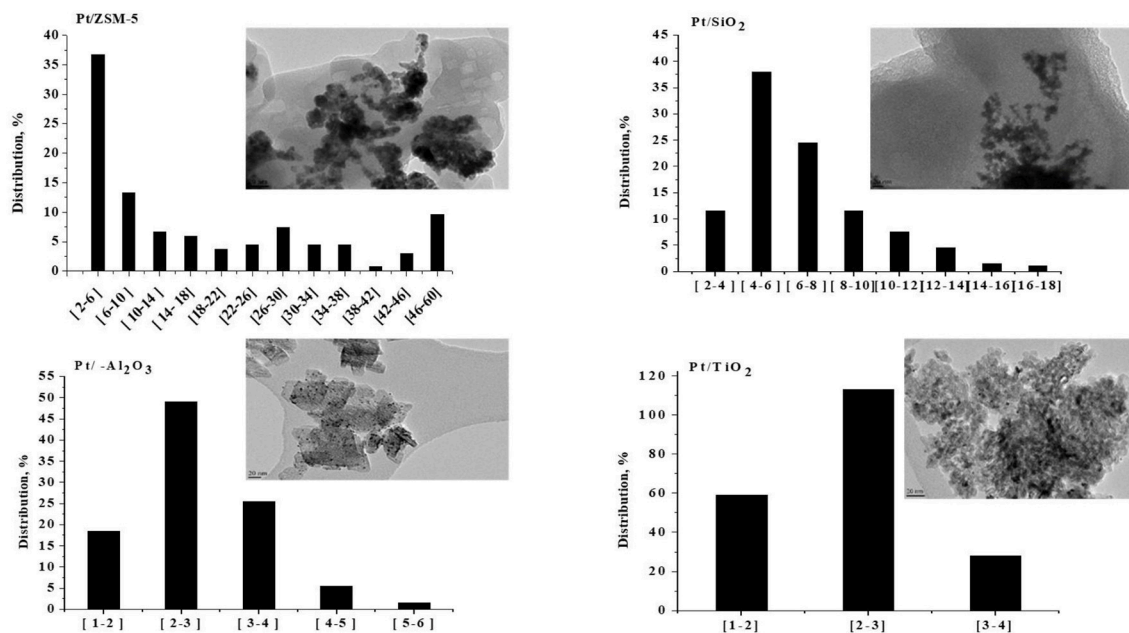
FIGURE 2 | TEM images and histograms of the metallic particle size distributions observed over the prepared catalysts.

are identical. The diffractogram of the SiO$_2$ MCM-41 support (**Figure 1C**) has a very large and low intensity line representative of the amorphous character of this support. The appearance of several additional peaks on the Pt/SiO$_2$ diffractogram is attributed to the presence of crystallized metallic platinum in a face-centered cubic lattice (JCPDS No. 04-0802). The diffractogram of the ZSM-5 support (**Figure 1D**) has well resolved diffraction peaks, characteristic of ZSM-5 zeolite. The appearance of additional peaks after Pt deposition (which are similar to those observed for silica MCM-41) is also attributed to the presence of crystallized metallic platinum (JCPDS No. 04-0802). According to the diffractogram analysis of the various catalysts, it can be concluded that the platinum supported on TiO$_2$ and γ-Al$_2$O$_3$ is predominantly present under the form of small particles (with XRD, particles with a size <5 nm can be hardly identified). The clear appearance of characteristic diffraction peaks assigned to metallic platinum over SiO$_2$ and ZSM-5 suggests the presence of Pt particles larger than 5 nm, which will be confirmed by TEM analysis (*vide supra*).

ICP & H$_2$ Chemisorption

The results of the elemental analysis of the catalysts prepared shown in **Table 1** confirm that the actual amount of deposited platinum is close to the theoretical one (i.e., 1.5 wt.%). Metal dispersions obtained by chemisorption of H$_2$ are summarized in **Table 1** as well. A very low platinum dispersion is obtained for Pt/SiO$_2$ and Pt/ZSM-5 (1 and 1.5%, respectively). On the other hand, the platinum dispersion on TiO$_2$ and γ-Al$_2$O$_3$ is much better, with respective values of 24.5 and 32.7%. These results suggest an agglomeration of the platinum particles on the two silicic supports. This is in agreement with the XRD analyzes

results (i.e., detection of a metallic Pt phase suggesting particle sizes larger than 5 nm).

TEM

Figure 2 presents the TEM images of supported platinum-based catalysts, as well as the particle size distribution. A non-homogeneous distribution and aggregations of platinum particles were observed for Pt/SiO$_2$. Over this sample, more than 50% of the particles have a size <6 nm, but the distribution extends to sizes larger than 18 nm. Note that we did not analyze all the agglomerated particles on the TEM pictures for that sample, which means that the actual number of very large agglomerates/particles is even underestimated. The TEM images of Pt/ZSM-5 catalyst show that the platinum particles' size distribution is not homogeneous over this sample with the presence of aggregates of platinum particles. One third of the population has a size between 2 and 6 nm, more than half is within the range of 6–36 nm and the remainder has a diameter larger than 36 nm. This agrees with the XRD observations as well. Concerning the Pt/TiO$_2$ catalyst, the particle size distribution is centered on 2–3 nm with 55% of the particles in this range. The largest size observed is 4 nm. This result agrees with the observed metal dispersion (24.44%) and the absence of Pd peaks on the XRD diffractograms. Finally, The Pt/γ-Al$_2$O catalyst has the best dispersion among all of the studied samples, with a particle size distribution centered on 2–3 nm, it gathered 50% of the total population. The largest size observed is 6 nm.

XPS

The chemical surface composition of the samples has been studied by XPS. This study is based, for platinum, on the analysis of the Pt 4f levels for Pt/SiO$_2$, Pt/TiO$_2$, and Pt/ZSM-5 and of

FIGURE 3 | XPS spectra of the Pt 4d or Pt 4f levels with the corresponding BE values observed over the prepared catalysts.

the Pt 4d level for Pt/γ-Al$_2$O$_3$. Indeed, for this latter, the Pt 4f photopeak overlaps that of Al 2p, which makes it unexploitable. It should be noted that the percentage of aluminum in the ZSM-5 support is lower than in the γ-Al$_2$O$_3$, and that it is therefore possible to separate the Pt 4f and Al 2p photopeaks for this sample. **Figure 3** shows the corresponding spectra obtained for all the catalysts. The spectrum of Pt/TiO$_2$ shows two photoelectron peaks at binding energies of 70.28 eV (Pt 4f$_{7/2}$) and 73.58 eV (Pt 4f$_{5/2}$). These binding energies correspond to those expected for Pt^O (Hu et al., 2010). The other two photoelectron peaks are located at binding energies of 75.30 eV (Pt 4f$_{7/2}$) and 78.60 eV (Pt 4f$_{5/2}$) and are characteristic of platinum in the oxidic form (Skrzynska et al., 2015; "X-ray Photoelectron Spectroscopy (XPS) Reference Pages, Element: Platinum, Home page: http://www.xpsfitting.com (access 15thSep. 2018).," n.d.). We determined that platinum oxide represents about 15% of the total platinum **Table 3**. Concerning the Pt/ZSM-5 catalyst, two photoelectrons peaks characteristic of platinum metal, located at binding energies of 71.65 eV (Pt 4f$_{7/2}$) and 74.95 eV (Pt 4f$_{5/2}$), and a photoelectron peak corresponding to Al 2p level, located at a binding energy of 74.66 eV, could be observed. The platinum analyzed in this catalyst was therefore 100% in the metallic form (Pt^O). As for Pt/SiO$_2$, the spectrum obtained is composed of two photoelectron peaks characteristic of Pt^O at binding energies of 71.0 eV (Pt 4f$_{7/2}$) and 74.33 eV (Pt 4f$_{5/2}$) and two photoelectron peaks characteristic of platinum in the oxidic form,

TABLE 2 | List of catalysts prepared with the acronyms, the actual platinum metal loading estimated by elemental analysis (ICP), and dispersion estimated by H$_2$-Chemisorption.

Catalyst name	Support		Catalyst	
	SSA_{BET} (N$_2$-BET)/m^2.g^{-1}		$V_{poresBJH}$ /cm^3.g^{-1}	d_{pores} (nm)
Pt/SiO$_2$	635	625	0.575	2.7
Pt/ZSM-5	361	358	0.165	8.2
Pt/TiO$_2$	173	167	0.396	6.5
Pt/γ-Al$_2$O$_3$	57	56	0.394	25.7

located at binding energies of 74.23 eV (Pt 4f$_{7/2}$) and 77.53 eV (Pt 4f$_{5/2}$). Regarding the Pt/γ-Al$_2$O$_3$ sample, two components characteristic of Pt in the metallic form (Pt 4d$_{5/2}$ and Pt 4d$_{3/2}$ localized at binding energies 314.55 and 331.93 eV, respectively) and two peaks characteristic of platinum in the oxidic form (at 320.08 and 339.72 eV, respectively), were observed. Furthermore, the presence of a photoelectron peak located at a binding energy of 305.04 eV was noted, corresponding to an impurity that could be magnesium (Mg Auger) present as impurity in one of the precursors used during the synthesis.

The results of the XPS analyses as well as the quantification of the different species are summarized in **Table 3**, below.

The Pt/M atomic ratios are larger for the Pt/TiO$_2$ and Pt/γ-Al$_2$O$_3$, which can be explained by the better dispersion of Pt over these catalysts.

Catalytic Performances

Evolution of Selectivity as a Function of Time

The evolution of the quantity of the different products formed during a catalytic oxidation reaction of glycerol in liquid phase, using a Pt/SiO2 sample as an example under 0.1 M glycerol solution with 2 bars of oxygen at 80°C, was studied. As well as that, the consumption of glycerol as a function of time are shown

TABLE 3 | Binding energies of the Pt 4f7/2 level for the Pt on SiO$_2$, TiO$_2$, ZSM-5 catalysts, and of the Pt 4d5/2 level for Pt/γ-Al$_2$O$_3$; Surface Pt/M atomic ratios with M = Si (2p), Ti (2p) ou Al (2p).

Catalyst	Pt 4f$_{7/2}$ metallic (eV)	Pt 4f$_{7/2}$ oxide (eV)	Mol% Pt metallic	Mol% Pt oxide	Pt/M (atom/atom)
Pt/SiO$_2$	71.0	74.2	87	13	0.008
Pt/TiO$_2$	70.3	75.3	85	15	0.022
Pt/ZSM-5	71.2	-	100	-	0.005
Pt/γ-Al$_2$O$_3$	**4d$_{5/2}$** 314.5	**4d$_{5/2}$** 320.0	76	24	0.014

*The bold text signifies that the XPS contribution was changed for this sample due to the fact that there was a significant overlap in 4f7/2 with the Al contribution.*

in **Figure 4** (right). Also, **Figure 4** (left) presents the same data in the form of glycerol conversion and selectivities to products. At the beginning of the reaction, the oxidation of the primary hydroxyl group first leads to the formation of glyceraldehyde with a very rapid increase in the number of moles in the first 5 min with 13 mmol.mol^{-1}Pt.h^{-1} as the initial formation rate. After 5 min, the rate of glyceraldehyde formation decreases. Further, the number of moles of glyceraldehyde remains stable after 300 min. On the other hand, glyceric acid appears after 8 min of reaction and its quantity progresses linearly. Two other minor products (i.e., glycolic acid and glyoxal) appear at the beginning of the reaction, without any subsequent evolution of their quantity with time. In terms of selectivity, **Figure 4** shows that the glyceraldehyde selectivity reaches 90% after 8 min and then progressively decreases to 58% after 340 min. The selectivity to glyceric acid increases gradually to 38% after 340 min.

Owing to the obtained results, a reaction scheme (**Figure 5**) was proposed to explain the formation of the products (Katryniok et al., 2011). The first step of the reaction is the oxidation of the primary hydroxyl to form glyceraldehyde (primary product). The latter can be oxidized to glyceric acid or undergo oxidative C-C cleavage to form glycolic acid and carbon dioxide, as secondary products.

Influence of the Support

The catalytic tests of the glycerol oxidation in the liquid phase were carried out for the four catalysts and the results are
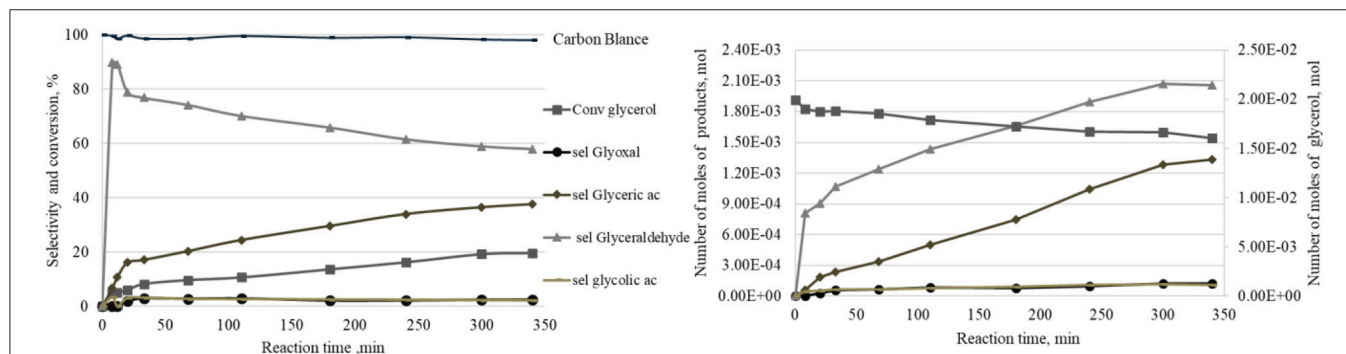
FIGURE 4 | Evolution of the products quantities as a function of time under the following reaction conditions: 0.5 g of Pt/SiO$_2$, 200 cm^3 of an aqueous 0.1 M GLY solution, 2 bars of oxygen, 1,000 rpm, temperature 80°C.
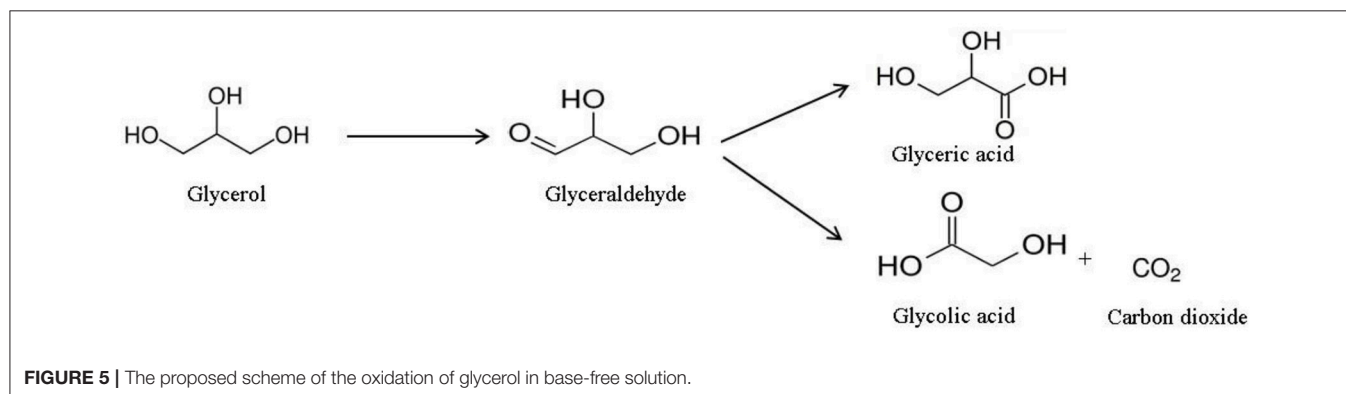

FIGURE 5 | The proposed scheme of the oxidation of glycerol in base-free solution.
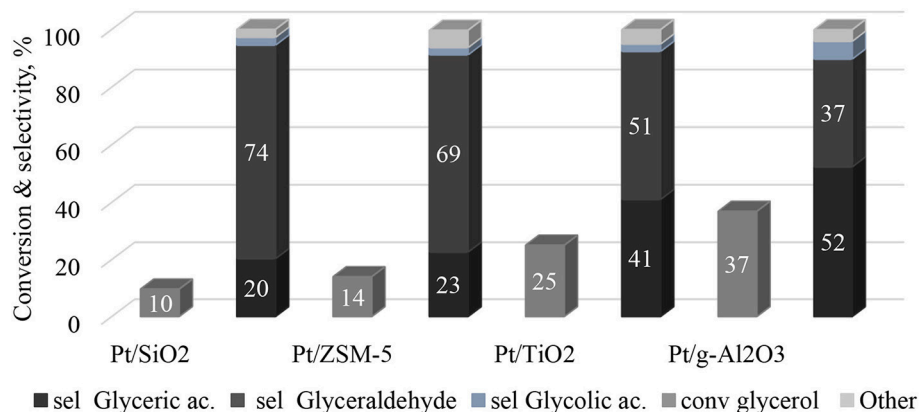
FIGURE 6 | Conversion and selectivity of products during glycerol partial oxidation over the prepared catalysts. Reaction conditions: 0.5 g of catalysts, 200 cm^3 of an aqueous 0.1 M GLY solution, 2 bars of oxygen, 1,000 rpm, temperature 80°C, 1 h.

presented in **Figure 6**. The best performance is obtained with Pt/γ-Al$_2$O$_3$ with a glycerol conversion of 37% after 60 min of the reaction (with an initial glycerol conversion speed of 48 mmol glycerol.mol^{-1}Pt.h^{-1}). After the same reaction time, the Pt/TiO$_2$ catalyst converts 25% of glycerol with an initial glycerol conversion rate of 52 mmol glycerol.mol^{-1}Pt.h^{-1}. Finally, the Pt/SiO$_2$ and Pt/ZSM-5 catalysts are much less active with glycerol conversions of 10 and 14%, respectively, after 1 h (and initial glycerol conversion rates of 16 and 14 mmol glycerol.mol^{-1}Pt.h^{-1}, respectively). These differences can be interpreted according to the aforementioned characterization results. The analysis of the platinum dispersion showed that the platinum on SiO$_2$ and on ZSM-5 is weakly dispersed, but well dispersed on TiO$_2$ and γ-Al$_2$O$_3$. This result was confirmed by TEM analysis, which showed an agglomeration of platinum over SiO$_2$ and ZSM-5. Therefore, this suggests that the number of active sites accessible on the Pt/SiO$_2$ and Pt/ZSM-5 catalysts is lower than on the Pt/TiO$_2$ and Pt/γ-Al$_2$O$_3$ catalysts. This result was further corroborated by XPS analysis, which showed that the atomic ratios (i.e., Pt/M, Atom/Atom) are lower for the Pt/SiO$_2$ and Pt/ZSM-5 catalysts (**Table 3**)

Figure 7 shows the relationship between the initial rate of glycerol conversion and the average particle size of Pt. It is evident that from ∼6 nm, the initial rate of transformation seems constant. According to **Figure 6**, the selectivity to glyceraldehyde (74%) is higher for the less active catalyst (Pt/SiO$_2$-10% glycerol conversion and 20% glycerol acid selectivity after 60 min of reaction). The Pt/γ-Al$_2$O$_3$ catalyst is the most active in the series studied with a 37% glycerol conversion after 60 min of the reaction, predominantly producing glyceric acid (52%). It clearly exists a dependence between glyceraldehyde and glycerol acid selectivity and glycerol conversion, which is common for successive reactions of the A→B→C type. To interpret these results, the evolution of glyceraldehyde selectivity was plotted as a function of conversion for all of the catalysts. **Figure 8** shows that the selectivity of the glyceraldehyde linearly decreases with the increase in conversion, and therefore the most active catalyst will have a low glyceraldehyde selectivity, which is the case for the Pt/Al$_2$O$_3$, Pt/TiO$_2$, and Pt/ZSM-5.
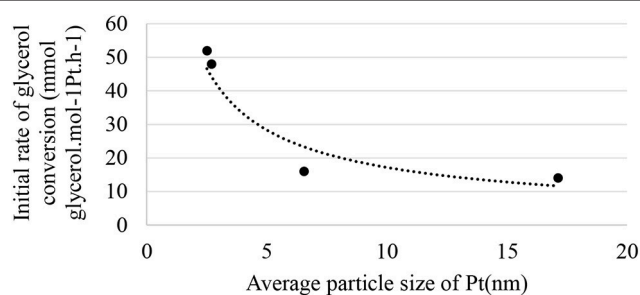
FIGURE 7 | Relationship between the initial rate of glycerol conversion and the average particle size of Pt.
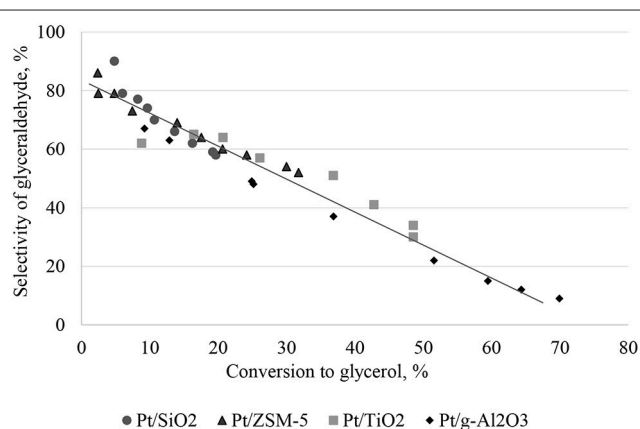
FIGURE 8 | Relationship between the selectivity of glyceraldehyde and the conversion to glycerol.

CONCLUSION

In this work, we synthesized four Pt based catalysts changing the support. XPS characterizations evidence that the platinum was mainly reduced but not totally for most used supports with a reduction level higher than 80%. The nature of the

catalytic support clearly influences the platinum particle size and the dispersion of the particles has been demonstrated. The silicic supports studied generate aggregation of the platinum particles leading to a high average particle size (i.e., 6.5 nm) Contrary to that, using TiO_2 or γ-Al_2O_3 as supports leads to very small particles (i.e., 2.7 nm) with a narrow size distribution. The average particle size leads to a significant change in the initial rates of glycerol oxidation in the liquid phase in a base-free solution. The catalyst having a low dispersion has a particle size distribution spread over a wide range and a larger average particle size (i.e., fewer active sites), inducing a lower glycerol conversion and initial transformation rate on these materials. We have also demonstrated a real dependence between target molecule selectivity (i.e., glyceraldehyde) and substrate conversion, where the selectivity of glyceraldehyde decreases with increasing glycerol conversion. At the same time, the oxidation of glyceraldehyde leads to the formation of glyceric acid, which does not seem to be transformed anymore in our reaction conditions. Thanks to our work, we have designed a series of catalysts able to transform glycerol either in glyceraldehyde or in glyceric acid in base free media, depending on material choice. In order to achieve high glyceraldehyde selectivity, low glycerol conversion is needed followed by a separation process. In this case, the Pt/SiO_2 is a good candidate due to the fact that its initial transformation rate is lower allowing an easier separation process. If the goal is to obtain glyceric acid with high selectivity, Pt/γ-Al_2O_3 is much more suitable.

DATA AVAILABILITY

All datasets generated for this study are included in the manuscript and/or the supplementary files.

AUTHOR CONTRIBUTIONS

AE: student who perform majority of the experiment; PF: contribution on the mechanism part; FD: contribution on the characterization part (XPS,...); MC: contribution on the reactivity part. All authors have contributed to the manuscript writing process.

REFERENCES

Alhanash, A., Kozhevnikova, E. F., and Kozhevnikov, I. V. (2008). Hydrogenolysis of glycerol to propanediol over Ru: polyoxometalate bifunctional catalyst. *Catal. Lett.* 120, 307–311. doi: 10.1007/s10562-007-9286-3

Carrettin, S., McMorn, P., Johnston, P., Griffin, K., and Hutchings, G. J. (2002). Selective oxidation of glycerol to glyceric acid using a gold catalyst in aqueous sodium hydroxide. *Chem. Commun.* 7, 696–697. doi: 10.1039/b201112n

Carrettin, S., McMorn, P., Johnston, P., Griffin, K., Kiely, C. J., and Hutchings, G. J. (2003). Oxidation of glycerol using supported Pt, Pd and Au catalysts. *Phys. Chem. Chem. Phys.* 5, 1329–1336. doi: 10.1039/b212047j

Díaz, J. A., Skrzynska, E., Girardon, J.-S., Capron, M., Dumeignil, F., and Fongarland, P. (2017). Glycerol oxidation in the liquid phase over a gold-supported catalyst: kinetic analysis and modelling. *ChemEngineering* 1, 1–14. doi: 10.3390/chemengineering1010007

El Doukkali, M., Iriondo, A., Cambra, J. F., Gandarias, I., Jalowiecki-Duhamel, L., Dumeignil, F., et al. (2014). Deactivation study of the Pt and/or Ni-based γ-Al2O3 catalysts used in the aqueous phase reforming of glycerol for H2 production. *Appl. Catal. Gen.* 472, 80–91. doi: 10.1016/j.apcata.2013.12.015

Ftouni, J., Villandier, N., Auneau, F., Besson, M., Djakovitch, L., and Pinel, C. (2015). From glycerol to lactic acid under inert conditions in the presence of platinum-based catalysts: the influence of support. *Catal. Today* 257, 267–273. doi: 10.1016/j.cattod.2014.09.034

Hu, W., Knight, D., Lowry, B., and Varma, A. (2010). Selective oxidation of glycerol to dihydroxyacetone over Pt–Bi/C catalyst: optimization of catalyst and reaction conditions. *Ind. Eng. Chem. Res.* 49, 10876–10882. doi: 10.1021/ie1005096

Katryniok, B., Kimura, H., Skrzynska, E., Girardon, J.-S., Fongarland, P., Capron, M., et al. (2011). Selective catalytic oxidation of glycerol: perspectives for high value chemicals. *Green Chem.* 13, 1960–1979. doi: 10.1039/C1GC15320J

Katryniok, B., Paul, S., Bellière-Baca, V., Rey, P., and Dumeignil, F. (2010). Glycerol dehydration to acrolein in the context of new uses of glycerol. *Green Chem.* 12, 2079–2098. doi: 10.1039/c0gc00307g

Katryniok, B., Paul, S., Capron, M., and Dumeignil, F. (2009). Towards the sustainable production of acrolein by glycerol dehydration. *ChemSusChem* 2, 719–730. doi: 10.1002/cssc.200900134

Lauriol-Garbey, P., Millet, J. M. M., Loridant, S., Bellière-Baca, V., and Rey, P. (2011). New efficient and long-life catalyst for gas-phase glycerol dehydration to acrolein. *J. Catal.* 281, 362–370. doi: 10.1016/j.jcat.2011.05.014

Li, Y., and Zaera, F. (2015). Sensitivity of the glycerol oxidation reaction to the size and shape of the platinum nanoparticles in Pt/SiO2 catalysts. *J. Catal.* 326, 116–126. doi: 10.1016/j.jcat.2015.04.009

Liebig, C., Paul, S., Katryniok, B., Guillon, C., Couturier, J.-L., Dubois, J.-L., et al. (2013). Glycerol conversion to acrylonitrile by consecutive dehydration over WO3/TiO2 and ammoxidation over Sb-(Fe,V)-O. *Appl. Catal. B Environ.* 132–133, 170–182. doi: 10.1016/j.apcatb.2012.11.035

Mimura, N., Hiyoshi, N., Daté, M., Fujitani, T., and Dumeignil, F. (2014). Microscope analysis of Au–Pd/TiO2 glycerol oxidation catalysts prepared by deposition–precipitation method. *Catal. Lett.* 144, 2167–2175. doi: 10.1007/s10562-014-1382-6

Purushothaman, R. K. P., van Haveren, J., Mayoral, A., Melián-Cabrera, I., and Heeres, H. J. (2014). Exploratory catalyst screening studies on the base free conversion of glycerol to lactic acid and glyceric acid in water using bimetallic Au–Pt nanoparticles on acidic zeolites. *Top. Catal.* 57, 1445–1453. doi: 10.1007/s11244-014-0316-2

Skrzynska, E., El Roz, A., Paul, S., Capron, M., and Dumeignil, F. (2019). Glycerol partial oxidation over Pt/Al2O3 catalysts under basic and base-free conditions – effect of the particles size. *J. Amer. Oil Chem. Soc.* 96, 63–74. doi: 10.1002/aocs.12159

Skrzynska, E., Ftouni, J., Mamede, A.-S., Addad, A., Trentesaux, M., Girardon, J.-S., et al. (2014). Glycerol oxidation over gold supported catalysts – "Two

faces" of sulphur based anchoring agent. *J. Mol. Catal. Chem.* 382, 71–78. doi: 10.1016/j.molcata.2013.11.007

Skrzynska, E., Zaid, S., Addad, A., Girardon, J.-S., Capron, M., and Dumeignil, F. (2016). Performance of Ag/Al$_2$O$_3$ catalysts in the liquid phase oxidation of glycerol – effect of preparation method and reaction conditions. *Catal. Sci. Technol.* 6, 3182–3196. doi: 10.1039/C5 CY01581B

Skrzynska, E., Zaid, S., Girardon, J.-S., Capron, M., and Dumeignil, F. (2015). Catalytic behaviour of four different supported noble metals in the crude glycerol oxidation. *Appl. Catal. Gen.* 499, 89–100. doi: 10.1016/j.apcata.2015.04.008

Wang, Y., Van de Vyver, S., Sharma, K. K., and Román-Leshkov, Y. (2014). Insights into the stability of gold nanoparticles supported on metal oxides for the base-free oxidation of glucose to gluconic acid. *Green Chem.* 16, 719–726. doi: 10.1039/C3GC41362D

Zaid, S., Skrzynska, E., Addad, A., Nandi, S., Jalowiecki-Duhamel, L., Girardon, J.-S., et al. (2017). Development of silver based catalysts promoted by noble metal M (M = Au, Pd or Pt) for glycerol oxidation in liquid phase. *Top. Catal.* 60, 1072–1081. doi: 10.1007/s11244-017-0800-6

Zhang, M., Liang, D., Nie, R., Lu, X., Chen, P., and Hou, Z. (2012). Oxidation of biodiesel glycerol over Pt supported on different sized carbon supports in base-free solution. *Chin. J. Catal.* 33, 1340–1346. doi: 10.1016/S1872-2067(11)60411-7

Conflict of Interest Statement: The authors declare that the research was conducted in the absence of any commercial or financial relationships that could be construed as a potential conflict of interest.

Esterification of Glycerol With Oleic Acid Over Hydrophobic Zirconia-Silica Acid Catalyst and Commercial Acid Catalyst: Optimization and Influence of Catalyst Acidity

Pei San Kong[1]*, Yolande Pérès[2], Wan Mohd Ashri Wan Daud[3], Patrick Cognet[2]* and Mohamed Kheireddine Aroua[4,5]*

[1] Sime Darby Research Sdn. Bhd., Pulau Carey, Malaysia, [2] Laboratoire de Génie Chimique, CNRS, INP, UPS, Université de Toulouse, Toulouse, France, [3] Department of Chemical Engineering, Faculty of Engineering, University of Malaya, Kuala Lumpur, Malaysia, [4] Centre for Carbon Dioxide Capture and Utilization, School of Science and Technology, Sunway University, Bandar Sunway, Malaysia, [5] Department of Engineering, Lancaster University, Lancaster, United Kingdom

Catalytic esterification of glycerol with oleic acid (OA) was optimized over hydrophobic mesoporous zirconia-silica heterogeneous acid catalyst (ZrO_2-SiO_2-Me&Et-$PhSO_3H$) and benchmarked with commercial catalysts (Aquivion and Amberlyst 15) in order to examine the effect of catalyst acidity on conversion, yield and product selectivity. The process optimisation results showed an 80% conversion with a 59.4% glycerol mono-oleate (GMO) and 34.6% glycerol dioleate (GDO) selectivities corresponding to a combined GMO and GDO selectivity of 94.8% at equimolar OA-to-glycerol ratio, 160°C reaction temperature, 5 wt% catalyst concentration with respect to the OA weight and 4 h reaction time. This work reveals that the hydrophobic and mild acidic ZrO_2-SiO_2-Me&Et-$PhSO_3H$ catalyst outperformed Amberlyst 15 and Aquivion with a yield of 82% and GMO selectivity of 60%. It is found that catalyst acidity is a key parameter for catalytic activity and conversion rate. Nevertheless, high acidity/acid strength reduced the product yield in the glycerol esterification of OA.

Keywords: hydrophobic silica-zirconia based catalyst, optimisation, acidity, selectivity, esterification, glycerol

INTRODUCTION

Glycerol mono, di-oleates (GMO, GDO) are lipids with amphiphilic, non-ionic and excellent emulsifying properties that widely applied in food, cosmetic, and pharmaceutical industries, and aqueous fiber finishing (Thengumpillil et al., 2002; Macierzanka and Szelag, 2004). GMO featuring a polar head group and a non-polar hydrocarbon chain which exhibits significant amphiphilic properties. Therefore, GMO could be self-assembled into different liquid crystalline structures under varying conditions of temperature and solvent composition (Kulkarni et al., 2011). The actively growing industries such as personal care, pharmaceuticals, and lubricants are the main outlets for GMO. Nevertheless, the demand of GMO is correlated to personal care or lubricant

market due to the gradual slowdown in the food and plastics sectors (Frost Sullivan Research Service, 2014). Meanwhile, GDO is mainly used in drug delivery applications and as safe plasticizers for the polymer industry (Barauskas et al., 2006; Zhang et al., 2017).

The esterification reaction between glycerol and fatty acids can be an economic process. Glycerol can be obtained from low costs feedstock such as co-product in the biodiesel industry. Extensive research investigations on glycerol conversion to value-added chemicals have been shepherded due to surplus glycerol production and its inevitably low value (Quispe et al., 2013; Kong et al., 2016a). Generally, acid catalytic system is employed in esterification, etherification, polymerization, dehydration, acetylation, or glycosylation reaction (Kong et al., 2015, 2016b; Karam et al., 2017). The catalytic esterification of glycerol with large molecular size of oleic acid (OA) can produce numerous high commercial value of glycerol mono-, di-, and tri-oleate (GMO, GDO, and GTO).

Mesoporous silica, metal oxide, modified zeolites, heteropolyacids-supported catalysts (Wee et al., 2013) and ion-exchange resins (Amberlyst 15, Amberlyst 16, Amberlyst 31) (Åkerman et al., 2011), double-metal cyanide complexes (Kotwal et al., 2011), hydrotalcite (Hamerski and Corazza, 2014; Hamerski et al., 2016) and sulfated metal oxides catalysts (Kong et al., 2015) have been investigated as potential catalysts for glycerol esterification with OA. It was reported that the use of DMC complex allowed to obtain a conversion of 63.4% together with a 67.3% GMO selectivity at reaction temperature (180°C), catalyst concentration (8 wt%), and equimolar glycerol-to-OA ratio in 8 h reaction time (Kotwal et al., 2011). Notably, the outstanding catalytic performance was not only ascribed to the available catalyst sites in enhancing the conversion but also to the catalyst structure for maximize the selectivity of desired product. In terms of process parameters, the selectivity toward GMO and GDO formation is higher when using higher glycerol concentration, shorter reaction time, and lower reaction temperature (preferably 1:4 molar ratio of OA to glycerol, 3–6 h, <180°C). On the contrary, the formation of GTO can be achieved by increasing reaction time and operating temperature at higher OA environment (3:1 molar ratio of OA to glycerol, >10 h, >180°C) (Kong et al., 2015).

It has been reported that catalyst surface structure together with operating parameters play an important role in controlling the selectivity of products, whereby the yields rely mainly upon catalyst properties, amongst which hydrophobicity is of great importance. Consequently, this work examines the optimization study of hydrophobic-enhanced ZrO_2-SiO_2-Me&Et-$PhSO_3H$ catalyst under various operating conditions such as reactants molar ratio, catalyst concentration, reaction temperature, and reaction time. The novelty of this work is to examine the influence of ZrO_2-SiO_2-Me&Et-$PhSO_3H$ catalyst acidity in yield and product selectivity in comparison to the commercial available catalysts with higher acidity (Amberlyst 15; Aquivion) at optimized conditions as effect of catalyst acidity has not been insight studied in literatures. Furthermore, this work investigates the combination catalyst properties as such hydrophobicity and acidity strength in order to obtain desired product yield

and color. Nevertheless, this work also provides interaction effect of important operating parameters to acquire higher product selectivity.

EXPERIMENTAL

Materials

Zirconium hydroxide powder [$Zr(OH)_4$, 97% purity, Sigma-Aldrich], ethanol (99%), ammonia solution (NH_4OH, 25%, Sigma-Aldrich), tetraethyl orthosilicate (TEOS, 98%, Sigma-Aldrich), trimethoxymethylsilane (TMMS, 98%, Sigma-Aldrich), dry toluene (99%, Sigma-Aldrich), 2-(4-Chlorosulfonylphenyl) ethyltrimethoxysilane (CSPETS, 50% in dichloromethane, Fisher Scientific) and sulfuric acid solution (H_2SO_4, 99.99%) were used to synthesize ZrO_2-SiO_2-Me&Et-$PhSO_3H$ hydrophobic-enhanced catalyst. Zirconium (IV) propoxide, $Zr(OCH_2CH_2CH_3)_4$ precursor (70% in 1-propanol, Sigma-Aldrich), 1-propanol (99.7%, Sigma-Aldrich), and 0.5 M aqueous H_2SO_4 were utilized to produce sol-gel method-prepared catalyst (SO_4^{2-}/ZrO_2 solgel). The precipitation method prepared-catalyst, (SO_4^{2-}/ZrO_2 precipitation) was synthesized using zirconium oxychloride precursor, ($ZrOCl_2.8H_2O$, 99.5%, Sigma-Aldrich) and sodium hydroxide solution (NaOH, Sigma-Aldrich). SO_4^{2-}/ZrO_2 commercial catalyst was prepared by using commercial available $Zr(OH)_4$ and aqueous H_2SO_4. Commercial catalyst such as Amberlyst 15 (Sigma-Aldrich) and Aquivion (Solvay) were used for comparison study. Reactants glycerol (≥99.5%) and OA (technical grade, 90%) were purchased from Sigma-Aldrich. All the analytical standard reagents such as monoolein (≥99%), diolein (≥99%), and triolein (≥99%) were purchased from Sigma-Aldrich for quantitative product formation analysis. Analytical grade solvents such as acetonitrile (ACN), methanol (MeOH) and tetrahydrofuran (THF) were used as mobile phase and trifluoroacetic acid (TFA) was used as mobile phase additive.

Catalyst Preparation

The preparation steps of catalyst featured with hydrophobic surface, which synthesized with tailored amount of TMMS hydrophobic agent (ZrO_2-SiO_2-Me&Et-$PhSO_3H$) were described in our published work (Kong et al., 2018). ZrO_2 was added into ethanol under vigorous mixing condition at ambient temperature for 30 min. Twelve milliliters of NH_4OH and 4 ml of TEOS were successively added and stirred for 24 h to generate white silica suspension environment. The produced ZrO_2-SiO_2 was then filtered, rinsed with ethanol and dried overnight under vacuum at room temperature. Meanwhile, modification of ZrO_2-SiO_2 to higher hydrophobicity level together with functionalization of sulfonic acid group into ZrO_2-SiO_2 surface were carried out using TMMS and CSPETS (hydrophobic and surface initiating agents) (Mobaraki et al., 2014). The functionalized catalyst (ZrO_2-SiO_2-Me&Et-$PhSO_2Cl$) was then washed with toluene and distilled water. Eventually, the functionalized ZrO_2-SiO_2-Me&Et-$PhSO_2Cl$ solids were suspended in H_2SO_4 solution for 2 h (0.5 M, 5 ml) for cation-anion exchange of Cl^- with H^+ cation to form of ZrO_2-SiO_2-Me&Et-$PhSO_3H$. It was washed several times with

water and dried overnight under vacuum at room temperature. The formed ZrO_2-SiO_2-Me&Et-PhSO$_3$H catalyst for glycerol catalytic esterification reaction.

Catalyst Characterization

N$_2$ physisorption method [BELSORP-max analyser (Japan)] was used to analyse the textural properties of catalysts by degassing the catalyst samples under vacuum condition at 200°C for 5 h. Meanwhile, the particle size distributions of catalysts were measured by dry Malvern MS3000 particle sizer at pressure of 2 bar. The acidity of catalyst (mmol/g) was determined by acid-base titration. Forty–Fifty milligrams of catalyst sample was degassed at 120°C for 3 h and subsequently suspended in 25 ml of NaCl (2 M) and stirred for 24 h at room temperature to achieve equilibrium and then to be titrated with 8.38×10^{-3} M NaOH solution. The fresh and spent catalyst was evaluated by hydrophobicity levels (water contact angle method) using KRUSS DSA100, N$_2$ physisorption, and Field Emission Scanning Electron Microscope (FESEM) at 1–30 kV acceleration voltage by instrument model JSM-7100F.

Catalytic Reaction

The catalytic esterification reaction of glycerol with OA was performed in a 250 ml batch reactor equipped with a temperature indicator and connected to a condenser and a vacuum system at 160°C, equimolar ratio of reactant and constant acidity (1.55 mmol H$^+$) for 8 h. The samples were analyzed using high performance liquid chromatography coupled to refractive index detection (HPLC-RI) through an isocratic method, equipped with Gemini C18 11OA column (100 × 2 mm × 3 μm). The OA and GMO groups of the sample were separated using a mobile phase consisted of ACN/water (80:20 v/v) with 0.1% TFA (v/v of total mobile phase). Meanwhile, GDO and GTO groups were separated using ACN/MeOH/THF (40:40:20 v/v/v) (Lee et al., 2013). The injection volume was 10 μL and the diluted samples were eluted at a 220 μL/min flow rate. The column and RI detector temperatures were set at 40°C. The conversion, yield and selectivity of the products are defined by Equations 1 to 3.

$$\text{Conversion} = \frac{mol_{OA_{consumed}}}{mol_{OA_{initial}}} \times 100\% \quad (1)$$

$$\text{Yield}_{total\ GMO,GDO,GTO} = \frac{mol_{total\ esters}}{mol_{OA_{initial}}} \times 100\% \quad (2)$$

$$\text{Selectivity}_{GMO} = \frac{mol_{GMO}}{mol_{total\ GMO+GDO+GTO}} \times 100\% \quad (3)$$

RESULTS AND DISCUSSION

Process Optimization

The ZrO_2-SiO_2-Me&EtPhSO$_3$H catalyst was used to study the effect of process operating parameters. The influences of reaction temperature, catalyst concentration, glycerol-to-OA molar ratio, and reaction time on the catalytic glycerol esterification with OA were investigated. The mass transfer limitation was evaluated prior to investigating the process variables to ensure that the esterification process was reaction controlled. Mechanism for esterification of glycerol with OA in GMO, GDO, and GTO production is presented in **Scheme 1**.

Effects of Mass Transfer

Mass transfer limitation was assessed at the reaction temperature of 100°C prior to temperature optimisation. The experiments were carried out at an equimolar OA-to-glycerol ratio, 100°C reaction temperature, 480 min and 3 wt% catalyst concentration with respect to the OA weight and solvent-less reaction conditions during mass transfer limitation study. The reaction yield and selectivity catalyzed by ZrO_2-SiO_2-Me&EtPhSO$_3$H catalyst were evaluated in two different stirring speeds (300 and 650 rpm). The high stirring speed 650 rpm resulted in a slightly increased yield (from 35.3 to 37.4%) compared with the 300 rpm reaction speed. The selectivity of GDO and GTO also slightly increased compared with the reaction at 300 rpm, but the difference was insignificant. Therefore, the maximum stirring speed of 650 rpm was proposed for further testing of process variables in the presence of ZrO_2-SiO_2-Me&EtPhSO$_3$H catalyst to eliminate the external mass transfer resistance. It was reported that external mass transfer resistance can be completely eliminated when a high stirring speed is applied, and external diffusion negligibly affects the overall reaction rate (Nanda et al., 2014).

Effects of Reaction Temperature

ZrO_2-SiO_2-Me&EtPhSO$_3$H catalyst was used to study the effects of reaction temperature. Various temperatures (100, 120, 140, and 160°C) were utilized under the stirring speed of 650 rpm, equimolar OA-to-glycerol ratio, 3 wt% catalyst concentration with respect to the OA weight and solvent-less reaction conditions. **Figure 1** presents the effects of reaction temperature on the catalytic esterification of glycerol with OA. Results indicated that the conversion increased with increased reaction temperature because high temperature favors a high equilibrium product yield in a typical endothermic reaction (Trinh et al., 2018). The initial rate of esterification also increased with increased reaction temperature. The reaction temperature of 160°C yielded the highest conversion level (86.7%) in this study. On the contrary, relatively low activities were observed at the beginning of reaction at 100° and 120°C. The activation energy required for successful conversion is difficult to exceed at low temperatures because the energy possessed by the reactant molecules is low; consequently, the effective collision is decreased because the kinetic energy in the reactant molecules and potential energy of molecules are decreased (Hoo and Abdullah, 2014).

The effects of reaction temperature on the selectivity of GMO, GDO, and GTO are shown in **Figure 2**. The GMO selectivity decreased by increasing the reaction temperature but both GDO and GTO selectivities increased. Notably, the selectivity percentage at 140° and 160°C were much alike, particularly at more than 360 min because ~60% of GMO and 36% of GDO were obtained. Therefore, 160°C was suggested as the optimal reaction temperature by considering
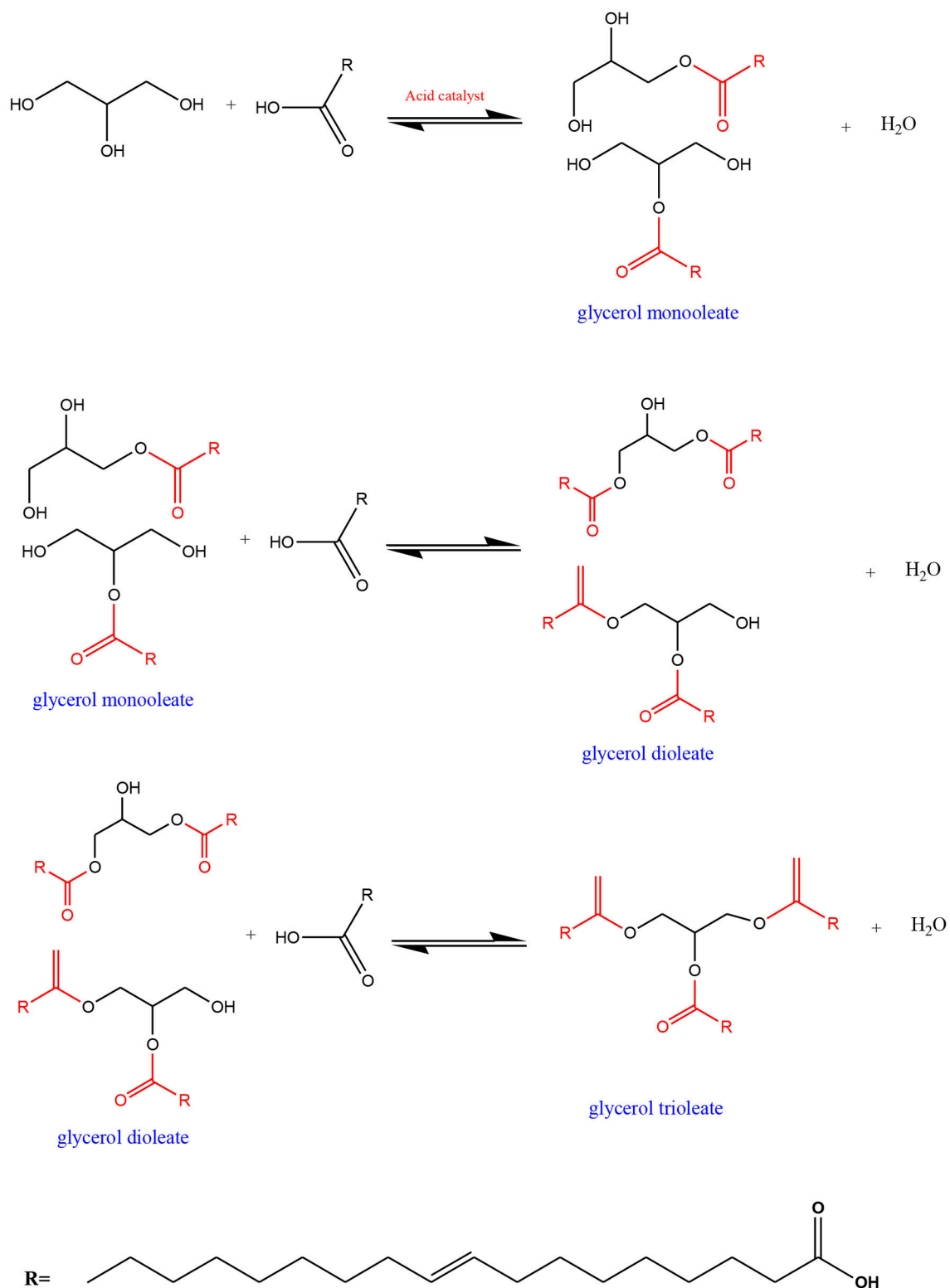
SCHEME 1 | Mechanism for esterification of glycerol with OA in GMO, GDO, and GTO production.

FIGURE 1 | Effects of reaction temperature on the catalytic esterification of glycerol with OA using ZrO_2-SiO_2-Me&EtPhSO$_3$H catalyst.
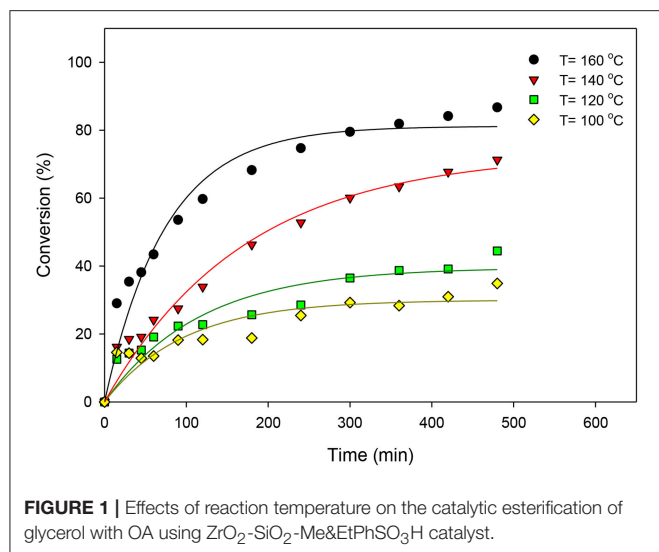
the obtained conversion and selectivity under the ZrO_2-SiO_2-Me&EtPhSO$_3$H-catalyzed esterification reaction of glycerol with OA.

The interaction effects of reaction time and reaction temperature on the conversion and selectivity of GMO. The highest conversion was obtained at 160°C after 480 min reaction time. The selectivity of GMO decreased with time and temperature. The intersection point corresponding to the highest conversion (74%) and GMO selectivity (63.6%) is obtained at 160°C and after 240 min reaction time, at equimolar OA-and-glycerol ratio and 3 wt% catalyst concentration. It is worthy to note that under these conditions the GMO and GDO combined selectivity is 91.6%.

Effects of the Oleic Acid-to-Glycerol Molar Ratio

The effects of excess glycerol on glycerol esterification with OA catalyzed by ZrO_2-SiO_2-Me&EtPhSO$_3$H were investigated at the constant reaction temperature of 160°C, catalyst concentration of 3 wt%, stirring speed of 650 rpm and solvent-less reaction conditions. At 480 min reaction time, the conversion increased slightly with increased glycerol amount in the following descending order: 91.6, 89.0, and 87.5% for 1:3, 1:2, and 1:1 OA-to-glycerol molar ratios, respectively. According to Le Chatelier's principle, the glycerol esterification with OA will shift to improve products formation with increased reactant concentration. The conversion and selectivity of various GMO, GDO, and GTO at 240 min reaction time are presented in **Figure 3** to evaluate the effects of excess glycerol on conversion and selectivity. The conversion of 1:1 OA to glycerol (75%) was nearly close to the 1:2 molar ratio of OA to glycerol (76%). Results revealed that the 1:3 OA-to-glycerol molar ratio produced the highest conversion of about 82% at 240 min reaction time. Similarly, Singh et al. (2013) stated that the significant reaction rate increases when the molar ratio increases from 1:2 (OA:glycerol) and insignificantly changes when excess glycerol is added at 1:6 OA-to-glycerol molar ratio.

The selectivity of GDO and GTO increased with the increased glycerol feeding ratio. Thus, the GMO selectivity was minimized

by increasing the loading amount of glycerol in the catalytic esterification of glycerol with OA. It has been reported that unreacted glycerol removal is necessary despite of an equimolar OA-to-glycerol ratio of reactant was used in reaction (Konwar et al., 2016). Therefore, it can be concluded that equimolar OA-to-glycerol ratio can produce high GMO and GDO yield and equimolar ratio is suggested to obtain maximum GMO and GDO yield.

The GMO, GDO and GTO selectivities at different molar ratios are illustrated in **Figure 4**. The GMO selectivity decreased with increased glycerol ratio; by contrast, increased glycerol concentrations improved GDO and GTO selectivity. Significant GDO and GTO increments were also observed at more than 240 min reaction time. This work revealed that the selectivity profiles for the OA-to-glycerol molar ratios of 1:1 and 1:2 were similar, which demonstrated that no significant effect was observed for excess glycerol amount in the glycerol:OA molar ratio range of 1–2.

Glycerol esterification with OA was conducted with excess OA to compare the different reaction behavior in the OA-to-glycerol molar ratio of 3:1 at 160°C and 3 wt% catalyst concentration of OA for 480 min. **Figure 5** shows the conversion and selectivity obtained at the OA-to-glycerol molar ratio with excess glycerol (1:1, 1:2, and 1:3) and OA (3:1) conditions. This work showed that excess OA caused the high formation of GTO (selectivity = 40%) and GDO (selectivity = 50%) and relatively low GMO yield. This work also confirmed that an equimolar OA-to-glycerol ratio resulted in an optimum yield of GMO, with 93% combined selectivity of GMO and GDO. The interaction effects of glycerol-to-OA molar ratio and reaction time on the conversion and selectivity of GMO are performed. It is clearly indicated that reaction time exerts stronger influence on selectivity and conversion than the molar ratio.

Effects of Catalyst Concentration

ZrO_2-SiO_2-Me&EtPhSO$_3$H catalyst (3, 5, and 8 wt%) was used to investigate the effects of catalyst concentration on the conversion and selectivity of the catalytic glycerol esterification with OA at the constant operation parameters of 160°C, equimolar ratio and 650 rpm. Catalyst loading was calculated with respect to the weight of the limiting reactant OA. **Figure 6** shows the effects of catalyst concentration on the conversion and selectivity at 240 min by using different concentrations of ZrO_2-SiO_2-Me&EtPhSO$_3$H catalyst. Catalyst concentrations 3, 8, and 5 wt% achieved the slowest reaction rate in sequence. At 240 min reaction time, the obtained conversion was 74.7, 80.0, and 78.8% for the catalyst concentrations of 3, 5, and 8 wt%, respectively. These results proved that 5 wt% catalyst concentration was the optimal level for this catalytic study. Increasing the catalyst concentration at more than 5 wt% was not recommended because such increase does not improve the conversion. A similar trend was also reported in a previous work on glycerol esterification with palmitic acid; the conversion is unaffected beyond a certain amount of catalyst loading (Yusoff and Abdullah, 2016).

Notably, the GMO selectivity trend decreased with increased catalyst concentration; the 3 wt%-produced selectivity was 64%, which was higher than that of the 5 wt% ($S_{GMO} = 61\%$) and 8
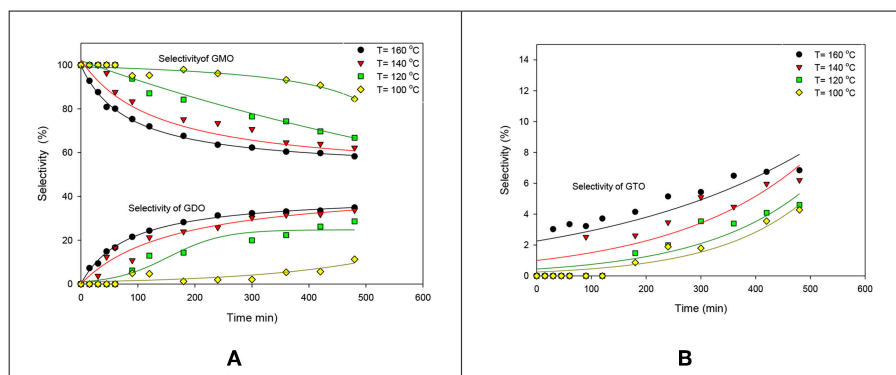
FIGURE 2 | Effects of reaction temperature on the selectivities of GMO, GDO **(A)**, and GTO **(B)**.
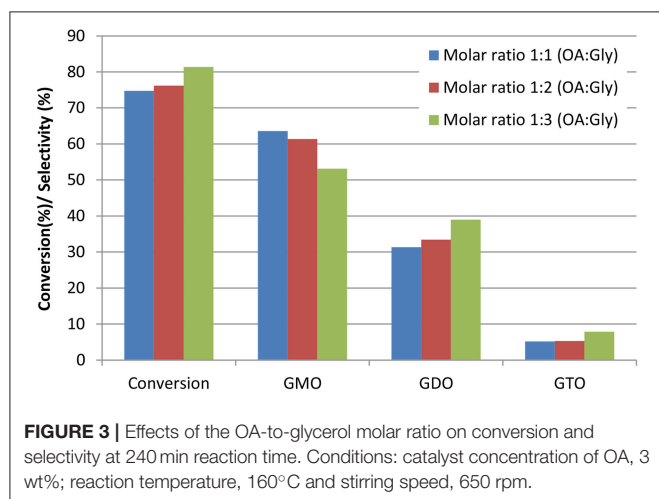
FIGURE 3 | Effects of the OA-to-glycerol molar ratio on conversion and selectivity at 240 min reaction time. Conditions: catalyst concentration of OA, 3 wt%; reaction temperature, 160°C and stirring speed, 650 rpm.

wt% (S_{GMO} = 53%). These findings clearly revealed that GMO was successfully converted to GDO and GTO. The increased effective interaction between the reactant molecules and GTO formation was highly attributed to the increased number of available acidic sites and acidity of the catalyst. At the end of reaction, generally after 420 min, a change in catalyst loading resulted in non-accelerated reaction rate. The conversion was insignificantly influenced with further increase in catalyst loading from 5 to 8 wt% due to the equilibrium limit (Tao et al., 2015).

The influence of catalyst concentration on the formation trend of GMO, GDO, and GTO in terms of selectivity is elaborated in **Figure 7**. The selectivity profile of GMO decreased with increased catalyst concentration. The GMO selectivity curve for the 8 wt% catalyst concentration markedly decreased, particularly from 15 min to 180 min. Moreover, 5 and 8 wt% catalyst concentrations achieved high tendency to form GDO and GTO. However, the formation ratios in terms of selectivity were almost identical. In brief, the conversion acquired from ZrO_2-SiO_2-Me&EtPhSO$_3$H-catalyzed glycerol esterification with OA was 88.2% with 53.5% of GMO and 39.6% of GDO selectivity at 5 wt% catalyst concentration, 160°C, equimolar reactant ratio and 480 min reaction time.

Interaction effects of catalyst concentration and reaction time
The interaction effects of catalyst concentration and reaction time on conversion and selectivity were also investigated. The aforementioned section reported that 3 wt% catalyst concentration, 240 min reaction time and an equimolar ratio of OA and glycerol resulted in 74% conversion and 63.6% of GMO selectivity (about 95% of combined selectivity of GMO and GDO).

The interaction plot in **Figure 8** indicates that a short reaction time (180 min), 5 wt% catalyst concentration and an equimolar ratio of reactants allowed to achieve a conversion of 74 and 62.5% selectivity of GMO (~95.8% combined selectivity of GMO and GDO). Additionally, extending the reaction time to 240 min under the same reaction parameters (5 wt% catalyst concentration, equimolar ratio of OA to glycerol and 650 rpm) led to a conversion of 80% and about 60% selectivity of GMO, with a low combined GMO and GDO selectivity (94.8%). Consequently, 240 min reaction time was suggested for the catalytic esterification of glycerol with OA in the presence of 5 wt% of ZrO_2-SiO_2-Me&EtPhSO$_3$H catalyst with the use of equimolar reactants.

Interaction effects of catalyst concentration and reaction temperature
The interaction effects of catalyst concentration and reaction temperature were studied comprehensively at 240 and 480 min in **Figures 9A,B**, respectively. These two response surface diagrams display a similar relation curve but different intersection points shown between the conversion and selectivity of GMO. At 240 and 480 min, the conversion can be increased in two ways: increasing the reaction temperature and the catalyst concentration. The effect of catalyst concentration was much significant at a short reaction time of 240 min.

An increased GMO selectivity can be obtained at a low reaction temperature and a high catalyst concentration. At 240 min, the GMO selectivity was highly dependent on the reaction temperature (an inclined curve was obtained). By contrast, the GMO selectivity was less dependent on the reaction temperature at a long reaction time. **Figure 9B** shows that at a low range of reaction temperature (100°-125°C).
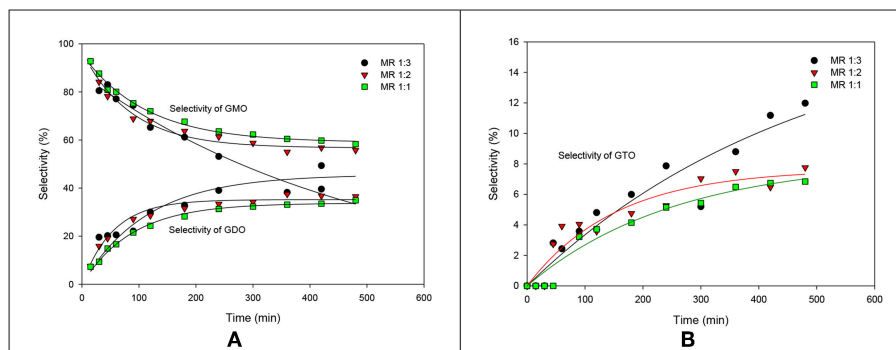
FIGURE 4 | Effects of OA-to-glycerol molar ratios on the selectivities of GMO, GDO **(A)**, and GTO **(B)**.
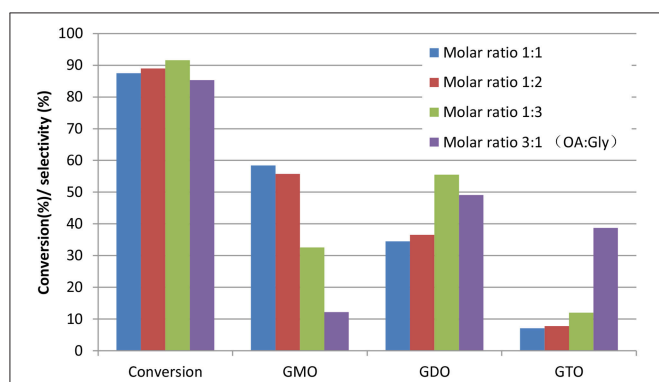
FIGURE 5 | Effects of OA-to-glycerol molar ratios at 480 min reaction time. Conditions: catalyst concentration of OA, 3 wt%; reaction temperature, 160°C and speed, 650 rpm.
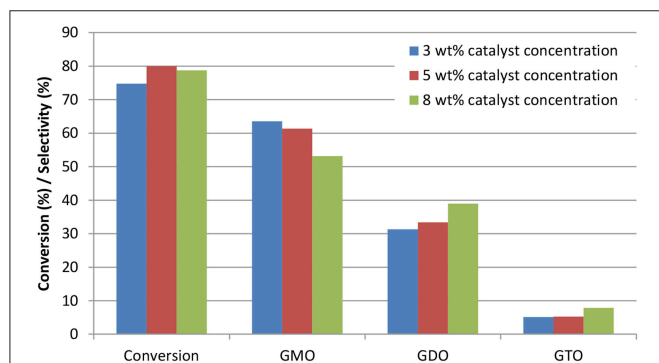
FIGURE 6 | Effects of catalyst concentration on the conversion and selectivity at 240 min reaction time. Conditions: equimolar glycerol-to-OA ratio; reaction temperature, 160°C and speed, 650 rpm.

The GMO selectivity was high when a high loading catalyst amount was used. In conclusion, a high conversion (more than 80%) and selectivity of GMO (about 60%) can be achieved at 480 min reaction time, equimolar reactant ratio, 160°C and 650 rpm.

Catalyst Characterizations

The Barrett-Joyner-Halenda (BJH) plots and N_2 adsorption–desorption isotherms for the fresh and spent catalysts of ZrO_2-SiO_2-Me&EtPhSO$_3$H are shown in **Figure 10**. The pore size distribution was unevenly distributed at the low surface area of the spent catalyst, which was most probably due to the existence of less-ordered structures of silica (Estevez et al., 2016) and the adherence of triglycerides/compounds within the pore of the spent samples (refer to FESEM image of spent catalyst, **Figure 11**). The contact angle analysis result of the spent catalyst was inferior (31.9°) to that of the newly developed catalyst with 41.5°.

Commercial Amberlyst 15 and Aquivion Characterisations and Performance Evaluations

A comparative study between ZrO_2-SiO_2-Me&Et-PhSO$_3$H and the commercially available Amberlyst 15 and polymeric perfluorosulfonic acid (PFSA) Aquivion was performed under optimized operating reaction conditions in the glycerol esterification with OA. Aquivion PFSA is a copolymer based on tetrafluoroethylene and the sulfonyl fluoride vinyl ether catalyst from Solvay Specialty Polymers. Aquivion is a perfluorosulfonic superacid resin with a relatively high acid strength, high thermal stability and ∼−12 Hammett acidity (comparable to the acid strength of H_2SO_4) (Fang et al., 2016). Amberlyst 15 is a conventional macroporous sulphonic ion exchange resin with 120°C thermal stability (Kong et al., 2015). The catalyst characteristics are summarized in **Table S1**. Although the ion exchange capacity of Aquivion PFSA (1.0 mequiv/g) used in this study is lower than that of Amberlyst 15 (4.7 mequiv/g), the Hammett acidity function of Amberlyst 15 ($H_0 = -2$) is considerably lower than that of the superacid Aquivion ($H_0 = -12$) (Karam et al., 2016). Thus, the influences of the different acidity strengths of catalysts were observed in the present work.

The surface area, pore volume, particle size distribution, and acidity strength of these three catalysts differed. The distribution phenomenon of each catalyst was also examined in a polar and non-polar solvent (within a layer of immiscible toluene–water phase), and result is demonstrated in **Figure S1**. Aquivion were located on the interface between toluene and water. Nevertheless,
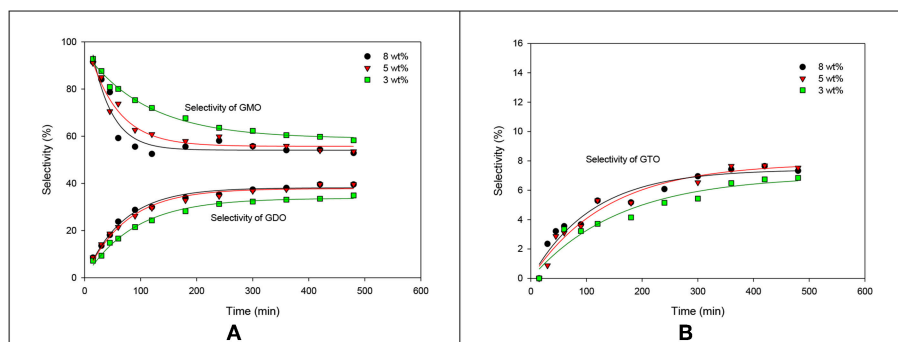
FIGURE 7 | Effects of the catalyst concentration of ZrO_2-SiO_2-Me&EtPhSO$_3$H on the selectivities of GMO, GDO **(A)**, and GTO **(B)**.

Aquivion exhibited an amphiphilic property because it was only located on the interface between toluene and water, unlike the Me&Et-PhSO$_3$H-SiO$_2$-ZrO$_2$, which was distributed in the toluene phase. By contrast, Amberlyst 15 was immersed in the bottom-water phase.

Three sets of experiments were performed under optimized conditions in glycerol esterification with OA in the presence of different catalysts, namely, ZrO$_2$-SiO$_2$-Me&EtPhSO$_3$H, Amberlyst 15 and Aquivion. Aquivion afforded the highest conversion, which was nearly 99% in 240 min reaction time (**Figure 12A**). Approximately 98% conversion was obtained within 120 min reaction time. The formation rates of GDO and GTO were the fastest for Aquivion (S_{GDO} = 69% and S_{GTO} = 30%), although an equimolar ratio of reactants was used. This result was attributed to the strong acidity of Aquivion. A relatively low selectivity of GMO was obtained for Aquivion-catalyzed reaction ($<$ 3%). This finding suggested that the superstrong acidity of Aquivion is suitable in producing large GTO molecules at the OA-to-glycerol molar ratio of 3:1. Further lowering the loading amount of Aquivion (optimisation of catalyst concentration) is necessary to attain high yield and selectivity of GMO. Superstrong acid potentially produces undesirable side reaction products, ~50% by-product was attained in this experiment; the possible by-products would be glycerol oligomers, polyglycerol, alkenes, acrolein, or polyglycerol esters. A long reaction time is unadvisable for Aquivion-catalyzed reaction because the yield and GTO selectivity were reduced (**Figure 12B**).

Results showed that Amberlyst 15 obtained a higher yield and selectivity for GDO and GTO (S_{GDO} = 65% and S_{GTO} = 12%) than those of the two other catalysts; this result can be attributed to the lower acidity strength of Amberlyst 15 (H_0 = -2) than that of Aquivion (H_0 = -12) and its larger pore size (28.8 nm) than that of ZrO$_2$-SiO$_2$-Me&EtPhSO$_3$H (3.77 nm). The undesirable by-product catalyzed by Amberlyst 15 is lesser (20%) than that of attained by Aquivion under identical reaction parameters. Prolonging the reaction time of Amberlyst 15–8 h increased the GDO and GTO selectivities (S_{GDO} = 74% and S_{GTO} = 16%). The water as a by-product from esterification reaction was reported can deactivate
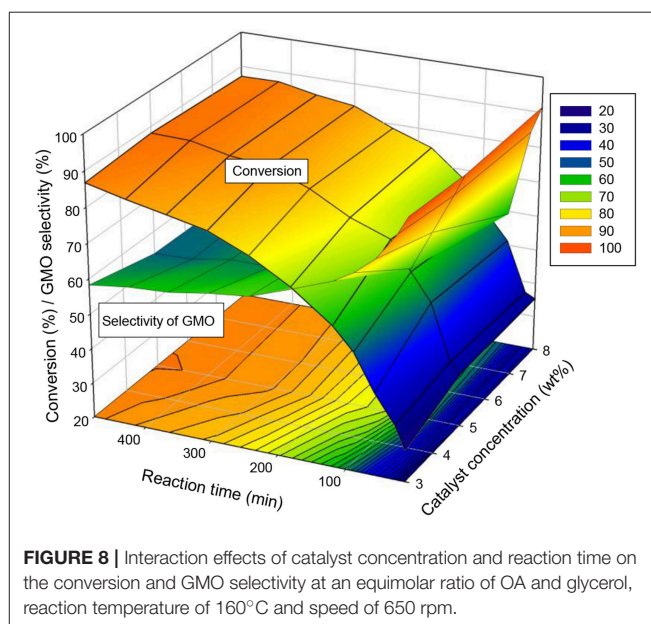
FIGURE 8 | Interaction effects of catalyst concentration and reaction time on the conversion and GMO selectivity at an equimolar ratio of OA and glycerol, reaction temperature of 160°C and speed of 650 rpm.

sulphonation exchanger of Amberlyst 15 by adsorbing water in its pores. It was reported addition higher amount of water in reaction resulted in slightly lower yield from 95 to 85% in synthesis of glucose esters using Amberlyst 15 (Ignatyev Igor et al., 2012).

Whereas, ZrO$_2$-SiO$_2$-Me&EtPhSO$_3$H obtained the highest yield and GMO selectivity (60%), which proved that catalyst acidity is vital in controlling the conversion rate and yield. Firstly, a moderate acidity level of catalyst or suitable loading amount of catalyst is required to produce a high-yield product, and excess acidity may lead to side reaction. Secondly, textural properties, such as pore size/pore volume, influence the selectivity of a product significantly by controlling the pore size of catalyst to form the desired selectivity product. Catalyst recyclability and stability experiment of ZrO$_2$-SiO$_2$-Me&EtPhSO$_3$H revealed that the yield decreased with the number of uses. The yield was reduced from 83, 74, and 69% in accordance with the number of times of usage. Herein, yield refers to the total GMO, GDO,
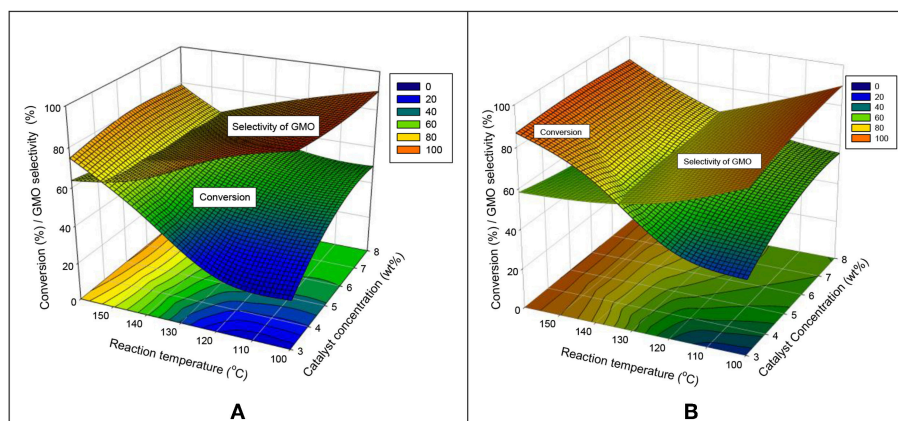
FIGURE 9 | Interaction effects of catalyst concentration and reaction temperature on the conversion and GMO selectivity at **(A)** 240 and **(B)** 480 min reaction time, equimolar ratio of OA and glycerol, reaction temperature of 160°C and speed of 650 rpm.
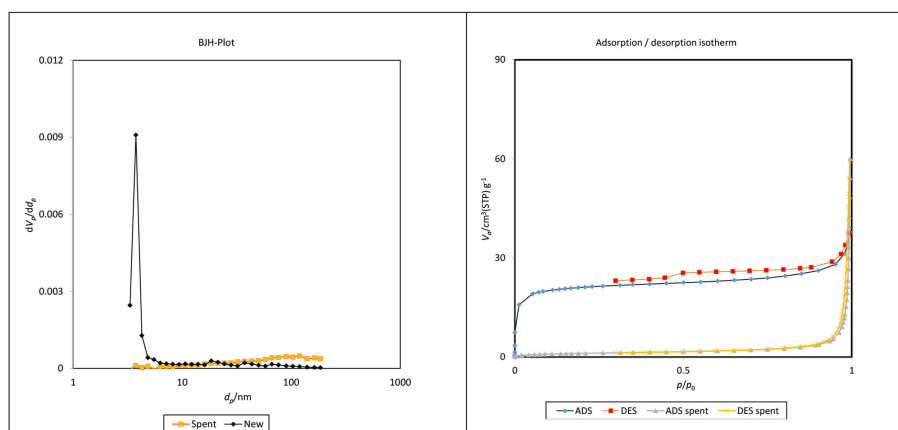

FIGURE 10 | BJH plot and N_2 adsorption–desorption isotherms of new and spent ZrO_2-SiO_2-Me&EtPhSO$_3$H catalyst.
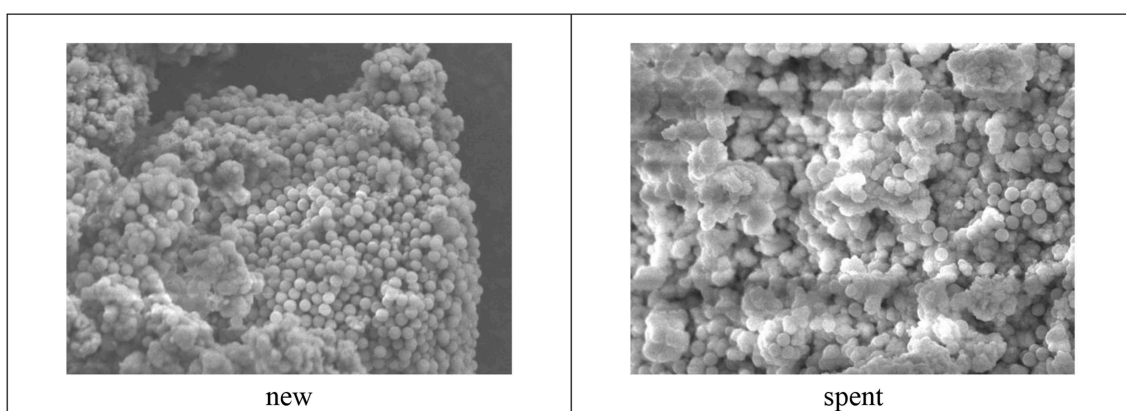
FIGURE 11 | FESEM images of new and spent ZrO_2-SiO_2-Me&EtPhSO$_3$H catalyst.

FIGURE 12 | Comparison of the catalytic activities of ZrO_2-SiO_2-Me&EtPhSO$_3$H, Amberlyst 15 and Aquivion catalysts. All reactions were conducted at the constant acidity of 1.55 mmol H$^+$, equimolar ratio of OA and glycerol, reaction temperature of 160°C and stirring speed of 650 rpm for 240 min **(A)** and 480 min **(B)**.
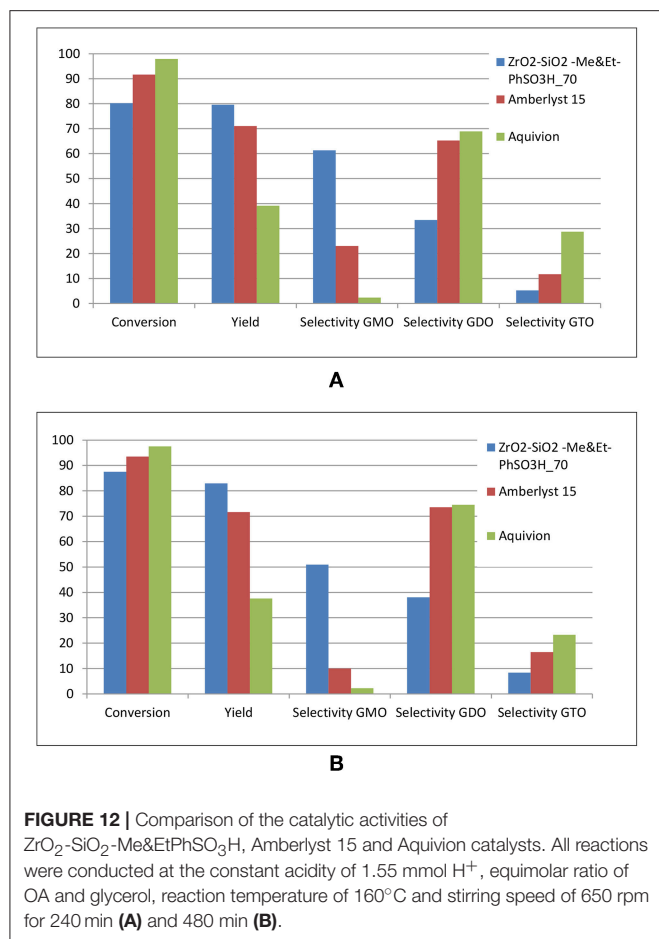
and GTO in product mixtures, respectively. This trend may be attributed to that the GTO product blocks the active centers of the catalyst or the hydrophobic properties are lost (Zhang et al., 2017). The chromatogram peaks for products are provided in supplementary material (**Figures S2, S3**).

CONCLUSIONS

In this work the esterification of oleic acid with glycerol was conducted on ZrO_2-SiO_2-Me&Et-PhSO$_3$H catalyst. The reaction achieved 80% conversion with GMO and GDO being the major products having a combined selectivity of 94.8% (GMO = 59.4% and GDO = 34.6 %) at equimolar ratio of OA-to-glycerol, 160°C reaction temperature, 5 wt% catalyst concentration with respect to OA and for a reaction time of 4 h. After prolonging the reaction time to 8 h under the same operating parameters, 88.2% conversion with 53.5% GMO selectivity and 40.0% GDO selectivity (combined GMO and GDO selectivity = 94%) were obtained. It is found that increasing the reaction temperature

accelerates the conversion rate but decreases the selectivity of GMO. The equimolar ratio of OA to glycerol was suggested to increase the selectivities of GMO and GDO. This work also confirmed that 5 wt% ZrO_2-SiO_2-Me&Et-PhSO$_3$H catalyst concentration is the optimal level for the catalytic study of glycerol with OA. Moreover, the GMO selectivity decreased with the increased catalyst concentration. This effect was highly attributed to the increased number of available acidic sites of the catalyst.

Therefore, a strongly acidic catalyst promoted the formation of a low-GMO-selectivity product mixture. Comparison of the performance of ZrO_2-SiO_2-Me&Et-PhSO$_3$H and commercially available Amberlyst 15 and Aquivion showed that catalyst acidity is a key parameter for catalytic activity and conversion rate. Nevertheless, high acidity/acid strength reduced the product yield in the glycerol esterification of OA. The mild acidity of ZrO_2-SiO_2-Me&Et-PhSO$_3$H with a hydrophobic surface was recommended for the catalytic esterification of glycerol with OA at equimolar ratio of reactants to attain a high selectivity of GMO. Superacid Aquivion was recommended to produce GTO at an OA-to-glycerol moral ratio of 3:1. This study proved that the textural properties (pore volume and pore size); acidity and hydrophobicity of heterogeneous acid catalysts play vital roles in controlling the activity and selectivity of reactions. Therefore, the acid strength and the number of available acid sites influence the conversion rate of reaction, and the hydrophobicity and pore volume of solid catalysts significantly affect the selectivity of the product.

AUTHOR CONTRIBUTIONS

PSK and YP contributed to the conception and design of the study, organized the database and performed the statistical analysis. PSK wrote the first draft of the manuscript. YP, PC, WMAWD, and MKA contributed to the manuscript revision, read and approved the submitted version.

ACKNOWLEDGMENTS

SUPPLEMENTARY MATERIAL

The Supplementary Material for this article can be found online at: https://www.frontiersin.org/articles/10.3389/fchem. 2019.00205/full#supplementary-material

REFERENCES

Åkerman, C. O., Gaber, Y., Ghani, N. A., Lämsä, M., and Hatti-Kaul, R. (2011). Clean synthesis of biolubricants for low temperature applications using heterogeneous catalysts. *J. Mol. Catal. B* 72, 263–269. doi: 10.1016/j.molcatb.2011.06.014

Barauskas, J., Misiunas, A., Gunnarsson, T., Tiberg, F., and Johnsson, M. (2006). "Sponge" Nanoparticle dispersions in aqueous mixtures of diglycerol

monooleate, glycerol dioleate, and polysorbate 80. *Langmuir.* 22, 6328–6334. doi: 10.1021/la060295f

Estevez, R., López, M. I., Jiménez-Sanchidrián, C., Luna, D., Romero-Salguero, F. J., and Bautista, F. M. (2016). Etherification of glycerol with tert-butyl alcohol over sulfonated hybrid silicas. *Appl. Catal. A* 526, 155–163. doi: 10.1016/j.apcata.2016.08.019

Fang, W., Fan, Z., Shi, H., Wang, S., Shen, W., Xu, H., et al. (2016). Aquivion[registered sign]-carbon composites via hydrothermal carbonization: amphiphilic catalysts for solvent-free biphasic acetalization. *J. Mater. Chem. A* 4, 4380–4385. doi: 10.1039/C5TA09705C

Frost and Sullivan Research Service (2014). *World Fatty Esters Markets (Technical Insights).*

Hamerski, F., and Corazza, M. L. (2014). LDH-catalyzed esterification of lauric acid with glycerol in solvent-free system. *Appl. Catal. A* 475, 242–248. doi: 10.1016/j.apcata.2014.01.040

Hamerski, F., Prado, M. A., da Silva, V. R., Voll, F. A. P., and Corazza, M. L. (2016). Kinetics of layered double hydroxide catalyzed esterification of fatty acids with glycerol. *React. Kinet. Mech. Catal.* 117, 253–268. doi: 10.1007/s11144-015-0942-0

Hoo, P.-Y., and Abdullah, A. Z. (2014). Direct synthesis of mesoporous 12-tungstophosphoric acid SBA-15 catalyst for selective esterification of glycerol and lauric acid to monolaurate. *Chem. Eng. J.* 250, 274–287. doi: 10.1016/j.cej.2014.04.016

Ignatyev Igor, A., Doorslaer Charlie, V., Mertens Pascal, G. N., Binnemans, K., and de Vos Dirk, E. (2012). Synthesis of glucose esters from cellulose in ionic liquids. *Holzforschung* 66:417. doi: 10.1515/hf.2011.161

Karam, A., De Oliveira Vigier, K., Marinkovic, S., Estrine, B., Oldani, C., and Jérôme, F. (2017). High catalytic performance of aquivion PFSA, a reusable solid perfluorosulfonic acid polymer, in the biphasic glycosylation of glucose with fatty alcohols. *ACS Catal.* 7, 2990–2997. doi: 10.1021/acscatal.6b03561

Karam, A., Sayoud, N., De Oliveira Vigier, K., Lai, J., Liebens, A., Oldani, C., et al. (2016). Heterogeneously-acid catalyzed oligomerization of glycerol over recyclable superacid Aquivion® PFSA. *J. Mol. Catal. A* 422, 84–88. doi: 10.1016/j.molcata.2016.03.001

Kong, P. S., Aroua, M. K., and Daud, W. M. A. W. (2015). Catalytic esterification of bioglycerol to value-added products. *Rev. Chem. Eng.* 31, 437–451. doi: 10.1515/revce-2015-0004

Kong, P. S., Aroua, M. K., and Daud, W. M. A. W. (2016a). Conversion of crude and pure glycerol into derivatives: a feasibility evaluation. *Renew. Sust. Energ. Rev.* 63, 533–555. doi: 10.1016/j.rser.2016.05.054

Kong, P. S., Aroua, M. K., Daud, W. M. A. W., Lee, H. V., Cognet, P., and Peres, Y. (2016b). Catalytic role of solid acid catalysts in glycerol acetylation for the production of bio-additives: a review. *RSC Adv.* 6, 68885–68905. doi: 10.1039/C6RA10686B

Kong, P. S., Cognet, P., Pérès, Y., Esvan, J., Daud, W. M. A. W., and Aroua, M. K. (2018). Development of a novel hydrophobic ZrO2–SiO2 based acid catalyst for catalytic esterification of glycerol with oleic acid. *Ind. Eng. Chem. Res.* 57, 9386–9399. doi: 10.1021/acs.iecr.8b01609

Konwar, L. J., Mäki-Arvela, P., Kumar, N., Mikkola, J.-P., Sarma, A. K., and Deka, D. (2016). Selective esterification of fatty acids with glycerol to monoglycerides over –SO3H functionalized carbon catalysts. *React. Kinet. Mech. Catal.* 119, 121–138. doi: 10.1007/s11144-016-1040-7

Kotwal, M., Deshpande, S. S., and Srinivas, D. (2011). Esterification of fatty acids with glycerol over Fe–Zn double-metal cyanide catalyst. *Catal. Commun.* 12, 1302–1306. doi: 10.1016/j.catcom.2011.05.008

Kulkarni, C. V., Wachter, W., Iglesias-Salto, G., Engelskirchen, S., and Ahualli, S. (2011). Monoolein: a magic lipid? *Phys. Chem. Chem. Phys.* 13, 3004–3021. doi: 10.1039/c0cp01539c

Lee, K. W., Porter, C. J., and Boyd, B. J. (2013). A simple quantitative approach for the determination of long and medium chain lipids in bio-relevant matrices by high performance liquid chromatography with refractive index detection. *AAPS PharmSciTech* 14, 927–934. doi: 10.1208/s12249-013-9976-7

Macierzanka, A., and Szelag, H. (2004). Esterification kinetics of glycerol with fatty acids in the presence of zinc carboxylates: preparation of modified acylglycerol emulsifiers. *Ind. Eng. Chem. Res.* 43, 7744–7753. doi: 10.1021/ie040077m

Mobaraki, A., Movassagh, B., and Karimi, B. (2014). Hydrophobicity-enhanced magnetic solid sulfonic acid: a simple approach to improve the mass transfer of reaction partners on the surface of the heterogeneous catalyst in water-generating reactions. *Appl. Catal. A* 472, 123–133. doi: 10.1016/j.apcata.2013.12.018

Nanda, M. R., Yuan, Z., Qin, W., Ghaziaskar, H. S., Poirier, M.-A., and Xu, C. C. (2014). Thermodynamic and kinetic studies of a catalytic process to convert glycerol into solketal as an oxygenated fuel additive. *Fuel* 117, 470–477. doi: 10.1016/j.fuel.2013.09.066

Quispe, C. A. G., C., and Coronado, J. R., Carvalho J. A. Jr. (2013). Glycerol: production, consumption, prices, characterization and new trends in combustion. *Renew. Sust. Energ. Rev.* 27, 475–493. doi: 10.1016/j.rser.2013.06.017

Singh, D., Patidar, P., Ganesh, A., and Mahajani, S. (2013). Esterification of oleic acid with glycerol in the presence of supported zinc oxide as catalyst. *Ind. Eng. Chem. Res.* 52, 14776–14786. doi: 10.1021/ie401636v

Tao, M.-L., Guan, H.-Y., Wang, X.-H., Liu, Y.-C., and Louh, R.-F. (2015). Fabrication of sulfonated carbon catalyst from biomass waste and its use for glycerol esterification. *Fuel Process. Technol.* 138, 355–360. doi: 10.1016/j.fuproc.2015.06.021

Thengumpillil, N. B. K., Penumarthy, V., and Ayyagari, A. L. (2002). *Process for the Preparation of a Monoglyceride,* Patents, U. S.

Trinh, H., Yusup, S., and Uemura, Y. (2018). Optimization and kinetic study of ultrasonic assisted esterification process from rubber seed oil. *Bioresour. Technol.* 247, 51–57. doi: 10.1016/j.biortech.2017.09.075

Wee, L. H., Lescouet, T., Fritsch, J., Bonino, F., Rose, M., Sui, Z., et al. (2013). Synthesis of monoglycerides by esterification of oleic acid with glycerol in heterogeneous catalytic process using tin–organic framework catalyst. *Catal. Lett.* 143, 356–363. doi: 10.1007/s10562-013-0970-1

Yusoff, M. H. M., and Abdullah, A. Z. (2016). Catalytic behavior of sulfated zirconia supported on SBA-15 as catalyst in selective glycerol esterification with palmitic acid to monopalmitin. *J. Taiwan Inst. Chem. Eng.* 60, 199–204. doi: 10.1016/j.jtice.2015.11.018

Zhang, Z., Huang, H., Ma, X., Li, G., Wang, Y., Sun, G., et al. (2017). Production of diacylglycerols by esterification of oleic acid with glycerol catalyzed by diatomite loaded SO42–/TiO2. *J. Ind. Eng. Chem.* 53, 307–316. doi: 10.1016/j.jiec.2017.05.001

Check for updates

Peculiarities of Glycerol Conversion to Chemicals Over Zeolite-Based Catalysts

Oki Muraza*

Center of Research Excellence in Nanotechnology and Chemical Engineering Department, King Fahd University of Petroleum and Minerals, Dhahran, Saudi Arabia

Many countries have opted to produce biodiesel from vegetable oils for energy security and climate change concerns. Consequently, the availability of abundant glycerol, as a by-product in biodiesel production, is more obvious. Many institutions and companies have explored different routes to convert glycerol to highly-added chemical products and fuel additives. As the addition of the second reactant to glycerol may end up with worse exergy calculation, the conversion of glycerol over solid acid catalysts without the addition of the second reactant is preferred in this mini-review. Glycerol aromatization and glycerol dehydration over zeolite catalysts were focused with an emphasis on recent papers in the past 3 years. The role of acidity, hydrophilicity-hydrophobicity, zeolite frameworks are highlighted. The presence of water in the glycerol feed affected the stability of the catalysts. Low cost and naturally abundant zeolite and minerals are proposed. Numerous low-cost catalysts such as natural zeolites and natural clays are potentially used for this purpose.

Keywords: Glycerol, biodiesel, aromatics, fuels, solid acid catalysts, hierarchical zeolites

INTRODUCTION

Sustainability is one of the most important issues this century. Sustainable production of fuels and chemicals are among the most studied topics in heterogeneous catalysis. Diesel is an important fuel for transportation and industry. According to ExxonMobil Outlook for Energy in 2017 (Exxonmobil, 2017), the demand for diesel will grow to 30% due to the surge in diesel demand for trucks and ships.

The worldwide production of biodiesel is continuously increasing due to the growth and demand for transportation fuels and industry. In 2017, more than 30 billion liters of biodiesel (FAME) were produced. Correspondingly, ∼6 billion liters of glycerol was produced (**Table 1**). Recently, many countries released higher blend mandates (Ren21, 2018). For instance, Indonesia recently released regulation for B20 (Biodiesel 20%). Thailand is targeting to use 9 million liters of biodiesel by 2020. This trend in biodiesel certainly will increase the production of glycerol, as a by-product in biodiesel plant. Glycerol (also known as glycerin, propane-1,2,3-triol, $C_3H_8O_3$) is produced with a ratio of 1:1 with the biodiesel main product (**Figure 1**). The worldwide production of glycerol increased five-fold from 2006 to 2018 to reach 36 billion liters (Quispe et al., 2013; Monteiro et al., 2018). The abundance of glycerol as renewable chemicals should be monetized to improve the economic feasibility of biodiesel industry. Different pathways to convert glycerol to chemicals and fuels depend on the progress of low-cost and affordable catalysts (Atabani et al., 2012; Zakaria et al., 2012; Bagheri et al., 2015; Galadima and Muraza, 2016a,b; Monteiro et al., 2018).

TABLE 1 | Worldwide production of biodiesel and glycerol in 2017 (Ren21, 2018).

Country	Biodiesel (FAME)	Glycerol	HVO/Green Diesel	Blend mandate
Unit	[billion liters]	[billion liters]	[billion liters]	% Biodiesel
USA	6.0	1.2	1.7	2 to 20
Brazil	4.3	0.86		8
Germany	3.5	0.7		
Argentina	3.3	0.66		10
China	1.0	0.2		
France	2.3	0.46		
Thailand	1.4	0.28		7 (9 million L by 2020)
Indonesia	2.5	0.5		20
Canada	0.5	0.1		2 to 4
the Netherlands	0.4	0.08	1.3	
Spain	1.3	0.26		11.3 (2020)
Poland	1.0	0.2		
Singapore		0	1.3	
India	0.2	0.04		15
Colombia	0.6	0.12		10
EU-28	11.8	2.36	3.5	
World	30.7	6.14	6.5	

Density of glycerol at 20°C is 1.26 kg/l, while the density of biodiesel is ∼ 0.99 kg/l. HVO is the abbreviation for hydrogenated vegetable oil.

This mini-review paper aims to emphasize the potential exploration of zeolites for glycerol conversion to two promising commercial products: acrolein and aromatics with an emphasis on recent open literature after 2010. Many cited works are recent papers in the past 3 years from the 2016 to 2018 period.

The conversions of glycerol to fuels and value-added chemicals have been explored via different schemes such as acetalization, acetylation, dehydration, oxidation, and many others. The schemes can be classified into two main trends: (i) with co-reactant and (ii) without co-reactant. Different chemicals have been targeted from glycerol, among others; aromatics, acrolein, acetal, and glycerol carbonate were studied extensively over porous solid acid catalysts (Galadima and Muraza, 2016a,b; Mahdi et al., 2016) (see **Figure 2**). **Table 2** presents the highlight of different conversion pathways from glycerol to chemicals over zeolite catalysts studied by different research groups recently. The explored co-reactants were acetone, n-butanal, benzyl alcohol, acetic acid, acetic anhydride, isobutylene, ketones, formaldehyde, acetaldehyde, benzaldehyde, and many others (Cornejo et al., 2017).

The valorization of glycerol to value-added products by addition of co-reactant have been explored with ketones, aldehydes, or alcohols as co-reactants (Cornejo et al., 2017). Most of the cases, the higher the concentrations of co-reactants, the higher yield of the products in glycerol valorization (Marimuthu et al., 2018; Chen et al., 2019). Unfortunately, the higher ratio on co-reactant to glycerol, the higher the exergy destruction rate (Gutiérrez Ortiz et al., 2012a,b; Hajjaji et al., 2014; Antonova

et al., 2015; Aghbashlo et al., 2018a,b, 2019; Gholami et al., 2018; Presciutti et al., 2018).

Without the addition of co-reactant, acrolein and aromatics are among the most studied chemical products over zeolite catalysts (Galadima and Muraza, 2016a,b). Numerous catalytic materials were evaluated for glycerol to acrolein such as oxides, heteropoly acids, zeolites, and silicoaluminates (Galadima and Muraza, 2016a). There are many reviews on the conversions of glycerol to acrolein and aromatics. This paper focused only on zeolite catalysts for dehydration and aromatization.

GLYCEROL-TO-AROMATICS OVER ZEOLITE CATALYSTS

Most of research groups reported that Brønsted acidity played important roles for the conversion of glycerol to aromatics over zeolite catalysts. **Table 3** summarizes the conversion of glycerol to aromatics reported recently. Zeolites with MFI framework are the most studied material for the conversion of glycerol and methanol to aromatics. Yang and coworkers incorporated tin (Sn) into the framework of MFI with Si/Al_2 of 200 (Yang et al., 2018). The Si/Al ratio plays critical role to tune the yield of aromatics (BTX). Higher Al content (low Si/Al) led to higher yield of aromatics (He et al., 2018). The addition of bentonite as a matrix increased the selectivity to benzene. However, coke deposition was significant and reduced the Brønsted acidity. The coke was removed in regeneration step at 600°C. During regeneration, some of the bentonite structures collapsed and the acid strength was reduced.

The effect of metal (M) modified zeolite, especially M-ZSM-5 was reported recently (Xiao and Varma, 2016). Without palladium (Pd), the main product was acrolein (54%) with 11% of aromatics. The Pd was responsible for hydrodeoxygenation (HDO) while H-ZSM-5 was in charge for aromatization. Pd was obviously more active than platinum (Pt) in hydrogenation. The metal improved the scission of C-O bond. The temperature was crucial to increase the conversion of glycerol. The optimum temperature was found to be ca. 400°C. The pressure has a negligible effect on the conversion of glycerol to aromatics.

Hierarchical ZSM-5 (MFI), fabricated by nitric acid dealumination and steam-treatment at 500°C, exhibited stable conversion of glycerol (ca.98%) to aromatics (ca. 32% - C-based BTX) (Wang et al., 2019). The strong acidity on the surface of ZSM-5 affected the stability negatively, the catalyst life-time for conventional H-ZSM-5 (Si/Al = 25) was very short. Strong acidity favored the formation of hydrocarbon pool species such as polymethylbenzenes inside the MFI intersection and resulted in more coke deposition. The H-ZSM-5 contains sinusoidal channels (0.51 × 0.5 nm), which are crossed with straight channels (0.53 x 0.56 nm) with intersection channel of 0.9 nm size (Corma et al., 2008; Lauriol-Garbay et al., 2011). The conversion of glycerol to aromatics was increased by the addition of appropriate amount of water to the system at
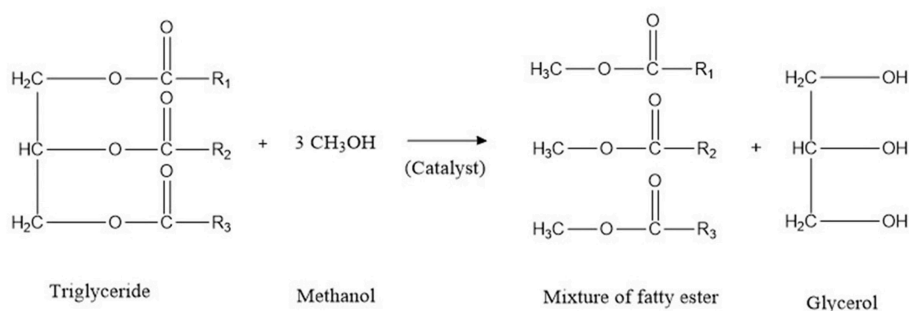
FIGURE 1 | Biodiesel (FAMA) and glycerol from triglyceride of vegetable oil. TRL = technology readiness level.
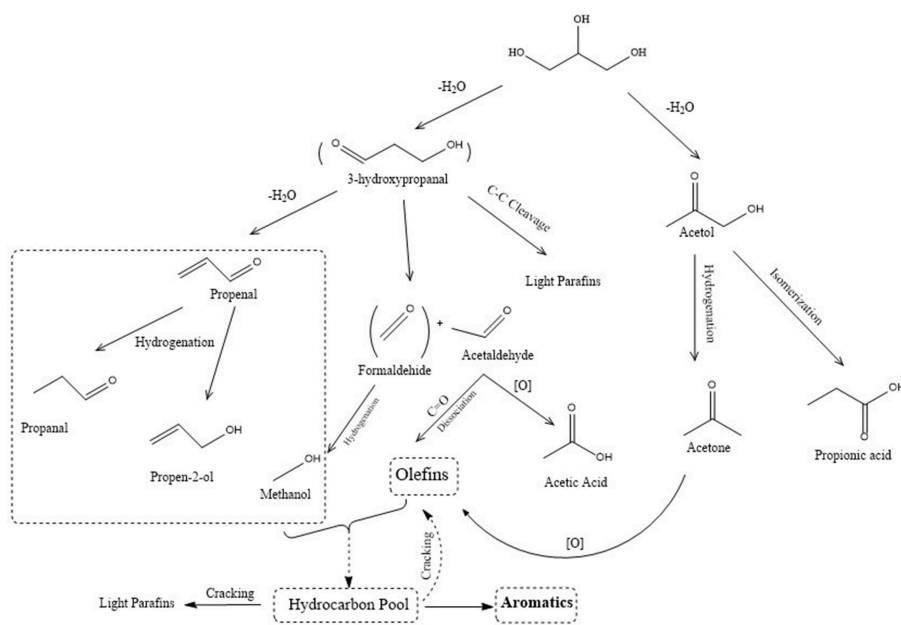
FIGURE 2 | Scheme of glycerol to acrolein and aromatics (Tamiyakul et al., 2015).

440°C under atmospheric pressure as reported by Jang and coworkers in 2014 (Jang et al., 2014). The maximum aromatic products were obtained approximately with 25 wt.% of glycerol in glycerol-water mixture. Mesoporosity has an important role to control the selectivity to aromatics (Wang et al., 2017). Hierarchical ZSM-5, fabricated by desilication with initial Si/Al of 25 has higher Brønsted acidity than its parent. The increase of Brønsted acidity favored higher selectivity to aromatics (benzene-toluene-xylene) with suppressed production of heavier aromatics. Pore topology was also crucial to adjust the selectivity to aromatics. The large pore FAU zeolite (with pore size of

0.74 nm) was less selective to aromatics, as compared to MFI (with pore size of approximately 0.55 nm (Hoang et al., 2010).

GLYCEROL-TO-ACROLEIN OVER ZEOLITES

The catalytic activity of zeolites in glycerol to acrolein was determined by some strong factors: (i) shape selectivity of medium pore zeolites, (easy access of active sites in hierarchical zeolites (i) the number of acid sites, (ii) the presence of

Conversion	Catalyst	Results	References
Glycerol conversion to aromatics via pyrolysis followed by aromatization	ZSM-5 (MFI) with SiO_2/Al_2O_3 of 23. The matrix of bentonite was varied from 10, 20 and 40 wt.%.	Crude glycerol with 2.4 wt.% of H_2O and 44.5 wt.% of free fatty acids was used as a feedstock. The pyrolysis (500°C) followed by aromatization (at 550°C). Conversion of glycerol = 100°C. The selectivity of aromatics (BTX) was 35% (Carbon) or 15 wt.%. $S_{Benzene}$ = 27%, $S_{Toluene}$ = 45 and S_{Xylene} = 28%. $S_{Benzene}$ changed to 40% (additional 10%) when bentonite was added as matrix.	(He et al., 2018)
Glycerol to aromatics	H-MFI, Zn/MFI, 2.34 wt.% Sn MFI, Ni/MFI, Mo/MFI and Ag/MFI.	BTX aromatics (21.1 wt.%) with 10 h stability. Parent H-ZSM-5 only resulted 13.9 wt.% aromatics with 5.5 h stability.	(Wang et al., 2016, 2017, 2019)
Glycerol to acrolein	Zeolite Y (FAU) was modified by La and Pd-La.	The yield of acrolein increased from 57 to 75% at 300°C due to the increase of Brønsted and Lewis acidity.	(Gonzalez-Arellano et al., 2015)
Acetalization glycerol with acetone	Hierarchical zeolites from different topologies such as MFI, MOR and BEA.	High conversion (above 80%) and high selectivity to solketal (nearly 100%).	(Kowalska-Kus et al., 2017)
Glycerol to glycerol carbonate	Natural clinoptilolite (HEU) was dealuminated by 1 N of HCl for 90 min.	Reaction parameters were studied. The conversion of glycerol increased with a decrease of catalyst diameter.	(Mahdi et al., 2016)
Glycerol to solketal with acetone as a co-reactant	Zeolite Beta(Si/Al_2 = 25) was compared with Y (FAU, Si/Al_2 = 30) and MOR (Si/Al_2 = 16).	Glycerol: acetone = 2:1. Beta was the most active ($X_{glycerol}$ = ca.74) and the most selective to solketal (ca.98%). Nano BEA exhibited higher activity and higher selectivity to desired product.	(Manjunathan et al., 2015)
Glycerol to allyl alcohol	Hierarchical ZSM-5 was fabricated from commercial ZSM-5 (Si/Al = 40). Ag-ZSM-5 was prepared by IWI (incipient wetness impregnation).	Gas phase reaction, glycerol to allyl alcohol was studied. P = 0.1–4 MPa. Dehydration was followed by hydrogenation. Lewis acidity was reduced to increase acrolein selectivity. The 5 wt.% Ag-hierarchical ZSM-5 was the best catalyst with $S_{allylalcohol}$ = 20%, $X_{glycerol}$ = 80%. Stable for 100 h reaction.	(Manjunathan et al., 2015)
Glycerol etherification with n-butanol	H-BEA was compared with H-MFI.	Etherification of glycerol using n-butanol at 140–180°C and 0.5 MPa. $X_{glycerol}$ = 55%. $S_{mono-butylglycerolether(MBGE)}$ = 98%. MBGE is an additive to biodiesel.	(Nandiwale et al., 2014; Aghbashlo et al., 2019)
Glycerol etherification with benzyl alcohol	Starting material: NH_4-ZSM-5 (MFI) with Si/Al = 40. Hierarchical MFI was prepared by NaOH desilication and HCl dealumination.	Higher acid sites were not linear with glycerol conversion. Three different acid sites resulted almost the same glycerol conversion in the range of 70 to 77%. Selectivity to bulky product di-benzyl-glycerol ether (DBG, 1,3-dibenzyloxy-2-propanol plus 1,2-dibenzyloxy-3-propanol) was higher for hierarchical MFI. Catalyst with higher Al content (Si/Al = ca 0.20) was more selective toward mono-benzyl-glycerol ether (MBG).	(Gonzalez-Arellano et al., 2015)

mesopores, (iii), and (iv) the hydrophobicity of the catalyst (as described in **Figure 3**). **Table 4** presents selected works on glycerol to acrolein over zeolites.

Carrico et al. reported the utilization of MWW, pillared MWW and delaminated MWW in glycerol to acrolein at 320°C (Carriço et al., 2016). The selectivity to acrolein increased with the increase of acid site density. ITQ-2, with the strongest of density of acid sites exhibited the best selective solid for acrolein. The mesopores were not linear with acrolein selectivity. More coke depositions were observed over ITQ-2 which had the largest mesopore pore volumes. The Brønsted/Lewis (B/L) ratio is a crucial parameter to maximize acrolein selectivity. The higher the B/L has the higher selectivity to acrolein. The low B/L was important if we need to maximize acetol (hydroxyacetone).

GLYCEROL CONVERSION OVER NATURAL MINERALS

Glycerol is an abundant and low-cost feedstock. To minimize the barrier in the valorization of glycerol, low-cost catalysts are targeted. Despite of their low-cost benefit, there are still limited works on the use of natural zeolites and natural clays for glycerol conversions to chemicals. Some notable works are cited in **Table 5**. The most common natural zeolites in solid-acid catalysts are from HEU frameworks. Mahdi et al reported clinoptilolite (HEU) in glycerol conversion to glycerol carbonate (Mahdi et al., 2016). Furthermore, recently our group also reported natural mordenite and hierarchical mordenites (Nasser et al., 2016b; Kurniawan et al., 2017a,b). Mild activation of natural zeolites and clays should be established to

Catalyst	Condition	$C_{glycerol}$ (%)	$S_{aromatics}$ (%)	Remark	References
Dealuminated H-ZSM-5 (MFI) with initial Si/Al = 25	$T = 400°C$, glycerol/methanol = 40 wt.%, $P = 0.1$ MPa, WHSV: 0.71 h^{-1}.	ca.98	ca.32 (C% BTX)	The most stable catalysts was the hierarchical ZSM-5 made by steam + acid dealumination = 11.5 h.	(Wang et al., 2019)
ZSM-5 ($SiO_2/Al_2O_3 = 30$)	$T = 400°C$. WHSV = 0.8 h^{-1}.	100	>30 (C% BTX)	In the presence of water as a contaminant, the catalyst was deactivated rapidly.	(Jang et al., 2014)
H-ZSM-5 ($Si/Al_2 = 200$)	$T = 400°C$ WHSV = 0.9 h^{-1}.	100	18	Only 3 h life-time.	(Yang et al., 2018)
Hierarchical Sn-ZSM-5	$T = 400 °C$ WHSV = 0.9 h^{-1}.	100	32 (BTX)	H-Sn-ZSM-5 was desilicated by 0.3 M NaOH. Longer catalyst lifetime.	(Yang et al., 2018)
Pd-H-ZSM-5	$T = 400°C$. H_2/glycerol = 10:1. $P = 1$ atm.	100	More than 50	Without Pd, the main product was acrolein with 11% aromatics. Pd was responsible for hydrodeoxygenation while H-ZSM-5 was for aromatization.	(Xiao and Varma, 2016)
Hierarchical ZSM-5. Starting material: ZSM-5 with Si/Al of 25. Different alkaline solutions were used for desilication.	$T = 400°C$. $P = 1$ atm. Feed = 40 wt.% glycerol in methanol. WHSV = 0.71 h^{-1}.	100	15 wt.%	Desilication induced the increase of Brønsted acidity. The BTW increased while heavier aromatics ere suppressed.	(Wang et al., 2017)
H-Y (FAU), Si/Al = 40	$T = 400°C$. $P = 2$ MPa. W/F = 0.5 h. H_2/glycerol = 15:1.	ca. 95	31	FAU was less selective to aromatics, as compared to MFI.	(Hoang et al., 2010)
H-ZSM-5 (MFI) with Si/Al = 45	$T = 400°C$. $P = 2$ MPa. W/F = 0.5 h. H_2/glycerol = 15:1.	ca. 95	59	Maximum yield of aromatics was ca. 60%.	(Hoang et al., 2010)

Glycerol to the second reactant ratio was presented as molar ratio. All conversions and selectivity values were rounded to the nearest whole number.

FIGURE 3 | Crucial factors in the applications of hierarchical zeolites in glycerol conversions.
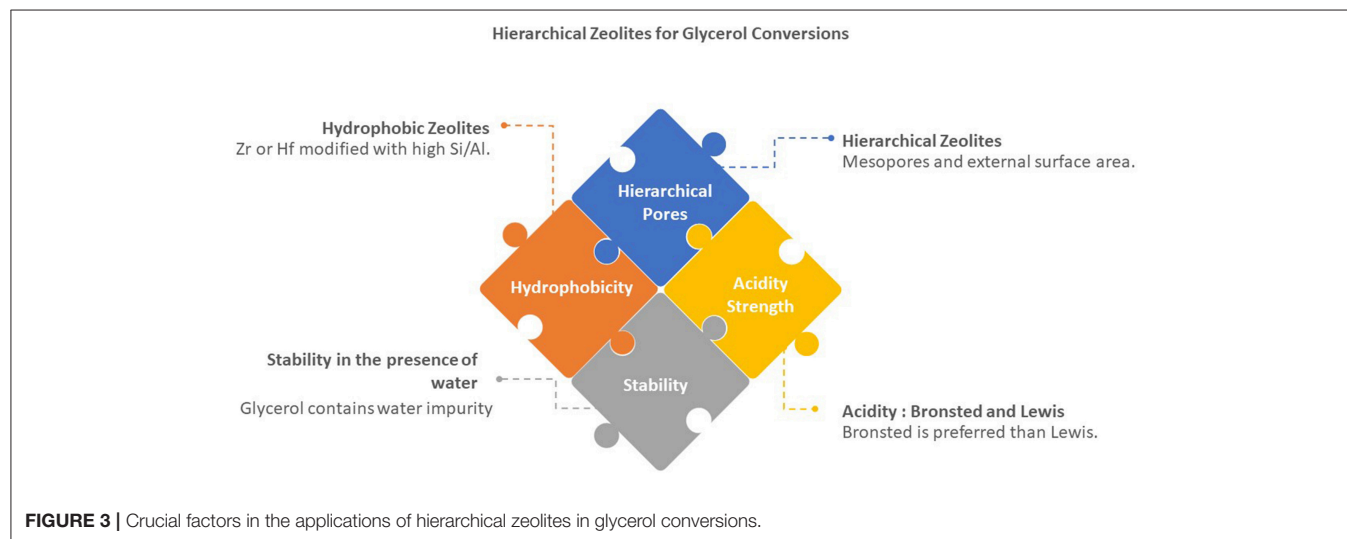
achieve industrial standards for safety and economic assessments (Pawar et al., 2015).

In addition to activation procedures, stability during chemical reactions, and possible regeneration are expected to suppress the catalyst cost. Ahmed and coworkers reported the decrease of crystallinity of hierarchical MRE zeolite (i.e., ZSM-48) (Ahmed et al., 2017). Typically, the crystallinity of zeolite-based catalysts decreased during regeneration. Before the hierarchical zeolites can be applied in glycerol conversions, improvements on the stability of structure and acidity after regeneration should be established.

The additions of boron and fluoride have been explored to improve the stability of zeolite catalysts in the presence of hot water or steam (Sanhoob et al., 2017). Boron has a weaker acidity as compared to aluminum acid sites. Appropriate level of boron content increased the stability of MFI framework (with zero aluminum) in steam-assisted reactions. The conversion in the presence of steam was maintained with the large external surface area with higher acid strength and high concentration of silanols. Proper compositions of minerals were crucial.

Considering the deactivation problems in glycerol conversion over zeolite catalysts, several cheaper catalysts are proposed:

TABLE 4 | Selected works on **glycerol-to-acrolein** over zeolites.

Catalyst	Condition	$X_{glycerol}$ (%)	$S_{acrolein}$ (%)	Remark	References
Hierarchical and conventional SAPO-40 (AFR)	$T = 320\ ^{\circ}C.\ P = 1$ atm. WHSV: $0.85\ h^{-1}$.	100	78	Hierarchical AFR was more active, more selective to acrolein. AFR was also more active as compared to SAPO-11 and SAPO-34.	(Fernandes et al., 2017)
MCM-22 (MWW) with $Si/Al2 = 28$	Feed: glycerol in water (36.6%), $T = 320^{\circ}C.\ T = 2$ h.	99.8	$\sim$50	Coke after 10 h = ca. 25%.	(Carriço et al., 2016)
Delaminated MCM-22 (ITQ-2, MWW) with $Si/Al2 = 37$	Feed: glycerol in water (36.6%), $T = 320^{\circ}C.\ T = 2$ h.	58	44	Delaminated MWW, ITQ-2 has the largest V_{meso}.	(Carriço et al., 2016)
Pillared MWW (MCM-36), $Si/Al2 = 51$)	Feed: glycerol in water (36.6%), $T = 320^{\circ}C.\ T = 2$ h.	89	ca.7	MCM-36 has B/L = 0.9.	(Carriço et al., 2016)
H-Na-mordenite (MOR), $Si/Al = 8$	$T = 400^{\circ}C.\ P = 2$ MPa. W/F $= 0.5$ h. H_2/glycerol $= 15:1$.	ca.93	27	MOR, is considered as 1D pore zeolite with larger size (12 MR, 0.65 x 0.7 nm) than TON zeolite.	(Hoang et al., 2010)
H-ZSM-22 (TON), $Si/Al = 45$	$T = 400^{\circ}C.\ P = 2$ MPa. W/F $= 0.5$ h. H_2/glycerol $= 15:1$.	100	ca. 80	TON is representing 1D pore zeolite with medium pore size (10 MR, 0.46 x 0.57 nm).	(Hoang et al., 2010)
ZSM-5 ($SiO_2/Al_2O_3 = 30$)	$T = 400^{\circ}C.$ WHSV $= 0.8\ h^{-1}$.	100	>30 (C% BTX)	In the presence of water as a contaminant, the catalyst was deactivated rapidly.	(Jang et al., 2014)

Glycerol to the second reactant ratio was presented as molar ratio. $C_{glycerol} = Conversion\ of\ glycerol.$ $S_{acrolein} = selectivity\ to\ acrolein.$

TABLE 5 | Glycerol conversion over natural zeolites and natural minerals.

Co-reactant	Catalyst	T (°C)	$X_{glycerol}$ (%)	Products	Remark	References
No co-reactant	Bentonite was added to ZSM-5 with different weight ratios: 10, 20 and 40 wt.%.	500°C (pyrolysis) or 550°C (aromatization).	100	aromatics BTX, 35%.	Bentonite was selective to benzene. $S_{Benzene}$ changed to 40% (additional 10%) when bentonite was added as matrix.	(He et al., 2018)
Benzaldehyde	montmorillonite	40	83%	Solketal (99%)	Glycerol:benzaldehyde dimethyl acetal = 1:1.1 for 6 h.	(Nanda et al., 2016)
Sodium bicarbonate	Hierarchical clinoptilolite	60–100	28	N.A.	The optimum conditions at molar ratio of glycerol: sodium bicarbonate: water equal to 3:1:3.	(Mahdi et al., 2016)
Acetone	montmorillonite	30	87%	Solketal (85%)	Glycerol:acetone = 1:6, catalyst weight: 3 wt.% of total reactant weight, for 2 h.	(Sandesh et al., 2015)

Glycerol to co-reactant ratio was highlighted as molar ratio.

(i) natural zeolites which need acid-base activation, (ii) OSDA-free zeolites, (iii) amine-templated zeolites. Those materials were considered due to cheaper production cost. OSDA-free zeolites are synthesized without template (without organic structure directing agent). Amines are low-cost OSDA as compared to ammonium hydroxide OSDAs.

PERSPECTIVE ON GLYCEROL OVER HIERARCHICAL ZEOLITES IN THE PRESENCE OF WATER

The crude glycerol obtained as byproduct in biodiesel production contains water (up to 10%), ash, matter organic non-glycerol (MONG) and trimethylene glycol (Tan et al., 2013). The presence of water, hot water or steam in glycerol conversions affects the stability of zeolites (including hierarchical zeolites). **Table 6** presents some notable research reports on the effect of water in glycerol conversions. High Si/Al (Si/Al=16) zeolite beta (BEA) with rich silicon content has resulted in the hydrophobic properties for the conversion of glycerol with formaldehyde in the presence of water (Da Silva et al., 2009). This may happen over BEA as this topology has the internal surface area almost similar with the external surface area. The authors claimed that the water molecules were prevented to reach the acid sites at the internal pore architectures. Surprisingly, zeolite FAU (USY) exhibited negligible conversion due to hydrophilic properties of FAU (Si/Al=28). Good stability was also observed over medium pore zeolite, such as MFI with Si/Al of 14 with the pore opening of ca. 0.56 nm, the formation glycerol acetals was prevented.

Bakare and co-workers reported that a one dimensional pore zeolite, MTT framework was stable in the presence of water vapor at 200°C under autogenous pressure of autoclave (Bakare et al., 2016). The addition of lanthanum (La) and cerium

TABLE 6 | Glycerol conversions over zeolites in the presence of water.

Co-reactant	Catalyst	T (°C)	$X_{glycerol}$ (%)	Selectivity to main product	Remark	References
No co-reactant, but different solvents were used.	ZSM-5 (MFI) with Si/Al_2 of 30.	440	>99.99	The carbon yield of aromatics reached 25 wt.% after ca. 5 h.	Different concentrations of water were used. Jang et al reported the positive effect of water in glycerol feed. The glycerol/(glycerol+water) was varied from 30 to 70 wt.%.	(Jang et al., 2014)
No co-reactant	MCM-22 (MWW) with Si/Al_2 28	320	99.8	$S_{acrolein}$ = ~50. Coke after 10 h = ca. 25%.	Feed: glycerol in water (36.6%), t = 2 h.	(Carriço et al., 2016)
No co-reactant	Delaminated MCM-22 (ITQ-2, MWW) with Si/Al_2 37	320	58	$S_{acrolein}$ = 44. Delaminated MWW, ITQ-2 has the largest Vmeso.	Feed: glycerol in water (36.6%), t = 2 h.	(Carriço et al., 2016)
No co-reactant	SAPO-40 (AFR) with 12 MR (0.67 nm).	320	89	$S_{acrolein}$ =72%.	P = 1 atm. WHSV: 0.85 h-1. T = 2.5 h. Feed: 10 wt.%.	(Fernandes et al., 2017)
No co-reactant	Hierarchical SAPO-40 (AFR)	320	100	$S_{acrolein}$ =78%.	Hierarchical SAPO-40 was more active and more stable.	(Fernandes et al., 2017)
Acetone, 20 wt.% of water	Zeolite Y (FAU), Si/Al = 2.6	70	36	Selectivity was not clearly reported.	Conversion in the presence of water decreased to 19% where glycerol/H_2O: 4:1.	(Li et al., 2012)
Formaldehyde and water with formaldehyde (37%)	Zeolite BEA with Si/Al = 16	70	95 after 60 min (0.5 h)	70% of 6 MR (membered rings) acetals and 30% of 5 MR.	Glycerol: formadehyde = 1: 1.2	(Da Silva et al., 2009)
No co-reactant	ZSM-5 (MFI) with Si/Al = 50, Particle size: 40–120 micron.	350	97	$S_{acrolein}$ = 59%.	Feed: 85 wt.% glycerol in the presence of water.	(Corma et al., 2008)
No co-reactant	ZSM-5 (MFI) with Si/Al = 50. Particle size: 40–120 micron.	350	100	$S_{acrolein}$ = 59%.	Feed: 50 wt.% glycerol in the presence of water.	(Corma et al., 2008)
No co-reactant	ZSM-5 (MFI) with Si/Al = 50. Particle size: 40–120 micron.	350	100	$S_{acrolein}$ = 62%.	Feed: 20 wt.% glycerol in the presence of water.	(Corma et al., 2008)
No co-reactant	Hierarchical ZSM-5 with similar Si/Al	250–320	100	$S_{acrolein}$ = 81%.	Selectivity to acrolein was relatively constant around 80%.	(Zhang et al., 2015)
No co-reactant	Hierarchical ZSM-5, intercrystalline mesopores	250–320	100	$S_{acrolein}$ = 86%.	Hierarchical ZSM-5 with intercrystalline mesopores has exhibited the highest selectivity to acrolein.	(Zhang et al., 2015)
No co-reactant	Hierarchical ZSM-5, intracrystalline mesopores	250–320	100	$S_{acrolein}$ = 85%.	Hierarchical ZSM-5 with intracrystalline mesopores showed lower stability than the hierarchical ZSM-5 with intracrystalline mesopores.	(Zhang et al., 2015)

$X_{glycerol}$ (%) = conversion of glycerol.

(Ce) improved the stability of MTT in hot water vapor. The most stable catalyst was cerium modified MTT. Stability of TON, another medium pore zeolite with one-dimensional pore architectures was reported by (Jamil et al., 2016).

Li et al. (2012) reported the presence of water reduced the catalytic activity of solid acid catalysts (up to 50%) in the acid-catalyzed glycerol conversions as compared with the activity with pure glycerol feed. They emphasized that strength and density of Brønsted and Lewis do not have linear relationship with catalyst activity. Hierarchical large pore zeolite (FAU) and mesoporous silica (Al-TUD-1) with high number Brønsted and Lewis acidity were not active enough in the conversion of glycerol to solketal, a fuel additive (Li et al., 2012). Hydrophobicity of the catalysts plays

an important role in solid-acid catalyzed reactions. In line with hydrophobicity strategy, the addition of zirconium and hafnium improved the stability of aluminosilicate TUD-1 and SBA-15 in glycerol conversions (Ammaji et al., 2018).

Prinsen and co-workers reported the activity of the solid acid catalyst is not always linear increase with acidity for the conversions of glycerol and fatty acids to chemicals (Prinsen et al., 2018). In the conversion of palmitic acid to methyl palmitate over zeolites, it was reported that zeolite Y (FAU) with high a Si/Al of 30 (SiO_2/Al_2O_3 = 60) was more active than Al-rich FAU (with SiO_2/Al_2O_3 of 5. FAU based catalyst was also more active as compared with medium pore ZSM-5 (MFI). Maximum 100% conversion was achieved at the temperature reaction of 70°C for

3 h. They concluded that the most important parameters were: (i) porosity of zeolites (hierarchical pores), (ii) hydrophobicity, (iii) acid strength and (iv) stability as shown in **Figure 3**. The importance of hierarchical pores was also reported by Zhang et al. (2015). Hydrophobicity of catalysts are tunable by adding metals such as zirconium and hafnium and by removing the aluminum from the zeolite frameworks.

The effects of types of mesopores, either intercrystalline mesopores or intracrystalline mesopores were reported by Zhang et al. (2015). The most suitable nanozeolites with intercrystalline mesopores followed by hierarchical ZSM-5 with intra crystalline mesopores. Selectivity to acrolein was slightly increased due to intrercrystalline and intracrystalline mesopores. Fernandes et al. (2017) reported the application of hierarchical SAPO-40 (AFR) zeolite for the conversion of glycerol to acrolein in the presence of high water content (10 wt.% of glycerol in water). The hierarchical SAPO-40 with higher mesopore volume promoted larger stability and less mass-transfer limitation. The hierarchical SAPO-40 contained less Brønsted acidity with almost similar Lewis acid strength. The unique SAPO-40 was synthesized using two different silica sources, including [3-(trimethoxysilyl) propyl] octadecyl dimethyl ammonium chloride (TPOAC) and fumed silica. In the conversion of glycerol to acrolein, SAPO-40 was more active than SAPO-11 (AEL) and SAPO-34 (CHA). Due to more open porosity, the coke found in hierarchical AFR was higher (23.5%). The presence water (10 wt.% glycerol) did not affect the stability of SAPO-40 negatively. Corma et al. (2008) reported interested fact about glycerol conversion that the addition of water increased the selectivity to acrolein over commercial zeolite Y in SiO_2-Al_2O_3 matrix and ZSM-5 in clay matrix.

The improvement of catalytic activity of zeolites in glycerol dehydration and aromatization by the creation of mesopores are reported in **Table 5**. Nanosized zeolites are also promising for glycerol conversions. The nanosized crystals can also form intercrystalline hierarchical zeolites (Kowalska-Kus et al., 2017; Possato et al., 2017; Feliczak-Guzik, 2018; Galadima and Muraza, 2018; Yang et al., 2018; Ahmed et al., 2019). Theoretically, the intercrystalline zeolites affect better diffusion properties to tackle mass-transfer limitations (Yu et al., 2013; Manjunathan et al., 2015; Huang et al., 2017). Hierarchical zeolites are fabricated by different approaches, however, to suppress catalyst cost (as part of variable cost in industrial scale), the templated methods are not proposed due to the expensive price of the bulky organic structure directing agents (OSDA). The low-cost desilication and dealumination routes are preferred. The demetalization processes changed the mesopore distribution, improved the access to active sites, reduced mass transfer limitation and acid distributions. Another route for cheap catalyst is OSDA free (without additional OSDA). The low-cost fabrication of hierarchical zeolites with different topologies were started with three-dimensional (3D) medium pore ZSM-5 (MFI) (Muraza et al., 2013, 2014; Bawah et al., 2018), 3D large Beta (BEA) and 3D large pore FAU. Later, some one-dimensional pore zeolites such as MTW (Sanhoob et al., 2016), MTT (Muraza et al., 2013, 2014), TON (Jamil et al., 2018), and MRE (Ahmed et al., 2017) were also reported elsewhere.

Considering the popularity and the stability of hierarchical zeolites for glycerol monetization in water, hot water, sub-critical water and super critical water, it is also beneficial to explore the applicability of low-cost zeolites with hierarchical pores. The manufacturing of zeolites is indeed possible by using organic-structure directing agent (OSDA) free synthesis. The absence of template or OSDA (Khalil and Muraza, 2016; Idris et al., 2019; Nasser et al., 2019) will suppress the catalyst cost as one of the variable costs in glycerol biorefinery. Pure MOR, for instance, was fabricated by using OSDA or without OSDA route. The synthesis parameters such as alkalinity (Na/Si) and Si/Al were found to be crucial to obtain pure mordenite (Idris et al., 2019). If higher Si/Al is targeted, the higher Na/Si ratio should be set in the synthesis mixture. Rapid fabrication of low-cost MOR zeolite was also possible under microwave irradiation (Khalil and Muraza, 2016).

In addition, the natural zeolites are also potential as a low-cost catalyst for glycerol conversions. Mostly, natural zeolites are presence as small pore zeolites such as clinoptilolite (HEU) and chabazite (CHA) (Aysan et al., 2016). There are more than 28 different zeolite frameworks found in nature (Stocker et al., 2017), mordenite (MOR) is a promising natural zeolites for industrial catalytic applications. Recently, Kurniawan and co-workers reported to the applications of MOR and hierarchical MOR from natural zeolites for catalytic reactions (Nasser et al., 2016a,b; Kurniawan et al., 2017b). Hierarchical mordenite was modified by zirconium and applied in glycerol conversion (i.e., esterification) (Popova et al., 2017). By this approach, natural zeolites can also be converted to hierarchical MOR as low-cost catalyst for glycerol conversions. Other medium pore natural zeolites are expected. In addition to natural zeolites, low-cost natural clays such as montmorillonite are expected to be applicable in the conversion of low-cost feedstock like glycerol. Montmorillonite, which was activated by sulfuric acid, was used as a catalyst support (Samudrala et al., 2018). Bentonite was reported as good matrix for ZSM-5 for glycerol conversions to aromatics (He et al., 2018). Bentonite contains approximately 80 wt.% of montmorillonite structured clay (Carniato et al., 2018; Pentrák et al., 2018).

PERSPECTIVE AND CONCLUSIONS

This mini review highlights recent development glycerol conversions to acrolein and aromatics over zeolite-based catalysts. Crude glycerol usually contains water and other impurities. Water is a critical factor for glycerol conversions over solid acid catalysts. The presence of water and coke formation affect the stability of zeolite catalysts in glycerol conversions. Therefore, it was proposed to consider some strategies to suppress catalyst costs by using OSDA-free zeolites or by applying natural zeolites. Proper activations of natural zeolites were proposed. Natural mordenite is a potential natural zeolite for glycerol conversions. Low-cost catalysts should be found for low cost feedstock (e.g. glycerol). Coking is one of the main problems in the conversion of glycerol to acrolein. Coke formation can be suppressed by selecting the appropriate pore opening, especially medium pore zeolites with mild acidity. In addition to pore

architectures of the catalysts, acidity is an important factor in glycerol to acrolein or aromatics over zeolite catalysts. This review will open plethora in designing better zeolite catalysts for glycerol conversions to acrolein and aromatics. Medium pore zeolite with shape selective catalysts are expected to perform better in glycerol to acrolein. Large pore zeolite with large cavity are expected to be ideal catalysts for glycerol to aromatics. Natural clays such as montmorillonite and natural zeolites are potential applied in commercial glycerol to aromatics.

AUTHOR CONTRIBUTIONS

The author confirms being the sole contributor of this work and has approved it for publication.

ACKNOWLEDGMENTS

REFERENCES

Aghbashlo, M., Hosseinpour, S., Tabatabaei, M., Rastegari, H., and Ghaziaskar, H. S. (2019). Multi-objective exergoeconomic and exergoenvironmental optimization of continuous synthesis of solketal through glycerol ketalization with acetone in the presence of ethanol as co-solvent. *Renew. Energy* 130, 735–748. doi: 10.1016/j.renene.2018.06.103

Aghbashlo, M., Tabatabaei, M., Hosseinpour, S., Rastegari, H., and Ghaziaskar, H. S. (2018a). Multi-objective exergy-based optimization of continuous glycerol ketalization to synthesize solketal as a biodiesel additive in subcritical acetone. *Energy Conver. Manage.* 160, 251–261. doi: 10.1016/j.enconman.2018.01.044

Aghbashlo, M., Tabatabaei, M., Rastegari, H., Ghaziaskar, H. S., and Roodbar Shojaei, T. (2018b). On the exergetic optimization of solketalacetin synthesis as a green fuel additive through ketalization of glycerol-derived monoacetin with acetone. *Renew. Energy* 126, 242–253. doi: 10.1016/j.renene.2018.03.047

Ahmed, M. H. M., Muraza, O., Galadima, A., Yoshioka, M., Yamani, Z. H., and Yokoi, T. (2019). Choreographing boron-aluminum acidity and hierarchical porosity in *BEA zeolite by in-situ hydrothermal synthesis for a highly selective methanol to propylene catalyst. *Micropor. Mesopor. Mater.* 273, 249–255. doi: 10.1016/j.micromeso.2018.06.036

Ahmed, M. H. M., Muraza, O., Nakaoka, S., Jamil, A. K., Mayoral, A., Sebastian, V., et al. (2017). Stability assessment of regenerated hierarchical ZSM-48 zeolite designed by post-synthesis treatment for catalytic cracking of light naphtha. *Energy Fuels* 31, 14097–14103. doi: 10.1021/acs.energyfuels.7b02796

Ammaji, S., Rao, G. S., and Chary, K. V. R. (2018). Acetalization of glycerol with acetone over various metal-modified SBA-15 catalysts. *Appl. Petrochem. Res.* 8, 107–118. doi: 10.1007/s13203-018-0197-6

Antonova, Z. A., Krouk, V. S., Pilyuk, Y. E., Maksimuk, Y. V., Karpushenkava, L. S., and Krivova, M. G. (2015). Exergy analysis of canola-based biodiesel production in Belarus. *Fuel Proc. Technol.* 138, 397–403. doi: 10.1016/j.fuproc.2015.05.005

Atabani, A. E., Silitonga, A. S., Badruddin, I. A., Mahlia, T. M. I., Masjuki, H. H., and Mekhilef, S. (2012). A comprehensive review on biodiesel as an alternative energy resource and its characteristics. *Renew. Sustain. Energy Rev.* 16, 2070–2093. doi: 10.1016/j.rser.2012.01.003

Aysan, H., Edebali, S., Ozdemir, C., CeliK Karakaya, M., and Karakaya, N. (2016). Use of chabazite, a naturally abundant zeolite, for the investigation of the adsorption kinetics and mechanism of methylene blue dye. *Micropor. Mesopor. Mater.* 235, 78–86. doi: 10.1016/j.micromeso.2016.08.007

Bagheri, S., Julkapli, N. M., and Yehye, W. A. (2015). Catalytic conversion of biodiesel derived raw glycerol to value added products. *Renew. Sustain. Energy Rev.* 41, 113–127. doi: 10.1016/j.rser.2014.08.031

Bakare, I. A., Muraza, O., Kurniawan, T., Yamani, Z. H., Shafei, E. N., Punetha, A. K., et al. (2016). Hydrothermal stability of MTT zeolite in hot water: the role of La and Ce. *Micropor. Mesopor. Mater.* 233, 93–101. doi: 10.1016/j.micromeso.2015.11.038

Bawah, A.-R., Malaibari, Z. O., and Muraza, O. (2018). Syngas production from CO2 reforming of methane over Ni supported on hierarchical silicalite-1 fabricated by microwave-assisted hydrothermal synthesis. *Int. J. Hydrog. Energy* 43, 13177–13189. doi: 10.1016/j.ijhydene.2018.05.073

Carniato, F., Bisio, C., Evangelisti, C., Psaro, R., Dal Santo, V., Costenaro, D., et al. (2018). Iron-montmorillonite clays as active sorbents for the decontamination of hazardous chemical warfare agents. *Dalton Trans.* 47, 2939–2948. doi: 10.1039/C7DT03859C

Carriço, C. S., Cruz, F. T., Dos Santos, M. B., Oliveira, D. S., Pastore, H. O., Andrade, H. M. C., et al. (2016). MWW-type catalysts for gas phase glycerol dehydration to acrolein. *J. Catal.* 334, 34–41. doi: 10.1016/j.jcat.2015.11.010

Chen, Z., Gao, L., Han, W., and Zhang, L. (2019). Energy and exergy analyses of coal gasification with supercritical water and O2-H2O. *Appl. Thermal Eng.* 148, 57–63. doi: 10.1016/j.applthermaleng.2018.10.050

Corma, A., Huber, G. W., Sauvanaud, L., and O'connor, P. (2008). Biomass to chemicals: catalytic conversion of glycerol/water mixtures into acrolein, reaction network. *J. Catal.* 257, 163–171. doi: 10.1016/j.jcat.2008.04.016

Cornejo, A., Barrio, I., Campoy, M., Lázaro, J., and Navarrete, B. (2017). Oxygenated fuel additives from glycerol valorization. main production pathways and effects on fuel properties and engine performance: a critical review. *Renew. Sustain. Energy Rev.* 79, 1400–1413. doi: 10.1016/j.rser.2017.04.005

Da Silva, C. X. A., Gonçalves, V. L. C., and Mota, C. J. A. (2009). Water-tolerant zeolitecatalyst for the acetalisation of glycerol. *Green Chem.* 11, 38–41. doi: 10.1039/B813564A

Exxonmobil (2017). *2018 Outlook for Energy: A View to 2040*. Exxonmobil.

Feliczak-Guzik, A. (2018). Hierarchical zeolites: synthesis and catalytic properties. *Micropor. Mesopor. Mater.* 259, 33–45. doi: 10.1016/j.micromeso.2017.09.030

Fernandes, A., Filipa Ribeiro, M., and Lourenço, J. P. (2017). Gas-phase dehydration of glycerol over hierarchical silicoaluminophosphate SAPO-40. *Catal. Commun.* 95, 16–20. doi: 10.1016/j.catcom.2017.02.015

Galadima, A., and Muraza, O. (2016a). A review on glycerol valorization to acrolein over solid acid catalysts. *J. Taiwan Inst. Chem. Eng.* 67, 29–44. doi: 10.1016/j.jtice.2016.07.019

Galadima, A., and Muraza, O. (2016b). Sustainable production of glycerol carbonate from by-product in biodiesel plant. *Waste Biomass Valorization* 8, 141–152. doi: 10.1007/s12649-016-9560-y

Galadima, A., and Muraza, O. (2018). Hydrocracking catalysts based on hierarchical zeolites: a recent progress. *J. Indust. Eng. Chem.* 61, 265–280. doi: 10.1016/j.jiec.2017.12.024

Gholami, A., Hajinezhad, A., Pourfayaz, F., and Ahmadi, M. H. (2018). The effect of hydrodynamic and ultrasonic cavitation on biodiesel production: an exergy analysis approach. *Energy* 160, 478–489. doi: 10.1016/j.energy.2018.07.008

Gonzalez-Arellano, C., Grau-Atienza, A., Serrano, E., Romero, A. A., Garcia-Martinez, J., and Luque, R. (2015). The role of mesoporosity and Si/Al ratio in the catalytic etherification of glycerol with benzyl alcohol using ZSM-5 zeolites. *J. Mol. Catal. A Chem.* 406, 40–45. doi: 10.1016/j.molcata.2015.05.011

Gutiérrez Ortiz, F. J., Ollero, P., Serrera, A., and Galera, S. (2012a). An energy and exergy analysis of the supercritical water reforming of glycerol for power production. *Int. J. Hydrogen Energy* 37, 209–226. doi: 10.1016/j.ijhydene.2011.09.058

Gutiérrez Ortiz, F. J., Ollero, P., Serrera, A., and Galera, S. (2012b). Process integration and exergy analysis of the autothermal reforming of glycerol using supercritical water. *Energy* 42, 192–203. doi: 10.1016/j.energy.2012.03.069

Hajjaji, N., Baccar, I., and Pons, M.-N. (2014). Energy and exergy analysis as tools for optimization of hydrogen production by glycerol autothermal reforming. *Renew. Energy* 71, 368–380. doi: 10.1016/j.renene.2014.05.056

He, S., Muizebelt, I., Heeres, A., Schenk, N. J., Blees, R., and Heeres, H. J. (2018). Catalytic pyrolysis of crude glycerol over shaped ZSM-5/bentonite catalysts for bio-BTX synthesis. *Appl. Catal. B Environ.* 235, 45–55. doi: 10.1016/j.apcatb.2018.04.047

Hoang, T. Q., Zhu, X., Danuthai, T., Lobban, L. L., Resasco, D. E., and Mallinson, R. G. (2010). Conversion of glycerol to alkyl-aromatics over zeolites. *Energy Fuels* 24, 3804–3809. doi: 10.1021/ef100160y

Huang, G., Ji, P., Xu, H., Jiang, J.-G., Chen, L., and Wu, P. (2017). Fast synthesis of hierarchical Beta zeolites with uniform nanocrystals from layered silicate precursor. *Micropor. Mesopor. Mater.* 248, 30–39. doi: 10.1016/j.micromeso.2017.03.060

Idris, A., Khalil, U., Abdulaziz, I., Makertihartha, I. G. B. N., Subagjo, L.aniwati, M., Al-Betar, A.-R., et al. (2019). Fabrication zone of OSDA-free and seed-free mordenite crystals. *Powder Technol.* 342, 992–997. doi: 10.1016/j.powtec.2018.09.041

Jamil, A. K., Muraza, O., Ahmed, M. H., Zainalabdeen, A., Muramoto, K., Nakasaka, Y., et al. (2018). Hydrothermally stable acid-modified ZSM-22 zeolite for selective propylene production via steam-assisted catalytic cracking of n-hexane. *Micropor. Mesopor. Mater.* 260, 30–39. doi: 10.1016/j.micromeso.2017.10.016

Jamil, A. K., Muraza, O., Osuga, R., Shafei, E. N., Choi, K.-H., Yamani, Z. H., et al. (2016). Hydrothermal stability of one-dimensional pore ZSM-22 zeolite in hot water. *J. Phys. Chem. C* 120, 22918–22926. doi: 10.1021/acs.jpcc.6b04980

Jang, H.-S., Bae, K., Shin, M., Kim, S. M., Kim, C.-U., and Suh, Y.-W. (2014). Aromatization of glycerol/alcohol mixtures over zeolite H-ZSM-5. *Fuel* 134, 439–447. doi: 10.1016/j.fuel.2014.05.086

Khalil, U., and Muraza, O. (2016). Microwave-assisted hydrothermal synthesis of mordenite zeolite: optimization of synthesis parameters. *Micropor. Mesopor. Mater.* 232, 211–217. doi: 10.1016/j.micromeso.2016.06.016

Kowalska-Kus, J., Held, A., Frankowski, M., and Nowinska, K. (2017). Solketal formation from glycerol and acetone over hierarchical zeolites of different structure as catalysts. *J. Mol. Catal. A Chem.* 426, 205–212. doi: 10.1016/j.molcata.2016.11.018

Kurniawan, T., Muraza, O., Hakeem, A. S., and Al-Amer, A. M. (2017a). Mechanochemical route and recrystallization strategy to fabricate mordenite nanoparticles from natural zeolites. *Cryst. Growth Des.* 17, 3313–3320. doi: 10.1021/acs.cgd.7b00295

Kurniawan, T., Muraza, O., Miyake, K., Hakeem, A. S., Hirota, Y., Al-Amer, A. M., et al. (2017b). Conversion of dimethyl ether to olefins over nanosized mordenite fabricated by a combined high-energy ball milling with recrystallization. *Ind. Eng. Chem. Res.* 56, 4258–4266. doi: 10.1021/acs.iecr.6b04834

Lauriol-Garbay, P., Millet, J. M. M., Loridant, S., Bellière-Baca, V., and Rey, P. (2011). New efficient and long-life catalyst for gas-phase glycerol dehydration to acrolein. *J. Catal.* 280, 68–76. doi: 10.1016/j.jcat.2011.03.005

Li, L., Korányi, T. I., Sels, B. F., and Pescarmona, P. P. (2012). Highly-efficient conversion of glycerol to solketal over heterogeneous lewis acid catalysts. *Green Chem.* 14, 1611–1619. doi: 10.1039/c2gc16619d

Mahdi, H. I., Irawan, E., Nuryoto, N., Jayanudin, J., Sulistyo, H., Sediawan, W. B., et al. (2016). Glycerol carbonate production from biodiesel waste over modified natural clinoptilolite. *Waste Biomass Valorization* 7, 1349–1356. doi: 10.1007/s12649-016-9495-3

Manjunathan, P., Maradur, S. P., Halgeri, A. B., and Shanbhag, G. V. (2015). Room temperature synthesis of solketal from acetalization of glycerol with acetone: effect of crystallite size and the role of acidity of beta zeolite. *J. Mol. Catal. A Chem.* 396, 47–54. doi: 10.1016/j.molcata.2014.09.028

Marimuthu, M., Marimuthu, P. S. K. A. K. Palanivelu, S., and Rajagopalan, V. (2018). Tuning the basicity of Cu-based mixed oxide catalysts towards the efficient conversion of glycerol to glycerol carbonate. *Mol. Catal.* 460, 53–62. doi: 10.1016/j.mcat.2018.09.002

Monteiro, M. R., Kugelmeier, C. L., Pinheiro, R. S., Batalha, M. O., and Da Silva César, A. (2018). Glycerol from biodiesel production: technological paths for sustainability. *Renew. Sustain. Energy Rev.* 88, 109–122. doi: 10.1016/j.rser.2018.02.019

Muraza, O., Bakare, I. A., Tago, T., Konno, H., Adedigba, A.-L., Al-Amer, A. M., et al. (2013). Controlled and rapid growth of MTT zeolite crystals with low-aspect-ratio in a microwave reactor. *Chem. Eng. J.* 226, 367–376. doi: 10.1016/j.cej.2013.04.072

Muraza, O., Bakare, I. A., Tago, T., Konno, H., Taniguchi, T., Al-Amer, A. M., et al. (2014). Selective catalytic cracking of n-hexane to propylene over hierarchical MTT zeolite. *Fuel* 135, 105–111. doi: 10.1016/j.fuel.2014.06.045

Nanda, M. R., Zhang, Y., Yuan, Z., Qin, W., Ghaziaskar, H. S., and Xu, C. (2016). Catalytic conversion of glycerol for sustainable production of solketal as a fuel additive: a review. *Renew. Sustain. Energy Rev.* 56, 1022–1031. doi: 10.1016/j.rser.2015.12.008

Nandiwale, K. Y., Patil, S. E., and Bokade, V. V. (2014). Glycerol etherification using n-butanol to produce oxygenated additives for biodiesel fuel over H-beta zeolite catalysts. *Energy Technol.* 2, 446–452. doi: 10.1002/ente.201300169

Nasser, G., Kurniawan, T., Miyake, K., Galadima, A., Hirota, Y., Nishiyama, N., et al. (2016a). Dimethyl ether to olefins over dealuminated mordenite (MOR) zeolites derived from natural minerals. *J. Nat. Gas Sci. Eng.* 28, 566–571. doi: 10.1016/j.jngse.2015.12.032

Nasser, G. A., Kurniawan, T., Tago, T., Bakare, I. A., Taniguchi, T., Nakasaka, Y., et al. (2016b). Cracking of n-hexane over hierarchical MOR zeolites derived from natural minerals. *J. Taiwan Inst. Chem. Eng.* 61, 20–25. doi: 10.1016/j.jtice.2015.11.025

Nasser, G. A., Muraza, O., Nishitoba, T., Malaibari, Z., Al-Shammari, T. K., and Yokoi, T. (2019). OSDA-free chabazite (CHA) zeolite synthesized in the presence of fluoride for selective methanol-to-olefins. *Micropor. Mesopor. Mater.* 274, 277–285. doi: 10.1016/j.micromeso.2018.07.020

Pawar, R. R., Gosai, K. A., Bhatt, A. S., Kumaresan, S., Lee, S. M., and Bajaj, H. C. (2015). Clay catalysed rapid valorization of glycerol towards cyclic acetals and ketals. *RSC Adv.* 5, 83985–83996. doi: 10.1039/C5RA15817F

Pentrák, M., Hronský, V., Pálková, H., Uhlík, P., Komadel, P., and Madejová, J. (2018). Alteration of fine fraction of bentonite from Kopernica (Slovakia) under acid treatment: a combined XRD, FTIR, MAS NMR and AES study. *Appl. Clay Sci.* 163, 204–213. doi: 10.1016/j.clay.2018.07.028

Popova, M., Lazarova, H., Kalvachev, Y., Todorova, T., Szegedi, Á., Shestakova, P., et al. (2017). Zr-modified hierarchical mordenite as heterogeneous catalyst for glycerol esterification. *Catal. Commun.* 100, 10–14. doi: 10.1016/j.catcom.2017.06.009

Possato, L. G., Chaves, T. F., Cassinelli, W. H., Pulcinelli, S. H., Santilli, C. V., and Martins, L. (2017). The multiple benefits of glycerol conversion to acrolein and acrylic acid catalyzed by vanadium oxides supported on micro-mesoporous MFI zeolites. *Catal. Today* 289, 20–28. doi: 10.1016/j.cattod.2016.08.005

Presciutti, A., Asdrubali, F., Baldinelli, G., Rotili, A., Malavasi, M., and Di Salvia, G. (2018). Energy and exergy analysis of glycerol combustion in an innovative flameless power plant. *J. Clean. Prod.* 172, 3817–3824. doi: 10.1016/j.jclepro.2017.06.022

Prinsen, P., Luque, R., and González-Arellano, C. (2018). Zeolite catalyzed palmitic acid esterification. *Micropor. Mesopor. Mater.* 262, 133–139. doi: 10.1016/j.micromeso.2017.11.029

Quispe, C. A. G., Coronado, C. J. R., and Carvalho, J. A. Jr (2013). Glycerol: Production, consumption, prices, characterization and new trends in combustion. *Renew. Sustain. Energy Rev.* 27, 475–493. doi: 10.1016/j.rser.2013.06.017

Ren21, T. (2018). "Renewables 2018 Global Status Report," in: *Renewables 2018 Global Status Report (GSR)*. The REN21 Network.

Samudrala, S. P., Kandasamy, S., and Bhattacharya, S. (2018). Turning biodiesel waste glycerol into 1,3-Propanediol: catalytic performance of sulphuric acid-activated montmorillonite supported platinum catalysts in glycerol hydrogenolysis. *Sci. Rep.* 8:7484. doi: 10.1038/s41598-018-25787-w

Sandesh, S., Halgeri, A. B., and Shanbhag, G. V. (2015). Utilization of renewable resources: condensation of glycerol with acetone at room temperature catalyzed by organic–inorganic hybrid catalyst. *J. Mol. Catal. A Chem.* 401, 73–80. doi: 10.1016/j.molcata.2015.02.015

Sanhoob, M. A., Muraza, O., Shafei, E. N., Yokoi, T., and Choi, K.-H. (2017). Steam catalytic cracking of heavy naphta (C12) to high octane naphta over B-MFI zeolite. *Appl. Catal. B Environ.* 210, 432–443. doi: 10.1016/j.apcatb.2017.04.001

Sanhoob, M. A., Muraza, O., Taniguchi, T., Tago, T., Watanabe, G., and Masuda, T. (2016). Steam catalytic cracking of n-hexane over modified MTW zeolites impregnated by extra-framework elements. *Energy Fuels* 30, 9679–9685. doi: 10.1021/acs.energyfuels.6b00857

Stocker, K., Ellersdorfer, M., Lehner, M., and Raith, J. G. (2017). Characterization and utilization of natural zeolites in technical applications. *BHM Berg und Hüttenmännische Monatshefte* 162, 142–147. doi: 10.1007/s00501-017-0596-5

Tamiyakul, S., Ubolcharoen, W., Tungasmita, D. N., Jongpatiwut, S. (2015). Conversion of glycerol to aromatic hydrocarbons over Zn-promoted HZSM-5 catalysts. *Catalysis Today* 256, 325–335. doi: 10.1016/j.cattod.2014.12.030

Tan, H. W., Abdul Aziz, A. R., and Aroua, M. K. (2013). Glycerol production and its applications as a raw material: a review. *Renew. Sustain. Energy Rev.* 27, 118–127. doi: 10.1016/j.rser.2013. 06.035

Wang, F., Chu, X., Zhu, F., Wu, F., Li, Q., Liu, B., et al. (2019). Producing BTX aromatics-enriched oil from biomass derived glycerol using dealuminated HZSM-5 by successive steaming and acid leaching as catalyst: reactivity, acidity and product distribution. *Micropor. Mesopor. Mater.* 277, 286–294. doi: 10.1016/j.micromeso.2018.11.015

Wang, F., Xiao, W., Gao, L., and Xiao, G. (2016). Enhanced performance of glycerol to aromatics over Sn-containing HZSM-5 zeolites. *RSC Adv.* 6, 42984–42993. doi: 10.1039/C6RA03358J

Wang, F., Zhou, M.-X., Yang, X.-H., Gao, L.-J., and Xiao, G.-M. (2017). The effect of hierarchical pore architecture on one-step catalytic aromatization of glycerol: Reaction routes and catalytic performances. *Mol. Catal.* 432, 144–154. doi: 10.1016/j.mcat.2017.01.017

Xiao, Y., and Varma, A. (2016). Conversion of glycerol to hydrocarbon fuels via bifunctional catalysts. *ACS Energy Lett.* 1, 963–968. doi: 10.1021/acsenergylett.6b00421

Yang, X., Wang, F., Wei, R., Li, S., Wu, Y., Shen, P., et al. (2018). Synergy effect between hierarchical structured and Sn-modified H[Sn, Al]ZSM-5 zeolites on the catalysts for glycerol aromatization.

Micropor. Mesopor. Mater. 257, 154–161. doi: 10.1016/j.micromeso.2017. 08.039

Yu, Q., Cui, C., Zhang, Q., Chen, J., Li, Y., Sun, J., et al. (2013). Hierarchical ZSM-11 with intergrowth structures: synthesis, characterization and catalytic properties. *J. Energy Chem.* 22, 761–768. doi: 10.1016/S2095-4956(13)60101-1

Zakaria, Z. Y., Linnekoski, J., and Amin, N. A. S. (2012). Catalyst screening for conversion of glycerol to light olefins. *Chem. Eng. J.* 207–208, 803–813. doi: 10.1016/j.cej.2012.07.072

Zhang, H., Hu, Z., Huang, L., Zhang, H., Song, K., Wang, L., et al. (2015). Dehydration of glycerol to acrolein over hierarchical ZSM-5 zeolites: effects of mesoporosity and acidity. *ACS Catal.* 5, 2548–2558. doi: 10.1021/cs5019953

A Novel Strategy for Selective *O*-Methylation of Glycerol in Subcritical Methanol

Sophie Bruniaux[1], Rajender S. Varma[2] and Christophe Len[1,3]*

[1] *Sorbonne Universités, Universite de Technologie de Compiegne, Compiègne, France,* [2] *Regional Center of Advanced Technologies and Materials, Palacky University, Olomouc, Czechia,* [3] *PSL University, Chimie ParisTech, Paris, France*

A new regioselective approach has been elaborated for the selective conversion of bio-based glycerol into the monomethyl derivative using sub/supercritical methanol. The reaction was realized in a batch process using three reactive components, namely, glycerol, methanol, and potassium carbonate to selectively produce the 3-methoxypropan-1,2-diol in mild yields; the mechanism of the *O*-methylation has been delineated using labeled methanol and GC-MS experiments.

Keywords: glycerol, glycerol *O*-methylation, critical methanol, green chemistry, mechanism

INTRODUCTION

To compensate for the constantly diminishing fossil-derived resources, the concept of biorefinery and the use of vegetable oils has emerged as a promising alternative to meet future challenges in both public and industrial sectors (Biermann et al., 2000; Behr et al., 2008). Glycerol, as a co-product of industrial oleochemistry, is an outstanding example that has significant potential for conversion into valuable products (Len et al., 1996, 1997, 2018; Rafin et al., 2000; DeSousa et al., 2011; Saggadi et al., 2014a,b, 2015; Galy et al., 2017a,b; Nguyen et al., 2017; Varma and Len, 2018). Among the target chemicals, monoalkyl glyceryl ethers (MAGE) are relative chemical inert, which renders them suitable as solvents, chemicals for inks, polymers, lubricants, and liquid detergents (Sutter et al., 2015). Moreover, MAGEs bearing short *O*-alkyl chains have an impact on the energy sector as exemplified by the good fuel additive properties of 3-methoxypropan-1,2-diol (**2**) (Chang et al., 2012). Nevertheless, the main drawback of the use of MAGE is the basic structure of glycerol, which is a symmetrical polyol encompassing three hydroxy (OH) groups, with two identical primary OH and one secondary OH having a similar pKa. To improve the regio- and stereoselectivity starting from glycerol, protection–deprotection steps using solketal (Vanlaldinpuia and Bez, 2011; Jiang et al., 2013; Jakubowska et al., 2015), as well as activation steps deploying glycidol (Cucciniello et al., 2016; Leal-Duaso et al., 2017; Ricciardi et al., 2017, 2018), were necessary to produce the target glycerol ethers, which limits the interest in view of the cost and sustainability. Starting from glycerol (**1**), the direct one-step synthesis of glycerol ethers has been reported using different conventional methods: the Williamson-type synthesis, catalytic *O*-telomerization, acid catalysis, and reductive alkylation (Sutter et al., 2012), among others. Recently, acid homogeneous and heterogeneous catalysts such as Bi(OTf)$_3$ (Liu et al., 2013), Amberlyst-15 (Pariente et al., 2009), and silica-supported sulfonic groups (Gu et al., 2008) have been used, with success, for the synthesis of MAGEs. Among the documented research on direct MAGE synthesis, the use of critical alcohol as a solvent and reagent in the presence of homogeneous bases has not been described. In order to provide a greener protocol for the selective etherification of glycerol, herein, we disclose a novel *O*-methylation of glycerol (**1**) into the corresponding 3-methoxypropan-1,2-diol and (**2**) in the presence of a common and widely available homogeneous base under subcritical methanol.

EXPERIMENTAL SECTION

Materials and Methods

Substrates and solvents were purchased from Acros and all materials were used without further purification. Reactions were monitored by TLC (Kieselgel 60F254 aluminum sheet), with detection carried out through the use of an acidic potassium permanganate solution. Column chromatography was performed on silica gel $40–60 \, \mu m$, while flash column chromatography was accomplished on an automatic apparatus, using silica gel cartridges. ^1H and ^{13}C NMR spectra were recorded on a 400 MHz/54 mm ultralong hold. Chemical shifts (δ) are quoted in parts per million (ppm) and are referenced to TMS as an internal standard with coupling constants (J) being quoted in hertz. Gas chromatography analyses are performed on a PerkinElmer gas chromatography (Autosystem XL GC), using an Altech AT HT column (30.0 m, 0.25 mm i.d., 0.1 μm film thickness), with a detector at $300°C$, an injector at $350°C$, and a constant flow of nitrogen of 1 mL min^{-1}. The column is heated at $50°C$ for 3 min, and then warmed to $270°C$ with a temperature gradient of $20°C$ min^{-1} before being held at that temperature for 5 min.

Synthesis of 3-methoxypropan-1,2-diol (2)

A batch autoclave reactor (100 mL) was charged with glycerol (**1**, 4.0 g, 43.4 mmol), K_2CO_3 (1.0 g, 7.2 mmol) and methanol (70 mL) and was sealed, placed in the heating collar, and heated to $220°C$ under magnetic stirring with an internal control of the temperature and an auto-generated pressure. After 15 h, the autoclave was cooled down to $40°C$, with the volatile chemicals subsequently evaporating. The crude product was purified over a column on silica and eluted with a gradient of cyclohexane/ethyl acetate (100:0–0:100, v/v) to afford the pure ether **2** (36%, 1.66 g, 15.6 mmol). ^1H NMR (400 MHz; CDCl$_3$), δ 4.19 (s, 2H, OH),

3.71 (s, 1H, H$_2$), 3.61–3.36 (m, 2H, H$_1$), 3.36–3.08 (m, 5H, H$_{3,4}$) ppm; ^{13}C NMR (100 MHz; CDCl$_3$), δ (ppm): 73.8 (CH, C$_3$), 70.6 (CH$_2$, C$_2$), 63.6 (CH$_2$, C$_4$), 58.9 (CH$_3$, C$_1$) ppm.

RESULTS AND DISCUSSION

The optimization of method for the selective *O*-alkylation of glycerol (**1**) was achieved with the glycerol (**1**) and a commercial homogeneous base in methanol. The reaction occurs in an autoclave with a 100 mL container under magnetic stirring under sub- and super-critical conditions. When methanol is subjected to a temperature and a pressure higher than its critical point, supercritical methanol is obtained. When both: (i) the temperature and/or the pressure are lower than that of the critical point; and (ii) the temperature is higher than that of the boiling point with a pressure higher than 1 bar, subcritical methanol is obtained. Subcritical methanol can be referred to as hot compressed methanol. Heating methanol under pressure deeply modifies some of their physical characteristics: density, viscosity, diffusivity, thermal conductivity, static dielectric constant, and ion dissociation constant. In this process, methanol had a dual role of a solvent and as a reagent. Initial studies were performed for glycerol (**1**, 4.0 g, 43.6 mmol) in the presence of K_2CO_3 (1.0 g, 7.2 mmol) in methanol (70 mL) for 15 h by varying the temperature from 180 to $260°C$ (**Table 1**) wherein the pressure was auto-generated. The use of supercritical methanol

TABLE 1 | *O*-Methylation of glycerol (**1**) in sub- and supercritical methanol under varying temperatures.

Entry	Temperature (°C)	Pressure (bar)	Yield of 2 (%)
1[a]	260	170	39
2[a]	240	160	40
3[b]	220	60	39
4[b]	200	60	18
5[b]	180	50	4

[a]*Supercritical methanol.*
[b]*Subcritical methanol.*

TABLE 2 | Variation of the nature of the base for the *O*-methylation of glycerol (**1**) in subcritical methanol.

Entry	Base (16 mol%)	Yield of 2 (%)
1	K_2CO_3	39
2	$CaCO_3$	0
3	Na_2CO_3	8
4	Cs_2CO_3	40
5	$(NH_4)_2CO_3$	0
6	NaOH	4
7	KOH	6
8	K_3PO_4	4
9	AcONa	11
10	DABCO	0
11	Ag_2O	0
12	Na	9

(temperature > 239°C and pressure > 81 bar) was not necessary for the O-methylation of glycerol (**1**) since a similar result (39%

Entry	Glycerol (g)	K_2CO_3 (mol%)	Yield of 2 (%)
1	1	66.3	11
2	2	33.2	20
3	3	22.10	30
4	4	16.6	39
5	5	13.3	32
6	6	11.0	29
7	4	8.3	33
8	4	33.4	25
9	1	16.5	19
10	1	66.0	37
11	8	16.7	36
12	16	16.6	23
13*	4	2 × 16.6	44

*Addition of the second amount of K_2CO_3 (16.6 mol%) after 15 h for a total reaction time of 30 h.

Entry	Water (mL)	$HC(OCH_3)_3$ (mol%)	Yield of 2 (%)
1	–	0	39
2	anhydrous	0	35
3	1	0	25
4	–	100	21

yield) could be obtained in subcritical methanol at 220°C and 60 bar (**Table 1**, entry 3). Nevertheless, a lower temperature and pressure did not allow the generation of the target O-ether (**2**) in a yield higher than 18% (**Table 1**, entries 4 and 5). The selective direct O-alkylation of glycerol (**1**) under our experimental conditions was possible, with the only product observed being the 3-methoxypropan-1,2-diol (**2**).

Based on these results, different strong and weak bases (16 mol%), including K_2CO_3, $CaCO_3$, Na_2CO_3, Cs_2CO_3, $(NH_4)_2CO_3$, NaOH, KOH, K_3PO_4, AcONa, DABCO, Ag_2O, and Na were evaluated under the initial optimized temperature (220°C). Notably, the strength of the base was not a key factor since strong bases such as NaOH and KOH and weak bases such as AcONa did not furnish the corresponding O-methyl derivative **2**. The solubility of the base in subcritical methanol appears to be a rather important parameter. Among the different bases, only K_2CO_3 and Cs_2CO_3 gave the target MAGE **2** in 39 and 40% yields, respectively. The other carbonate bases did not generate the O-ether **2** in satisfactory yields. A plausible explanation may be that the increasing ionic radius among the sodium and the cesium ions could permit a best dissociation of the corresponding salt. Furthermore, this dissociation may be enhanced by the particular properties of the methanol at 220°C and at a 50–70 bar. However, K_2CO_3 will be the preferred base in the subsequent evaluations because Cs_2CO_3 is more expensive than the corresponding potassium derivative for a rather similar yield (39 vs. 40%). In case of other carbonates explored, the dissociation of the calcium, which is a divalent ion, is harder than the monovalent ion. In case of ammonium counterion, the possibility of the formation of the acid form, and consequently a counter balance of the basic conditions, might be an explanation for the non-formation of 3-methoxypropan-1,2-diol (**2**) with $(NH_4)_2CO_3$. The use of Na in methanol furnished the corresponding CH_3ONa base, which gave a poor yield (9%), similar to those obtained with Na_2CO_3 and NaOH (**Table 2**, entry 12).

To attain the most efficient process conditions, the highest concentration of glycerol (**1**) in methanol was determined; the variation of glycerol concentration was explored in the presence of K_2CO_3 (1.0 g, 7.2 mmol) at 220°C for 15 h. The yield of 3-methoxypropan-1,2-diol (**2**) increased with an increasing glycerol (**1**) concentration to an optimum of 39% yield for a concentration of 57 g L^{-1}; a higher concentration of glycerol (**1**, 71 and 86 g L^{-1}) produced lower yields of 32 and 29%, respectively. Nevertheless, the O-ether productivity was higher when deploying a higher glycerol concentration (5 10^{-6} vs. 4.5 10^{-6} mol s^{-1} L^{-1}) (**Table 2**, entries 4 and 6). Starting with a fixed quantity of glycerol (**1**, 4.0 g), the variation of the amount of K_2CO_3 (8.3, 16.6, and 33.4 mol%) showed that 16.6 mol% was the optimum (**Table 3**, entries 4, 7, and 8); too high an amount of K_2CO_3 in methanol may result in the saturation of the media thus impeding the solubility of glycerol (**1**). A scale-down and scale-up study was subsequently undertaken. When a dilution factor of 4 was applied, the reaction was less efficient and only a 19% yield was obtained (**Table 3**, entry 9), which may be counterbalanced by the increasing base quantity (**Table 3**, entry 10). On the other hand, when the reaction was scaled up with a
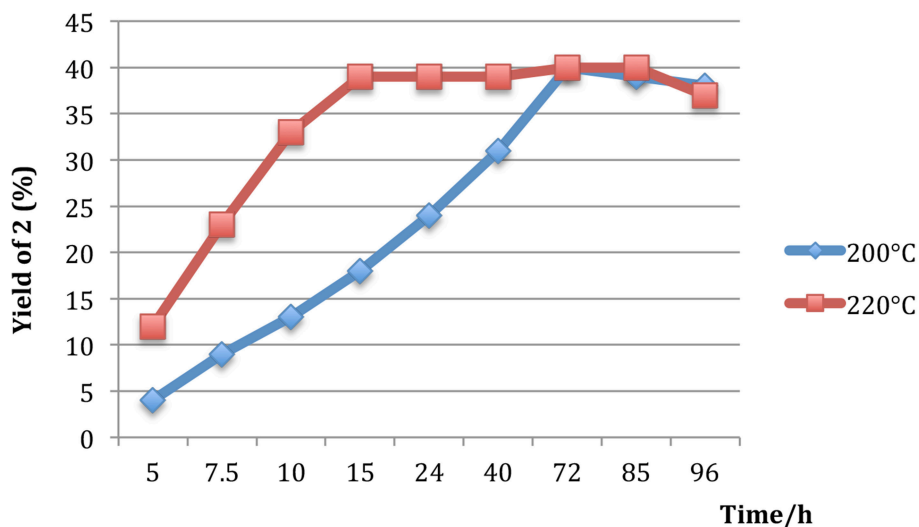
FIGURE 1 | Reaction profile of glycerol conversion to 3-methoxypropan-1,2-diol (**2**) at 200 and 220°C.

TABLE 5 | Scale down and scale up study for the *O*-methylation of glycerol (**1**) in subcritical methanol.

Entry	Methanol (mL)	Yield of 2 (%)
1	20	29
2	50	30
3	70	39
4	350	35

factor 2, a similar yield was achieved (36 vs. 39%) (**Table 3**, entries 4 and 11). Unfortunately, the scale up with a factor 4 resulted in a decreasing yield (**Table 3**, entries 4 and 12). Furthermore, a test was conducted with the addition of a second lot of K_2CO_3 after the first 15 h (**Table 3**, entry 13). This test gave a better result (44 vs. 39%) but does not justify the additional amount of K_2CO_3 and a prolonged reaction time, twice as long.

Since the present *O*-methylation process is a dehydration-type reaction, the effect of the presence of water was probed; the addition of water (1.4%) in the reaction turned out to be damaging as the yield decreased (**Table 4**, entries 1 and 3). On the other hand, the use of anhydrous reagents, i.e., glycerol (**1**), K_2CO_3 and methanol without water traces was not

advantageous because the same results were obtained when the starting materials were not anhydrous (**Table 4**, entries 1 and 2). This means that the ensuing water during this dehydration was not a critical negative point necessary to make a significant difference. However, a decrease of the reaction yield was noticed when a dryer agent, methyl orthoformiate, was used (**Table 4**, entry 4), which also means that the water produced may be essential for the reaction.

The variation of reaction time was next studied at 220 and 200°C; a faster kinetic was observed at 220°C rather than at 200°C. A plateau (40%) was reached with a temperature of 220°C after 15 h and more time (72 h) was required at 200°C to attain a similar yield (**Figure 1**). In our hands, a longer reaction time was not necessary to acquire a significant increase in the reaction yield.

Based on these results, a scale-down and scale-up study was performed using the following optimized conditions, glycerol (**1**, 4.0 g, 43.6 mmol) in the presence of K_2CO_3 (1.0 g, 16.6 mol%) in MeOH (70 mL) at 220°C and at a 50–70 bar for 15 h. Two different reactors (100 and 450 mL) were used to accomplish these evaluations. Indeed, a reactor of 100 mL was used for 20, 50, and 70 mL of methanol and the scale-up with 350 mL was performed in a reactor of 450 mL in size (**Table 5**). Only a difference of six points (29 vs. 35%) between the smallest volume and the highest volume was discerned, meaning that the results were slightly affected by the scale-down and the scale-up of the reaction.

With our optimized reaction conditions in hand, a range of alcohols as substrate and the reagent were screened (**Figure 2**). Propan-1,3-diol, propan-1,2-diol, erythritol, butan-1,4-diol, and butan-1-ol were evaluated instead of glycerol (**1**) and ethanol and butan-1-ol were evaluated instead of methanol. Changing glycerol (**1**) by another substrate afforded poor yields (<4%), except for propan-1,2-diol, which furnished the corresponding *O*-methyl ether **4** in a 10% yield; the close proximity of two
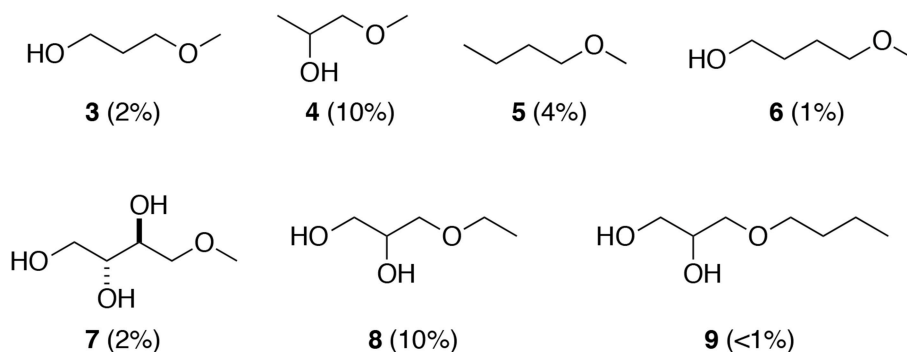
FIGURE 2 | Applications of the *O*-alkylation in subcritical alcohol.
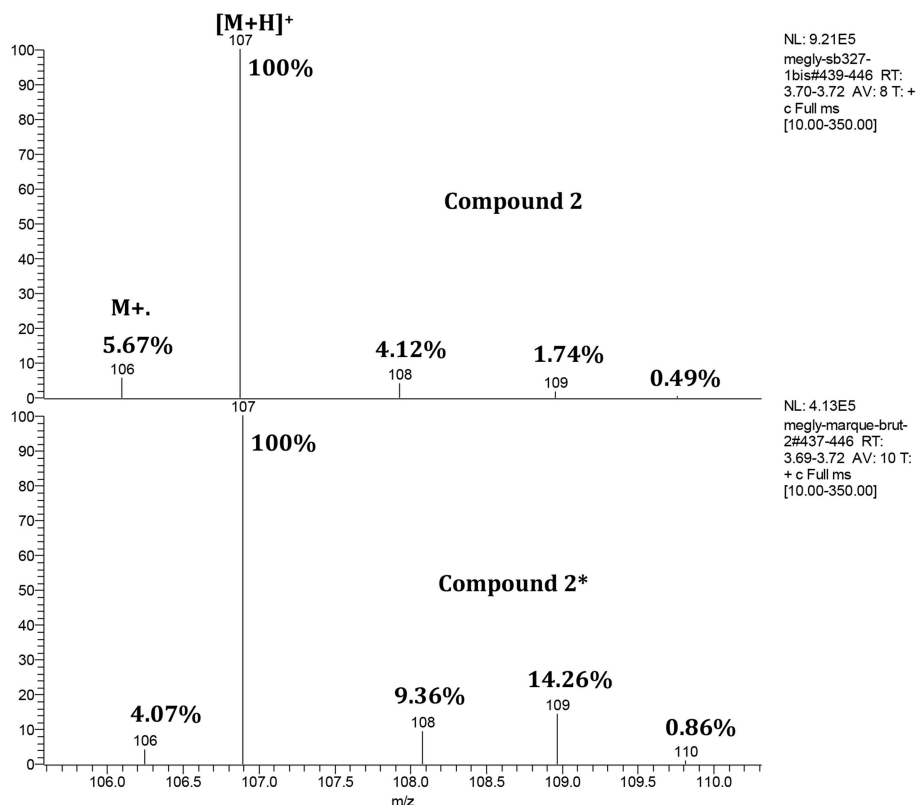
FIGURE 3 | Zoom of the isotopic cluster concerning the GC-MS analysis of compound 2 and compound 2*.

hydroxyl groups could have had a specific role in the mechanism. However, an unexpected result was obtained with erythritol, which has a structural similarity to glycerol (**1**). The deployment of another solvent other than methanol, notably for ethanol, resulted in a collapse of the yield from 39 to 10%, with only traces of product obtained when butanol was used. Although the low yields were obtained (<10%) in aforementioned cases, only the exclusive regioselective *O*-alkylation of the primary hydroxyl group was observed. One explanation may be the difference of solubility of glycerol (**1**) in the different alcohol, which decreased with the increasing length of the alcohol.

In order to propose a plausible mechanism for this new selective *O*-methylation of glycerol (**1**), the origin of the oxygen atom of the *O*-ether functionality was studied by using methanol labeled with ^{18}O. The *O*-alkylation was performed in the presence of glycerol (**1**, 1.14 g) and K_2CO_3 (16.6 mol%) in a mixture of methanol MeOH-Me^{18}OH (20.4:2.4, v/v) for 15 h at 220°C. After treatment, a GC-MS analysis of the crude target ether **2*** was undertaken to identify the oxygen origin of the methoxy group in position 1 of the glycerol moiety (**Figure 3**). The analysis of the commercial non-labeled 3-methoxypropan-1,2-diol (**2**) showed a signal of the [M+1] which was the corresponding ion
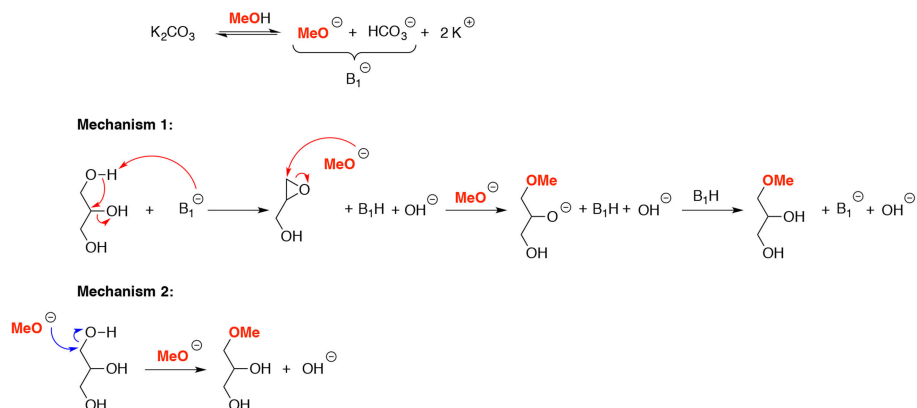
SCHEME 1 | Plausible mechanism for *O*-methylation of glycerol in sucritical methanol.

with an adding H+ at m/z of 107. An apparition of a signal corresponding to the [M+2] was noticed for the analysis of the crude target ether **2*** that matched with the presence of the labeled 3-methoxypropan-1,2-diol (**2***). To directly access the labeled percent of ^{18}O of the 3-methoxypropan-1,2-diol (**2***), the study was based on the M+2 of the [M+H]$^{+}$. In our case, 12.5% (14.26–1.74%) of labeled ether **2*** was obtained, corresponding almost to the introduced Me^{18}OH for the *O*-alkylation. Consequently, the oxygen atom of the ether function came from the methanol, which was used as a solvent and a reagent.

Two possible reaction mechanisms may be suggested based under these basic conditions: (i) one with the direct regioselective nucleophile attack of the methoxide to the primary hydroxyl group of glycerol (**1**); (ii) one with the regioselective epoxide ring opening (**Scheme 1**). In this case, the glycerol epoxide was an intermediate obtained by successive formation of the glycerolate, followed by an internal nucleophilic addition of the oxygen atom to the carbon atom at position 2 to form the corresponding epoxide.

CONCLUSIONS

A simple batch protocol has been developed for the regioselective *O*-methylation of glycerol in the presence of an inexpensive commercial base K_2CO_3 in subcritical methanol. Moreover, a scale-up of the process can be achieved using autoclaves without a loss in neither reactivity nor selectivity; a 39% yield

was obtained starting from glycerol (**1**, 4.0 g) vs. a 35% yield from the higher amount of glycerol (**1**, 20.0 g). Conventional flash chromatography was carried out with success to obtain the pure target methyl ether without further purification. A mechanistic pathway has been delineated to determinate the origin of the oxygen of the methoxy group, which came from the methanol following the results of the labeled reaction. To date, the additional tests to extend the method to other substrates have not provided significant results (<10%). A more in-depth study is warranted to enhance the scope of the proposed environmentally friendly *O*-alkylation of glycerol to different alcohols in batch reactors as well as in continuous flow operations.

AUTHOR CONTRIBUTIONS

SB, RV, and CL analyzed the bibliography. SB performed the experiment. RV and CL wrote the paper.

ACKNOWLEDGMENTS

REFERENCES

Behr, A., Westfechtel, A., and Perez Gomez, J. (2008). Catalytic processes for the technical use of natural fats and oils. *Chem. Eng. Technol.* 31, 700–714. doi: 10.1002/ceat.200800035

Biermann, U., Friedt, W., Lang, S., Luhs, W., Machmuller, G., Metzger, J. O., et al. (2000). New syntheses with oils and fats as renewable raw materials for the chemical industry. *Angew. Chem. Int. Ed.* 39, 2206–2224. doi: 10.1002/1521-3773(20000703)39:13<2206::AID-ANIE2206>3.0.CO;2-P

Chang, J. S., Lee, Y. D., Chou, L. C. S., Ling, T. R., and Chou, T. C. (2012). Methylation of glycerol with dimethyl sulfate to produce a new oxygenate additive for diesels. *Ind. Eng. Chem. Res.* 51, 655–661. doi: 10.1021/ie201612t

Cucciniello, R., Ricciardi, M., Vitiello, R., Di Serio, M., Proto, A., and Capacchione, C. (2016). Synthesis of monoalkyl glyceryl ethers by ring opening of glycidol with alcohols in the presence of Lewis acids. *ChemSusChem* 9, 1–5. doi: 10.1002/cssc.201600989

DeSousa, R., Thurier, C., Len, C., Pouilloux, Y., Barrault, J., and Jerome, F. (2011). Regioselective functionalization of glycerol with a dithiocarbamate moiety: an environmentally friendly route to safer fungicides. *Green Chem.* 13, 1129–1132. doi: 10.1039/c1gc15053g

Galy, N., Nguyen, R., Blach, P., Sambou, S., Luart, D., and Len, C. (2017a). Glycerol oligomerization in continuous flow reactor. *J. Ind. Eng. Chem.* 51, 312–318. doi: 10.1016/j.jiec.2017.03.020

Galy, N., Nguyen, R., Yalgin, H., Thiebault, N., Luart, D., and Len, C. (2017b). Glycerol in subcritical and supercritical solvents. *J. Chem. Technol. Biotechnol.* 92, 14–26. doi: 10.1002/jctb.5101

Gu, Y., Azzouzi, A., Pouilloux, Y., Jérôme, F., and Barrault, J. (2008). Heterogeneous catalyzed etherification of glycerol : new pathway for transformation of glycerol to more valuable chemicals. *Green Chem.* 10, 164–167. doi: 10.1039/B715802E

Jakubowska, A., Zuchowski, G., and Kulig, K. (2015). Cyclic sulfates as useful tools in the asymmetric synthesis of 1-aminocyclopropane-1-carboxylic acid derivatives. *Tetrahedron Asymmetry* 26, 1261–1267. doi: 10.1016/j.tetasy.2015.09.013

Jiang, G., Inoue, A., Aoki, J., and Prestwich, G. D. (2013). Phosphorothioate analogs of sn-2 radyl lysophosphatidic acid (LPA): stabilized LPA receptor agonists. *Bioorg. Med. Chem. Lett.* 23, 1865–1869. doi: 10.1016/j.bmcl.2013.01.002

Leal-Duaso, A., Caballero, M., Urriolabeitia, A., Mayoral, J. A., Garcia, J. I., and Pires, E. (2017). Synthesis of 3-alkoxypropan-1,2-diols from glycidol: experimental and theoretical studies for the optimization of the synthesis of glycerol derived green solvents. *Green Chem.* 19, 4176–7185. doi: 10.1039/c7gc01583f

Len, C., Delbecq, F., Corpas, C. C., and Ramos, E. R. (2018). Continuous flow conversion of glycerol into chemicals: an overview. *Synthesis* 50, 723–740. doi: 10.1055/s-0036-1591857

Len, C., Merlot, A. S., Postel, D., Ronco, G., Villa, P., Goubert, C., et al. (1996). Synthesis and antifungal activity of novel bis(dithiocarbamate) derivatives of glycerol. *J. Agric. Food Chem.* 44, 2856–2858. doi: 10.1021/jf950751y

Len, C., Postel, D., Ronco, G., Villa, P., Goubert, C., Jeufrault, E., et al. (1997). Synthesis of carbamic esters derivatives of itols: antifungal activity against various crop diseases. *J. Agric. Food Chem.* 45, 3–6. doi: 10.1021/jf9607371

Liu, F., Vigier, K. D. O., Pera-Titus, M., Pouilloux, Y., Clacens, J. M., Decampo, F., et al. (2013). Catalytic etherification of glycerol with short chain alkyl alcohols in the presence of Lewis acids. *Green Chem.* 15, 901–909. doi: 10.1039/c3gc36944g

Nguyen, R., Galy, N., Singh, A., Paulus, F., Stoebener, D., Schlesser, C., et al. (2017). A simple and efficient process for large scale glycerol oligomerization by microwave irradiation. *Catalysts* 7, 123–134. doi: 10.3390/catal7040123

Pariente, S., Tanchoux, N., and Fajula, F. (2009). Etherification of glycerol with ethanol over solid acid catalysts. *Green Chem.* 11, 1256–1261. doi: 10.1039/b905405g

Rafin, C., Veignie, E., Sancholle, M., Postel, D., Len, C., Villa, P., et al. (2000). Synthesis and antifungal activity of novel bisdithiocarbamate derivatives of carbohydrates against *Fusarium oxysporum* f. sp. Lini. *J. Agric. Food Chem.* 48, 5283–5287. doi: 10.1021/jf0003698

Ricciardi, M., Passarini, F., Capacchione, C., Proto, A., Barrault, J., Cucciniello, R., et al. (2018). First attempt to glycidol-to-monoalkyl glyceryl ethers conversion by acid heterogeneous catalysis: synthesis and simplified sustainability assessment. *ChemSusChem* 11, 1829–1837. doi: 10.1002/cssc.201800530

Ricciardi, M., Passarini, F., Vassura, I., Proto, A., Capacchione, C., Cucciniello, R., et al. (2017). Glycidol, a valuable substrate for MAGEs synthesis: a simplified life cycle approach. *ChemSusChem* 10, 2291–2300. doi: 10.1002/cssc.20170 0525

Saggadi, H., Luart, D., Thiebault, N., Polaert, I., Estel, L., and Len, C. (2014a). Toward the synthesis of 6-hydroxyquinoline starting from glycerol via improved microwave-assisted modified Skraup reaction. *Catal. Commun.* 44, 15–18. doi: 10.1016/j.catcom.2013.07.029

Saggadi, H., Luart, D., Thiebault, N., Polaert, I., Estel, L., and Len, C. (2014b). Quinoline and phenanthroline preparation starting from glycerol via improved microwave-assisted modified Skraup reaction. *RSC Adv.* 4, 21456–21464. doi: 10.1039/C4RA00758A

Saggadi, H., Polaert, I., Luart, D., Len, C., and Estel, L. (2015). Microwaves under pressure for the continuous production of quinoline from glycerol. *Catal. Today* 255, 66–74. doi: 10.1016/j.cattod.2014.10.050

Sutter, M., Da Silva, E., Duguet, N., Raoul, Y., Metay, E., and Lemaire, M. (2015). Glycerol ether synthesis: a bench test for green chemistry concepts and technologies. *Chem. Rev.* 115, 8609–8651. doi: 10.1021/cr5004002

Sutter, M., Dayoub, W., Metay, E., Raoul, Y., and Lemaire, M. (2012). Selective synthesis of 1-O-alkyl(poly)glycerol ethers by catalytic reductive alkylation of carboxylic acids with a recyclable catalytic system. *ChemSusChem* 5, 2397–2409. doi: 10.1002/cssc.201200447

Vanlaldinpuia, K., and Bez, G. (2011). Useful methods for the synthesis of isopropylidenes and their chemoselective cleavage. *Tetrahedron Lett.* 52, 3759–3764. doi: 10.1016/j.tetlet.2011.05.050

Varma, R. S., and Len, C. (2018). Glycerol valorization under continuous flow conditions-Recent advances. *Curr. Opin. Green Sustain. Chem.* 15, 83–90. doi: 10.1016/j.cogsc.2018.11.003

Check for
updates

Recent Progress in Synthesis of Glycerol Carbonate and Evaluation of Its Plasticizing Properties

Pascale de Caro[1], Matthieu Bandres[1], Martine Urrutigoïty[2], Christine Cecutti[1] and Sophie Thiebaud-Roux[1]*

[1] Laboratoire de Chimie Agro-industrielle, LCA, Université de Toulouse, INRA, Toulouse, France, [2] Laboratoire de Chimie de Coordination, LCC, Université de Toulouse, CNRS, Toulouse, France

The state of the art on the glycerol carbonate (GC) synthesis has been updated since the last published reviews in 2012, 2013, and 2016. Three types of reactions continue to be studied: glycerolysis of urea, transcarbonation of DMC, DEC, or cyclic carbonates with glycerol and reaction using CO_2. Among these different routes, DMC and glycerol were selected as the raw materials for the GC synthesis in this work since the transcarbonation from these green reagents leads to high yields and selectivities, using mild conditions including a less energy consuming GC separation process. Catalytic conditions using Na_2CO_3 seem to be a good compromise to achieve a high yield of GC, leading to an easier purification step without GC distillation. Mild temperatures for the reaction (73–78°C) as well as a low waste amount confirmed by the E-factor calculation, are in favor of controlled costs. Plasticizing properties of synthesized GC were compared to the behaviors of a commercial plasticizer and natural dialkyl carbonates, for a colorless nail polish formulation. The resulting films subjected to mechanical and thermal stresses (DMA and Persoz pendulum) showed the high plasticizing effect of GC toward nitrocellulose based films, probably due to hydrogen bond interactions between GC and nitrocellulose. The GC efficiency gives the possibility to decrease the content of the plasticizer in the formulation. Glycerol carbonate can be thus considered as a biobased ingredient abiding by the green chemistry concepts, and safe enough to be used in an ecodesigned nail polish formulation.

Keywords: glycerol, glycerol carbonate, transcarbonatation, plasticizer, green chemistry

INTRODUCTION

The global warming of our planet is a major danger for humanity and its environment. Greenhouse gas emissions are the primary cause of this climate change and far from being reduced increases year by year because of the growing of the population. Consequently needs in both food and industrial development regularly increase. In this context, solutions emerge to replace fossil energy sources with renewable energies that are more respectful of the environment. Especially in the transport sector, the biodiesel obtained from plant resources has been developed as a fuel in substitution for traditional petroleum energies. Over the last twenty years, the level of diester production in many countries has led to a significant production of glycerol (GL) as by-product of the process. This crude glycerol is thus produced in large quantities and available on the market at a lost cost.

Among the twelve platform chemicals recommended by the US Department of Energy, glycerol is the fastest growing industrial molecule (Averous et al., 2017)[1].

Glycerol is particularly interesting as a building block to produce bio-based molecules with added value. In the chemicals market, the production of bio-based products has become a priority in the industries of plastics, lubricants, solvents and surfactants: an increase is expected at a CAGR (compound annual growth rate) of 16.67% over the forecast period of 2019–2027 (Global bio-based chemicals market forecast, 2018). Indeed, the manufacture of bio-based molecules offers a good alternative/opportunity to reduce the dependence on petroleum, to improve the environmental balance due to the reduction of CO_2 emissions, to meet the growing of consumers demand for safer and healthier products and for companies, to set themselves apart from the competition.

Among the molecules derived from glycerol, glycerol carbonate (GC) (**Figure 1**), is a five membered cyclic carbonate remarkable for its physical and chemical properties as it gets an interesting chemical reactivity thanks to its two different functions (hydroxyl and cyclic carbonate). Indeed it can be used as a platform molecule to lead to others value-added products which find applications in a wide variety of fields such as cosmetics, detergents, intermediates for chemistry and polymer synthesis as illustrated in **Figure 2**. GC is chemically stable, non-flammable (Flash Point >204°C), water-soluble and presents ecofriendly properties: low toxicity (no R-phrase in its material Safety data Sheet), good biodegradability, very low volatility (bp 110–115°C at 0.1 mmHg) and a high renewable content ranging between 76 and 100% depending on its synthesis route (Clements, 2003).

The development of synthetic routes for obtaining GC follows in parallel the growing interest for its applications (Sonnati et al., 2013). Several conversion schemes exist (**Figure 3**), involving various reagents as a carbonyl source such as phosgene, carbon monoxide, urea, carbon dioxide, or organic carbonates. However, some of these processes are limited because of the toxicity of the reagents and difficulty to implement the chemical reactions, as it is the case for phosgene and carbon monoxide. So in this contribution we provide an overview on the synthesis of glycerol carbonate based on the three main routes: carbon dioxide, urea and organic carbonates including dimethyl carbonate. A focus on the green aspects of the reactions, their industrial feasibility according to the raw material (crude glycerol obtained directly from biodiesel plants or pure glycerol) and an example of one glycerol carbonate application as plasticizer is also given.

MATERIALS AND METHODS

Chromatographic Analysis

For the GC synthesis, the composition of the reaction mixture was analyzed by HPLC, Spectra System P 1500 Spectra-Physics

Analytical. The injector system was Spectra System AS 3000 Spectra-Physics Analytical and the detector was a refractometer (Varian Prostar Model 350 RI detector). The column was apolar (Car-H). The following conditions were used: an eluant corresponding to an aqueous solution of H_2SO_4 (0.004 N), a flow at 0.80 mL/min, a column temperature at 35°C and an injection volume of 20 μL.

For the dialkyl carbonates synthesis, the composition of the reaction mixture was analyzed by GC (Chrompack 9002). An on-column injector and a FID detector were used with a polar column CP WAX 25 m*0.32 mm*1.2 μm. Samples were diluted 1,000 times in acetone.

Synthesis of Glycerol Carbonate

Dimethyl carbonate (DMC) (45 g, 0.5 mol), 15.3 g glycerol (0.167 mol) and 0.053 g Na_2CO_3 (5.10^{-4} mol) were introduced simultaneously into a 250 mL three-neck flask equipped with a condenser, a temperature sensor and a mechanical stirring system. The mixture was stirred and refluxed (75°C). After 2 h of reflux, the conversion rate of glycerol, measured by HPLC, reached 98%. After cooling the reaction medium, the catalyst was filtered off on Buchner and the excess of dimethyl carbonate and the methanol formed were distilled under atmospheric pressure. The glycerol carbonate was obtained as a colorless viscous liquid (19.7 g) with a purity of 98%.

^{1}H NMR (400 MHz, CDCl$_3$): δ (ppm) = 5.29 (t, 1H, OH), 4.82–4.77 (m, 1H, CH), 4.49 (dd, 1H, OCH_2), 4.29 (dd, 1H, OCH_2CH), 3.66 (ddd, 1H, CH_2OH), 3.49 (ddd, 1H, CH_2OH).

Synthesis of Dialkyl Carbonates

In a 250 mL three-neck reactor connected to a long distillation column and equipped with a mechanical stirrer and a thermometer, were added 10 g of DMC (10.111 mol), 49 g of isoamyl alcohol (0.555 mol), and 5 g K_2CO_3. The mixture was heated for 4 h at 140°C corresponding to a high reflux in the reactor. A mixture of DMC-methanol azeotrope of mass composition 30–70 was recovered at the top of the distillation column ($T = 63$–64°C). The kinetic of the reaction was followed by gas chromatography and the reaction was stopped when DMC has totally reacted. The diisoamyl carbonate was obtained with a selectivity of 99% relative to the intermediate carbonate. A distillation under reduced pressure (92–94°C, 3.8 mmHg) led to
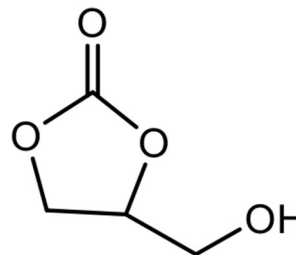
FIGURE 1 | Structure of the glycerol carbonate (GC).
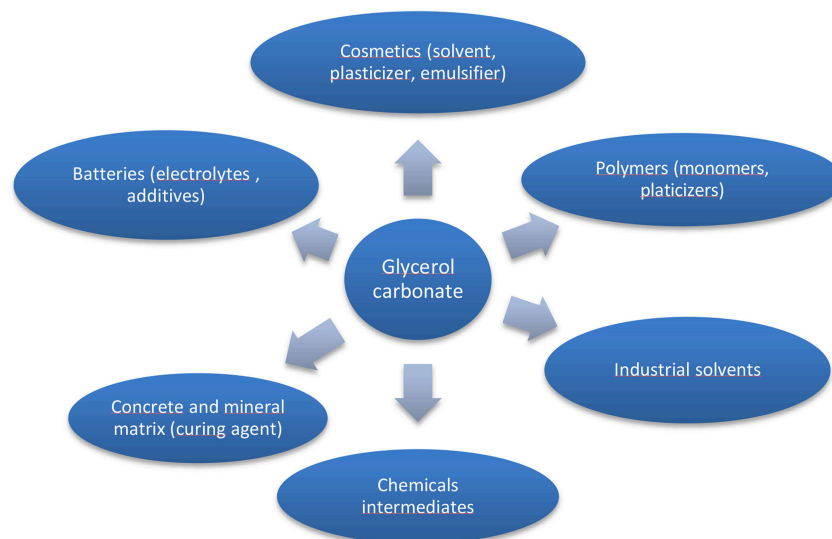
FIGURE 2 | Applications of glycerol carbonate (adapted from references Sonnati et al., 2013; Algoufi et al., 2017).
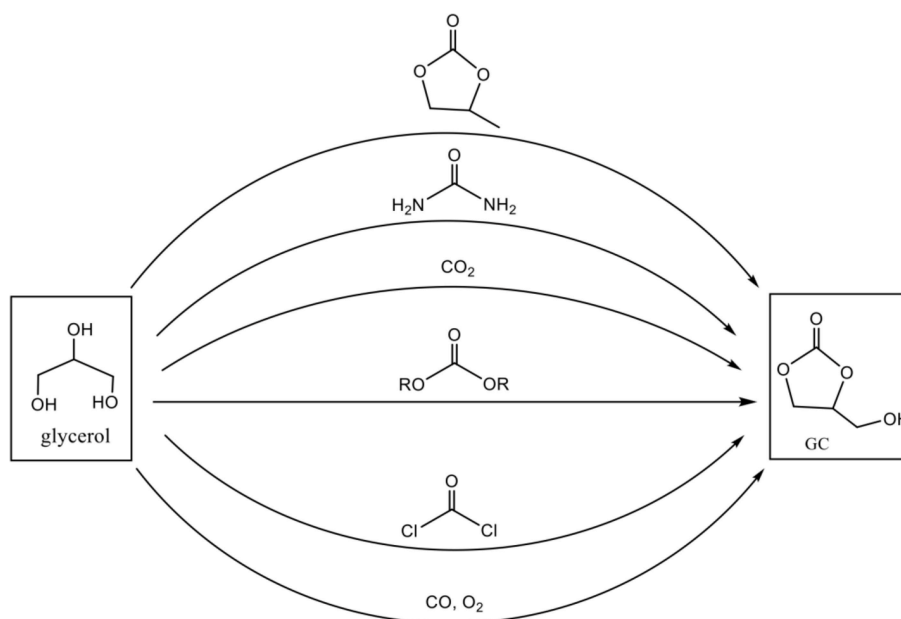
FIGURE 3 | Different conversion routes for synthesis of glycerol carbonate (adapted from reference Van Mileghem et al., 2018).

diisoamyl carbonate (17.44 g, overall yield 76%) in the form of a colorless and odorless liquid.

^{1}H NMR (400 MHz, CDCl$_3$): δ (ppm) = 4.11–4.12 (t, 2H, OCH_2), 1.69–1.71 (dd, H, CH), 1.55 (t, 2H, OCH$_2$CH_2), 0.90–0.92 (d, 6H, CH$_3$).

Synthesis of Didodecyl Carbonate

In a 250 mL three-neck reactor connected to a cooler, equipped with a mechanical stirrer and a thermometer, were added 15 g of DMC (0.167 mol) and 93.2 g of dodecanol (0.5 mol) and 5 g of K$_2$CO$_3$. The mixture is heated for 5 h at reflux of DMC. These conditions led to the symmetrical carbonate with a selectivity of

85% relative to the mixed carbonate. The purification is carried out by distillation under reduced pressure (180°C, 1 mbar) to distill only the dodecanol and recover a mixture of composition (dilauryl carbonate: methyl lauryl carbonate 94: 6). 33.3 g of dilauryl carbonate (48%) is obtained as a viscous colorless liquid.

^{1}H NMR (400 MHz, CDCl$_3$): δ (ppm) = 4.12 (t, 2H, OCH_2), 1.55 (t, 4H, OCH$_2$CH_2), 1.26–1.32 (m, 18H, CH$_2$), 0.87–0.90 (t, 3H, CH$_3$).

Pendulum Hardness Test

Persoz hardness is measured with a pendulum of Persoz according to the protocol that meets the standards ASTM D
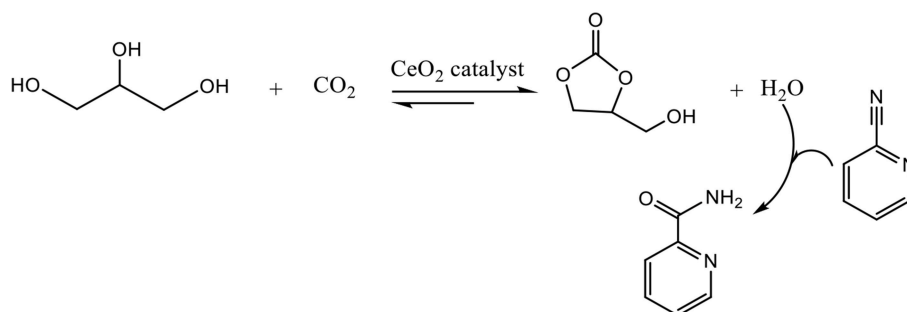
FIGURE 4 | Reaction of glycerol and CO_2 with CeO_2 in presence of 2-cyano-pyridine.

4366 and EN ISO 1522. The apparatus used is an ERICHSEN Pendulum Damping Tester model 299/300. Oscillations of a pendulum in contact with the tested surface have a damping time directly proportional to the hardness of this surface.

A 300 μm wet film was applied to a glass plate. The measurements were made at regular intervals (30 min, 1, 2, 4, 24 h) after drying the varnish film in a thermostatically controlled chamber at 20°C. The plasticizing properties of a molecule is therefore inversely proportional to the number of oscillations made by the pendulum.

Dynamical and Mechanical Temperature Analysis (DMA)

The sample was prepared by pouring the formulation into a teflon matrix and then dried on a plate thermostated at 30°C for 24 h under room humidity. Specimens (200 μm thick, 10 mm wide and 7 mm long) were cut from the resulting molded film. A pre-stressing of 0.5 N was imposed on the sample before the beginning of the measurement in order to put the film under tension. Tensile tests and small deformations were applied at the 1 Hz frequency while imposing a sinusoidal displacement of 8 microns. The sample was subjected to a temperature sweep (3°C/min) over the range −50 to 60°C.

RESEARCH UPDATE ON GC SYNTHESIS

Synthesis of GC From Glycerol and CO_2

The use of CO_2 as C1 chemical feedstock to prepare useful products such as organic carbonates, methanol and polycarbonates on a large scale would be ideal for industrial applications, resulting in the consumption of million tons of CO_2 per year (Dabral and Schaub, 2019). Performing CO_2 conversion is a great promise for recycling CO_2, as only a small proportion of the total abundance is currently being consumed by the chemical industry (Song Q. W. et al., 2017). Therefore, preparation of GC directly from glycerol and CO_2 is an ideal strategy for dealing with these two by-products, commercially available at low price. The atom efficiency of the reaction could be high if we consider H_2O as the only side product. Thus, much attention has been focused on this reaction which is in line with the concept of green and sustainable development.

The direct carbonylation of glycerol with CO_2 was carried out in homogeneous and heterogenous catalysis. The first experiments in presence of metal alkoxides such as n-$Bu_2Sn(OMe)_2$ and n-Bu_2SnO, were done using various experimental conditions (Aresta et al., 2006). Unfortunately, the reaction was unsuccessful with low conversion of glycerol due to the low CO_2 reactivity. Moreover, the original catalysts were converted into oligomers showing a moderate catalytic activity. When the same reaction was carried out in methanol as solvent, the yield was increased to 35% (George et al., 2009). Following these poor results and the thermodynamic stability and kinetic inertness of CO_2, solid metallic oxides were used for their potential activity in the transformation of CO_2 due to the surface adsorption and activation of CO_2.

CeO_2 nanoparticles or nanorods were employed as catalyst in the presence of 2-cyanopyridine, which was used as a dehydration reagent to remove water and shift the chemical equilibrium to the glycerol carbonate side (**Figure 4**) (Liu et al., 2016). 2-cyanopyridine reveals to be a better dehydrant than acetonitrile which can gives the formation of by-products with the resulting hydrolysis product and glycerol (Li et al., 2015). Moreover, the hydration of the resulting amine into acid does not occur over CeO_2 catalysts resulting in a higher selectivity toward GC (Liu et al., 2016).

The system showed good catalytic performances in the carbonylation of glycerol and CO_2 with the efficient hydration of 2-cyanopyridine and solvent effect of DMF, obtaining a 21% yield of GC. The redox properties of CeO_2 played an important role on the activity. The reaction conditions were 3 times the stoichiometric value of 2-cyanopyridine, 150°C, 4 MPa and 5 h. The catalyst could be easily recycled through the calcination process at 400°C for 5 h, and the activity of the regenerated catalyst stayed constant after recycling for five times. To enhance the catalytic performances, Zr doped CeO_2 was used and the influence of molar ratio of Zr/Ce on the crystalline structure, surface composition, redox and acid-base properties were studied (Liu et al., 2018). The conversion of glycerol increases to 40% and the yield of GC to 36.3% in presence of a 0.02 molar fraction of Zr. This good performance is explained by the acid-base properties of the catalyst, knowing that the Lewis acid sites are appropriate to the absorption and activation of OH

FIGURE 5 | Reaction of glycerol in presence of CO_2 and PO.

FIGURE 6 | Reaction of glycerol in presence of urea and urea synthesis from NH_3 and CO_2.
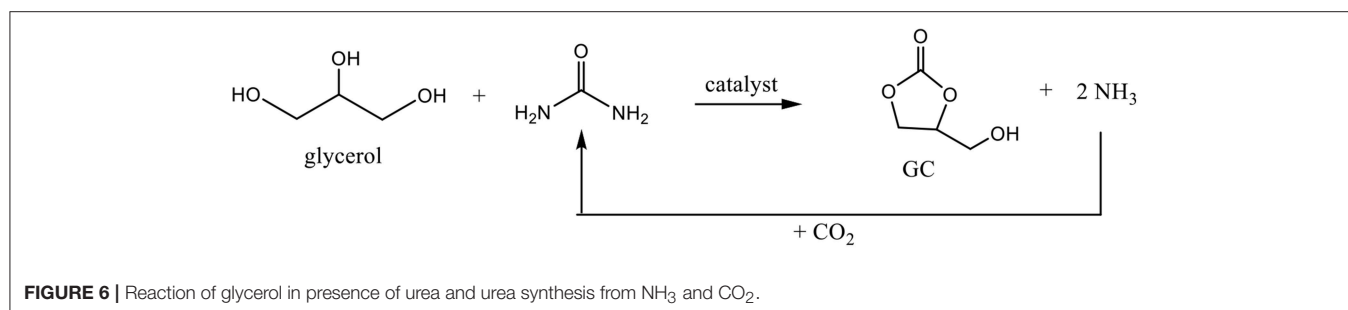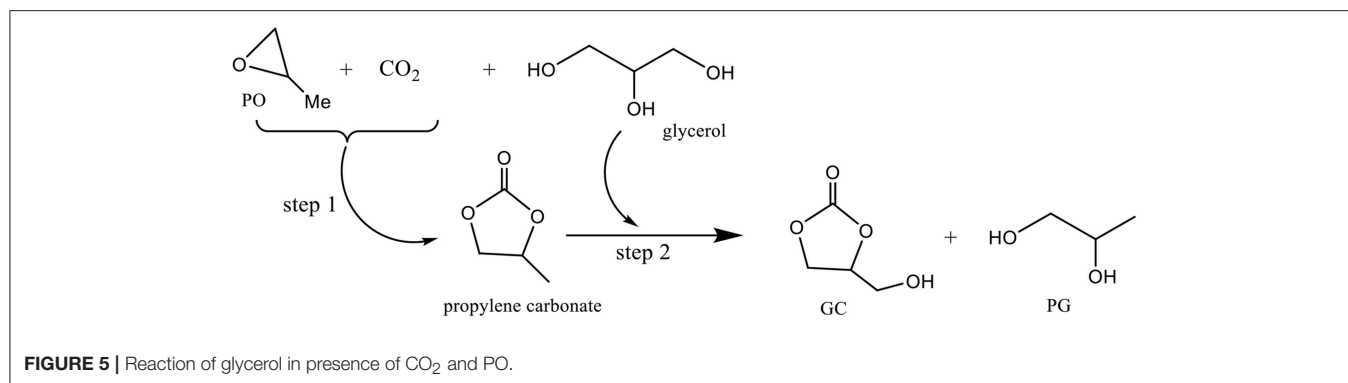
group of glycerol and the basic sites favor the CO_2 absorption and activation.

Besides acetonitrile and 2-cyanopyridine introduced as chemical dehydrating agents to eliminate the formed water, 13X zeolite and molecular sieves were used as physical dehydrating agents to absorb water but the results were unsatisfactory (George et al., 2009). New strategies have emerged for the carbonylation of glycerol with CO_2. Pioneering work on the preparation of GC using KI as a highly efficient homogeneous catalyst and propylene oxide (PO) as a coupling agent to make the reaction thermodynamically favorable has been published (Ma et al., 2012). The coupling reaction between PO, glycerol and CO_2 consists of a cycloaddition of CO_2 with PO (step 1, **Figure 5**) and a subsequent transesterification of glycerol with carbonate to form GC and propylene glycol (PG) (step 2, **Figure 5**). The simultaneous conversion of glycerol and CO_2 via the coupled reaction can be carried out very effectively using KI as the catalyst since 78% glycerol conversion was achieved with a yield of 40% glycerol carbonate. Despite the good catalytic performance of KI, its usage is limited due to the difficulty in separating it from the reaction system.

Therefore, an efficient strategy for developing a heterogeneous, reusable and easily recoverable catalyst from the reaction system has been studied (Song et al., 2018). A functionalized heterogeneous catalyst was developed by introduction of imidazole-based ionic liquids into the structure of a DVB-based polymer showing, in presence of PO, a satisfying activity toward both the coupling of PO with CO_2 and the transesterification of PC with glycerol could be achieved, implying the high catalytic performance of ionic liquid groups in the coupling reaction of PO with CO_2. The conversion of

PO reached up to 96% with a GC yield of 81% in presence of the prepared PDVB-(vIm-BuBr) catalyst. Moreover, this latter showed excellent stability during the reaction, and maintained its catalytic activity after five cycles. The high activity and remarkable stability of this heterogeneous polymer P-DVB-(vIm-BuBr) catalyst represent interesting features for future industrial applications.

Synthesis of GC From Glycerol and Urea

Beside the direct synthesis of GC from glycerol and CO_2, the exploration of another indirect synthesis approaches using urea as a CO_2 donor may simplify the glycerol production and may lead to a more economical process (Claude et al., 2000; Nguyen and Demirel, 2013). Urea glycerolysis represents an attractive alternative method to produce GC because it is a biobased reactant containing an activated form of CO_2. The reaction was run under a reduced pressure in order to remove the ammonia formed during the reaction and move the equilibrium to a maximum conversion. Furthermore, ammonia formed can be easily converted to urea since urea synthesis is performed from ammonia and carbon dioxide (**Figure 6**).

Heterogeneous catalysts have been developed and they have been particularly efficient for carbonylation of glycerol with urea affording good yield under moderate reaction conditions. Recently the carbonylation of glycerol with urea was reported at 145°C using MgO and CaO basic oxides, Al/Mg and Al/Li mixed oxides derived from hydrotalcites with adequate acid–base pairs. About 72% of glycerol carbonate yield was achieved in 5 h of reaction time with 82% of glycerol conversion (Climent et al., 2010). The results showed that catalysts exhibiting adequate acid-base properties were efficient to the synthesis of GC. The effect

of Zr doping on the acidic-basic properties of calcined Mg-Al hydrotalcite and their catalytic performance for the GC synthesis have been demonstrated as a 85% yield of GC could be obtained with a glycerol conversion of 97% and a selectivity of 90%. The Zr content could affect significantly the acidic-basic property (Wan D. et al., 2018).

The impact of these acidic and basic properties had already been shown in the study involving γ-zirconium phosphate catalyst exhibiting about 80% glycerol conversion with 100% selectivity toward GC (Aresta et al., 2009). The presence of Lewis acid sites able to activate the carbonyl group of urea makes the nucleophilic attack of the glycerol absorbed on the Lewis basic sites easier. The reaction mechanism describing the role of the basic and acidic active sites is proposed by Fernandes and Yadav (2013) based on their experiment observations and the effect of different parameters during their study on the glycerolysis using combustion synthesized magnesium oxide as catalyst. A well-balanced acidic-basic property was important to obtain high GC yield with good selectivity.

A series of tin-tungsten mixed oxides with different Sn to W molar ratio were synthesized and characterized by various spectroscopic techniques and were involved in the carbonylation of glycerol (Jagadeeswaraiah et al., 2014).The catalysts were active for selective formation of glycerol carbonate and the best one was the catalyst Sn/W ratio 2:1 calcined at 500°C giving 52% glycerol conversion with >99% GC selectivity. The catalyst without any pre-treatment was recycled with a consistent activity.

An interesting study on a green co-generation of high purity of zinc glycerolate and glycerol carbonate was published using glycerol as reactant and as a raw material to prepare the catalyst (Zhang et al., 2016) The zinc glycerolate obtained by mixing Zn acetate with glycerol was decomposed to ZnO by calcination. ZnO was highly active toward the reaction, yielding 85.97% of GC. The study revealed that the ZnO catalysts have the advantages of high activity, high recyclability, high stability, and environmental friendliness that can be appropriately applied in industrial settings.

The dual catalysis over ZnAl mixed oxides consisting of ZnO and ZnAl$_2$O$_4$ phases was investigated. The ZnAl mixed oxides showed much higher glycerol conversion and GC yield than the ZnO and ZnAl$_2$O$_4$. The ZnO phase provided a homogeneous reaction route via the dissolved Zn species, resulting in the zinc isocyanate Zn(NCO) complex formed in the liquid phase suggested as a main active site (Fujita et al., 2013). The Zn(NCO) complex also adsorbs on the ZnAl$_2$O$_4$ phase and acts as a supplementary heterogeneous active site, in addition to the original Lewis acid-base active site of ZnAl$_2$O$_4$. The combination of these homogeneous and heterogeneous reaction routes enhances the catalytic performance of the ZnAl mixed oxide (Nguyen-Phu et al., 2018).

Despite these many promising results achieved in the study in the urea glycerolysis, most of the works either utilized commercial glycerol as a starting material. Indeed the main reason is due to the presence of impurities in the crude glycerol which can affect the transformation of glycerol into the targeted value-added product. Few studies have been reported on the production of GC through the direct use of crude glycerol.

Recently, an economical and green synthesis approach using boiler ash (BA) from palm oil industry as catalyst for the reaction of producing GC from crude glycerol and urea, has been studied (Paroo Indran et al., 2014). It was the first example on the use of waste material, containing many metals of those being major are potassium, calcium, and magnesium, as catalyst for the production of GC. Various catalysts calcinated at different temperatures showed relatively comparable glycerol conversion of about 90%. The potassium silicate BA 900 (calcination at 900°C) gave the highest GC selectivity and yield of 90 and 84.3% respectively. The authors explained this result by the presence of potassium ion (higher metal content with a percentage of 86%) which acts as a weak Lewis acid to catalyze the reaction. Moreover, the presence of oxide ion (O^{2-}) certainly plays a role of strong base to activate glycerol to form GC. In a similar study, boiler ash containing BA 900 and potassium silicate (K$_2$SiO$_3$) were proven to be feasible Lewis acid catalysts for the synthesis of GC. The catalytic system was reusable for three consecutive reaction cycles without the loss of activity (Indran et al., 2016). In another study, the same catalytic system was involved in the glycerolysis of crude glycerol from two different sources obtained from the commercial biodiesel plant depending on the catalyst used either sodium methylate or potassium methylate (Paroo Indran et al., 2017) The results confirmed the activity of the catalytic system but the selectivity and yield C are lower than those obtained using commercial glycerol. The water and methanol present in the crude glycerol, even in small quantities, are responsible, knowing the instability of GC in water and methanol can cause decomposition of GC into glycidol (Teng et al., 2014). Nevertheless, the current results suggest that the crude glycerol can be directly transformed using boiler ash as catalyst, even if the optimal yield of GC cannot be obtained. This study is interesting because it represents an example of a totally green synthesis approach.

Transcarbonatation of Alkyl or Cyclic Carbonate With Glycerol
Chemical Catalysis

Glycerol carbonate (GC) can also be synthesized by transesterification of cyclic carbonates (most often ethylene or propylene carbonate) or aliphatic carbonates (dimethyl carbonate or diethyl carbonate) (**Figure 7**) with glycerol in the presence of a basic catalyst, the acid catalysts having proved to be slightly effective (Teng et al., 2016). The addition of solvent is not necessary since the carbonates, reactants in excess of glycerol, also play the role of solvent in these transcarbonation reactions. This excess (carbonate:glycerol molar ratio generally between 2:1 and 5:1) makes it possible to shift the reaction equilibrium toward GC synthesis: this method is more effective than the addition of molecular sieves to remove the methanol formed (Lanjekar and Rathod, 2013).

Numerous synthesis conditions of this transcarbonation reaction have been compared in the reviews of Ochoa-Gómez et al. (2012); Sonnati et al. (2013), and Teng et al. (2016), and in particular, the basic catalysts. For transesterification reactions from dimethyl carbonate DMC or diethyl carbonate
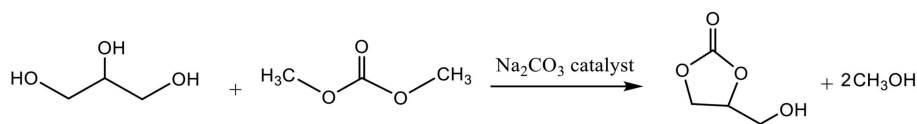
FIGURE 7 | Transcarbonatation of glycerol with dimethyl carbonate.

DEC were tested CaO, MgO, K_2CO_3, $CaCO_3$, KOH, NaOH, K_2CO_3/MgO, Mg/Al/Zr mixed oxides, Al/Mg hydrotalcites, KF-hydroxyapatite, lipases and ionic liquids including 1-n-butylimidazole (Naik et al., 2009). It is important to point out that this latter catalyst allows to convert efficiently crude glycerol (purity of 88 wt%–contaminants: water and traces of alkaline salts) while most of the syntheses have been studied from pure glycerol or containing <2% water (Rokicki et al., 2005). Water can cause deactivation of catalysts such as extruded CaO/Al2O3 (Lu et al., 2013). However, according to Bai et al. (2011), the KF-hydroxyapatite-based catalyst may not be degraded by the presence of water and soap, which suggests that synthesis of GC from crude glycerol could be achieved without the need to implement an expensive distillation process after the production of biodiesel.

For reactions from ethylene carbonate (EC), the catalysts CaO, Al/Ca mixed oxides, Li-hydrotalcite, basic resins of the type Amberlyst A26 (HCO_3^-), immobilized ionic liquids have been studied (Ochoa-Gómez et al., 2012; Sonnati et al., 2013; Teng et al., 2016). The results have shown that regardless of the homogeneous or heterogeneous basic catalyst tested, conversions of glycerol and reaction selectivities are high: conversions are >95% from DMC and >85% from EC and selectivities are generally ranged between 95 and 99% from DMC and between 84 and 99% from EC. According to (Ochoa-Gómez et al., 2012), the transcarbonation route from DMC or EC with glycerol is suitable for industrial production and involves uncalcined CaO as this heterogeneous catalyst is cheap and can be easily separated by filtration. Although its performance is slightly lower than that of the calcined catalyst due to the presence of impurities such as $Ca(OH)_2$ and $CaCO_3$, the calcined catalyst is deactivated and must be regenerated after reaction.

Although the reaction temperatures used are lower for the transcarbonation of EC with glycerol (35–80°C vs. 75–120°C for the reaction with DMC) due to a decrease in the constants of chemical equilibrium as a function of temperature (Li and Wang, 2011), DMC could be preferentially selected industrially (Hirotsu and Kaneko, 2001; Hérault et al., 2003) because the purification step of the GC is less energy consuming. Indeed, the boiling temperatures of DMC (90°C) and methanol (65°C) are much lower than those of EC (261°C) and ethylene glycol EG (197°C). In addition, reactions with DMC are usually carried out at atmospheric pressure while, for reactions from EC, a reduced pressure (35 mmHg) is often applied to remove EG and displace reaction equilibrium.

Since 2014, the date of the last review on the synthesis of glycerol carbonate, other work about transcarbonatation with

glycerol has been published and highlight the strong catalytic activity of other bases such as:

- The calcined silicates (Wang et al., 2017) (Na_2SiO_3) that can be reused 5 times without significant decrease of its catalytic activity,
- Li doped La_2O_3 (Li Y. et al., 2018) or ZnO (Song X. et al., 2017) or $Mg_4AlO_{5.5}$ (Liu et al., 2015). Li doping was shown to improve the catalytic activity due to its positive effect on the basic properties and the interaction between Li and the metal oxide supports.
- Other mixed oxides catalysts such as Ce-NiO (Wu et al., 2017), CeO_2-CdO (Wu et al., 2018), Sr/Al mixed oxides and in particular the catalyst With Sr/Al ratio of 0.5 (Algoufi et al., 2017): high reaction selectivity (91–100%) and glycerol conversion (94–97%) were also obtained for the GC synthesis from diethyl carbonate (instead of DMC) for the two former catalysts.
- Basic resins such as Ambersep® 900 (hydroxide functional resin) filling glass column reactor in a continuous flow process. High glycerol conversion and reaction selectivity with a short residence time (10 min) are resulted from this process (Van Mileghem et al., 2018).
- DABCO embedded porous organic polymer (Wan Y, et al., 2018): the efficiency of this catalyst can be explained by its porous structure and its amphiphile characteristic which is supposed to make a miscible microenvironment while reactants are immiscible. It has been reused up to 13 times without obvious deactivation.

All the studies using all heterogeneous catalytic materials previously mentioned show the key parameters for a catalyst to be effective in GC synthesis: the strength of basic sites and the porous structure allowing mass transfer and diffusion of reagents to active sites (Okoye and Hameed, 2016).

- Amidines based ionics liquids (Ishak et al., 2017). The results depend on both cation and anion used, knowing that the anion activates hydroxyl groups of glycerol through an hydrogen bonding interaction (Ishak et al., 2016). 1,8-diazabicyclo[5.4.0]undec-7-ene (DBU) based ionic liquid was proved to be the best catalyst for converting 98% glycerol to produce GC with a selectivity of 96% and a high turnover number (TON = 9408 within 7.5 h and 0.01 mol% of catalyst loading) (Munshi et al., 2014a,b).
- Homogeneous ammonium catalysts: tetraethylammonium pipecolinate gives the best results in terms of glycerol conversion and reaction selectivity (Van Mileghem et al., 2018).

Biocatalysis

Another catalytic route of glycerol transesterification reactions with DMC to synthesize GC is the biocatalytic route with the use of lipase type enzymes. These reactions under kinetic control lead to high yields according to the experimental conditions. Studies showed (Du et al., 2018) the optimization of the reaction with the immobilized *Candida Antartica* lipase B as biocatalyst at a concentration of 5 g/L, a GL/DMC molar ratio (1:20), at 50°C. After 24 h the yield in GC is 89%. Under these conditions the authors showed that the presence of organic solvents could be harmful to the reaction and worked in a solvent-free system.

Netherless other authors (Jung et al., 2012) relate the positive effect of hydrophilic solvents, such as THF, tert-butanol, and acetonitrile. These solvents would play a favorable role by reducing the coating effect of insoluble glycerol on the surface of the immobilized enzyme. Thus, a maximum yield of 77% could be achieved with the solvent acetonitrile and the surfactant Tween 80 helping the mixing of the reagents. On the other hand, hydrophobic solvents such as hexane, toluene, and xylene did not allow the reaction.

The role of water in the biocatalytic transformation of GL is not so obvious (Kim and Lee, 2018): beyond 0.5% v/v it seems to have a negative effect on the reaction by inhibition of enzymatic activity. However, small quantities of water could play a positive role by improving interfacial availability by preserving the 3D structure of the enzyme in non-aqueous media.

If we switch to the feasibility of achieving the biocatalytic conversion of crude glycerol to GC, the adverse effect of water on enzyme activity by hydrolysis could be effectively reduced through pre-treatment processes, keeping a low amount of moisture favorable to the reaction by improvement of the enzymatic catalytic activity. Thus, prospects for the use of crude glycerol containing traces of water for biocatalyzed reactions (Tudorache et al., 2014; Luo et al., 2016 are opened, whether for the synthesis of GC or other value-added chemicals.

Crude Glycerol as Starting Material

The transformation of crude glycerol into hydrogen, polyglycerols, epichlorohydrin, or polyols for polyurethane foam synthesis can be interesting and competitive in comparison with results obtained from pure glycerol (Kong et al., 2016). This added value finds a significant meaning with the esterification or transesterification reactions like in glycerol carbonate synthesis.

During the production of biodiesel, the crude glycerol obtained as a byproduct has a very different composition depending on the technology used or the sourcing of the oils. The glycerol content can vary from 30 to 70% depending on the process and the oil and reaches 80% after acid treatment (Nanda et al., 2014; Kong et al., 2016). The main impurities present which can interfere with the transformation of crude glycerol, are water, methanol, soaps, free fatty acids (FFAs), fatty acid methyl esters (FAMEs), glycerides, and ashes. The

TABLE 1 | Compositions of colorless nail polishes.

Ingredients	Composition 1 (%)	Composition 2 (%)
Solvents*	62.6	59.1
Isopropanol	14.4	–
Nitrocellulose	10.2	17.9
Polyester resin	7.2	13.3
Plasticizer	5.6	9.9

*A mixture of ethyl acetate, butyl acetate and isopropanol.

FIGURE 8 | Continuous process proposed for glycerol carbonate production.
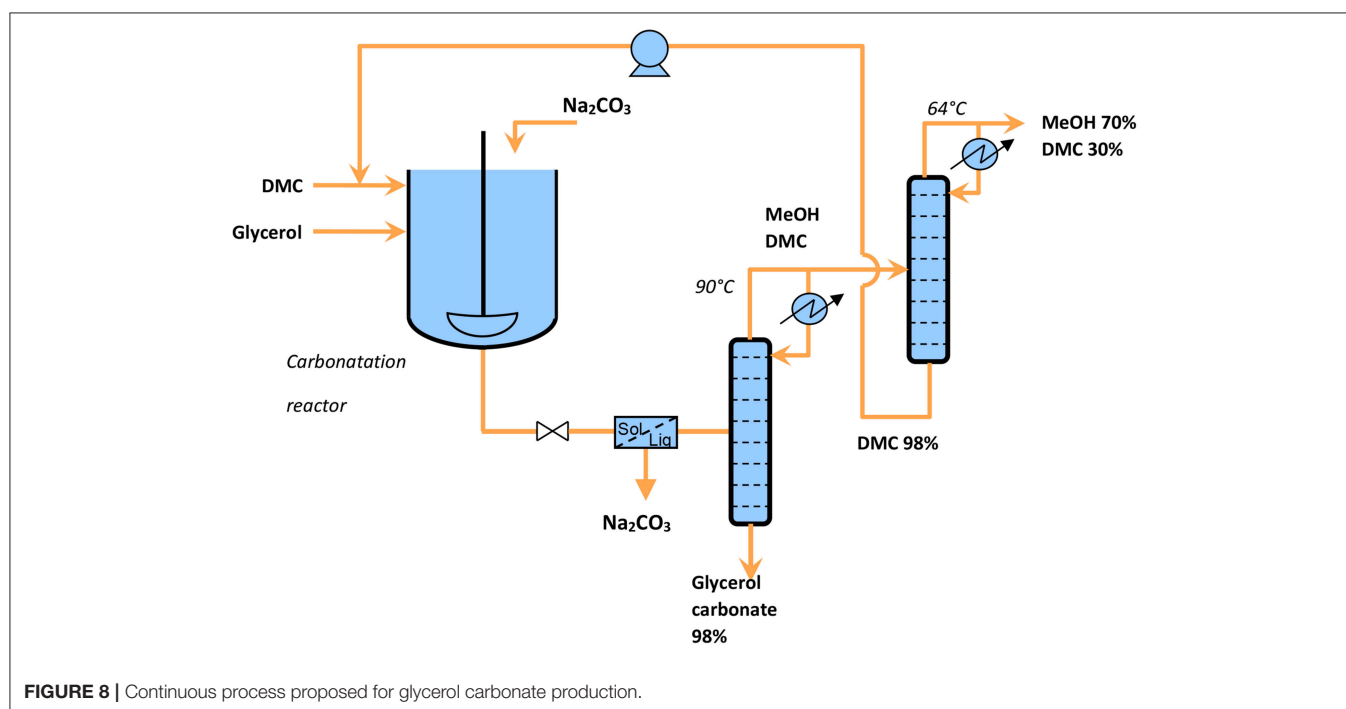
economic advantage of the use of crude glycerol has led to a deeper knowledge (Hu et al., 2012) of these impurities and the understanding of their effects on glycerol performance, especially during transesterification reactions.

Studies show that from 10% w/w of water, GC becomes instable and has a significant influence on crude glycerol conversion (Paroo Indran et al., 2017). Similarly, a 5% w/w methanol content interferes with the selectivity of the reaction.

But these conditions are extreme and in reality the crude glycerol may not reach this content of impurities. On the contrary, the potassium and calcium methylate residues resulting of the biodiesel production process, can effectively act as a catalyst in its transformation into GC. In fact, very high conversion and selectivity rates have been demonstrated on PG by a joint effect of Ca and Mg species in the catalyst structure (Zheng et al., 2015).

CaO is a very good catalyst in transesterification reactions and can be easily used in industrial processes. For example, GC synthesis from crude glycerol containing 1% CaO with a 2: 1 ratio of DMC / glycerol is optimized with microwave activation for 5 min at 65°C to give a 93% yield, while under the same conditions the pure glycerol leads to only a 5% yield after 90 min of reaction (Teng et al., 2016). These better performances of crude glycerol transesterification compared with pure glycerol are also shown with conventional heating activation conditions (84 vs. 10%).

RESULTS AND DISCUSSION

A New Catalyst System for Transcarbonatation of Glycerol

Although in terms of sustainable chemistry, CO_2 is a reagent of choice for GC synthesis, its reaction with methanol is thermodynamically limited, which leads to relatively low conversions and yields compared to other methods of GC synthesis. As for the glycerolysis process of urea, a reduced pressure in the reactor is necessary to remove the ammonia and shift the equilibrium. In addition, the GC purification process coupled to this reaction tends to be the most complex because it requires a multistep GC purification process (liquid-liquid extraction, evaporation and then vacuum distillation).

In this work, we preferred to use the DMC for the GC synthesis because the transcarbonation involves mild conditions and leads to high yields and selectivities. We can also expect the GC separation process to be less energy consuming than the one using cyclic carbonates because of the higher boiling points of cyclic alkylene carbonates and byproducts (glycols).

To test the properties of glycerol carbonate as a plasticizer for a nail polish, glycerol carbonate has been synthesized by transcarbonatation with DMC, with a heterogeneous catalyst.

Unlike K_2CO_3, the catalysts CaO and Na_2CO_3 are insoluble in the hot medium composed of DMC, glycerol and glycerol carbonate. Note that a supported catalyst K_2CO_3/MgO prepared by dry impregnation was also tested with good results (Du et al., 2012).

It was found that 3 wt. % of CaO (relative to glycerol weight) added to a DMC to glycerol molar ratio of 3:1, gave a GC yield of 92% after 2 h, a yield measured without isolating the synthesized GC (Roschat et al., 2018). When the reactant molar ratio was 1:1, an azeotropic agent (benzene) was used to remove continuously the produced methanol during the reaction (Li and Wang, 2010). In these conditions, it was

TABLE 2 | Glass transition temperatures of the nitrocellulosic films according to the plasticizer.

Plasticizer	T_g obtained by DMA (°C)
No plasticizer	38.7
Diisoamyl carbonate	36.5
Dilauryl carbonate	35.2
Ethylene carbonate	30.9
Propylene carbonate	26.1
Acetyl tributyl citrate	22.3
Glycerol carbonate	17.4
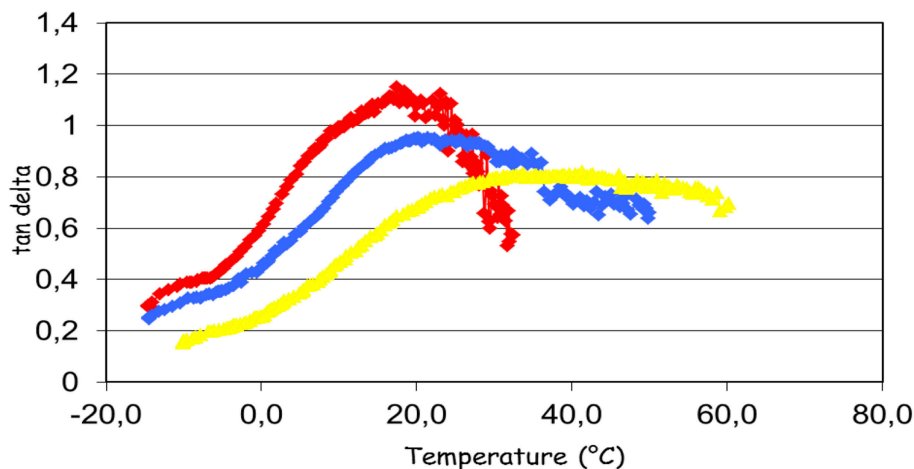
FIGURE 9 | Effect of plasticizers on glass temperature of nitrocellulosic films. Tg = 17.4°C no plasticizer (red line); Tg = 22.3°C with addition of acetyl tributyl citrate (blue line); Tg = 38.7°C with glycerol carbonate addition (yellow line).

FIGURE 10 | Effect of the plasticizers on the Persoz hardness. ✗ no plasticizer, ■ diisoamyl carbonate, ▲ dilauryl carbonate, ◆ acetyl tributyl citrate, ● glycerol carbonate.
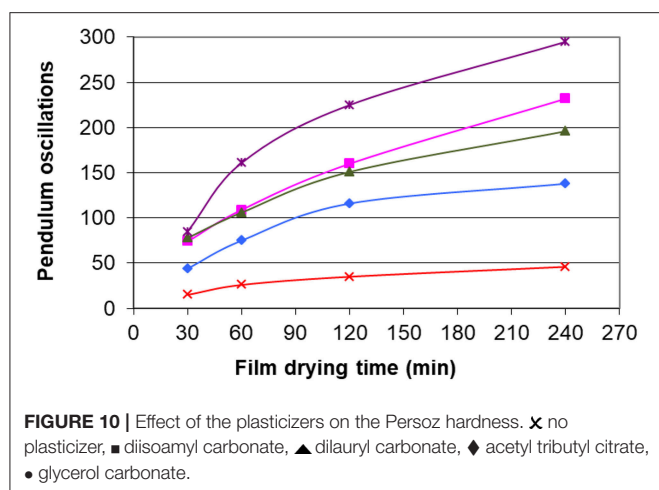
possible to reach a GC yield of 98% with a CaO: glycerol molar ratio of 2%.

Another work (Li W. et al., 2018) proposed the perevaporation as an alternative technology to purify the final medium resulting from transesterification between glycerol and dimethyl carbonate. It was thus possible to separate the four components of the mixture (methanol as a by-product, DMC in excess, non-reacted glycerol and GC) and to break the methanol:DMC azeotrope. However, it was concluded that the selective recovery of methanol remains a future objective.

The reaction was implemented with the selected catalyst, Na_2CO_3 (2.9 wt%), with a ratio DM: glycerol equal to 3, under a reflux at 75°C for 2 h. This system showed a great efficiency since glycerol conversion reached 98% (Bandres et al., 2010).

This process presents several advantages compared to usual processes since it generates pure glycerol carbonate (low residual glycerol). Catalyst was recovered by filtration before the distillation of a light fraction composed of MeOH:DMC (azeotrope at 63.5°C).

Calculation of green metrics leads to an atom economy of 65%, an environmental factor of 0.77 and a reaction mass efficiency of 56%. These results can be compared with the performances of same reaction catalyzed by K_2CO_3, generating lower green metrics (AE = 43%, RME = 29.5%) and a higher e-factor (E-factor = 2.4). The heterogeneous process using urea and catalyzed by Zn_2CO_3, has only improved atom economy (AE = 77%), while E-factor = 1.7 and RME = 37% are once again penalized.

For the reaction catalyzed by Na_2CO_3, the easy purification and the low production of waste lead to a very interesting E-factor (and a high reaction mass efficiency), conditions which are suitable for scaling-up. The collected data allow to design a continuous process as shown in **Figure 8**. The reactor outlet flow analyzed by HPLC, is composed of glycerol (0.5%), glycerol carbonate (32.1%), dimethyl carbonate (50.1%), and methanol (17.3%). The second distillation column allows to separate the excess of DMC to recycle it as a reactant. GC collected at the bottom of the distillation column was a viscous, colorless liquid with a purity of 98%. Moreover, these operating conditions, in

particular in terms of reduced wastes and moderate temperatures, seem to meet the technical and environmental requirements expected by industry.

Assessment of GC Plasticizing Properties

Glycerol carbonate was already used as a plasticizer of polymer electrolyte (Yuan, 2015). During the polymerization, glycerol carbonate was added to P(AN-MMA) to form the gel electrolyte. The effect of the plasticizer on the conductivity of the copolymer electrolyte was then studied. Glycerol carbonate was also mentioned in a composition for plasticization of aliphatic and aromatic polyesters (Wypych, 2017).

Our work dealt with the study of plasticizing effect of the synthesized glycerol carbonate within a nitrocellulosic film. Glycerol carbonate was incorporated in a nail polish formulation as an additive (5.6%). The properties of different organic carbonates including natural carbonates are compared with a commercial plasticizer (acetyl tributyl citrate) taken as a standard. **Table 1** indicates the composition of the formulation used to prepare the film.

Glycerol carbonate was perfectly solubilized in the formulation and the resulting film was transparent, unlike the film obtained with dilauryl carbonate which tends to whiten.

The film samples prepared using composition 1 were analyzed by Dynamic Mechanical Analysis. Under the sinusoidal mechanical stress applied to samples, the deformation amplitude of a viscoelastic material is shifted by a phase angle δ.

Nitrocellulose is a thermoplastic polymer; the behavior of plasticized nitrocellose was studied by Baker et al. (1984). The glass transition temperature of nitrocellulose is close to 40°C, as indicated by the maximum of the tan δ curve as a function of temperature (**Figure 9**). The reduction of Tg for nitrocellulose plasticized with glycerol carbonate or with acetyl tributyl citrate is distinctly observed. The decrease of Tg reflects the action of a plasticizer. It is also noted that at the same concentration, the plasticizing effect of glycerol carbonate is higher than for citrate. Glass transition temperatures of nitrocellulosic films are presented in **Table 2**.

The results show that the glass transition temperature of the film with the glycerol carbonate is lower than Tg of the film with the commercial plasticizer. The other carbonates have variable performances, without achieving the performance of glycerol carbonate. To avoid the formation of a film too soft, a plasticizer must reach a state of equilibrium, that is to say a constant Persoz hardness. The Persoz pendulum is used to study the change of the hardness of the formulations as a function of time (**Figure 9**). The test was carried out with the composition 2 (**Table 1**).

Figure 10 shows that the film containing the glycerol carbonate dampens the oscillations of the pendulum. We can check that the film without plasticizer does not dampen the oscillations. We find that the classification of plasticizers according to their hardness is the same as that obtained with the measurement of the glass transition temperatures. The results thus confirm a moderate plasticizing effect for dilauryl carbonate and diisoamyl carbonate while for glycerol carbonate, plasticizing properties revealed better than those of
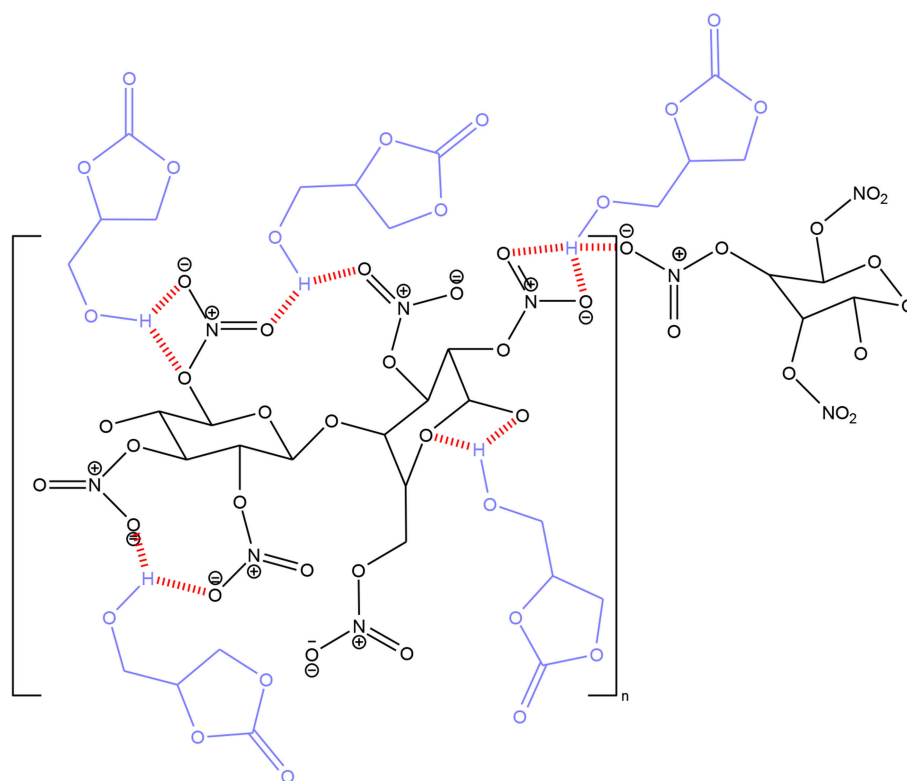
FIGURE 11 | Arrangement of glycerol carbonate molecules within nitrocellulose chains.

the commercial plasticizer. Glycerol carbonate content can thus be reduced below 10% to meet the specification of nail polishes.

Finally, results obtained in terms of hardness are in agreement with the decrease of Tg: both approaches show the effectiveness of glycerol carbonate as a plasticizer.

These performances suggest that the OH group of glycerol carbonate plays a role in the plasticization of nitrocellulose. Indeed, it can be assumed that the formation of hydrogen bonds between the hydroxyl function and the NO_2 groups of the nitrocellulose generates an orderly and stable arrangement of the carbonate molecules within the polymeric network, as shown by **Figure 11**. This characteristic helps to maintain a large and well-distributed free volume between the nitrocellulose chains, thus leading to a high plasticizing effect.

CONCLUSION

The state of art on the GC synthesis has been updated since the last published reviews in 2012, 2013 and 2016. Three types of reactions continue to be studied: glycerolysis of urea, transcarbonation of DMC, DEC, or cyclic carbonates with glycerol and reaction using CO_2. Among these different routes, in this work, DMC and glycerol were selected as the raw materials for the GC synthesis since the transcarbonation from these biobased reagents uses mild conditions including a less energy consuming for GC separation process and leads to high yields

and selectivities. Catalytic conditions using Na_2CO_3 seem to be a good compromise to achieve a high yield of GC, leading to an easier purification step. Compared to industrial processes, the high glycerol conversion and total selectivity avoid the GC distillation for the application targeted in this work. Mild temperatures for the reaction (73–78°C) as well as a low waste amount confirmed by the E-factor calculation are in favor of controlled costs.

Plasticizing properties of synthesized GC were compared to the behaviors of a commercial plasticizer and natural dialkyl carbonates, for a colorless nail polish formulation. The resulting films subjected to mechanical and thermal stresses (DMA and Persoz pendulum) showed the high plasticizing effect of GC toward nitrocellulose based films, probably due to hydrogen bond interactions between GC and nitrocellulose. The GC efficiency gives the possibility to decrease the content of the plasticizer in the formulation.

GC can be thus considered as a biobased ingredient abiding by the green chemistry concepts, and safe enough to be used in an ecodesigned nail polish formulation.

DATA AVAILABILITY

All datasets generated for this study are included in the manuscript and/or the supplementary files.

AUTHOR CONTRIBUTIONS

PdC wrote the evaluation of plasticizing properties and the results and discussion on this part. MB was the Ph.D. student who worked on this subject. CC wrote the introduction and conclusion and the "mini-review" part on synthesis of glycerol carbonate by biocatalysis and from crude glycerol. MU wrote the "mini-review" part on synthesis of glycerol carbonate by glycerolysis with urea and reaction from CO_2. ST-R wrote the abstract, the mini-review part on synthesis of glycerol carbonate by transcarbonatation, and the results and discussion on the improvement of this route.

ACKNOWLEDGMENTS

REFERENCES

Algoufi, Y. T., Akpan, U. G., Kabir, G., Asif, M., and Hameed, B. H. (2017). Upgrading of glycerol from biodiesel synthesis with dimethyl carbonate on reusable Sr-Al mixed oxide catalysts. *Energy Conv. Manag.* 138, 183–189. doi: 10.1016/j.enconman.2017.01.078

Aresta, M., Dibenedetto, A., Nocito, F., and Ferragina, C. (2009). Valorization of bio-glycerol: new catalytic materials for the synthesisof glycerol carbonateviaglycerolysis of urea. *J. Catal.* 268, 106–114. doi: 10.1016/j.jcat.2009.09.008

Aresta, M., Dibenedetto, A., Nocito, F., and Pastore, C. (2006). A study on the carboxylation of glycerol to glycerol carbonate with carbon dioxide: the role of the catalyst, solvent and reaction conditions. *J. Mol. Catal. A Chem.* 257, 149–153. doi: 10.1016/j.molcata.2006.05.021

Averous, L., Caillol, S., and Cramail, H. (2017). Polymères biosourcés; perspectives et enjeux. *Actualité Chimique*, 422-423, 68–75.

Bai, R., Wang, S., Mei, F., Li, T., and Li, G. (2011). Synthesis of glycerol carbonate from glycerol and dimethyl carbonate catalyzed by KF modified hydroxyapatite. *J. Ind. Eng. Chem.* 17, 777–781. doi: 10.1016/j.jiec.2011.05.027

Baker, F. S., Jones, M., Lewis, T., J., Privett, G., Crofton, D. J., and Pethrick, R. A. (1984). Dielectric studies of nitrocellulose-nitroglycerine mixtures. *Polymer 25*, 6, 815–820. doi: 10.1016/0032-3861(84)90012-0

Bandres, M., Deswartvaegher, A., de Caro, P., Senet, J.-P., and Thiebaud-Roux, S. (2010). *Plasticizer of Natural Origin for Nail Polish*. U.S. Patent US 2010158835; French patent FR2895905, WO 2007080172. Bergerac: Chromadurlin.

Claude, S., Mouloungui, Z., Yoo, J.-W., and Gaset, A. (2000). *Method for Preparing Glycerol Carbonate*. United state patent US 6025504. (Paris: Onidol).

Clements, J. H. (2003). Reactive applications of cyclic alkylene carbonates. *Ind. Eng. Chem. Res.* 42, 663–674. doi: 10.1021/ie020678i

Climent, M. J., Corma, A., Frutos, P., Iborra, S., Noy, M., Velty, A., et al. (2010). Chemicals from biomass: synthesis of glycerol carbonate by transesterification and carbonylation with urea with hydrotalcite catalysts. The role of acid-base pairs. *J. Catal.* 269, 140–149. doi: 10.1016/j.jcat.2009.11.001

Dabral, S., and Schaub, T. (2019). The use of carbon dioxide (CO2) as a building block in organic synthesis from an industrial perspective. *Adv. Syn. Catal.* 361, 223–246. doi: 10.1002/adsc.201801215

Du, M., Li, Q., Dong, W., Geng, T., and Jiang, Y. (2012). Synthesis of glycerol carbonate from glycerol and dimethyl carbonate catalyzed by K2CO3/MgO. *Res. Chem. Intermed.* 38, 1069–1077. doi: 10.1007/s11164-011-0443-3

Du, Y., Gao, J., Kong, W., Zhou, L., Ma, L., and He, Y., et al. (2018). Enzymatic synthesis of glycerol carbonate using a lipase immobilized on magnetic organosilica nanoflowers as a catalyst. *ACS Omega* 3, 6642–6650. doi: 10.1021/acsomega.8b00746

Fernandes, G. P., and Yadav, G. D. (2013). Selective glycerolysis of urea to glycerol carbonate using combustion synthesized magnesium oxide as catalyst. *Catal. Today* 309, 153–160. doi: 10.1016/j.cattod.2017.08.021

Fujita, S. I., Yamanishi, Y., and Arai, M. (2013). Synthesis of glycerol carbonate from glycerol using zinc-containing solid catalysts: a homogeneous reaction. *J. Catal.* 297, 137–141. doi: 10.1016/j.jcat.2012.10.001

George, J., Patel,Y., Pillai, M. S., and Munshi, P. (2009). Methanol assisted selective formation of 1,2-glycerol carbonate from glycerol and carbon dioxide using nBu2SnO as a catalyst. *J. Mol. Catal.* 304, 1–7. doi: 10.1016/j.molcata.2009.01.010

Global Bio-Based Chemicals Market Forecast 2019–2027. Report February 2018. Available online at: https://www.reportlinker.com/p05001382/Global-Bio-Based-Chemicals-Market-Forecast.html (accessed February 28, 2019).

Hérault, D., Boutty, B., Zander, L., and Strube, A. (2003). *Method for Producing Glycerol Carbonate*. International patent WO 03022829. (Düsseldorf: Cognis Deutschland GmbH).

Hirotsu, K., and Kaneko, T. (2001). *Method for Producing 4-Hydromethyl-1,3-Dioxolan-2-One*. Japanese patent JP2001172277. (Yamaguchi: Ube Industries Ltd.)

Hu, S., Luo, X., Wan, C., and Li, Y. (2012). Characterization of crude glycerol from biodiesel plants. *J. Agric. Food Chem.* 60, 5915–5921. doi: 10.1021/jf3008629

Indran, V. P., Saud, A. S., Maniam, G. P., Yasoff, M. M., Taufiq-Yap, Y. H., and Rahim, M. H. A. (2016). Versatile boiler ash containing potassium silicate for the synthesis of organic carbonates. *RSC Adv.* 6, 34877–34884. doi: 10.1039/C5RA26286K

Ishak, Z. I., Sairi, N. A., Alias, Y., Aroua, M. K. T., and Yusoff, R. (2016). Production of glycerol carbonate from glycerol with the aid of ionic liquid as catalyst. *Chem. Eng. J.* 297, 128–138. doi: 10.1016/j.cej.2016.03.104

Ishak, Z. I., Sairi, N. A., Alias, Y., Aroua, M. K. T., and Yusoff, R. (2017). A review of ionic liquids as catalysts for transesterification reactions of biodiesel and glycerol carbonate production. *Catal. Rev.* 59, 44–49. doi: 10.1080/01614940.2016.1268021

Jagadeeswaraiah, K., Ch Ramesh, K., Sai Prasad, P. S., Loridant, S., and Lingaiah, N. (2014). Synthesis of glycerol carbonate from glycerol and urea over tin-tungsten mixed oxide catalysts. *App.Catal. A Gen.* 469, 165–172. doi: 10.1016/j.apcata.2013.09.041

Jung, H., Lee, Y., Kim, D., Han, S., Kim, O. S. W., Lee, J., et al. (2012). Enzymatic production of glycerol carbonate from by-product Park. *Enzyme Microb. Technol.* 51, 143–147. doi: 10.1016/j.enzmictec.2012.05.004

Kim, K. H., and Lee, E. Y. (2018). Simultaneous production of transformer insulating oil and value-added glycerol carbonates from soybean oil by lipase-catalyzed transesterification in dimethyl carbonate. *Energies* 11:82. doi: 10.3390/en11010082

Kong, P. S., Aroua, M. K., and Wan Daud, W. M. A. (2016). Conversion of crude and pure glycerol into derivatives: a feasibility evaluation. *Renew. Sust. Energy Rev.* 63, 533–555. doi: 10.1016/j.rser.2016.05.054

Lanjekar, K., and Rathod, V. K. (2013). Use of glycerol for the production of glycerol carbonates through the greener route. *J. Environ. Chem. Eng.* 1, 1231–1236. doi: 10.1016/j.jece.2013.09.015

Li, H., Jiao, X., Li, L., Zhao, N., Xiao, F., Wei, W., et al. (2015). Synthesis of glycerol carbonate by direct carbonylation of glycerol with CO2 over solid catalysts derived from Zn/Al/La and Zn/Al/La/M(M = Li, Mg and Zr) hydrotalcites. *Catal. Sci. Technol.* 5, 989–1005. doi: 10.1039/C4CY01237B

Li, J., and Wang, T. (2010). Coupling reaction and azeotropic distillation for the synthesis of glycerol carbonate from glycerol and dimethyl carbonate. *Chem. Eng. Proc.* 49, 530–535. doi: 10.1016/j.cep.2010.04.003

Li, J., and Wang, T. (2011). Chemical equilibrium of glycerol carbonate synthesis from glycerol. *J. Chem. Thermodyn.*43, 731–736. doi: 10.1016/j.jct.2010.12.013

Li, W., Sreerangappa, R., Estager, J., Monbaliu, J.-C., Debecker, D. P., and Luis, P. (2018). Application of perevaporation in the bio-production of glycerol carbonate. *Chem. Eng. Proc. Intensif.* 132, 127–136. doi: 10.1016/j.cep.2018.08.014

Li, Y., Liu, J., and He, D. (2018). Catalytic synthesis of glycerol carbonate from biomass-based glycerol and dimethyl carbonate over Li-La2O3. *Appl. Catal. A Gen.* 564, 234–242. doi: 10.1016/j.apcata.2018.07.032

Liu, J., Li, Y., Liu, H., and He, D. (2018). Transformation of CO2 and glycerol to glycerol carbonate over CeO2/ZrO2 solid solution-effect of Zr doping. *Biomass Bioenergy* 118, 74–83. doi: 10.1016/j.biombioe.2018.08.004

Liu, J., Li, Y., Zhang, J., and He, D. (2016). Glycerol carbonylation with CO2 to glycerol carbonate over CeO2 catalyst and the influence of CeO2

preparation methods and reaction parameters. *Appl. Catal. A Gen.* 513, 9–18. doi: 10.1016/j.apcata.2015.12.030

Liu, Z., Wang, J., Kang, M., Yin, N., Wang, X., and Tan, Y. (2015). Structure activity correlations of LiNO3/ Mg4AlO5.5 catalysts for glycerol carbonate synthesis from glycerol and dimethyl carbonate. *J. Ind. Eng. Chem.* 21, 394–399. doi: 10.1016/j.jiec.2014.02.051

Lu, P., Wang, H., and Hu, K. (2013). Synthesis of glycerol carbonate from glycerol and dimethyl carbonate over the extruded CaO-based catalysts. *Chem. Eng. J.* 228, 147–154. doi: 10.1016/j.cej.2013.04.109

Luo, X., Ge, X., Cui, S., and Li, Y. (2016). Value-added processing of crude glycerol into chemicals and polymers. *Biores. Technol.* 215, 144–154. doi: 10.1016/j.biortech.2016.03.042

Ma, J., Song, J., Liu, H., Liu, J., Zhang, Z., Jiang, T., et al. (2012). One-pot conversion of CO2 and glycerol to value-added products using propylene oxide as the coupling agent. *Green Chem.* 14, 1743–1748. doi: 10.1039/c2gc35150a

Munshi, M. K., Biradar, P. S., Gade, S. M., Rane, V. H., and Kelkar, A. A. (2014a). Efficient synthesis of glycerol carbonate/glycidol using 1,8-diazabicyclo[5.4.0]undec-7-ene (DBU) based ionic liquids as catalyst. *RSC Adv.* 4, 17124–17128. doi: 10.1039/c3ra47433j

Munshi, M. K., Gade, S. M., Mane, V. M., Mishra, D., Pal, S., Vanka, K., et al. (2014b). 1,8-diazabicyclo[5.4.0]undec-7-ene (DBU): a highly efficient catalyst in glycerol carbonate synthesis. *J. Mol.Catal. A Chem.* 391, 144–149. doi: 10.1016/j.molcata.2014.04.016

Naik, U., Petitjean, L., Refes, K., Picquet, M., and Plasseraud, L. (2009). Imidazolium-2-carboxylate as an efficient, expeditious and eco-friendly organocatalyst for glycerol carbonate synthesis. *Adv. Synth. Catal.* 351, 1753–1756. doi: 10.1002/adsc.200900280

Nanda, M. R., Yuan, Z., Qin, W., Poirier, M. A., and Chunbao, X. (2014). Purification of crude glycerol using acidification: effects of acid types and product characterization. *Austin J. Chem. Eng.* 1, 1–7. Available online at: https://scholar.google.com/scholar_lookup?title=Purification%20of%20crude%20glycerol%20using%20acidification%3A%20effects%20of%20acid%20types%20and%20product&characterization&publication_year=2014&author=M.%20Nanda&author=Z.%20Yuan&author=W.%20Qin.

Nguyen, N., and Demirel, Y. (2013). Economic analysis of biodiesel and glycerol carbonate production plant by glycerolysis. *J. Sust. Bioenergy Syst.* 3, 209–216. doi: 10.4236/jsbs.2013.33029

Nguyen-Phu, H., Park, C., and Woo Shin, E. (2018). Dual catalysis over ZnAl mixed oxides in the glycerolysis of urea: homogeneous and heterogeneous reaction routes. *Appl. Catal. A Gen.* 552, 1–10. doi: 10.1016/j.apcata.2017.12.018

Ochoa-Gómez, J. R., Gómez-Jiménez-Aberasturi, O., Ramirez-López, C., and Belsué, M. (2012). A brief review on industrial alternatives for manufacturing of glycerol carbonate, a green chemical. *Org. Process Res. Dev.* 16, 389–399.. doi: 10.1021/op200369v

Okoye, P. U., and Hameed, B. H. (2016). Review on recent progress in catalytic carboxylation and acetylation of glycerol as a byproduct of biodiesel production. *Renew. Sust. Energy Rev.* 53, 558–574. doi: 10.1016/j.rser.2015.08.064

Paroo Indran, V., Sajidah Haji Saud, A., Pragas Maniam, G., Taufiq-Yap,Y., Hasbi Ab., and Rahim, M. (2017). Viable glycerol carbonate synthesis through direct crude glycerol utilization from biodiesel industry. *Waste Biomass Valor.* 8, 1049–1059. doi: 10.1007/s12649-016-9681-3

Paroo Indran, V., Syuhada Zuhaimi, N., Asyrak Deraman, M., Pragas Maniam, G., Mohd Yusoff, M., Yun Hin, T., et al. (2014). An accelerated route of glycerol carbonate formation from glycerol using waste boiler ash as catalyst. *RSC Adv.* 4, 25257–25267. doi: 10.1039/C4RA02910K

Rokicki, G., Rakoczy, P., Parzuchowski, P., and Sobiecki, M. (2005). Hyperbranched aliphatic polyethers obtained from environmentally benign monomer: glycerol carbonate. *Green Chem.* 7, 529–539. doi: 10.1039/b501597a

Roschat, W., Phewphong, S., Kaewpuang, T., and Promarak, V. (2018). Synthesis of glycerol carbonate from transesterication of glycerol with dimethyl carbonate catalyzed by CaO from natural sources as green and economical catalyst. *Mater. Today Proc.* 5, 3909–3915. doi: 10.1016/j.matpr.2018.02.039

Song, Q. W., Zhou, Z. H., and He, L. N. (2017). Efficient, selective and sustainable catalysis of carbon dioxide. *Green Chem.* 19, 3707–3728. doi: 10.1039/C7GC00199A

Song, X., Wu, Y., Cai, F., Pan, D., and Xiao, G. (2017). High efficiency and low-cost Li/ZnO catalysts for synthesis of glycerol carbonate from glycerol

transesterification: the role of Li and ZnO interaction. *Appl.Catal. A Gen.* 532, 77–85. doi: 10.1016/j.apcata.2016.12.019

Song, X., Wu, Y., Pan, D., Zhang, J., Xu, S., Gao, L., et al. (2018).Functionalized DVB-based polymer catalysts for glycerol and CO2 catalytic conversion. *J. CO2 Utiliz.* 28, 326–334. doi: 10.1016/j.jcou.2018.10.015

Sonnati, M. O., Amigoni, S., Taffin de Givenchy, E. P., Darmanin, T., Choulet, O., and Guittard, F. (2013). Glycerol carbonate as a versatile building block for tomorrow: synthesis, reactivity, properties and applications. *Green Chem.* 15, 283–306. doi: 10.1039/C2GC36525A

Teng, W. K., Ngoh, G. C., Yusoff, R., and Aroua, M. K. (2014).A review on the performance of glycerol carbonate production via catalytic transesterification: effects of influencing parameters. *Energy Convers. Manag.* 88, 484–497. doi: 10.1016/j.enconman.2014.08.036

Teng, W. K., Ngoh, G. C., Yusoff, R., and Aroua, M. K. (2016). Microwave-assisted transesterification of industrial grade crude glycerol for production of glycerol carbonate. *Chem. Eng. J.* 284, 469–477. doi: 10.1016/j.cej.2015.08.108

Tudorache, M., Negoi, A., Tudora, B., and Parvulescu, V. I. (2014). Environmental-friendly strategy for biocatalytic conversion of waste glycerol to glycerol carbonate. *Appl. Catal. B Env.* 146, 274–278. doi: 10.1016/j.apcatb.2013.02.049

Van Mileghem, S., De Borggraeve, W. M., and Baxendale, I. R. (2018). A robust and scalable continuous flow process for glycerol carbonate, demonstrating that GC could be produced continuously at a pilot scale although the industrial processes currently used are batch ones. *Chem. Eng. Technol.* 41, 2014–2023. doi: 10.1002/ceat.201800012

Wan, D., Zhang, X., Cong, X., Liu, S., and Zhou, D. (2018). Influence of Zr on the performance of Mg-Al catalysts via hydrotalcite-like precursors for the synthesis of glycerol carbonate from urea and glycerol. *Appl. Catal. A Gen.* 555, 36–46. doi: 10.1016/j.apcata.2018.02.009

Wan, Y., Lei, Y., Lan, G., Liu, D., Li, G., and Bai, R. (2018). Synthesis of glycerol carbonate from glycerol and dimethyl carbonate over DABCO embedded porous organic polymer as a bifunctional and robust catalyst. *Appl. Catal. A Gen.* 562, 267–275. doi: 10.1016/j.apcata.2018.06.022

Wang, S., Hao, P., Li, S., Zhang, A., Guan, Y., and Zhang, L. (2017). Synthesis of glycerol carbonate from glycerol and dimethyl carbonate catalyzed by calcined silicates. *Appl. Catal. A Gen.* 542, 174–181. doi: 10.1016/j.apcata.2017.05.021

Wu, Y., Song, X., Cai, F., and Xiao, G. (2017). Synthesis of glycerol carbonate from glycerol and diethyl carbonate over Ce-NiO catalyst: the role of multiphase Ni. *J. Alloys Comp.* 720, 360–368. doi: 10.1016/j.jallcom.2017.05.292

Wu, Y., Song, X., Zhang, J., Li, S., Yang, X., Wang, H., et al. (2018). Synthesis of glycerol carbonate from glycerol and diethyl carbonate over CeO2-CdO catalyst: the role of Ce4+ doped into CdO lattice. *J. Taïwan Inst. Chem. Eng.* 87, 131–139. doi: 10.1016/j.jtice.2018.03.023

Wypych, G. (2017). *Handbook of Plasticizers, 3rd edn*. Toronto, ON: ChemTec Publishing. doi: 10.1016/B978-1-895198-96-6.50005-5

Yuan, Y. A. (2015). Effect of glycerol carbonate as plasticizer on P(AN-MMA) polymer electrolyte. *Appl. Mech. Mater.* 713–715, 2658–2662. doi: 10.4028/www.scientific.net/AMM.713-715.2658

Zhang, P., Liu, L., Fan, M., Dong, Y., and Jiang, P. (2016). The value-added utilization of glycerol for the synthesis of glycerol carbonate catalyzed with a novel porous ZnO catalyst. *RSC Adv.* 6, 76223–76230. doi: 10.1039/C6RA14288E

Zheng, I., Xia, S., Lu, X., and Hou, Z. (2015). Transesterification of glycerol with dimethyl carbonate over calcined Ca-Al hydrocalumite. *Chin. J. Catal.* 36, 1759–1765. doi: 10.1016/S1872-2067(15)60915-9

Two-Step Purification of Glycerol as a Value Added by Product From the Biodiesel Production Process

Abdul Aziz Abdul Raman*, Hooi W. Tan and Archina Buthiyappan

Department of Chemical Engineering, University of Malaya, Kuala Lumpur, Malaysia

For every ton of biodiesel produced, about 100 kg of glycerol is also generated as a by-product. The traditional method of removing glycerol is mainly by gravity separation or centrifugation. This method generates crude glycerol, which may still contain impurities such as methanol, oil, soap, salt, and other organic materials at ppm levels. The effective usage of crude glycerol is important to improve the economic sustainability of the biodiesel industry while reducing the environmental impacts caused by the generated waste. The application and value of crude glycerol can be enhanced if these impurities are removed or minimized. Thus, it is important to develop a method which can increase the economic and applicable value of crude glycerol. Therefore, in the present study, the dual step purification method comprised of acidification and ion exchange techniques has been used to purify the crude glycerol and convert it into higher-value products. The acidification process started with the pH adjustment of the crude glycerol, using phosphoric acid to convert soap into fatty acid and salts. Then, the pretreated glycerol was further purified by ion exchange with a strong cation H+ resin. Gas chromatography (GC) was used to analyze both crude and purified glycerol and expressed as the weight percentage of glycerol content. A maximum glycerol purity of 98.2% was obtained after the dual step purification method at the optimized conditions of 60% of solvent, the flow rate of 15 mL/min and 40 g of resin. Further, the glycerol content measured being within the accepted amount of BS 2621:1979. Therefore, this study has proven that the proposed crude glycerol purification process is effective in improving the glycerol purity and could enhance the applicability of glycerol in producing value-added products which bring new revenue to the biodiesel industry.

Keywords: biodiesel, crude glycerol, purification, acidification, ion exchange, optimization

INTRODUCTION

Biodiesel is a biodegradable and renewable fuel produced by transesterification from renewable sources such as soybean, microalgae, palm cooking oil, and jatropha (da Silva César et al., 2018; Corach et al., 2019). Recently, biodiesel is attracting many researchers as it is one of the most commonly explored biofuel that could reduce the global dependence on fossil fuels and the greenhouse effect. The biodiesel production is estimated to increase annually by 4.5% and reaching 41 Mm^3 in 2022 (Monteiro et al., 2018).

Crude glycerol is the main byproduct produced during the transesterification process in the biodiesel plant, with the generation of 10 wt.% of the biodiesel product (Samul et al., 2014). Based

on the analysis, about 1 kg of crude glycerol is generated with every 10 kg of biodiesel production (Hajek and Skopal, 2010; Tan et al., 2013; Chol et al., 2018). The current market value of pure glycerol is US$ 0.27–0.41 per pound; however, the crude glycerol with 80% purity is as low as US$ 0.04–0.09 per pound. This proved that excessively produced glycerol, affect the price of the glycerol in the market. Therefore, utilization of the crude glycerol for value-added products has become a serious issue in the biodiesel industry.

Glycerol with high purity has a wide application in various industry such as pharmaceutical, cosmetic, and food products. However, the percentage of purity of the glycerol from the biodiesel industry is limiting its conversion to a high valued product (Samul et al., 2014; Talebian-Kiakalaieh et al., 2018). The crude glycerol contains a large number of contaminants such as soap, salts, ethanol, methanol, water, fatty acid, methyl esters, glycerides, and ash (Tan et al., 2013; Dhabhai et al., 2016). Yang et al. (2012) stated that the impurities in the crude glycerol could greatly influence its conversion into other value-added products (Yang et al., 2012). Venkataramanan et al. (2012) also reported that soaps in the crude glycerol have a strong inhibitory effect on the utilization of the glycerol by bacteria, which affects the performance of crude glycerol as the carbon source in the fermentation process (Venkataramanan et al., 2012). As a conclusion, the impurities present in the crude glycerol creates a significant challenge to convert them into a value-added product. Therefore, it is important to purify crude glycerol to avoid market saturation and increase profits of biodiesel production.

In the literature, the most commonly used processes are distillation, ion exchange resin, membrane separation technology, acidification, followed by neutralization and solvent extraction. Acidification is a commonly used technique to neutralize the impurities like catalyst into inorganic salt. Besides acidification, it is also able to reduce the amount of soaps by converting them into insoluble free fatty acid as they can adversely impact the separation and cause loss of yield (Hajek and Skopal, 2010; Kovács et al., 2012). Since acidification process does not remove all impurities, it needs a further purification step to remove other impurities like methanol, oil, water, and ester. However, the distillation process has some limitation over others as it requires high energy input for vaporization and causes thermal decompositions (Lancrenon and Fedders, 2008). Besides, high vacuum is also required in distillation to prevent high-temperature denaturation of glycerol through acrolein formation (Manosak et al., 2011). Furthermore, this process involves high capital investment and maintenance cost, accompanied by considerable losses of glycerol (Sdrula, 2010). In comparison with distillation process, ion exchange process is gaining wide acceptance due to simplicity of operation, low power consumption and energy requirement, as well as the fact it has also proven efficient in removing traces of impurities, color, and odor (Carmona et al., 2009, 2012). Besides, Xiao et al. (2013) suggested that the multiple-step purification process of the crude glycerol could increase the purity make it viable for various usage (Xiao et al., 2013).

This study is aimed to obtain crude glycerol with the highest purity via two-step purification using acidification and ion exchange techniques, with the aid of the Taguchi method. In this study, statistical analysis, including an L_9 orthogonal array of Taguchi, signal-to-noise ratio, analysis of mean, analysis of variance, and regression analyses were used to identify the optimum conditions of the purification processes.

MATERIALS, CHEMICALS, AND METHODS

Materials

The crude glycerol was collected from a local biodiesel plant, in Malaysia. A strong cation exchange resin H^+, Amberlyst 15 was purchased from Sigma Aldrich Sdn. Bhd. The properties of the resin are shown in **Table 1**. Phosphoric acid (85 wt.%), sodium hydroxide pellets and methanol were purchased from Merck Sdn. Bhd. Distilled water was used for chemical solutions preparation.

Glycerol Purification Process

First Step: Acidification

The crude glycerol was pretreated based on the procedure adopted from Manosak et al. (2011). The experiments were conducted in the 500 ml Erlenmeyer flasks and equilibrated using a magnetic stirrer. Initially, the crude glycerol was acidified by using phosphoric acid to the desired pH value and then stirred at a constant rate of 200 rpm for 1 h. The solution was then left idle for phase separation. It was separated into three layers which are a free fatty acid, glycerol, and inorganic salt layers, respectively. The first layer, which is rich in fatty acid was separated through decantation, and the precipitated salt was removed by filtrations using 0.45 μm filter. The middle layer, which is glycerol-rich, was neutralized (pH 7) by adding NaOH. The inorganic and fatty acid salts that formed in the neutralization stage were removed by 0.45 μm filter. The input parameters selected for this design were pH, temperature, and reaction time, which were designated as parameters A, B, and C, respectively (**Table 2**). The L_9 orthogonal array was used to design the experiments in this work (**Table 3**).

Second Step: Ion Exchange

In the ion exchange process, the pretreated glycerol obtained from the acidification process with optimized operating conditions was used. The ion exchange resins were investigated by passing the feed through a 300 ml column of resin-supported

TABLE 1 | Properties of cation-exchange resins.

Appearance	Dry, spherical beads
Active group	Sulfonic
Matrix	Styrene—divinylbenzene (macroreticular)
Ionic form	Hydrogen
Particle size (mm)	0.600–0.850
Pore size (nm)	40–80
Surface area (m²/g)	50
Bulk density (kg/m³)	608
Moisture (by weight)	<1%

Properties listed in this table were originated in the product specification sheet from resin manufacture.

TABLE 2 | Operating parameters and levels.

Parameters	Level 1	Level 2	Level 3
A:pH	2	4	6
B:Temperature (°C)	30	50	70
C:Reaction time (min)	20	40	60

TABLE 3 | L_9 orthogonal array experimental design and results of the acidification experiments.

Run	pH	Temperature (°C)	Reaction time (min)	Glycerol purity (wt.%)*	S/N ratio
	A	B	C		
1	2	30	20	64.12	36.14
2	4	50	40	73.57	37.33
3	6	70	60	76.18	37.64
4	2	50	60	61.16	35.73
5	4	70	20	65.67	36.35
6	6	30	40	67.18	36.54
7	2	70	40	51.37	34.21
8	4	30	60	53.28	34.53
9	6	50	20	58.83	35.39

*Values are average from the repetition experiments.

TABLE 4 | Operating parameters and levels.

Parameters	Level 1	Level 2	Level 3
Amount of resin (g)	30	40	50
Amount of solvent (%)	20	40	60
Flow rate (mL/min)	15	30	45

TABLE 5 | L_9 orthogonal array experimental design and results of the ion exchange experiments.

Run	Amount of resin (g)	Amount of solvent (%)	Flow rate (mL/min)	Glycerol purity (wt.%)*	S/N ratio
1	20	20	25	89.25	39.01
2	20	40	50	88.13	38.90
3	20	60	75	87.04	38.79
4	30	40	75	90.14	39.10
5	30	60	25	88.68	38.96
6	30	20	50	97.87	39.77
7	40	60	50	88.36	38.93
8	40	20	75	94.89	39.54
9	40	40	25	92.47	39.32

*Values are average from the repetition experiments.

in a glass tube. Ion exchange resins type Amberlyst 15 hydrogen form was used for free ions removal. The resin was preliminarily swelled with methanol (25 wt.%) in a glass vessel and packed into the column. Besides, silica beads were also packed inside the column to remove excess moisture content. The ion exchange resins were used to adsorb the free anions and cations in the pretreated glycerol. The pretreated glycerol was then charged into the feed tank, and a pump was used to circulate the crude glycerol through the ion exchange resin bed at the predetermined operating conditions. The temperature of the fixed bed experiment was set up at room temperature (22°C). Then the sample has been put into the rotary evaporator for the methanol removal process. The effluents were collected and analyzed. The input parameters selected for this design were the amount of resin, flow rate and amount of solvents. A standard L_9 orthogonal array (OA) was selected, and nine experimental studies were performed to optimize the process. The L_9 orthogonal array is meant for understanding the effect of independent factors, each having 3-factor level values. Taguchi experimental design of experiments suggests L_9 orthogonal array, where nine experiments are enough to optimize the parameters. Each parameter at three levels for this study is shown in **Table 4. Table 5** shows the experimental runs with different combinations of parameters at different levels.

Analytical Methods

Agilent 6890 gas chromatography (GC) attached with a flame ionization detector (FID) was used to identify the concentration of glycerol under the following conditions: (i) capillary column (DB 5HT), 0.32 mm internal diameter, 15 m length with 0.1 μm of liquid film, (ii) carrier gas helium at 1.0 mL/min, and (iii) injector temperature 200°C, and (iv) total run time of 5 min. The water content of glycerol was measured using Karl Fisher titrator. Standard method (ISO 2098-1972) was used to calculate the ash content. The organic non-glycerol (MONG) of glycerol was measured by subtracting the sum of the contents of glycerol, ash and water based on the standard method (ISO 2464-1973). Determinations of pH for the crude and purified glycerol was conducted using a pH meter (Cyberscan pH 300, 19 Eutectic instruments).

Design of Experiments Using the Taguchi Method

In this study, the Taguchi method was used to design and optimize the crude glycerol two-step purification process. Minitab 16 software package was used to assist the design of experiments and statistical analysis in determining the optimum operating conditions. In this study, glycerol content (wt.%) was used as the parameter to evaluate the effectiveness of the acidification process under different operating conditions. The data obtained for each experiment in OA were analyzed by Signal-to-noise ratio (*S/N* ratios) to investigate the impact of influential factors and determine the optimum configuration of parameters set within the experimental design. The *S/N* ratio can be optimized using several criteria including the larger-the better, the smaller-the better, or the nomina-the better.

In this study, the larger-the better approach was employed to evaluate the experimental response for the purification of glycerol. The S/N ratio was calculated using Equation (1) (Park,

1996; Sharma et al., 2005):

$$\frac{S}{N} = -10 \log \left(\frac{1}{n} \sum_{i=i}^{n} \frac{1}{Y_i^2} \right) \qquad (1)$$

where "n" *represents* total number of replications of each test run and Yi represents the glycerol purity in replication experiment "i" carried out under the same experimental conditions of each test run. The *S/N* ratio was calculated for each experiment. The significant parameters were identified based on the *S/N* ratio of the glycerol purity.

Analysis of Mean

In this study, Analysis of Mean (ANOM) was used to determine the optimal operating condition of the acidification process (Chary and Dastidar, 2012). The mean of the S/N ratio shows the effect of each parameter, independently. The mean of the S/N ratio was calculated by averaging the value of the S/N ratio [calculated using Equation (1)] of all the experiments.

The mean of the S/N ratio of an individual parameter "*F*" at level "*I*" was calculated using Equation (2):

$$M_i^F = \frac{1}{n_{Fi}} \sum_{j=1}^{n_{Fi}} \left[\left(\frac{S}{N} \right)_i^F \right]_j \qquad (2)$$

Where n_{Fi} is the number of appearances of parameter "*F*" at level "*i*" and $\left[(S/N)_i^F \right]_j$ represents the *S/N* ratio of parameter "*F*" at level "*i*" in its jth value (where j = 1,2,3…, *n*).

Analysis of Variance

The Analysis of variance (ANOVA) analysis was carried out to statistically assess the effect of different parameters on the performance of the process. ANOVA was performed by calculating the sum of squares (SS), variance (V), degrees of freedom (DOF), variance ratio (F factor), and contribution percentage (ρ_F). In ANOVA, the significance of all parameters and the interaction among the parameters were investigated using the equations listed below. According to Taguchi method, the percentage contribution of all the studies parameter was used to evaluate the influence of each parameter on the acidification process and to investigate which parameters significantly affected the process response through the ANOVA analysis (Roy, 2001).The percentage contribution of each parameter, ρ_F, was calculated using the equation below:

$$\rho_F = \frac{SS_F - (DOF_F \times V_e)}{SS_T} \times 100 \qquad (3)$$

In Equation (3), V_e is the variance due to error, DOF_F is the degree of freedom of the studied parameter, and it can be calculated by subtracting one from the number of level of the parameter (*L*).

The sums of squares due to factor, SS$_F$ was calculated using Equation (4):

$$SS_F = \frac{\sum (\eta_t)^2}{m} - \frac{(\sum \eta_i)^2}{n} \qquad (4)$$

Which, η_t = the total of the S/N ratio of each parameter in i$_{th}$ level, η_i is the S/N ratio of the experimental results and *m* is the repeating number of each level of the parameter.

The SS_T in Equation (3) was calculated using Equation (5). SS$_T$ is the total of sum squares, *N* is the number of all observations,

$$SS_T = \sum \eta_i^2 - \frac{\left(\sum \eta_i \right)^2}{n} \qquad (5)$$

Sum of squares due to error, SS_e, was calculated by Equation (6):

$$SS_e = SS_T - \sum SS_F \qquad (6)$$

The variance of the parameter, Vp was calculated by Equation (7):

$$V_p = \frac{SS_F}{DOF_F} \qquad (7)$$

The Fisher ratio (F) which determines the meaningfulness of a parameter was calculated by Equation (8):

$$F = \frac{V_p}{V_e} \qquad (8)$$

Confirmatory Experiments

Confirmation test was carried out to verify optimal conditions proposed by ANOM and ANOVA analysis. The predicted glycerol purity and S/N ratio were calculated using Equation (9):

$$Y = Y_m + \sum_{i=1}^{K} \left(\overline{Y_i} - Y_m \right) \qquad (9)$$

where Y_m = The total mean of S/N ratio, $\overline{Y_i}$ = S/N ratio at the optimal level, and k = number of parameters.

RESULTS AND DISCUSSION

Characterization of Crude Glycerol

The crude glycerol was a dark brown liquid with a pH of 9.6. It has a higher pH compared to commercial glycerol. The crude glycerol contains a small amount of glycerol (46.8 wt.%), but high ash, water, and MONG content, as can be seen in **Table 6**. It is shown that the main impurity in the crude glycerol is the MONG content (50.4 wt.%). The MONG is composed of impurities such as soap, alcohol and methyl esters in the glycerol from the biodiesel processing steps (Kongjao et al., 2010). The free fatty acids formed will be released as a soluble soap. Moreover, the methyl esters will be suspended in the glycerol phase during the phase separation process (Kongjao et al., 2010). These organic compounds also possibly react with the excess alkaline catalyst such as NaOH or KOH, which remains in the glycerol solution to reform soap. The ash content (4.7 wt.%) is composed of inorganic matters originating from the utilization of alkali catalysts like NaOH and KOH during the transesterification process. The water content of 9.3 wt.% in the crude glycerol sample is maybe because of the hygroscopic nature of glycerol that absorbs moisture from surrounding during transesterification process.

TABLE 6 | Characteristics of crude glycerol obtained from biodiesel production and commercial glycerol.

Parameters	Commercial glycerol[a]	Crude glycerol	Pretreated glycerol[b]	Purified glycerol[c]
Glycerol content (wt.%)	99.98	35.60	77.42	98.20
Ash content (wt.%)	0.002	4.73	0.34	0.39
Water content (wt.%)	0.01	9.38	1.81	0.63
Mong content (wt.%)	0.001	50.29	20.43	0.78
pH	7	9.6	7.05	7.08
Color	Clear	Dark brown	Light brown	Clear

[a]Data obtained from the supplier.
[b]Glycerol purity after acidification process.
[c]Glycerol purity after ion exchange process.

Acidification

Taguchi method was used to study the effect of parameters on the performance of the acidification process and identify the optimal operating condition. Three controllable parameters (pH, temperature, and reaction time) with each parameter at three different levels were used to design the experiment. Based on the selected parameters, levels and degrees of freedom, a standard L_9 OA was chosen. Based on the Taguchi method, the results of the experiments were calculated in the term of the S/N ratio and then interpreted. The S/N ratios measure the deviations of the quality characteristics from the desired value and calculate the optimal conditions (Karabas, 2013). The objective of this study is to maximize the glycerol purity. Thus, higher quality characteristics are better desired. Equation (1) was used to determine the S/N ratio. The *S/N* ratios of each experimental run were obtained by substituting the values of glycerol purity and several replicates of each experimental run "*n*" into Equation (1).

Optimal Conditions by ANOM Approach

ANOM is used to identify the effect on the individual parameters and identify the optimum condition for the acidification process (Chary and Dastidar, 2012). This analysis was performed by averaging all the S/N ratios of that particular parameter used in the experiments. Equation (2) was applied to calculate the mean of S/N ratio and the values obtained for each experiment are presented in **Table 7**. The optimum operating conditions were determined based on the maximum *S/N* ratio at a certain level. The higher mean of S/N ratio indicates that the parameter has a stronger effect on the acidification process. As can be seen **Figure 1**, the optimum operating conditions for carrying out acidification to obtain the maximum glycerol purity were identified as follows: pH at level 2 (2), reaction temperature at level 3 (70°C) and reaction time at level 2 (40 min). The results obtained from ANOM were further verified by ANOVA.

Effect of Parameters on Acidification

The mean of S/N ratios reflects the level of the parameters on the acidification process. As shown in **Figure 1**, pH is the dominant parameter affecting the acidification process and quality of the product, followed by temperature and reaction time. This indicates that the parameter of pH is critically affected by the acidification process and the quality of a product obtained. The

TABLE 7 | Response table of the mean of S/N ratios for glycerol purity.

Level	Mean of S/N ratios		
	pH	Temperature(°C)	Reaction time (min)
1	37.04[b]	35.36	35.74
2	36.21	36.07	36.15[b]
3	34.71	36.52[b]	36.07
Delta[a]	2.32	1.16	0.41
Rank	1	2	3

[a]Delta represents the deviation of the highest value from the lowest value.
[b]Optimum level of the parameter.

significance of the parameters was also obtained quantitatively from ANOM. It was calculated by calculating the deviation of the highest value from the lowest value. The highest rank was assigned to the parameter that carried the highest value of deviation. A large deviation indicates significant contribution and effect of that particular parameter on the performance of the acidification process. As shown in **Table 7**, pH was the most significant parameter with a deviation of 2.32 and reaction time was the least significant parameter with a deviation of 0.41.

Percentage Contribution of Parameters by ANOVA

According to Taguchi method, the percentage contributed by each parameter was evaluated to accurately quantify the effect of the parameter on acidification in terms of the glycerol purity (Roy, 2001). The results of the ANOVA analysis and the percentage contributions of each parameter is shown in **Table 8**. It was observed that pH had a dominant effect on the acidification process, with the percentage contribution of 76.37%. The contribution of the parameters was found in the following order: pH (76.37%) > temperature (19.44%) > reaction time (2.72%). This result was in agreement with the results obtained from ANOM analysis.

Confirmation Experiments

Confirmation experiment is an important step in the Taguchi design method. This step must be carried out at the end of the optimization study to verify whether the optimized operating conditions, which are identified using ANOM, produce the desired experimental output. The combination of the identified optimal operating conditions was not included in the nine experimental runs of the orthogonal array. As such, a confirmatory experiment was performed for the acidification process by using the optimized value of each parameter and the S/N ratio was calculated. The purity of glycerol was estimated using Equation (9) and the comparison between the actual and predicted glycerol purity is presented in **Table 9**. As can be seen from **Table 9**, the S/N ratio obtained from the confirmation experiment is in good agreement with the predicted ones. These results showed that the optimization of the acidification process to yield glycerol of the highest purity was successful.

Ion Exchange

Three controllable parameters (amount of resin, amount of solvent, and flow rate) with each parameter at three different
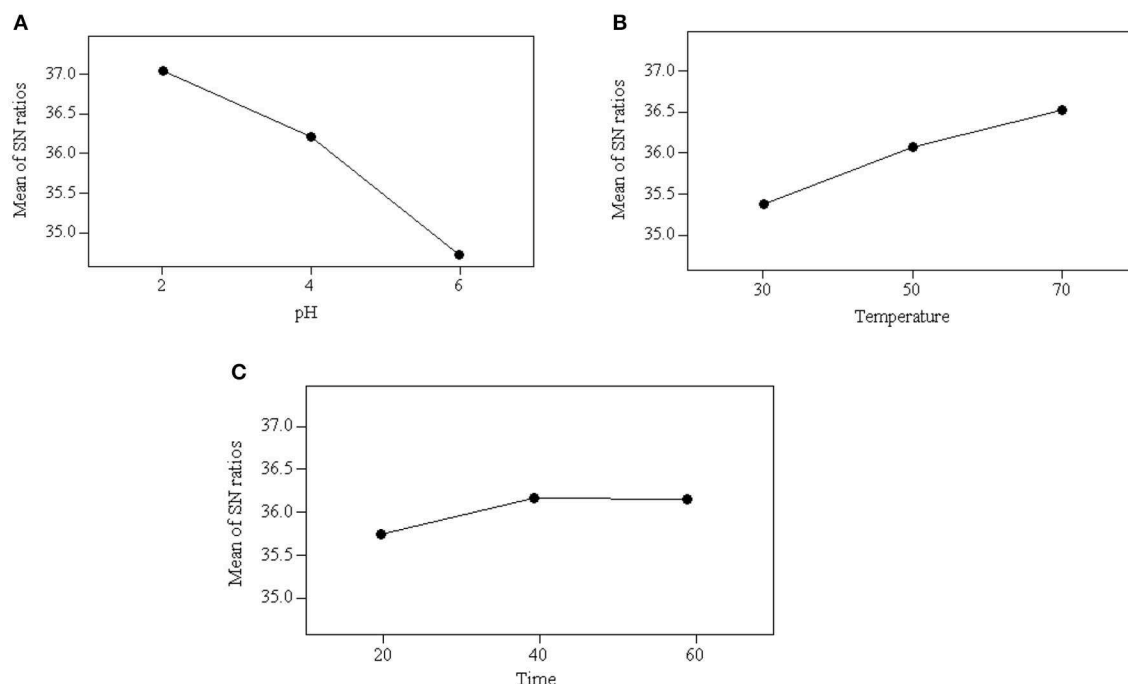
FIGURE 1 | Average value of S/N ratio at level 1–3 of each parameter: **(A)** effect of pH, **(B)** effect of temperature, and **(C)** effect of reaction time.

TABLE 8 | Results of ANOVA analysis.

Parameter	Degree of freedom	Sum of square	Variance	F-test	Contribution (%)
pH	2	429.52	214.76	208.95	76.37
Temperature	2	110.85	55.43	53.93	19.44
Reaction time	2	17.27	8.64	8.40	2.72
Error	2	2.06	1.03		1.47
Total	8	559.69			

TABLE 9 | Optimal conditions, actual, and predicted value for the response (glycerol purity).

pH	Reaction temperature (°C)	Reaction time (min)	Glycerol purity (wt.%)		S/N ratio	
			Actual	Predicted	Actual	Predicted
Optimal 2 condition	70	40	77.42	76.58	37.85	37.74

levels were optimized using the Taguchi orthogonal arrays experimental design. Based on the identified number of parameters, several levels, and the degrees of freedom, a standard L$_9$ OA was selected in the current study. A total of twenty-seven experimental runs were conducted based on the L$_9$ OA with three replications. For each experimental run, the response of the process in terms of glycerol purity (wt.%) was determined and further analyzed by the statistical approach. The collected data

on the glycerol purity were presented in **Table 5**. Based on the obtained results, the glycerol purity (wt.%) of the experiments were found to vary from 87.04 to 97.87 wt.%. This indicates that the ion exchange process is dependent on all controllable parameters (amount of resin, the amount of solvent, and flow rate), and this finding was further proven by the statistical analysis. The results of the experiments were converted into the S/N ratio. This study aims to maximize the glycerol purity obtained from the ion exchange process. Thus, higher quality characteristics [was given in Equation (1)] is used to calculate the S/N ratio.

Optimal Conditions by ANOM Approach

The mean of S/N ratio obtained for the experiment are presented in **Table 10**. The optimum operating conditions were selected based on the maximum value of the S/N ratio at a certain level of a parameter. A stronger effect on the ion exchange process is indicated by a higher mean of S/N ratio. Therefore, the optimum operating conditions for the parameters were obtained at the level with the largest mean of S/N ratios. As shown in **Figure 2**, the optimal operating conditions for the ion exchange process to achieve the maximum glycerol purity were identified as follows: the amount of resin at level 3 (40 g), the flow rate at level 1 (15 mL/min), and the amount of solvent at level 3 (60%). The results obtained from ANOM was further verified by ANOVA.

Effect of Parameters on Ion Exchange

The range of the mean of S/N ratios reflects the influence level of the parameters on the ion exchange process. As shown in **Figure 2**, the flow rate was the dominant parameter affecting

the ion exchange process and product quality, followed by the amount of resin and amount of solvent. The significance of these parameters was also be obtained quantitatively from ANOM. It was determined by calculating the deviation of the highest value from the lowest value. The highest rank was assigned to the parameter carrying the highest deviation value. A substantial deviation indicates significant contribution and effect of that particular parameter on the performance of the ion exchange process. As shown in **Table 10**, the flow rate was the main contributing parameter and the amount of solvent was the least contributing parameter.

Percentage Contribution of Parameters by ANOVA

The results of ANOVA on the glycerol purity and the percentage of contributions of each parameter is presented in **Table 11**.

It was clear from the result that flow rate exhibited a dominant effect on the ion exchange process with the percentage contribution of 51.02%. The contribution of the parameters in ascending order as follows: flow rate (51.02%) > amount of resin (28.42%) > amount of solvent (12.33%). The experimental results were in good agreement with the results obtained from the ANOM analysis.

Confirmation Experiment

The model predicted 96.91% of glycerol purity, and S/N ratio of 39.72 under the optimal conditions of 60% of solvent, the flow rate of 15 mL/min, and 40 g of resin. The experimentally obtained values were compared with the value predicted by the model to confirm the validity of the optimization procedure under the established operating conditions. The result shows

TABLE 10 | Response table of the mean of S/N ratios for ion exchange.

Level	Mean of S/N ratios		
	Amount of resin (g)	Amount of solvent (%)	Flow rate (mL/min)
1	38.56	38.88	39.42[b]
2	39.21	39.04	39.00
3	39.28[b]	39.13[b]	38.63
Delta[a]	0.72	0.26	0.79
Rank	2	3	1

[a]Delta represents the deviation of the highest value from the lowest value.
[b]Optimum level of the parameter.

TABLE 11 | Results of ANOVA analysis for ion exchange process.

Parameter	Degree of freedom	Sum of Square	Variance	F-test	Contribution (%)
Amount of resin	2	29.61	14.80	14.83	28.42
Amount of solvent	2	13.98	6.99	7.00	12.33
Flow rate	2	51.57	25.79	25.84	51.02
Error	2	2.00	1.00		8.23
Total	8	97.16			
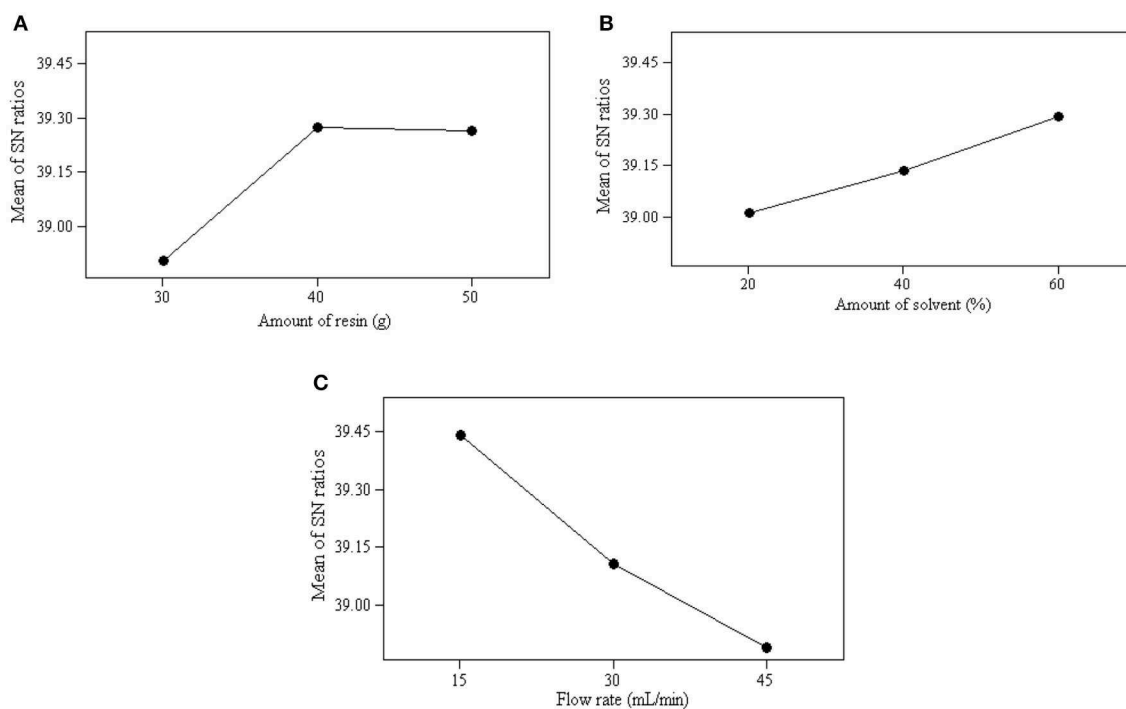
FIGURE 2 | Average value of S/N ratio at level 1–3 of each parameter: **(A)** effect of amount of resin, **(B)** effect of amount of solvent, and **(C)** effect of flow rate.

TABLE 12 | Comparison of characteristics of purified glycerol with other works.

Parameters	(Hajek and Skopal, 2010)	(Manosak et al., 2011)	(Kongjao et al., 2010)	(Saifuddin et al., 2013)	This work
Glycerol content (wt.%)	86.0	96.20	93.30	94.20	98.20
Ash content (wt.%)	–	2.08	0.05	0.01	0.19
Water content (wt.%)	–	0.06	0.45	10.50	0.63
Mong content (wt.%)	–	1.50	0.56	1.30	0.78
pH	–	–	7.03	7.40	7.08
Color	–	Clear	Light brown	Clear	Clear

that a maximum glycerol purity (98.2%), and the S/N ratio of 39.78 were obtained using the optimized operating conditions. The results of the confirmation experiments revealed that the actual experimental value and the S/N ratio obtained were in good agreement with the predicted ones. Therefore, it can be concluded that the optimization of the ion exchange process to improve glycerol purity was successful.

Comparison of the Characteristic of Purified Glycerol With Other Works

The result obtained in this work has been compared with previous studies and presented in the **Table 12**. Comparison table shows that the dual step purification method comprised of acidification and ion exchange techniques applied in this work successfully produced glycerol with the higher purity compared to other work. The percent of purified crude glycerol obtained from this study was 98%. Saifuddin et al. (2013) achieved lower yield of glycerol with the purity of 93.1–94.2% by using both acidification and adsorption treatment compared to this work. Besides, our two step purification techniques were more effective and superior compared to chemical and physical treatment used by Manosak et al. (2011) and Kongjao et al. (2010) in terms of glycerol purity.

CONCLUSION

This aim of this work is to obtain high purity glycerol through the two-step purification process with the aid of the Taguchi optimization tool. The acidification process and followed by ion exchange have produced glycerol with the purity of 98.20 wt.%. At the optimized conditions of pH (2), temperature (70°C), and

reaction time (40 min), the acidification process has obtained glycerol with a purity of 76.18 wt.%. In the ion exchange process, the pretreated glycerol, which was obtained from the acidification process with optimized operating conditions, was used. The ion exchange process has obtained glycerol with the purity of 98.20 wt.% at the optimized conditions of 60% of solvent, the flow rate of 15 mL/min, and 40 g of resin. The predicted values by Taguchi method was compared with that of the actual experimental results, and the actual result was found to be in good agreement with the predicted result. It is demonstrating that Taguchi was successfully applied to optimize the two-step for purification of biodiesel-derived crude glycerol. This study shows an improvement in the glycerol purity from 35.60 to 98.20 wt.% after optimization of the acidification and ion exchange processes, with the glycerol content being in the amount accepted based on BS 2621:1979.

AUTHOR CONTRIBUTIONS

HT: design of the work, experimental work, analysis and interpretation of data, and writing of the manuscript. AA: concept of the study, design of the work, and revising the manuscript. AB: analysis and interpretation of data and writing of the manuscript.

ACKNOWLEDGMENTS

REFERENCES

Carmona, M., Garcia, M. T., Alcazar, A., Carnicer, A., and Rodriguez, J. F. (2012). Combining ion exchange and water adsorption processes for high grade glycerol from biodiesel. *J. Chem. Sci. Technol.* 1, 14–20.

Carmona, M. L.,Valverde, J., Perez, A., Warchol, J., and Juan Rodriguez, F. (2009). Purification of glycerol/water solutions from biodiesel synthesis by ion exchange: sodium removal Part I. *J. Chem. Technol. Biotechnol.* 84, 738–744. doi: 10.1002/jctb.2106

Chary, G. H. V. C., and Dastidar, M. G. (2012). Investigation of optimum conditions in coal–oil agglomeration using Taguchi experimental design. *Fuel* 98, 259–264. doi: 10.1016/j.fuel.2012.03.027

Chol, C. G., Dhabhai, R., Dalai, A. K., and Reaney, M. (2018). Purification of crude glycerol derived from biodiesel production process: experimental studies and techno-economic analyses. *Fuel Process. Technol.* 178, 78–87. doi: 10.1016/j.fuproc.2018.05.023

Corach, J., Galván, E. F., Sorichetti, P. A., and Romano, S. D. (2019). Estimation of the composition of soybean biodiesel/soybean oil blends from permittivity measurements. *Fuel* 235, 1309–1315. doi: 10.1016/j.fuel.2018.08.114

da Silva César, A., Conejero, M. A., Barros Ribeiro, E. C., and Batalha, M. O. (2018). Competitiveness analysis of "social soybeans" in biodiesel production in Brazil. *Renew. Energy* 133, 1147–1157. doi: 10.1016/j.renene.2018.08.108

Dhabhai, R., Ahmadifeijani, E., Dalai, A. K., and Reaney, M. (2016). Purification of crude glycerol using a sequential physico-chemical treatment, membrane filtration, and activated charcoal adsorption. *Separat. Purificat. Technol.* 168, 101–106. doi: 10.1016/j.seppur.2016.05.030

Hajek, M., and Skopal, F. (2010). Treatment of glycerol phase formed by biodiesel production. *Bioresour. Technol.* 101, 3242–3245. doi: 10.1016/j.biortech.2009.12.094

Karabas, H. (2013). Biodiesel production from crude acorn (*Quercus frainetto* L.) kernel oil: an optimisation process using the Taguchi method. *Renew. Energy* 53, 384–388. doi: 10.1016/j.renene.2012.12.002

Kongjao, S., Damronglerd, S., and Hunsom, M. (2010). Purification of crude glycerol derived from waste used-oil methyl ester plant. *Korean J. Chem. Eng.* 27, 944–949. doi: 10.1007/s11814-010-0148-0

Kovács, A., Czinkota, I., and Tóth, J. (2012). Improving acid number testing of biodiesel feedstock and product. *J. Am. Oil Chem. Soc.* 89, 409–417. doi: 10.1007/s11746-011-1929-2

Lancrenon, X., and Fedders, J. (2008, June 2008). An innovation in glycerin purification. *Biodiesel Magazine*.

Manosak, R., Limpattayanate, S., and Hunsom, M. (2011). Sequential-refining of crude glycerol derived from waste used-oil methyl ester plant via a combined process of chemical and adsorption. *Fuel Process. Technol.* 92, 92–99. doi: 10.1016/j.fuproc.2010.09.002

Monteiro, M. R., Kugelmeier, C. L., Pinheiro, R. S., Batalha, M. O., and da Silva César, A. (2018). Glycerol from biodiesel production: technological paths for sustainability. *Renew. Sust. Energy Rev.* 88, 109–122. doi: 10.1016/j.rser.2018.02.019

Park, S. H. (1996). *Robust Design and Analysis for Quality Engineering*. London: Chapman and Hall.

Roy, R. K. (2001). *Design of Experiments Using the Taguchi Approach: 16 Steps to Product and Process Inprovement*. John Wiey and Sons.

Saifuddin, N., Refal, H., and Kumaran, P. (2013). Rapid purification of glycerol byproduct from biodiesel production through combined process of microwave assisted acidification and adsorption via chitosan immobilized with teast. *J. Appl. Sci. Eng. Technol.* 7, 593–602. doi: 10.19026/rjaset.7.295

Samul, D., Leja, K., and Grajek, W. (2014). Impurities of crude glycerol and their effect on metabolite production. *Ann. Microbiol.* 64, 891–898. doi: 10.1007/s13213-013-0767-x

Sdrula, N. (2010). A study using classical or membrane separation in the biodiesel process. *Desalination* 250, 1070–1072. doi: 10.1016/j.desal.2009.09.110

Sharma, P., Verma, A., Sidhu, R. K., and Pandey, O. P. (2005). Process parameter selection for strontium ferrite sintered magnets using Taguchi L_9 orthogonal design. *J. Mater. Process. Technol.* 168, 147–151. doi: 10.1016/j.jmatprotec.2004.12.003

Talebian-Kiakalaieh, A., Amin, N. A. S., Najaafi, N., and Tarighi, S. (2018). A review on the catalytic acetalization of bio-renewable glycerol to fuel additives. *Front. Chem.* 6:573. doi: 10.3389/fchem.2018.00573

Tan, H. W., Abdul Aziz, A. R., and Aroua, M. K. (2013). Glycerol production and its applications as a raw material: a review. *Renew. Sust. Energy Rev.* 27, 118–127. doi: 10.1016/j.rser.2013.06.035

Venkataramanan, K. P., Boatman, J. J., Kurniawan, Y., Taconi, K. A., Bothun, G. D., and Scholz, C. (2012). Impact of impurities in biodiesel-derived crude glycerol on the fermentation by Clostridium pasteurianum ATCC 6013. *Appl. Microbiol. Biotechnol.* 93, 1325–1335. doi: 10.1007/s00253-011-3766-5

Xiao, Y., Xiao, G., and Varma, A. (2013). A universal procedure for crude glycerol purification from different feedstocks in biodiesel production: experimental and simulation study. *Ind. Eng. Chem. Res.* 52, 14291–14296. doi: 10.1021/ie402003u

Yang, F., Hanna, M. A., and Sun, R. (2012). Value-added uses for crude glycerol-a byproduct of biodiesel production. *Biotechnol. Biofuels* 5, 1–10. doi: 10.1186/1754-6834-5-13

Techno-Economic Analysis of Glycerol Valorization via Catalytic Applications of Sulphonic Acid-Functionalized Copolymer Beads

Luma Sh. Al-Saadi*, Valentine C. Eze and Adam P. Harvey

School of Engineering, Newcastle University, Newcastle upon Tyne, United Kingdom

The design of experiments response surface analysis was employed for the first time to study the effect of divinylbenzene (DVB) (20–80 wt. %), diluent (0–100 wt.%), and mixing (200–900 rpm) on the beads' physical properties and on swelling ability. The beads with the highest performances, in terms of mechanical stability, surface area, and swelling ability, were sulphated, and tested in converting glycerol to a valuable product "solketal." Process options for glycerol valorization to solketal using synthesized sulphonic acid-functionalized styrene-divinylbenzene (ST-DVB-SO$_3$H) copolymer beads and techno-economic analysis of the processes have been investigated. Three processes were evaluated: two one-stage processes at 8.5 wt.% catalyst and 50°C, based on either 6:1 acetone to glycerol molar ratio (87% conversion) or 12:1 (98% glycerol to solketal conversion), and a two-stage route (two acetone additions), where ≥98% conversion can be achieved with lower overall acetone use (10:1 acetone to glycerol molar ratio and 50°C). Techno-economic analyses of the three solketal options were performed using Aspen (HYSYS), based on a fixed capacity of 100,000 te/y and 20-years lifetime. The techno-economic analyses showed that the net present values for the solketal process options were $707 M for the two-stage, $384 M for the one-stage at 6:1 acetone to glycerol molar ratio, and $703 M for the one-stage at 12:1 acetone to glycerol molar ratio. The break-even prices for these solketal processes were $2,058/ ton for the one-stage at 12:1 of acetone and two-stage and $2,088/ton for the one-stage at 6:1 of acetone, which is lower than the current price of solketal at $3,000/ton. The two-stage process was found to be the most effective method of glycerol valorization production to solketal.

Keywords: glycerol, valorization, sulphonic acid, copolymer beads, solketal

INTRODUCTION

Rapid depletion of fossil fuel and the harmful effects of its combustion on the environment have motivated the quest to find an economic and effective method to produce renewable fuels with less harmful environmental effects. Bio-fuels, such as biodiesel, have emerged as an environmentally friendly and sustainable substitute to petro-diesel (Demirbas, 2008; Helwani et al., 2009). Biodiesel is most commonly produced via triglyceride transesterification, which produces fatty acid alkyl

esters as the main product and crude glycerol as a by-product (Melero et al., 2009; Patil et al., 2009; Kim et al., 2011; Park et al., 2015). It is envisaged that the use of metal oxides, and hydroxide and sulphonic acid-functionalized resin catalysts for biodiesel production, will produce glycerol of high market value, increasing the commercial viability of biodiesel production. The co-production of glycerol in the conventional biodiesel processes has little economic advantage on biodiesel plants as the huge rise in global glycerol production has caused its oversupply, significantly reducing the glycerol price (Rodrigues et al., 2012). Glycerol surplus has increased from 200,000 tons in the year 2003 to over 2 million tons in 2011, and this is predicted to rise to over 6 million tons in 2025 (Ciriminna et al., 2014). Therefore, it is important to find a way to upgrade glycerol into valuable products. Indeed many alternatives have been suggested to utilize glycerol in many fields such as animal food, drugs, cosmetics, tobacco, fuel additives, waste treatment, and production of different chemicals (Knothe et al., 2010; Leoneti et al., 2012; Yang et al., 2012). It also can be used to reduce the free fatty acid content in biodiesel feedstocks, which could help to reduce many of problems related to separation duties and toxicity (Leung et al., 2010). Previous studies have shown that crude glycerol could be converted via a biological process to produce valuable chemicals such as 1,3-propanediol (Mu et al., 2006), citric acid (Papanikolaou et al., 2002), and polyhydroxyalkanoates (Ashby et al., 2004). A promising route for glycerol utilization is reaction with acetone in the presence of an acid catalyst to form 2,2-dimethyl 1,3-dioxalane-4-methanol, also called "solketal" (Mota et al., 2010). The reaction of acetone and glycerol to produce solketal is shown in **Figure 1**. The reaction is limited by the thermodynamic equilibrium, as complete glycerol conversion cannot be achieved due to water formation (Li et al., 2012; Nandan et al., 2013; Rossa et al., 2017), and long residence time and high amount of acetone are required to overcome this problem (Khayoon and Hameed, 2013). Solketal is a valuable product used as an additive to improve the fuel properties of gasoline and biodiesel, in pharmaceutical industry, and as a plasticizer in the polymer industry (Nanda et al., 2014a).

Conventional processes for solketal production use homogeneous acid catalysts such as p-toluenesulfonic acid (Suriyaprapadilok and Kitiyanan, 2011) and sulfuric acid (Dmitriev et al., 2016), which leads to an increase in the cost of production due to the extra costs of downstream separation of the homogenous catalyst as well as damage to the equipment due to its corrosive ability; thus it cannot be reused. Some homogenous acid catalysts can be easily recovered such as SnF_2-catalyst (da Silva et al., 2017) and $SnCl_2$-catalyst (Menezes et al., 2013), although the presence of chlorides from $SnCl_2$ in the reactor can cause corrosion in reactors and pipes. To overcome this problem, heterogeneous catalysts can be used as it is more environmentally friendly than homogenous catalysts; thus, it can be recycled and reused many times, which turn the production process to "green." Glycerol acetalization was researched using heterogeneous acid catalysis such as Ni–Zr supported on mesoporous activated carbon (Khayoon and Hameed, 2013), zeolite H-BEA (SAR 19) (Rossa et al., 2017), Zr- and Hf-TUD-1 and Sn-MCM-41 (Li et al., 2012), and sulfonic mesostructured

silica (Vicente et al., 2010). However, these catalysts have lower rates of reaction than homogeneous catalysts. An alternative is to use an ion-exchange resin supported catalyst, produced from co-polymerization of styrene and divinylbenzene (DVB). Due to the presence of DVB in the structure, the polymeric resin beads swell during the reaction, providing easy access of reactants to the catalytic active sites (Sharma et al., 2011; Boz et al., 2015), such that high reaction rates can be achieved. Ion-exchange resins can be regenerated (Tesser et al., 2010) and reused many times (Huang et al., 2012). Above all, Amberlyst resins, such as Amberlyst 35, exhibit excellent performance in glycerol acetalization (Nanda et al., 2014b). Resin catalysts have been synthesized with variety of physical properties, as the cross linking level has been varied from low for Dowex HCR-W2 and Amberlyst-16 to high for Amberlyst-15 and Amberlyst-35 (Özbay et al., 2008). Different structures (macro-porous and gel-type) were used in the transesterification reaction of biodiesel production; different surface areas, pore diameters, and porosities were produced (Fu and Borges, 2015). The results showed that the physical properties of catalyst such as pores and surface area have more effect on catalytic performance than that of cross-linking level. The catalyst types in order of decreasing activity are A-15 > A-35 > A-16 > Dowex HRC-W2 (Özbay et al., 2008). The authors revealed that the difference between using the abovementioned catalysts as a particle or as a powder is only 10% (Özbay et al., 2008). More study is required to investigate the feasibility of the use of other types of resin structures, such as non-porous and large porous structures.

In the resin synthesis, the organic phase (discrete phase) consists of monomer (i.e., styrene), cross linker (DVB), initiator (benzoyl peroxide), and a porogen, which can be either a solvent, such as toluene, or a non-solvent, such as heptane. The aqueous phase consists of emulsion stabilizer such as hydroxyethyl cellulose, gelatine, and sodium chloride (Gokmen and Du Prez, 2012; Yussof, 2012). The volume of the aqueous to the organic phase is usually fixed above 3:1 (Coutinho et al., 1998).

When toluene was used as a solvent in discrete phase, adding of monomer droplet leads to building a crosslinking continuously. When the crosslinking becomes rigid, it enables to absorb toluene at "a gelation point." After that the de-swelling (separation) phase occurs. The predominant beads in this case are micro or meso-pores with high surface area and low pore volume (Gokmen and Du Prez, 2012).

Conversely, a non-solvent porogen (such as n-heptane) cannot dissolve or swell the polymer chain, so the separation phase occurs before gelation point. In this case, large pore volumes and very low surface areas of macroporous particles were obtained (Gokmen and Du Prez, 2012) (see the chemical structure of ST-DVB in **Figure 2**).

However, the styrene-divinylbenzene (ST-DVB) copolymerization must be optimized for the production of copolymers of desirable particle sizes, surface area, and physical properties.

In this study, process options for glycerol valorization to solketal using sulphonic acid-functionalized (ST-DVB-SO_3H) copolymer beads and techno-economic analysis of the processes were investigated. The solketal processes evaluated were one-
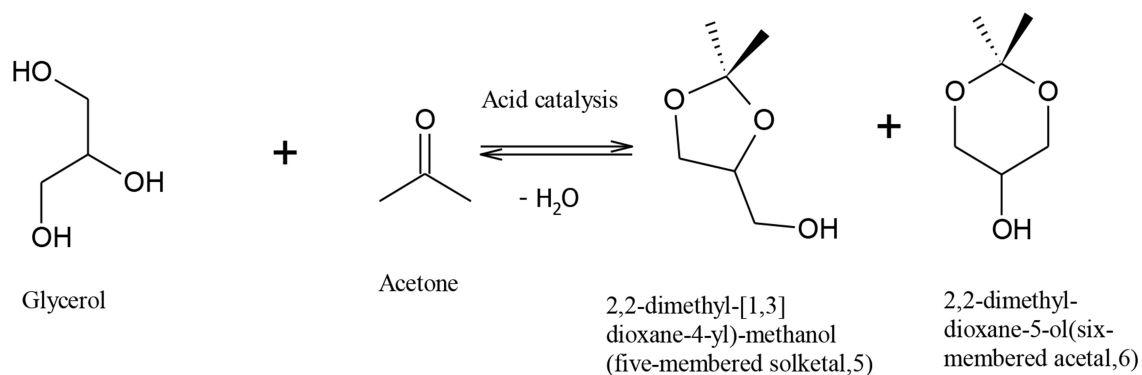
FIGURE 1 | Producing solketal from glycerol (Khayoon and Hameed, 2013).
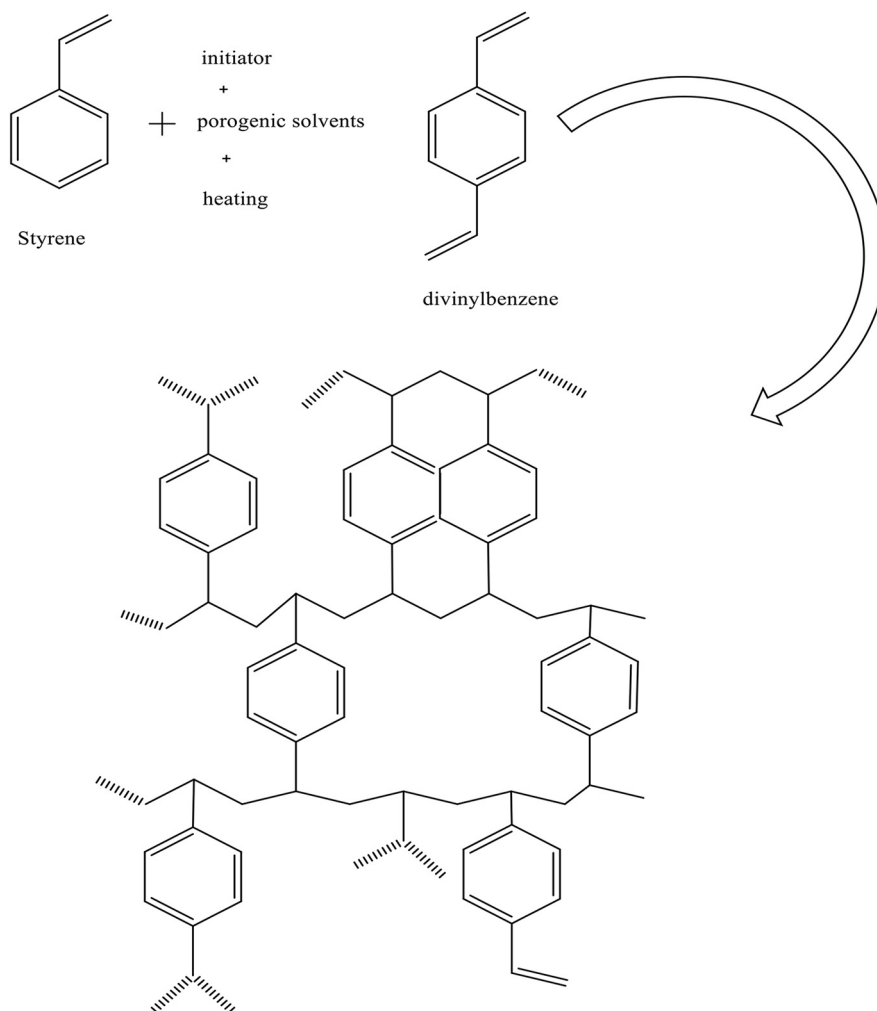
FIGURE 2 | Chemical structure of ST-DVB resin.

and two-stage acetalization processes using synthesized and sulphonic acid-functionalized ST-DVB copolymer beads of desirable properties. The glycerol acetalization process was optimized to overcome the equilibrium limitation and ensure high solketal yields. The ST-DVB copolymer beads were chosen as the sulphonic acid support because the polymerization process

could be tailored to achieve copolymer beads of different physical properties. Techno-economic analysis based on Aspen (HYSYS) was applied to evaluate the different process options for glycerol valorization to solketal.

MATERIALS AND METHODS

Materials

The chemicals used in the experiments were styrene (>99%), divinylbenzene (80%), benzoyl peroxide (75%), gelatine from bovine skin (99.5%), heptane (99.9%), toluene (99.9%), 2-hydroxyl ethyl cellulose, vinyl benzene chloride (97%), poly(vinyl alcohol) (>99% hydrolysed), 2,2′-Azobis(2-methylpropionitrile) of 0.2 M in toluene, and sodium chloride (>99%). These chemicals were purchased from Sigma-Aldrich, UK. Amberlyst^{TM} 70, supplied by Dow Chemical Company, Netherlands, was used for catalytic activities comparison, with the synthesized ST-DVB-SO$_3$H copolymer beads.

Synthesis and Characterization of Sulphonic Acid-Functionalized ST-DVB Copolymer Beads

The ST-DVB copolymer beads were produced by suspension polymerization of the styrene and divinylbenzene monomers. Copolymerization was carried out in a 500-ml three-necked batch reactor equipped with a heater–stirrer (IKA RCT basic), a reflux condenser, and a nitrogen inlet pipe (**Figure 3**) was used to carry out the copolymer synthesis. The heater–stirrer was used to control the reaction temperature and the mixing speed.

The copolymerization mixture contained organic phase with monomer compositions of 36 wt.% styrene and 64 wt.% divinylbenzene and the 84 wt.% diluent based on the total monomers solution. The diluent used was a solution of 40:60 toluene-to-heptane volume ratio. The aqueous phase in the suspension polymerization contained de-ionized water with 0.2 wt.% hydroxyl ethyl cellulose, 0.5 wt.% gelatine, and 0.5 wt.% sodium chloride. About 1 wt.% of benzoyl peroxide was added to monomers as an initiator before starting each batch of polymerization.

Copolymerization was conducted using 3:1 aqueous-to-organic phase volume ratio, 90°C temperature, mixing intensity of 900 rpm, and reaction time of 24 h. Preliminary investigations, using design of experiment methodology, showed that these experimental conditions are optimal in achieving the desired ST-DVB copolymer particle sizes and properties. The copolymer beads were washed three times with de-ionized water (until the water became clear) and with ethanol to remove the aqueous phase or any unreacted monomers (Coutinho et al., 1998; Kangwansupamonkon et al., 2002). The ST-DVB beads were also washed with methanol, dried under 60°C for 48 h (Yussof, 2012), and stored for characterization and sulphonic acid functionalization. Design of experiments, using a response surface method, with stepwise analysis was used to investigate the copolymerization conditions.

The styrene-DVB copolymer beads in each polymerization batch were characterized in terms of their morphology, particle size distributions, bead density, surface area, and swelling ratio. Morphology of the resin beads was measured by mounting the samples on aluminum stubs, followed by analysis of their micro-structure in low-vacuum mode at 2 kV, using an environmental scanning electron microscope (Hitachi S2400) equipped with a field emission gun (FEI X30 ESEM-FEG). Sieves with mesh sizes from 2 mm at the upper and 1 mm, 425, 335, 212, and 75 µm at the lower were used. The amount of copolymer beads retained in each sieve and the percentage weights used to calculate the average particle size diameter were obtained. The apparent density of the copolymer beads was determined using Equations 1–3 by gravity method based on the physical properties of the polymers as reported elsewhere (Kangwansupamonkon et al., 2002). The experimental swelling ratio of polymer (S) was obtained using Equation 4 by immersing the polymer in excess toluene for 24 h in a tube covered and sealed with aluminum foil (Kangwansupamonkon et al., 2002). The surface area of the beads was calculated based on particle radius and apparent density using Equation 5.

$$\text{Regular particles} = \frac{\text{mass of the polymer}}{\text{volume of occupied container}} \tag{1}$$

$$\text{Small particles or powder} = \frac{\text{mass of the polymer}}{\text{volume of the polymer from mark of cylinder}} \tag{2}$$

$$\text{Irregular particles} = \frac{\text{mass of the polymer}}{\text{volume of displaced water}} \tag{3}$$

$$S = 1 + \left(\frac{W_s}{W_p} - 1\right)\frac{\rho_p}{\rho_s} \tag{4}$$

$$\text{surface area} = \frac{\text{area of the particles } (4\pi\ R^2)}{\text{volume of the particles } \left(\left(\frac{4}{3}\right)*\pi\ R^3\right)} * \left(\frac{1}{\rho_p}\right)$$

$$= \frac{3}{R*\rho_p} \tag{5}$$

where W_s and W_p are the weights of the fully swollen polymer and the dry polymer, respectively. ρ_p and ρ_s are the densities of polymer and solvent, respectively, while R represents the average radius of polymer particles.

The dried ST-DVB copolymer beads were functionalized with sulphonic acid sites by treatment with hot, concentrated sulphuric acid. About 5 g of the copolymer beads were transferred into 200 ml concentrated sulphuric acid at 90°C and sulphonated for 160 min. On completion of the sulphonation, the reaction mixture was poured over ice to quench the reaction, and the sulphonated copolymer beads were washed up to four times with de-ionized water, acetone, and methanol and dried at 60°C for 48 h. The ST-DVB-SO$_3$H copolymer beads were characterized, and the active sites content was quantified through sulfur content analysis using Elementar Vario Max CNS Analyser. The synthesized ST-DVB-SO$_3$H copolymer beads were applied as heterogeneous catalysts for glycerol acetalization to solketal. In the catalytic applications, the spent ST-DVB-SO$_3$H copolymer beads were regenerated by treatment with 0.1 M HCl, washing three times with water, and drying at 120°C.

FIGURE 3 | Schematic diagram of copolymerization of styrene and DVB.
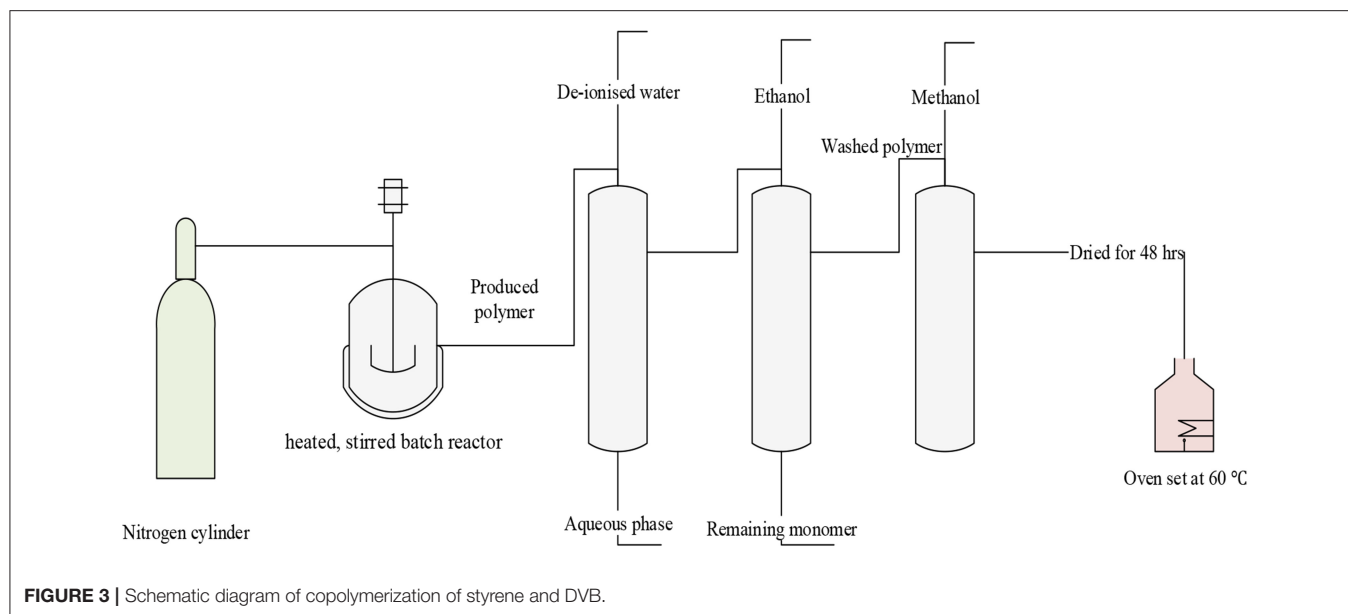
Glycerol Valorization to Solketal Using the ST-DVB-SO₃H Catalyst

Heterogeneously catalyzed glycerol acetalization to solketal by catalytic applications of the synthesized ST-DVB-SO$_3$H copolymer beads was investigated using a statistical design of experiments, response surface methodology with stepwise analysis. The reaction conditions investigated were acetone to glycerol molar ratios of 2:1–6:1, 1–20 min residence time, reaction temperatures of 30–50°C, fixed catalyst of 8.5 wt.% (based on the glycerol feed), and 800 rpm mixing intensity to ensure that the reactions were kinetically controlled. The glycerol acetalization experiments were performed in a 250-ml batch reactor equipped with a heater–stirrer and reflux condenser. In each experiment, 92.09 g of glycerol and 232.32 g of acetone (for 4:1 acetone to glycerol molar ratio) were charged into the reactor and heated to the reaction temperature. This was followed by adding 7.83 g of the ST-DVB-SO$_3$H copolymer catalyst and mixing at 800 rpm.

More experiments were carried out based on the observations from the abovementioned experimental design to investigate other process options for solketal production using one- and two-stage processes at 6:1–12:1 acetone to glycerol molar ratios and 30 min offixed reaction time. Two cases of one-stage glycerol acetalization process were investigated at 6:1 and 12:1 acetone to glycerol molar ratios, using 8.5 wt.% of ST-DVB-SO$_3$H copolymer catalyst and at 50°C. The two-stage process was performed using a first-step glycerol acetalization at 10:1 of acetone to glycerol molar ratio, 8.5 wt.% ST-DVB-SO$_3$H copolymer catalyst, and 50°C, followed by flash distillation at 10 mbar and 40°C, and a second glycerol acetalization step using fresh acetone. About 1 ml of sample was collected at various time intervals during the reactions using a micropipette, and these were filtered through a 150-µm stainless steel wire mesh in 2-ml vials. All the samples collected were analyzed immediately using gas chromatography.

Sample Analysis Using Gas Chromatography

The collected samples were analyzed using a 6890 Hewlett Packard gas chromatograph (GC). About 50–80 mg of the homogenized sample was measured into a 2-m GC vial, followed by the addition of 1 ml of 10 mg mL^{-1} of methyl heptadecanoate prepared in 2-propanol. The prepared samples were analyzed using GC by injection of 1 µl of sample with a 5-µl SGE GC syringe. The GC was equipped with a fused silica capillary column of 30 m length, 0.32 mm internal diameter, and film thickness of 0.25 µm. The GC oven temperature program was 120°C for 5 min initially and ramping up from 120 to 260°C at a heating rate of 15°C/min, which was held for another 15 min. The injector and flame ionization detector temperatures were set at 250°C and 260°C, respectively. The glycerol and solketal contents were quantified using a calibration data which were obtained from the response factors of the solutions of glycerol/solketal and methyl heptadecanoate standard prepared in 2-propanol. Glycerol and solketal conversions were calculated using Equations 6, 7, respectively.

$$\text{Glycerol conversion (\%)} = \frac{\text{Glycerol content of the sample}}{\text{Initial glycerol content}} * 100 \tag{6}$$

$$\text{Solketal yield (\%)} = \frac{\text{Solketal content of the sample}}{\text{Maximum theoretical solketal}} * 100 \tag{7}$$

Techno-Economic Analysis of the Glycerol Acetalization Process Options

Aspen (HYSYS) was used to simulate the three process options that have been investigated to produce solketal from the heterogeneously catalyzed acetalization of glycerol in the presence of the synthesized ST-DVB-SO$_3$H copolymer catalyst.

In this study, the process plants were simulated at fixed capacity of 100,000 *tons/year*, 20 years lifetime, and fixed residence time of 30 min. The flowsheet in **Figure 4** was proposed for all three solketal process plants. The one-stage solketal process plants operated at 8.5 wt.% ST-DVB-SO$_3$H copolymer catalyst and 50°C, based on either 6:1 with 87% glycerol to solketal yield (based on the experimental data; **Figure 4A**) or 12:1 of acetone to glycerol molar ratio with 98% glycerol to solketal yield (based on the experimental data; shown in **Figure 4B**). **Figure 4C** shows the third solketal process, which was based on glycerol acetalization at 10:1 of acetone to glycerol molar ratio, 8.5 wt.% ST-DVB-SO3H copolymer catalyst, and 50°C with 84% glycerol to solketal yield in the first step (based on the experimental data), followed by removal of reactively formed water, and another glycerol acetalization step at the same reaction conditions to achieve a total of 98% glycerol to solketal yield (based on the experimental data). The NRTL model was chosen to model this process (Sakdasri et al., 2018). The economic viability of these glycerol acetalization processes were evaluated based on the 20-years net present values (NPV) and the sensitivities of the plants' profit margins to the fluctuations in the reactant and product market prices.

The sensitivity analyses were determined by varying the price of the reactants and the products from −50 to +50% and calculating the effect of price changing on the net present value. The NPV is the cumulative discounted free cash at the end of the project (in this study, it was based on 20 years of operation and 1 year of construction); it was calculated using Equation 8. The trends in reactant and product prices lead to changes in the break-even price of the produced biodiesel, which is measured as the minimum selling price of biodiesel to achieve positive NPV.

$$NPV = \sum_{t=1}^{T} \frac{C_{in,t}}{(1+r)^t} - C_{out} \qquad (8)$$

where $C_{in,\,t}$ represents net cash inflow in time t, C_{out} represents initial capital expenditure, and r is the discount rate.

The economic analysis of the various biodiesel processes in this study was based on the following assumptions:

I   RSO feed of 100,000 tons/years was chosen as a case study
II   Plant lifetime of 20 years
III   Pump efficiency of 75%
IV   Equipment purchase costs from the HYSYS database
V   The total investment cost was calculated based on the investment cost required to build the plant in addition to operating cost.

RESULTS AND DISCUSSION

Synthesis, Functionalization, and Characterization of the Copolymer Beads

Table 1 shows the properties of the copolymer beads produced at various process conditions. The data were analyzed using the stepwise response surface method, implemented in Minitab 17. This analysis was applied to evaluate the effects of the operating parameters and generate empirical models for the average particle size, surface area, and swelling ratio. The experiments carried out at 200 rpm were ignored as no particles were formed at that mixing condition. All of the experiments were repeated twice.

The average particle size, the swelling ratio, and the surface area for the styrene-DVB copolymer beads are predicted by the empirical models in Equations 9–11, respectively.

Particle size (mm) $= 1.9734 - 0.05624\ X - 0.00547\ Y - 0.000523\ Z + 0.000718\ X^2 - 0.000102\ X^*Y + 0.000011\ Y^*Z.$

$$R^2 = 96.3\% \qquad (9)$$

Swelling ratio $= 3{,}150 - 18.89\ X - 56.71\ Y - 6.221\ Z - 0.1711\ X^2 + 0.05423\ Y^2 + 0.000576\ Z^2 - 1.456\ X^*Y + 0.08621\ X^*Z + 0.1396\ Y^*Z.$

$$R^2 = 95.3\% \qquad (10)$$

Surface area$^*10^{-5}$(m^2/gm) $= -1.961 + 0.1625\ X + 0.01182\ Y + 0.000213^*\ Z - 0.001611\ X^2 - 0.000096\ Y^2 - 0.000149\ X^*Y + 0.000006\ Y^*Z$

$$R^2 = 99\% \qquad (11)$$

where X is the weight percent of DVB, Y is the weight percent of the diluent, and Z is the mixing speed in revolution per minute.

Contour plots of the experimental data in **Figure 5** and data in **Table 1** show that mixing has a clear effect on particle size. This is because mixing is required to overcome the reactants' viscosities to generate small monomer beads. There was no substantial change in average particle size when increasing the value of diluent from 0 to 50% as the average particle sizes that obtained from empirical equation were ranged (0.42–0.62 mm) (see **Figure 5A**), which is consistent with what has been reported elsewhere (Kangwansupamonkon et al., 2002).

Whereas increasing the diluent above 50 wt.% can lead to synthesis of styrene-DVB particles of smaller sizes due to substantial reduction in solution viscosity [see entries (3, 4) and (6, 7) in **Table 1** and **Figure 6**]. To obtain small particle size (≤0.3 mm) at high diluent (80–100%), little mixing is required as shown in **Figure 5A** as increasing the diluent leads to reduced concentrations. For example, at diluent (80–100%), a particle size of ≤0.27 mm can be obtained at only 550–650 rpm of mixing intensity.

Increasing the DVB contents led to increased solution viscosity and consequent formation of beads of large average size [as can be observed in entries (4, 9) in **Table 1**], such that high diluent amount and high mixing intensity are required to overcome solution density to get small particle size (high surface area). However, because the effect of DVB on the particle size was more than that of mixing and diluent on the bead size, the interaction between the mixing, diluent, and DVB is not significant as shown in **Figures 5B,C**.

It was observed that at DVB concentrations of 20–30%, the particle size ranged from 0.52 to 0.7 mm at 0–100 wt.% of diluent and 550–900 rpm of mixing intensity as shown in
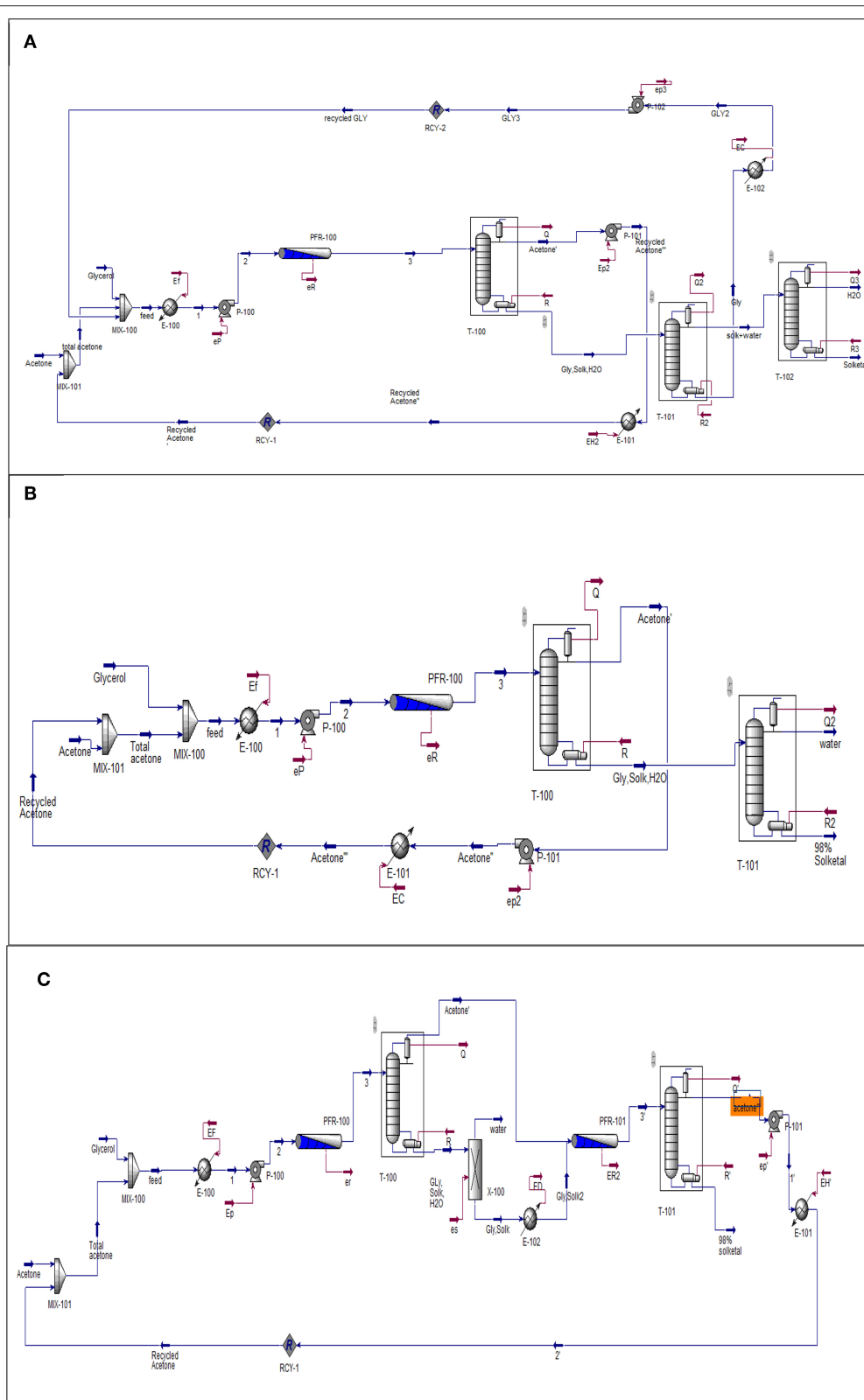
FIGURE 4 | Flowsheet diagram of glycerol acetalization *reaction.* **(A)** One-stage process (low acetone), **(B)** one-stage process (high acetone), and **(C)** two-stage process. Gly is glycerol, Solk is solketal, Mix is mixture, E is heat exchanger; T-100, T-101, and T-102 are distillation columns, PFR is a plug flow reactor. P-100, P-101, and P-102 and pumps and all the streams in red lines represent the energy required by the equipment.

Characteristics of ST-DVB copolymer beads produced at different reaction conditions.

Run number	DVB wt.%	Diluent (wt.%)	Mixing (rpm)	Average particle diameter (mm)	Swelling ratio	Surface area (m²/gm)	Particle shape
1	20	50	900	0.753	491.0	132	Spherical
2	20	50	200	–	133.0	–	No particles
3	20	0	550	0.856	337.7	76	Spherical
4	20	100	550	0.69	264.5	103	Spherical
5	50	50	550	0.416	174.0	240	Spherical
6	50	0	900	0.493	288.0	233	Spherical
7	50	100	900	0.393	455.0	237	Spherical
8	80	50	200	–	391.0	–	No particles
9	80	100	550	1	593.0	22	Spherical
10	80	0	550	1.78	1082	42	Spherical
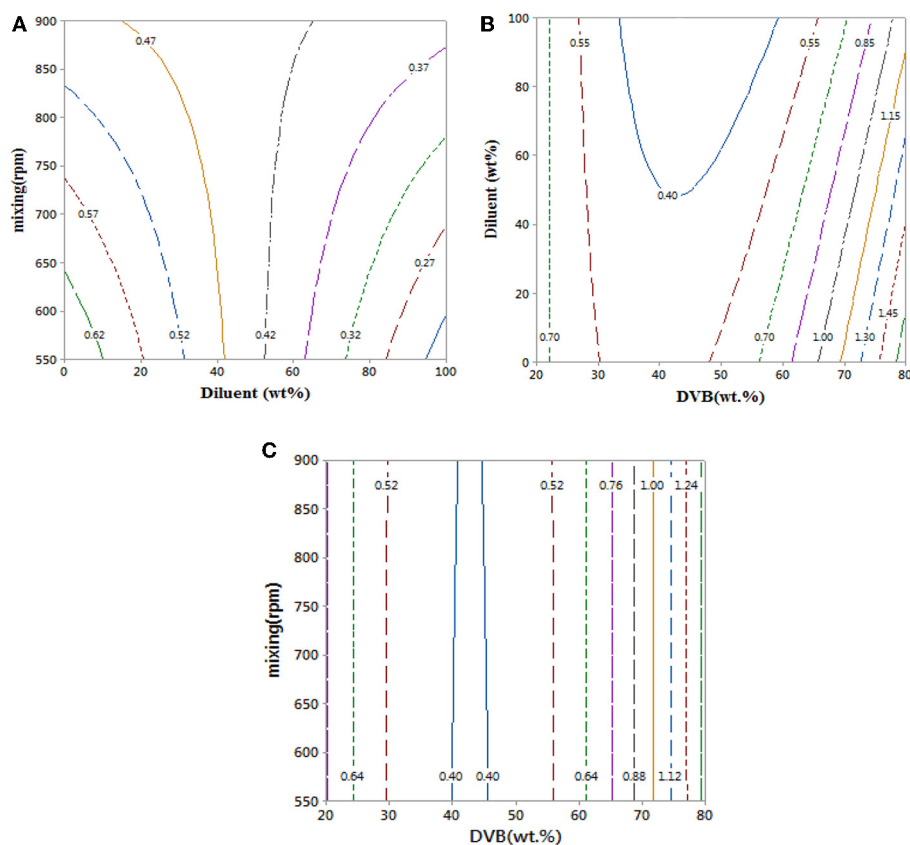
FIGURE 5 | (A–C) Contour plots showing the effect of reaction parameters on bead particle sizes. At hold values of DVB 50 wt.%, 50 wt.% of diluent: monomer (wt.%), and 725 rpm.

Figures 5B,C. However, under the same operating conditions at 40–50% of DVB, the particle sizes reduced to 0.4 mm; this is because at very small amounts of DVB (20–30 wt.%), the crosslinking between the particles is weak; therefore, the particles agglomerated to form larger particles than at higher DVBs (40–50 wt.%). They increased again to ≥0.85 mm at high crosslinking beads of DVB (60–80 wt.%) due to the increasing of solution viscosity.

It has been reported that high DVB and diluent contents led to the formation of highly cross-linked styrene-DVB particles, whereas the level of crosslinking was lower in the copolymer particles produced at lower DVB contents (Kangwansupamonkon et al., 2002).

In summary, increasing the DVB content leads to higher degrees of crosslinking in the styrene-DVB particles and higher viscosity of the polymerization solutions. Therefore, to control
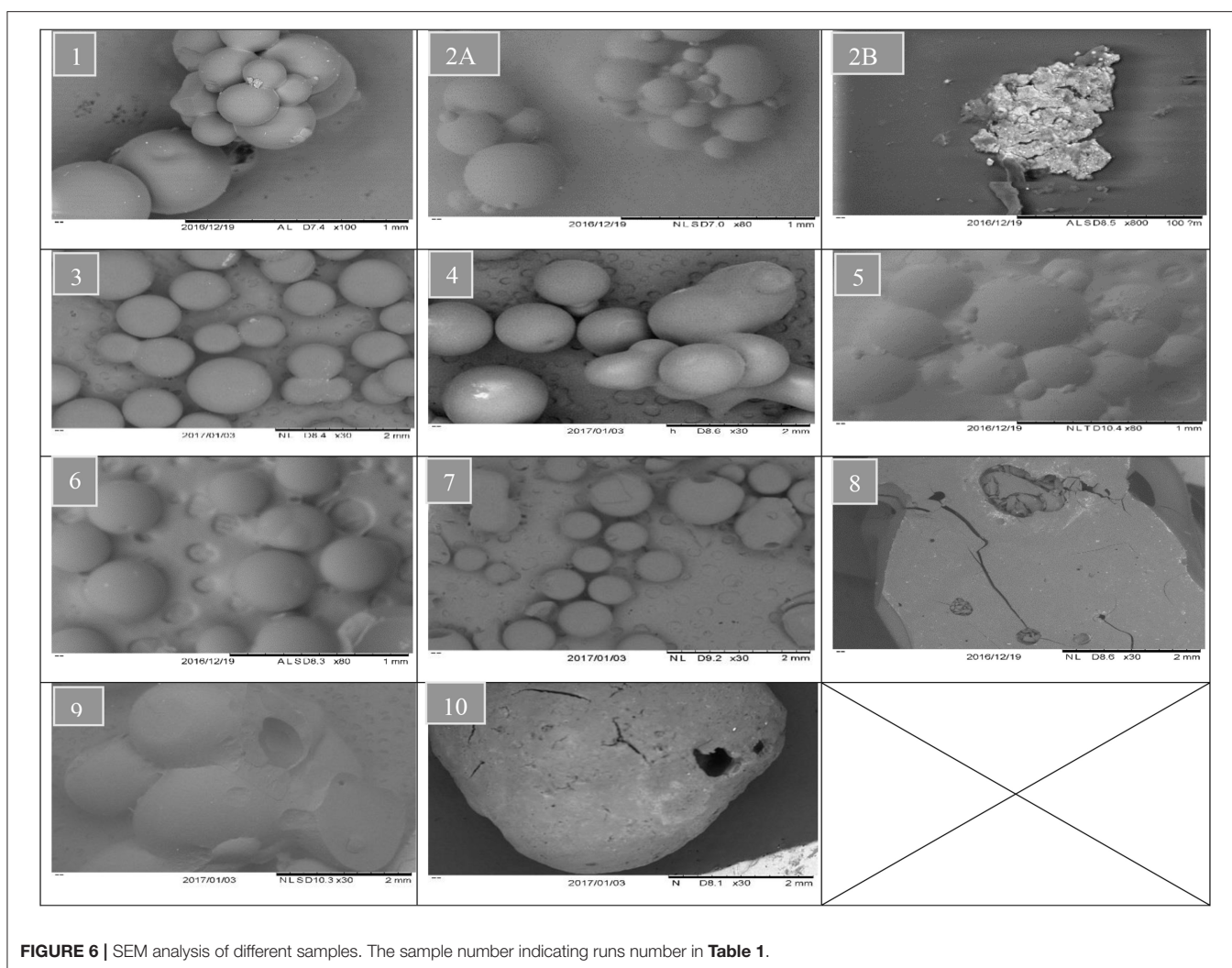
FIGURE 6 | SEM analysis of different samples. The sample number indicating runs number in **Table 1**.

the particle sizes and to synthesis styrene-DVB copolymer beads with substantial degrees of crosslinking, the mixing speed, DVB, and diluent contents must be controlled. For instance, high mixing and diluent content were required to produce small particle sizes in the range of 0.3–0.6 mm, while low diluent contents and mild mixing produced large particle sizes >1 mm.

Depending on the particle size, the surface area of the bead varied. As can be seen in **Table 1**, the surface area of the beads is inversely proportional to the particle diameters, as when the particle diameter decreased from 0.75 mm (run 1) to 0.39 mm (run 7) for example, the surface area increased from 132 to 237 m^2/gm, respectively; so to obtain high surface area particles, small bead diameters are required.

An empirical model for the styrene-DVB beads swelling ratio in Equation 10 was used to obtain the contour plots in **Figure 7**, which shows the effects of the copolymer bead synthesis conditions on their swelling ratio. Swelling ratio in the copolymer beads take place via solvation of the network chain and filling of pores (Kangwansupamonkon et al., 2002).

The swelling ratio of the copolymer particles increased with mixing intensity. This is attributed to the formation

of styrene-DVB beads of small particle sizes at high mixing intensity, which translates to higher particle surface area exposed to toluene and consequently higher swelling ratio as shown in **Figures 7A,C**. At low DVB content (20 wt.%), increasing the amount of diluent reduces the solution viscosity, such that porous copolymer beads of small size could be achieved, even at mild mixing conditions, and consequently higher values of swelling ratio were achieved as shown in **Figure 7B**. When DVB contents of more than 50% were used, the copolymer beads produced were highly cross-linked, leading to low porosity (Kangwansupamonkon et al., 2002), which explains the lower swelling ratio of the styrene-DVB copolymers at >50% content of DVB in **Figures 7B,C**.

At high DVB content (80 wt.%), the particles are non-porous (Kangwansupamonkon et al., 2002), so the swelling ratio is small, but when no diluent was used the particles tended to be fragile due to their high porosity as shown in **Figure 6** (3, 6, 10), which increased the swelling ratio (**Figure 7B**). At zero diluent, the polymer had a high porosity (Durie et al., 2002), so the swelling ratio was high even at high crosslinking (**Figure 7C**). This decreased with increasing diluent ratio >30 wt.% and
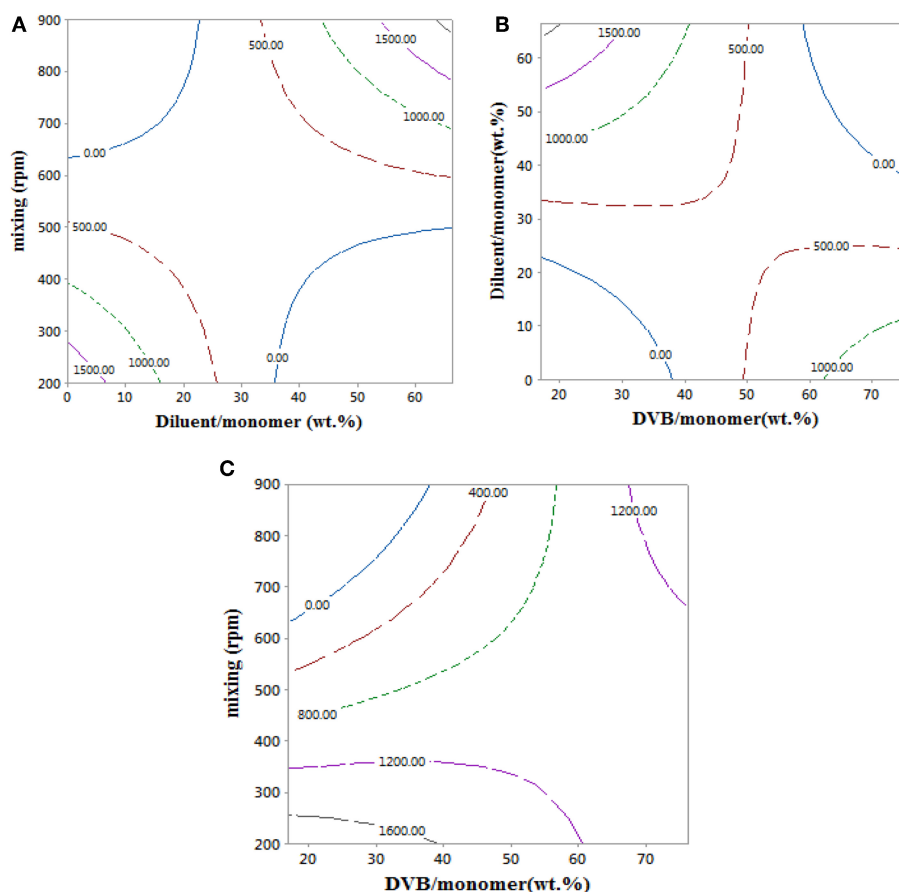
FIGURE 7 | Contour plots showing the effect of reaction parameters on swelling ratio at 0 wt.% of diluent/monomer, 17 wt.% of DVB/monomer, and 900 rpm.

increased again at high mixing speed due to the formation of copolymer beads of small particle sizes as shown in **Figure 7A**. At high mixing agitation, small particle sizes are formed, such that small swelling ratio can be achieved and increased again at diluent (>30 wt.%) and low cross-linking particle (DVB < 60 wt.%) as shown in **Figures 7A,C**.

The properties of the copolymer beads produced for the copolymerization using monomer compositions of 36 wt.% styrene and 64 wt.% divinylbenzene, 84 wt.% diluent based on the total monomers' solution, 90°C temperature, 900 rpm mixing intensity, and 24 h reaction time. The mean particle diameter for the ST-DVB-SO$_3$H beads using sieves was 340 μm. Elemental analysis of the ST-DVB-SO$_3$H copolymer beads showed that it contained 8.63 wt.% of sulfur, corresponding to 2.64 mmol -SO$_3$H per gram.
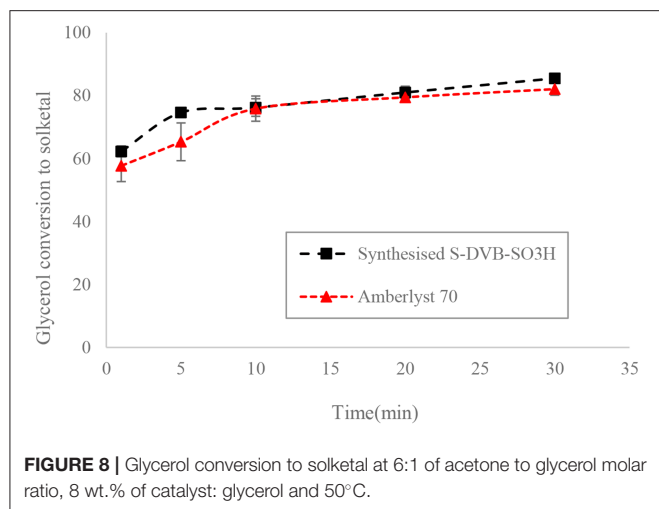
Catalytic Activity and Solketal Productions Using the ST-DVB-SO$_3$H Catalyst

The ST-DVB-SO$_3$H copolymer beads were characterized for their physical and chemical properties. The ST-DVB-SO$_3$H beads were spherical with 340 μm mean particle diameter. Elemental analysis of the ST-DVB-SO$_3$H copolymer beads showed that it contained 8.63 wt.% of sulfur, corresponding to 2.64 mmol -SO$_3$H per gram of copolymer beads. The active site density

of the synthesized ST-DVB-SO$_3$H copolymer catalyst beads was similar to that measured for the Amberlyst^{TM} 70, which has an acidic capacity of 2.59 mmol H$^+$/g as measured by sulfur content elemental analysis (Eze and Harvey, 2018). It was also observed that the ST-DVB-SO$_3$H had similar catalytic activity as the Amberlyst^{TM} 70 (as shown in **Figure 8**).

Results for the design of experiment investigations of solketal production using the ST-DVB-SO$_3$H copolymer beads for glycerol acetalization at 2:1–6:1 acetone to glycerol molar ratio, residence times of 1–20 min, 8.5 wt.% of catalyst, and 30–50°C reaction temperatures, are shown in **Table 2**. The experimental data in **Table 2** were analyzed by stepwise response surface methods using a Minitab 17 statistical software to obtain an empirical model for glycerol conversion to solketal (*X*; shown in Equation 12), where MR is the acetone-to-glycerol molar ratio, *t* is reaction time (min), and *T* is reaction temperature in °C. Experimental error for the data in **Table 1** was ±2%, and this was obtained from the three repeated experiments at run numbers 10, 11, and 15.

$$\mathbf{X}(\%) = 25.43 + 1.325\, \text{MR} + 0.391\, t + 0.637\, T + 0.1615\, \text{MR}^*t$$

(12)

FIGURE 8 | Glycerol conversion to solketal at 6:1 of acetone to glycerol molar ratio, 8 wt.% of catalyst: glycerol and 50°C.

TABLE 2 | Experimental data for glycerol conversions to solketal.

Run number	Acetone/ glycerol molar ratio	Residence time (min)	Temperature (°C)	Glycerol conversion to solketal (%)	
				Experimental values	**Predicted values**
1	4	20	50	81	83.3
2	6	20	40	87	86
3	4	1	50	62	63.6
4	6	10.5	50	83	79.5
5	2	20	40	70.9	67.8
6	2	10.5	30	54.4	54.7
7	6	10.5	30	66.7	66.7
8	4	1	30	55	50.9
9	6	1	40	56.4	60
10	4	10.5	40	71.65	67
11	4	10.5	40	69.96	67
12	4	20	30	66.3	70.6
13	2	1	40	52.5	54.3
14	2	10.5	50	67.2	67.4
15	4	10.5	40	67.8	67

The empirical model in Equation 12 was used to generate the contour plots in **Figure 9**, showing the effects of the process variables. It is clear from Equation 12 that acetone to glycerol molar ratio has the strongest positive effect on the conversion of glycerol to solketal as the acetone to glycerol ratio can enhance the forward reaction (Nanda et al., 2014b) (see **Figures 9A,B**). A steady increase in the conversion of solketal can be observed from **Figures 9B,C**, when the reaction temperature increased. This is attributed to both the increasing inherent rate of reaction (Khayoon and Hameed, 2013) and decreased glycerol viscosity at high temperature. Similarly, high residence time was required to obtaine high glycerol to solketal conversion as shown in **Figure 9C**. The empirical equation for glycerol conversions to solketal was experimentally validated at the process conditions, and the results showed that the experimental conversions agreed well with predicted values.

Glycerol conversion to solketal is limited by thermodynamic equilibrium. This, for example, limits conversion to 81% at 4:1 of acetone to glycerol molar ratio and 50°C and to 87% at 6:1 and 40°C in the presence of 8.5 wt.% of ST-DVB SO_3H (as shown in **Table 1**). Other studies showed that solketal yield was 63.21% at 4:1 and 60°C with 1 wt.% of zeolite H-BEA (SAR 19) catalyst (Rossa et al., 2017) and 81% at 6:1, 70°C, and 5 wt.% of sulfonated carbon–silica catalyst after 30 min (Nandan et al., 2013). Clearly, the process conditions must be adjusted to overcome the equilibrium limitations. There is a need to increase solketal production from glycerol above the equilibrium conversions in the range of 75–80%, commonly obtained in a single-stage process in the industry (Dmitriev et al., 2016).

Investigations of glycerol acetalization using the synthesized ST-DVB-SO3H catalyst indicate that high glycerol conversion to solketal could be obtained in a few minutes, with maximum conversion occurring in the range 2–20 min at 7:1 of acetone to glycerol molar ratio and 50°C as shown in **Figure 10A**, contrary to existing reports that equilibrium glycerol conversion to solketal requires residence times over 6 h at 1:2 of acetone to glycerol molar ratio and 80°C when mesoporous silicate Hf-TUD-1 catalyst was used (Li et al., 2012) and 30 min at 6:1 of

acetone to glycerol molar ratio and 70°C when sulfonic acid-modified mesostructured silica (Ar-SBA-15) catalyst was used (Vicente et al., 2010). This indicated the catalytic activity of St-DVB catalyst for this reaction.

Previous studies have reported that 4:1 of acetone to glycerol molar ratio was an optimum condition to achieve ≈ 75% of glycerol conversion to solketal after 2 h using $SnCl_2$ catalyst (Menezes et al., 2013) and 80% conversion after 1 h with amphiphilic catalysts (Souza et al., 2015). In this work, it was found that by increasing the acetone to glycerol molar ratio to 12:1, complete conversion (up to 98% of glycerol conversion) was obtained in only 30 min (as shown in **Figure 10C**). This is because, in addition to the high catalysis rate by the ST-DVB-SO3H catalyst, the use of acetone in excess shifts the thermodynamic equilibrium toward greater solketal formation, in accordance with Le Chatelier's principle.

Another effective route for achieving higher glycerol to solketal conversions was found to be through a two-stage acetalization process, which requires shorter reaction times under an economic reaction condition. The two-stage route applied a reaction at 10:1 acetone to glycerol molar ratio, with 8.5 wt.% ST-DVB-SO3H copolymer catalyst, and 50°C for 10 min in the first step, followed by catalyst separation and drying in vacuum distillation at 40°C and 10 mbar for 1 h, and a second step reaction with the same amount of acetone of 10:1 molar ratio was added, 8.5 wt.% catalyst, and 50°C for another 10 min. The two-stage process achieved about 99% glycerol to solketal conversion after a total reaction time of 20 min (as shown in **Figure 10B**). A multi-stage batch process has been used to slightly drive forward glycerol conversion to solketal at reaction temperature of 70°C and 5 wt.% of propyl sulphonic acid-functionalized mesostructured silica catalyst, where 89.5%
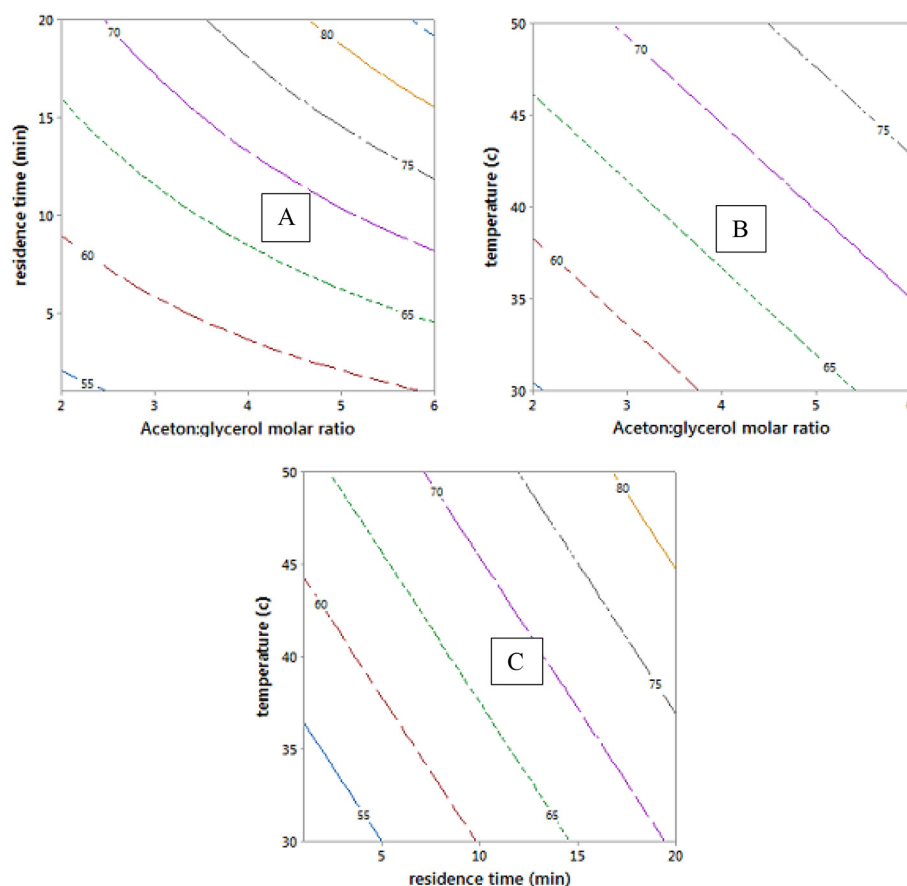
FIGURE 9 | Contour plots of glycerol conversion to solketal at hold values of 4:1 of acetone to oil molar ratio, 10.5 min of residence time, and 40°C.

of glycerol conversion was obtained after the third step (Vicente et al., 2010). The lower solketal conversion in that study could be attributed to the higher temperature of 70°C, which is well above the acetone boiling point, such that excessive loss of acetone during the reaction resulted in lower equilibrium solketal yield.

Figure 10D shows the results for the regeneration and reusability study for the ST-DVB-SO₃H copolymer catalyst. The average glycerol conversion to solketal was about 81% for the fresh catalyst. Subsequent solketal conversions using the regenerated catalyst were 80% for the first recycle, 79% for the second recycle, and 81% for the third recycle. The results demonstrate that the catalyst can be regenerated by treatment with 0.1 M HCl, followed by washing with de-ionized water and drying at 120°C. CNS analysis performed on the fresh and spent ST-DVB-SO₃H showed no change in composition for the fresh and spent catalysts, with the sulfur content remaining consistent between 8.6 and 8.63 wt.% after three cycles.

These findings are consistent with an existing study, which reported that acid-functionalized ion-exchange resins are reusable (Pico et al., 2013; Eze et al., 2017). Therefore, the synthesized ST-DVB-SO₃H copolymer catalyst could be an ideal catalyst for continuous solketal production from glycerol by-product in biodiesel processing.

Techno-Economic Analysis of the Glycerol Acetalization Processes

Techno-economic analysis was used to evaluate the viability of the three process conditions for solketal production as investigated in this study. These solketal process options were one-stage processes at low acetone molar ratio (6:1 of acetone to glycerol molar ratio) to achieve 87% solketal conversion, another one-stage process at higher acetone molar ratio (12:1) to achieve 98% solketal conversion, and a two-stage solketal process using 10:1 of acetone to glycerol molar ratio to obtain 98% solketal conversion. The techno-economic analysis of these three processes using the Aspen (HYSYS) showed that the total capital investment cost for the two-stage process was $27.5 M, $28.7 M for the one-stage process at 12:1 acetone to glycerol molar ratio, and $29.42 M for the one-stage process at 6:1 acetone to glycerol molar ratio (as shown in **Table 3**).

As shown in **Table 3**, the net revenue from the two-stage process was $119.36 M, which was slightly higher than $118.85 M for the one-stage process at 12:1 acetone to glycerol molar ratio, and $67.2 M for the one-stage process at 6:1 acetone to glycerol molar ratio. The NPV for the three glycerol acetalization process options follows similar trends as the net revenue. The NPV of the two-stage process was $707 M, which was higher than $703 M for
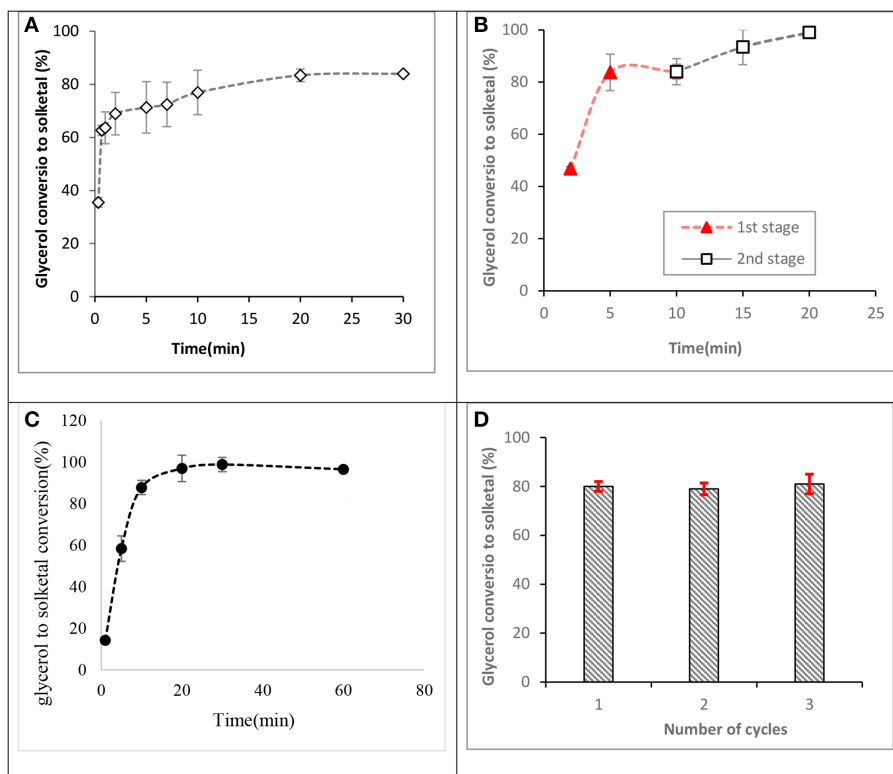
FIGURE 10 | Glycerol conversions to solketal at 50°C. **(A)** Reaction profile for a fresh catalyst at 7:1 of acetone to glycerol molar ratio and 8.5 wt.% of catalyst to glycerol, **(B)** a two-stage process at 10:1 of acetone to glycerol molar ratio and 8.5 wt.% of ST-DVB-SO3H catalyst to glycerol, **(C)** 12:1 of acetone to glycerol molar ratio and 8.5 wt.% of ST-DVB-SO3H catalyst, and **(D)** reusability of the styrene-DVB copolymer catalyst at 12:1 of acetone to glycerol molar ratio, and 5 wt.% of ST-DVB-SO$_3$H catalyst to glycerol at 2 h.

TABLE 3 | Economic evaluation of three different plants to produce solketal from glycerol acetalization (100,000 tons/year).

Techno-economic parameters	One-stage process (12:1 molar ratio)	One-stage process (6:1 molar ratio)	Two-stage process (10:1 molar ratio)
TCI ($ /M)	28.7	29.42	27.5
Operating cost ($ /M)	17.2	13.8	15.7
Utility cost ($/M)	14.7	11.4	13.26
Annual net revenue ($/ M)	118.85	67.2	119.36
NPV($/M) at 20 years	703	384	707
Break-even price ($/ton)	2,058	2,088	2,058

the one-stage process at 12:1 acetone to glycerol molar ratio, and $384 M for the one-stage process at 6:1 acetone to glycerol molar ratio. This was attributed to the higher cost of the distillation columns that were used in the purification steps of solketal in one-stage process (6:1 of acetone to glycerol molar ratio) to separate solketal from the high amount of glycerol and water. Only one distillation column was used in the purification step of solketal in the one-stage process (12:1 of acetone to glycerol) to separate (98% solketal and 2% of glycerol) from water. No purification step was required in the two-stage process as the formed product was separated from the first step and only a small amount of water (0.16% ≈ 0) was formed in the last stage.

Consequently, the break-even prices of solketal for these processes were reduced to $2,058/ton for the one-stage at 12:1 acetone molar ratio and two-stage process and to $2,088/ton for the one-stage at 6:1 acetone molar ratio, which are all lower than the current price of $3,000/ton for solketal (Alibaba, 2018).

The sensitivity analysis of acetone, glycerol, and solketal were evaluated by varying their prices from −50 to 50% for 20 years at 15.3% discount rate (**Figure 11**). As shown in **Figures 11A–C**, increase in glycerol prices by 10% resulted in decrease in the NPV by about $52.53 M for the one-stage process at 12:1 acetone, $59.18 M for the one-stage process at 6:1 acetone, and $52.53 M for the two-stage process at 10:1 acetone. Increasing the acetone price also had a huge effect on the plant's NPV. For instance, a 10% increase in the acetone price resulted in reductions of the NPV by $27.6 M, $31.1 M, and $ 27.6 M for the one-stage process at 12:1 acetone, one-stage process at 6:1 acetone, and two-stage process at 10:1 acetone, respectively. On the contrary, increasing
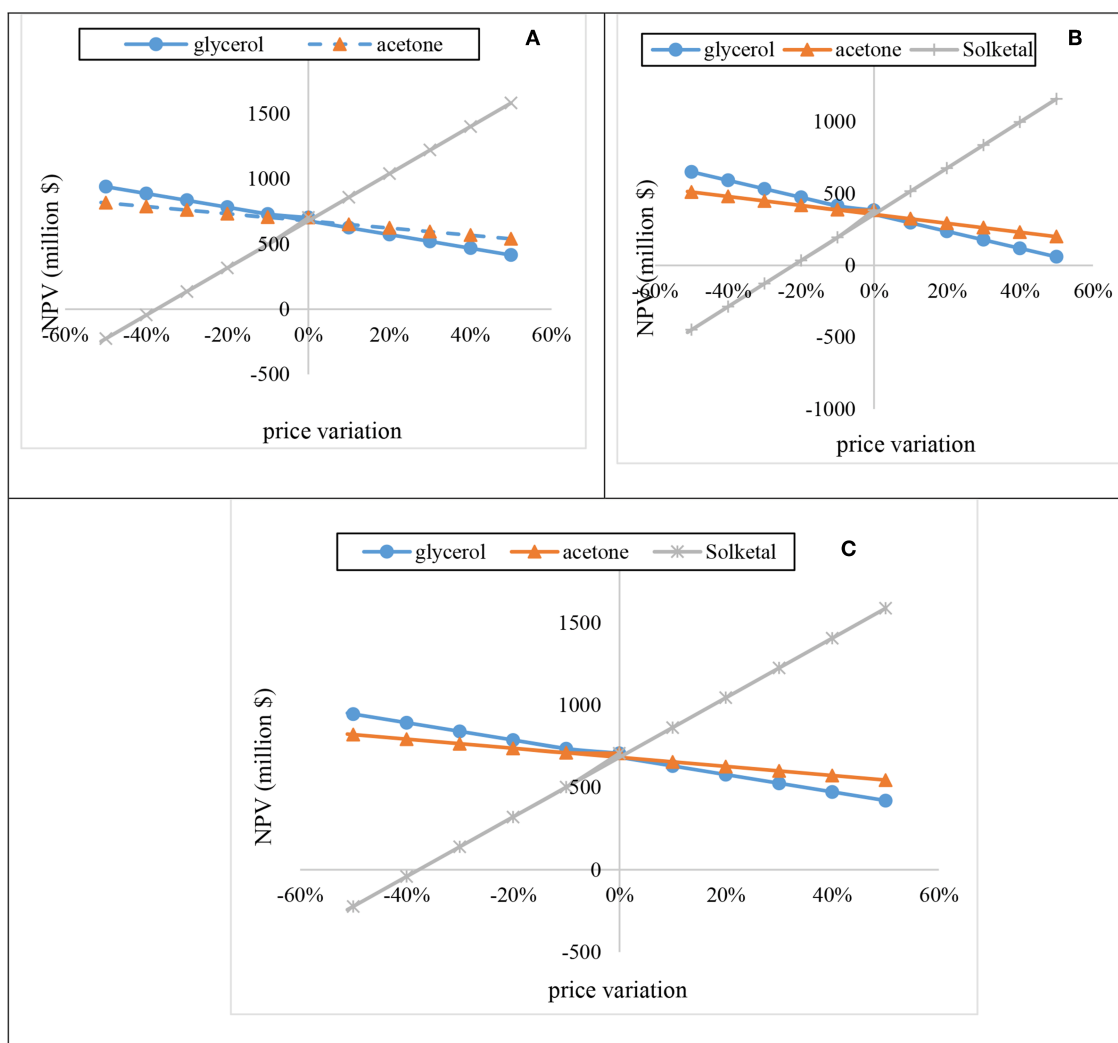
FIGURE 11 | Sensitivity of the process NPV to fluctuations in reactants (acetone and glycerol) and product (solketal) prices.

the solketal price by 10% resulted in a substantial rise in the NPV. As shown in **Figures 11A–C**, a 10% rise in the solketal price resulted in NPV rise by ∼$181 M for one-stage (12:1) and two-stage plants.

CONCLUSION

Styrene-divinylbenzene copolymer beads of desired physical properties were synthesized and functionalized for catalytic application in glycerol conversion to solketal. Mixing intensity had a profound effect on the particle size of the copolymer beads, while the DVB and diluent contents determined the degrees of crosslinking and porosity of the beads, respectively. The copolymer beads with the most desirable physical properties (high mechanical stability, porosity, and surface area) were derivatized with sulphonic acid and used in the catalysis of glycerol acetalization with acetone under mild reaction conditions (30–50°C, 2–30 min reaction time,

8.5 wt.% of the catalyst, and 2:1–12:1 acetone to glycerol molar ratio. Both the synthesis of the copolymer beads and the glycerol acetalization processes were investigated using design of experiments (response surface methodology), leading to empirical models for optimization of particle sizes, beads surface area, and swelling ratio. The sulphonic acid-functionalized styrene-divinylbenzene copolymer beads synthesized in this work were found to be catalytically active. This catalyst has similar catalytic activity as the AmberlystTM 70 obtained from Dow Chemical Company, Netherlands. Generally, the glycerol conversion to solketal increased with reaction temperature, residence time, and acetone to glycerol molar ratio.

Three process conditions for glycerol valorization to solketal using a synthesized sulphonic acid-functionalized styrene-divinylbenzene (ST-DVB-SO$_3$H) copolymer catalyst were investigated. The ST-DVB-SO$_3$H copolymer beads were obtained by copolymerization of 36 wt.% styrene and 64 wt.%

divinylbenzene monomer mixture in 84 wt.% diluent based on the total monomer solution, followed by sulphonic acid site functionalization. The ST-DVB-SO$_3$H beads produced were spherical of 340 μm mean particles diameter and 2.64 mmol of SO$_3$H active sites per gram were produced. Under three processes at 50°C and 8.5 wt.% of ST-DVB: single-stage process (1) 6:1 of acetone to glycerol molar ratio, (2) 12:1 of acetone to glycerol molar ratio to achieve 87% and ≥98% of solketal yield from each process, respectively, and two stages process at 10:1 of acetone to glycerol molar ratio to obtain ≥98%.

Techno-economic analysis was performed using Aspen (HYSYS) for a fixed capacity of 100,000 ton/years and 20-years lifetime, based on the 30-min reaction time. The techno-economic analysis of the three solketal process options at fixed capacity of 100,000 ton/years and 20-years lifetime showed that the net present values for the solketal process options were $707 M for the two-stage, $703 M for the one-stage at 6:1 acetone to glycerol molar ratio, and $384 M for one-stage at 12:1 acetone to glycerol molar ratio.

AUTHOR CONTRIBUTIONS

LA-S collected all the data and wrote the first draft of the paper. This work was done under VE and AH supervision.

ACKNOWLEDGMENTS

REFERENCES

Alibaba (2018). *Chemicals Categories*. Available online at: www.alibaba.com

Ashby, R., Solaiman, D. Y., and Foglia, T. (2004). Bacterial poly(hydroxyalkanoate) polymer production from the biodiesel co-product stream. *J. Polym. Environ.* 12, 105–112. doi: 10.1023/B:JOOE.0000038541.54263.d9

Boz, N., Nebahat, D., and Kalyon, D. M. (2015). Esterification and transesterification of waste cooking oil over Amberlyst 15 and modified Amberlyst 15 catalysts. *Appl. Catal. B Environ.* 165, 723–730. doi: 10.1016/j.apcatb.2014.10.079

Ciriminna, R., Della Pina, C., Rossi, M., and Pagliaro, M. (2014). Understanding the glycerol market. *Eur. J. Lipid Sci. Technol.* 116, 1432–1439. doi: 10.1002/ejlt.201400229

Coutinho, F. M. B., Teixeira, V. G., and Barbosa, C. R. (1998). Synthesis and characterization of styrene–divinylbenzene loaded with di(2-ethylhexyl)phosphonic acid. I. Influence of diluent mixture on the porous structure of the copolymer. *J. Appl. Polymer Sci.* 67, 781–787. doi: 10.1002/(SICI)1097-4628(19980131)67:5<781::AID-APP2>3.0.CO;2-P

da Silva, M. J., Ávila Rodrigues, F., and Júlio, A. A. (2017). SnF2-catalyzed glycerol ketalization: a friendly environmentally process to synthesize solketal at room temperature over on solid and reusable Lewis acid. *Chem. Eng. J.* 307, 828–835. doi: 10.1016/j.cej.2016.09.002

Demirbas, A. (2008). *A Realistic Fuel Alternative for Diesel Engines. 1st Edn.* London: Springer. p. 1–208.

Dmitriev, G. S., Terekhov, A. V., Zanaveskin, L. N., Khadzhiev, S. N., Zanaveskin, K. L., Maksimov, A. L. (2016). Choice of a catalyst and technological scheme for synthesis of solketal. *Russian J. Appl. Chem.* 89, 1619–1624. doi: 10.1134/S1070427216100094

Durie, S., Jerabek, K., Mason, C., and Sherrington, D. C. (2002). One-pot synthesis of branched poly(styrene–divinylbenzene) suspension polymerized resins. *Macromolecules* 35, 9665–9672. doi: 10.1021/ma0209794

Eze, V. C., and Harvey, A. P. (2018). Continuous reactive coupling of glycerol and acetone—a strategy for triglyceride transesterification and in-situ valorisation of glycerol by-product. *Chem. Eng. J.* 347, 41–51. doi: 10.1016/j.cej.2018.04.078

Eze, V. C., Phan, A., and Harvey, P. A. (2017). Intensification of carboxylic acid esterification using a solid catalyst in a mesoscale oscillatory baffled reactor platform. *Chem. Eng. J.* 322, 205–214. doi: 10.1016/j.cej.2017.04.038

Fu, J., and Borges, M. E. (2015). Free fatty acids esterification for biodiesel production using self-synthesized macroporous cation exchange resin as solid acid catalyst. *Fuel* 154, 1–8. doi: 10.1016/j.fuel.2015.03.048

Gokmen, M. T., and Du Prez, F. E. (2012). Porous polymer particles—a comprehensive guide to synthesis, characterization, functionalization and applications. *Progr. Polymer Sci.* 37, 365–405. doi: 10.1016/j.progpolymsci.2011.07.006

Helwani, Z., Othman, M. R., Aziz, N., Fernando, W. J. N., and Kim, J. (2009). Technologies for production of biodiesel focusing on green catalytic techniques: a review. *Fuel Proc. Technol.* 90, 1502–1514. doi: 10.1016/j.fuproc.2009.07.016

Huang, D., Wang, Z., and Yuan, Z. (2012). Pretreatment of trap grease with Amberlyst-15 for biodiesel production. *Adv. Mater. Res.* 347–353, 2528–2531. doi: 10.4028/www.scientific.net/AMR.347-353.2528

Kangwansupamonkon, W., Damronglerd, S., and Kiatkamjornwong, S. (2002). Effects of the crosslinking agent and diluents on bead properties of styrene-divinylbenzene copolymers. *J. Appl. Polymer Sci.* 85, 654–669. doi: 10.1002/app.10620

Khayoon, M. S., and Hameed, B. H. (2013). Solventless acetalization of glycerol with acetone to fuel oxygenates over Ni–Zr supported on mesoporous activated carbon catalyst. *Appl. Catal. A Gen.* 464–465(Suppl. C), 191–199. doi: 10.1016/j.apcata.2013.05.035

Kim, M. J., Kim, M. Y., Kwon, O. Z., and Seo, G. (2011). Transesterification of vegetable oils over a phosphazenium hydroxide catalyst incorporated onto silica. *Fuel Proc. Technol.* 92, 126–131. doi: 10.1016/j.fuproc.2010.09.015

Knothe, G., Krahl, J., and Van Gerpen, J. (2010). *The Biodiesel Handbook, 2nd Edn.* Biodiesel Handbook. p. 1–501.

Leoneti, A. B., Aragão-Leoneti, V., and Oliveira, S. V. W. B. (2012). Glycerol as a by-product of biodiesel production in Brazil: alternatives for the use of unrefined glycerol. *Renew. Energy* 45, 138–145. doi: 10.1016/j.renene.2012.02.032

Leung, D. Y. C., Wu, X., and Leung, K. H. (2010). A review on biodiesel production using catalyzed transesterification. *Appl. Energy* 87, 1083–1095. doi: 10.1016/j.apenergy.2009.10.006

Li, L., Korányi, T. I., and Hensen, E. J. M. (2012). Highly-efficient conversion of glycerol to solketal over heterogeneous Lewis acid catalysts. *Green Chem.* 14, 1611–1619. doi: 10.1039/c2gc16619d

Melero, J. A., Iglesias, J., and Morales, G. (2009). Heterogeneous acid catalysts for biodiesel production: current status and future challenges. *Green Chem.* 11, 1285–1308. doi: 10.1039/b902086a

Menezes, F. D. L., Guimaraes, M. D. O., and da Silva, M. J. (2013). Highly selective SnCl2-catalyzed solketal synthesis at room temperature. *Industr. Eng. Chem. Res.* 52, 16709–16713. doi: 10.1021/ie402240j

Mota, C. J. A., da Silva, C. X., Rosenbatch, N., Costa, J., and da Silva, F. (2010). Glycerin derivatives as fuel additives: the addition of glycerol/acetone ketal (solketal) in gasolines. *Energy Fuels* 24, 2733–2736. doi: 10.1021/ef9015735

Mu, Y., Teng, H., Zhang, D. J., Wang, W., and Xiu, Z.-L. (2006). Microbial production of 1,3-propanediol by *Klebsiella pneumoniae* using crude glycerol from biodiesel preparations. *Biotechnol. Lett.* 28, 1755–1759. doi: 10.1007/s10529-006-9154-z

Nanda, M. R., Yuan, Z., Qin, W., Ghaziaskar, H. S., Poirier, M. A., and Xu, C. (2014a). Catalytic conversion of glycerol to oxygenated fuel additive in a continuous flow reactor: process optimization. *Fuel* 128, 113–119. doi: 10.1016/j.fuel.2014.02.068

Nanda, M. R., Yuan, Z., Qin, W., Ghaziaskar, H. S., Poirier, M. A., and Xu, C. (2014b). Thermodynamic and kinetic studies of a catalytic process to convert glycerol into solketal as an oxygenated fuel additive. *Fuel* 117 (Part A), 470–477. doi: 10.1016/j.fuel.2013.09.066

Nandan, D., Peta, S., Konathala, L. N. S., Kumar, M., and Nagabhatla, V. (2013). Acid functionalized carbon–silica composite and its application for solketal production. *Microp. Mesop. Mater.* 179, 182–190. doi: 10.1016/j.micromeso.2013.06.004

Özbay, N., Oktar, N., and Tapan, N. A. (2008). Esterification of free fatty acids in waste cooking oils (WCO): role of ion-exchange resins. *Fuel* 87, 1789–1798. doi: 10.1016/j.fuel.2007.12.010

Papanikolaou, S., Muniglia, L., Chevalot, I., Aggelis, G., and Marc, I. (2002). Yarrowia lipolytica as a potential producer of citric acid from raw glycerol. *J. Appl. Microbiol.* 92, 737–744. doi: 10.1046/j.1365-2672.2002.01577.x

Park, S.-H., Park, J.-H., Gobikrishnan, S., Jeong, G.-T., and Park, D.-H. (2015). Biodiesel production from palm oil using a non-catalyzed supercritical process. *Korean J. Chem. Eng.* 32, 2290–2294. doi: 10.1007/s11814-015-0203-y

Patil, P. D., Gude, V. G., and Deng, S. (2009). Biodiesel production from Jatropha curcas, waste cooking, and Camelina sativa oils. *Ind. Eng. Chem. Res.* 48, 10850–10856. doi: 10.1021/ie901146c

Pico, M. P., Rosas, J. M., Rodriguos, S., Santos, A., and Romero, A. (2013). Glycerol etherification over acid ion exchange resins: effect of catalyst concentration and reusability. *J. Chem. Technol. Biotechnol.* 88, 2027–2038. doi: 10.1002/jctb.4063

Rodrigues, R., Isoda, N., Goncalves, M., Figueiredo, F. C. A., Mandelli, D., and Carvalho, W. A. (2012). Effect of niobia and alumina as support for Pt catalysts in the hydrogenolysis of glycerol. *Chem. Eng. J.* 198–199, 457–467. doi: 10.1016/j.cej.2012.06.002

Rossa, V., Pessanha, Y. S. P., Diaz, G., Diogenes, L., Camara, T., Pergher, S. B. C., et al. (2017). Reaction kinetic study of solketal production from glycerol ketalization with acetone. *Industr. Eng. Chem. Res.* 56, 479–488. doi: 10.1021/acs.iecr.6b03581

Sakdasri, W., Sawangkeaw, R., and Ngamprasertsith, S. (2018). Techno-economic analysis of biodiesel production from palm oil with supercritical methanol at a low molar ratio. *Energy* 152, 144–153. doi: 10.1016/j.energy.2018.03.125

Sharma, Y. C., Singh, B., and Korstad, J. (2011). Advancements in solid acid catalysts for ecofriendly and economically viable synthesis of biodiesel. *Biofuels Bioprod. Bioref.* 5, 69–92. doi: 10.1002/bbb.253

Souza, T. E., Padula, I. D., Teodoro, M. M. G., Chagas, P., Resende, J. M., Souzza, P. P., et al. (2015). Amphiphilic property of niobium oxyhydroxide for waste glycerol conversion to produce solketal. *Catalysis Today* 254, 83–89. doi: 10.1016/j.cattod.2014.12.027

Suriyaprapadilok, N., and Kitiyanan, B. (2011). Synthesis of solketal from glycerol and its reaction with benzyl alcohol. *Energy Proc.* 9, 63–69. doi: 10.1016/j.egypro.2011.09.008

Tesser, R., Di Serio, M., Casale, L., Sannino, L., Ledda, M., and Santacesaria, E. (2010). Acid exchange resins deactivation in the esterification of free fatty acids. *Chem. Eng. J.* 161, 212–222. doi: 10.1016/j.cej.2010.04.026

Vicente, G., Melero, J. A., Morales, G., Paniagua, M., and Martin, E. (2010). Acetalisation of bio-glycerol with acetone to produce solketal over sulfonic mesostructured silicas. *Green Chem.* 12, 899–907. doi: 10.1039/b923681c

Yang, F., Hanna, M. A., and Sun, R. (2012). Value-added uses for crude glycerol a byproduct of biodiesel production. *Biotechnol. Biofuels* 5:13. doi: 10.1186/1754-6834-5-13

Yussof, W. M. H. W. (2012). *Evaluation of Heterogeneous Quaternary Ammonium Catalysts for Transesterification of Triglycerides.* Newcastle University.

Advantages of publishing in Frontiers

OPEN ACCESS
Articles are free to read
for greatest visibility
and readership

FAST PUBLICATION
Around 90 days
from submission
to decision

HIGH QUALITY PEER-REVIEW
Rigorous, collaborative,
and constructive
peer-review

TRANSPARENT PEER-REVIEW
Editors and reviewers
acknowledged by name
on published articles

Frontiers
Avenue du Tribunal-Fédéral 34
1005 Lausanne | Switzerland

Visit us: www.frontiersin.org
Contact us: info@frontiersin.org | +41 21 510 17 00

REPRODUCIBILITY OF RESEARCH
Support open data
and methods to enhance
research reproducibility

DIGITAL PUBLISHING
Articles designed
for optimal readership
across devices

FOLLOW US
@frontiersin

IMPACT METRICS
Advanced article metrics
track visibility across
digital media

EXTENSIVE PROMOTION
Marketing
and promotion
of impactful research

LOOP RESEARCH NETWORK
Our network
increases your
article's readership